Early Triassic Palaeoenvironmental and Floral Changes on North Gondwana

---

Dissertation

zur

Erlangung der naturwissenschaftlichen Doktorwürde
(Dr. sc. nat.)

vorgelegt der

Mathematisch-naturwissenschaftlichen Fakultät

der

Universität Zürich

von

Elke Hermann

aus

Deutschland

Promotionskomitee

Prof. Dr. Peter A. Hochuli
(Leiter der Dissertation, Vertreter der Universität Zürich)
Prof. Dr. Hugo Bucher
Prof. Dr. Helmut Weissert

Zürich, 2011

Contents

Abstract

The end-Permian mass extinction is preceding the Early Triassic representing the time period of biotic recovery. The recovery patterns of the different marine faunal groups show great differences. Ammonoids and conodonts are the two marine clades that recovered quickly after the end-Permian extinction event. Their recovery was interrupted by Early Triassic marine extinction events such as the late Smithian event. The recovery of benthic organism was rather slow (reefs) or repeatedly reset by multiple minor extinction events during the Early Triassic (gastropods and bivalves). Consequences of the end-Permian event proposed for the continental vegetation range from a rapid and total collapse of terrestrial ecosystems to a rather long-term gradual change. The recovery patterns in the marine realm and terrestrial ecosystem changes are thought to be closely linked to environmental perturbation triggered by late pulses of the Siberian Trap volcanism and reflected in the Early Triassic C-isotope records, which are characterised by recurrent positive and negative anomalies.

In order to investigate changes in marine palaeoenvironments, and their link to carbon cycle perturbations, late Permian to Middle Triassic deposits have been studied with a combined approach of sedimentology, palynology, palynofacies, carbon isotopes and organic geochemistry. The sedimentary sequences from the Trøndelag and Finnmark platforms (Norway) represent the most expanded Permian-Triassic boundary sections containing well preserved organic matter. In order to assess the timing of ecosystem changes across the Permian-Triassic transition in Norway a high-resolution $\delta^{13}C_{org}$ dataset has been generated. This dataset allowed the establishment of a chemostratigraphic scheme that could be correlated to other globally distributed Permian-Triassic boundary sections. The global correlation reveals that the extinction of marine organisms occurred during the stepwise negative decline of C-isotopes across the Permian-Triassic boundary.

A reference area for the Early Triassic of the North Indian Margin is located in Pakistan. The sedimentary archives from the Nammal, Chhidru, Chitta-Landu and Narmia gorges in the Salt Range and Surghar Range have been studied to describe the marine environmental conditions in the aftermath of the end-Permian extinction. The sections are characterised by excellently preserved organic matter. Sedimentological and palynofacies data reveals several seal-level changes during the Early Triassic that could be correlated to a global Early Triassic sea-level curve. For the Dienerian poor oxygenation levels are indicated by high amounts of amorphous organic matter in the particulate organic matter assemblages. In contrast to previous studies our results do not support an anoxic event in the Griesbachian. Biomarker studies of a few samples suggest proliferating bacteria during the Early Triassic.

In order to investigate short-termed climatic and vegetation patterns from the late Permian to the Middle Triassic, terrestrial palynomorph assemblages from the sedimentary archives of the North Indian Margin have been studied. Changing humidity conditions have been inferred from the spore-pollen ratios of the palynological records from Pakistan and South Tibet. The results demonstrate increased humidity in the

Griesbachian persisting with short-termed fluctuations up to the middle Smithian. In the late Smithian, climate changed abruptly, humidity decreased and dryer climates prevailed in the Spathian and Anisian. Comparison to previous climate interpretations on Early Triassic palynological datasets from Norway reveals that the late Smithian climate change is not a local phenomenon of the North Indian Margin but has global significance. This climate change coincides with a major extinction event of ammonoids and conodonts. Probable causes for the observed climatic patterns are elevated atmospheric CO_2 levels combined with orbital forced insolation changes that influenced the monsoon intensity on the North Indian Margin. The vegetation patterns on North Gondwana inferred from the palynological records from Pakistan document high lycopod abundances from the Griesbachian to the middle Smithian where the climax of lycopods is reflected in a spore spike. This spore spike is closely associated with a C-isotope negative excursion and followed by a marine faunal extinction event (late Smithian event). The striking similarities with the end-Permian spore spike documented in previous studies support the conclusion that both events (end-Permian and late Smithian) are driven by comparable environmental perturbations. The resurgence of gymnosperms in the Spathian 2.1 Ma after lycopod dominated ecosystems suggests the fading of volcanically induced environmental stress.

Based on the palynological dataset the Early Triassic palynostratigraphy of Pakistan could be refined. Eight successive assemblage zones are distinguished and calibrated against ammonoid biostratigraphy and C-isotope chemostratigraphy. A comparison with other floral provinces reveals distinct local differences in the floral assemblages in the Permian and in the Spathian to Anisian interval. During the Griesbachian to Smithian time interval, floral assemblages show a more cosmopolitan character.

Keywords: Permian-Triassic boundary, Early Triassic, palynology, carbon isotopes, sedimentology, palynofacies, vegetation history, Norway, Pakistan

Zusammenfassung

Das Massenaussterben am Ende des Perms stellt das grösste Aussterbeereignis der Erdgeschichte dar. Die Erholung der Diversität nach diesem Ereignis verlief in den verschiedenen marinen Faunengruppen unterschiedlich schnell. Ammonoideen und Conodonten sind zwei Gruppen, die sich in der Frühen Trias schnell erholten. Durch nachfolgende Aussterbeeignisse (wie zum Beispiel im späten Smithium) zeigen sie jedoch komplexe Aussterbe- und Diversifizierungsmuster. Die Erholung benthischer Organismen war eher langsam (Riffe) oder wurde wiederholt von kleineren, aufeinanderfolgenden Aussterbeereignissen in der Frühen Trias unterbrochen (Gastropoden und Bivalven). Die vermuteten Auswirkungen des Massenaussterbens am Ende des Perms auf die Flora reichen von einem katastrophalen Zusammenbruch der terrestrischen Ökosysteme bis hin zu einem graduellen langfristigen Florenübergang. Die Erholung mariner Organismen und die Änderungen in terrestrischen Ökosystemen der Frühen Trias hingen stark von den vorherrschenden Umweltbedingungen ab. Die Kohlenstoffisotopendaten sind durch wiederkehrende positive und negative Anomalien gekennzeichnet, die auf periodische vulkanische Aktivität der Sibirischen Traps zurückgeführt werden können. Die dabei freigesetzten Gase führten zu klimatischen und ökologischen Veränderungen.

Um Änderungen in der marinen Paläoökologie und deren Beziehungen zu Veränderungen im Kohlenstoffkreislauf zu untersuchen, wurden Abfolgen des Späten Perms bis zur Mittleren Trias herangezogen. Diese wurden mit verschiedenen Methoden wie Sedimentologie, Palynofaziesanalyse, Kohlenstoffisotopen-Geochemie und organischer Geochemie untersucht. Die sedimentären Abfolgen der Trøndelag und Finnmark Plattformen in Norwegen sind expandierte Abfolgen des Perm-Trias-Überganges, die sich durch ihr gut erhaltenes organisches Material auszeichnen. Um die zeitliche Abfolge der Änderungen in den terrestrischen Ökosystemen zu bestimmen, wurde ein hochauflösender $\delta^{13}C_{org}$ Datensatz gemessen. Das daraus entstandene chemostratigraphische Muster konnte weltweit korreliert werden und zeigt, dass sich das Aussterben mariner Organismen während einer stufenweise auftretenden Kohlenstoffisotopenanomalie ereignete.

Ein Referenzgebiet für die Frühe Trias des Nord Indischen Kontinentalrandes ist in Pakistan zu finden. Die sedimentären Abfolgen der Nammal, der Chhidru, der Chitta-Landu und der Narmia Schlucht zeichnen sich durch ihr gut erhaltenes organisches Material aus. Sediment- und Palynofaziesdaten dokumentieren Meeresspiegelschwankungen, die mit der globalen Meeresspiegelkurve der Frühe Trias korreliert werden können. Die Zusammensetzung des partikulären organischen Materials zeigt, dass im Dienerium der Sauerstoffgehalt des Meeres niedrig war. Im Gegensatz zu früheren Studien konnte für das Griesbachium jedoch keine Anoxia festgestellt werden.

Um kurzzeitige Klimaschwankungen und Änderungen in der Vegetationszusammensetzung vom Späten Perm bis in die Mittlere Trias zu dokumentieren, wurden die Sporen und Pollen Assoziationen aus diesen Profilen untersucht. Änderungen der Humidität des Klimas in Nord Gondwana konnten aus den Sporen-Pollen-Verhältnissen der Profile abgeleitet werden. Humides Klima herrschte vom Griesbachium bis ins

mittlere Smithium. Im späten Smithium wurde das Klima schlagartig trockener. Tendenziell arideres Klima überwog im Spathium und Anisium. Der Vergleich mit früheren Klimastudien in Norwegen zeigt, dass der schnelle klimatische Wechsel im späten Smithium kein lokales Phänomen Nord Gondwanas ist, sondern globale Bedeutung hat. Der Klimaumschwung fällt mit dem marinen Aussterbeereignis des späten Smithium zusammen, von dem Ammonoideen und Conodonten betroffen waren. Der Grund für die beobachteten Klimaänderungen ist vermutlich eine Kombination aus erhöhtem CO_2-Gehalt der Atmosphäre und orbital gesteuerten Änderungen der Sonneneinstrahlung, welche die Monsunintensität Nord Gondwanas steuerte. Der palynologische Datensatz diente ausserdem dazu, Änderungen in der Vegetationszusammensetzung zu erfassen. Vom Griesbachium bis ins mittlere Smithium war die Vegetation der Region von Lycopodiengewächsen bestimmt. Im mittleren Smithium war die Vegetation fast vollständig von dieser Pflanzengruppe dominiert, was sich in einem markanten „Sporen-Peak“ zeigt. Dieser ist mit einer negativen Kohlenstoffisotopenanomalie assoziiert. Unmittelbar danach ereignete sich ein markantes marines Aussterbeereignis (spätes Smithium). Die Ähnlichkeiten mit dem in früheren Studien dokumentierten „Sporen-Peak“ am Ende des Perms ist verblüffend und lässt den Schluss zu, dass für beide Ereignisse ähnliche Änderungen der Umweltbedingungen verantwortlich sein könnten. Nach ca. 2,1 Ma begann sich die Florenzusammensetzung zugunsten der Gynmospermen zu ändern. Dies deutet darauf hin, dass sich der durch vulkanische Aktivität verursachte Stress legte.

Basierend auf den palynologischen Datensätzen konnte die Palynostratigraphie der Frühen Trias Pakistans revidiert werden. Acht Palynozonen wurden beschrieben und mit Hilfe von Ammonoideen-Biostratigraphie und Kohlenstoffisotopen-Chemostratigraphy kalibriert. Der Vergleich mit anderen Florenprovinzen zeigt, dass sich die lokalen palynologischen Assoziationen des Perms und im Zeitabschnitt vom Spathium bis Anisium stark unterscheiden. Im Zeitabschnitt Griesbachium bis Smithium dagegen haben die Assoziationen einen eher kosmopolitischen Charakter.

Schlüsselwörter: Perm-Trias Grenze, Frühe Trias, Palynologie, Kohlenstoffisotopen, Sedimentologie, Palynofazies, Florenentwicklung, Norwegen, Pakistan

Introduction

1. The end-Permian mass extinction

The Phanerozoic history of life is marked by five dramatic mass extinctions, of which the end-Permian event was the most severe biotic crises with a loss of 52% marine families (Raup and Sepkoski, 1982) (Fig. 1). Terrestrial tetrapod families were reduced by 70 to 80 % (Maxwell, 1992, Benton et al., 2004). In summary that means a loss of 80-96% of all animal species on earth (Benton and Twitchett, 2003). The recovery after the end-Permian event has long been assumed to be unusually long taking the entire Early Triassic (Hallam, 1991, Pruss and Bottjer, 2005). To study this peculiar time interval a multidisciplinary project has been launched at Institute and Museum of Palaeontology of the University of Zurich, which address several aspects of the Early Triassic recovery interval. Ongoing research in this project includes the study of terrestrial ecosystems of the northern hemisphere (Peter A. Hochuli); evolutionary trends, palaeobiogeography and biostratigraphy of ammonoids (Hugo Bucher, Thomas Brühwiler, and David Ware); Early Triassic conodonts (Nicolas Goudemand); the recovery of fish and the study of oxygen isotopes (Carlo Romano and Winand Brinkmann); the recovery patterns of benthic organism (Michael Hautmann and Richard Hofmann). The combined approach allows determining the recovery patterns of various clades in the aftermath of the end-Permian extinction and their relationship to environmental perturbations, such as climatic and oceanographic changes.

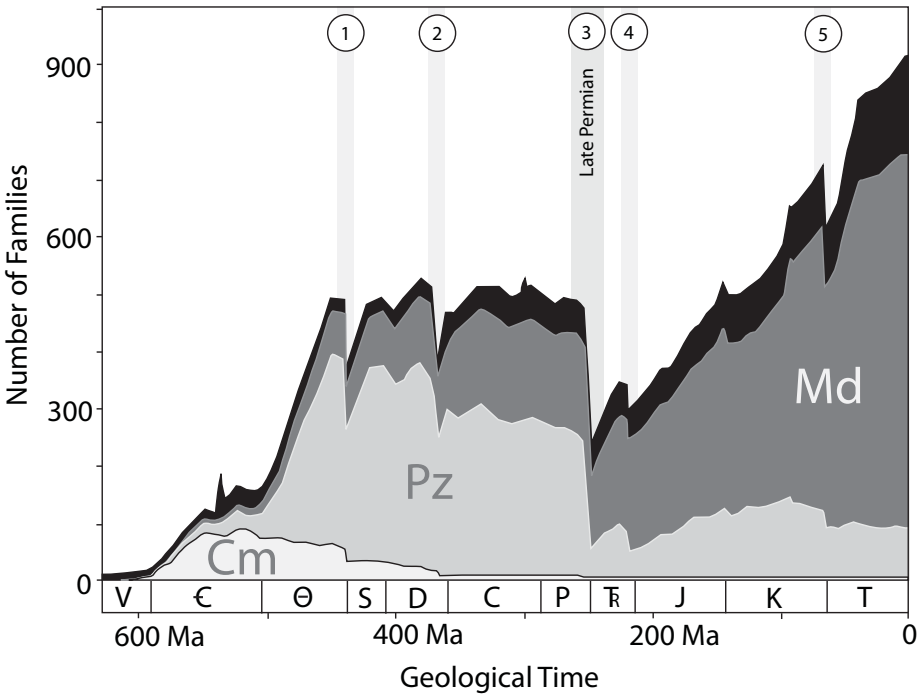

Figure 1. Marine diversity during the Phanerozoic. Cm: Cambrian fauna; Pz: Palaeozoic fauna; Md: Mesozoic-Cenozoic, or modern fauna after Sepkoski (1984).

The present thesis is a contribution to the aforementioned project and focuses on the palaeoenvironmental changes of the North Indian Margin and Norway as well as on climatic changes and the recovery of terrestrial ecosystems on North Gondwana.

The inferred causes for the end-Permian mass extinction and the observed floral changes range from a major sea level regression (Holser et al., 1989), massive volcanic activity (Renne and Basu, 1991;Renne et al., 1995), ocean acidification caused by volcanic degassing (Heydari et al., 2008), global warming caused by CO_2 (Kidder and Worsley, 2004; Kiehl and Shields, 2005; Wignall 2001), oceanic anoxia (Grice et al., 2005; Isozaki, 1997; Kump et al., 2005;Wignall and Hallam, 1992, 1993, Wignall and Twitchett, 1996; 2002), hypercapnia (Knoll et al., 1996) to an extraterrestrial impact (Becker et al., 2004). Beside the theory of an extraterrestrial impact all of the mentioned causes are more of less related to volcanism (Siberian Traps). The volcanic activity of the Siberian Traps induced profound environmental changes in the ocean-atmosphere system. CO_2 from volcanic degassing, from dissociation of methane clathrates (Retallack and Krull, 2006) or released from heating of organic rich sediments during emplacement of magmatic sills also affected the global carbon cycle (Svensen et al., 2009 Retallack and Jahren, 2008). The end-Permian mass extinction is associated with a negative carbon isotope spike reflecting fundamental changes in the budgets of the carbon pools (Baud et al., 1989; 1996; Hermann et al., in press).

After the great diversity loss the Early Triassic recovery patterns vary significantly between the marine faunal groups. Two marine clades that recovered quickly are ammonoids (Brayard et al, 2005; 2006; 2009) and conodonts (Orchard, 2007; Goudemand et al., 2008).

However, their rapid diversification was interrupted by a major biotic crisis of these clades in the late Smithian about 2.1 Ma (Ovtcharova et al., 2006; Galfetti et al., 2007a) after the end- Permian mass extinction. In contrast, recovery patterns of bottom dwelling organisms are totally different. Reefs for example began to recover only in the Middle Triassic and reached pre-extinction diversity levels not before the Late Triassic (Pruss and Bottjer, 2005). Molluscs and gastropods were also thought to recovery rather slowly (e. g. Fraiser and Bottjer, 2004). Recent studies demonstrated that multiple minor extinction events followed the main crisis at the Permian-Triassic boundary and repeatedly reset the recovery of marine ecosystems (Hautmann et al. in press; Hofmann et al. submitted, Twitchett et al., 2004). The recovery patterns of ammonoids are closely linked to anomalies in the carbon isotope cycle (Galfetti et al., 2007b). The multiple carbon cycle perturbations in the Early Triassic records have been interpreted to reflect volcanic activity pulses, adding CO_2 to the atmosphere (Payne and Kump, 2007). As a result the Early Triassic climate was not persistent hot and ever-dry but marked by multiple climate changes (Galfetti et al., 2007b, Hochuli et al., 2010b, Hochuli and Vigran 2010). These climatic perturbations might be the cause for the observed recovery patterns of marine biotas (Galfetti et al., 2007b).

2. End Permian event and recovery in the plant fossil record

The impact of the end-Permian mass extinction on the terrestrial flora is still matter of ongoing dispute. Numerous scientists agree that and important floral turnover coincides with the Permian-Triassic transition. However, views of the severity of the plant diversity loss as well as on the mode and tempo of the event are very divergent.

A different magnitude of diversity loss is reflected in megafossil plant records compared to palynological records of Australia (Retallack, 1995). In the megafossil record the change from the Late Permian *Glossopteris* flora to the Triassic *Dicroidium* flora is profound with a loss of 97% of leave species.

However, palynological data across the Permian-Triassic boundary are marked by a greater continuity of species. The loss of the peat forming *Glossopteris* flora is reflected by the loss of striate bisaccate pollen taxa in the palynological record. The total loss of palynomorph species (about 30%) is remarkably lower than that of plant leave species (Retallack, 1995). Deeply affected plant communities have also been interpreted from the palynological record from East Greenland. There, a distinct spore spike marks the onset of loss of woody biomass and the beginning dominance of opportunistic herbs and shrubs (Looy et al., 2001). *Reduviasporonites* WILSON 1962 (synonyms are *Chordecystia* FOSTER 1979 and *Tympanicysta* BALME, 1980, see Foster et al., 2002) has been interpreted to represent fungal spores. Their occurrence near the Permian-Triassic boundary is thought to be indicative of the "excessive dieback of arboreous vegetation" and the "collapse of terrestrial ecosystems" (p. 2155 in Visscher et al., 1996, Sephton et al., 2009). However the botanical affinity of *Reduviasporonites* is by far not clear, Foster et al. (2002) demonstrated that the spore is rather of algal origin than of fungal origin.

Another floral phenomenon of the Permian-Triassic boundary is the common occurrence of unseparated spore tetrads and anormal pollen grains, reflecting the prevailing environmental stress during the Permian-Triassic transition (Looy et al., 2001, Foster and Afonin, 2005). One of these environmental stress factors could be increase UV-B radiation induced by the depletion or destruction of the ozone layer. The increased UV-B radiation is thought to cause genetic changes so that mutant spore tetrads loose the ability to separate and probably reduce the efficiency of their reproductive efforts (Beerling, 2007, Visscher et al. 2004). Causes for the ozone layer destruction are probably volcanically induced releases of H_2S and halocarbons (Kump et al., 2005, Svenson et al., 2009, Visscher et al., 2004).

In contrast to the aforementioned catastrophic views of plant extinction across the Permian-Transition transition other authors advocate a gradual floral transition (Knoll, 1984, McElwain and Punyasena, 2007). They emphasise compared to animals the fact that plants have physiological advantages to cope with environmental perturbation. Therefore, the floral changes near the Permian-Triassic boundary reflect adaptations to environmental changes. In recent studies it has emerged that the flora is less affected by a significant loss of diversity, but reacts to the environmental perturbations causing the faunal mass extinctions (Hochuli et al., 2010b; Lindström and McLoughlin, 2007).

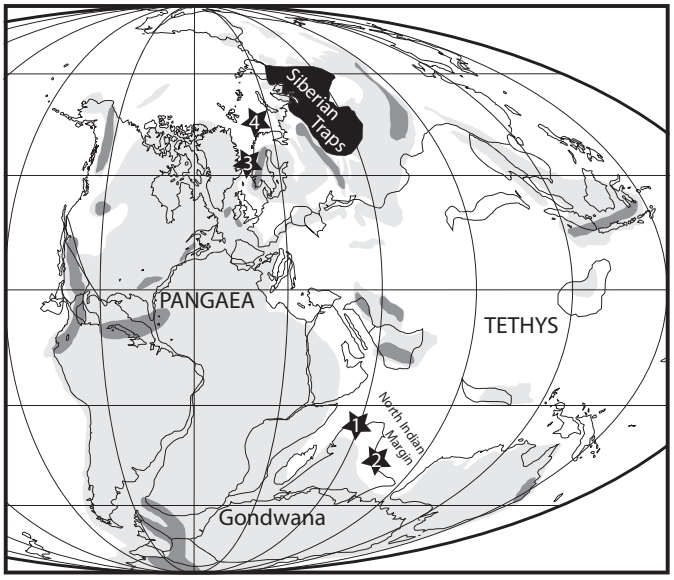

Figure 2: Palaeogeography during the Late Permian to Early Triassic modified after (Golonka and Ford, 2000; Smith et al., 1994), grey = landmass, dark grey = mountains. Asterisks mark the position of studied sites: (1) Salt Range and Surghar Range in Pakistan, (2) Tulong in South Tibet, (3) Trøndelag platform and (4) Finnmark platform in Norway.

3. Main objectives and general outline

Early Triassic palynological records with a firm marine biostratigraphic framework are rare. The independent dating is essential for the interpretation of data obtained in qualitative and quantitative palynological studies. The Early Triassic successions of the Salt Range and Surghar Range in Pakistan offer the opportunity to study well preserved organic matter including sporomorphs derived from the North Gondwanan continent together with contemporaneous marine fauna, such as ammonoids, conodonts, gastropods and molluscs. The main purpose of this thesis is to study changes in the marine depositional environment, changes in terrestrial ecosystems, and climatic conditions in the aftermath of the end-Permian mass extinction. In the present study a multidisciplinary approach including sedimentology, palynology, palynofacies and stable carbon isotope studies have been combined to **i)** obtain a chemostratigraphic framework of the Permian-Triassic boundary, **ii)** to describe the marine depositional environment of the North Indian Margin, **iii)** to reconstruct the terrestrial ecosystems and the timing of the floral recovery on North Gondwana in the aftermath of the end-Permian mass extinction, and **iv)** to demonstrate how changes in the terrestrial ecosystem are linked to climatic changes and turnovers in marine biotas.

The Norwegian sections of the Trøndelag and Finnmark platforms in Norway represent the most expanded Permian-Triassic sections and have been sampled in detail for establishing a bulk organic carbon isotope dataset. In **Chapter 1** the high resolution $\delta^{13}C_{org}$ has been subdivided into several chemostratigraphic units that can be correlated on a global scale. The new carbon isotope curve shows a distinct stepwise decline of $\delta^{13}C_{org}$ values to a first isotope minimum. After an intermittent positive excursion a second negative minimum follows up-section. This chemostratigraphic pattern has been used to locate the stratigraphic position of the end-Permian mass extinction events and the first appearance datum of *H. parvus* defining the Permian-Triassic boundary (Yin et al., 2001) with respect to the isotope curve. Furthermore the chemostratigraphic pattern allows assessing the timing of biotic events in the marine realm the recovery of terrestrial ecosystems (Hochuli et al., 2010a).

The Early Triassic sedimentary succession from the Salt Range and Surghar Range, Pakistan together with its well preserved organic matter has been studied in order to document changes in the depositional environment during the Early Triassic recovery phase of the North Indian Margin. In **Chapter 2** is a comprehension of the results of sedimentology, chemostratigraphy, palynofacies, biomarker, and Rockeval analysis. The data revealed several second order and third order sea-level changes within the studied sections. The well oxygenated condition prevailed during most of the Early Triassic, with the exception of the Dienerian time interval, in which poor oxygenation prevailed. The meaning of these environmental conditions for the recovery of marine organism is discussed this chapter.

The focus of **Chapter 3** is the climatic conditions during the Early Triassic. The climate in this area was determined by the supercontinent Pangae. In combination with the equatorial Tethys this palaeogeographic configuration resulted in strong monsoon circulation across the Tethys (e. g. Gallimore and Kutzbach, 1989; Parrish, 1993). The spore pollen ratios from the Late Permian to Middle Triassic sedimentary sequences of Pakistan (Nammal, Chhidru, Chitta-Landu and Narmia) and South Tibet (Tulong, Fig. 2) are used to demonstrate changes in humidity in the region of the North Indian Margin. These results are compared and correlated with the late Smithian climate change in the Boreal realm that has been inferred from similar proxies (Galfetti et al., 2007b). The probable causes for the observed climate changes in these distant areas be increased CO_2 levels induced from volcanism combined with orbitally forced insolation changes.

The palynological record from the Salt Range and Surghar Range has been studied with respect to the botanic affinities of the recovered sporomorph taxa. Thus, in **Chapter 4** the vegetation changes on North Gondwana during the Early Triassic could be described. These changes reflect the responses of terrestrial ecosystems to the Early Triassic environmental perturbations such as climate change. A prominent spore peak in the middle Smithian is recorded. It is associated with a negative excursion in the carbon isotope record and immediately followed by the late Smithian marine extinction event. The observed biotic and geochemical trends during this spore spike are very similar to the spore spike reported from the Permian-Triassic boundary (Hochuli et al., 2010a) Probable reasons for these recurrent patterns are discussed.

In **Chapter 5** the palynological assemblages from the Late Permian to Middle Triassic of the sections from Nammal, Chhidru, Chitta-Landu and Narmia gorge are described in detail. The palynological biostratigraphic scheme has been calibrated against ammonoid biostratigraphy and the carbon isotope curve. The stratigraphic significance of the Pakistani record is revealed in its correlation with other records from Gondwana. After the end-Permian event the microflora is dominated by relatively low diversity lycopod spore assemblages. Early recovery pulses have been observed about 1.4 Ma and about 2.1 Ma later, which contrasts the delayed recovery of 4.5 millions years that has been proposed for Central European floras (Looy et al., 1999).

The following chapters of the present thesis are discrete manuscripts, which are in review or have already been published in international peer-reviewed journals. Repetitions are therefore unavoidable.

References

Baud, A., Atudorei, V., and Sharp, Z., 1996. Late Permian and Early Triassic evolution of the Northern Indian margin: carbon isotope and sequence stratigraphy: Geodinamica Acta 9: 57-77.

Baud, A., Magaritz, M., and Holser, W.T., 1989. Permian-Triassic of the Tethys: Carbon isotope studies: Geologische Rundschau 78: 649-677.

Becker, L., Poreda, R.J., Basu, A.R., Pope, K.O., Harrison, T.M., Nicholson, C., and Iasky, R., 2004. Bedout: A possible end-Permian impact crater offshore of Northwestern Australia: Science 304: 1469-1476.

Beerling, D.J., 2007. The emerald planet - how plants changed Earth's history: Oxford, Oxford University Press, 288 p.

Benton, M.J., and Twitchett, R.J., 2003. How to kill (almost) all life: the end-Permian extinction event: Trends in Ecology and Evolution 18: 358-365.

Benton, M.J., Tverdokhlebov, V.P., and Surkov, M.V., 2004. Ecosystem remodelling among vertebrates at the Permian-Triassic boundary in Russia: Nature 432: 97-100.

Brayard, A., Bucher, H., Escarguel, G., Fluteau, F., Bourquin, S., and Galfetti, T., 2006. The Early Triassic ammonoid recovery: Paleoclimatic significance of diversity gradients: Palaeogeography, Palaeoclimatology, Palaeoecology 239: 374-395.

Brayard, A., Escarguel, G., and Bucher, H., 2005. Latitudinal gradient of taxonomic richness: combined outcome of temperature and geographic mid-domains effects?: Journal of Zoological Systematics and Evolutionary Research 43: 178-188.

Brayard, A., Escarguel, G., Bucher, H., Monnet, C., Brühwiler, T., Goudemand, N., Galfetti, T., and Guex, J., 2009. Good genes and good luck: Ammonoid diversity and the end-Permian mass extinction: Science 325: 1118-1121.

Foster, C.B., Stephenson, M. H., Marshall, C., Logan, G. A., Greenwood, P. F., 2002. A revision of Reduviasporonites Wilson 1962: Description, illustration, comparison and biological affinities: Palynology 26: 35-58.

Foster, C.B., and Afonin, S.A., 2005. Abnormal pollen grains: an outcome of deteriorating atmospheric conditions around the Permian-Triassic boundary: Journal of the Geological Society, London 162: 653-659.

Fraiser, M.L., and Bottjer, D.J., 2004. The Non-Actualistic Early Triassic Gastropod Fauna: A Case Study of the Lower Triassic Sinbad Limestone Member: Palaios 19: 259-275.

Galfetti, T., Bucher, H., Ovtcharova, M., Schaltegger, U., Brayard, A., Brühwiler, T., Goudemand, N., Weissert, H., Hochuli, P.A., Cordey, F., and Goudun, K., 2007a. Timing of the Early Triassic carbon cycle perturbations inferred from new U-Pb ages and ammonoid biochronozones: Earth and Planetary Science Letters 258: 593-604.

Galfetti, T., Hochuli, P.A., Brayard, A., Bucher, H., Weissert, H., and Vigran, J.O., 2007b. Smithian/Spathian boundary event: Evidence for global climatic change in the wake of the end-Permian biotic crisis: Geology 35: 291-294.

Golonka, J., and Ford, D., 2000. Pangean (Late Carboniferous-Middle Jurassic) paleoenvironment and lithofacies: Palaeogeography, Palaeoclimatology, Palaeoecology 161: 1-34.

Goudemand, N., Orchard, M., Bucher, H., Brayard, A., Brühwiler, T., Galfetti, T., Hochuli, P.A., Hermann, E., and Ware, D., 2008. Smithian-Spathian boundary: The biggest crisis in Triassic conodont history, GSA Joint Annual Meeting: Houston, Texas, Paper no. 318-3.

Grice, K., Cao, C., Love, G.D., Böttcher, M.E., Twitchett, R.J., Grosjean, E., Summons, R.E., Turgeon, S.C., Dunning, W., and Jin, Y., 2005. Photic zone euxinia during the Permian-Triassic superanoxic event: Science 307: 706-709.

Hallam, A., 1991. Why was there a delayed radiation after the end-Palaeozoic extinction?: Historical Biology 5: 257-262.

Hautmann, M., Bucher, H., Brühwiler, T., Goudemand, N., Kaim, A., Nützel, A., in press, And unusually divers mollusc fauna from the earliest Triassic of South China and its implication for benthic recovery after the end-Permian biotic crises. Geobios.

Hermann, E., Hochuli, P.A., Méhay, S., Bucher, H., Brühwiler, T., Hautmann, M., Ware, D., Roohi, G., ur-Rehman, K., and Yaseen, A., in press. Organic matter and palaeoenvironmental signals during the Early Triassic biotic recovery: the Salt Range and Surghar Range records: Sedimentary Geology doi:10.1016/j.sedgeo.2010.11.003.

Heydari, E., Arzani, N., and Hassanzadeh, J., 2008. Mantle plume: The invisible serial killer - application to the Permian - Triassic boundary mass extinction: Palaeogeography, Palaeoclimatology, Palaeoecology, 264: 147-162.

Hochuli, P.A., and Vigran, J.O., 2010. Climate variations in the Boreal Triassic - Inferred from palynological records from the Barents Sea: Palaeogeography, Palaeoclimatology, Palaeoecology 290: 20-42.

Hochuli, P.A., Hermann, E., Vigran, J.O., Bucher, H., and Weissert, H., 2010a. Rapid demise and recovery of plant ecosystems across the end-Permian extinction-event: Global and Planetary Change.

Hochuli, P.A., Vigran, J.O., Hermann, E., and Bucher, H., 2010b. Multiple climatic changes around the Permian Triassic boundary event revealed by an expanded palynological record from Mid Norway: GSA Bulletin 122: 884-896.

Hofmann, R., Goudemand, G., Wasmer, M., Bucher, H. & Hautmann, M. submitted. New trace fossil evidence indicates fast recovery from the end-Permian mass extinction.

Holser, W.T., Schönlaub, H.-P., Attrep, M., Boekelmann, K., Klein, P., Magaritz, M., Orth, C.J., Fenninger, A., Jenny, C., Kralik, M., Mauritsch, H., Pak, E., Schramm, J.-M., Stattegger, K., and Schmöller, R., 1989. A unique geochemical record at the Permian/Triassic boundary: Nature 337: 39-44.

Isozaki, Y., 1997. Jurassic accretion tectonics of Japan: The Island Arc 6: 25-51.

Kidder, D.L., and Worsley, T.R., 2004. Causes and consequences of extreme Permo-Triassic warming to globally equable climate and relation to the Permo-Triassic extinction and recovery: Palaeogeography, Palaeoclimatology, Palaeoecology 203: 207-237.

Kiehl, J.T., and Shields, C.A., 2005. Climate simulation of the latest Permian: Implications for mass extinction: Geology 33: 757-760.

Knoll, A.H., 1984. Patterns of extinction in the fossil record of vascular plants, in: Nitecki, M. H. (ed): Extinctions: Chicago, The University of Chicago Press: 21-68.

Knoll, A.H., Bambach, R.K., Canfield, D.E., and Grotzinger, J.P., 1996. Comparative Earth history and Late Permian mass extinction: Science 273: 452-457

Kump, L.R., Pavlov, A., and Arthur, M.A., 2005. Massive release of hydrogen sulfide to the surface ocean and atmosphere during intervals of oceanic anoxia: Geology 33:. 397-400.

Kutzbach, J.E., and Gallimore, R.G., 1989. Pangean climates: Megamonsoons of the megacontinent: Journal of Geophysical Research 94: 3341-3357.

Lindström, S., and McLoughlin, S., 2007. Synchronous palynofloristic extinction and recovery after the end-Permian event in the Prince Charles Mountains, Antarctica: Implications for palynofloristic turnover across Gondwana: Review of Palaeobotany and Palynology 145: 89-122.

Looy, C.V., Brugman, W.A., Dilcher, D.L., and Visscher, H., 1999. The delayed resurgence of equatorial forests after the Permian-Triassic ecologic crisis: Proceedings of the National Academy of Sciences of the United States of America 96: 13857-13862.

Looy, C.V., Twitchett, R.J., Dilcher, D.L., Van Konijnenburg-VanCittert, J.H.A., and Visscher, H., 2001. Life in the end-Permian dead zone: PNAS - Proceedings of the National Academy of Sciences 98: 7879-7883.

Maxwell, D., 1992. Permian and Early Triassic extinction of non-marine tetrapods: Palaeontology 35: 571-583.

McElwain, J.C., and Punyasena, S.W., 2007. Mass extinction events and the plant fossil record: Trends in Ecology and Evolution 22: 548-557.

Orchard, M.J., 2007. Conodont diversity and evolution through the latest Permian and Early Triassic upheavals: Palaeogeography, Palaeoclimatology, Palaeoecology 252: 93-117.

Ovtcharova, M., Bucher, H., Schaltegger, U., Galfetti, T., Brayard, A., and Guex, J., 2006. New Early to Middle Triassic U-Pb ages from South China: Calibration with ammonoid biochronozones and implications for the timing of the Triassic biotic recovery: Earth and Planetary Science Letters 243: 463-475.

Parrish, J.T., 1993. Climate of the Supercontinent Pangea: The Journal of Geology 101: 215-233.

Payne, J.L., and Kump, L.R., 2007. Evidence for recurrent Early Triassic massive volcanism from quantitative interpretation of carbon isotope fluctuations: Earth and Planetary Science Letters 256: 264-277.

Pruss, S.B., and Bottjer, D.J., 2005, The reorganization of reef communities following the end-Permian mass extinction: Comptes Rendus Palevol, v. 4, p. 553-568.

Raup, D.M., and Sepkoski, J.J., 1982. Mass extinction in the Marine Fossil Record: Science 215: 1501-1503.

Renne, P.R., and Basu, A.R., 1991. Rapid eruption of the Siberian Traps flood basalts at the Permo-Triassic boundary: Science 253: 176-179.

Renne, P.R., Zhang, Z., Richards, M.A., Black, M.T., and Basu, A.R., 1995. Synchrony and causal relations between Permian-Triassic Boundary Crisis and Siberian Flood Volcanism: Science 269: 1413-1416.

Retallack, G.J., 1995. Permian-Triassic life crisis on land: Science 267: 77-80.

Retallack, G.J., and Jahren, A.H., 2008. Methane release from igneous intrusion of coal during Late Permian extinction events: The Journal of Geology 116: 1-20.

Retallack, G.J., and Krull, E.S., 2006. Carbon isotopic evidence for terminal-Permian methane outbursts and their role in extinctions of animals, plants, coral reefs, and peat swamps: Geological Society of America, Special Paper 399: 249-268.

Sephton, M.A., Visscher, H., Looy, C.V., Verchovsky, A.B., and Watson, J.S., 2009. Chemical constitution of a Permian-Triassic disaster species: Geology 37: 875-878.

Sepkoski, J.J., 1984. A kinetic model of Phanerozoic taxonomic diversity. III. Post-Palaeozoic families and mass extinctions: Paleobiology 10: 246-267.

Smith, A.G., Smith, D.G., and Funnell, B.M., 1994. Atlas of Mesozoic and Cenozoic Coastlines: Cambridge, Cambridge University Press, 109 pp.

Svensen, H., Planke, S., Polozov, A.G., Schmidbauer, N., Corfu, F., Podladchikov, Y., and Jamtveit, B., 2009. Siberian gas venting and the end-Permian environmental crisis: Earth and Planetary Science Letters 277: 490-500.

Twitchett, R.J., Krystyn, L., Baud, A., Wheeley, J.R., and Richoz, S., 2004. Rapid marine recovery after the end-Permian mass-extinction event in the absence of marine anoxia: Geology 32: 805-808.

Visscher, H., Brinkhuis, H., Dilcher, D.L., Elsik, W.C., Eshet, Y., Looy, C.V., Rampino, M.R., and Traverse, A., 1996. The terminal Paleozoic fungal event: Evidence of terrestrial ecosystem destabilization and collapse: Proceedings of the National Academy of Sciences 93: 2155-2158.

Visscher, H., Looy, C.V., Collinson, M.E., Brinkhuis, H., van Konijenburg-van Cittert, J.H.A., Kürschner, W.M., and Sephton, M.A., 2004. Environmental mutagenesis during the end-Permian ecologial crisis: Proceedings of the National Academy of Sciences of the United States of America 101: 12952-12956.

Wignall, P.B., 2001. Large igneous provinces and mass extinctions: Earth-Science Reviews 53: 1-33.

Wignall, P.B., and Hallam, A., 1992. Anoxia as a cause of the Permian/Triassic mass extinction: facies evidence from northern Italy and the western United States: Palaeogeography, Palaeoclimatology, Palaeoecology 93: 21-46.

Wignall, P.B., and Hallam, A., 1993. Griesbachian (Earliest Triassic) palaeoenvironmental changes in the Salt Range, Pakistan and southeast China and their bearing on the Permo-Triassic mass extinction: Palaeogeography, Palaeoclimatology, Palaeoecology 102: 215-237.

Wignall, P.B., and Twitchett, R.J., 1996. Oceanic anoxia and the end Permian mass extinction: Science 272: 1155-1158.

Wignall, P.B., and Twitchett, R.J., 2002. Extent, duration, and nature of the Permian-Triassic superanoxic event: Geological Society of America, Special Paper 356: 395-413.

Yin, H., Zhang, K., Tong, J., Yang, Z., and Shunbao, W., 2001, The Global Stratotype Section and Point (GSSP) of the Permian-Triassic Boundary: Episodes, v. 24, p. 102-114.

Chapter 1:

Close-up view of the Permian Triassic boundary based on extended organic carbon isotope records from Norway (Trøndelag and Finnmark Platform)

with Peter A. Hochuli, Hugo Bucher, Jorunn O. Vigran,
Helmut Weissert, Stefano M. Bernasconi

Global and Planetary Change 2010, 74(3-4): 156-167

Global and Planetary Change 74 (2010) 156–167

Contents lists available at ScienceDirect

Global and Planetary Change

journal homepage: www.elsevier.com/locate/gloplacha

A close-up view of the Permian–Triassic boundary based on expanded organic carbon isotope records from Norway (Trøndelag and Finnmark Platform)

Elke Hermann [a,*], Peter A. Hochuli [a], Hugo Bucher [a], Jorunn O. Vigran [b], Helmut Weissert [c], Stefano M. Bernasconi [c]

[a] Institute and Museum of Palaeontology, University of Zurich, Karl Schmid-Str. 4, CH-8006 Zurich, Switzerland
[b] SINTEF Petroleum Research, NO-7465 Trondheim, Norway
[c] Department of Earth Sciences, ETH Zurich Sonneggstrasse 5, CH-8092 Zurich, Switzerland

ARTICLE INFO

Article history:
Received 20 April 2010
Accepted 18 October 2010
Available online 26 October 2010

Keywords:
Permian–Triassic
organic carbon isotopes
particulate organic matter
Norway

ABSTRACT

High-resolution carbon isotope records of organic carbon ($\delta^{13}C_{org}$) across the Permian–Triassic boundary (PTB) from the expanded sections of the Trøndelag and Finnmark platforms in Norway demonstrate that the negative carbon isotope excursion around the PTB begins with a stepwise 8‰ negative decline to a first minimum. After a subsequent positive excursion, a second minimum follows in the basal Griesbachian. Particulate organic matter (POM) is dominated by terrestrial particles with changing marine contributions. Intervals with minor C-isotope fluctuations coincide with homogeneous terrestrial POM assemblages, whereas intervals with pronounced C-isotope fluctuations correspond to heterogeneous marine–terrestrial POM assemblages, suggesting that the C-isotope curve represents a global signal with superimposed local variations of carbon sources. The $\delta^{13}C_{org}$ of the contributing organic carbon ranges from −32‰ (marine organic carbon) to −22‰ (terrestrial organic carbon). Comparison of the new record, divided into 10 chemostratigraphic intervals with other, globally distributed sections suggests the presence of gaps in several classical PTB sections. Detailed chemostratigraphic correlation reveals that the extinction of marine organisms occurred during the stepwise negative shift and the end-Permian floral turnover occurred prior to the first C-isotope minimum. The correlation also shows that the marker of the recently defined Global Stratotype Section and Point PTB occurs within a broad interval ranging from most negative $\delta^{13}C$ values up to the subsequent isotopic increase.

1. Introduction

The end-Permian mass extinction affected marine and terrestrial life dramatically. About 95% of all species on Earth went extinct (Benton and Twitchett, 2003). The mode and severity of the effects of the end-Permian extinction on flora are intensely debated. The end-Permian extinction coincides with a prominent, globally recorded negative C-isotope shift with an estimated duration of 165 ka (Bowring et al., 1998). The combined sections of Late Permian–Early Triassic age from the Trøndelag Platform and the Finnmark Platform represent the most expanded Late Permian–Early Triassic boundary record documented so far and therefore allow a close-up view of this short time interval. Because of the essentially siliciclastic composition of these series and the scarcity of age-diagnostic fossils, it has been difficult to pinpoint the exact position of the Permian–Triassic boundary (PTB) and to assess the precise temporal framework of associated changes in the biosphere.

This study provides a detailed carbon isotope stratigraphy across the PTB in sections with very high sedimentation rates. The high resolution allows the recognition of 10 chemostratigraphic intervals, which can be correlated across marine and terrestrial C-isotope records worldwide: East Greenland (Stemmerik et al., 2001; Twitchett et al., 2001), Arctic Canada (Grasby and Beauchamp, 2008), Austria (Holser et al., 1989), Iran (Heydari et al., 2008), South China (Jin et al., 2000; Krull et al., 2004; Peng et al., 2005), and Australia (Morante, 1996). With the new organic carbon isotope data, ecological changes linked to the PTB could be chronologically resolved with high resolution, thus allowing the construction of a succession of floral changes and marine events during the studied time interval.

2. Geological setting and dating

Two shallow cores from the Trøndelag Platform (6611/09-U-01 and 6611/09-U-02 drilled by IKU/SINTEF Petroleum research, Fig. 1), comprise together 750 m of Late Permian and Early Triassic strata of which the upper 500 m have been sampled for organic carbon isotope measurements. The studied Permian interval (ca. 50 m) consists of alternating massive and fining-upward sandstones and siltstones,

* Corresponding author. Tel.: +41 44 634 23 29; fax: +41 44 634 49 23.
E-mail address: ehermann@pim.uzh.ch (E. Hermann).

0921-8181/$ – see front matter © 2010 Elsevier B.V. All rights reserved.
doi:10.1016/j.gloplacha.2010.10.007

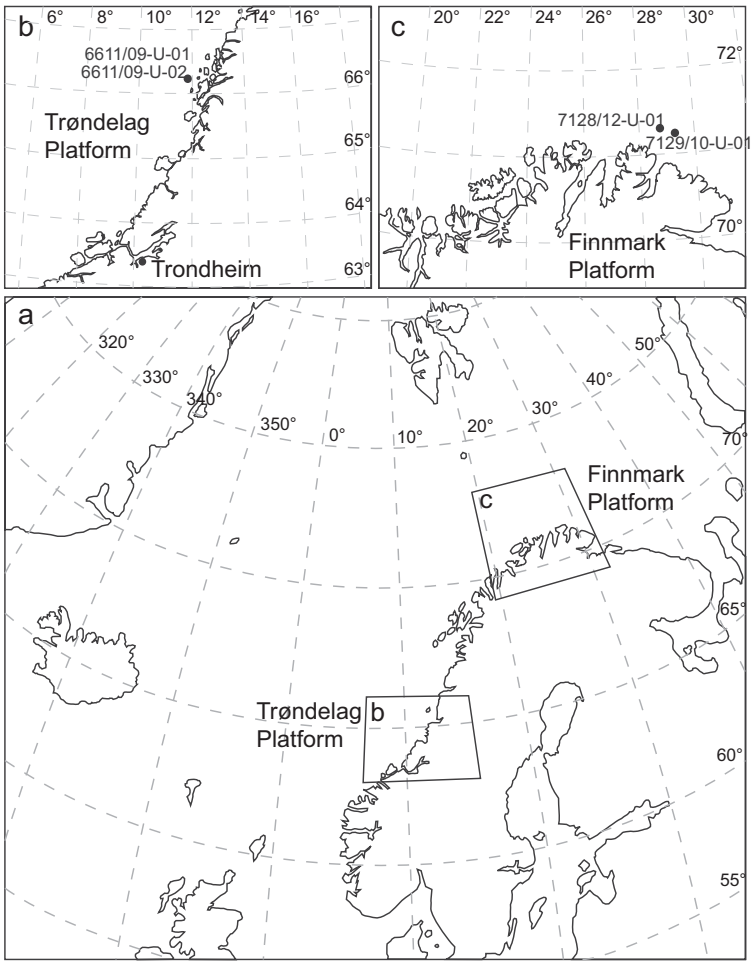

Fig. 1. Location of the Trøndelag platform and the Finnmark platform (a). Detailed maps of the Trøndelag core site (b) and the Finnmark core site (c).

interpreted as turbidites (Bugge et al., 2002). Palynological assemblages indicate a Lopingian (Late Permian) age for this interval (Bugge et al., 2002). As assemblages indicative of Changhsingian or earliest Griesbachian have not been recovered, a considerable gap marks the PTB of the Trøndelag platform. The 400 m of Griesbachian deposits consists of siltstones, sandstones, and conglomerates also interpreted as turbidites (Bugge et al., 2002). Rare ammonoids, bivalves, and palynological data indicate a Griesbachian age (Bugge et al., 2002; Hochuli et al., 2010). A distinct interval rich in evaporite beds within the Griesbachian permits confident correlation between the two cores. A detailed lithological description of cores 6611/09-U-01 and 02 can be found in (Bugge et al., 2002). Core pictures and additional information are stored on the SINTEF web site:http://www.sintef.no/static/pe/produkt/shadripro/corephotos/area_pages/helgeland.htm.

The shallow cores from the Finnmark Platform 7128/12-U-01(ca. 100 m) and 7129/10-U-01 (ca. 40 m, Fig. 1) comprise both Late Permian and Early Triassic rocks. The geological setting and the lithological succession of these sections have been described in several publications (Mangerud, 1994; Bugge et al., 1995; Larssen et al., 2005). The Permian part of the sections is marked by a predominance of carbonates and siltstones deposited in a shallow to outer shelf environment. The carbonates are overlain by a phosphoritic layer in 7129/10-U-01, which corresponds to a prominent gamma peak in core 7128/12-U-01 where this interval was not recovered. Deeper depositional environments are indicated by cherts in core 7128/12-U-01 above the gamma ray peak (Bugge et al., 1995). A pebbly shale with chert clasts and glauconite on top of the phosphoritic layer (7129/10-U-01) and the chert (7128/12-U-01), respectively, corresponds to a seismic marker interpreted as top of the Permian (Fig. 3). In 7129/10-U-01, this layer includes black phosphorite and a crack filled with sediments of the overlying rocks, which have been interpreted to represent subaerial exposure (Bugge et al., 1995). Palynological data indicate a Tatarian (Changhsingian) age of the studied interval including the phosphoritic horizon (Mangerud, 1994). The overlaying sequence of alternating silty sandstones and sandstones is interpreted as a shallow, storm-influenced shelf (Bugge et al., 1995). Here, a Griesbachian age is indicated by palynology (Mangerud, 1994). Core pictures and additional information are stored on the SINTEF web site:http://www.sintef.no/static/pe/produkt/shadripro/corephotos/area_pages/finnmark_east.htm.

3. Materials and methods

Sampling focused on siltstone and mudstone with a high preservation potential for organic matter. All samples from the Trøndelag cores (370 samples) and the Finnmark cores (45 samples) have been ground and treated with 3 N HCl for at least 24 h to remove all carbonates. The residue was homogenised and analysed with a ThermoFisher Flash-

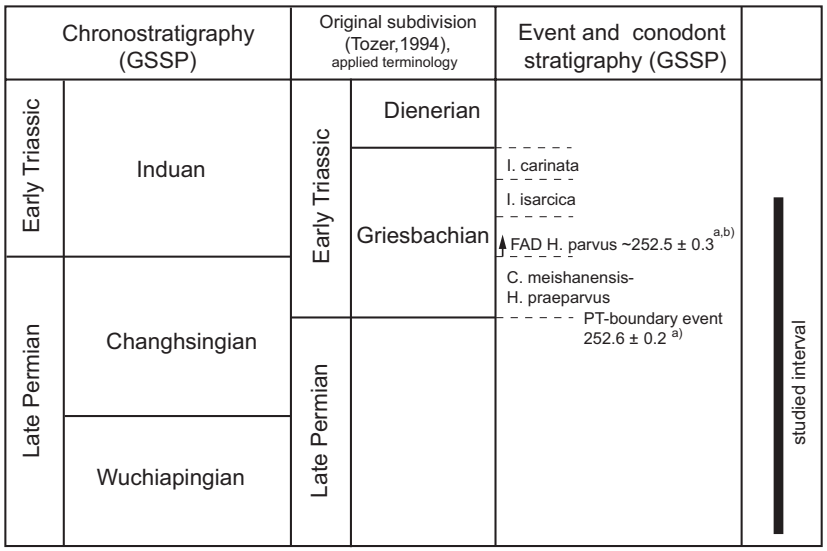

Fig. 2. Chronostratigraphy of the PTB at the GSSP in Meishan and subdivision after Tozer (1994). Radiometric ages after a) Mundil et al. (2004) and b) Mundil et al. (2001).

EA1112 elemental analyser coupled with a Conflo IV interface to a ThermoFisher Delta V isotope ratio mass spectrometer. Isotope ratios are reported in the conventional δ-notation with respect to V-PDB (Vienna Pee Dee Belemnite) standard. The system was calibrated with NBS22 ($\delta^{13}C = -30.03‰$) and IAEA CH-6 ($\delta^{13}C = -10.46‰$). Reproducibility of the measurements is better than ±0.15‰ for both nitrogen and carbon.

The applied terminology of the chronostratigraphic units Permian, Triassic and PTB follows the usual subdivisions of Tozer (1994) (Fig. 2).

4. Results

The high-resolution organic carbon isotope record ($\delta^{13}C_{org}$) of 415 samples and palynological data of the Trøndelag and Finnmark sites allows constructing a composite record (Fig. 3). The $\delta^{13}C_{org}$ record has been subdivided into 10 chemostratigraphic intervals "a" to "j" (Fig. 3) according to their characteristic C-isotope patterns (increase, decrease, or stable $\delta^{13}C_{org}$ values). Very rapid shifts, probably biased by sedimentary gaps, are regarded as transitions between two intervals.

In the Late Permian, the $\delta^{13}C_{org}$ profile starts with high values (−23‰ and −22‰; Fig. 3, interval "a"). In the Finnmark cores, these high values are followed by a first negative shift of about 5‰ (Fig. 3, interval "b"). The curve decreases towards the top of interval "b" until stable values (around −28.5‰) are reached in interval "c" (Fig. 4B). This first negative shift is missing in the Trøndelag record. There the Permian $\delta^{13}C_{org}$ values of −22‰ drop abruptly to values around −27‰. The record continues with values fluctuating around −27‰ in the upper part of interval "c". In the Finnmark record (7128/12-U-01), a minor positive shift marks the top of interval "c" (Fig. 4B). The final and more rapid drop of the $\delta^{13}C_{org}$ curve reaches values of −31‰ to −30‰ (Fig. 3, interval "d"). After this drop (interval "d"), low $\delta^{13}C_{org}$ values were measured in a 48-m-thick siltstone-dominated section (interval "e"). In the Trøndelag cores, interval "e" which is marked by very low C-isotope values is followed by a rapid shift to C-isotope values around −22‰ (Fig. 3, interval "f"). These values are comparable with those of the latest Permian. Towards the top of interval "f", C-isotope values start to decrease before they abruptly drop again to values around −30‰ (transition "f" to "g"). Subsequently, the $\delta^{13}C_{org}$ curve shifts to values around −28‰ (Fig. 3, interval "g") and the following interval "h" is marked by values scattering around −28‰ (Fig. 1, interval "h"). Values are gradually shifting to −27‰ (Fig. 3, interval "i") and the C-isotope curve fluctuates around −27‰ in the uppermost interval "j".

In conclusion, the Permian–Triassic transition in Norway is marked by a stepwise decrease of the $\delta^{13}C_{org}$ values with a first drop in interval "b" and a pronounced drop in interval "d" with a total decrease of about 8‰. After a positive excursion in interval "f", a second minimum is reached in interval "g".

The $\delta^{13}C_{org}$ record is supported by the particulate organic matter (POM) analysis of the Trøndelag record (6611/09-U-01). There, pollen, spores, fungal remains, degraded terrestrial organic matter, inertinite, membranes, cuticles, and opaque and translucent phytoclasts have been assigned to the terrestrial POM fraction. Acritarchs, AOM, prasinophyceae and foraminiferal linings form the marine POM fraction (Supplementary Fig. 2). The results of the POM analysis are summarised in column *C* of Fig. 3. We differentiated two POM assemblages, a pure terrestrial one and a mixed terrestrial marine assemblage. The POM of the Finnmark cores has been documented in Hochuli et al., this volume). There, the POM consists only of terrestrial POM with the exception of one sample in interval "b" (pebbly shale horizon) where an acritarch peak is documented.

5. Comparison and discussion

5.1. Comparison with other PTB records worldwide

The described stepwise negative shift across the PTB has been recorded in other expanded marine sections (Fig. 4A–P): Buchanan Lake, Arctic Canada, (Grasby and Beauchamp, 2008) Shahreza, Iran, (Heydari et al., 2008), Svalbard, (Wignall et al., 1998), from one rather

Fig. 3. Simplified lithologies of the Finnmark cores (7128/12-U-01 and 7129/10-U-01, Bugge et al., 1995) and Trøndelag cores (6611/09-U-01, 6611/09-U-02, Bugge et al., 2002) and composite $\delta^{13}C_{org}$ record. Black arrow indicates radiometric dated ash layers at in the GSSP section in Meishan, see text for details. Use of period terminology after Tozer (1994, see Fig. 2). *A*: Chemostratigraphic intervals "a" to "j". *B*: Dominant lithology of cores 6611/09-U-01, 6611/09-U-02 after (Bugge et al., 2002). *C*: main palynofacies changes in core 6611/09-U-01 (Peter A. Hochuli) for details see Supplementary Fig. 2. *D*: spore/pollen ratio of cores 6611/09-U-01, 6611/09-U-02 (Hochuli et al., 2010). *E*: spore/pollen ratio of core 7128/12-U-01 (Hochuli et al., this volume).

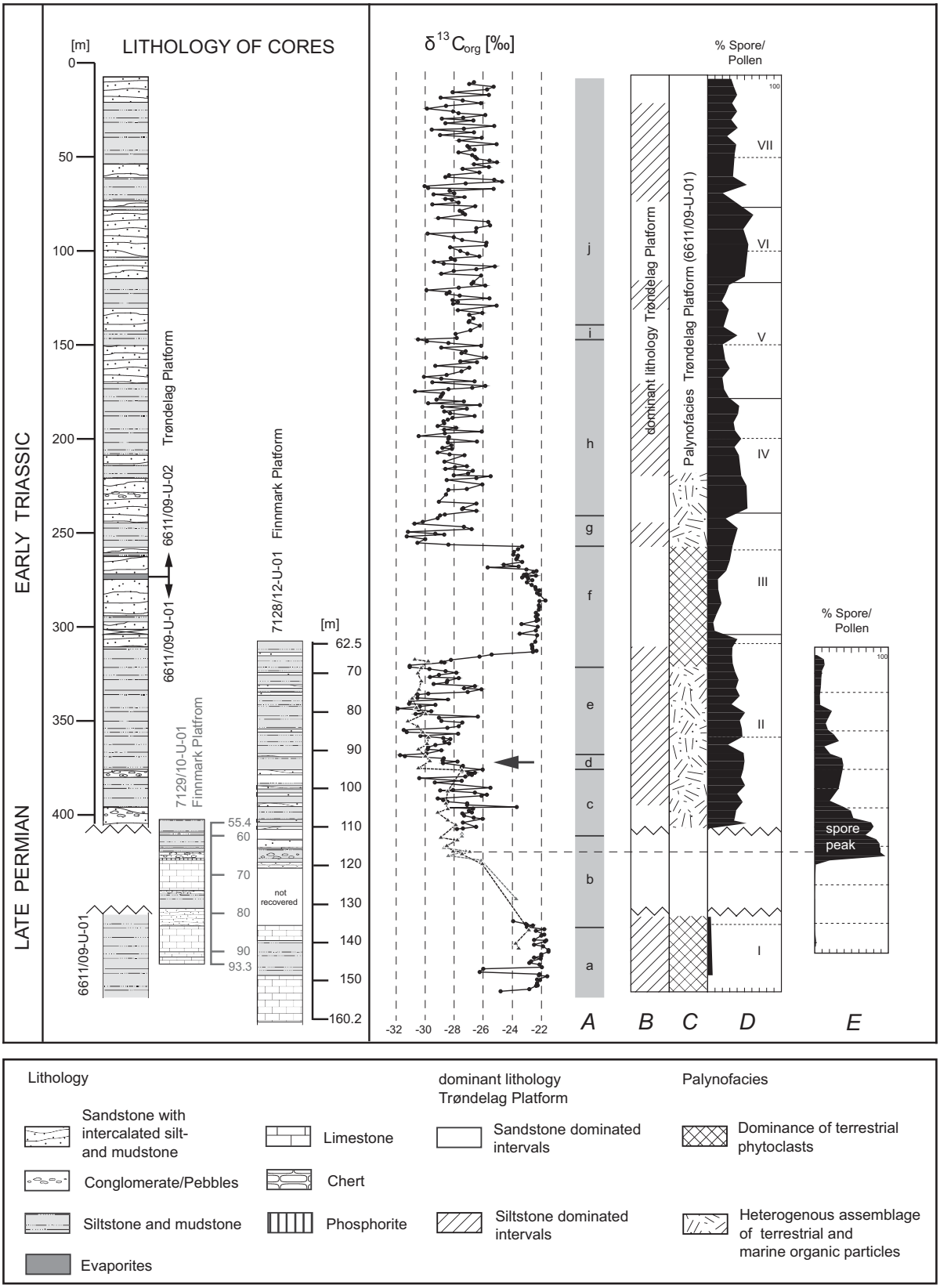
LITHOLOGY OF CORES
[m]
0
50
100
150
200
250
300
350
400
EARLY TRIASSIC
LATE PERMIAN
6611/09-U-01
6611/09-U-02
Trøndelag Platform
7129/10-U-01
Finnmark Platfrom
55.4
60
70
80
90
93.3
7128/12-U-01
Finnmark Platform
[m]
62.5
70
80
90
100
110
120
130
140
150
160.2
not recovered
δ13Corg [‰]
-32
-30
-28
-26
-24
-22
% Spore/ Pollen
100
VII
VI
V
IV
III
II
I
j
i
h
g
f
e
d
c
b
a
A
B
C
D
E
dominant lithology Trøndelag Platform
Palynofacies Trøndelag Platform (6611/09-U-01)
% Spore/ Pollen
100
spore peak
Lithology
Sandstone with intercalated silt- and mudstone
Conglomerate/Pebbles
Siltstone and mudstone
Evaporites
Limestone
Chert
Phosphorite
dominant lithology Trøndelag Platform
Sandstone dominated intervals
Siltstone dominated intervals
Palynofacies
Dominance of terrestrial phytoclasts
Heterogenous assemblage of terrestrial and marine organic particles

condensed section in East Greenland (Stemmerik et al., 2001) as well as from the terrestrial records of the Chahe section in Southwest China (Peng et al., 2005) and the Australian Bowen Basin (Morante, 1996). For the palaeogeographic position of the mentioned sections, see Supplementary Fig. 1. The most distinct common feature of these C-isotope records is the rapid negative shift close to the end-Permian extinction event (interval "d").

In the following, the considered sections are compared interval by interval with focus on completeness of the sections, differences between the sections and the floral and faunal events documented in each interval.

The Late Permian stable interval "a" is recorded in almost all sections considered. Most $\delta^{13}C_{carb}$ profiles show stable positive values of +3‰ to +4‰ in the Late Permian (see Fig. 4). $\delta^{13}C_{org}$ values are ranging between −25‰ in the Buchanan Lake record, Sverdrup Basin, Arctic Canada (Fig. 4E, Grasby and Beauchamp, 2008) and −23‰ in the Jameson Land record (Greenland, Fig. 4D, Twitchett et al., 2001). In Greenland, the end-Permian marine extinction event is documented within the top of interval "a". The marine extinction level is immediately followed by the increase in spore abundance (spore peak) and a sudden drop of C-isotope values (Fig. 5). Intervals "b" and "c" are not recorded and therefore the onset of the spore peak is concealed. In the Australian Bowen Basin (Fig. 4P, Morante, 1996), the author combined the $\delta^{13}C_{org}$ record with palynological data. The *P. microcorpus* zone starts at the top of our interval "a" and lasts up to the top of interval "d". Within this zone, spore contents reach relative abundances of up to 80% (Foster, 1982) comparable to the coeval spore peak of the Northern hemisphere. In contrast to the abovementioned $\delta^{13}C_{org}$ records, the detailed $\delta^{13}C_{org}$ record from the Global Stratotype Section and Point (GSSP) at Meishan, South China (Cao et al., 2002, Fig. 4K) shows more negative organic C-isotope values in the Permian interval. Although several publications described the palynological and biomarker content of the Meishan sections, no data of the POM analysis is available for the samples measured by Cao et al. (2002). A peculiar composition of the organic matter might explain the low values.

Interval "b" is characterised by a protracted negative shift of about −2‰ in $\delta^{13}C_{carb}$ profiles, and about −3‰ to −5‰ in $\delta^{13}C_{org}$ profiles (Fig. 4). In the stratigraphically complete $\delta^{13}C_{org}$ record from the Fiskegrav section, Jameson Land, East Greenland (Fig 4C, Stemmerik et al., 2001), a pronounced extinction event is documented in the uppermost part of interval "b", which reduces the Permian fauna (agglutinating foraminifera, brachiopods, ammonoids) dramatically (Stemmerik et al., 2001). This event coincides with a major increase in spore abundance (onset of spore peak) and a dramatic reduction of gymnosperms in Greenland (Stemmerik et al., 2001) and Northern Norway (Hochuli et al., this volume). In the Iranian Shahreza section, the end Permian extinction event is also documented in the top of interval "b". Both extinction events (Iran and Greenland) occur within the top of interval "b" and are chronologically close or even contemporaneous (Fig. 5).

With the exception of the $\delta^{13}C_{carb}$ record from the Shahreza section (Iran, Heydari et al., 2008) and the recently published high-resolution chemostratigraphy of further Iranian sections (Richoz et al., 2010), the stable interval "c" has been observed exclusively in $\delta^{13}C_{org}$ records. Interval "c" corresponds to the interval between the isotopic events IE2 to IE3 of the generalised isotope curve of Richoz et al. (2010). It also corresponds to the isotopic interval below the Late Permian Extinction defined in the $\delta^{13}C_{org}$ records of Buchanan Lake (Fig. 5 in Grasby and Beauchamp, 2008) except that we lowered the top boundary of interval "c" to the short-lived increase of $\delta^{13}C_{org}$ isotopes. The sediments deposited on a carbonate ramp in the Carnic Alps (Gartnerkofel core 1) yield the most expanded carbonate C-isotope record across the PTB (Holser et al., 1989, Fig. 4G). Due to sedimentary gaps, which have been recognised in the nearby outcrop, the stable interval "c" is missing (see also Grasby and Beauchamp, 2008). In the Gartnerkofel core 1, the Tesero Horizon, a 6-m-thick fossil-poor oolithic interval is considered to represent the end Permian extinction (Jenny-Deshusses, 1991). This horizon includes the top of interval "b" and the lower part of interval "d". The short-lived positive peak marking the top of interval "c" is also documented in the Finnmark record and the Fiskegrav section in Greenland (Stemmerik et al., 2001). Similar short-lived $\delta^{13}C_{org}$ increases after stable intervals have been observed near the Palaeocene–Eocene Thermal Maximum (Sluijs et al., 2007) and the Cretaceous OAE1a (Méhay et al., 2009) while the carbonate record displays a continued negative trend. In these records, this small positive shift has been explained by an increase in sea surface temperatures. A temperature increase leads to decreased fractionation between dissolved inorganic carbon and dissolved CO_2. Therefore, the isotopic signal of marine algae increases (Hayes, 1993; Hayes et al., 1999). In terrestrial plants, environmental stress such as reduced water availability, salinity, decreased sunlight and temperature lead to $\delta^{13}C$ enrichment of plant material (Ivlev, 2004; Jahren et al., 2008).

Interval "d" is recorded in all the sections considered in this study. The correlation of interval "d" with the globally recognised negative spike at the PTB is based on the comparison of our chemostratigraphic intervals with the chemostratigraphic pattern of the Buchanan Lake records given by Grasby and Beauchamp (2008). Our interval "d" overlaps with the top of their isotopic interval below the Late Permian extinction event and the base of their isotopic interval above this event (see Fig. 5 in Grasby and Beauchamp, 2008; and Fig. 4F). A common feature of most records is a protracted decrease in interval "b" $\delta^{13}C_{carb}$ curves followed by a pronounced rapid decrease of about −1.5‰ to −2.5‰, which we define as interval "d" (e.g. Gartnerkofel Holser et al., 1989; Iran, Heydari et al., 2008; Meishan, Jin et al., 2000). Most $\delta^{13}C_{carb}$ records show a negative excursion with an amplitude of 2‰ to 4‰ (e.g. Kaiho et al., 2009). In the corresponding interval of the Finnmark and the Trøndelag Platforms, the $\delta^{13}C_{org}$ records display a total negative shift of 8‰. Similar $\delta^{13}C_{org}$ excursions are known from Australia (6‰ to 10‰, Morante, 1996), Arctic Canada (5‰, Grasby and Beauchamp, 2008), and other areas (Retallack and Krull, 2006). The strongly condensed GSSP PTB section in Meishan (South China) has been repeatedly studied. Here, the thickness from the top of the well-defined interval "d" to the maximum C-isotope values in interval "f" is 0.4 m compared to the 20 m for the same interval in the Gartnerkofel core 1 and about 70 m in the Trøndelag record. For the various Meishan sections, several carbon isotope records exist with partly differing results (Xu and Yan, 1993; Jin et al., 2000; Riccardi et al., 2007; Xie et al., 2007; Kaiho et al., 2009). Kaiho et al. (2009) describes the individual sections, especially the GSSP Meishan D section as being altered through weathering. The most detailed C-isotope record of organic matter has been published by Cao et al. (2002, Fig. 4K) and of carbonates by Jin et al. (2000, Meishan B, Fig.4D). In Meishan, some of the isotope intervals defined in this study are poorly expressed or even absent (e.g. interval "c" and "e"). In this section, the last documented extinction event coincides with the negative shift of the C-isotopes (interval "d") in bed 25 ($\delta^{13}C_{org}$, (Cao et al., 2002) and $\delta^{13}C_{carb}$ (Jin et al., 2000)). An extinction event at the same stratigraphic position has been documented at Buchanan Lake (Grasby and Beauchamp, 2008), in the Nanpanjiang Basin, (Krull et al., 2004) and the Gartnerkofel core 1 (Holser et al., 1989; Jenny-Deshusses, 1991, Fig. 5). In the same interval ("d"), the oldest occurrence of the first appearance datum (FAD) of the conodont *Hindeodus parvus*, which is used as a marker for the base of the Triassic (Yin et al., 2001) is documented in the Kamura section (Japan, Fig. 4O, Musashi et al., 2001), the Nanpanjiang basin (South China, Krull et al., 2004), and the Shahreza section (Iran, Heydari et al., 2008, Fig. 5).

In interval "e" the $\delta^{13}C_{org}$ values range around −30‰ in most records with the exception of Kamura (−27‰, Musashi et al., 2001) and Chahe (−28‰, Peng et al., 2005). In most $\delta^{13}C_{carb}$ records, interval "e" (varying between 0‰ and −1.5‰) is condensed to a few

centimetres (e.g. in Meishan) compared to a thickness of about 50 m in the Trøndelag record. The carbonate record of interval "e" of Jameson Land (Twitchett et al., 2001) is exceptionally ^{13}C-depleted (−11‰) but shows positive shifts of up to 4‰. For this case, the chemostratigraphic correlation is rather loose. In this section, the FAD of *H. parvus* occurs within this interval.

The amplitude of the positive shift in interval "f" of about +8‰ in the Trøndelag core is not reached in any carbonate record [Iran, ca. +1.5‰ (Heydari et al., 2008); Austria, +2‰ (Holser et al., 1989); and Meishan, +2‰ (Xie et al., 2007)]. The only comparable $\delta^{13}C_{org}$ record with a positive shift of about +6‰ is the Meishan section (Cao et al., 2002). Assuming a constant sedimentation rate for the Gartnerkofel and Trøndelag record, the comparison of the duration of the positive shift relative to the duration of the total interval "f" reveals that the steep increase in $\delta^{13}C_{org}$ in interval "f" in the Trøndelag section is probably due to sedimentary gaps. In the generalised isotope curve of Iran and Oman (Richoz et al., 2010), the stable interval between IE2 and IE3 corresponding to interval "c" is followed by a negative shift. The following negative interval is interrupted by smaller positive peaks. One of these peaks (IE6) can be compared with the Shahreza section of Heydari et al. (2008) and might correspond to our interval "f". In contrast to the majority of PTB-sections where the FAD of *H. parvus* is reported within the negative shift or the following minimum values (interval "d" and "e"), it is located in a stratigraphically higher position (interval "f") in the GSSP of Meishan, suggesting a diachronous FAD of the index species.

The second minimum and subsequent increase of C-isotope values in interval "g" is also recorded in Austria (Gartnerkofel, Holser et al., 1989), Iran (Heydari et al., 2008), and Meishan (Xie et al., 2007). In the $\delta^{13}C_{carb}$ record of Meishan (Xie et al., 2007, Fig. 4I) interval "g" is 13 m thick, indicating increased sedimentation rates compared to the underlying intervals. In the Trøndelag record, the rapid drop of C-isotope values between interval "f" and "g" suggests a sedimentary gap between these intervals (Hochuli et al., 2010).

Based on the high-resolution $\delta^{13}C_{org}$ record of the Norwegian sites, it is possible to correlate the abovementioned sections confidently and to link the stepwise negative shift with several faunal extinction events and floral changes.

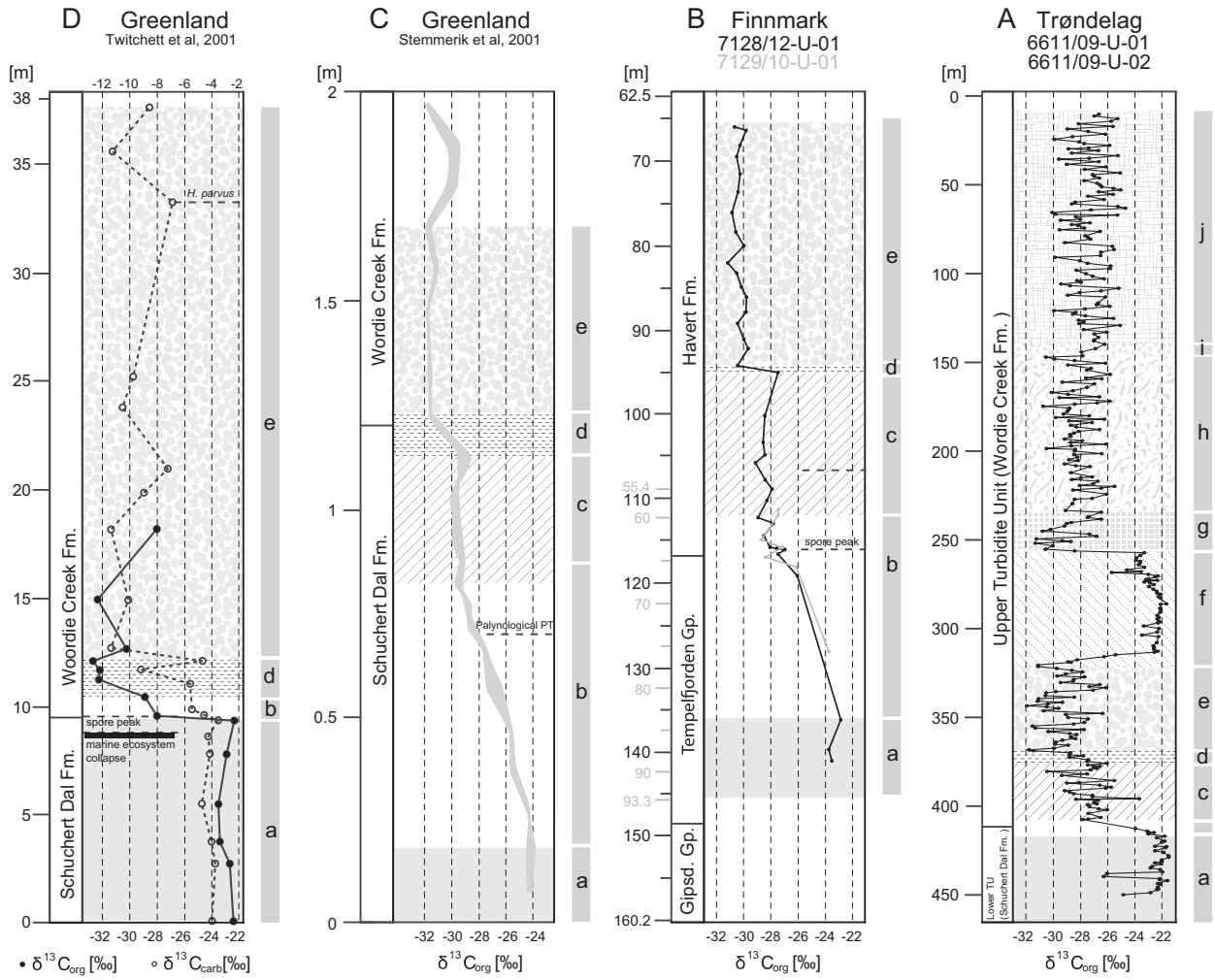

Fig. 4. C-isotope records and chemostratigraphic subdivision of the Trøndelag cores (A), the Finnmark cores (B), the East Greenland section (C, Stemmerik et al., 2001), the Greenland section (D, Twitchett et al., 2001), the Svalbard section (E, Wignall et al., 1998), the Buchanan Lake section, Canada (F, Grasby and Beauchamp, 2008), the Gartnerkofel section, Austria (G, Holser et al., 1989), the Shareza section, Iran (H, Heydari et al., 2008), the Meishan section, China (I, Xie et al., 2007), the GSSP section in Meishan (J, Jin et al., 2000) with conodont stratigraphy after (Chen et al., 2007; Yin et al., 2007), the Meishan section (K, Cao et al., 2002), section from the Nanpanjiang basin (L, M, Krull et al., 2004), the Chahe section (N, Peng et al., 2005), the Kamura section, Japan (O, Musashi et al., 2001), and the section from the Bowen Basin, Australia (P, Morante, 1996).

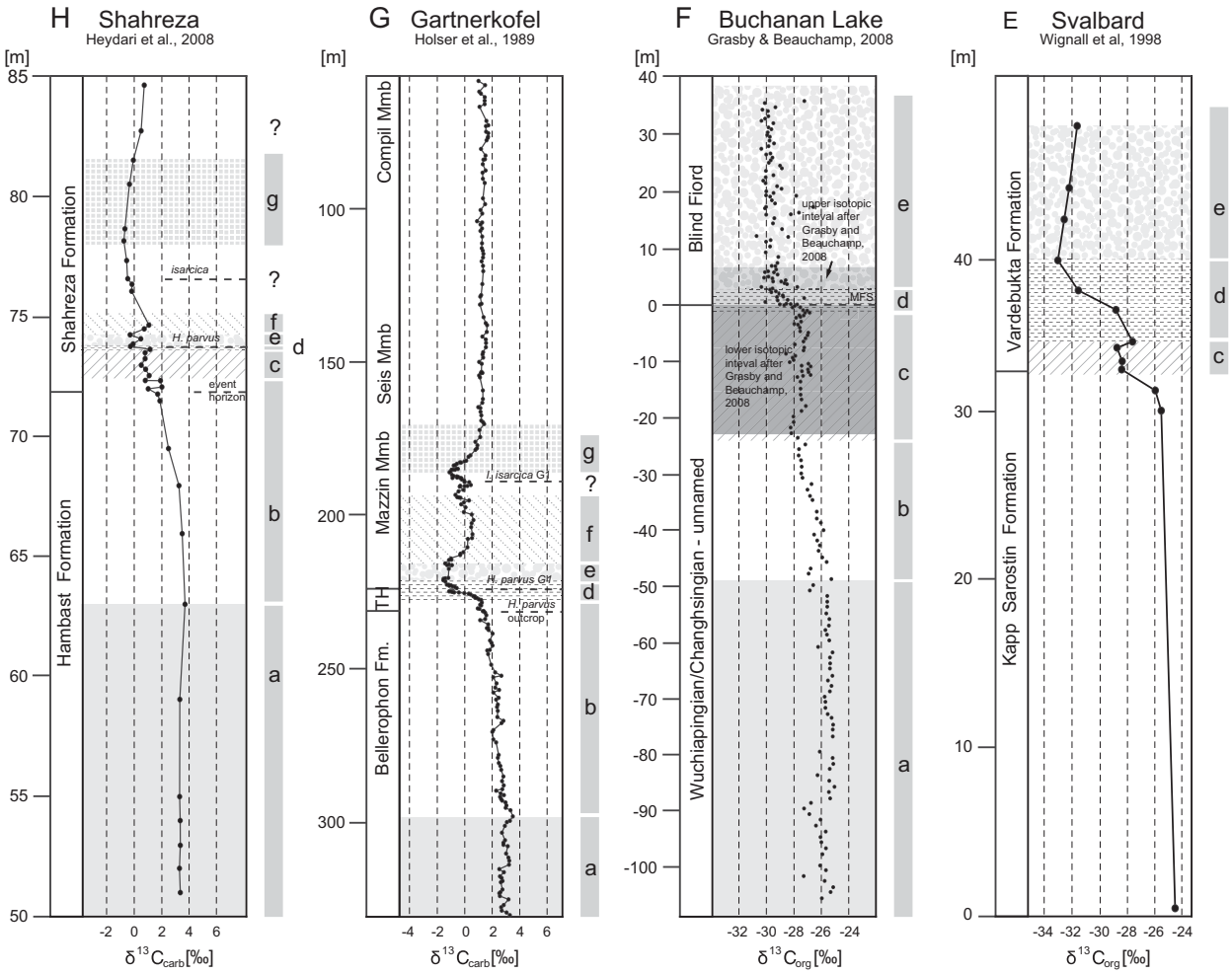

Fig. 4 (*continued*).

Our results differ from recently published works on the PTB chemostratigraphy by the following two points. First, the comparison of the Norwegian chemostratigraphic pattern with other PTB sections documents a series of extinction events during a stepwise decline of carbon isotope values in agreement with the multiphase end-Permian extinction as previously documented in Meishan (Jin et al., 2000). Our results and those of Jin et al. (2000) stand in marked contrast with the isochronous extinction event horizon, which has been suggested to predate the carbon isotope negative spike by Korte and Kozur (2010).

Second, the diachronous occurrence of the FAD of *H. parvus* has been previously suspected (e.g. Shevyrev, 2006), which is also supported by the comparison of our data with other published PTB carbon isotope records. Furthermore, evidence from recently published carbon isotope data of several PTB sections from South China show the inconsistent position of the FAD of *H. parvus* with respect to the carbon isotope signal (Cao et al., 2010). However, Korte and Kozur (2010) postulated that the FAD of *H. parvus* coincides with the negative carbon isotope spike of several PTB sections and is therefore suggested to be isochronous. In addition, the amended positions of the FAD of *H. parvus* used by these authors are ambiguous with respect to the original data (e.g. Schönlaub, 1991 and Krull et al., 2004).

5.2. Possible causes for the observed chemostratigraphic patterns in the Norwegian $\delta^{13}C_{org}$ record

As marine and terrestrial organic matter have different carbon isotopic compositions, the isotopic end-members of marine and terrestrial organic matter have to be considered when interpreting bulk $\delta^{13}C_{org}$ curves. In our record, the pure terrestrial POM assemblages (interval "a" and "f") show relatively positive $\delta^{13}C_{org}$ values of −22‰ to −23‰. We can estimate the composition of the marine end-member by simple mass balance calculations. If we take a sample at ca. 335 m depth at Trøndelag with $\delta^{13}C_{org} = -27$‰ and a marine to terrestrial ratio of 0.5 (see POM distribution of core 6611/09-U-01 in Supplementary Fig. 2, the depth of ca. 335 m in the composite section in Fig. 3 corresponds to ca.125 m original core depth) and a terrestrial end-member $\delta^{13}C_{org}$ of −22‰, the end-member marine composition is −32‰. These two values are tentative end-members to discuss our results. The isotopic composition of terrestrial and marine organic matter depends on the isotopic composition of the atmosphere and the isotopic composition of the dissolved organic carbon in the ocean. Changes in the isotopic composition of these two carbon pools would therefore cause synchronous changes of the $\delta^{13}C_{org}$ values of the calculated end-members. In their Early Triassic records of the Perth Basin, Thomas et al.

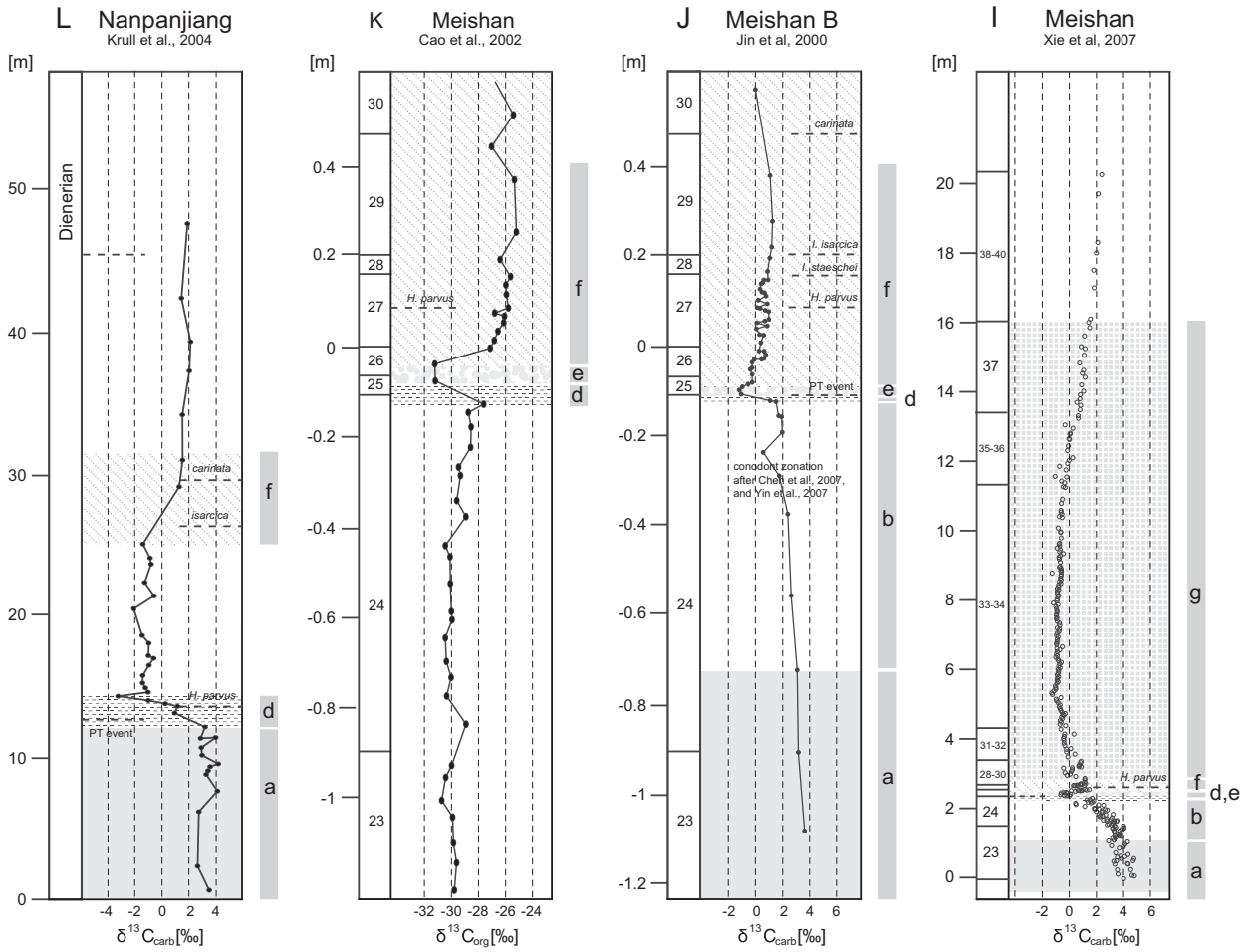

Fig. 4 (*continued*).

(2004) and Foster et al. (1997) explained the isotopic variations across the PTB by changes in the ratio of marine vs. terrestrial organic matter. Thomas et al. (2004) demonstrated that Permian POM is dominated by a terrestrial charcoal-wood assemblage with a $\delta^{13}C_{org}$ of −23.5‰. In contrast, Early Triassic POM is essentially composed of marine algal-amorphous matter with C-isotope values of −31‰. Hence, these values are interpreted to represent isotopic end-members of marine and terrestrial organic matter (Thomas et al., 2004) very similar to our end-members.

Because of the difference between marine and terrestrial C-isotope composition, some authors have expressed reservations against the correlative usefulness of $\delta^{13}C_{org}$ records (e.g. Corsetti et al., 2005). Differences between the $\delta^{13}C_{org}$ and $\delta^{13}C_{carb}$ records from Meishan and Shanghsi demonstrate that the shifts in the two records are not synchronous (Riccardi et al., 2007), suggesting that the negative shift in $\delta^{13}C_{org}$ is not a reliable marker for the end-Permian mass extinction event. For these measured sections, no POM data is available. Thus, it is unclear if the observed changes might have been caused by changes in the deposition of sedimentary organic matter. However, numerous studies corroborate the value of $\delta^{13}C_{org}$ records for chemostratigraphic correlation (e.g. Gröcke, et al., 1999; Heimhofer et al., 2003; Weissert et al., 2008). Because of the absence of reliable biostratigraphic markers in the Norwegian siliciclastic succession, $\delta^{13}C_{org}$ record combined with data on POM composition is the best approach to assess the chronology of events. In the Finnmark cores, no significant POM compositional variation influenced the isotopic signal (Hochuli et al., this volume); therefore, our palynofacies-supported $\delta^{13}C_{org}$ data of the PTB from Norway suggest that the C-isotopes of organic matter reflect real global changes of the carbon cycle. Fluctuations in intervals “c” to “e” and “g” to “j” in the Trøndelag cores indicate that this global C-isotope signal is combined with a local signal generated by fluctuating respective contributions of sedimentary terrestrial and marine POM. Hence, the negative shift (interval “b” to interval “d”) cannot be caused by changing POM composition. Proposed causes for the global negative (carbonate and organic) C-isotope shift at the PTB include: (i) marine productivity collapse caused by anoxia (Wignall and Twitchett, 1996); (ii) regression and oxidation of organic carbon on the exposed shelf (Holser et al., 1989); (iii) destabilisation of methane hydrates (Morante, 1996; Krull et al., 2004; Retallack and Krull, 2006); (iv) volcanic CO_2 degassing (Renne et al., 1995); (v) heating of organic-rich sediments by volcanism and release of light carbon (Svensen et al., 2009); or (vi) a combination of several of the abovementioned causes (Berner, 2002).

In Norway, Late Permian $\delta^{13}C_{org}$ values are stable around −22‰ (interval “a”). For this interval, palynofacies of the Trøndelag section (6611/09-U-01, Supplementary Fig. 2) indicates the influx of a homogenous assemblage of mainly opaque and translucent phytoclasts into the sedimentary record. Compared to C-isotope values of recent terrestrial organic matter (C3 plants −28‰, Derry and France-Lanord, 1996), these values are very heavy. C-isotope fractionation of

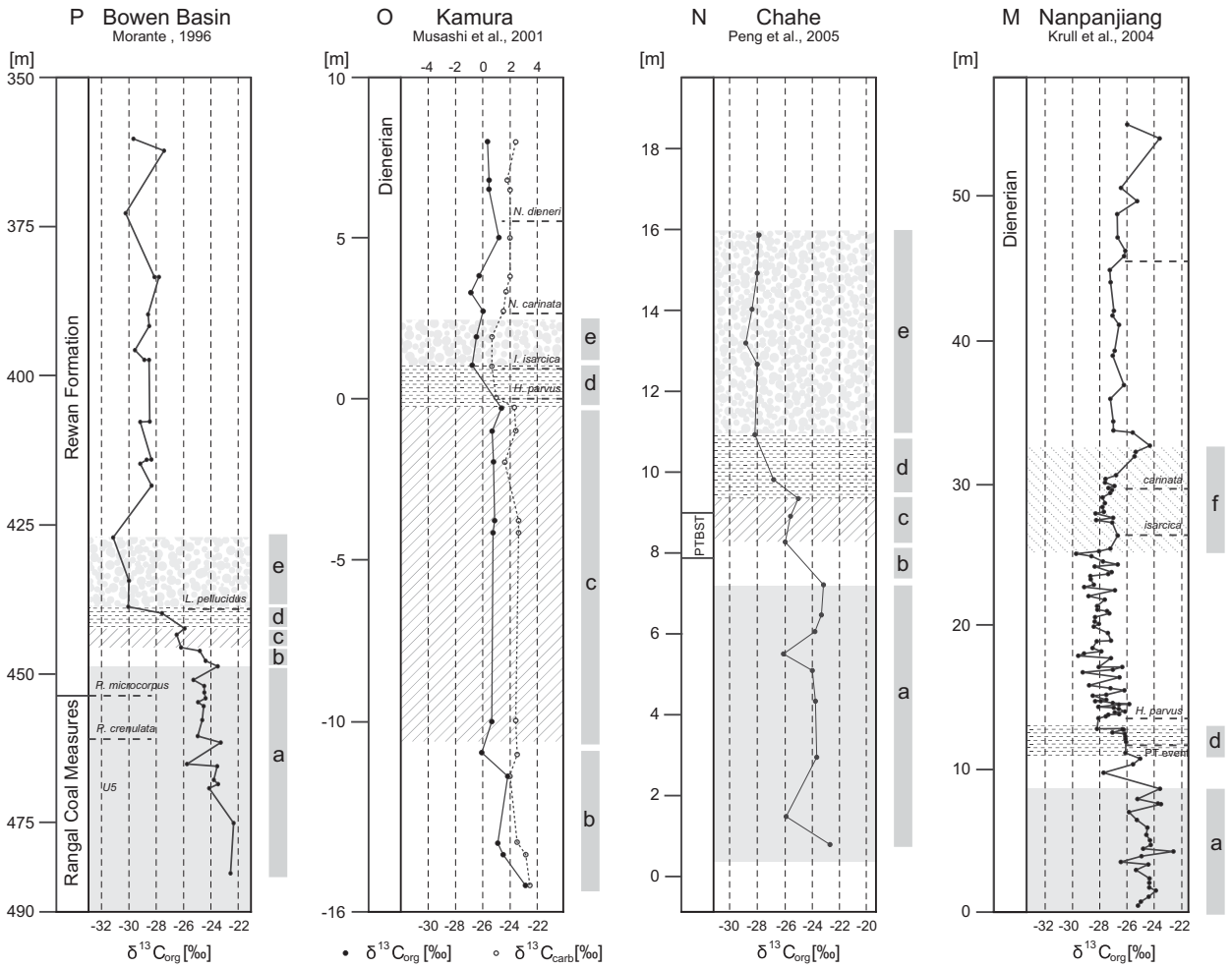

Fig. 4 (*continued*).

terrestrial plants is sensitive to environmental conditions. As Late Permian climate prior to the negative $\delta^{13}C$ shift is characterised by the waning of the late Palaeozoic cool and dry icehouse climate (Kiehl and Shields, 2005), these climatic conditions might have been one of the causes for the high C-isotope values. A recent study by Diefendorf et al. (2010) emphasises a strong correlation of carbon isotope fractionation by leaves with water availability.

In the Trøndelag cores, interval "b" and the lower part of interval "c" are missing due to a sedimentary gap, which is indicated by a lithological break and an abrupt change in palynological assemblages (Bugge et al., 2002; Hochuli et al., 2010). In the Finnmark cores, the upper part of interval "b" coincides with the phosphoritic layer in 7129/10-U-01 and the overlying pebbly shale layer, a seismic marker for the top of the Permian. The refilled crack structures in this bed have been interpreted as a feature of subaerial exposure (Bugge et al., 1995). On the other hand, palynological data (acritarch peak) from the pebbly shale layer imply a flooding of the Late Permian carbonate platform in this interval (Hochuli et al., this volume). Thus, we interpret the succession of phosphoritic layer and the pebbly shale layer rather as being deposited during a transgressive interval than during emersion. The amplitude of the negative shift (of 5‰ to 6‰) in interval "b" is not reached in any of the considered $\delta^{13}C_{carb}$ records (Fig. 4). Increases in pCO_2 due to volcanism have only a minor influence on the isotopic composition of carbonates (e.g. Kump and Arthur, 1999), but increased pCO_2 can lead to decreased isotopic composition of the organic matter by several per mill, thus increasing the difference between inorganic and organic $\delta^{13}C$ (commonly expressed as Δ). Zircon U/Pb radiometric dating of the negative C-isotope spike in Meishan (252.4 ± 0.3 Ma (Mundil et al., 2004) to 251.4 ± 0.3 Ma (Bowring et al., 1998)) and the Siberian magmatic activity (252.0 ± 0.4 Ma (Svensen et al., 2009), to 251.1 ± 0.3 Ma (Kamo et al., 2003)) overlap in a time interval of 1.3 Ma. Therefore, the first decrease (interval "b") of $\delta^{13}C_{org}$ is most probably caused by a first massive eruptive phase of the Siberian Traps, a concomitant release of CO_2 and increase of atmospheric pCO_2. Additional input of light carbon from methane of other sources (e.g. released by the heating of organic-rich sediments during Siberian Trap emplacement) has to be considered (Svensen et al., 2009). Interval "c" of the Norwegian $\delta^{13}C_{org}$ record suggests that conditions stabilise after the first negative shift and a new equilibrium between increased pCO_2, volcanic activity, and fractionation is established.

The second negative shift (interval "d") is recorded worldwide in carbonate and organic carbon isotope records with nearly the same magnitude of about −3‰ to −4‰ (e.g. Grasby and Beauchamp, 2008; and Section 5.2). The simultaneous rapid negative excursions in the organic and inorganic carbon must have been triggered by an event affecting both the marine and terrestrial carbon pools. Probably methane release caused by increased temperatures or heating of

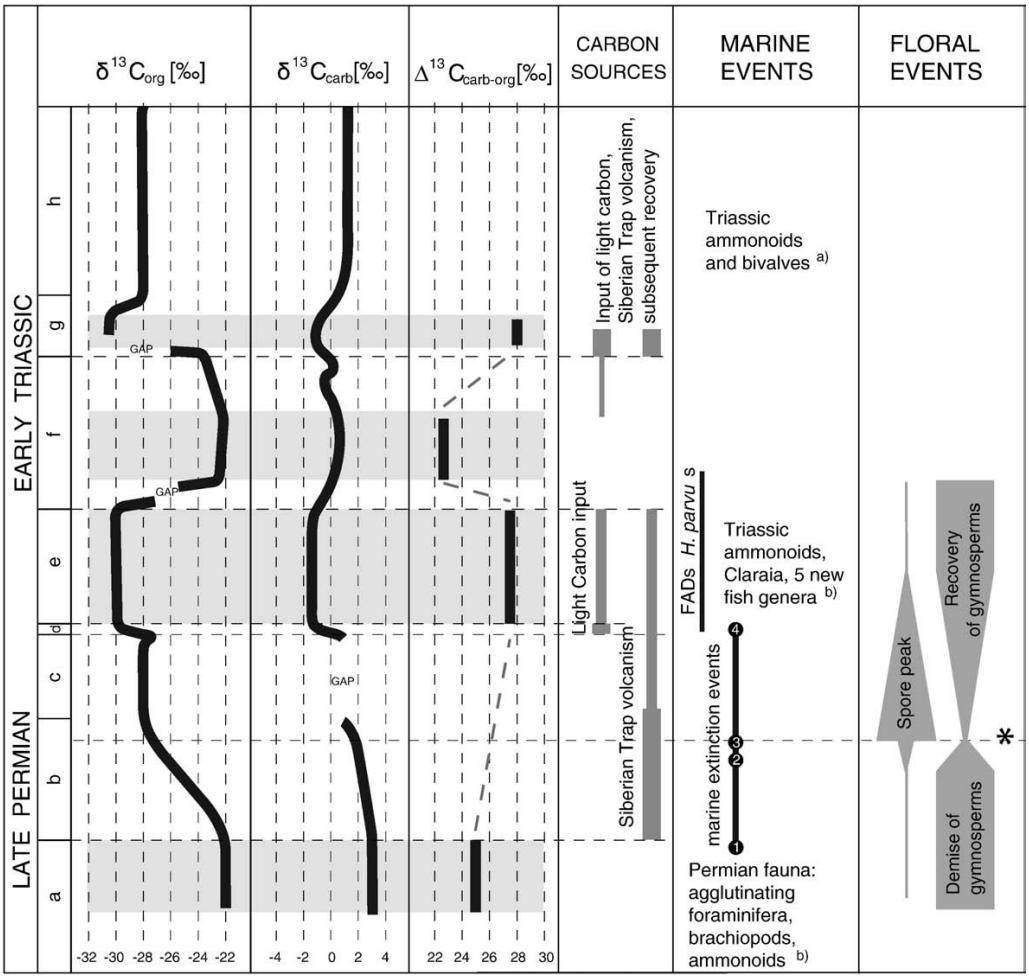

Fig. 5. Schematic C-isotope composite records: $\delta^{13}C_{org}$ (this study), $\delta^{13}C_{carb}$ Gartnerkofel core 1 modified after Holser et al. (1989) and $\Delta = \delta^{13}C_{carb\text{-}org}$. Marine faunal events after a) Bugge et al. (2002) and b) Stemmerik et al. (2001) Chemostratigraphic position of extinction events: (1) East Greenland (Twitchett et al., 2001); (2) Shahreza, Iran, (Heydari et al., 2008); (3) East Greenland, (Stemmerik et al., 2001); (4) Meishan, China (Jin et al., 2000), Gartnerkofel, Austria (Holser et al., 1989; Jenny-Deshusses, 1991), Buchanan Lake, Canada (Grasby and Beauchamp, 2008). Range of FADs of *H. parvus* according to their different chemostratigraphic position in various sections (see Fig. 4). Floral events (Hochuli et al., this volume and Stemmerik et al., 2001), * extinction of glossopterids (Morante, 1996).

organic matter–rich sediments (dispersed organic matter, coal beds, or petroleum reservoirs) underlying the Siberian Traps (Svensen et al., 2009) triggered the negative shift in interval "d". Evidence for a further increase of atmospheric pCO_2 can be inferred from the difference between inorganic and organic $\delta^{13}C$. To obtain a rough picture of this difference, we calculated $\Delta = \delta^{13}C_{carb} - \delta^{13}C_{org}$ after e.g. Kump and Arthur (1999) for intervals "a", "d", "f", and "g" using the $\delta^{13}C_{carb}$ record from the Gartnerkofel core 1 (Austria, Holser et al., 1989; Fig. 5 and Table 1) since the lithology of the Trøndelag cores does not allow a parallel $\delta^{13}C_{carb}$ curve. From interval "a" to interval "d" Δ increases by 2.5‰ supporting an increase in pCO_2 derived from the Siberian Trap eruption.

Table 1
Difference between $\delta^{13}C_{carb}$ and $\delta^{13}C_{org}$.

Interval	$\delta^{13}C_{org}$ [‰] Norway, this study	$\delta^{13}C_{carb}$ [‰] Austria, (Holser et al., 1989)	Δ [‰]
"a"	−22.0	+3.0	25.0
"d"	−29.0	−1.5	27.5
"f"	−22.0	+0.5	22.5
Base "g"	−29.0	−1.0	28.0

Intervals "c" to "e" coincide roughly with a silt- and mudstone-dominated interval (Fig. 3). The heterogeneous POM assemblage of core 6611/09-U-01 consisting of terrestrial phytoclasts and degraded terrestrial organic matter ($\delta^{13}C_{org}$ −22‰) with contributions of acritarchs and amorphous organic matter (AOM, $\delta^{13}C_{org}$ −32‰; Supplementary Fig. 2), explains the C-isotope fluctuations of ±3‰ within these intervals.

As there is no ^{13}C-enriched carbon pool which could release large quantities of ^{13}C-rich carbon to trigger high-amplitude positive shifts, the increase in $\delta^{13}C_{org}$ in interval "f" must have been caused by a combination of regional and global causes. At least parts of the positive shift, as expressed in the carbonate records (Fig. 4G, H, I, J, L) can be explained by the demise of light carbon input and an increase in burial of organic matter leading to an increase in the carbon isotope composition of the ocean–atmosphere carbon pool. The anoxia-phosphate feedback pathway implies that the burial of organic matter under anoxic conditions leads to the preferential recycling of

phosphate into the water column, which enables marine productivity to continue during high rates of organic carbon burial (Payne and Kump, 2007). PTB sequences are often described as being deposited under anoxic conditions (e.g. Wignall and Twitchett, 2002), which would favour an anoxia-phosphate feedback; however, the accurate age and relation to the C-isotope curve has not been confidently established. However, the POM composition in interval "f" supports neither anoxia nor increased marine productivity for the Trøndelag platform. Instead, the POM consists of homogenous assemblages of opaque and translucent phytoclasts with $\delta^{13}C_{org}$ values of −22‰. A change to dryer climate might increase isotopic values of terrestrial organic matter. In fact, palynology suggests dryer conditions for interval "f" (Hochuli et al., 2010). However, the onset of this dryer phase is delayed with respect to the isotope shift. Therefore, dry climates probably stabilised the $\delta^{13}C$ values at high levels but could not have triggered the positive shift.

The second phase with minimum values around −30‰ (interval "g") can also be observed in several $\delta^{13}C_{carb}$ records and suggests a renewed input of light carbon. Additionally, the increase of Δ values from 22.5‰ to 28‰ points to a renewed intensive pulse of CO_2 input (Fig. 5 and Table 1), probably from a late eruptive pulse of the Siberian Traps. The abrupt decrease of $\delta^{13}C_{org}$ values in the Trøndelag record is probably due to discontinuous deposition, which is also supported by the abrupt changes in the dominant lithology (change from sandstone- to siltstone-dominated succession) and palynofacies (change from homogenous to heterogeneous POM assemblage, Fig. 3 and Supplementary Fig. 2).

The following intervals "g" to "j" are characterised by the alternation of small positive shifts (intervals "g" and "i") with relative stable phases in-between (intervals "h" and "j"). The fluctuations within these intervals are probably caused by variations in composition of organic matter as shown for intervals "c" to "e". The composition of the marine and terrestrial end-members (marine, −32‰; terrestrial, −22‰) causing these fluctuations are the reverse of recent marine organic matter (−21‰) and terrestrial C3 plants (−28‰; Derry and France-Lanord, 1996), but marine organic matter lighter than the terrestrial is also common in Cretaceous and pre-Cretaceous sediments (Arthur et al., 1985). The increased fractionation of pre-Cretaceous marine organic matter compared to the fractionation of modern organic matter is caused by high levels of atmospheric CO_2 (Arthur et al., 1985; Hayes, 2004). Late Permian pCO_2 levels are estimated 10 times higher than present day values (Kiehl and Shields, 2005) or even higher (Kidder and Worsley, 2004). An additional increase of atmospheric CO_2 is proposed for the transition to the Triassic (Berner, 2002, 2003). Therefore, we propose a combination of high pCO_2 and probably dry climate as a reasonable explanation for the highly depleted C-isotope values of marine organic matter and the relative ^{13}C-enrichment of terrestrial organic matter.

6. Conclusions

The high-resolution chemostratigraphy combined with analysis of the POM composition of the expanded Norwegian sections and closely comparable trends in other globally distributed sections show that $\delta^{13}C_{org}$ data reflect real changes in the global carbon cycle. High frequency fluctuations of the record can be explained by heterogeneous POM assemblages with contribution of marine organic carbon (−32‰) and terrestrial organic carbon (−22‰) to the $\delta^{13}C_{org}$ record. We subdivide the typical chemostratigraphic pattern of the composite $\delta^{13}C_{org}$ record from Norway into 10 intervals ("a" to "j") that can be correlated worldwide. A stepwise negative shift leads to a first minimum (interval "e"), which is separated by a positive excursion (interval "f") from a subsequent second minimum (interval "g"). Both negative shifts are probably caused by a combination of volcanism (Siberian Traps) and input of light carbon from other sources (methane and/or heating of organic-rich sediments). Beside the records from Norway, the second negative shifts (interval "g") can also be observed in Meishan (Xie et al., 2007), Gartnerkofel (Holser et al., 1989), and Iran (Heydari et al., 2008). The general trend of stepwise negative shifts is also documented in the PTB sections of Greenland (Stemmerik et al., 2001), Arctic Canada (Grasby and Beauchamp, 2008), Australia (Morante, 1996), and China (Peng et al., 2005). The comparison of the results of the expanded Norwegian sections with other data confirms the assumption that several classical PTB sections are incomplete, as advocated by other authors (e.g. Grasby and Beauchamp, 2008). The stepwise negative shift – near the top of interval "b" – coincides with a floral turnover where the palynological records from Greenland (Stemmerik et al., 2001) and Norway (Hochuli et al., this volume) reflect a change from gymnosperm-dominated to spore-dominated assemblages (spore peak). At these sites – Northern mid latitudes – floral associations of interval "c" are characterised by the recovery of conifers and pteridosperms. The distribution of faunal events relative to the C-isotope curve shows a series of extinctions in the marine realm coinciding with the stepwise negative shift—from the top of interval "a" to the top of interval "d"). The detailed chemostratigraphic correlation of various sections shows that the biostratigraphic event – FAD of the conodont *H. parvus* – used to define the base of the Mesozoic has a diachronous distribution. This event coincides with the youngest extinction event (e.g. Gartnerkofel) or occurs after the extinction period (e.g. Meishan). The diachrony of the FAD of *H. parvus* obscures biostratigraphic correlation between different basins (Shevyrev, 2006), and moreover, the ecological differentiation between coeval pelagic and neritic conodont assemblages is a significant hindrance for the use of *H. parvus*, which is rare in pelagic settings and detrital series of the Boreal realm (Orchard and Krystyn, 1998).

Acknowledgments

SINTEF is thanked for the access to core samples. We are grateful to H. Weiss for his assistance in the core storage in Trondheim. We thank N. Goudemand for valuable discussions on conodont stratigraphy. We are grateful for the constructive comments on the manuscript by Lee Kump, Hedi Oberhänsli and for the remarks provided by an anonymous reviewer. This research was supported by the Swiss NSF project 200020-113554 (to H. Bucher).

Appendix A. Supplementary data

Supplementary data to this article can be found online at doi:10.1016/j.gloplacha.2010.10.007.

References

Arthur, M.A., Dean, W.E., Claypool, G.E., 1985. Anomalous ^{13}C enrichment in modern marine organic carbon. Nature 315, 216–218.
Benton, M.J., Twitchett, R.J., 2003. How to kill (almost) all life: the end-Permian extinction event. Trends Ecol. Evol. 18, 358–365.
Berner, R.A., 2002. Examination of hypotheses for the Permo-Triassic boundary extinction by carbon cycle modelling. Proc. Natl. Acad. Sci. USA 99 (7), 4172–4177.
Berner, R.A., 2003. The long-term carbon cycle, fossil fuels and atmospheric composition. Nature 426, 323–326.
Bowring, S.A., Erwin, D.H., Jin, Y.G., Martin, M.W., Davidek, K., Wang, W., 1998. U/Pb Zircon geochronology and tempo of the end-Permian mass extinction. Science 280, 1039–1045.
Bugge, T., Mangerud, G., Elvebakk, G., Mørk, A., Nilsson, I., Fanavoll, S., Vigran, J.O., 1995. The Upper Palaeozoic succession on the Finnmark Platform, Barents Sea. Nor. Geol. Tidsskr. 75, 3–30.
Bugge, T., Ringas, J.E., Leith, D.A., Mangerud, G., Weiss, H.M., Leith, T.L., 2002. Upper Permian as a new play model on the mid-Norwegian continental shelf: investigated by shallow stratigraphic drilling. AAPG Bull. 86 (1), 107–127.
Cao, C., Wang, W., Jin, Y., 2002. Carbon isotope excursions across the Permian-Triassic boundary in the Meishan section, Zhejiang Province, China. Chin. Sci. Bull. 47 (13), 1125–1129.

Cao, C.Q., Yang, Y.C., Shen, S.Z., Wang, W., Zheng, Q.F., Summons, R.E., 2010. Pattern of $\delta^{13}C_{carb}$ and implications for geological events during the Permian-Triassic transition in South China. Geol. J. 45, 186–194.
Chen, Z.Q., Tong, J., Kaiho, K., Kawahata, H., 2007. Onset of biotic and environmental recovery from the end-Permian mass extinction within 1-2 million years: a case study of the Lower Triassic of the Meishan section, South China. Palaeogeogr. Palaeoclimatol. Palaeoecol. 252, 176–187.
Corsetti, F.A., Baud, A., Marenco, P.J., Richoz, S., 2005. Summary of Early Triassic carbon isotope records. C. R. Palevol 4, 473–486.
Derry, L.A., France-Lanord, C., 1996. Neogene growth of the sedimentary organic carbon reservoir. Paleoceanography 11 (3), 267–275.
Diefendorf, A.F., Mueller, K.E., Wing, S.L., Koch, P.L., Freeman, K.H., 2010. Global patterns in leaf ^{13}C discrimination and implication for studies of past and future climate. Proc. Natl. Acad. Sci. USA 107 (13), 5738–5743.
Foster, C.B., 1982. Spore-pollen assemblages of the Bowen Basin, Queensland (Australia): their relationship to the Permian/Triassic boundary. Rev. Palaeobot. Palynol. 36, 165–183.
Foster, C.B., Logan, G.A., Summons, R.E., Gorter, J.D., Edwards, D.S., 1997. Carbon isotopes, kerogen types and the Permian-Triassic boundary in Australia: implications for exploration. Aust. Petrol. Prod. Explor. Assoc. J. 37, 472–489.
Grasby, S.E., Beauchamp, B., 2008. Intrabasin variability of the carbon-isotope record across the Permian-Triassic transition, Sverdrup Basin, Arctic Canada. Chem. Geol. 253, 141–150.
Gröcke, D.R., Hesselbo, S., Jenkyns, H.C., 1999. Carbon-isotope composition of Lower Cretaceous fossil wood: ocean-atmosphere chemistry and relation to sea-level change. Geology 27, 155–158.
Hayes, J.M., 1993. Factors controlling ^{13}C contents of sedimentary organic compounds: principles and evidence. Mar. Geol. 113, 111–125.
Hayes, J.M., 2004. Isotopic order, biogeochemical processes, and earth history. Geochim. Cosmochim. Acta 68 (8), 1691–1700.
Hayes, J.M., Strauss, H., Kaufmann, A.J., 1999. The abundance of 13C in marine organic matter and isotopic fractionation in the global biogeochemical cycle of carbon during the past 800 Ma. Chem. Geol. 161, 103–125.
Heimhofer, U., Hochuli, P.A., Burla, S., Andersen, N., Weissert, H., 2003. Terrestrial carbon-isotope records from coastal deposits (Algarve, Portugal): a tool for chemostratigraphic correlation on an intrabasinal and global scale. Terra Nova 15, 8–13.
Heydari, E., Arzani, N., Hassanzadeh, J., 2008. Mantle plume: the invisible serial killer—application to the Permian–Triassic boundary mass extinction. Palaeogeogr. Palaeoclimatol. Palaeoecol. 264, 147–162.
Hochuli, P.A., Vigran, J.O., Hermann, E., Bucher, H., 2010. Multiple climatic changes around the Permian Triassic boundary event revealed by an expanded palynological record from Mid Norway. AAPG Bull. 122 (5/6), 884–896.
Hochuli, P.A., Hermann, E., Vigran, J.O., Bucher, H., Weissert, H. (this volume). Rapid demise and recovery of plant ecosystems across the end-Permian extinction event.
Holser, W.T., Schönlaub, H.-P., Attrep, M., Boekelmann, K., Klein, P., Magaritz, M., Orth, C.J., Fenninger, A., Jenny, C., Kralik, M., Mauritsch, H., Pak, E., Schramm, J.-M., Stattegger, K., Schmöller, R., 1989. A unique geochemical record at the Permian/Triassic boundary. Nature 337, 39–44.
Ivlev, A.A., 2004. Contribution of photorespiration to changes of carbon isotope characteristics in plants affected by stress factors. Russ. J. Plant Physl. 51 (2), 271–280.
Jahren, A.H., Arens, N.C., Harbeson, S.A., 2008. Prediction of atmospheric $\delta^{13}CO_2$ using fossil plant tissues. Rev. Geophys. 46, RG I002. doi:10.1029/2006RG000219.
Jenny-Deshusses, C., 1991. The Permian-Triassic of the Gartnerkofel-1 Core (Carnic Alps, Austria): foraminifera and algae of the core and the outcrop section. Abh. Geol. Bundesanstalt 45, 99–108.
Jin, Y.G., Wang, Y., Wang, W., Shang, Q.H., Cao, C.Q., Erwin, D.H., 2000. Pattern of marine mass extinction near the Permian-Triassic boundary in South China. Science 289, 432–436.
Kaiho, K., Chen, Z.Q., Sawada, K., 2009. Possible causes for a negative shift in the stable carbon isotope ratio before, during and after the end-Permian mass extinction in Meishan, South China. Aust. J. Earth Sci. 56 (6), 799–808.
Kamo, S.L., Czamanske, G.K., Amelin, Y., Fedorenko, V.A., Davis, D.W., Trofimov, V.R., 2003. Rapid eruption of Siberian flood-volcanic rocks and evidence for coincidence with the Permian-Triassic boundary and mass extinction at 251 Ma. Earth Planet. Sci. Lett. 214, 75–91.
Kidder, D.L., Worsley, T.R., 2004. Causes and consequences of extreme Permo-Triassic warming to globally equable climate and relation to the Permo-Triassic extinction and recovery. Palaeogeogr. Palaeoclimatol. Palaeoecol. 203, 207–237.
Kiehl, J.T., Shields, C.A., 2005. Climate simulation of the latest Permian: implications for mass extinction. Geology 33 (9), 757–760.
Korte, C., Kozur, H.W., 2010. Carbon-isotope stratigraphy across the Permian–Triassic boundary: a review. J. Asian Earth Sci. 39, 215–235.
Krull, E.S., Lehrmann, D.J., Druke, D., Kessel, B., Yu, Y., Li, R., 2004. Stable carbon isotope stratigraphy across the Permian-Triassic boundary in shallow marine carbonate platforms, Nanpanjiang Basin, south China. Palaeogeogr. Palaeoclimatol. Palaeoecol. 204, 297–315.
Kump, L.R., Arthur, M.A., 1999. Interpreting carbon-isotope excursions: carbonates and organic matter. Chem. Geol. 161, 181–198.
Larssen, G.B., Elvebakk, G., Henriksen, L.B., Kristensen, S.-E., Nilsson, I., Samuelsberg, T.J., Svånå, T.A., Stemmerik, L., Worsley, D., 2005. Upper Palaeozoic lithostratigraphy of the southern part of the Norwegian Barents Sea. Norg. Geol. Unders. Bull. 444, 3–43.
Mangerud, G., 1994. Palynostratigraphy of the Permian and lowermost Triassic succession, Finnmark Platform, Barents Sea. Rev. Palaeobot. Palynol. 82, 317–349.
Méhay, S., Keller, C.E., Bernasconi, S.M., Weissert, H., Erba, E., Bottini, C., Hochuli, P.A., 2009. A volcanic CO2 pulse triggered the Cretaceous Oceanic Anoxic Event 1a and a biocalcification crisis. Geology 37, 819–822.
Morante, R., 1996. Permian and Early Triassic isotopic records of carbon and strontium in Australia and a scenario of events about the Permian-Triassic boundary. Hist. Biol. 11, 289–310.
Mundil, R., Metcalfe, I., Ludwig, K.R., Renne, P.R., Oberli, F., Nicoll, R.S., 2001. Timing of the Permian-Triassic biotic crisis: implications from new zircon U/Pb age data (and their limitations). Earth Planet. Sci. Lett. 187, 131–145.
Mundil, R., Ludwig, K.R., Metcalfe, I., Renne, P.R., 2004. Age and timing of the Permian mass extinctions: U/Pb dating of closed-system zircons. Science 305, 1760–1763.
Musashi, M., Isozaki, Y., Koike, T., Kreulen, R., 2001. Stable carbon isotope signature in mid-Panthalassa shallow-water carbonates across the Permo-Triassic boundary: evidence for ^{13}C-depleted superocean. Earth Planet. Sci. Lett. 191, 9–20.
Orchard, M., Krystyn, L., 1998. Conodonts of the lowermost Triassic of Spiti, and new zonation based on Neogondolella successions. Rev. Ital. Paleontol. Strat. 104 (3), 341–368.
Payne, J.L., Kump, L.R., 2007. Evidence for recurrent Early Triassic massive volcanism from quantitative interpretation of carbon isotope fluctuations. Earth Planet. Sci. Lett. 256, 264–277.
Peng, Y., Zhang, S., Yu, T., Yang, F., Gao, Y., Shi, G.R., 2005. High-resolution terrestrial Permian-Triassic eventostratigraphic boundary in western Guizhou and eastern Yunnan, southwestern China. Palaeogeogr. Palaeoclimatol. Palaeoecol. 215, 285–295.
Renne, P.R., Zhang, Z., Richards, M.A., Black, M.T., Basu, A.R., 1995. Synchrony and causal relations between Permian-Triassic boundary crisis and Siberian flood volcanism. Science 269, 1413–1416.
Retallack, G.J., Krull, E.S., 2006. Carbon isotopic evidence for terminal-Permian methane outbursts and their role in extinctions of animals, plants, coral reefs, and peat swamps. Geol. Soc. Am. Spec. Pap. 399, 249–268.
Riccardi, A., Kump, L.R., Arthur, M.A., D'Hondt, S., 2007. Carbon isotopic evidence for chemocline upward excursions during the end-Permian event. Palaeogeogr. Palaeoclimatol. Palaeoecol. 248, 73–81.
Richoz, S., Krystyn, L., Baud, A., Brandner, R., Horacek, M., Mohtat-Aghai, P., 2010. Permian–Triassic boundary interval in the Middle East (Iran and N. Oman): progressive environmental change from detailed carbonate carbon isotope marine curve and sedimentary evolution. J. Asian Earth Sci. 39, 236–253.
Schönlaub, H.P., 1991. The Permian-Triassic of the Gartnerkofel-1 Core (Carnic Alps, Austria): Conodont Biostratigraphy. Abh. Geol. Bundesanstalt 45, 75–98.
Shevyrev, A.A., 2006. Triassic biochronology: state of the art and main problems. Stratigr. Geol. Correl. 14 (6), 629–641.
Sluijs, A., Brinkhuis, H., Schouten, S., Bohaty, S.M., John, C.M., Zachos, J.C., Reichart, G.-J., Sinninghe Damsté, J.S., Crouch, E.M., Dickens, G.R., 2007. Environmental precursors to rapid light carbon injection at the Palaeocene/Eocene boundary. Nature 450, 1218–1221.
Stemmerik, L., Bendix-Almgreen, S.E., Piasecki, S., 2001. The Permian-Triassic boundary in central East Greenland: past and present views. Bull. Geol. Soc. Denmark 48, 159–167.
Svensen, H., Planke, S., Polozov, A.G., Schmidbauer, N., Corfu, F., Podladchikov, Y., Jamtveit, B., 2009. Siberian gas venting and the end-Permian environmental crisis. Earth Planet. Sci. Lett. 277, 490–500.
Thomas, B.M., Willink, R.J., Grice, K., Twitchett, R.J., Purcell, R.R., Archbold, N.W., George, A.D., Tye, S., Alexander, R., Foster, C.B., Barber, C.J., 2004. Unique marine Permian-Triassic boundary section from Western Australia. Aust. J. Earth Sci. 51, 423–430.
Tozer, E.T., 1994. Canadian Triassic ammonoid faunas. Geological Survey of Canada, Ottawa.
Twitchett, R.J., Looy, C.V., Morante, R., Visscher, H., Wignall, P.B., 2001. Rapid and synchronous collapse of marine and terrestrial ecosystems during the end-Permian biotic crisis. Geology 29 (4), 351–354.
Weissert, H., Joachimski, M., Sarnthein, M., 2008. Chemostratigraphy. Newsl. Stratigr. 42, 145–179.
Wignall, P.B., Twitchett, R.J., 1996. Oceanic anoxia and the End Permian mass extinction. Science 272, 1155–1158.
Wignall, P.B., Twitchett, R.J., 2002. Extent, duration, and nature of the Permian-Triassic superanoxic event. Geol. Soc. Am. Spec. Pap. 356, 395–413.
Wignall, P.B., Morante, R., Newton, R., 1998. The Permo-Triassic transition in Spitsbergen: $\delta^{13}C_{org}$ chemostratigraphy, Fe and S geochemistry, facies, fauna and trace fossils. Geol. Mag. 135 (1), 47–62.
Xie, S., Pancost, R.D., Huang, J., Wignall, P.B., Yu, J., Tang, X., Chen, L., Huang, X., Lai, X., 2007. Changes in the global carbon cycle occurred as two episodes during the Permian Triassic crisis. Geology 35, 1083–1086.
Xu, D.-Y., Yan, Z., 1993. Carbon isotope and iridium event markers near the Permian/Triassic boundary in the Meishan section, Zhejiang Province, China. Palaeogeogr. Palaeoclimatol. Palaeoecol. 104, 171–176.
Yin, H., Zhang, K., Tong, J., Yang, Z., Shunbao, W., 2001. The Global Stratotype Section and Point (GSSP) of the Permian-Triassic Boundary. Episodes 24 (2), 102–114.
Yin, H., Feng, Q., Lai, X., Baud, A., Tong, J., 2007. The protracted Permo-Triassic crisis and multi-episode extinction around the Permian-Triassic boundary. Glob. Planet. Change 55, 1–20.

Supplementary Data

Supplementary Figure 2: Palaeogeographic position of correlated PTB sections modified after Smith et al. (1994) and Golonka and Ford (2000). Capital letters refer to the sections in Supplementary Figure 1.

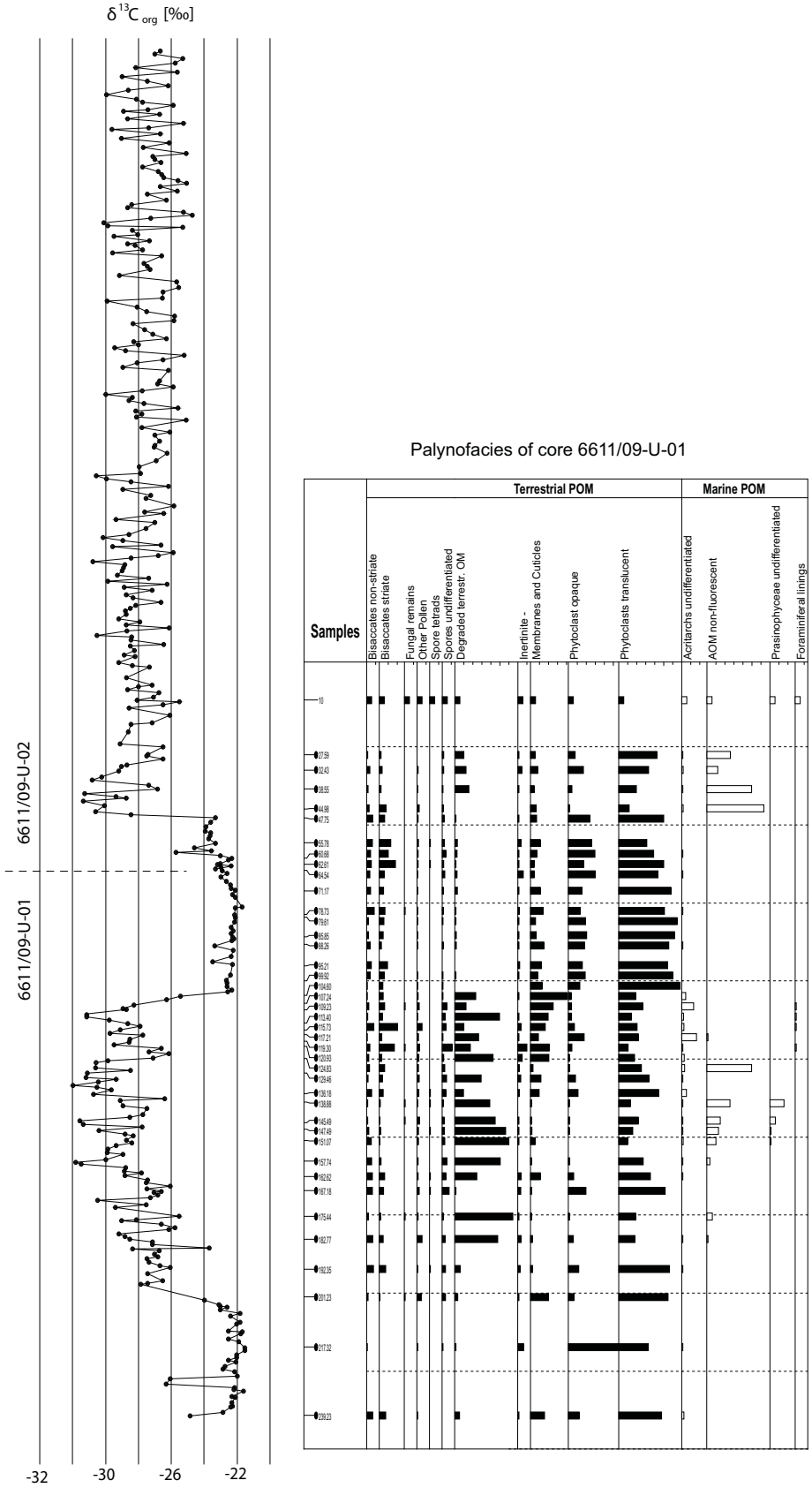

Supplementary Figure 3: Palynofacies of core 6611/09-U-01 together with the C-isotope curve of cores 6611/09-U-01, -02.

Chapter 2:

Organic matter and palaeoenvironmental signal during the Early Triassic biotic recovery: the Salt Range and Surghar Range records

with Peter A. Hochuli, Sabine Méhay, Hugo Bucher, Thomas Brühwiler, David Ware, Michael Hautmann, Ghazala Roohi, Khalil-ur-Rehman, Aamir Yaseen

Sedimentary Geology, in press, doi:10.1016/j.sedgeo.2010.11.003

ARTICLE IN PRESS
SEDGEO-04273; No of Pages 23

Sedimentary Geology xxx (2010) xxx–xxx

Contents lists available at ScienceDirect

Sedimentary Geology

journal homepage: www.elsevier.com/locate/sedgeo

Organic matter and palaeoenvironmental signals during the Early Triassic biotic recovery: The Salt Range and Surghar Range records

Elke Hermann [a,*], Peter A. Hochuli [a], Sabine Méhay [b], Hugo Bucher [a], Thomas Brühwiler [a], David Ware [a], Michael Hautmann [a], Ghazala Roohi [c], Khalil ur-Rehman [c], Aamir Yaseen [c]

[a] Institute and Museum of Palaeontology, University of Zurich, Karl Schmid-Str. 4, 8006 Zurich, Switzerland
[b] Massachusetts Institute of Technology, Department of Earth, Atmospheric, and Planetary Sciences, 45 Carleton Street, Cambridge, MA 02139, USA
[c] Pakistan Museum of Natural History, Garden Avenue, Islamabad 44000, Pakistan

ARTICLE INFO

Article history:
Received 23 June 2010
Received in revised form 15 November 2010
Accepted 19 November 2010
Available online xxxx

Editor: B. Jones

Keywords:
Early Triassic
Palynofacies
Palaeoenvironment
Sequence stratigraphy
Molecular biomarkers

ABSTRACT

Latest Permian to the Middle Triassic mixed siliciclastic–carbonate shelf deposits of the northern Gondwana margin have been studied in four sections (Nammal, Chhidru, Chitta–Landu, and Narmia) in the Salt Range and Surghar Range of Pakistan. Sedimentological and palynofacies patterns combined with a high resolution ammonoid based age control have been used to assess environmental changes such as sea-level change, distance from the shore, and oxygenation conditions of the sections in the aftermath of the end-Permian mass extinction.

The base and the top of the Early Triassic are marked by second order sequence boundaries (SRT1, SRT8). Within the Early Triassic two third order sequence boundaries could be delineated by means of palynofacies analysis and sedimentology, one near the Dienerian–Smithian (SRT2) and the second one near the Smithian–Spathian boundary (SRT5). The extinction event at the Smithian–Spathian boundary seems to be closely associated to the latter globally recorded sea-level low stand. Five additional sequences of undetermined order (SRT3, SRT 4, SRT5/1, SRT6, and SRT7) are reflected in the sedimentological record of the studied sections.

The observed changes in the composition of the particulate organic matter (POM) indicate a general shallowing upward trend, which is modulated by smaller transgressive–regressive cycles supporting the sedimentologically defined sequences. The POM is mostly dominated by terrestrial phytoclasts and sporomorphs. The strongest marine signal is reflected by increased abundance of amorphous organic matter (AOM) in the lower part of the Ceratite Marls at Nammal (late Dienerian) and Chhidru (earliest Smithian) and the Lower Ceratite Limestone at Chitta–Landu (late Dienerian). AOM of marine origin is characteristic for deeper, distal basinal settings and is preferentially preserved under dysoxic and anoxic conditions, indicating reduced oxygen conditions during these intervals. Up-section transgressive events are reflected by increased numbers of acritarchs, reaching up to 50% of the POM. Well oxygenated conditions and low total organic carbon contents (TOC) continue up to the top of the Early Triassic (Mianwali Formation). The most pronounced terrestrial influx is expressed in the Middle Triassic.

Organic carbon isotope data parallel the carbonate carbon isotope records from the Tethyan realm; therefore, they reflect real global changes in the carbon cycle independent of the OM composition. The biomarker study of the apolar hydrocarbons of three samples from the Nammal section indicates an enhanced bacterial productivity, especially in the Smithian and Spathian, reflected in high relative abundances of hopanes. POM, TOC data and redox sensitive biomarkers together with high resolution biostratigraphy demonstrate that well-oxygenated environmental conditions prevailed in the Early Triassic with the exception of the Dienerian to earliest Smithian interval. The POM assemblages of Late Permian to late Griesbachian age indicate well oxygenated conditions during this time interval. There is no evidence in support of an anoxic event in the late Griesbachian in these sections.

1. Introduction

Mass extinctions have attracted the attention of scientists for a long time starting with the recognition of mass extinctions by Cuvier in the mid 18th century. The search for the possible causes of the most severe end-Permian mass extinction resulted in a number of

* Corresponding author. Tel.: +41 44 634 2329; fax: +41 44 634 4923.
E-mail address: ehermann@pim.uzh.ch (E. Hermann).

0037-0738/$ – see front matter © 2010 Elsevier B.V. All rights reserved.
doi:10.1016/j.sedgeo.2010.11.003

Please cite this article as: Hermann, E., et al., Organic matter and palaeoenvironmental signals during the Early Triassic biotic recovery: The Salt Range and Surghar Range records, Sediment. Geol. (2010), doi:10.1016/j.sedgeo.2010.11.003

hypotheses. Most of them call for a single overarching cause (e. g. the Siberian Traps) to account for the extinction. The cascading effects triggered by such a single cause are still not fully understood, thus a complex combination of several causes was also proposed for the drastic reduction of biodiversity (e. g. Berner, 2002; Erwin, 2006 and references therein). One of the most frequently proposed cause is a global superanoxic event, which is thought to have affected shallow water areas of the equatorial Tethys and Perigondwanan shelf between the latest Permian and the basal Triassic (Griesbachian). Evidence for this superanoxia has been postulated for the Pakistani sections (Wignall and Hallam, 1993; Wignall and Twitchett, 2002), which are the subject of the present study. These sections offer the rare opportunity to study excellently preserved organic matter (OM), which allows identifying oxygenation conditions and testing the anoxia hypothesis for the entire Early Triassic. Furthermore, in this well preserved OM, lipid biomarkers could be used to support results of the optically investigated POM results. Lipid biomarkers are biosynthetic molecules preserved in the form of resistant hydrocarbon skeletons in sedimentary rocks over geologic time. The molecules represent more or less specifically their precursor organisms and the diagenetic transformations they might have undergone. Hence, they are useful palaeoenvironmental and palaeobiological indicators (Eglinton and Eglinton, 2008; Peters et al., 2005).

During the last decade the focus of research expanded from the extinction event to the time during which life recovered, asking for the duration and key factors of the recovery and the environmental conditions throughout this time. During the initial recovery phase, the diversity of marine ecosystems was still low and only few marine clades recovered rather quickly, such as ammonoids and conodonts (Brayard et al., 2006, 2009; Goudemand et al., 2008; Orchard, 2007). Radiation of these groups started in the Dienerian and continued in discontinuous steps up to the Spathian. Both ammonoids and conodonts suffered a major extinction event in the latest Smithian. Benthic organisms (bivalves and gastropods) recovered at least locally already in the late Griesbachian (Hautmann and et al., in press), but it appears that this early recovery pulse did not form the basis of the main recovery phase that started towards the end of the Smithian (Posenato, 2008). In the Spathian, the number of newly evolved bivalve genera doubled without indication of a major crisis at the Smithian–Spathian boundary (Hautmann et al., 2008). Recovery of reef building organisms such as corals was relatively slow and did not start until the Middle Triassic (Flügel, 2002; Posenato, 2008).

Several proxies indicate profound environmental changes affecting marine ecosystems. Sedimentary records of the basal Triassic show unusual facies development such as microbialites, seafloor precipitated carbonate fans, flat pebble conglomerates and wrinkle structures, which can be explained by unusual ocean chemistry (Baud et al., 2007). These peculiar facies are known from various parts of the globe such as South China (Galfetti et al., 2008), Turkey, and the United States (Pruss et al., 2006).

Within the Early Triassic, changes of ammonoid diversity in time and space have been interpreted as fluctuations of the global temperature gradient (Brayard et al., 2005, 2006). Palynological records from Norway and Pakistan suggest changing climatic conditions during the Griesbachian (Hochuli et al., 2010a,b) and a distinct climatic change from humid to dryer climate around the Smithian–Spathian boundary (Galfetti et al., 2007a; Hermann et al., 2008). Multiple perturbations of the carbon cycle began with the negative spike at the Permian Triassic boundary and continued throughout the entire Early Triassic indicating changes in the biogeochemical cycles (e.g. Atudorei, 1999; Baud et al., 1996; Galfetti et al., 2007a,b; Payne et al., 2004; Richoz, 2006). Positive shifts coincide with substage boundaries such as the Dienerian–Smithian boundary, the Smithian–Spathian boundary, and the Spathian–Anisian boundary. A major negative excursion is recorded in the middle Spathian.

This study contributes to the understanding of the Early Triassic marine and non-marine palaeoenvironment including new data from lithology, particulate organic matter (POM), total organic carbon (TOC), and biomarker analysis. Sedimentological successions are presented together with sequence stratigraphic interpretation and biostratigraphic dating. New C-isotope data (organic and inorganic) allow the correlation with other Tethyan sections (e. g. South China). The Early Triassic in the Salt Range and Surghar Range is a unique archive providing excellent data on C-isotopes, biostratigraphy, sequence stratigraphy, palynofacies, and palynology. This strengthens the role of these areas as a reference area for the study of the Tethyan Early Triassic record.

2. Palaeogeography

The Late Permian palaeogeography with the supercontinent Pangaea located approximately symmetrical to the equator continued to exist throughout the Early Triassic (Stampfli and Borel, 2002; Ziegler et al., 1983). The Salt Range and Surghar Range were situated on the Northern Gondwanan shelf about 30° south (Golonka and Ford, 2000; Smith et al., 1994). The Salt Range and Surghar Range are located about 200 km southwest of Islamabad (Fig. 1a). The mixed siliciclastic–carbonate shelf of the Indian subcontinent was bordered to the northeast by the Neotethyan rift zone. As a result of the Himalayan orogeny, the sequence of Cambrian to Pliocene rocks was thrusted southward along the Salt Range Thrust onto late Tertiary sediments during Quaternary times (Gee, 1989). Permian and Early Triassic rocks are exposed in a structural stack of narrow thrusted plates more or less parallel to the Salt Range and the Surghar Range, respectively. The dextral Kalabagh strike-slip fault separates the Salt Range East of the Indus from the Surghar Range West of it. Permian and Triassic strata are well exposed in several transecting gorges, among which Chitta–Landu and Narmia in the Surghar Range and Nammal and Chhidru in the Salt Range were studied (Fig. 1).

3. Methods

3.1. Carbonate and organic carbon isotopes

To analyse the carbon isotope composition ($\delta^{13}C$) of bulk carbonate carbon, 128 samples (51 Nammal, 31 Chhidru, 46 Chitta–Landu) were drilled to produce a fine powder, which was treated with phosphoric acid at 90 °C in a Kiel IV preparation device and Gasbench, respectively. Subsequently, the liberated CO_2 gas was analysed with a Thermo-Scientific Delta V Plus isotope ratio mass spectrometer.

For determination of $\delta^{13}C$ of bulk organic carbon, 280 silt and shale samples (100 Nammal, 68 Chhidru, 98 Chitta–Landu, and 14 Narmia) were powdered with a ceramic mortar and treated with 1 N and 3 N hydrochloric acid respectively for at least 24 h to remove carbonates. The homogenised residue was analysed with an elemental analyser connected in continuous flow to a Thermo-Finnigan MAT 253 isotope ratio mass spectrometer. Average reproducibility of analyses, based on repeated measurements of laboratory standards calibrated to NBS 22 ($\delta^{13}C = -30.03‰$), is better than $\pm 0.2‰$.

All $\delta^{13}C$ values are expressed in the standard δ notation in per mil (‰) relative to the international VPDB isotope standard.

3.2. Palynofacies

184 cleaned samples (67 Nammal, 59 Chhidru, 7 (+2) Narmia, and 49 (+3) Chitta–Landu) were crushed and weighed (5–25 g) and subsequently treated with hydrochloric and hydrofluoric acid according to standard palynological preparation techniques (Traverse, 2007). The residues were sieved with an 11 μm mesh screen and mounted for the analysis of the POM. From strew mounts a

Please cite this article as: Hermann, E., et al., Organic matter and palaeoenvironmental signals during the Early Triassic biotic recovery: The Salt Range and Surghar Range records, Sediment. Geol. (2010), doi:10.1016/j.sedgeo.2010.11.003

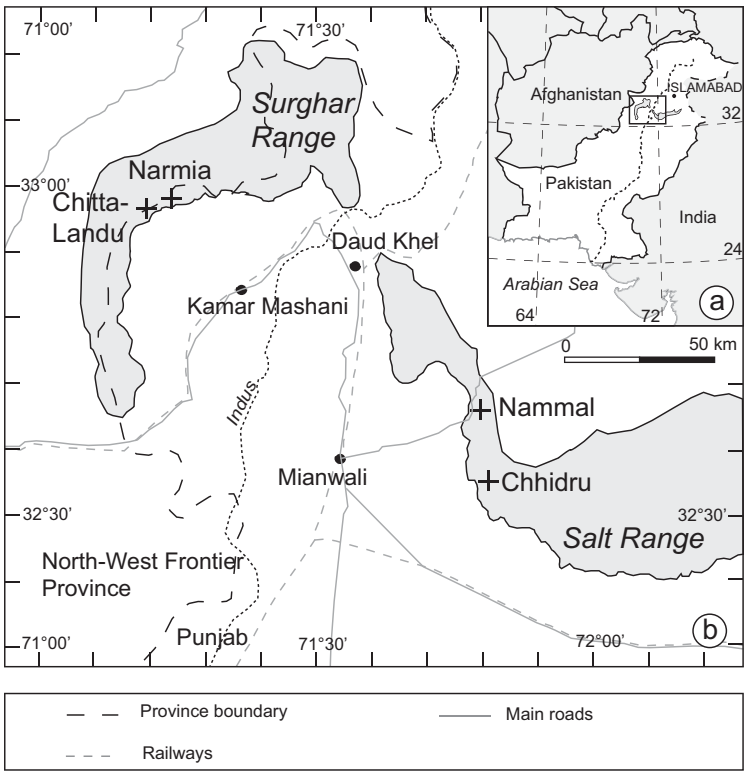

Fig. 1. a) Location of the Salt Range and Surghar Range in Pakistan; b) Location of the studied sections of Chitta–Landu and Narmia (Surghar Range) and Nammal and Chhidru (Salt Range).

minimum of 250 particles per sample were counted. Selected samples have also been used for palynological analysis.

Palynofacies reflects the depositional environment based on the total assemblage of POM (Tyson, 1995). Relative abundances of the different groups reflect firstly oxygenation condition and are therefore a tool to discriminate between oxic and anoxic conditions and secondly document changes in sea level (transgressive–regressive trends), and distance from the shore (Combaz, 1964; Tyson, 1993, 1995). Palynofacies has also been used as a tool for sequence stratigraphic interpretations (e. g. Götz et al., 2008; Pittet and Gorin, 1997; Steffen and Gorin, 1993). To analyse palynofacies patterns, the POM has been grouped into a fraction of terrestrial derived particles and a marine fraction. The terrestrial POM includes translucent and opaque woody particles, intertinite, cuticles, membranes, spores, striate and non-striate bisaccate pollen, and other pollen. The marine fraction includes amorphous organic matter (AOM), acritarchs, foraminiferal test linings, prasinophyceae and other algal remains. AOM consists of structureless aggregates of organic matter derived from phytoplankton or bacteria (Lewan, 1986; Tyson, 1995); dissolved organic matter and faecal pellets can also contribute to the formation of AOM (Tyson, 1995).

3.3. Total organic carbon and Rock Eval analysis

48 samples from the Nammal site were analysed for total organic carbon (TOC) content. Total carbon contents were measured on a CNS Elemental Analyser (Carlo Erba Instruments) and the inorganic carbon contents were determined using a UIC CM 5012 Coulometer. The TOC was calculated from the difference between total and inorganic carbon contents. 12 samples from Nammal were pulverised, and about 100 mg were analysed using a Rock Eval/TOC analyser. The samples are pyrolysed at 300 °C for 3–4 min, and the amount of hydrocarbon liberated from 1 g of rock is noted as parameter S1. Parameter S2 is the amount of hydrocarbon released during the temperature programmed pyrolysis (300–600 °C). TOC is determined by oxidising the pyrolysis residue in a second oven (600 °C in air).

3.4. Lipid biomarkers

Three samples from Nammal were ground to a fine powder (60 to 70 g), and organic compounds were extracted with an accelerated solvent extractor (ASE 200/DIONEX) using a solvent mixture of dichloromethane (DCM) and methanol (MeOH) (4:1, v/v) at 1500 psi and 100 °C. The solvents were evaporated to dryness under a gentle stream of nitrogen (N_2) at 35 °C. The total lipid extracts were fractionated by column chromatography (SiO_2). Two fractions were recovered by the elution of DCM and a mixture of DCM/MeOH (1:1, v/v), respectively. The first fraction was further separated by column chromatography (SiO_2) to yield a fraction of apolar hydrocarbons by elution with n-hexane. Elemental sulphur was removed with activated copper. The apolar hydrocarbon fractions were then analysed by gas chromatography coupled to mass spectrometry (GC–MS).

GC–MS analysis was carried out on a Hewlett Packard 6890 gas chromatograph equipped with an on-column injector and coupled to a Hewlett Packard 5973 Mass Selective Detector mass spectrometer operating in the electron impact mode (70 eV). A fused silica capillary column (DB5ms 30 m × 0.32 mm, 0.25 μm film thickness) with helium as a carrier gas was used. The samples were injected at 70 °C. The GC oven temperature was subsequently raised to 120 °C at 10 °C/min and to 300 °C at 4 °C/min, followed by 20 min isothermal.

Please cite this article as: Hermann, E., et al., Organic matter and palaeoenvironmental signals during the Early Triassic biotic recovery: The Salt Range and Surghar Range records, Sediment. Geol. (2010), doi:10.1016/j.sedgeo.2010.11.003

4. Stratigraphy and lithology

4.1. Terminology

The geology of the Salt Range and Surghar Range was first studied in the early and middle 19th century. The most important contributions defining and describing the Early Triassic stratigraphy of the Salt Range were published by Waagen (1891, 1895). His lithological subdivision of the Early Triassic sequence is extremely robust and is used in this paper with the minor modifications suggested by Guex (1978) and Kummel and Teichert (1966) (Fig. 2). Subsequent studies concerning brachiopods, conodonts, palynology and ammonoids contributed detailed information about Early Triassic fauna and flora, and the Permian–Triassic-boundary (PTB) interval (Balme, 1970; Kummel, 1966; Kummel and Teichert, 1970; Pakistani-Japanese Research Group (PJRG), 1985; Schindewolf, 1954; Teichert, 1966).

The Early Triassic Mianwali Formation has been divided into six lithological units, which include in ascending order: the Kathwai Member, Lower Ceratite Limestone (LCL), Ceratite Marls (CM), Ceratite Sandstone (CS), Upper Ceratite Limestone (UCL) including the Bivalve Beds (BB), *Niveaux Intermédiaires* (NI) and Topmost Limestone (TL). The lithologies of the Mianwali Formation consist of siltstones, sandstones, limestones and dolomites. LCL, UCL and TL include several packages of carbonate beds, whereas the CM, CS and the NI are dominated by silt- and sandstones. Several erosional horizons underlined by intraformational breccias and karst features can be observed in some restricted intervals of the sequence. The base of the Middle Triassic (Landa Member) has been included in this study. All formation names for the Early Triassic series are used in the sense of Kummel and Teichert (1966), with modifications of Guex (1978). The latter restricted the Narmia Member to the Topmost Limestone and excluded the Niveaux Intermédiaires and Bivalve Beds (Fig. 2). The "Chidru beds" of Waagen (1891) were formally named Chhidru Formation by Teichert (1966).

The PTB is officially defined by the FAD (First Appearance Datum) of the conodont *Hindeodus parvus* at the GSSP in Meishan, South China (Yin et al., 2001). Based on the lithological succession and the fossil content, the PJRG (1985) split the Kathwai Member in the Salt Range into three units considering the lowermost brachiopod bearing unit of the Kathwai Member as latest Permian in age. This part of the section is separated from the middle unit by a hiatus. *H. parvus* is reported to occur in the middle unit of the Kathwai Member at Nammal and Zaluch, thus placing the PTB between the lower and middle unit of the Kathwai Member (PJRG, 1985). We could locate a significant hiatus between the Chhidru Formation and the Kathwai Member, but none within the Kathwai Member. According to the evidence given by the PJRG, 1985 the PTB, in the sense of the GSSP definition, should be located within the middle unit of the Kathwai Member. Kummel and Teichert (1970) placed the PTB between the Chhidru Formation and the Kathwai Member. This formational boundary coincides with the main faunal turnover (Schindewolf, 1954). However, our palynological data from the Salt Range and Surghar Range indicate diachronism of the formational boundary between the two units (see below).

4.2. Sections and correlation

Three main sections have been studied, namely Nammal and Chhidru in the Salt Range, and Chitta–Landu and a smaller stratigraphic interval at Narmia in the Surghar Range (Fig. 1b). All lithological units (Fig. 2) can be traced laterally across the Salt Range and Surghar Range, with the exception of Chhidru where Triassic rocks younger than the BB have been eroded. Biostratigraphic and C-isotope data allow dating and precise correlation of the sections.

4.2.1. Nammal gorge

The studied section at Nammal ranges from the topmost part of the Chhidru Formation to the lithological change between the Topmost Limestone and the Landa Member. Total thickness of the studied section at Nammal is 120 m of which the Early Triassic encompasses 118 m. The POM record includes the interval from the Kathwai Member up to the base of the Landa Member. The Chhidru Formation is most probably of late Wuchiapingian age, thus suggesting that most of the Changhsingian stage is missing in the Salt Range although it cannot be excluded that the youngest Permian deposits might be represented by the lower unit of the Kathwai Member (PJRG, 1985). In the LCL of Nammal and Chitta–Landu *Gyronites frequens* has been reported by Guex (1978), indicating a Dienerian age. Younger Dienerian ammonoid assemblages with *Ambites* or *Prionolobus* occur within the CM where they are followed by Smithian ammonoid faunas (*Flemingites bhargavai* and *Kashmirites* sp., Fig. 3). A friable yellow weathering dolomitic limestone bed is associated with the change in ammonoid assemblage occurring below the *Kashmirites* bed. This bed is probably of similar age as the dolomitic limestone bed at the top of the LCL at Chitta–Landu and Narmia, which separates Dienerian and Smithian ammonoid faunas. Four metres below the top of the CS, *Flemingites flemingianus* indicates a Smithian age. The Smithian UCL can be subdivided by ammonoid faunas into the *Nammalites* beds, *Prionites* beds, *Wasatchites–Anasibirites* beds and *Glyptophiceras* beds (from base to top). The positive shift in the carbonate carbon isotope record at the Smithian–Spathian boundary, which has been reported

<table>
<tr><th>Age</th><th colspan="2">Formation</th><th>this study</th><th>Guex, 1978</th><th>Waagen, 1895</th></tr>
<tr><td>M.T.</td><td>Tredian Fm.</td><td>Landa Member</td><td>Landa Member</td><td></td><td></td></tr>
<tr><td rowspan="9">Early Triassic</td><td rowspan="8">Mianwali Fm.</td><td>Narmia Member</td><td>Topmost Limestone</td><td>Topmost Limestone</td><td>Topmost Limestone</td></tr>
<tr><td rowspan="6">Mittiwali Member</td><td>Niveaux Intermédiaires</td><td>Niveaux Intermédiaires</td><td>Dolomite Beds</td></tr>
<tr><td>Bivalve Beds</td><td rowspan="2">Upper Ceratite Limestone</td><td>Bivalve Beds</td></tr>
<tr><td>Upper Ceratite Limestone incl. BB</td><td>Upper Ceratite Limestone</td></tr>
<tr><td>Ceratite Sandstone</td><td>Ceratite Sandstone</td><td>Ceratite Sandstone</td></tr>
<tr><td>Ceratite Marls</td><td>Ceratite Marls</td><td>Ceratite Marls</td></tr>
<tr><td>Lower Ceratite Limestone</td><td>Lower Ceratite Limestone</td><td>Lower Ceratite Limestone</td></tr>
<tr><td>Kathwai Member</td><td>Kathwai</td><td>Kathwai</td><td rowspan="2">Upper Productus Limestone</td></tr>
<tr><td>P.</td><td>Chhidru Fm.</td><td></td><td></td><td></td></tr>
</table>

Fig. 2. Lithological units of the Mianwali Formation.

Please cite this article as: Hermann, E., et al., Organic matter and palaeoenvironmental signals during the Early Triassic biotic recovery: The Salt Range and Surghar Range records, Sediment. Geol. (2010), doi:10.1016/j.sedgeo.2010.11.003

from this area and other Tethyan sections (Baud et al., 1996; Galfetti et al., 2007b; Payne et al., 2004) could be confirmed and precisely positioned in the lowermost bed of the BB in all three main sections (Nammal, Chhidru, and Chitta–Landu, Figs. 3–6). The *Procolumbites* fauna near the top of the BB indicates an early middle Spathian age for the top of the UCL; therefore the Smithian/Spathian boundary lies in the topmost metres of the UCL. Comparison of the ammonoid faunas of Nammal and Chitta Landu above the positive carbon isotope shift indicates a sedimentary gap between the lowermost BB and the *Procolumbites* fauna at Nammal. The *Procolumbites* fauna in the BB at Nammal is younger than the *Tirolites* fauna from the base of the NI at Chitta–Landu. At Nammal, age control of the transition to the Landa Member is suggested by increasing $\delta^{13}C_{org}$ values.

In the Nammal section several reworking horizons and erosional surfaces with characteristic relief and tool marks have been observed. The bases of the CS and TL and the sandstone bed in the middle NI are marked by erosional surfaces (Fig. 3). Reworking horizons mark the base of the UCL and the top of the BB and the TL. Some of these horizons have also been recognised at Chhidru and Chitta–Landu. Erosional features at the base of the CS recognised at Nammal are clearly developed at Chhidru but have not been observed at Chitta–Landu. The erosional surface between the sandstone beds of the topmost NI and the first TL limestone bed at Nammal is also recognisable at Chitta–Landu within the uppermost few sandstone beds of the NI.

4.2.2. Chhidru gorge

At Chhidru the thickness from Kathwai Member to top of BB is about 90 m, thus slightly thicker than the corresponding interval at Nammal (72 m). Here, the Triassic units above the BB are not preserved. At Chhidru it was possible to take palynological samples from the Chhidru Formation up to the BB. Palynological assemblages from the Chhidru Formation indicate a Permian age for this interval. The presence of *Ophiceras* in the Kathwai Member indicates a basal late Griesbachian age; the early Griesbachian ammonoid zone (*Otoceras woodwardi*) has not been recognised. At Chhidru, the transition from LCL to CM is marked by two successive ammonoid-rich limestone beds bracketing the Dienerian–Smithian boundary. The lower limestone bed yields a Dienerian *Prionolobus* fauna and the upper bed a Smithian fauna including *Flemingites planatus* (Brühwiler et al., in press and Fig. 3). The Smithian ammonoid faunal succession with *Flemingites* beds, *Nammalites* beds, *Prionites* beds and *Glyptophiceras* beds in the CS and the UCL allows for precise biostratigraphic correlations with the Nammal section (Fig. 3).

4.2.3. Chitta and Landu gorges

The two sites are located close together on the southern slope of the Surghar Range. The lithological succession can be traced laterally bed by bed. Here we present a composite section of the two sites. The section ranges from the Chhidru Formation up into the Landa Member. Only minor faults and folds disrupt the section and a total thickness of 155.3 m has been logged, of which 130.3 m are Early Triassic in age. Sampling focused on the Spathian–Anisian interval. In contrast to Chhidru gorge, palynological assemblages from the uppermost part of the Chhidru Formation at Chitta–Landu have a Griesbachian affinity (high abundance of spores, esp. *Kraeuselisporites* spp.) thus indicating regional diachronism of the lithological boundary between the Chhidru Formation and the Kathwai Member. At Landu gorge ammonoids of the top limestone bed of the Kathwai Member indicate time-equivalence of these beds to the LCL at Nammal (Dienerian). In contrast to Nammal, the topmost thin-bedded limestone of the LCL at Chitta–Landu and Narmia contains *Kashmirites* sp. indicating a Smithian age hence indicating diachronism of the LCL–CM transition. Remarkable is a yellow weathering dolomitic limestone below the *Kashmirites* bed, which is also found at Nammal in the same stratigraphic position but within the CM.

The ammonoid fauna found below the BB (*Anasibirites* sp./*Wasatchites* sp. and *Glyptophiceras* sp.) allow for a correlation of the upper UCL with the UCL at Nammal. The *Procolumbites* fauna present in the upper BB at Nammal has not been found in the upper UCL at Chitta–Landu. The *Anasibirites*/*Wasatchites* fauna is followed by a *Tirolites* fauna in the lower part of the NI, which is older than the *Procolumbites* fauna of the BB at Nammal (Fig. 3). In the absence of an adequate ammonoid record in this part of the section, age control for the Early/Middle Triassic boundary is given by palynological assemblages and chemostratigraphy.

4.2.4. Narmia gorge

At Narmia sampling focused on the Permian–Triassic transition ranging from the upper Chhidru Formation to the basal part of the CM. Total thickness of the studied part of the Narmia section is 17.80 m, with 10.30 m of Early Triassic sediments. Similar to Chitta–Landu, palynological assemblages from the Chhidru Formation have a Griesbachian affinity. Ammonoids in the top limestone beds of the Kathwai Member indicate a Dienerian age. Similar to the Chitta–Landu section, the Dienerian–Smithian boundary falls within the topmost beds of the LCL in Narmia.

4.3. Lithological description

The following lithological description focuses on the Nammal section, complemented and compared to the Chhidru and Chitta–Landu sections.

4.3.1. Chhidru Formation

The uppermost part of the Late Permian Chhidru Formation consists of sandy limestone and white sandstone (White Sandstone Unit of Kummel and Teichert, 1970). The limestones are rich in fossils, especially brachiopods and gastropods. At Chhidru the White Sandstone Unit is replaced by a 3.5 m thick succession of alternating white to grey parallel laminated sandstone and dark grey siltstone. At Chitta–Landu, the transition to the Kathwai Member is marked by a 10 cm thick white medium-grained parallel laminated sandstone with two thin siltstone bands at its bottom and top. At Narmia, the topmost metres of the Chhidru Formation consist of an alternation of limestone and light coloured medium grained sandstone. Two horizons of dark coloured fine-grained sandstone could be sampled, one 80 cm below the Kathwai Member and the other between the Chhidru Formation and Kathwai Member. About seven metres below the Kathwai Member a poorly preserved organic rich siltstone lense is intercalated into the sandstone–limestone alternations (for OM description see Section 5.2.10).

4.3.2. Kathwai Member

At Nammal the 3.5 m thick Kathwai Member consists of sandy dolomites, limestones and calcareous sandstones. The lower part is dominated by brown to rusty weathering, middle to coarse grained and poorly bedded dolomite. Several coquinoid layers can be observed. In all sections the lower dolomitic part exceeds in thickness than the upper part. Towards the top of the Kathwai Member the thickness of beds decreases and the grey to greenish fine grained sandstones/limestones are better sorted. Glauconite can be observed macroscopically. Sandstone occurs in the Kathwai Member of the Salt Range but not in the Surghar Range sections. At Chhidru the 3.8 m thick Kathwai Member comprises intercalated siltstone lenses in the dolomitic beds. Alternating sandstones and sandy dolomites represent the upper part of the member. In the sections of the Surghar Range the thickness of the Kathwai Member is reduced to about 2 m. Here, the massive orange to purple weathering dolomite is directly overlain by limestone (20 cm at Chitta–Landu and 70 cm thin-bedded at Narmia).

Please cite this article as: Hermann, E., et al., Organic matter and palaeoenvironmental signals during the Early Triassic biotic recovery: The Salt Range and Surghar Range records, Sediment. Geol. (2010), doi:10.1016/j.sedgeo.2010.11.003

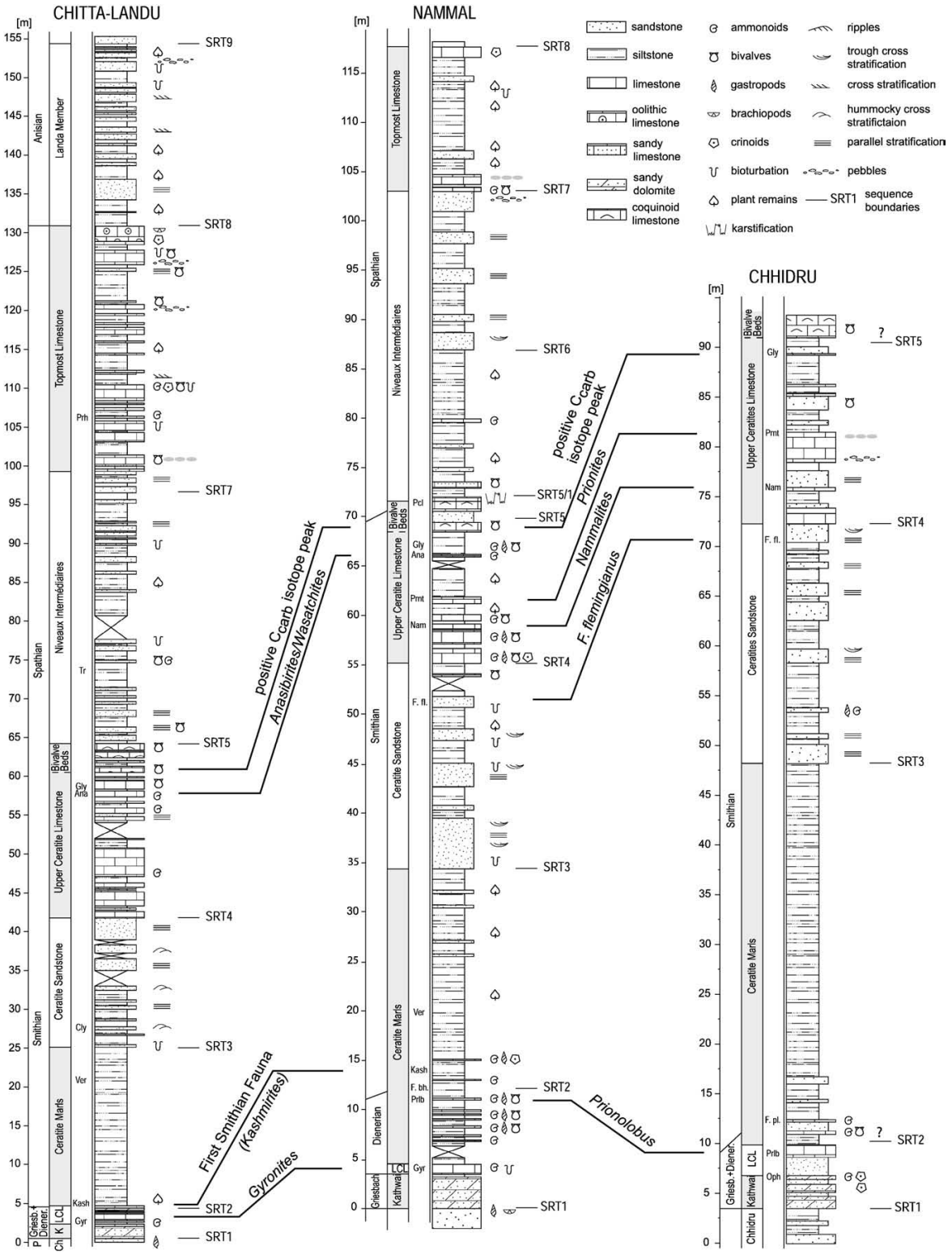

Fig. 3. Sedimentology and age of the sections and sequence stratigraphic interpretation. Prh = *Prohungarites* (occurrence after Guex, 1978); ammonoid faunas (Brühwiler et al., in press and ongoing work of Ware et al., Bucher et al.,): Tr = *Tirolites*; Pcl = *Procolumbites*; Gly = *Glyptophiceras*; Ana = *Anasibirites/Wasatchites*; Prnt = *Prionites*; Nam = *Nammalites*; F. pl. = *Flemingites planatus*; F. fl. = *Flemingites flemingianus*, Ver = *Vercherites*; Cly = *Clypeoceras*; Par = *Paranorites*; Kash = *Kashmirites*; F. bh. = *Flemingites bhargavai*; Prlb = *Prionolobus*; Gyr = *Gyronites* (occurrence after Guex, 1978); Oph = *Ophiceras*. Additionally the Smithian-Spathian positive peak of the carbonate carbon isotope record is marked.

Please cite this article as: Hermann, E., et al., Organic matter and palaeoenvironmental signals during the Early Triassic biotic recovery: The Salt Range and Surghar Range records, Sediment. Geol. (2010), doi:10.1016/j.sedgeo.2010.11.003

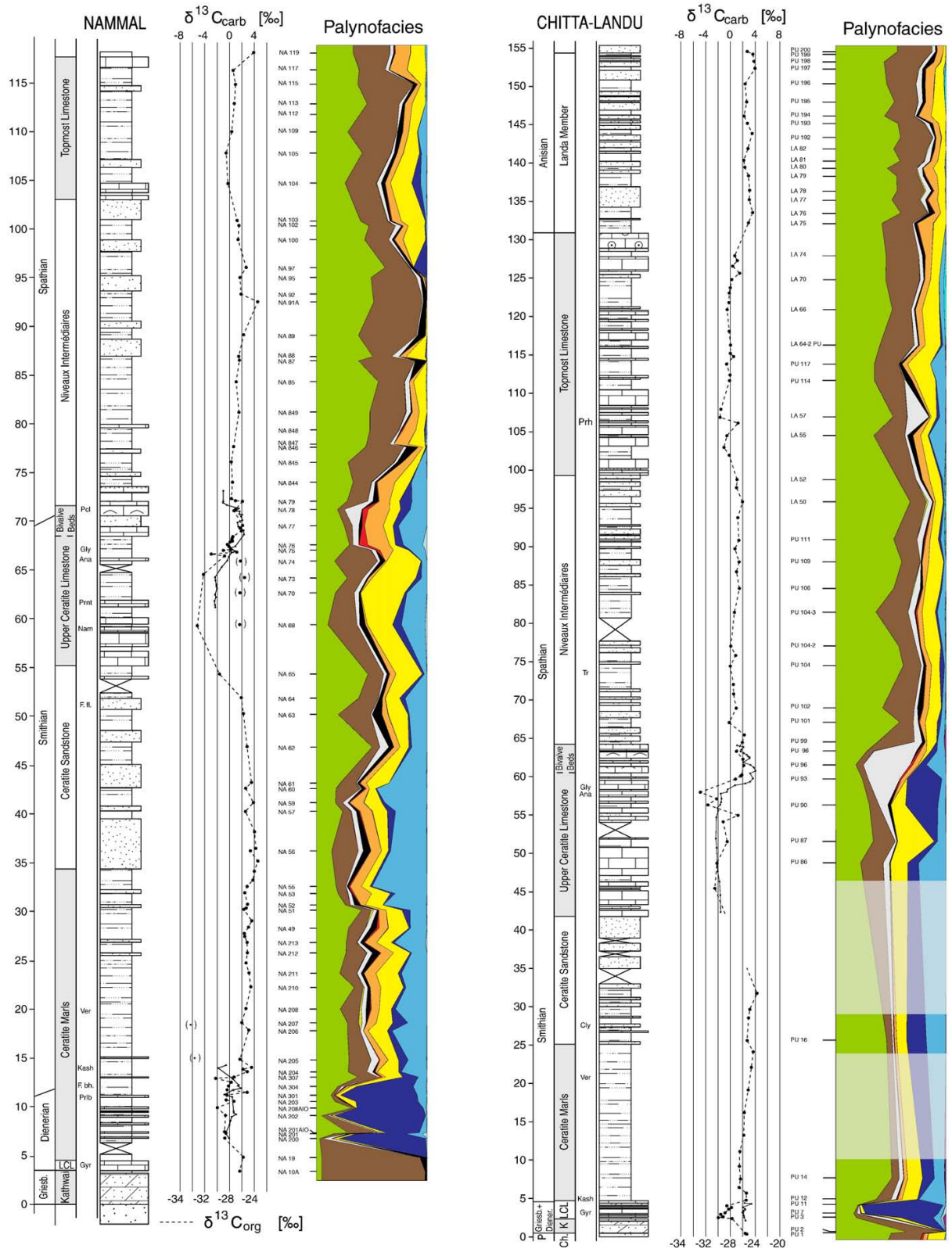

Fig. 4. Lithology, $\delta^{13}C_{org}$ and $\delta^{13}C_{carb}$ data and palynofacies record of the Nammal and Chitta–Landu section. Pattern/colour code: see Fig. 5. For lithological signature: see Fig. 3.

Please cite this article as: Hermann, E., et al., Organic matter and palaeoenvironmental signals during the Early Triassic biotic recovery: The Salt Range and Surghar Range records, Sediment. Geol. (2010), doi:10.1016/j.sedgeo.2010.11.003

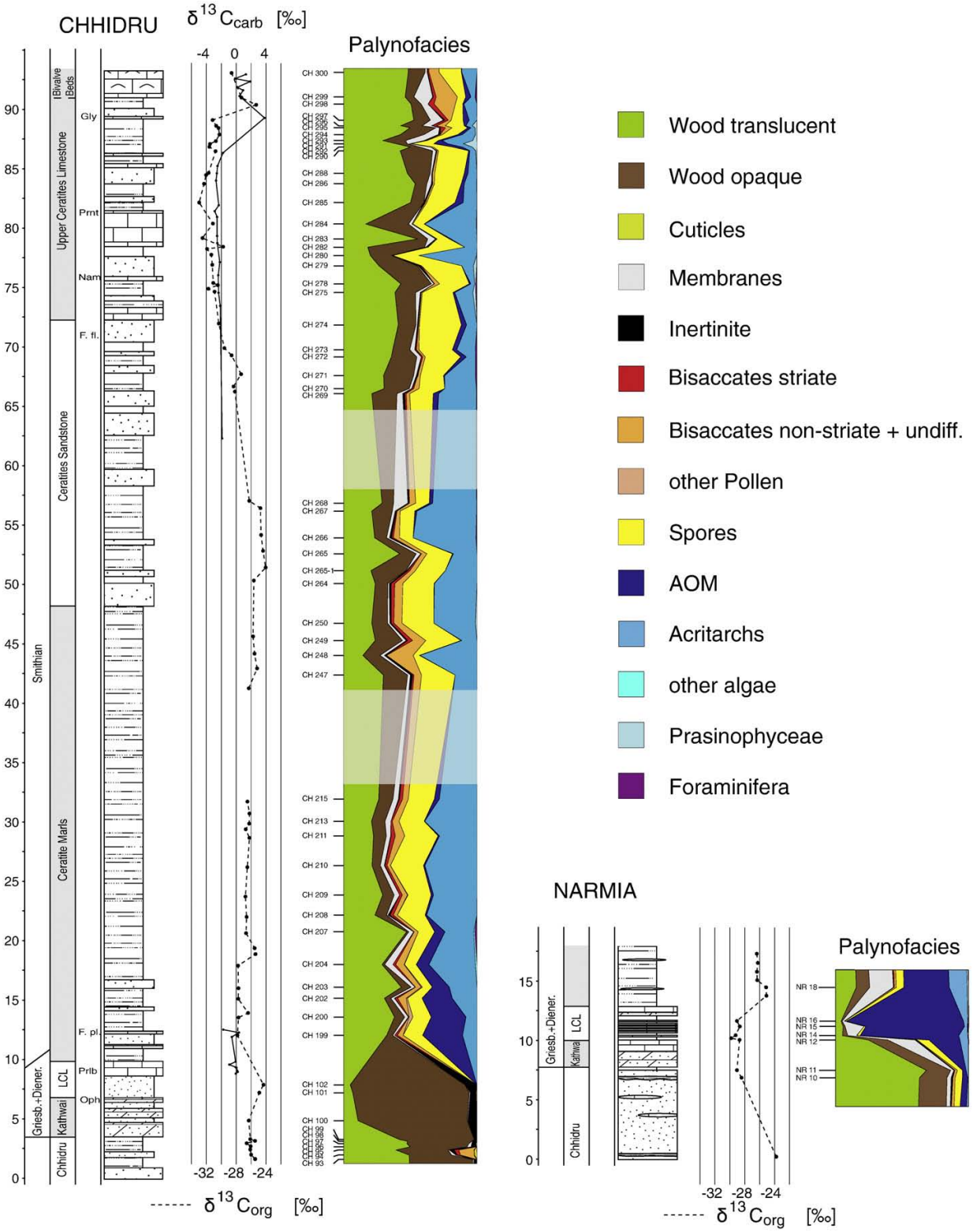

Fig. 5. Lithology, $\delta^{13}C_{org}$ and $\delta^{13}C_{carb}$ data and palynofacies record of the Chhidru and Narmia sections. For lithological signature: see Fig. 3.

Please cite this article as: Hermann, E., et al., Organic matter and palaeoenvironmental signals during the Early Triassic biotic recovery: The Salt Range and Surghar Range records, Sediment. Geol. (2010), doi:10.1016/j.sedgeo.2010.11.003

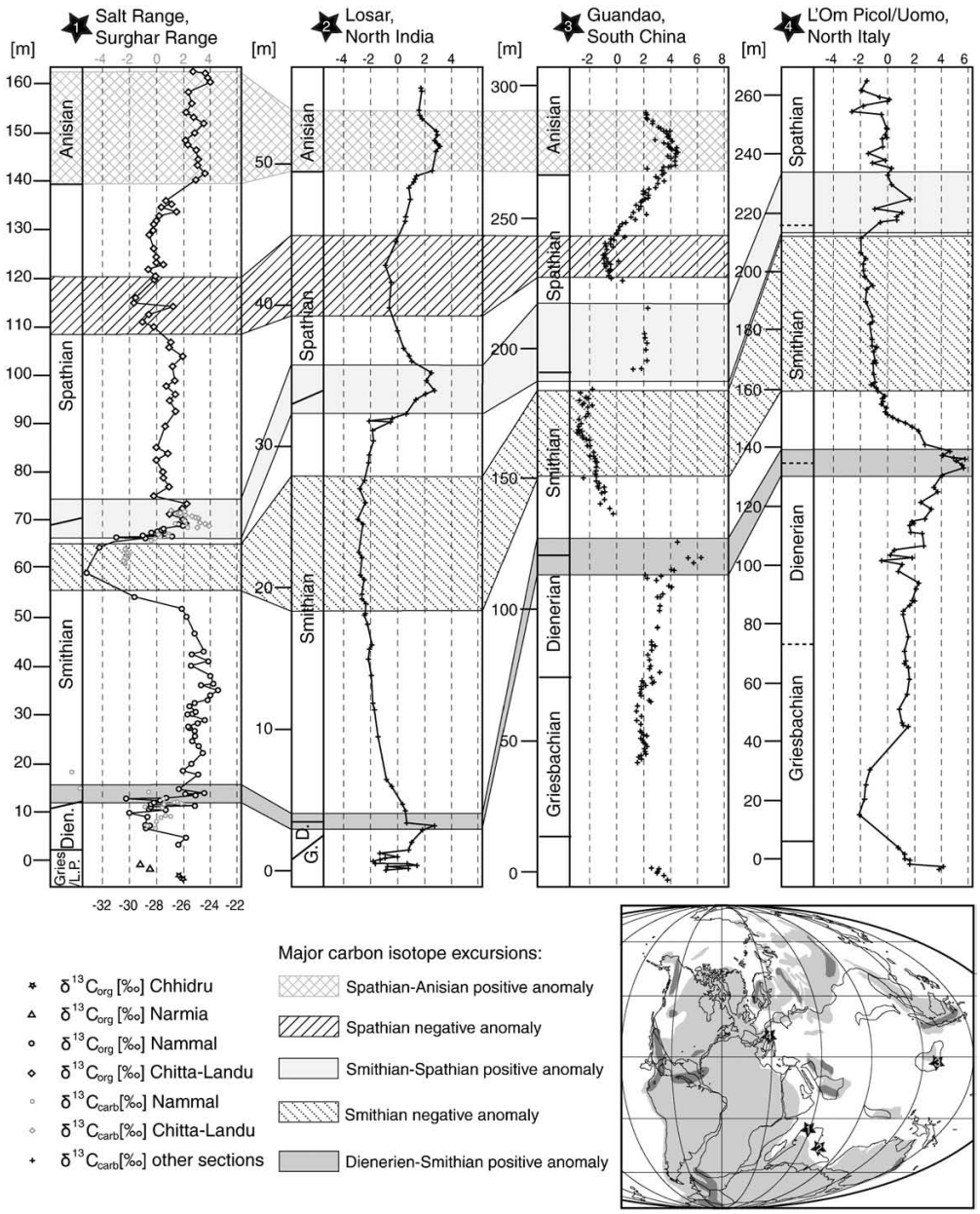

Fig. 6. Correlation of the major carbon isotope anomalies of the composite carbon isotope record from the Salt Range and Surghar Range sections with the carbon isotope records from Losar (North India, after Galfetti et al., 2007b), Guandao (South China, after Payne et al., 2004), and L'Om Picol/Uomo (North Italy, after Horacek et al., 2007), Palaeogeography modified after Smith et al. (1994) and Golonka and Ford (2000).

4.3.3. Lower Ceratite Limestone (LCL, Mittiwali Member)

At Nammal the LCL is 1.2 m thick and consists of greyish–greenish limestone with coquinoid lenses, and intervals with alternating sandstone and limestone beds. Stylolithes are present in the lower limestone beds. A 5 to 15 cm thick breccia layer is intercalated approximately 0.8 m above the base of the LCL. This grey to rusty coloured breccia consists of angular, poorly sorted limestone intraclasts of up to 10 cm in diameter and shell fragments. Coquinoid limestone beds of bivalve shell fragments, ammonoids and gastropods are found above the breccia. In these beds ammonoids are very unevenly distributed and show obvious signs of mechanical accumulations. In some cases the limestone is laminated. Small scaled burrowing is abundant on several bedding surfaces. At Chhidru, sandstone beds with intercalated limestone layers and lenses characterise the base and the top of the LCL, whose thickness locally amounts to 4.5 m. The middle limestone interval is about 1.2 m thick and contains common bivalve fragments and ammonoids. At Chitta–Landu and Narmia the LCL thickness ranges between 2.4 m and 3.1 m, respectively. It consists of thin limestone beds alternating with dark grey siltstone and lenses with high organic content. Rounded extraclasts and irregular distribution of the OM indicates reworking of these sediments (see Section 5.2.10). The top of the LCL is formed

Please cite this article as: Hermann, E., et al., Organic matter and palaeoenvironmental signals during the Early Triassic biotic recovery: The Salt Range and Surghar Range records, Sediment. Geol. (2010), doi:10.1016/j.sedgeo.2010.11.003

by two prominent marker beds; the lower one is a yellow weathering dolomitic limestone and the upper one consists of thin-bedded limestone, which can both be traced laterally throughout the entire Surghar Range.

4.3.4. Ceratite Marls (CM, Mittiwali Member)

At Nammal the thickness of the CM reaches 29.7 m. The term "marls" is somewhat misleading as the CM also contain a large proportion of thin bedded siltstone and fine grained siltstone. These commonly display either parallel lamination or cross bedding. Greenish to grey limestone lenses and lenticular limestone beds are intercalated in the lower third of the CM. Sandy layers can be observed at the upper and lower boundaries of most limestone beds. These sandstone layers are laminated or even cross bedded. The carbonate beds vary laterally in thickness. In the lower CM the lenticular limestone beds contain numerous, sometimes imbricated ammonoids. Bivalves are also common. Few coquinoid layers with distinct bases and fining upward grain size are observed. In some horizons small gastropods and fish scales are present. The middle part of the CM is dominated by siltstone; the upper part consists of siltstone with intercalated beds and lenses of micaceous sandstone; carbonate almost become absent as micaceous sandstone appear in the CM. The sandstones and siltstones are mostly of dark grey or green colour. Occasionally plant remains can be found in the siltstones. The much thicker CM at Chhidru (36.1 m) are dominated by grey siltstone with few limestone and sandstone lenses at its base. Additionally the overall grain size appears to be finer and the section comprises only few limestone and sandstone beds (Fig. 3). At Chitta–Landu the CM consist of a 20.4 m thick, dark grey siltstone with fine- to medium-grained mica-rich sandstone lenses. In contrast to Nammal there are no limestone beds in its lower part at Chitta–Landu. Compared to Nammal and Chhidru the thickness of the unit is considerably reduced. Macrofossils are rare except for a few horizons rich in ammonoids and small plant remains in the lower part. Similar lithologies are found at Narmia. There, intercalated mica-rich fine-grained sandstones display occasionally hummocky cross stratification.

4.3.5. Ceratite Sandstone (CS, Mittiwali Member)

At Nammal the contact between CM and CS is characterised by a sudden increase in thickness and frequency of sandstone beds. Total thickness of the CS at Nammal is 20.9 m. Medium grained sandstone alternates with fine grained sandstone and siltstone. Sandstone beds are massive, parallel laminated or show trough cross stratification; in a few beds of the upper part hummocky cross stratification is observed. The basal sandstone interval reaches 2.2 m in thickness; individual sandstone beds are up to 50 cm thick. Some beds including the basal one show erosional bases and are followed by fining upward cycles (1.5–2 m scale). Small sized bioturbation is present in several horizons. In the upper part of the CS few limestone beds/lenses are intercalated. Fossils are generally rare, ammonoids and fish teeth (*Colobodus*) were found in the upper part. Small plant remains can be commonly found in the siltstones. A bivalve rich layer occurs 1 m below the top of the CS. At Chhidru the CS is slightly thicker (23.6 m). The thickness of individual sandstone beds and overall sandstone content is lower than at Nammal. The sandstone beds are parallel laminated or show trough cross stratification. A few sandy limestone beds are rich in fish remains. 7 m above the base of the unit two successive sandy limestone beds contain abundant specimens of the bellerophonid gastropod *Warthia* (Kaim and Nützel, 2010, which were referred to as "Stachella" since Waagen, 1895).

The lower part of the 18.5 m thick CS at Chitta–Landu is characterised by an alternation of siltstone, thin sandstone, and limestone beds and limestone lenses. The sandstone beds are massive, parallel laminated or display hummocky cross stratifications; some are bioturbated. The sandstone fraction is increasing towards the top of the unit with alternating fine-grained and medium-grained sandstones. Hummocky cross stratification, trough cross stratification and parallel lamination characterise the sandstone beds. The thickness of individual sandstone beds increases upward. Compared to the Nammal section the total thickness of the CS and thickness of individual beds is lower at Chitta–Landu. Another distinct feature of the latter section is the occurrence of several limestone beds in the lower part of the CS and the abundance of sandstone in the upper part. This differs from Nammal, where the CS includes only very few limestone lenses and horizons of diagenetic limestone pods within the sandstones, with a sandstone–siltstone ratio decreasing upward.

4.3.6. Upper Ceratite Limestone (UCL, Mittiwali Member)

At Nammal the 16.4 m thick UCL shows a sharp contact with the underlying CS. At some but not all places, this boundary is and erosional surface marked by a bed containing rusty brown to purple coloured clasts (up to 10 cm in diameter), abundant small bivalve fragments, and small gastropods. The lower part of the UCL is dominated by limestone beds, which are interrupted by few sand- and siltstone beds. The limestone is light grey in colour showing in parts nodular structures. Several coquinoid bivalve layers are present with imbricated shells. The silt- and sandstone fraction is increasing in the middle part of the unit. The upper part of the UCL, termed Bivalve Beds, is again dominated by limestone alternating with sandstone. Here, the limestone is nodular except for the lowermost bed of the BB which is distinguished by its sharp and planar boundaries. Numerous coquinoid bivalve layers (bivalve packstone) are present; in some beds bioclasts show graded bedding. The BB can be recognised in all sections where the UCL has been studied. At the top of the BB an approximately 20 cm thick limestone bed contains pebbles and clasts in Nammal. In some outcrops of the Nammal gorge this bed shows a corroded surface with open dissolution cavities lined with iron oxides. Elongated but smooth clasts with the same coating of iron oxides occur in this bed. They represent the residues of this karstification episode. At Narmia the top of the BB is also affected by karstification. There, the decimetric karstic cavities are filled with sparry calcite (Supplementary Fig. 1). In the lower part of the UCL ammonoids are common; gastropods occur as accumulations in thin (few centimetres thick) layers. Crinoids and plant remains are rare, the latter increase towards the top. Compared to the Nammal section the UCL is thicker at Chhidru (20.6 m). Limestone, sandy limestone and sandstone are alternating with fine-grained parallel laminated sandstone and siltstone. The sandstone fraction is generally higher at Chhidru than at Nammal. The top of the lowermost bed of the BB is characterised by wave ripples at Chhidru. At Chitta–Landu the UCL is as thick as at Chhidru (20.6 m). Here, the UCL consists of thin-bedded limestone with some massive or parallel laminated sandstone beds. The intercalated siltstones contain limestone lenses, and, in a restricted interval just below the BB, siltstone lenses with high OM content. A thin section of this interval reveals that the OM is distributed heterogeneously and lamination is not orientated uniformly, which indicates reworking (see also Section 5.2.10). Within the BB bivalve shells are more fragmented at Chitta–Landu and of smaller size than at Nammal. Compared to the Salt Range sections, the Surghar Range sections show a higher proportion of limestone throughout the UCL, and the sandstone fraction is reduced. If the uppermost part of the BB is clearly karstified at Narmia, no such indication was found in Landu. This suggests a deeper bathymetry in Landu than in Narmia.

4.3.7. Niveaux Intermédiaires (NI, Mittiwali Member)

At Nammal the 31.4 m thick NI overlay the Fe-crusts of the topmost UCL beds. Their lower part consists of siltstone, sandy siltstone and sandstone beds (20–30 cm thick). At Nammal an approximately 2.5 m thick prominent sandstone bed with limestone pods containing ammonoids occurs in the middle of the NI, showing tool marks at their base. It is partly massive or shows trough cross

Please cite this article as: Hermann, E., et al., Organic matter and palaeoenvironmental signals during the Early Triassic biotic recovery: The Salt Range and Surghar Range records, Sediment. Geol. (2010), doi:10.1016/j.sedgeo.2010.11.003

stratification. This bed marks the transition to the upper part of the NI where the sandstone beds increase in number and thickness. The uppermost beds of the NI contain sandstone pebbles of few centimetres in diameter. Here, the grey, yellow, rusty and purple coloured beds show a variety of sedimentary features such as parallel lamination, channel fills, soft sediment deformation structures and hummocky cross stratification. The thickness of the beds varies laterally. The 35.1 m thick NI consists of an alternation of siltstone and sandstone beds; the latter showing parallel lamination, trough cross stratification and bioturbation. A few intercalated calcareous sandstone lenses and diagenetic pods in the lower part contain abundant bivalve coquina and ammonoids. A thick sandstone bed at the boundary with the TL displays a marked erosional base. In the intercalated siltstones of the upper NI in both sections, plant remains up to 3 cm in length have been observed.

4.3.8. Topmost Limestone (TL, Narmia Member)

At Nammal the contact between the 14.8 m thick TL and the underlying NI shows an erosional surface. The TL is dominated by an alternation of siltstone and sandstone with few limestone intervals. The fine to medium grained sandstone beds are massive or show occasional hummocky cross stratification. Some of the sandstone beds have an erosional base; large scaled bioturbation occurs frequently. Fining upward cycles can be observed on a 0.2–1.0 m scale. The base and the top of the TL are dominated by limestone. Several coquinoid layers (bivalve fragments) and bioturbated horizons have been observed. At Nammal a characteristic feature of the TL is a red coloured bed containing crinoid columnalia within the lower limestone interval. This 15 to 20 cm thick bed can be traced throughout the entire Nammal gorge area. The uppermost part of the TL consists again of a 1 m thick limestone/dolomite bed with a reworking horizon at its top, containing crinoid columnalia accumulated in relief lows. They are associated with common rounded limestone pebbles up to 2 cm in diameter. Ammonoids are found only in the lowest part of this unit together with bivalve remains and crinoid stems. Plant fragments are present in the siltstones. At Chitta–Landu, the TL is twice as thick (31.9 m) as at Nammal. The top and base of the unit are dominated by limestone, whereas the middle part of the TL is represented by a mixture of prominent limestone beds, siltstone and few sandstone beds. The lowermost limestone interval is thin- to medium bedded and in parts nodular. Bedding surfaces of the limestone are rich in glauconite. Crinoid columnalia, bivalves and bioturbation are concentrated in some horizons, ammonoids are rare. Siltstones are intercalated between the larger limestone intervals. Towards the top of the TL, the limestone beds show increased evidence for reworking with rounded limestone pebbles and shell fragments. Bedding surfaces often show bioturbation. The upper limestone interval consists of a pisolithic limestone with common occurrence of brachiopods.

4.3.9. Landa Member

The 23.5 m of the Landa Member, studied in Chitta and Landa, respectively, consists of sandstone and siltstone. The medium- to coarse-grained sandstone beds are mostly purple, sometimes orange in colour. They are parallel or cross laminated; in one case they display pillow-structures. Most sandstone beds are bioturbated. The thickness of the individual sandstone beds increases towards the top of the Landa Member. The dark grey mica-rich siltstones and fine-grained sandstones contain abundant and large plant remains (up to 3 cm). The unit is overlain by the white sandstone of the Khatkiara Member. The transition is marked by a distinct disconformity.

4.4. Interpretation

The most obvious difference between the studied sections is the variability of the thickness of the individual units. A difference is most distinctly expressed in the CM with a variation of 16 m between Chitta–Landu and Chhidru. The CS has similar thicknesses in all sections. Compared to Nammal, the UCL is slightly expanded at Chhidru and Chitta–Landu. The NI and the TL are thicker at Chitta–Landu. Therefore, accommodation rate obviously varied in space and time. The Chitta–Landu section is generally more expanded and probably represents a more distal setting. This is in agreement with the smaller size of the bivalve fragments in the BB and the absence of karstifications at the top of the same unit at this locality.

The disappearance of marine invertebrate fossils and the presence of large plant remains in the TL and the Landa Member indicate a general shallowing upward trend, reflecting several sequences with distinct boundary surfaces (SRT1–SRT9, Fig. 3). Not all mentioned erosional surfaces and reworking horizons necessarily correspond to higher-order sequence boundaries (SB). The distinct breaks in sedimentation associated with significant lithological changes are interpreted as SB, such as at the lithological change around the boundary between the Chhidru Formation and the Kathwai Member (SRT1), the sedimentary gap within the BB at Nammal and the lithological change between the BB and the NI at Chitta–Landu (SRT5), and the boundary between the TL and the Landu Member (SRT8). Other surfaces represent SB of undetermined order. All recognised sequences are listed and described in Table 1.

5. Carbon isotopes and organic matter

5.1. Carbonate and organic carbon isotopes

The detailed C-isotope data of the individual sections are displayed in Figs. 4 and 5 and in the Supplementary Table 1. Carbonate carbon isotopes ($\delta^{13}C_{carb}$) of Nammal and Landu have been reported by Atudorei (1999) and Baud et al. (1996). Our data confirm these earlier values and allow a detailed biostratigraphic positioning of the positive $\delta^{13}C_{carb}$ shift at the Smithian–Spathian boundary. The mixed siliciclastic–carbonate lithology of the Mianwali Formation allows only for a fragmentary $\delta^{13}C_{carb}$ record. The more complete organic carbon isotope ($\delta^{13}C_{org}$) record features the same chemostratigraphic signal (positive shifts at the Dienerian–Smithian, Smithian–Spathian and Spathian–Anisian boundary, negative shifts in the Smithian and Spathian) as many other C-isotope records (e. g. Galfetti et al., 2007a,b; Payne et al., 2004; Richoz, 2006).

5.2. Palynofacies

Palynofacies analysis has been performed on 184 samples and the results for Nammal, Chhidru and Chitta–Landu are shown in Figs. 4 and 5, and in more detail in Fig. 7 and Supplementary Figs. 2 and 3. The POM is well preserved and shows no indication of thermal alteration (alteration scale 2, Batten, 1996).

5.2.1. Chhidru Formation

Appropriate lithologies for palynological studies are rare in the upper Chhidru Formation. The oldest palynofacies (probably late Wuchiapingian age according to PJRG, 1985) of this study is reported from the Chhidru site (Supplementary Fig. 2). The POM assemblages are dominated by translucent and opaque phytoclasts; additionally bisaccate pollen grains (up to 11% at Chhidru) and spores (up to 15% at Chitta–Landu) occur in most samples. Marine influence is minor, only few acritarchs could be observed at Narmia and Chitta–Landu.

5.2.2. Kathwai Member

The palynofacies of the Kathwai member has also a terrestrial character. In contrast to the Chhidru Formation, the assemblages are clearly dominated by opaque phytoclasts (Fig. 7). Palynomorphs are absent from most samples. Only a few remains of bisaccate pollen have been observed in one sample from Chhidru. The assemblages at

Please cite this article as: Hermann, E., et al., Organic matter and palaeoenvironmental signals during the Early Triassic biotic recovery: The Salt Range and Surghar Range records, Sediment. Geol. (2010), doi:10.1016/j.sedgeo.2010.11.003

Table 1
Sequence stratigraphy of the studied sections.

Sequence (Fig. 2)	Lithological units	Sequence boundary (SB)	Dating of SB and sequence
SRT9	Khatkiara Member	Erosional surface and lithological change from dark grey siltstone–purple sandstone alternation to white coarse grained sandstone.	Top of the studied section — probably Anisian
SRT8	Landa Member	Lithological change from pisolithic limestone of the TL to dark grey siltstone–purple sandstone alternation of the Landa Member (Chitta–Landu), reworking horizon on top of the TL (Nammal).	Spathian–Anisian boundary — positive C-isotope shift and palynological data
SRT7	TL	Erosional relief between NI and TI, reworking at the base of the TL, change from sandstone to limestone sedimentation.	Spathian
SRT6	Upper part of the NI	Erosional surface at the base of the thick sandstone bed in the middle NI at Nammal.	Spathian
SRT5/1	Lower part of the NI	Reworking (bioclasts and pebbles) in the top of the BB, Fe-crusts and karst features.	Early middle Spathian
SRT5	BB (including lower part of NI at Chitta Landu)	Significant sedimentary gap at Nammal; change from bivalve packstone to siltstone–sandstone alternation at Chitta–Landu, reworking (bioclasts and pebbles) in the BB, Fe-crusts and karst features.	Smithian–Spathian boundary — positive C-isotope peak, change from Smithian to Spathian ammonoid faunas
SRT4	UCL including lowermost bed of the BB	Reworking horizon (reworked bioclasts) at the base of the UCL.	Smithian — ammonoid faunas
SRT3	CS	Erosional surface at the base of the CS, change form siltstone dominated to sandstone dominated sedimentation. Sandstone ratio increases up-section at Chhidru and Chitta–Landu, indicating a shallowing upward trend.	Smithian — ammonoid faunas
SRT2	• Chitta–Landu: complete CM • Chhidru: almost complete CM • Nammal: upper part of CM	Yellow weathering dolomitic limestone bed at Nammal, Chitta–Landu and Narmia.	Dienerian–Smithian boundary — positive C-isotope shift and change from Dienerian to Smithian ammonoid faunas
SRT1	• Chitta–Landu, Narmia: Uppermost part of the Chhidru Formation (White Sandstone Unit) and LCL excluding the topmost limestone bed. • Nammal, Chhidru: Kathwai Member and LCL • Nammal: Lower part of the CM.	• Nammal: erosional relief, change from coarse grained sandstone to dolomite. • Chhidru: sedimentary gap, change from siltstone–sandstone alternation to dolomite. • Chitta–Landu, Narmia: change from sandstone–limestone alternation to sandstone with siltstones.	Permian–Triassic boundary. Kathwai Member: Triassic ammonoids. Uppermost Chhidru Formation: Palynological assemblages with Permian and Griesbachian affinities, respectively.

Chhidru and Nammal are almost identical. No appropriate samples could be obtained at Chitta Landu and Narmia.

5.2.3. Lower Ceratite Limestone (LCL)

The POM composition described for the Kathwai Member of Nammal and Chhidru continues unchanged into the LCL of Nammal and Chhidru. In contrast to that the palynofacies of the LCL at Narmia and Chitta–Landu in the Surghar Range is characterised by high abundances of AOM. At Narmia AOM contributes up to 88% to the POM. In these two localities minor components are acritarchs, sporomorphs, and phytoclasts (Fig. 5 and Supplementary Fig. 3).

5.2.4. Ceratite Marls (CM)

At Nammal and Chhidru the lithological change from LCL to CM coincides with a distinct change in palynofacies (Supplementary Figs. 2, 3). The lower third of the CM at Nammal shows a clear predominance of AOM (up to 82%, mean value 54%), phytoclasts and palynomorphs occur regularly. The main interval of the CM at Nammal is characterised by minor traces of AOM. Here, the composition of the POM is strongly dominated by phytoclasts (mainly translucent woody particles), sporomorphs and acritarchs (mean 21%). In the topmost CM samples acritarch contents increase abruptly to about 50%. At Chhidru (Fig. 5, Supplementary Fig. 2) the predominance of AOM is not as pronounced as in Nammal. Peak values of AOM reach 30% at the very base of the CM and decrease rapidly. Acritarchs and translucent phytoclasts are prominent elements of the POM composition and sporomorphs occur in limited quantities in this lower part. With decreasing AOM content, acritarchs increase and remain at mean values of 29%. The spore content (up to 26%) increases up-section. The POM of the basal CM at Chitta–Landu is characterised by translucent woody particles. Acritarchs, spores and bisaccate pollen are common, whereas AOM represents only a minor component. Compared to the high AOM values in the LCL the sample from the lowest part of the CM at Narmia displays reduced AOM contents (34%) associated with increased acritarch percentages. Membranes of uncertain origin amount to 17% of the POM.

5.2.5. Ceratite Sandstone (CS)

At Nammal the basal interval of the CS is dominated by acritarchs (mean 35%) without changes to the topmost CM. Phytoclasts and sporomorphs are regularly recorded. Towards the top of the CS acritarch numbers decrease and phytoclasts are dominant. At Chhidru the POM assemblage of the CS are comparable to those of the underlying CM. Remarkable is an acritarch spike in the lower third of the unit with values up to 47%. Towards the top of the CS the spore content increases reaching values up to 30%. A single sample from the CS from Chitta–Landu shows a similar composition to those from the basal CM.

5.2.6. Upper Ceratite Limestone (UCL)

The dominance of phytoclasts continues into the UCL at Nammal. Spores reach their highest abundances in the lower half of the UCL (up to 40%). The upper half of the UCL displays slightly increased values of acritarchs, bisaccate pollen and minor amounts of AOM. At Chhidru the assemblage shows relatively high spore abundances at the base of the UCL decreasing slightly towards the top of the unit. Two acritarch spikes (up to 42%) have been recorded within the UCL. The POM in the lower part of the UCL at Chitta Landu consists of nearly equal parts of spores (up to 33%), opaque and translucent wood and acritarchs together with low percentages of AOM and membranes. The upper part of the UCL is characterised by increased numbers of AOM and a distinct membrane spike, which ranges up to the UCL–NI transition.

5.2.7. Niveaux Intermédiaires (NI)

The NI are characterised by almost exclusive terrestrial palynofacies assemblages with high abundances of translucent and opaque

Please cite this article as: Hermann, E., et al., Organic matter and palaeoenvironmental signals during the Early Triassic biotic recovery: The Salt Range and Surghar Range records, Sediment. Geol. (2010), doi:10.1016/j.sedgeo.2010.11.003

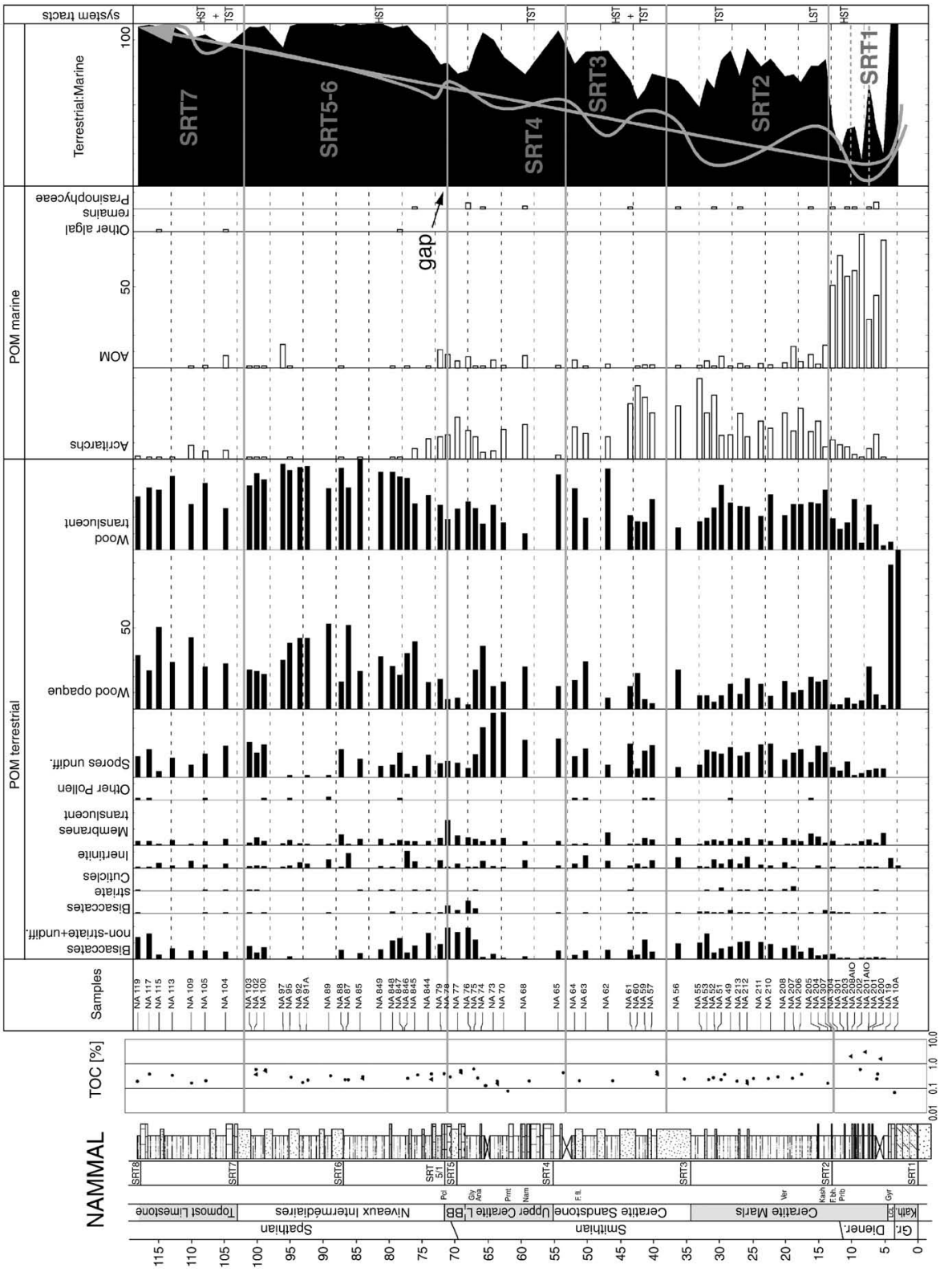

Fig. 7. Lithology, TOC and detailed palynofacies record of the Nammal section. Relative abundances of individual organic particle categories are displayed together with TOC values. The ratio of terrestrial (black) to marine (white) is given together with the sequence stratigraphic interpretation. Dashed grey lines in SRT1 indicate lower order sequences. LST = lowstand system tract, TST = trangressive system tract, HST = high stand system tract. For lithological signature: see Fig. 3.

Please cite this article as: Hermann, E., et al., Organic matter and palaeoenvironmental signals during the Early Triassic biotic recovery: The Salt Range and Surghar Range records, Sediment. Geol. (2010), doi:10.1016/j.sedgeo.2010.11.003

phytoclasts and sporomorphs. Due to coarser grained lithologies and therefore poor preservation some assemblages consist exclusively of plant debris. Low percentages of acritarchs and AOM are found in the basal and topmost part of the Nammal section and throughout the NI of the Chitta–Landu section (Supplementary Fig. 3).

5.2.8. Topmost Limestone (TL)

The palynofacies of the TL of Nammal and Chitta–Landu is dominated by woody particles. Sporomorphs are common and acritarchs occur in smaller numbers (8% at Nammal and 15% at Chitta–Landu).

5.2.9. Landa Member

The POM of the Landa Member at Chitta–Landu is dominated by translucent and opaque woody particles. Among the sporomorphs the non-striate bisaccates are well represented in all samples (Supplementary Fig. 3). In all samples spores are present with variable abundances. Large particles of cuticles with well preserved stomata are a distinct feature of the POM samples of the upper part of the Landa member. Acritarchs are only few but do persist throughout the member. A single sample from the basal part of the Landa Member at Nammal shows a similar POM composition as described above.

5.2.10. Organic rich rocks

A 30 cm thick, continuous, organic rich siltstone horizon within the late Smithian has been traced laterally from Landu to Narmia. It is bracketed by the *Wasatchites* fauna below and the *Glyptophiceras* fauna above. It was previously recognised by the PJRG (1985) only in Narmia area and was then referred to as “coaly shale”. Thinner and laterally more limited similar organic rich siltstone horizons also occur in the LCL of Narmia and Landu area. These horizons may locally contain angular to subangular extraclasts several millimetres in size. Two samples from Narmia and three samples from Chitta–Landu have been prepared in order to determine the POM. The POM is characterised by strongly degraded amorphous organic matter. The dark brown colour of the POM corresponds to a medium stage of maturation (oil window level). Phytoclasts and palynomorphs are very rare and badly preserved. Hence, it is difficult to determine the age of the OM. The difference in thermal alteration and preservation of this OM contrasts with that from enclosing rocks. All of the available evidence suggests that this OM is laterally transported and even possibly reworked. Therefore, these samples were excluded from the palynofacies data in Figs. 4–6 and Supplementary Figs. 2 and 3.

5.3. Interpretation of palynofacies results

Sedimentary sequences are reflected in changing dominance of the two main POM groups (marine/terrestrial ratio, Fig. 7, Supplementary Figs. 2 and 3) and the characteristic succession of POM assemblages within the sequences. Lowstand deposits are characterised by predominance of terrestrial POM. Increasing marine POM indicates transgressive deposits and early highstand deposits. Highstand deposits show decreasing marine influence up-section and corresponding increase of terrestrial POM. Palynofacies together with sedimentological observations can be used to describe the succession of sequences in a sedimentary sequence. However, the amount and composition of the terrestrial POM fraction depend not only on sea-level but also on hydrological features of the catchment area. For the studied sections measurements of palaeocurrent directions (ranging between NNE and NW at Nammal, Narmia, and Chhidru) indicate relatively stable directions of sediment supply (PJRG, 1985). In our material several minima and maxima of the marine/terrestrial ratio coincide with, or occur close to lithological changes.

In the studied sections the composition of the POM indicates a general shallowing upward trend (Fig. 7, Supplementary Figs. 2 and 3), which is modulated by smaller transgressive–regressive cycles (Fig. 7, Supplementary Figs. 2 and 3).

The distribution of the POM indicates lowstand deposits of the lowermost sequence SRT1 in the Kathwai Member and the LCL of Nammal and Chhidru, which are characterised by phytoclast dominance. A rapid transgression is expressed by high abundances of AOM in the LCL of Chitta–Landu and Narmia and the lowermost CM at Nammal and Chhidru. In the studied sections the abundance of AOM indicates not only the strongest marine signal but also dysoxic conditions. The proportion of AOM in shallow shelf settings is generally low but increases towards offshore basinal settings (Leckie et al., 1990; Steffen and Gorin, 1993; Tyson 1993, 1995; Wood and Gorin, 1998). During transgressions, shelf areas may fall below the storm wave base, and thus reducing water mass mixing. This may allow the establishment of water mass stratification and increase the preservation for AOM (Tyson, 1995). The top of SRT1 is indicated by the decrease of the AOM content at Nammal and Chitta–Landu coinciding with a yellowish dolomitic limestone bed near the Dienerian–Smithian boundary. At Nammal the high sampling resolution allows for discrimination of lower order sequences within SRT1. The corresponding sequence boundaries are reflected in the higher terrestrial to marine ratios of the sampled limestone beds (NA 201AIO and NA208AIO); they are marked with dashed grey lines in Fig. 7. At Chhidru the top of SRT1 is not clearly expressed (Fig. 5). Here AOM is gradually replaced by acritarchs and therefore the marine POM signal remains constant throughout the CM. Dysoxic conditions can be inferred for the late Dienerian of Nammal, the Dienerian of Narmia and Chitta–Landu and to a lesser degree in the lowermost Smithian of Chhidru. AOM is rapidly degraded under oxic condition (Jannasch, 1991; Pilskaln, 1991) but is well preserved under dysoxic to anoxic conditions in modern marine settings and ancient anoxic basins (Tissot and Pelet, 1981; Tyson, 1993, 1995). Since the establishment of dysoxic to anoxic conditions depends on various factors, such as climate and oceanographic constraints, we also consider sedimentological features to support our palynofacies interpretation. One of the possible processes that could lead to enhanced deposition of AOM during stable sea-level could be the upward migration of the oxygen minimum zone, thus providing the low oxygen environment for the preservation of AOM. Considering the sedimentary record of the aforementioned intervals (Sections 4.3) the increase in AOM abundance is accompanied by the disappearance of glauconite, as observed in the Kathwai Member, by a change to fine-grained lithologies as in the LCL (Chitta–Landu and Narmia) and lower CM (Chhidru and Nammal), and the absence of sedimentary structures indicating shallow water settings, such as hummocky cross stratification as documented in the CS. Therefore, in these cases the high AOM abundances can be directly related to deepening of the depositional environment.

At Nammal and Chhidru, the subsequent SRT2 is characterised by reduced marine influence in the middle part of the CM (lowstand) followed by acritarch dominated transgressive and highstand deposits in the uppermost CM. Hence, AOM occurs only in minor percentages or is absent in the POM up-section. Together with rich marine faunas, the absence of AOM indicates well oxygenated conditions from the middle CM onward. As indicated by sedimentological data, the base of the CS marks the SRT3 SB. The palynofacies data show increased terrestrial influence in this interval (Fig. 7, Supplementary Fig. 2). At Nammal and Chhidru, the POM lowstand signal of SRT4 can be observed in the lowermost UCL corresponding to the sedimentologically defined sequence in the UCL. Transgressive and highstand deposits are indicated by increased acritarch abundances in the UCL at Nammal, Chhidru and Chitta–Landu (Fig. 7, Supplementary Figs. 2 and 3). Because of the sedimentary gaps within the BB the SRT5 SB is weakly expressed in the palynofacies record since lowstand and transgressive deposits are missing; the signal of SRT 4 highstand is immediately followed by the SRT 5 highstand. Because of the terrestrial POM predominance in the NI SRT5, SRT5/1, and SRT6 are undistinguishable based on palynofacies data. Transgressive and highstand deposits of SRT6 are expressed in the

Please cite this article as: Hermann, E., et al., Organic matter and palaeoenvironmental signals during the Early Triassic biotic recovery: The Salt Range and Surghar Range records, Sediment. Geol. (2010), doi:10.1016/j.sedgeo.2010.11.003

TL at Nammal and Chitta–Landu by increased numbers of acritarchs. Compared to Nammal the NI at Chitta–Landu displays a higher acritarch content, which confirms a more distal position of the latter section. The SRT8 SB is close to the lithological change between the TL and the Landa Member coinciding with the SB defined by lithology.

5.4. Total organic carbon (TOC) content and Rock Eval analysis

The TOC values at Nammal are generally low, ranging between 0.07% and 0.61%, with a mean value of 0.28% (Fig. 7). TOC normally correlates well with the relative abundance of AOM in the sediment (Tyson, 1995), meaning that high TOC values usually indicate the presence of well preserved AOM. Therefore, the very low TOC values of the AOM-rich intervals (Dienerian) of the section are unexpected. Three samples from the AOM-rich interval have also been analysed using Rock Eval pyrolysis (Table 2). These TOC values of the AOM-rich interval range between 1.63% and 3.08%, which is in agreement with the higher AOM abundances (Table 2, Fig. 7). The TOC values of Smithian and Spathian samples could be confirmed by Rock Eval analysis (Table 2, Fig. 7).

The high Hydrogen Index (HI) and low Oxygen Index (OI) values of samples NA 200, NA 202 and NA 301 (upper Dienerian) indicate a marine origin of the OM. Low HI and high OI values of samples NA 57, NA 77 (Smithian), NA 100 and NA 102 (Spathian) indicate kerogen type IV (terrestrial and/or oxidised). T_{max} as an indicator for the maturity of the samples could only be determined in samples with high enough TOC. T_{max} ranging between 429 °C and 441 °C (averaging 435 °C) indicates a thermal maturity on the upper limit of the oil window (T_{max} of top oil window 435–445 °C after Peters, 1986). As T_{max} is influenced not only by thermal maturity but also by the composition of the OM and the mineral matrix of the samples, interpretations of T_{max} should be supported by other data, such as the application of optical thermal alteration scales. OM of kerogen type IV (NA 57, NA 77, NA 100, and NA 102) for example usually shows higher T_{max} values and T_{max}, which are combined with very low S2 peaks (<0.2 mg hydrocarbon/gram rock) are not reliable (Peters, 1986). Optical considerations confirm an immature state of the OM (2 on the thermal alteration scale after Batten, 1996).

5.5. Lipid biomarkers

Three samples from the Nammal section were analysed for molecular biomarkers: a relatively high TOC sample from the late Dienerian (NA 202, CM, TOC 3.08%), and two samples from the early Smithian (NA 55, CM) and the lower part of the Spathian (NA 88, NI, both with TOC around 0.2%). The distribution of the apolar hydrocarbons of the three samples is shown on Fig. 8. They are mainly constituted by n-alkanes, some isoprenoids, steranes and hopanes. The major molecular features are summarised in Table 3.

In NA 202, the apolar hydrocarbon fraction is dominated by pristane i-C_{19} (Pr) and phytane i-C_{20} (Ph) with Pr>Ph (Table 3). Regular isoprenoids were also identified from i-C_{17} to i-C_{23}. The n-alkane distribution ranges from n-C_{13} to n-C_{36}. There is a slight dominance of short-chain n-alkanes and an odd-over-even predominance is detected within the long-chain n-alkanes (>n-C_{24}) as indicated by the carbon preference index (CPI) (Table 3).

On the fragmentogram m/z 191, tricyclic terpanes and tetracyclic terpanes were detected in low abundance and hopanes (pentacyclic terpanes) from C_{27} to C_{35} in high abundance. The hopane distribution is dominated by the C_{30} homologue and shows a progressive decrease with increasing lateral chain-length up to the hopanes in C_{35}. The mature configuration (17α, 21β-hopane (αβ)) is predominant for all homologues. However, the immature stereochemistry (βα) is still present. Isomerisation at position 22 in the C_{32} αβ-hopanes reaches 0.46 (S/(R+S) ratio, Table 3). Ts (C_{27} 18α-neohopane) is present in relative low abundance compared to its immature precursor Tm (C_{27} 17α-hopane). The sterane distribution shows the presence of the C_{27}, C_{28} and C_{29} homologues, dominated by the immature stereochemistry 5α, 14α, 17α, 20R-sterane (ααα R), and of the corresponding diasteranes. Remarkably, the relative abundance of hopanes is much higher (about five times) compared to steranes.

In samples NA 55 and NA 88 the distribution of apolar hydrocarbons is very similar. n-alkane distributions range from n-C_{15} to n-C_{36}, dominated by short-chain n-alkanes, in particular the n-alkane in C_{20}. There is a slight odd-over-even predominance within the long-chain n-alkanes as shown by the CPI (Table 3). Some isoprenoids were detected in low abundance, with Ph>Pr (Table 3). An unresolved complex mixture (UCM) observed in the mass range from 254 (n-C_{18}) to 324 (n-C_{23}) suggests the presence of numerous isomers of short-chain branched alkanes.

In samples NA 55 and NA 88 the relative abundance of hopanes is extremely high compared to steranes (up to 15 times). The hopane distributions are dominated by the C_{29} homologue and show a progressive decrease with increasing lateral chain-length up to the hopanes in C_{33}. αβ and βα hopane configurations are observed in equal abundance. The mature configuration of the C_{27} hopane, i.e. Ts, is not detectable. However, the C_{32} 22S/(22S+22R)-hopanes ratio is about 0.55 (Table 3). No tricyclic and tetracyclic terpanes were found. The sterane distributions mainly consist of the ααα R-C_{27} to C_{29} homologues and diasteranes were not detected.

5.6. Interpretation of biomarkers

During OM diagenesis the original biological configuration of some biomarkers evolves to thermally stable stereochemistries. Thus ratios of isomers give an insight into the level of maturity reached in the studied samples. The maturity of the OM is most reliably reflected in the ratio S/(S+R) for C_{32}β-hopanes since isomerisation at the C_{22}-R position occurs very early during OM diagenesis, leading to a mixture of R and S stereomers (up to 0.62 for highly mature OM, Peters et al., 2005). The ratios calculated for our samples (Table 3) indicate that they have been exposed to a light thermal stress, with the slightest

Table 2
Rock Eval analysis of 12 samples from Nammal.

Lithological unit	Sample	TOC [%]	HI [mg HC/g TOC]	OI [mg CO_2/g TOC]	Tmax [°C]	S1 [mg HC/g]	S2a [mg HC/g]	S2b [mg HC/g]	S3
Niveaux Intermédiaires	NA102	0.37	3	105	437	0.00	0.01	0.00	0.39
Upper Ceratite Limestone	NA100	0.53	11	83	439	0.00	0.06	0.00	0.45
	NA85	0.25	0	161	−22	0.00	0.00	0.00	0.40
	NA844	0.23	0	167	−20	0.00	0.00	0.00	0.38
	NA77	0.45	62	92	438	0.00	0.28	0.00	0.41
	NA73	0.15	0	208	−22	0.00	0.00	0.00	0.30
Ceratite Sandstone	NA57	0.37	39	112	437	0.00	0.14	0.00	0.42
Ceratite Marls	NA55	0.10	0	231	−23	0.00	0.00	0.00	0.23
	NA213	0.16	0	196	−21	0.32	0.00	0.00	0.32
	NA301	2.07	263	25	429	0.02	5.44	0.00	0.52
	NA202	3.08	443	14	430	0.18	13.61	0.00	0.42
	NA200	1.63	213	59	441	0.04	3.47	0.00	0.97

Please cite this article as: Hermann, E., et al., Organic matter and palaeoenvironmental signals during the Early Triassic biotic recovery: The Salt Range and Surghar Range records, Sediment. Geol. (2010), doi:10.1016/j.sedgeo.2010.11.003

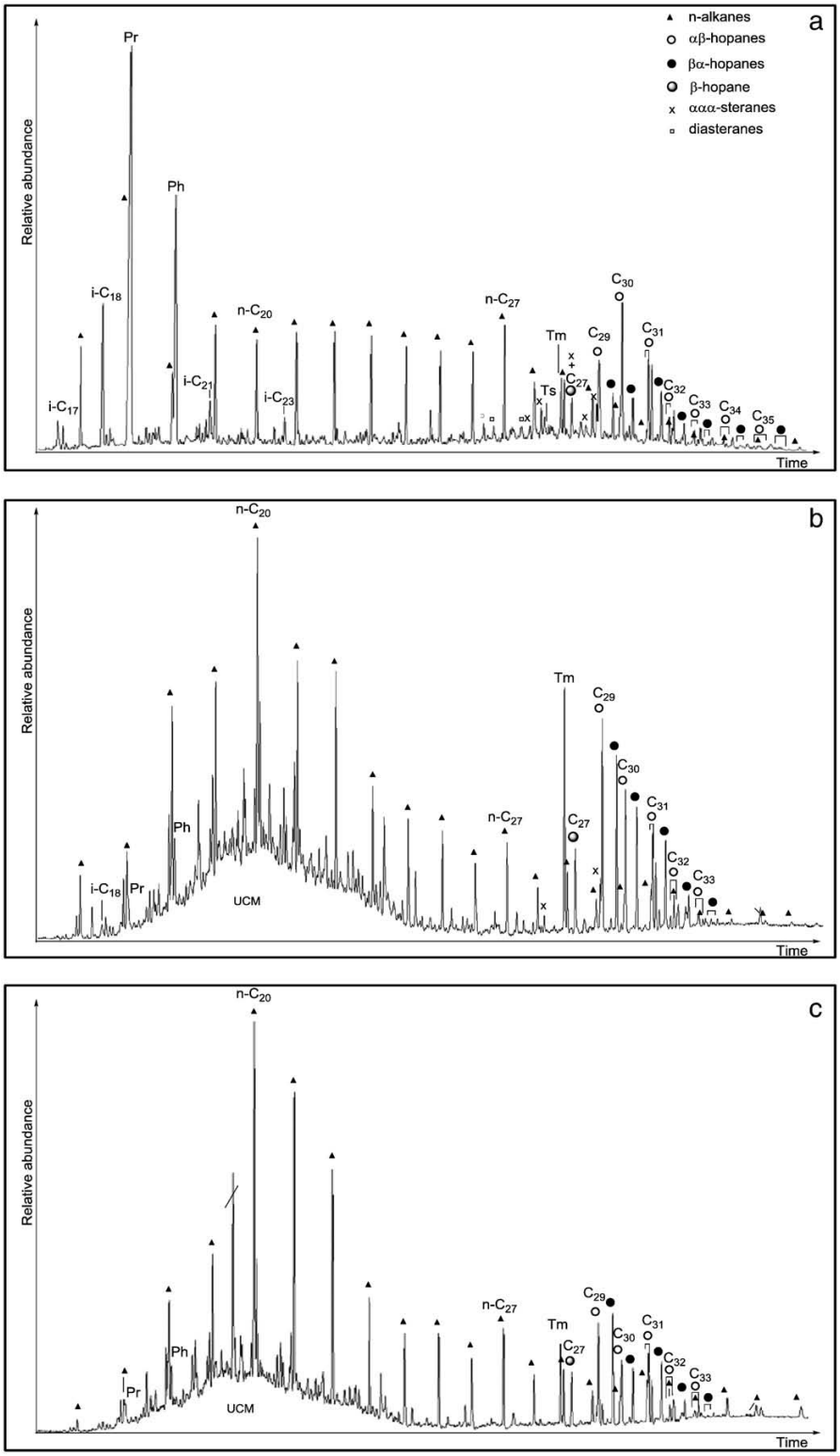

Fig. 8. Total ion currents of the apolar hydrocarbon fraction of the samples NA 202 (a), NA 55 (b) and NA 88 (c) from the Nammal sections. UCM = unresolved complex mixture. For each hopane homologue, the αβ stereochemistry is followed by the βα stereochemistry.

Please cite this article as: Hermann, E., et al., Organic matter and palaeoenvironmental signals during the Early Triassic biotic recovery: The Salt Range and Surghar Range records, Sediment. Geol. (2010), doi:10.1016/j.sedgeo.2010.11.003

Table 3
Molecular parameters of samples NA 202, NA 55 and NA 88 from Nammal.

Samples	CPI[a]	Pr/Ph[b]	Ts/(Tm + Ts)[c]	C_{29}/C_{30} αβ-hopane[c]	C_{30} βα/(βα + αβ)-hopanes[c]	C_{32} αβ 22S/(22R + 22S)-hopanes[c]	C_{27}/C_{29} αααR-sterane[d]	C_{28}/C_{29} αααR-sterane[d]
NA 202	1.29	2.7	0.17	0.60	0.25	0.46	0.91	0.79
NA 55	1.31	0.6	n.a.	1.27	0.48	0.56	0.77	0.65
NA 88	1.35	0.6	n.a.	1.18	0.47	0.55	1.19	0.71

n.a., not applicable.
[a] CPI = Carbon preference index Bray and Evans, 1961 defined as:

$$\mathrm{CPI} = \frac{1}{2} \times \left(\frac{nC_{25} + nC_{27} + nC_{29} + nC_{31} + nC_{33}}{nC_{24} + nC_{26} + nC_{28} + nC_{30} + nC_{32}} + \frac{nC_{25} + nC_{27} + nC_{29} + nC_{31} + nC_{33}}{nC_{26} + nC_{28} + nC_{30} + nC_{32} + nC_{34}} \right).$$

The index was calculated based on the area of the peaks of the n-alkanes measured on the ion current m/z 57.
[b] The ratio was calculated based on the corresponding peak areas measured on the ion currents m/z 268 and 282.
[c] The ratios of hopanes were calculated based on the corresponding peak areas measured on the ion current m/z 191.
[d] The ratios of steranes were calculated based on the corresponding peak areas measured on the ion current m/z 217.

thermal alteration observed in sample NA 202. However, other parameters commonly used to assess OM thermal maturity seem to conflict with a lowest level of maturity for NA 202. In NA 55 and NA 88, the αβ and βα configurations of hopanes occur in equal proportion for all homologues, indicating a relative immaturity of the OM (Seifert and Moldowan, 1980). In addition, the absence of Ts, the mature configuration of the C_{27} hopane, suggests a low level of maturity for these two samples. Accordingly sterane distributions, in NA 55 and NA 88, are dominated by the immature stereochemistry (αααR). In NA 202 the presence of Ts and the predominant mature configuration (αβ) of hopanes point to a higher maturity. At low maturity levels, βα/(βα + αβ)-hopanes and Ts/(Ts + Tm) ratios are known to poorly correlate with thermal stress (Grantham, 1986; Pan et al., 2008). The observed anomaly in hopane-based maturity parameters, as also observed by Wang (2007), has been attributed to a terrestrial input. However, Cao et al. (2009), reporting a similar feature in the hopane distribution, ascribed it to a significant variability in the pathways of OM diagenesis. Additionally, one might envisage that a mature OM migrated from an allochthonous source overprinting the autochthonous OM in sample NA 202. Diasteranes are believed to be formed by acidic catalysed rearrangement of steranes usually provided by clay minerals (Rubinstein et al., 1975), which is compatible with the siltstone to mudstone lithology of the late Dienerian at Nammal (sample NA 202). The presence of diasteranes only in NA 202 supports the fact that βα/(βα + αβ)-hopanes and Ts/(Ts + Tm) ratios might have also been differently affected by the lithology of the rocks in NA 202 and in NA 88 and NA 55. The overall biomarker distribution indicates immaturity to low maturity for the three samples.

In the studied samples a terrestrial contribution to the OM is shown by the odd-over-even predominance in the long-chain n-alkanes (CPI > 1) derived from higher plants (Eglinton and Hamilton, 1967). The steroid distribution also suggests a terrestrial input. Steranes result from the diagenetic reduction of sterols, widespread lipids biosynthesised by photosynthetic eukaryotes (Volkman, 1986, 2005). A strong contribution of higher plants can lead to a relatively elevated C_{29} sterane abundance (Peters et al., 2005). Hence, the low ratio C_{27}/C_{29} sterane in the studied samples suggests a strong terrestrial contribution.

In NA 202 the high abundance of Pr and Ph often considered as derived from the side chain of the chlorophyll of phototrophic organisms contrasts with the low abundance of steranes and could indicate another origin for Pr and Ph. This is also suggested by the absence of a significant amount of porphyrin in the organic extracts and the presence of isoprenoids >i-C_{20} (Ph). Other precursors such as archaea (Chappe et al., 1982; Rowland, 1990) or tocopherols (Goossens et al., 1984) are also known to produce isoprenoid hydrocarbons in the sedimentary record. The low amount of isoprenoids in NA 55 and NA 88 suggests that one or more of their precursors might have disappeared from the basin after the Dienerian. Given the decrease of the marine fraction in the POM assemblages after the Dienerian, the isoprenoid hydrocarbons in NA 202 are most likely of marine origin.

The relative amount of hopanes compared to steranes is a generalised proxy for the relative contribution of bacterial versus eukaryotic biomass. Compared to NA 202 this ratio is about five times higher in NA 55 and about 15 times higher in NA 88. High bacterial input has also been recorded in sediment preceding the end-Permian mass extinction event (Cao et al., 2009). Bacteria are ubiquitous in marine and terrestrial environments. However, a high hopane/sterane ratio is more indicative of a terrigenous or microbially reworked OM. In addition, some specific characteristics in the hopane distribution are usually associated with a land plant dominated sedimentary environment such as low tricyclic terpanes compared to hopanes, a high C_{31}/C_{32}-hopane ratio, and as in NA 55 and NA 88, a high C_{29}/C_{30}-hopane and Tm/C_{30}-hopane ratios (Fig. 8 and Table 3). However, these ratios might have also been affected by the lithology (Peters et al., 2005). Even if the bacterial input is confirmed by the biomarker record its origin (marine or terrestrial) cannot be confidently determined.

At low level of OM maturity, the predominance of short chain n-alkanes, slight in NA 202 and stronger in NA 55 and NA 88, suggests a substantial contribution of marine OM. However, according to the palynofacies study, the marine contribution is expected to be higher in NA 202. Short-chain n-alkanes are most commonly interpreted as being synthesised by marine algae, but bacterial precursors are also known (Collister et al., 1994). Given the high hopane/sterane ratio in NA 55 and NA 88, bacteria, whether terrestrial or marine, might be the main precursors of the short-chain n-alkanes.

When exclusively derived from the lateral chain of chlorophyll, the Pr/Ph is used to describe redox conditions in the depositional environment (Didyk et al., 1978; Peters et al., 2005). However, in immature samples this ratio is believed to be unreliable to assess redox conditions (Alexander et al., 1981; Volkman, 1986) but mainly depends on the origin of the OM. Therefore, in NA 202 the high Pr > Ph is unlikely to reflect oxic palaeoenvironmental conditions. The detection of hopanes up the C_{35} homologue (Fig. 8) indicates instead favourable conditions of OM preservation.

In NA 55 and NA 88 low amounts of Pr and Ph associated with a low Pr/Ph suggest low oxygen levels, although dependence on source and maturity cannot be ruled out. However, the detection of hopanes only up to C_{33} suggests a less well preserved OM in these two samples compared to NA 202.

Although the OM is well preserved in the three samples there is no indication for anoxia. Biomarker distribution indicates that the level of oxygen might have been slightly higher during deposition of samples NA 55 and NA 88.

Please cite this article as: Hermann, E., et al., Organic matter and palaeoenvironmental signals during the Early Triassic biotic recovery: The Salt Range and Surghar Range records, Sediment. Geol. (2010), doi:10.1016/j.sedgeo.2010.11.003

6. Discussion

6.1. Sequence stratigraphy (see Table 1)

Both sedimentological data and palynofacies analysis indicate changes in sea-level during deposition of the Early Triassic sequence in the Salt Range and Surghar Range. In the studied sections nine sequences have been identified. A comparison of these sequences with the global sequence framework of the Triassic (Embry, 1997) and the sequence interpretation of the Early Triassic in the Nammal gorge after Haq et al. (1988) shows their position within the global sea-level curve (Fig. 9). Gianolla and Jacquin (1998) compared the detailed sequence stratigraphy of the boreal realm with the framework of the Tethyan realm, which allows linking our sequences to a global sequence stratigraphic scheme. Two second order and two third order sequences can be identified with relatively high confidence. The significance of five additional sequences is less clear. They might represent fourth order sequences or parasequences.

In the Canadian Sverdrup Basin Embry (1997) described four sequence boundaries between the Permian–Triassic boundary and the Spathian–Anisian boundary. These sequences could be recognised in many other sections such as Svalbard, Germany, Italian Alps, East Siberia, Northern Himalayas, and Western USA and are therefore interpreted as sequence boundaries of global significance (see also Gianolla et al., 1998; Gianolla and Jacquin, 1998; Skjold et al., 1998). The basal Triassic second order sequence is marked globally by a major depositional shift at the PTB. In the Pakistani sections the transition from the Chhidru Formation to the Kathwai Member near the PTB is marked by an erosional surface and a change from a sandstone–limestone alternation to the dolomite lithologies and sandstone–siltstone succession (SRT1, Table 1 and Fig. 9).

The third order sequence boundary in the latest Dienerian or at the Dienerian–Smithian boundary, respectively, is marked by a change in depositional regime or conformable transgressive surfaces (Embry, 1997). This sequence boundary, which corresponds to the European T1–3 or to the In 2 sequence boundary (Gianolla and Jacquin, 1998,

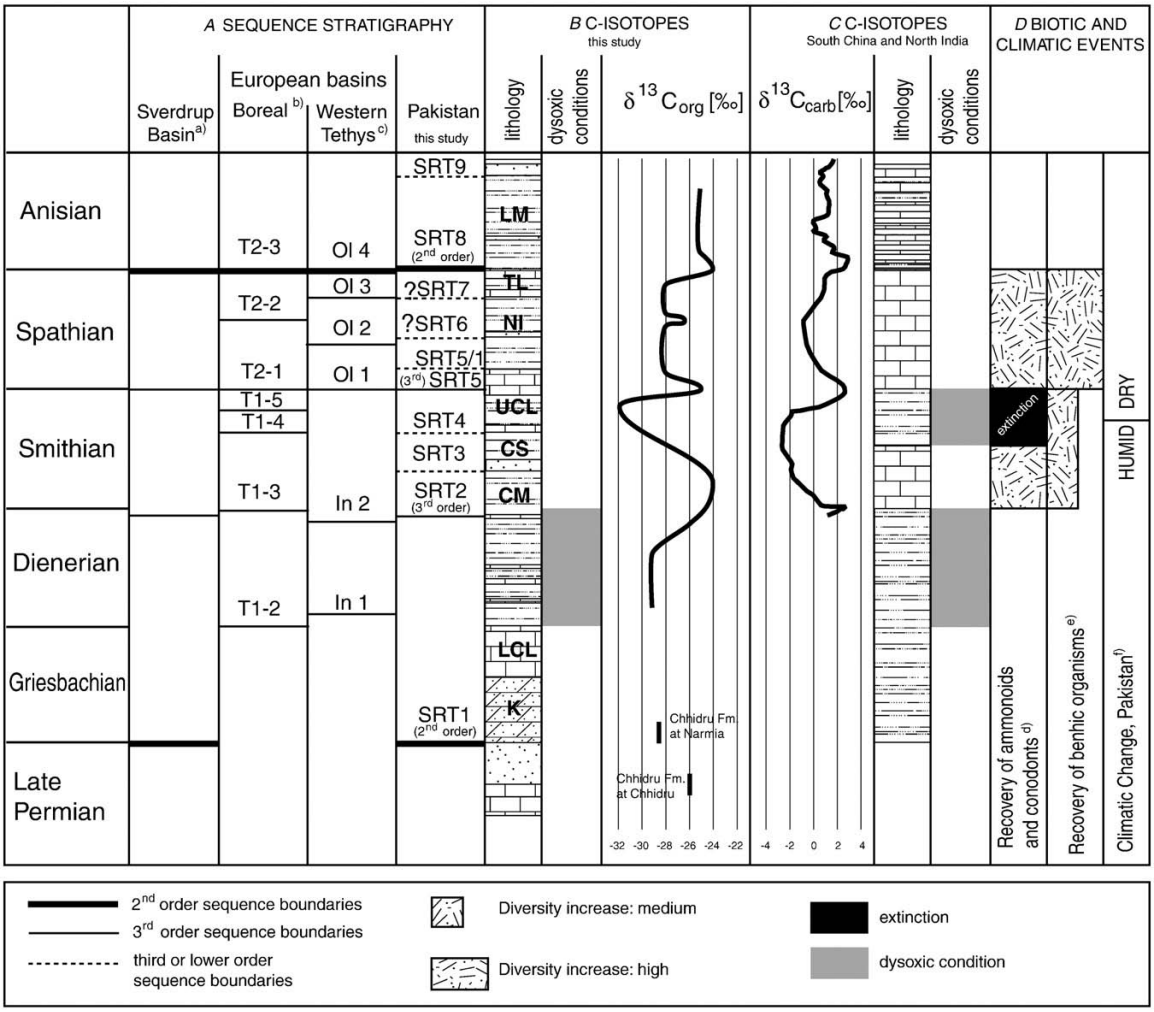

Fig. 9. A) Sequences stratigraphy of the studied sections in comparison with sequence stratigraphy of a) Sverdrup Basin (Embry, 1997); b) Barents Sea (Gianolla and Jacquin, 1998; Skjold et al., 1998); c) Western Tethys (Gianolla and Jacquin, 1998; Gianolla et al., 1998); B) Schematic $\delta^{13}C_{org}$ data, lithology and oxygenation conditions of the studied sections, LM = Landa Member; C) Schematic $\delta^{13}C_{carb}$ data, lithology oxygenation conditions of the Jinya section (South China) and Losar section (North India) modified after (Galfetti et al., 2007b), D) Biotic and climatic events d) ammonoid and conodont diversification (Brayard et al., 2006; Orchard, 2007); e) benthic diversification (Hautmann et al., 2008), f) climatic change in Pakistan (Hermann et al., 2008); see Fig. 3 for lithological legend.

Please cite this article as: Hermann, E., et al., Organic matter and palaeoenvironmental signals during the Early Triassic biotic recovery: The Salt Range and Surghar Range records, Sediment. Geol. (2010), doi:10.1016/j.sedgeo.2010.11.003

see also Fig. 9) is less distinct in the sedimentological record of the Salt Range and Surghar Range. However, the yellow weathering dolomitic limestone bed below the early Smithian *Kashmirites* fauna, near the top of the LCL at Chitta–Landu, and in the same biostratigraphic position in the CM at Nammal, coincide with a significant change from AOM dominated to more terrestrial POM dominated assemblages. This coincidence suggests that the global third order sequence boundary near the Dienerian–Smithian boundary (T1–3, In2) is expressed in the two sections (SRT2, Fig. 9). At Chhidru the sequence boundary could not be located with certainty. It may correspond to the local LCL–CM transition.

Another global third order sequence boundary is reported from the latest Smithian along with a moderate shift in the depositional regime of the above mentioned areas (Embry, 1997); it corresponds to the European T2–1 and Ol 1 (Gianolla and Jacquin, 1998) respectively. At Nammal and Chitta–Landu, a sequence boundary could be discriminated above the lowermost bed of the BB and at the top of the BB, respectively (SRT5, Figs. 3, 9).

The second order sequence boundary near the Spathian–Anisian corresponding to the EuropeanT2–3 and Ol 4 (Gianolla and Jacquin, 1998) is marked globally by a distinct change in depositional regime, and in some cases the development of this sequence boundary seems to be tectonically influenced (Sverdrup Basin and Italian Alps; Embry, 1997). At Nammal and Chitta–Landu a marked lithological change occurring between the TL and the Landa Member probably corresponds to this sequence boundary (SRT8, Fig. 9).

The identification of the SB SRT3, SRT4, SRT5/1, SRT6 and SRT7 recognised in sequence stratigraphic framework of the Tethyan and boreal basins is less clear. The boreal *romunduri* zone corresponds approximately to the ammonoid faunas found in the topmost part of the CS and the lower UCL. Therefore, the reworking at the base of the UCL (SRT4) could correspond to the T1–4 sequence boundary described from the boreal realm (Skjold et al., 1998). T1–5 coinciding with the *tardus* zone in the boreal realm could not be recognised in the Pakistani sections. Two of the erosional surfaces described in the Spathian of Nammal might correlate with the Ol 2 and Ol 3 sequence boundaries in the western Tethys. However, this correlation is rather tentative because of the loose ammonoid age control in the NI and TL in the studied sections.

A first sequence stratigraphic interpretation of the Nammal gorge has been established by Haq et al. (1988) based on the lithological description biostratigraphy of the PJRG (1985). Haq et al. (1988) described three sequences within the sedimentological record of the Nammal gorge. The first includes the Chhidru Formation, the Kathwai Member, the LCL and the lower part of the CM. The second one ranges from the upper part of the CM up to the middle NI. The third sequence includes the upper part of the NI and the TL. According to Haq et al. (1988), the lowermost SB in the sedimentary succession of the Nammal section is located in the middle CM and is indicated by "increased terrigenous input of coarser grained sandstones", which, however, disregards the discontinuous record and the depositional gaps near the Permian–Triassic boundary (SRT1), which after Haq et al. (1988) corresponds to a transgressive surface and not to a SB. Limestone beds are absent in the upper part of the CM and are substituted by rare fine-grained sandstone beds and lenses; the mentioned coarse-grained sandstones or even a dominance of sandstones could not be confirmed. Therefore, a more reasonable interpretation of the upper CM would be HST rather than LST deposits. The second sequence of Haq et al. (1988) ranges up into the middle NI ignoring the base of the CS (SRT3), the base of the UCL (SRT4), the sedimentary gap in the BB (SRT5), and the emersion features in the BB (SRT5/1); according to Haq et al. (1988) the BB represent early HST deposits. The base of the UCL (SRT4) is again interpreted as transgressive surface and not as a SB. The SB in the middle part of the NI of Haq et al. (1988) probably corresponds to SRT6. The third SB after Haq et al. (1988), at the top of the Mianwali Formation, correspond to the second order SB near the Spathian–Anisian boundary of Embry (1997) and our SRT8. The statement of Haq et al. (1988) that the Tredian Formation consists of continental deposits could not be confirmed. Samples of the Landa Member (lower Member of the Tredian Formation) contain marine palynomorphs (*Micrhystridium* spp.) confirming a marine depositional environment.

Therefore, the interpretation of the sedimentological record of the Nammal gorge by Haq et al. (1988) contrasts with the sequence framework of Embry (1997) and the results and sequence interpretation of this study. Our results suggest that the transgressive surfaces of Haq et al. (1988) should be reinterpreted as SB.

Baud et al. (1996) subdivided the Early Triassic succession of the Salt Range and Surghar Range into three third order sequences (S6, S7, and S8) placing the SB of S6 at the transition from the Chhidru Formation to the Kathwai Member similar to our interpretation (SRT1). The SB of S7 is located at the base of the CS corresponding to our SRT 3. The position of the SB to S8 is not clear as it occurs on top of BB or within the BB (Figs. 4 and 5 of Baud et al., 1996); therefore, it might correspond to our SRT5 or to SRT5/1.

6.2. Palaeoenvironment

Palaeoenvironmental studies on the Permian–Triassic sections of the Salt Range and Surghar Range (Nammal, Chhidru, Narmia and Zaluch) have previously been carried out by Wignall and Hallam (1993). These authors argued in favour of an anoxic event in this region, which they regarded as the principal kill mechanism of the end-Permian extinction event (Wignall and Twitchett, 2002). Three of their four sections are included in the present study. The stratigraphic framework and lithological units of Wignall and Hallam (1993) are based on the study of the PJRG (1985) but have been inaccurately implemented. The PJRG (1985) applied the stratigraphic framework and lithological units of Waagen (1895) and Guex (1978) but named the lithological units differently. Unit 1, in the sense of the PJRG (1985) corresponds to the LCL in the sense of Waagen (1895) and Guex (1978). However, the PJRG (1985) attributed Unit 1 to the "Griesbachian *Gyronites frequens* zone", which contradicts the standard ammonoid biostratigraphy. The *Gyronites frequens* zone represents the basal Dienerian (e.g. Guex, 1978); therefore Unit 1 is of Dienerian age. Fig. 3 of Wignall and Hallam (1993) implies that the authors apply Unit 1 in the sense of the PJRG (1985); however, they included parts of the CM (unit 2 of the PJRG, 1985) into their Unit 1 (Figs. 5 and 7 of Wignall and Hallam, 1993) and attributed Unit 1 to the Griesbachian *Ophiceras* Zone in Fig. 3, erroneously citing the PJRG (1985). Hence, Wignall and Hallam (1993) extended their "Griesbachian" up into the CM, thus in fact up to the top of the ammonoid-defined Dienerian.

According to previous documentations and our findings the Kathwai Member in the Salt Range contains *Ophiceras connectens* Schindewolf and therefore can be attributed to the mid to early late Griesbachian (Kummel, 1970; Schindewolf, 1954). So far *Otoceras* sp., which would indicate an early to middle Griesbachian age has not been reported from the area. Therefore, either the early Griesbachian is absent or local environment was inappropriate (too shallow) for ammonoids.

The LCL (or Unit 1 in the sense of the PJRG, 1985) can be attributed to the Dienerian at Narmia, Chitta–Landu, and Chhidru. It is dated as early Dienerian at Nammal based on the presence of *Gyronites frequens* (e. g. Guex, 1978 and ongoing studies of D. Ware and H. Bucher). At Narmia, Chitta–Landu, and Chhidru the basal part of the overlying CM is of Smithian age and of late Dienerian at Nammal (Brühwiler et al., in press). Therefore, the onset of anaerobic conditions proposed by Wignall and Hallam (1993) would not correspond to a Griesbachian event but fall within the Dienerian or late Dienerian at Nammal. Our palynofacies data show that the late

Please cite this article as: Hermann, E., et al., Organic matter and palaeoenvironmental signals during the Early Triassic biotic recovery: The Salt Range and Surghar Range records, Sediment. Geol. (2010), doi:10.1016/j.sedgeo.2010.11.003

Dienerian (lower third of CM) at Nammal, the earliest Smithian (lowermost CM) at Chhidru and the Dienerian (LCL) at Chitta–Landu and Narmia are marked by POM assemblages with increased AOM contents, reflecting poor oxygenation. The relatively high TOC values (Fig. 8) and the rare occurrences of laminated beds suggest oxygen deficient conditions during the Dienerian and the earliest Smithian time interval. Biomarker distribution confirms good preservation conditions of the OM in the late Dienerian sample (NA 202) implying low oxygen levels. Palynofacies samples from the Chhidru Formation (at Chitta–Landu and Narmia) containing palynological assemblages with Griesbachian affinity document well oxygenated conditions. Thus the hypothesis of Wignall and Hallam (1993) that the end-Permian extinction event was delayed until the late Griesbachian in the Salt Range and Surghar Range and caused by the combination of a flooding event (Kathwai Member) and a severe and widespread anoxia in the late Griesbachian is not supported by our data.

6.3. The carbon isotope record

Our data from the Early Triassic of Pakistan (sedimentology, C-isotopes, POM, TOC and biomarkers) allow linking recovery events to coeval environmental changes. For the correlation with other sections we use our new organic C-isotope record. Bulk organic C-isotope data are known to be strongly dependent on the composition of the organic matter and physical factors during plant growth, such as temperature, water availability, insolation etc. (Jahren et al., 2008). Therefore, it is essential to know the composition of the OM as well as the isotopic end-members of marine and terrestrial OM respectively. Our studies of OM across the PTB from Norway show that the Early Triassic primary C-isotope signal of terrestrial OM varies around −22‰ and marine OM around −32‰ (Hermann et al., 2010). This contrasts with the C-isotope signal of recent marine organic matter (−21‰) and terrestrial C3 plants (−28‰) (Derry and France-Lanord, 1996). Therefore, the composition of the organic matter has to be considered when using organic C-isotope records as a correlation tool. In this study the C-isotope data is shown together with the palynofacies record in Figs 4 and 5.

In the studied sections several shifts in the $\delta^{13}C_{org}$ can be observed. In the Nammal section the positive shift around the Dienerian–Smithian boundary is not related to a corresponding change in the POM composition. However, the AOM abundance decreases abruptly near the Dienerian–Smithian boundary, contrasting with the rather protracted $\delta^{13}C_{org}$ change (Fig. 4). There is also no correlation between the composition of the POM and the negative shift in the Smithian and the positive shift at the Smithian–Spathian boundary. At Nammal the positive shift at the Smithian–Spathian boundary is slightly obscured by four single data points around −26‰, which are probably due to poor preservation. Detailed re-sampling of this interval in a nearby section resulted in a coherent curve. The positive shift at the Spathian–Anisian boundary cannot be caused by the demise of marine OM, since marine OM is already reduced in the Spathian and the positive shift is also seen in other Tethyan C-isotope records (Fig. 6). The two most negative data points in the carbonate carbon isotope record in the CM of the Nammal section (Fig. 4) have not been recorded in the Chhidru and Chitta–Landu sections. These samples are relatively heterogeneous therefore biogenic carbonate might have obscured the isotope signal.

According to several authors effects of diagenesis on the variability of the bulk organic carbon isotope values are thought to be minor (~1‰; e. g. Freudenthal et al., 2001, Meyers et al., 1995). However, changes of the early diagenetic conditions such as the variability of productivity, and changing redox conditions of bottom waters can have significant impact on the preservation of the isotope signal of organic matter (Freudenthal et al., 2001). As a consequence several studies documented significant changes in $\delta^{13}C_{org}$ values (up to 4‰) due to selective preservation of refractory terrestrial material (e.g. Dean et al., 1986) or of non-metabolisable organic matter during anoxic anaerobic degradation (e.g. Benner et al., 1987). However, since the isotopic end-members of marine and terrestrial organic matter differ significantly, one of the most important factors that could mask $\delta^{13}C_{org}$ records are changes in the composition of the POM as discussed above. Thus, the parallel study of bulk organic carbon isotopes and POM allows a good control on possible compositional effects on the carbon isotope record.

In chemostratigraphic studies of Cretaceous successions a close relationship between sea-level changes and carbon isotope records has been demonstrated (e.g. Jarvis et al., 2006, Weissert et al., 1998). Sea-level rises, as documented in the chalk series of southern and eastern England, correspond to positive shifts in the carbonate carbon records of these series. Regressions match with negative isotope shifts. These correspondences are induced by changes in the partitioning of the carbon between the two major carbon sinks — the carbonate carbon sink and the organic carbon fixation by marine phytoplankton and terrestrial vegetation. During transgressive phases the area of flooded shallow seafloor is increased, sediments and soils are reworked and promote increased nutrient availability, thus enhancing productivity and burial of isotopically light organic matter (Jarvis et al., 2002). During sea level fall these areas are exposed to erosion and oxidation, which induces the release of ^{13}C depleted carbon into the carbon cycle.

In this study we identified several concurrences between sea-level changes and the isotope record. The positive shift at the Dienerian–Smithian boundary correlates with a sea-level rise (transgression). A similar correlation is observed during the Spathian–Anisian transition, where a positive isotope shift across the TL–Landu Member boundary concurs with a sea-level rise. However, the hypothesis fails to explain the negative–positive carbon isotope excursion couplet at the Smithian–Spathian transition. The negative shift in the Smithian might correspond to a regressive phase, however, the following positive shift does not coincide with a sea-level rise. Jarvis et al. (2002) noted that the relationship between sea-level changes and carbon isotope curve is not always straightforward. In Cretaceous records intervals with a mismatch of the two records have been assigned to a release of mantel derived light CO_2 during enhanced sea floor spreading (e.g. Gröcke et al., 1999). Changes in the marine primary productivity or changes in the preservation of organic matter might also influence the isotopic composition independent of the sea-level curve (Kump and Arthur, 1999). Faster processes, such as rapid releases of CO_2, e.g. from metamorphosed organic rich sediments during the Siberian Trap emplacement (Payne and Kump, 2007; Svensen et al., 2009), could explain why the couplet of rapid negative and positive isotope excursion across the Smithian–Spathian transition might be unrelated to the development of the sequences.

6.4. Comparison with other sections

The aforementioned considerations suggest that the organic C-isotope record of the studied sections reflects real global changes independent of the OM composition. Therefore, we can use the organic C-isotope chemostratigraphy to compare our results with other sections such as the Jinya/Waili area in South China, the Losar section in North India (Galfetti et al., 2007b), and the Tulong area in South Tibet (Brühwiler et al., 2009).

Recent studies demonstrate that the early/middle Smithian and Spathian time intervals in the Loulou Formation were times of deposition of well oxygenated carbonates (Nanpanjiang Basin, Guangxi Province, South China (Galfetti et al., 2008)). The same time intervals are marked by increased rates of diversity and abundance of skeletal material (Galfetti et al., 2008) and coincide with the highest values in taxonomic richness of ammonoids (Brayard et al., 2006; Brühwiler et al., 2010) and conodonts (Orchard, 2007). In contrast, the Dienerian and late Smithian time intervals are marked by predominantly mixed

Please cite this article as: Hermann, E., et al., Organic matter and palaeoenvironmental signals during the Early Triassic biotic recovery: The Salt Range and Surghar Range records, Sediment. Geol. (2010), doi:10.1016/j.sedgeo.2010.11.003

siliciclastic–carbonate depositional environments with dark, suboxic, laminated mudstones and organic-rich shales and limited bioturbation, suggesting an overarching causal mechanism leading simultaneously to low sea water oxygenation levels and slow downs or even set backs of the course of the biotic recovery (Galfetti et al., 2008).

Similar to the South China and Indian records our data demonstrate that dysoxic conditions, suggested by AOM abundance and high TOC, prevailed during the Dienerian interval and coincided with low diversity of benthic organisms (Hautmann et al., 2008). From the Smithian onward oxygenated conditions prevailed in the Mianwali Formation of the Salt Range and Surghar Range. Global diversity increase of benthic organisms in the Smithian (Hautmann et al., 2008) coincided with the pronounced recovery phase of ammonoids (Brayard et al., 2006; Brühwiler et al., 2010) and conodonts (Orchard, 2007). Additionally, the abundance of hopanes in the Smithian (NA 55) and Spathian samples (NA 88) indicates proliferation of bacteria from the Smithian onward. However, the decline of isoprenoids from the Dienerian (NA 202) to the Smithian sample (NA 55) indicates that the precursor organisms, probably of marine origin, disappeared or became reduced after the Dienerian. In contrast to South China and the Spiti area, the oxic conditions in the Mianwali Formation were not interrupted during the late Smithian. The continuous shallowing upward trend within the Mianwali Formation probably prevented the formation of a dysoxic water–sediment interface during Early Triassic. Well oxygenated conditions during late Smithian are also reported from the Tulong area in South Tibet (Brühwiler et al., 2009). However, in the Spiti area dysoxic conditions are documented during the late Smithian (Galfetti et al., 2007b). During Early Triassic, the Salt Range and Surghar Range, the Tulong and Spiti area were all situated on the northern margin of the Indian subcontinent.

The identical and synchronous changes in the Early Triassic records from Spiti on the northern Gondwanan margin and from Guangxi–Guizhou Province in the equatorial, palaeogeographically isolated South China block strongly suggest that the absence of late Smithian dysoxic conditions in the Salt Range and Surghar Range may result from the local Early Triassic tectonic configuration of this area (Galfetti et al., 2007b). The unusually thick and clastic-dominated nature of the Spathian record of the Salt Range also concurs with this interpretation.

The above mentioned recovery of ammonoids and conodonts in the Smithian was interrupted by an extinction event at the Smithian–Spathian boundary (Brayard et al., 2006; Orchard, 2007). Our sequence stratigraphic interpretation demonstrates that this extinction event is closely associated to a sea-level low stand near the Smithian–Spathian boundary (SRT5), which is recognised globally (Embry, 1997; Gianolla and Jacquin, 1998; Gianolla et al., 1998; Skjold et al., 1998). It also coincides with a global positive shift of C-isotopes (Galfetti et al., 2007a,b), and climatic changes inferred from ammonoid distribution (Brayard et al., 2005, 2006) and palynology (Hermann et al., 2008; Fig. 9). Benthic faunas are still not well enough documented to distinguish between extinction or absence of extinction during the late Smithian global disruption of the recovery (Hautmann et al., 2008).

Early Triassic terrestrial ecosystems are thought to be heavily affected by the end Permian extinction event (Benton and Twitchett, 2003; Retallack et al., 1996). It has been proposed that the recovery of equatorial conifer forests was delayed until the beginning of the Middle Triassic, whereas Early Triassic terrestrial ecosystems were continuously dominated by lycopods (Looy et al., 1999). However, recent studies demonstrate that terrestrial ecosystems recovered rather quickly already in the Griesbachian of Norwegian sections (Hochuli et al., 2010b). In the Pakistani palynofacies data, the continuous record of sporomorphs and plant debris reflects prolific ecosystems in the hinterland of the Salt Range and Surghar Range during Early Triassic times. Within the sporomorph group the continuous abundance of striate and non-striate bisaccate pollen suggests that pteridosperms and conifers proliferated on the Indian subcontinent already during the Early Triassic.

7. Conclusions

The interpretation of the succession of marine palaeoenvironments of the Early Triassic sections in the Salt Range and Surghar Range are based on sedimentological observation combined with palynofacies data, C-isotopes records, TOC, and biomarkers.

(1) Sea level changes are reflected in the sedimentological and palynofacies record. Two second order SB (SRT1 near the Permian–Triassic boundary, SRT8 near the Spathian–Anisian boundary) and two third order SB (SRT2 near the Dienerian–Smithian boundary, SRT5 near the Smithian–Spathian boundary) have been identified. Six SB of undetermined order (in the Smithian SRT3 at the base of CS and SRT4 the base of UCL, in the Spathian SRT5/1 at the top of the BB, SRT6 in the middle NI and SRT7 at the base of TL, and in the Anisian SRT9 at the top of the Landa Member) could be differentiated.

(2) The sequence boundaries defined in this study differ from the interpretation of the Nammal section of Haq et al. (1988), but are consistent with the global sequence boundaries established by Embry (1997) and Gianolla and Jacquin (1998).

(3) The composition of the POM reflects changing ecological conditions such as a protracted shallowing upward combined with short-termed sea-level changes, oxygenation conditions, and proximity to the shore. These results are supported by the molecular biomarker results. Dysoxic conditions are recorded in the Dienerian of Chitta–Landu and Narmia, in the late Dienerian at Nammal, and in the earliest Smithian at Chhidru. The results show that the patterns of the Early Triassic recovery were closely linked to the prevailing environmental conditions, such as carbon cycle, sea-level and oxygenation levels.

(4) The POM suggests well oxygenated conditions in the Late Griesbachian. The proposed late Griesbachian shallow water anoxia as kill mechanism for the Permian fauna as postulated for the Salt Range and Surghar Range (Wignall and Hallam, 1993) is refuted.

(5) The observed low oxygenation levels in the Dienerian are also documented from coeval marine sediments of South China and North India (Galfetti et al., 2007b, 2008) and are probably responsible for low diversity of benthic organisms during this time interval.

(6) From the Smithian onward well oxygenated conditions prevailed in the Early Triassic of Pakistan coinciding with the onset of the explosive radiation of ammonoids (Brayard et al., 2006, 2009; Brühwiler et al., 2010, in press) and conodonts (Orchard, 2007) as well as a diversity increase of benthic organisms, and the proliferation of bacteria as inferred from the biomarker data.

(7) The positive shift of C-isotopes and the SB SRT5 near the Smithian–Spathian boundary coincides with a major extinction of ammonoids and conodonts and a change from humid to dryer climate (Brayard et al., 2005, 2006; Galfetti et al., 2007a; Hermann et al., 2008). Accumulation of OM-rich shales during the late Smithian, as documented from other Tethyan sections, is not recorded in the Salt Range and Surghar Range. The OM rich siltstone horizon deposited in the Surghar Range during this time interval probably originates from an accumulation of older OM that has been reworked during this regression episode.

(8) Early Triassic terrestrial ecosystems in the hinterland of the Salt Range and Surghar Range proliferated and constantly shed OM onto the Northern Gondwanan shelf. Continuous terrestrial primary production is documented for the entire Early Triassic.

Please cite this article as: Hermann, E., et al., Organic matter and palaeoenvironmental signals during the Early Triassic biotic recovery: The Salt Range and Surghar Range records, Sediment. Geol. (2010), doi:10.1016/j.sedgeo.2010.11.003

Supplementary materials related to this article can be found online at doi:10.1016/j.sedgeo.2010.11.003.

Acknowledgements

This project was funded by Swiss NSF project 200020-127716 to HB. We are grateful to Thierry Adatte (University of Lausanne) for Rock Eval analysis. Many thanks go to Stefano Bernasconi and Helmut Weissert for access to the stable isotope laboratory of the Geology Department of the ETH Zurich and discussions on Early Triassic chemostratigraphy. We are grateful to Steve Kershaw and an anonymous reviewer for their constructive comments and valuable suggestions that significantly improved an earlier version of this work.

References

Alexander, R., Kagi, R.I., Woodhouse, G.W., 1981. Geochemical correlation of Windalia oil and extracts of Winning Group (Cretaceous) potential source rocks, Barrow subbasin, Western Australia. Bulletin of the American Association of Petroleum Geology 65, 235–250.

Atudorei, V., 1999. Constraints on the Upper Permian to Upper Triassic marine carbon isotope curve. Case studies from the Tethys. PhD Thesis, University of Lausanne, Switzerland, 161 pp.

Balme, B.E., 1970. Palynology of Permian and Triassic strata in the Salt Range and Surghar Range, West Pakistan. In: Kummel, B., Teichert, C. (Eds.), Stratigraphic Boundary Problems: Permian and Triassic of West Pakistan. Department of Geology, University of Kansas, pp. 305–453.

Batten, D.J., 1996. In: Jansonius, J., McGregor, D.C. (Eds.), Palynofacies and Petroleum Potential. : Palynology: Principles and Applications, Vol. 3. American Association of Stratigraphic Palynologists Foundation, pp. 1065–1084.

Baud, A., Atudorei, V., Sharp, Z., 1996. Late Permian and Early Triassic evolution of the Northern Indian margin: carbon isotope and sequence stratigraphy. Geodinamica Acta 9 (2), 57–77.

Baud, A., Richoz, S., Pruss, S., 2007. The lower Triassic anachronistic carbonate facies in space and time. Global and Planetary Change 55, 81–89.

Benner, R., Fogel, M.L., Sprague, E.K., Hodson, R.E., 1987. Depletion of ^{13}C in lignin and its implication for stable carbon isotope studies. Nature 329, 708–710.

Benton, M.J., Twitchett, R.J., 2003. How to kill (almost) all life: the end-Permian extinction event. Trends in Ecology & Evolution 18, 358–365.

Berner, R.A., 2002. Examination of hypotheses for the Permo-Triassic boundary extinction by carbon cycle modeling. Proceedings of the National Academy of Sciences 99, 4172–4177.

Bray, E.E., Evans, E.D., 1961. Distribution of n-paraffins as a clue to recognition of source beds. Geochimica et Cosmochimica Acta 22, 2–15.

Brayard, A., Escarguel, G., Bucher, H., 2005. Latitudinal gradient of taxonomic richness: combined outcome of temperature and geographic mid-domains effects? Journal of Zoological Systematics and Evolutionary Research 43 (3), 178–188.

Brayard, A., Bucher, H., Escarguel, G., Fluteau, F., Bourquin, S., Galfetti, T., 2006. The Early Triassic ammonoid recovery: paleoclimatic significance of diversity gradients. Palaeogeography, Palaeoclimatology, Palaeoecology 239, 374–395.

Brayard, A., Escarguel, G., Bucher, H., Monnet, C., Brühwiler, T., Goudemand, N., Galfetti, T., Guex, J., 2009. Good genes and good luck: ammonoid diversity and the end-Permian mass extinction. Science 325, 1118–1121.

Brühwiler, T., Goudemand, N., Galfetti, T., Bucher, H., Baud, A., Ware, D., Hermann, E., Hochuli, P.A., Martini, R., 2009. The Lower Triassic sedimentary and carbon isotope records from Tulong (South Tibet) and their significance for Tethyan palaeoceanography. Sedimentary Geology 222, 314–332.

Brühwiler, T., Bucher, H., Brayard, A., Goudemand, N., 2010. High-resolution biochronology and diversity dynamics of the Early Triassic ammonoid recovery: the Smithian faunas of the Northern Indian Margin. Palaeogeography, Palaeoclimatology, Palaeoecology 297, 491–501.

Brühwiler, T., Bucher, H., Ware, D., Hermann, E., Hochuli, P.A., Roohi, G., ur-Rehman, K., and Yaseen, A., in press. Smithian (Early Triassic) ammonoids from the Salt Range, Pakistan. Special Papers in Palaeontology.

Cao, C., Love, G.D., Hays, L.E., Wang, W., Shen, S., Summons, R.E., 2009. Biogeochemical evidence for euxinic oceans and ecological disturbance presaging the end-Permian mass extinction event. Earth and Planetary Science Letters 281, 188–201.

Chappe, B., Albrecht, P., Michealis, W., 1982. Polar lipids of achaebacteria in sediments and petroleum. Science 217, 65–66.

Collister, J.W., Lichtfouse, E., Hieshima, G., Hayes, J.M., 1994. Partial resolution of sources of n-alkanes in the saline portion of the Parachute Creek Member, Green River Formation (Piceance Creek Basin, Colorado). Organic Geochemistry 21, 645–659.

Combaz, A., 1964. Les palynofaciès. Revue de Micropaléontologie 7 (3), 205–218.

Dean, W.E., Arthur, M.A., Claypool, G.E., 1986. Depletion of ^{13}C in Cretaceous marine organic matter: source, diagenetic, or environmental signal? Marine Geology 70, 119–157.

Derry, L.A., France-Lanord, C., 1996. Neogene growth of the sedimentary organic carbon reservoir. Paleoceanography 11 (3), 267–275.

Didyk, B.M., Simoneit, B.R.T., Brassel, S.C., Eglinton, G., 1978. Organic geochemical indicators of paleoenvironmental conditions of sedimentation. Nature 272, 216–222.

Eglinton, T.I., Eglinton, G., 2008. Molecular proxies for paleoclimatology. Earth and Planetary Science Letters 275, 1–16.

Eglinton, G., Hamilton, C.P., 1967. Leaf epicuticular waxes. Science 156, 1322–1335.

Embry, A.F., 1997. Global sequence boundaries of the Triassic and their identification in the Western Canada Sedimentary Basin. Bulletin of Canadian Petroleum Geology 45 (4), 415–433.

Erwin, D.L., 2006. Extinction. How Life on Earth Nearly Ended 250 Million Years Ago. Princeton University Press, Princeton.

Flügel, E., 2002. Triassic reef patterns. In: Kiessling, S.E., Flügel, H., Golonka, J. (Eds.), Phanerozoic Reef Patterns: SEPM Special Publication, 72, pp. 391–463.

Freudenthal, T., Wagner, T., Wenzhöfer, F., Zabel, M., Wefer, G., 2001. Early diagenesis of organic matter from sediments of the eastern subtropical Atlantic: evidence from stable nitrogen and carbon isotopes. Geochimica et Cosmochinica Acta 65, 1795–1808.

Galfetti, T., Hochuli, P.A., Brayard, A., Bucher, H., Weissert, H., Vigran, J.O., 2007a. Smithian/Spathian boundary event: evidence for global climatic change in the wake of the end-Permian biotic crisis. Geology 35, 291–294.

Galfetti, T., Bucher, H., Brayard, A., Hochuli, P.A., Weissert, H., Goudun, K., Atudorei, V., Guex, J., 2007b. Late Early Triassic climate change: insights from a carbonate carbon isotopes, sedimentary evolution and ammonoid paleobiogeography. Palaeogeography, Palaeoclimatology, Palaeoecology 243, 394–411.

Galfetti, T., Bucher, H., Martini, R., Hochuli, P.A., Weissert, H., Crasquin-Soleau, S., Brayard, A., Goudemand, N., Brühwiler, T., Goudun, K., 2008. Evolution of Early Triassic outer platform paleoenvironments in the Nanpanjiang Basin (South China) and their significance for the biotic recovery. Sedimentary Geology 204, 36–60.

Gee, E.R., 1989. Overview of the geology and structure of the Salt Range, with observations on related areas of northern Pakistan. Geological Society of America Special Paper 232, 95–112.

Gianolla, P., Jacquin, T., 1998. Triassic sequence stratigraphic framework of western European basins. In: de Graciansky, P.-C., Hardenbol, J., Jacquin, T., Vail, P.R. (Eds.), Mesozoic and Cenozoic Sequence Stratigraphy of European Basins: SEPM Special Publication, 60, pp. 643–650. Tulsa SEPM (Society for Sedimentary Geology).

Gianolla, P., de Zanche, V., Mietto, P., 1998. Triassic sequence stratigraphy in the southern Alps (Northern Italy): definition of sequences and basin evolution. In: de Graciansky, P.-C., Hardenbol, J., Jacquin, T., Vail, P.R. (Eds.), Mesozoic and Cenozoic Sequence Stratigraphy of European Basins: SEPM Special Publication, 60, pp. 719–747. Tulsa SEPM (Society for Sedimentary Geology).

Golonka, J., Ford, D., 2000. Pangean (Late Carboniferous–Middle Jurassic) paleoenvironment and lithofacies. Palaeogeography, Palaeoclimatology, Palaeoecology 161, 1–34.

Goossens, H., de Leeuw, J.W., Shenk, P.A., Brassell, S.C., 1984. Tocopherols as likely precursors of pristine in ancient sediments and crude oils. Nature 312, 440–442.

Götz, A.E., Feist-Burkhardt, S., Ruckwied, K., 2008. Palynofacies and sea-level changes in the Upper Cretaceous of the Vocontian Basin, southeast France. Cretaceous Research 29, 1047–1057.

Goudemand, N., Orchard, M., Bucher, H., Brayard, A., Brühwiler, T., Galfetti, T., Hochuli, P.A., Hermann, E., Ware, D., 2008. Smithian–Spathian boundary: the biggest crisis in Triassic conodont history. Joint Annual Meeting, GSA, Houston, Paper No. 318-3.

Grantham, P.J., 1986. Sterane isomerization and moretane/hopane ratios in crude oils derived from Tertiary source rocks. Organic Geochemistry 9, 293–304.

Gröcke, D.R., Hesselbo, S.P., Jenkyns, H.C., 1999. Carbon-isotope composition of Lower Cretaceous fossil wood: ocean–atmosphere chemistry and relation to sea-level change. Geology 27, 155–158.

Guex, J., 1978. Le Trias intérieur des Salt Ranges (Pakistan): problèmes biochronologiques. Eclogae Geologicae Helvetiae 71 (1), 105–141.

Haq, B.U., Hardenbol, J., Vail, P.R., 1988. Mesozoic and Cenozoic chronostratigraphy and cycles of sea-level change. In: Wilgus, C.K., Hastings, B.S., Kendall, C.G.St.C., Posamentier, H.W., Ross, C.A., Van Wagoner, J.C. (Eds.), Sea-Level Changes: An Integrated Approach. : Special Publication, No. 42. Society of Economic Paleontologists and Mineralogists, Tulsa, Oklahoma, pp. 71–108.

Hautmann, M., Bucher, H., Brühwiler, T., Goudemand, N., Kaim, A. & Nützel, A. (in press): An unusually diverse mollusc fauna from the earliest Triassic of South China and its implications for benthic recovery after the end-Permian biotic crisis. Geobios.

Hautmann, M., Bucher, H., Nützel, A., Brühwiler, T., Goudemand, N., Brayard, A., 2008. Recovery of benthos versus nekton after the end-Permian mass extinction event — a preliminary comparison. Joint Annual Meeting, GSA, Houston, Paper No. 285-14.

Hermann, E., Hochuli, P.A., Bucher, H., Brühwiler, T., Goudemand, N., Roohi, G., 2008. Major climatic change at the Smithian/Spathian boundary — evidence from low palaeolatitudinal records. Joint Annual Meeting, GSA, Houston, Paper No. 318-1.

Hermann, E., Hochuli, P.A., Bucher, H., Vigran, J.O., Weissert, H., Bernasconi, S.M., 2010. Close-up view on the Permian–Triassic boundary based on extended organic carbon isotope records from Norway (Trøndelag and Finnmark Platform). Global and Planetary Change. doi:10.1016/j.gloplacha.2010.10.007.

Hochuli, P.A., Vigran, J.O., Hermann, E., Bucher, H., 2010a. Multiple climatic changes around the Permian Triassic boundary event revealed by an expanded palynological record from Mid Norway. American Association of Petroleum Geologists Bulletin 122 (5/6), 884–896.

Hochuli, P.A., Hermann, E., Vigran, J.O., Bucher, H., Weissert, H., 2010b. Rapid demise and recovery of plant ecosystems across the end-Permian extinction-event. Global and Planetary Change. doi:10.1016/j.gloplacha.2010.10.004.

Horacek, M., Brandner, R., Abart, R., 2007. Carbon isotope record of the P/T boundary and the Lower Triassic in the Southern Alps: evidence for rapid changes in storage of organic carbon. Palaeogeography, Palaeoclimatology, Palaeoecology 252, 347–354.

Jahren, A.H., Arens, N.C., Harbeson, S.A., 2008. Prediction of atmospheric $\delta^{13}CO_2$ using fossil plant tissues. Review of Geophysics 46, RG I002. doi:10.1029/2006RG000219.

Please cite this article as: Hermann, E., et al., Organic matter and palaeoenvironmental signals during the Early Triassic biotic recovery: The Salt Range and Surghar Range records, Sediment. Geol. (2010), doi:10.1016/j.sedgeo.2010.11.003

Jannasch, H.W., 1991. Microbial processes in the Black Sea water column and top sediment: and overview. In: Izdar, E., Murray, J.W. (Eds.), Black Sea Oceanography: NATO Advanced Studies Institute Series, C351, pp. 271–281.

Jarvis, I., Mabrouk, A., Moody, R.T.J., de Cabrera, S., 2002. Late Cretaceous (Campanian) carbon isotope events, sea-level change and correlation of the Tethyan and Boreal realms. Palaeogeography, Palaeoclimatology, Palaeoecology 188, 215–248.

Jarvis, I., Gale, A.S., Jenkyns, H.C., Pearce, M.A., 2006. Secular variation in Late Cretaceous carbon isotopes: a new $\delta^{13}C$ carbonate reference curve for the Cenomanian–Campanian (99.6–70.6 Ma). Geological Magazine 143, 561–608.

Kaim, A., Nützel, A., 2010. Dead bellerophontids walking — the short Mesozoic history of the Bellerophontoidea (Gastropoda). Palaeogeography, Palaeoclimatology, Palaeoecology. doi:10.1016/j.palaeo.2010.04.008.

Kummel, B., 1966. The Lower Triassic formations of the Salt Range and Trans-Indus Ranges, West Pakistan. Bulletin of the Museum of Comparative Zoology 134 (10), 361–429.

Kummel, B., 1970. Ammonoids from the Kathwai Member, Mianwali Formation, Salt Range, West Pakistan. In: Kummel, B., Teichert, C. (Eds.), Stratigraphic Boundary Problems: Permian and Triassic of West Pakistan. Department of Geology, University of Kansas, pp. 177–192.

Kummel, B., Teichert, C., 1966. Relations between the Permian and Triassic formations in the Salt Range and Trans-Indus ranges, West Pakistan. Neues Jahrbuch für Geologie und Paläontologie Abhandlungen 125, 297–333.

Kummel, B., Teichert, C., 1970. Stratigraphy and paleontology of the Permian–Triassic boundary beds, Salt Range and Trans-Indus Ranges, West Pakistan. In: Kummel, B., Teichert, C. (Eds.), Stratigraphic Boundary Problems: Permian and Triassic of West Pakistan. Department of Geology, University of Kansas, pp. 1–110.

Kump, L.R., Arthur, M.A., 1999. Interpreting carbon-isotope excursions: carbonates and organic matter. Chemical Geology 161, 181–198.

Leckie, D.A., Singh, C., Goodarzi, F., Wall, J.H., 1990. Organic-rich, radioactive marine shale: a case study of a shallow-water condensed section, Cretaceous Shaftesbury Formation, Alberta, Canada. Journal of Sedimentary Petrology 60, 101–117.

Lewan, M.D., 1986. Stable carbon isotopes of amorphous kerogens from Phanerozoic sedimentary rocks. Geochimica et Cosmochinica Acta 50, 1583–1591.

Looy, C.V., Brugman, W.A., Dilcher, D.L., Visscher, H., 1999. The delayed resurgence of equatorial forests after the Permian–Triassic ecologic crisis. Proceedings of the National Academy of Sciences of the United States of America 96, 13857–13862.

Meyers, P.A., Leenheer, M.J., Bourbonniere, R.A., 1995. Diagenesis of vascular plant organic matter components during burial in lake sediments. Aquatic Geochemistry 1, 35–52.

Orchard, M.J., 2007. Conodont diversity and evolution through the latest Permian and Early Triassic upheavals. Palaeogeography, Palaeoclimatology, Palaeoecology 252, 93–117.

Pakistani-Japanese Research Group, 1985. Permian and Triassic systems in the Salt Range and Surghar Range, Pakistan. In: Nakazawa, K., Dickins, J.M. (Eds.), The Tethys: Her Paleogeography and Paleobiogeography from Paleozoic to Mesozoic. Tokai University Press, Tokyo, Japan, pp. 221–312.

Pan, C., Peng, D., Zhang, M., Yu, L., Sheng, G., FuPan, J., 2008. Distribution and isomerization of C_{31}–C_{35} homohopanes and C_{29} steranes in Oligocene saline lacustrine sediments from Qaidam Basin, Northwest China. Organic Geochemistry 39, 646–657.

Payne, J.L., Kump, L.R., 2007. Evidence for recurrent Early Triassic massive volcanism from quantitative interpretation of carbon isotope fluctuations. Earth and Planetary Science Letters 256, 264–277.

Payne, J.L., Lehrmann, D.J., Wei, J., Orchard, M.J., Schrag, D.P., Knoll, A.H., 2004. Large perturbations of the carbon cycle during recovery from the end-Permian extinction. Science 305, 506–509.

Peters, K.E., 1986. Guideline for evaluating petroleum source rock using programmed pyrolysis. American Association of Petroleum Geologists Bulletin 70 (3), 318–329.

Peters, K.E., Walters, C.C., Moldowan, J.M., 2005. The Biomarker Guide. Cambridge University Press, Cambridge.

Pilskaln, C.H., 1991. Biogenic aggregate sedimentation in the Black Sea. In: Izdar, E., Murray, J.W. (Eds.), Black Sea Oceanography: NATO Advanced Studies Institute Series, C351, pp. 271–281.

Pittet, B., Gorin, G.E., 1997. Distribution of sedimentary organic matter in a mixed carbonate–siliciclastic platform environment: Oxfordian of the Swiss Jura Mountains. Sedimentology 44, 915–937.

Posenato, R., 2008. Patterns of bivalve biodiversity from Early to Middle Triassic in the Southern Alps (Italy): regional vs. global events. Palaeogeography, Palaeoclimatology, Palaeoecology 261, 145–159.

Pruss, S.B., Bottjer, D.J., Corsetti, F.A., Baud, A., 2006. A global marine sedimentary response to the end-Permian mass extinction: examples from southern Turkey and the western United States. Earth Science Reviews 78, 193–206.

Retallack, G.J., Veevers, J.J., Morante, R., 1996. Global coal gap between Permian–Triassic extinction and Middle Triassic recovery of peat-forming plant. GSA Bulletin 108 (2), 195–207.

Richoz, S., 2006, Stratigraphie et variations isotopiques du carbone dans le Permien supérieur et le Trias inférieur de quelques localités de la Néotéthys (Turquie, Oman et Iran). PhD Thesis, University of Lausanne, 251 pp.

Rowland, S.J., 1990. Production of acyclic isoprenoid hydrocarbons by laboratory maturation of methanogenic bacteria. Organic Geochemistry 15, 9–16.

Rubinstein, I., Sieskind, O., Albrecht, P., 1975. Rearranged steranes in a shale: occurrence and simulated formation. Journal of the Chemical Society, Perkin I 1833–1836.

Schindewolf, O.H., 1954. Über die Faunenwende vom Paläozoikum zum Mesozoikum. Zeitschrift der Deutschen Geologischen Gesellschaft 105, 154–183.

Seifert, W.K., Moldowan, J.M., 1980. The effect of thermal stress on source-rock quality as measured by hopane stereochemistry. In: Douglas, A.G., Maxwell, J.R. (Eds.), Advances in Organic Geochemistry. Oxford Press, Oxford, pp. 229–237.

Skjold, L.J., van Veen, P.M., Kristensen, S.-E., Rasmussen, A.R., 1998. Triassic sequence stratigraphy of the southwestern Barents Sea. In: de Graciansky, P.-C., Hardenbol, J., Jacquin, T., Vail, P.R. (Eds.), Mesozoic and Cenozoic Sequence Stratigraphy of European Basins: SEPM Special Publication, 60, pp. 651–666. Tulsa SEPM (Society for Sedimentary Geology).

Smith, A.G., Smith, D.G., Funnell, B.M., 1994. Atlas of Mesozoic and Cenozoic Coastlines. Cambridge University Press, Cambridge.

Stampfli, G.M., Borel, G.D., 2002. A plate tectonic model for the Paleozoic and Mesozoic constrained by dynamic plate boundaries and restored synthetic oceanic isochrons. Earth and Planetary Science Letters 196, 17–33.

Steffen, D., Gorin, G.E., 1993. Sedimentology of organic matter in Upper Tithonian–Berriasian deep-sea carbonates of Southeast France: evidence of eustatic control. In: Katz, B.J., Pratt, L.M. (Eds.), Source Rocks in a Sequence Stratigraphic Framework: AAPG Studies on Geology, Tulsa, 37, pp. 49–65.

Svensen, H., Planke, S., Polozov, A.G., Schmidbauer, N., Corfu, F., Podladchikov, Y., Jamtveit, B., 2009. Siberian gas venting and the end-Permian environmental crisis. Earth and Planetary Science Letters 277, 490–500.

Teichert, C., 1966. Stratigraphic nomenclature and correlation of the Permian "Productus limestone", Salt Range, West Pakistan. Geological Survey of Pakistan 15 (1), 1–19.

Tissot, B.P., Pelet, R., 1981. Sources and fate of organic matter in ancient sediments. Oceanologica Acta, Actes 26e Congrès International de Géologie, colloque Géologie des Océan Special Issue, pp. 97–103.

Traverse, A., 2007. Paleopalynology. : Topics in Geobiology, 28. Springer, Dordrecht.

Tyson, R.V., 1993. Palynofacies analysis. In: Jenkins, D.G. (Ed.), Applied Micropaleontology. Kluwer, Dordrecht, pp. 153–191.

Tyson, R.V., 1995. Sedimentary organic Matter — Organic Facies and Palynofacies. Chapman & Hall, London.

Volkman, J.K., 1986. A review of sterol markers for marine and terrigenous organic matter. Organic Geochemistry 9, 83–99.

Volkman, J.K., 2005. Sterols and other triterpenoids; source specificity and evolution of biosynthetic pathways. Organic Geochemistry 36, 139–159.

Waagen, W., 1891. Salt Range fossils: geological results. Palaeontologia Indica 4 (pt. 2), 89–242.

Waagen, W., 1895. Salt Range fossils II. Fossils from the Ceratite formation. Palaeontologia Indica 2, 1–323.

Wang, C., 2007. Anomalous hopane distribution at the Permian–Triassic boundary, Meishan, China — evidence for the end-Permian marine ecosystem collapse. Organic Geochemistry 38, 52–66.

Weissert, H., Lini, A., Föllmi, K.B., Kuhn, O., 1998. Correlation of Early Cretaceous carbon isotope stratigraphy and platform drowning events: a possible link? Palaeogeography, Palaeoclimatology, Palaeoecology 137, 189–203.

Wignall, P.B., Hallam, A., 1993. Griesbachian (Earliest Triassic) palaeoenvironmental changes in the Salt Range, Pakistan and southeast China and their bearing on the Permo-Triassic mass extinction. Palaeogeography, Palaeoclimatology, Palaeoecology 102, 215–237.

Wignall, P.B., Twitchett, R.J., 2002. Extent, duration, and nature of the Permian–Triassic superanoxic event. Geological Society of America Special Paper 356, 395–413.

Wood, S.E., Gorin, G.E., 1998. Sedimentary organic matter in distal clinoforms of Miocene slope sediments: Site 903 of ODP Leg 150, offshore New Jersey (U.S.A.). Journal of Sedimentary Research 68, 856–868.

Yin, H., Zhang, K., Tong, J., Yang, Z., Wu, S., 2001. The Global Stratotype Section and Point (GSSP) of the Permian–Triassic boundary. Episodes 24 (2), 102–114.

Ziegler, A.M., Scotese, C.R., Barrett, S.F., 1983. Mesozoic and Cenozoic paleogeographic maps. In: Brosche, P., Sündermann, J. (Eds.), Tidal Friction and the Earth's Rotation II. Springer Verlag, Berlin, pp. 240–252.

Please cite this article as: Hermann, E., et al., Organic matter and palaeoenvironmental signals during the Early Triassic biotic recovery: The Salt Range and Surghar Range records, Sediment. Geol. (2010), doi:10.1016/j.sedgeo.2010.11.003

Supplementary Data

For Supplementary Table 1 see Appendix 6 on page 215.

Comment on the biostratigraphic constraints of SRT3:

In Text-Fig. 15 of Brühwiler et al. (in press) *Flemingites nanus* is shown to occur in the top of the CM at Nammal and in the basal part of the CS at Chhidru. This would imply that the lithological boundary between the CM and the CS is diachronous, obscuring the interpretation of this horizon as a sequences boundary of undetermined order. However the $\delta^{13}C_{org}$ record of both sections show maximum values in the lower CS. The siliciclastic lithology at Chhidru probably prevents ammonoid findings in the lower part of the CS and the topmost CM, and prevents findings of *F. nanu*s in this interval of the Chhidru section.

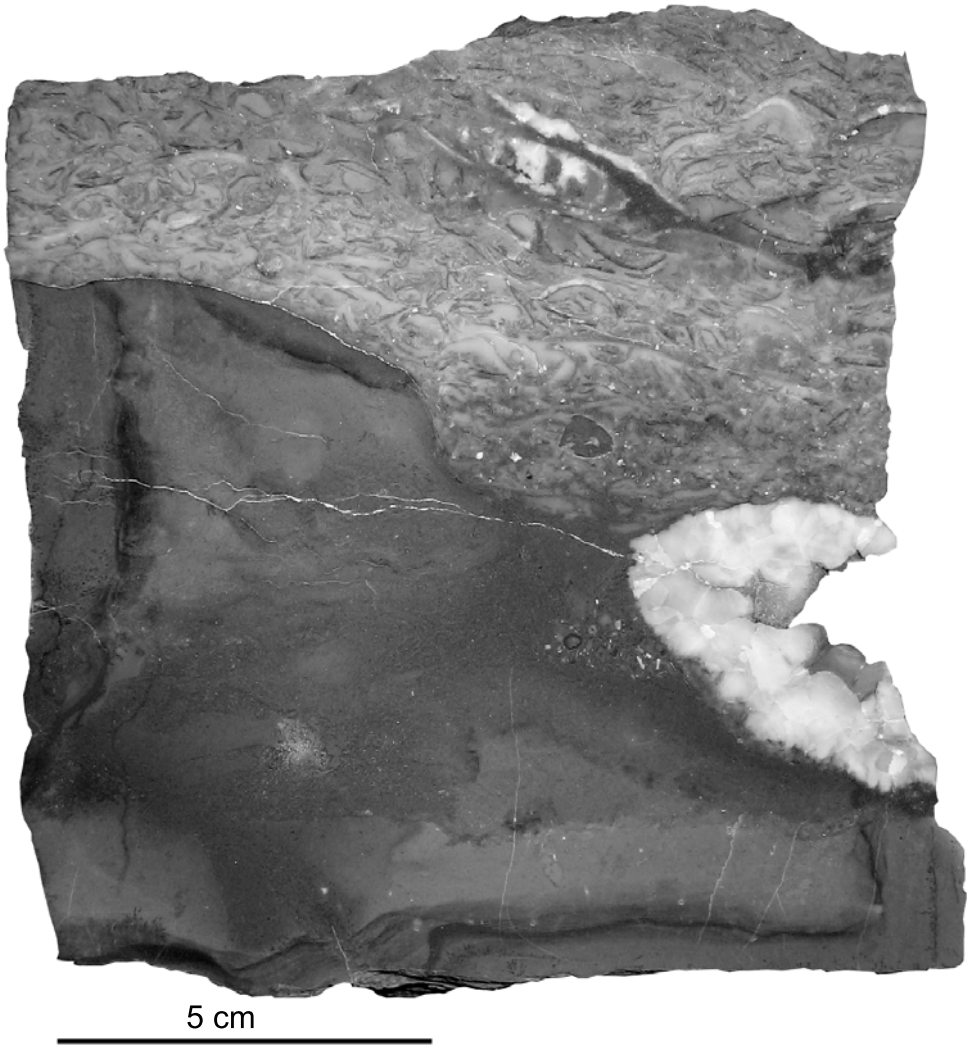

Supplementary Figure 1: At Narmia the top of the BB is affected by karstification. Karstic cavities are filled with sparry calcite.

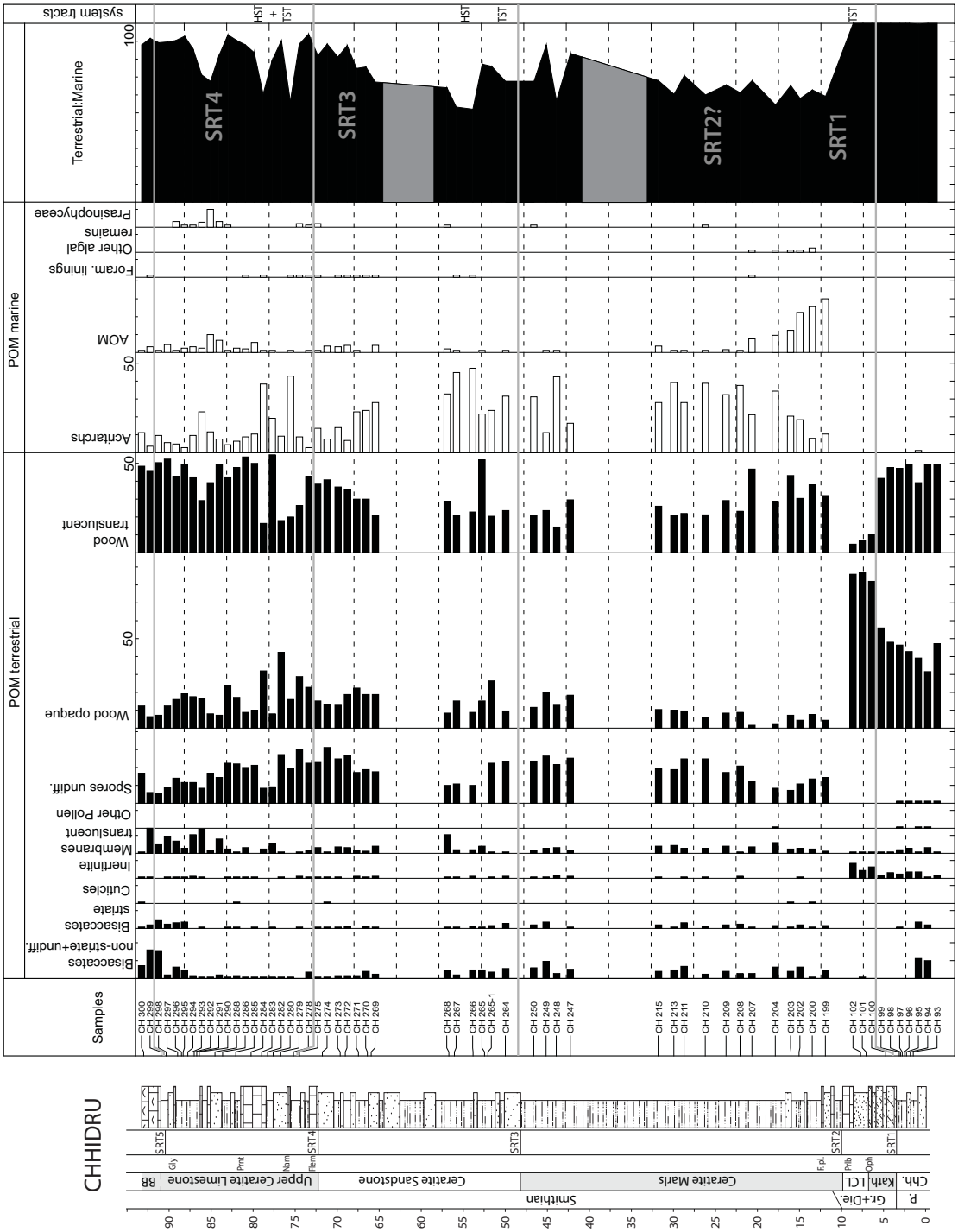

Supplementary Figure 2: Detailed palynofacies of Chhidru with relative abundances of individual organic particle categories. The ratio of terrestrial (black) to marine (white) is given with sequence stratigraphic interpretation. C1 – C3 correspond to TR-cycles mentioned in the text. LST (POM indicating lowstand system tract), TST (POM indicating transgressive system tract), HST (POM indicating high stand system tract). For lithological signature: see Fig. 3.

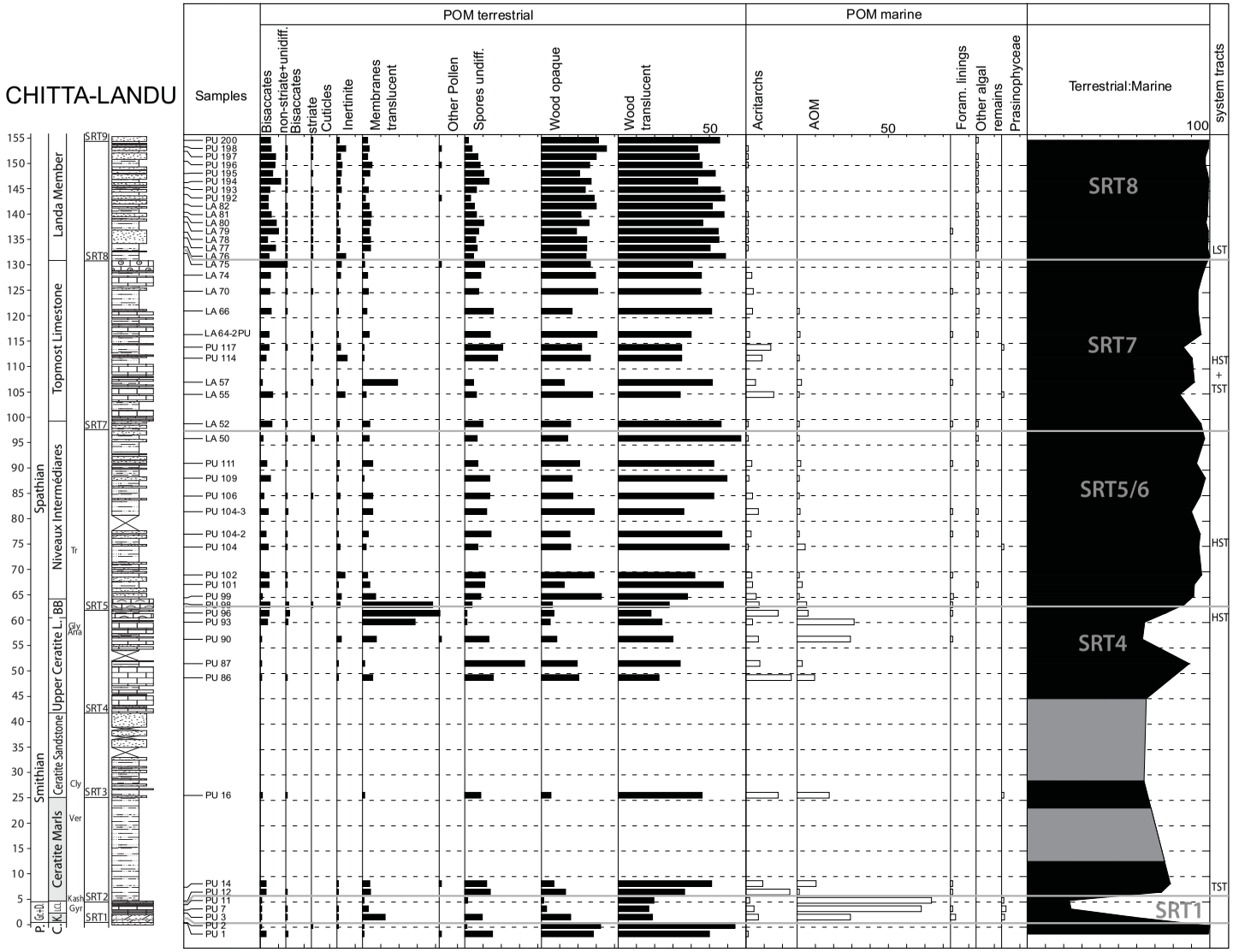

Supplementary Figure 3: Detailed palynofacies of Chitta-Landu with relative abundances of individual organic particle categories. The ratio of terrestrial (black) to marine (white) is given with sequence stratigraphic interpretation. C1 – C5 correspond to TR-cycles mentioned in the text. LST (POM indicating lowstand system tract), TST (POM indicating transgressive system tract), HST (POM indicating high stand system tract). For lithological signature see: Fig.

Chapter 3:

Climatic oscillations at the onset of the Mesozoic inferred from palynological records from the North Indian Margin

with Peter A. Hochuli, Hugo Bucher, Thomas Brühwiler, Michael Hautmann, David Ware, Helmut Weissert, Ghazala Roohi, Aamir Yaseen, Khalil-ur-Rehman

submitted to the Journal of the Geological Society of London

The beginning of the Mesozoic - the Early Triassic - is characterised by several ecological perturbations following the end-Permian mass extinction. They are reflected in multiple C-isotope excursions coupled with change in climate.

Here we present palynological data from two accurately dated mixed siliciclastic-carbonate sections from the Northern Indian Margin (Pakistan and South Tibet). The spore-pollen ratios, used as a proxy for climatic changes (humidity), indicate several distinct climatic shifts, which are closely related to C-isotope excursions. Comparison with the palynological data from the Barents Sea and other proxies reveal that the profound climatic change around the Smithian/Spathian boundary represents a global event, which affected also the northern mid-latitudes and coincides with an ammonoid and conodont major extinction event. The climatic boundary conditions for the Early Triassic were given by persistent monsoon circulation. Comparison with climate model simulations reveals that the climatic shifts were probably induced by orbital cycles and/or increased greenhouse gas concentration due to recurring volcanic pulses. Our data strongly support a link between C-isotope excursions, climatic changes and biotic responses such as ammonoid and conodont recovery patterns.

Keywords: Early Triassic, climate change, spore-pollen, carbon isotope excursions

1. Introduction

The Early Triassic is a peculiar time interval during which marine biota started to recover from the end-Permian mass extinction. It is marked by recurrent high magnitude excursions in organic and inorganic carbon isotope records, which record changes in global carbon cycling and coupled perturbation of climate and of marine and terrestrial environments. It is often assumed that recurring volcanic pulses of the Siberian Traps were responsible for the C-isotope excursions (Ovtcharova et al., 2006; Payne and Kump, 2007) and climatic variability (Galfetti et al., 2007b).

One of the few stable elements of this time interval was the palaeogeographic persistence of the supercontinent Pangaea extending almost from pole to pole (e.g. Ziegler et al., 1983). The latitudinal arrangement of the merged continents disrupted the atmospheric zonal circulation and the huge landmasses in northern and southern mid-latitude determined climatic conditions combined with the tropical Tethys as moisture source (Parrish, 1993). Climate models and sensitivity experiments demonstrated that Pangaean palaeogeography provided the disposition for a monsoonal circulation with strong seasonality of temperatures and rainfall (e. g. Gibbs et al., 2002; Kutzbach and Gallimore, 1989; Parrish, 1993). The main features of this monsoon system were a strong seasonality with distinct northern and southern intertropical convergence zones (Fig. 1) causing seasonal rainfall maxima on the Tethyan coasts on both hemispheres during summer and seasonal aridity in the mid-latitude continent interior on the winter-hemisphere. Besides the western Pangaea coast, where the strong monsoon circulation reversed the easterlies and drew moisture into the continent interior, the tropics were all-year arid. Moist conditions prevailed in middle and high latitudes year-round with winter rainfall maximum in western mid-latitudes (Kutzbach and Gallimore, 1989; Parrish, 1993). These models are based on simplifications with respect to palaeogeography, geographic resolution, vegetation feedback and dynamic ocean/atmosphere coupling; however, they give a reasonable overview of the global climatic conditions during the Early Triassic (Kutzbach, 1994; Kutzbach and Gallimore, 1989). Models incorporating mountain ranges and inland lakes simulate the same basic monsoon circulation, however, with increased humidity in the tropics and extenuated seasonal temperature extremes of the continent's interiors (as modelled for the Late Permian by Kutzbach and Ziegler, 1993). Evidence for the monsoonal circulation can be inferred from various sedimentary records. Red beds are assumed to indicate areas with seasonal rainfall (Parrish, 1993). Ziegler et al. (2003) established a zone of high evaporation in the tropics by mapping the global distribution of evaporites, reef carbonate, and coals deposits (see also Scotese, 2001) (Fig. 1). General palaeophytogeographic considerations, however based on Permian floras, also support the proposed climate models (Gibbs et al., 2002; Rees et al., 2002).

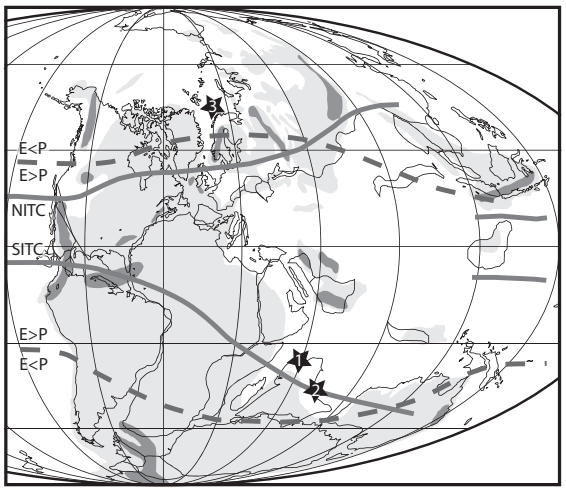

Figure 1: Palaeogeography of Pangaea in the Early Triassic after Golonka and Ford (2000); Smith et al., (1994). 1) Pakistan, 2) South Tibet, 3) Norway. Precipitation/Evaporation ratio (P<E, P>E) after Ziegler et al. (2003). Northern and Southern intertropical convergence zones (NITC, SITC) after Kutzbach and Gallimore (1989).

However, new palaeontological and isotope data suggest that Early Triassic climate might have

been more variable than generally assumed. Considerable climatic oscillations have been suggested based on palynological and faunal evidence (Brayard et al., 2005; 2006; Galfetti et al., 2007b; Hochuli and Vigran, 2010; Hochuli et al., 2010; Mutti and Weissert, 1995). In this paper we present palynological data from the Early Triassic of the North Indian Margin (NIM) suggesting climatic oscillations in the subtropics of the southern hemisphere. The high resolution data are based on excellently preserved material from the Salt Range and Surghar Range sections in Pakistan, which represent the reference area for the Early Triassic of the Tethyan realm and the subtropical Gondwana. Additional data from the Tulong area (South Tibet) support the records from Pakistan. The area offers the rare opportunity to study the recovery of marine and terrestrial biota after the end-Permian mass extinction in the same sections.

2. Geological setting - Methods

The studied sections are part of a mixed carbonate-siliciclastic system deposited on the NIM (southern Tethys coast, Fig. 1). The sections form the Salt Range and Surghar Range (Pakistan) were situated about 30°S (Golonka and Ford, 2000; Smith et al., 1994). The Tulong section (South Tibet) was located southeast of Pakistan, about 40°S (Ogg and von Rad, 1994) (Fig. 1). Clastic sediments and terrestrial organic matter were shed from the Indian subcontinent (Northern Gondwanan shelf) into the basin.

In the Salt Range and Surghar Range, the Early to Middle Triassic mixed siliciclastic- carbonate sediments are represented by the Chhidru, Mianwali and the Tredian Formations. The detailed ammonoid age control of the outcrops (Brühwiler et al., 2010 in press) allowed establishing a composite section of the localities of the Chhidru gorge, Narmia and Nammal gorge and Chitta-Landu gorges. In this paper we present a complete palynological succession compiled from these sections.

The Chhidru Formation consists of limestone and sandstone with intercalated siltstones. It was dated as late Wuchiapingian based on brachiopods and foraminifera (Pakistani-Japanese Research Group, 1985). Our study of the uppermost part of the Chhidru Formation reveals palynological assemblages with Permian as well as Griesbachian affinities (Hermann et al., in press). The basal Mianwali Formation is dominated by dolomites and limestone and has been dated as middle to late Griesbachian based on ammonoids. It is followed by an alternation of siltstone and limestone rich in ammonoid faunas of Dienerian age. The early Smithian interval is dominated by siltstones, which are replaced by sandstone-siltstone and siltstone-limestone alternations in the middle and late Smithian. The early Spathian siliciclastics sequence is overlain by fossil-rich limestones of late Spathian age. The Anisian Tredian Formation is again characterised by a predominant siltstone/sandstone alternation. The sedimentary organic material is mainly of terrestrial origin, thermally unaltered, and exceptionally well preserved (Hermann et al., in press).

The studied composite section of the Tulong area in South Tibet comprises the interval from the Permian up to the Early-Middle Triassic boundary (Brühwiler et al., 2009). The mixed siliciclastic-carbonate lithologies are very similar to those described from the Salt Range and Surghar Range. The Griesbachian consists of dolomites and is followed by thin-bedded, ammonoid-rich limestones in the early Dienerian and shales and siltstones from the late Dienerian up to the early Smithian.

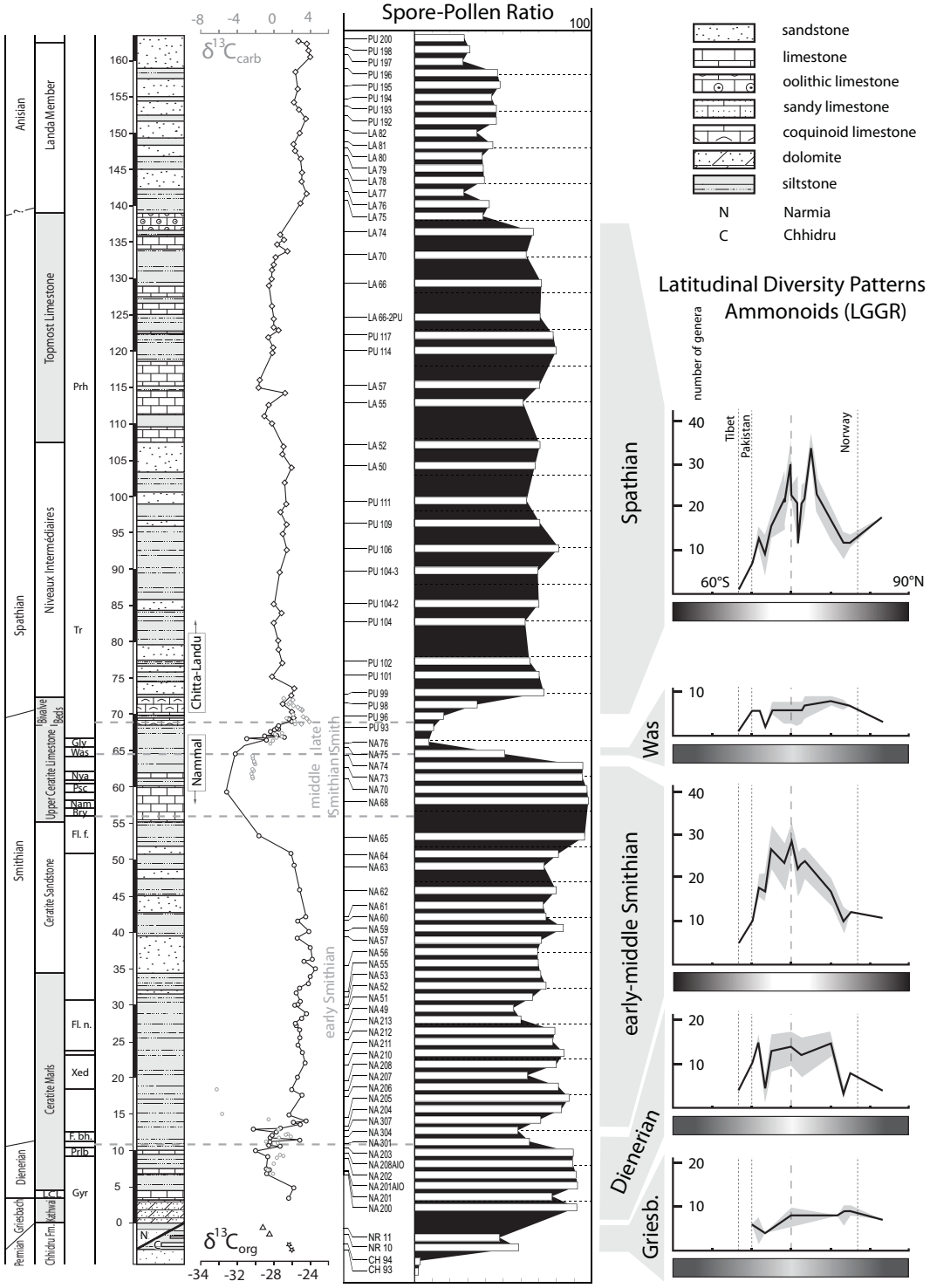

Figure 2: Palynological and carbon isotope record of Pakistan. Ammonoid zones after Brühwiler et al. (2010 in press), Guex (1978), and ongoing work of Bucher, H. and Ware, D.: Prh = Prohungarites beds; Tr = Tirolites beds; löschen: Pcl = Procolumbites beds; Gly = Glyptophiceras sinatum beds; Was = Wasatchites distractus beds; Nya = Nyalamites angustecostatus beds; Psc = Pseudoceltites multiplicatus beds; Nam = Nammalites pilatoides beds; Bry = Brayardites compressus beds; Fl. f. = Flemingites flemingianus beds; Fl. n. = Flemingites nanus beds; Xed = Xenodiscoides perplicatus beds; F. bh. Flemingites bhargavai beds; Prbl. = Prionolobus rotundatus beds; Gyr = Gyronites beds; Smithian subdivision after Brühwiler et al. (submitted). Latitudinal diversity patterns of ammonoids (LGGR) after Brayard et al. (2006). Carbon isotopes after Hermann et al. (in press).

The middle-late Smithian consists of fossil-rich limestones, which are overlain by early Spathian shales. The two major shale intervals (early Smithian and early Spathian) have been sampled for palynology. Brown to black colored palynomorphs indicate a high thermal maturity of the organic matter (Brühwiler et al., 2009).

The chronological timeframe is provided by high resolution ammonoid biostratigraphy (Brühwiler et al., 2009; 2010; 2010 in press; ongoing work Bucher, H.; Ware, D) and carbon isotope chemostratigraphy (Hermann et al., in press). The C-isotope records of the studied sections are closely comparable to the patterns known from various other Early Triassic sections (e. g. Atudorei, 1999; Galfetti et al., 2007a; Payne et al., 2004) providing an excellent tool to correlate and compare the sections.

3. Results

The spore-pollen ratio of the subtropical palynological records from the Salt Range and Surghar Range is displayed in Fig. 2. Data from Tulong and the correlation of the Pakistani and Norwegian sections are presented in the Supplementary Data Fig. S 1. In the Salt Range and Surghar Range two markedly different assemblages occur in the uppermost part of the Chhidru Formation: One of these assemblages contains typical Permian floral elements, dominated by conifer and pteridosperm pollen with rare spores (< 5%). In contrast, the Griesbachian assemblages are dominated by lycopod spores (up to 60%). The assemblages of Dienerian age are characterised by further increase of spores (up to 80%). From the Dienerian-Smithian boundary onwards spore pollen ratios show oscillations between spore dominated and pollen dominated assemblages combined with a general trend of pollen abundance increase, which reaches up to (55%). This trend is reversed above the top of the *Flemingites nanus* beds (Fig. 2, Fl. n.). Spore dominance increases up-section up to the middle Smithian, where it reaches up to 95 % in the interval between the *Flemingites flemingianus* and *Nyalamites angustecostatu*s beds (Brühwiler et al., 2010 in press). An abrupt change from spore-dominated to pollen-dominated assemblages occurs in the upper Smithian, across the *Wasatchites distractus* beds. After the peak abundance of pollen (90%), percentages of spores increase again up-section to level off at around 65% in the Spathian. The onset of the Middle Triassic (Anisian Tredian Formation) is characterised by relatively low spore contents (around 45%).

The Tulong section has been sampled at a lower resolution; the scarcity of limestones within the two sampled shale intervals does not allow a detailed ammonoid age control, thus a detailed correlation with the Pakistan record is not feasible. However, the *Wasatchites distractus* beds are clearly developed and two distinct palynological assemblages have been recovered from the two major shale intervals. The assemblages from the Smithian shale interval below the *Wasatchites distractus* beds contain up to 80 -90% spores with a slight increasing trend up-section. In the assemblages from the Spathian shales immediately above the *Wasatchites distractus* beds spore contents are reduced to about 30-60%.

4. Spore-pollen ratios and inferred climatic changes

Since Early Triassic sporomorphs are difficult to assign to individual plant taxa and therefore limiting the possibility of ecological reconstructions we use spore-pollen ratios as a proxy for water availability for terrestrial plants. Physiological characteristics of the two major plant groups, pteridophytes and gymnosperms, are determined by their ecological requirements such as water availability. From the dominance of pteridophyte spores we infer at least seasonally humid conditions and form the dominance of gymnosperms dry conditions similar to the differentiation of hygrophytes and xerophytes used by other authors (Visscher and van der

Zwan, 1981). Limits of the application of the spore-pollen ratio are described in the Supplementary Data. In the studied interval the spore fraction mainly consists of cavate trilete and cavate monolete spores derived from lycopods. Smooth and ornamented spores are also commonly present; they are assigned to Equisetales and Filicopsids. The rare alete spores are associated with bryophytes. Pollen assemblages are dominated by bisaccate pollen derived from conifers and seed ferns. Other pollen groups are rare, e.g. monosaccate (conifers), monosulcate pollen grains of heterogeneous origin, and Circumpolles (conifers).

Early Triassic climatic models suggest seasonal precipitation for the NIM determined by monsoon circulation. The described spore-pollen ratios document climatic oscillations and improve our view of the environmental/climatic conditions of this area. The pollen dominated Permian assemblages indicate comparatively dry climates. The increased spore contents of the Griesbachian assemblages, however, point toward increased humidity during this time interval. Within the same time interval the values of bulk organic C-isotopes shift from values around -26‰ in the Permian to values in the order of -29‰ in the Griesbachian, suggesting a stratigraphic level near the negative carbon isotope peak marking Permian-Triassic boundary sections worldwide. Very humid conditions are reflected in the spore dominated Dienerian assemblages from Pakistan as well as in the early Smithian shale interval of the Tulong area. In the Salt Range and the Surghar Range a change in the palynological assemblages at the Dienerian-Smithian boundary marks the onset of a trend towards more arid conditions modified by small scaled humidity oscillations (Fig. 2). At this boundary $\delta^{13}C_{org}$ values shift from about -28‰ to about -25‰. Subsequently $\delta^{13}C_{org}$ values continue to increase slightly to -24‰. In the Salt Range and Surghar Range area, between the $\delta^{13}C_{org}$ maximum (-24‰) and the top of the *Flemingites nanus* beds the palynological trend is reversed and increasing spore abundances suggest humidity increase. Synchronously $\delta^{13}C_{org}$ values decrease gradually. The most humid conditions can be inferred from highest spore contents in the late Smithian below the *Wasatchites distractus* beds. Above the *Wasatchites distractus* beds the extreme reduction of spore abundance suggests a dramatic aridity increase. It coincides with the onset of the positive shift in the organic and inorganic carbon isotope records ($\delta^{13}C_{org}$: -32‰ to -26‰ and $\delta^{13}C_{carb}$: -2‰ to 4‰). Compared to the Smithian, the Spathian assemblages show generally more stable and arid conditions, up-section increasing spore abundances suggest a slight humidity increase. At Tulong, spore contents of the assemblages from the Spathian shale interval point towards even dryer conditions. In the Salt Range and Surghar Range, Spathian $\delta^{13}C_{org}$ values range around -28‰ up to another positive shift of about 3‰, which marks the Spathian/Anisian boundary. The associated decrease in spore abundance suggests another aridity increase.

5. Discussion

The end-Permian extinction event is often assumed to have affected terrestrial ecosystems dramatically; leaving devastated areas in the Early Triassic, which were only habitable for opportunistic plant taxa (Retallack 1995; 1997; Looy et al., 2001). Recovery of terrestrial ecosystems was thought to have lasted until the middle Triassic (Retallack, 1995; Looy et al., 1999). However, palynological data from the Griesbachian of mid latitudinal sites (Norway, Australia, Antarctica?) are exceptionally diverse and at variance with the view of a devastated flora (Hochuli et al., 2010; de Jersey, 1979; Lindström and Mc Loughlin, 2007). They also imply that the observed global floral patterns in the Early Triassic are primarily determined by climatic conditions rather than by the loss of entire plant clades. During the Early Triassic large parts of Pangaea interiors were rather dry and inhibited development of diverse plant communities whereas climatic conditions in coastal areas and mid-latitudes allowed proliferating terrestrial

ecosystems. Here we presented the spore-pollen ratios from the NIM, which reflect changes in the net water balance i. e. changes in the balance between evaporation and precipitation. According to climate models the climate of this area was determined by the monsoonal circulation and characterised by high seasonality of precipitation (Kutzbach and Gallimore, 1989). A record with similar stratigraphic resolution has been described from the Barents Sea, Norway (Galfetti et al., 2007b; Hochuli and Vigran, 2010). These authors used the xerophyte/ hygrophyte ratio as a proxy for changes in humidity. The spore-pollen ratio used in this study is almost identical to the xerophyte/ hygrophyte ratio but less afflicted with uncertain palaeobotanical interpretations. The Barents Sea area (Norway) was situated in the northern mid-latitudes and its climate was characterised by year-round humid conditions (Kutzbach and Gallimore, 1989). Nevertheless the palynological data also reflect a similar palynological shift across the *Wasatchites* beds boundary associated with the onset of a positive C-isotope shift (supplementary Fig.). This coeval change in the composition of the sporomorph assemblages coincides with a distinct faunal turnover featuring a mass extinction of ammonoids and conodonts (Brayard et al., 2005; 2006; Orchard, 2007). The late Smithian extinction event represents the most significant biotic turnover until the end-Triassic mass extinction. Ammonoids and conodonts belong to the rare marine clades that recovered rather quickly from the end-Permian extinction, but suffered a great diversity reduction during the late Smithian. The cosmopolitan *Wasatchites* fauna characterises this interval of reduced diversity. This implies that the observed climatic change in the palynological records from the NIM and the Barents Sea corresponds to a global environmental and climatic change in distant palaeogeographic regions. This finding raises several questions: Which environmental feature can trigger a change in the evaporation/precipitation ratio in such distant localities under different palaeogeographic and climatic premises? And concerning the NIM: What factors influence the intensity of the monsoon in a stable palaeogeographic situation?

5.1 Ammonoid palaeobiogeography

Global temperature and latitudinal temperature gradients influence global and regional evaporation patterns and in the case of land-sea temperature gradients also monsoon intensity. Evidence for sea-surface temperature changes is suggested by the palaeobiogeographic distribution of ammonoids. Their distribution and diversity in space and time, introduced as latitudinal gradient of generic richness (LGGR), have been interpreted to reflect latitudinal sea surface temperature gradients (SSTG) (Brayard et al., 2005; Brayard et al., 2006) (Fig. 2). The low LGGR in the Griesbachian was initially interpreted as being induced by a warm equable global climate corresponding to flat SSTG. However, the low diversity and cosmopolitanism of Griesbachian ammonoids also represents the effect of the mass extinction, and may not univocally be the product of a warm and equal climate. Both effects may be combined and virtually impossible to disentangle without additional independent evidence. However palynological data with increased spore abundances indicate increased humidity in this time interval. As opposed to the unclear Griesbachian case, the rise of a LGGR from the Dienerian on unambiguously supports the presence a steeped SSTG.

The LGGR of most of the Smithian points towards increased SSTG and therefore more differentiated climate. The palynological data however indicate increased aridity in the early Smithian and decreased aridity towards the late Smithian. As the global ammonoid data are compiled over the early and middle Smithian, further comparison with the highly resolved spore-pollen ratio is limited. Small scaled changes in the early Smithian spore-pollen assemblages indicate several climatic changes in this time interval. The late Smithian extinction event

induced the diversity reduction in ammonoids and conodonts as it is reflected in the flat LGGR of the *Wasachites* beds. The cosmopolitan ammonoid fauna of these beds indicates a very low SSTG and it coincides with the onset of a prominent positive $\delta^{13}C_{org}$ shift. The most distinct change of the spore-pollen ratio occurs across these *Wasatchites* beds (late Smithian).Associating warm climates with increased humidity would imply that the increasing relative spore abundance would reflect a warming trend within this interval. This would suggest the existence of a short hot period (*Wasatchites* beds), which was followed by a rapid drop of temperatures leading to cooler and dryer conditions in the Spathian. For Permian sedimentary and $\delta^{13}C_{org}$ records from Australia, Birgenheier et al., (2010) demonstrated the existence of a strong correlation between positive bulk organic C-isotope shifts and the onset of glacial intervals. For our record this correlation implies that the Early Triassic greenhouse climate was not persistently hot and dry, as commonly postulated, but showed marked oscillations in temperature and humidity especially at the Smithian-Spathian boundary.

5.2 Volcanism

Global temperature changes might be induced by changes of insolation intensity and greenhouse gas concentration. In the following we discuss firstly how volcanism might have influenced the climate system and secondly how the monsoon circulation may respond to orbital forced insolation changes.

The Siberian Traps are widely assumed to be the driving force of the end Permian mass extinction (Renne et al., 1995), for enhanced global warming (Kidder and Worsley, 2004) and for recurrent carbon cycle perturbations in the Early Triassic (Ovtcharova et al., 2006; Payne and Kump, 2007). Volcanism can affect climate in two different ways, firstly by releasing large amounts of the greenhouse gas CO_2 it can trigger global warming. Secondly it can cause cooling by the release of aerosols reducing insolation or by an increased draw-down of pCO_2 through enhanced primary productivity stimulated by increased iron availability from silicic volcanic ashes or through enhanced silicate weathering (Cather et al., 2002; Goddéris et al., 2008). As there is no evidence for explosive silicic volcanic activity during Siberian trap emplacement (Bryan et al., 2002) we consider only the possible effects of increased atmospheric CO_2 concentrations, which has long been recognised as a climate driver (e.g. Kump, 2002). Pangaea sensitivity experiments with a fivefold increase of pCO_2 predicted increased global annual land surface temperatures and amplified seasonal temperature extremes in continent interiors by several degrees, even if luminosity is reduced by 1%. However, these changes do not influence the balance between precipitation and evaporation but intensify the hydrological cycle (Kutzbach and Gallimore, 1989). For the ecosystems of both areas, Barents Sea area and NIM, this implies increased annual temperatures, precipitation and evaporation. Coupled atmosphere/ocean models simulate increased high latitude sea surface temperatures (Kutzbach et al., 1990) resulting in low sea surface temperature gradients for a fivefold increase of pCO_2. This may strengthen the role of the high latitude sea surfaces as moisture source for adjacent land areas. Low SSTG caused by volcanic greenhouse gas release has also been postulated for the late Smithian (*Wasatchites* beds), prior to the significant drop in humidity as indicated by the palynological data (Galfetti et al., 2007b). Increased greenhouse gas concentration alone does not explain the humidity changes that are inferred from the palynological records of Norway and the NIM, but it may enhance the sensitivity of the global climate system.

5.3 Orbital forcing

Orbitally forced changes of seasonal insolation intensity cause increased seasonality when perihelion occurs in the summer hemisphere. Seasonal temperature differences are bound to

increase and the land-sea temperature contrast to intensify, and profoundly affecting the monsoon circulation (Kutzbach, 1994). For the hemisphere with increased seasonality (perihelion in summer) climate models simulate increased rainfall and runoff in the tropics, subtropical continental interiors, and along the Tethyan coast. In areas on the hemisphere with reduced seasonality, rainfall and runoff decreases (Kutzbach, 1994).

For the subtropical NIM sections (Pakistan and South Tibet) this implies increased seasonality, with increased precipitation and runoff for periods when perihelion occurs in the southern hemisphere summer. For mid-latitudes on both hemispheres these models predict only minor changes in precipitation and runoff, but temperatures in mid-latitudinal continent interiors are thought to increase on the hemisphere with increased seasonality. Therefore, orbitally forced insolation changes should have minor or no effect on the climate of the Norwegian sites. Thus, the observed changes in the Norwegian records cannot be explained by insolation changes due to precession cycles. However, the considered climate simulations and frequency analyses (Kutzbach, 1994; Olsen and Kent, 1996) did not include obliquity cycles, which influence annual and seasonal insolation, especially in higher latitudes, and could explain the observed climatic changes in the Norwegian record.

Astronomically controlled changes in precipitation and evaporation have been documented in the lacustrine sedimentary record of the Late Triassic Newark Group. Besides high frequency cycles low frequency eccentricity cycles with a period time of ~2 Ma have been documented (Olsen and Kent, 1996). Eccentricity affects insolation by modulating the precession cycle (Clemens and Tiedemann, 1997). Therefore, the climatic signal recorded in the Newark Group reflects a combined signal of precession and eccentricity cycles (Olsen and Kent, 1996) and can be compared to the orbitally forced climatic changes modelled by Kutzbach (1994).

The limited resolution of the studied records hampers the recognition of orbital periodicities or the performance of a frequency analysis to test any orbital forcing of the Early Triassic climate. Hence, a comparison with the modelled climatic changes induced by precessional cycles is difficult. However, cyclicity might be detected in our data by the fact that the climate record of the Salt Range and the Surghar Range starts off with dry conditions in the Late Permian and reaches similar condition after about 2.1 Ma at the Smithian-Spathian boundary, and again about 2.4 Ma later around the Spathian-Anisian boundary. Even periodicities with higher frequencies might be reflected in the distinct pattern of the spore-pollen ratios in the early Smithian indicating oscillating humidity changes.

Orbitally forced changes of seasonal insolation alone does not explain the inferred climatic changes in both distant regions (NIM and Norway), but it has the potential to explain the observed changes on the NIM. Most probably a combination of several factors (pCO_2 increase and orbital forcing) induced the climatic oscillation in the Early Triassic.

6. Conclusions

The Early Triassic palynological data from Pakistan and South Tibet document changes in the spore-pollen record, which are interpreted to reflect humidity changes within a climate system determined by monsoon circulation. These climatic changes coincide with or might be closely related to C-isotope variations such as the positive shifts at the Dienerian-Smithian boundary, the Smithian-Spathian boundary, and the Spathian-Anisian boundary. Around these boundaries the palynological record suggests the onset of decreasing or abruptly reduced humidity. The drastic and synchronous changes in humidity, C-isotopes and diversity of ammonoids and conodonts at the Smithian Spathian boundary (Brayard et al., 2005; 2006; Orchard, 2007) in distant areas (NIM and Norway) imply a close relationship between environmental changes and

ecological responses. Considering the distance and the synchronicity of events implies that the trigger of these changes acted globally.

Volcanism and related greenhouse gas releases might have increased the sensitivity of the climate system. Recurring CO_2 releases are reflected in the Early Triassic C-isotope perturbations probably by late protracted pulses of the Siberian Trap emplacement (Ovtcharova et al., 2006; Payne and Kump, 2007). Despite an inappropriate resolution our data suggest a combination of changing greenhouse gas concentration and orbital forcing as the most plausible causes for the observed Early Triassic climatic changes on the NIM and Norway.

Acknowledgments

We acknowledge financial support from the Swiss National Science Foundation project 200020-127716/1 (to H. Bucher).

Appendix A. Supplementary material

Supplementary data associated with this article can be found on page 73.

References

Atudorei, V., 1999, Constraints on the Upper Permian to Upper Triassic marine carbon isotope curve. Case studies from the Tethys [PhD Thesis], University of Lausanne, Switzerland, 161 pp.

Birgenheier, L.P., Frank, T.D., Fielding, C.R., and Rygel, M.C., 2010, Coupled carbon isotopic and sedimentological records from the Permian system of eastern Australia reveal the response of atmospheric carbon dioxide to glacial growth and decay during the late Palaeozoic Ice Age. Palaeogeography, Palaeoclimatoloy, Palaeoecology, v. 286, p. 178-193.

Brayard, A., Bucher, H., Escarguel, G., Fluteau, F., Bourquin, S., and Galfetti, T., 2006, The Early Triassic ammonoid recovery: Paleoclimatic significance of diversity gradients. Palaeogeography, Palaeoclimatoloy, Palaeoecology, v. 239, p. 374-395.

Brayard, A., Escarguel, G., and Bucher, H., 2005, Latitudinal gradient of taxonomic richness: combined outcome of temperature and geographic mid-domains effects?, Journal of Zoological Systematics and Evolutionary Research, v. 43, p. 178-188.

Brühwiler, T., Bucher, H., Brayard, A., and Goudemand, N., submitted to Palaeogeography, Palaeoclimatology, Palaeoecology, High-resolution biochronology and diversity dynamics of the Early Triassic ammonoid recovery: the Smithian faunas of the Northern Indian Margin.

Brühwiler, T., Bucher, H., and Goudemand, N., 2010, Smithian (Early Triassic) ammonoids from Tulong, South Tibet, Geobios, v. 43, p. 403-431.

Brühwiler, T., Bucher, H., Ware, D., Hermann, E., Hochuli, P.A., Roohi, G., ur-Rehman, and K., Yaseen, A., 2010 in press, Smithian (Early Triassic) ammonoids from the Salt Range, Pakistan, Special Papers in Palaeontology

Brühwiler, T., Goudemand, N., Galfetti, T., Bucher, H., Baud, A., Ware, D., Hermann, E., Hochuli, P.A., and Martini, R., 2009, The Lower Triassic sedimentary and carbon isotope records from Tulong (South Tibet) and their significance for Tethyan palaeoceanography. Sedimentary Geology, v. 222, p. 314-332.

Bryan, S.E., Riley, T.R., Jerram, D.A., Stephens, C.J., and Leat, P.T., 2002, Silicic volcanism: An undervalued component of large igneous provinces and volcanic rifted margins, in: Menzies, M.A., Klemperer, S.L., Ebinger, and C.J., and Baker, J. (Eds.), Volcanic Rifted Margins. Boulder, Colorado, Geological Society of America Special Paper 362, p. 97-118.

Cather, S.M., Dunbar, N.W., McDowell, F.W., McIntosh, W.C., and Scholle, P.A., 2009, Climate forcing by iron fertilization from repeated ignimbrite eruptions: The icehouse-silicic large igneous province (SLIP) hypothesis, Geosphere, v. 5, p. 315-324.

De Jersey, N.J., 1979, Palynology of the Permian-Triassic transition in the Western Bowen

Basin, Geological Survey of Queensland publication, v. 374, 67 pp.

Galfetti, T., Bucher, H., Brayard, A., Hochuli, P.A., Weissert, H., Goudun, K., Atudorei, V., and Guex, J., 2007a, Late Early Triassic climate change: Insights from a carbonate carbon isotopes, sedimentary evolution and ammonoid paleobiogeography, Palaeogeography, Palaeoclimatoloy, Palaeoecology, v. 243, p. 394-411.

Galfetti, T., Hochuli, P.A., Brayard, A., Bucher, H., Weissert, H., and Vigran, J.O., 2007b, Smithian/Spathian boundary event: Evidence for global climatic change in the wake of the end-Permian biotic crisis, Geology, v. 35, p. 291-294.

Gibbs, M.T., Rees, P., Kutzbach, J.E., Ziegler, A.M., Behling, P.J., and Rowley, D.B., 2002. Simulations of Permian climate and comparisons with climate-sensitive sediments, The Journal of Geology, v. 110, p. 33-55.

Goddéris, Y., Donnadieu, Y., de Vargas, C., Pierrehumbert, R.T., Dromart, G., and van de Schootbrugge, B., 2008, Causal or casual link between the rise of nannoplankton calcification and a tectonically-driven massive decrease in Late Triassic atmospheric CO_2?, Earth and Planetary Science Letters, v. 267, p. 247-244.

Golonka, J. and Ford, D., 2000, Pangaean (Late Carboniferous-Middle Jurassic) paleoenvironment and lithofacies, Palaeogeography, Palaeoclimatoloy, Palaeoecology, v. 161, p. 1-34.

Hermann, E., Hochuli, P.A., Méhay, S., Bucher, H., Brühwiler, T., Hautmann, M., Ware, D., Roohi, G., ur-Rehman, K., and Yaseen, A., in press. Organic matter and palaeoenvironmental signals during the Early Triassic biotic recovery: the Salt Range and Surghar Range records. Sedimentary Geology. doi:10.1016/j.sedgeo.2010.11.003.

Hochuli, P.A., and Vigran, J.O., 2010, Climate variations in the Boreal Triassic - Inferred from palynological records from the Barents Sea, Palaeogeography, Palaeoclimatoloy, Palaeoecology, v. 290, p.20-42.

Hochuli, P.A., Vigran, J.O., Hermann, E., and Bucher, H., 2010, Multiple climatic changes around the Permian Triassic boundary event revealed by an expanded palynological record from Mid Norway, GSA Bulletin, v. 122, p. 884-896.

Kidder, D.L. and Worsley, T.R., 2004, Causes and consequences of extreme Permo-Triassic warming to globally equable climate and relation to the Permo-Triassic extinction and recovery, Palaeogeography, Palaeoclimatoloy, Palaeoecology, v. 203, p. 207-237.

Kump, L.R., 2002, Reducing uncertainty about carbon dioxide as a climate driver, Nature, v. 419, p. 188-190.

Kutzbach, J.E., 1994, Idealized Pangean climates: Sensitivity to orbital change, in: Klein, G. D. (Ed.), Pangae: Paleoclimate, tectonics, and sedimentation during accretion, zenith and breakup of a supercontinent. Boulder, Colorado, Geological Society of America Special Paper 288, p. 41-55.

Kutzbach, J.E. and Gallimore, R.G., 1989, Pangaean climates: Megamonsoons of the megacontinent, Journaln of Geophysical Research, v. 94, p 3341-3357.

Kutzbach, J.E. and Ziegler, A.M., 1993, Simulation of Late Permian climate and biomes with an atmosphere-ocean model: comparisons with observations, Philosophical Transactions of the Royal Society of London. Series B, Biological Sciences, v. 341, p. 327-340.

Kutzbach, J.E., Guetter, P.J., and Washington, W.M., 1990, Simulated circulation of an idealized ocean for Pangaean time, Paleoceanography, v. 5, p. 299-317.

Lindström, S. and McLoughlin, S., 2007, Synchronous palynofloristic extinction and recovery after the end-Permian event in the Prince Charles Mountains, Antarctica: Implications for palynofloristic turnover across Gondwana, Review of Palaeobotany and Palynology, v. 145, p. 89-122.

Looy, C.V., Brugman, W.A., Dilcher, D.L. and Visscher, H., 1999, The delayed resurgence of equatorial forests after the Permian-Triassic ecologic crisis, Proceedings of the National Academy of Sciences of the United States of America, v. 96, p. 13857-13862.

Looy, C.V., Twitchett, R.J., Dilcher, D.L., Van Konijnenburg-Van Cittert, J.H.A., and Visscher, H., 2001, Life in the end-Permian dead zone, Proceedings of the National Academy of Sciences of the United States of America, v. 98, p. 7879-7883.

Mutti, M. and Weissert, H., 1995, Triassic Monsoonal Climate and its signature in Ladinian–Carnian carbonate platforms (Southern Alps, Italy), Journal of Sedimentary Research, v. 65, p. 357–367.

Ogg, J.G. and von Rad, U., 1994, The Triassic of the Thakkhola (Nepal). II: Paleolatitudes and Comparison with other Eastern Tethyan Margins of Gondwana. Geolische Rundschau, v. 83, p. 107-129.

Olsen, P.E. and Kent, D.V., 1996, Milankovitch climate forcing in the tropics of Pangaea during the Late Triassic, Palaeogeography, Palaeoclimatoloy, Palaeoecology, v. 122, p. 1-26.

Orchard, M.J., 2007, Conodont diversity and evolution through the latest Permian and Early Triassic upheavals, Palaeogeography, Palaeoclimatoloy, Palaeoecology, v. 252, p. 93-117.

Ovtcharova, M., Bucher, H., Schaltegger, U., Galfetti, T., Brayard, A., and Guex, J., 2006. New Early to Middle Triassic U-Pb ages from South China: Calibration with ammonoid biochronozones and implications for the timing of the Triassic biotic recovery, Earth and Planetary Science Letters, v. 243, p. 463-475.

Pakistani-Japanese Research Group, 1985, Permian and Triassic systems in the Salt Range and Surghar Range, Pakistan, in: Nakazawa, K., and Dickins, J.M., (Eds.), The Tethys: Her Paleogeography and Paleobiogeography from Paleozoic to Mesozoic, Tokai University Press, Tokyo, p. 221-312.

Parrish, J. T., 1993, Climate of the Supercontinent Pangea, The Journal of Geology, v. 101, p. 215-233.

Payne, J.L. and Kump, L.R., 2007, Evidence for recurrent Early Triassic massive volcanism from quantitative interpretation of carbon isotope fluctuations, Earth and Planetary Science Letters, v. 256, p. 264-277.

Payne, J.L., Lehrmann, D.J., Wei, J., Orchard, M.J., Schrag, D.P., and Knoll, A.H., 2004, Large pertubations of the carbon cycle during recovery from the end-Permian extinction, Science, v. 305, p. 506-509.

Rees, P., Ziegler, A.M., Gibbs, M.T., Kutzbach, J.E., Behling, P.J., and Rowley, D.B., 2002, Permian Phytogeographic Patterns and Climate Data/Model Comparison, The Journal of Geology, v. 110, p. 1-31.

Renne, P.R., Zhang, Z., Richards, M.A., Black, M.T., and Basu, A.R., 1995, Synchrony and causal relations between Permian-Triassic Boundary Crisis and Siberian Flood Volcanism, Science, v. 269, p. 1413-1416.

Retallack, G.J., 1995, Permian-Triassic life crisis on land, Science, v. 267, p. 77-80.

Retallack, G.J., 1997, Earliest Triassic origin of Isoetes and Quillwort evolutionary radiation, Journal of Paleontology, v. 71, p. 500-521.

Scotese, C. R., 2001. Atlas of Earth History, Volume 1, Paleogeography, PALEOMAP Project, Arlington, Texas, 52 pp

Smith, A.G., Smith, D.G., and Funnell, B.M., 1994, Atlas of Mesozoic and Cenozoic Coastlines. Cambridge University Press, Cambridge, 109 pp.

Visscher, H. and van der Zwan, C.J., 1981, Palynology of the circum-Mediterranean Triassic: Phytogeographical andpalaeoclimatological Implications, Geologische Rundschau, v. 70, p. 625-634.

Ziegler, A.M., Eshel, G., McAllister Rees, P., Rothfus, T.A., Rowley, D.B., and Sunderlin, D., 2003, Tracing the tropics across land and sea: Permian to present, Lethaia, v. 36, p. 227-254.

Ziegler, A.M. and Scotese, C.R., Barrett, S.F., 1983, Mesozoic and Cenozoic Paleogeographic Maps, in: Brosche, P., Sündermann, J. (Eds.), Tidal Friction and the Earth's Rotation II, Springer Verlag, Berlin p. 240-252.

Supplementary Data

Preparation Technique:

Samples (80 Salt Range and Surghar Range, Pakistan, 12 Tulong, South Tibet) were crushed and weighed (5-25 g) and subsequently treated with hydrochloric and hydrofluoric acid according to standard palynological preparation techniques (Traverse, 2007). A short oxidation with nitric acid was performed on the Pakistan samples. The Tibetan samples were additionally treated with Schulze's reagent. The residues were sieved with an 11 µm mesh screen. From strew mounts a minimum of 250 spores and pollen per sample were counted.

Limiting Factors

As the majority of sporomorphs are transported into the marine environment by rivers it is essential considering changes of the local hydrological regime and the depositional environment as these factors might be responsible for the observed changes in the palynological record, i. e. sporomorphs may be derived from different source areas. A possible source area bias can be minimised by including several parallel records from the same climatic and floral zone. For this study we included several sections from the Salt Range and the Surghar Range (Nammal, Chhidru and Chitta-Landu), which are and were located by a distance of about 60 km and about 1500 km for the Tulong section. For the Pakistani sections, measurements of palaeocurrent direction (ranging between NNE and NW at Nammal, Narmia, and Chhidru) indicate for the Mianwali Formation relatively stable sediment supply (Pakistani- Japanese Research Group, 1985). As an exceptional phase with counter currents seem to exist for the middle part of the Smithian (CS) in one section (Chhidru). The parallel records from Nammal, Chhidru and Chitta-Landu show similar trends in the composition of the spore-pollen assemblages indicating that they represent a genuine climatic signal rather than a random mixture influenced by hydrological features. Even in the Tulong section, probably separated from the Pakistani sections by 1500 km, we see the same change across the Smithian Spathian boundary.

Since spores and pollen behave differently during transport and deposition (Tyson, 1995) sea-level changes (i.e. proximity to shore) might also influence the composition of the palynomorph assemblages. For the Pakistani sections several sea level changes are documented in the sedimentary record and the particulate organic matter composition, which reflects the depositional environment such as the proximity to the shore (Hermann et al., submitted for publication). A comparison of the particulate organic matter record with the studied spore pollen record from Pakistan shows that there might be some bias caused by sea level changes but the changes in the two records are not synchronous. Therefore the spore pollen ratio can be regarded as "independent record" reflecting climatic changes.

References:

Brayard, A., Bucher, H., Escarguel, G., Fluteau, F., Bourquin, S., Galfetti, T., 2006. The Early Triassic ammonoid recovery: Paleoclimatic significance of diversity gradients. Palaeogeogr. Palaeoclimat., Palaeoecol. 239, 374-395.

Brühwiler, T., Bucher, H., Brayard, A., Goudemand, N., submitted to Palaeogeography, Palaeoclimatology, Palaeoecology. High-resolution biochronology and diversity dynamics of the Early Triassic ammonoid recovery: the Smithian faunas of the Northern Indian Margin.

Brühwiler, T., Bucher, H., Goudemand, N., 2010. Smithian (Early Triassic) ammonoids from Tulong, South Tibet: Geobios 43,403-431.

Brühwiler, T., Bucher, H., Ware, D., Hermann, E., Hochuli, P.A., Roohi, G., ur-Rehman, K., Yaseen, A., 2010 in press. Smithian (Early Triassic) ammonoids from the Salt Range, Pakistan. Spec. Pap. Palaeontol.

Brühwiler, T., Goudemand, N., Galfetti, T., Bucher, H., Baud, A., Ware, D., Hermann, E., Hochuli, P.A., Martini, R., 2009. The Lower Triassic sedimentary and carbon isotope records from Tulong (South Tibet) and their significance for Tethyan palaeoceanography. Sediment. Geol. 222, 314-332.

Galfetti, T., Hochuli, P.A., Brayard, A., Bucher, H., Weissert, H., Vigran, J.O., 2007. Smithian/Spathian boundary event: Evidence for global climatic change in the wake of the end-Permian biotic crisis. Geology 35, 291-294.

Guex, J., 1978. Le Trias intérieur des Salt Ranges (Pakistan): problèmes biochronologiques. Eclogae geologicae Helvetiae 71, 105-141.

Hermann, E., Hochuli, P.A., Méhay, S., Bucher, H., Brühwiler, T., Hautmann, M., Ware, D., Roohi, G., ur-Rehman, K., Yaseen, A., in press. Organic matter and palaeoenvironmental signals during the Early Triassic biotic recovery: the Salt Range and Surghar Range records. Sedimentary Geology, doi:10.1016/j.sedgeo.2010.11.003.

Pakistani-Japanese Research Group, 1985. Permian and Triassic systems in the Salt Range and Surghar Range, Pakistan, in Nakazawa, K., Dickins, J.M., (Eds.), in: The Tethys: Her Paleogeography and Paleobiogeography from Paleozoic to Mesozoic. Tokai University Press, Tokyo, p. 221-312.

Traverse, A., 2007. Paleopalynology. Springer, Dordrecht.

Tyson, R. V., 1995. Sedimentary organic matter - organic facies and palynofacies. Chapman & Hall, London.

Figure S 1: Correlation of the palynological records from Tibet, Pakistan and Norway. Ammonoid zones after Brühwiler et al. (2009; 2010; 2010 in press), Guex (1978) and ongoing work of Bucher and Ware. Prh = Prohungarites beds, Tr = Tirolites beds; Gly = Glyptophiceras sinatus beds; Was = Wasachites disctractus beds; Nya = Nyalamites angustecostatus beds; Psc = Pseudoceltites multiplicatus beds; Nam = Nammalites pilatoides beds; Bry = Brayarditescompressus beds; Fl. f. = Flemingites flemingianus beds; Fl. n. = Flemingites nanus; Xed = Xenodiscoides perplicatus beds; F. bh. Flemingites bhargavai beds; Prbl. = Prionolobus rotundatus beds; Gyr = Gyronites beds and Tibet ammonoid zones after Brühwiler et al., 2009. Hel = Hellenites beds; Par = Paragoceras beds; Fen = Fengshanites beds; alb = albanitid n. gen. beds; Col = Columbites beds; Nor = Nordophiceras beds; Owe = Owenites beds. Smithian subdivision after Brühwiler et al., (submitted). Latitudinal diversity patterns of ammonoids (LGGR) after Brayard et al. (2006). Carbon isotope data from Pakistan after Hermann et al. (in press). Paynological record and stratigraphy from Norway after Galfetti et al., 2007.

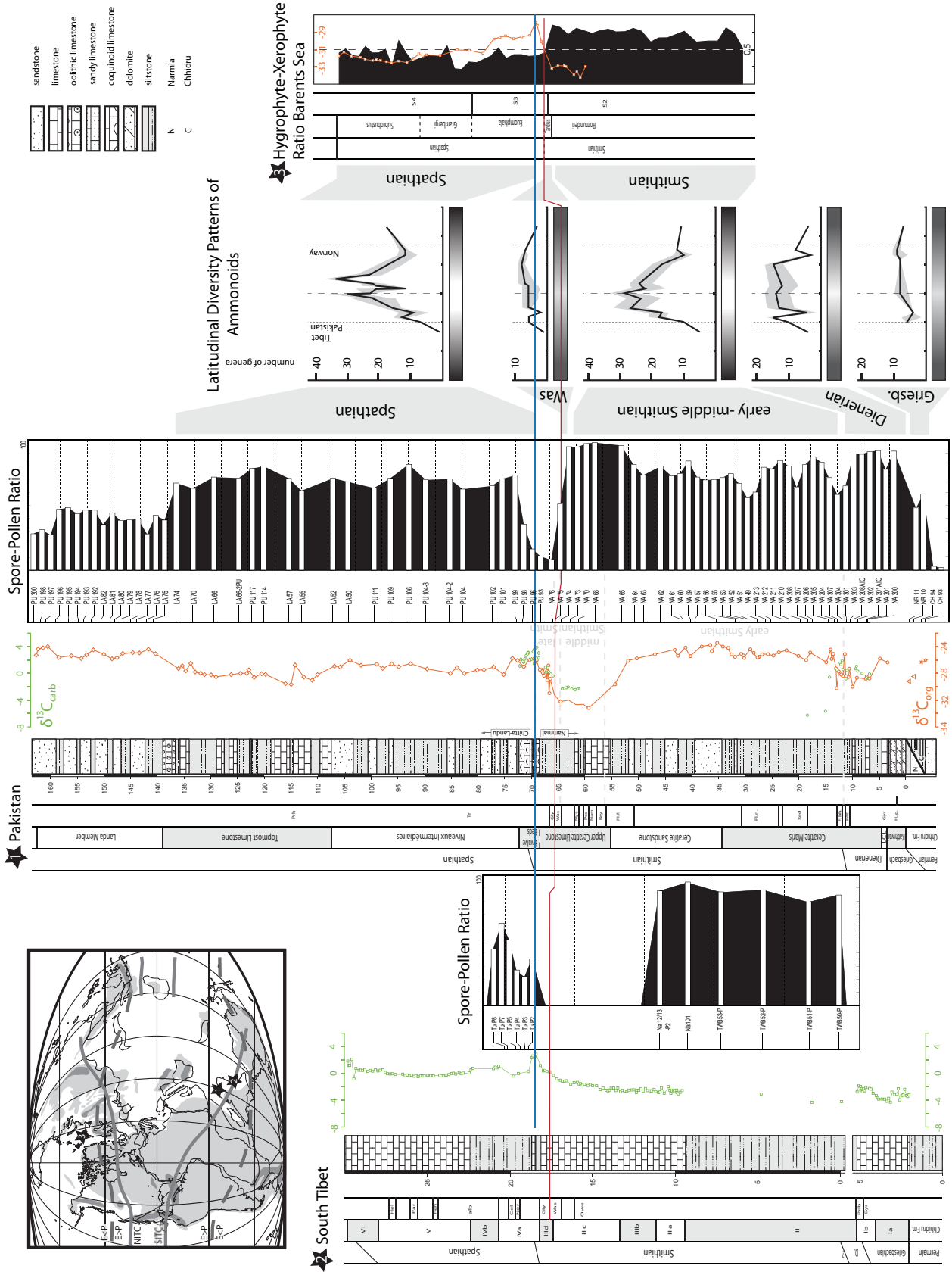
sandstone
limestone
oolithic limestone
sandy limestone
coquinoid limestone
dolomite
siltstone
N
C
Narmia
Chhidru
Hygrophyte-Xerophyte Ratio Barents Sea
Latitudinal Diversity Patterns of Ammonoids
number of genera
Tibet
Pakistan
Norway
Griesb.
Dienerian
early -middle Smithian
Was
Spathian
Smithian
Spathian
Spore-Pollen Ratio
Pakistan
Topmost Limestone
Niveaux intermédiaires
Upper Ceratite Limestone
Ceratite Sandstone
Ceratite Marls
Landa Member
Dienerian
Smithian
Spathian
Chidru Fm.
Kathmai
Gastach.
Permian
Spore-Pollen Ratio
South Tibet
Chidru Fm.
Permian
Griesbachian
Dienerian
Smithian
Spathian

Chapter 4:

Terrestrial ecosystems on North Gondwana in the aftermath of the end-Permian mass extinction

with Peter A. Hochuli, Hugo Bucher, Thomas Brühwiler, Michael Hautmann, David Ware, Ghazala Roohi

submitted to Gondwana Research

The impact of the end-Permian mass extinction on terrestrial ecosystems is still highly controversial. Here, new high-resolution palynological data from biostratigraphically well-dated Late Permian to Middle Triassic sections of the Salt Range and Surghar Range (Pakistan) are presented. Our results reveal seven successive floral phases between the Late Permian and the Middle Triassic. At the onset of the Mesozoic the flora is characterised by high abundances of lycopods associated with pteridosperms and conifers. This association prevails up to the middle Smithian and is followed by a prominent spore spike similar to the global spore spike reported from the Permian-Triassic boundary. Similar to the end-Permian spore spike the middle Smithian spore spike is associated with a negative isotope excursion and is succeeded by a major marine faunal extinction event in the late Smithian. The recurrent patterns observed at the Permian-Triassic boundary and in the middle-late Smithian suggest a common cause such as massive injections of gases of volcanic origin. The increasing abundance of conifers still associated with common lycopods in the Spathian suggests fading of volcanically induced environmental perturbations and stabilisation of terrestrial ecosystems ca. 2.1 Ma after the end-Permian event.

1. Introduction

The end-Permian mass extinction about 252 Ma ago was the largest crisis in the Phanerozoic history of marine life. However, the impact of this event on terrestrial plant communities is still debated and the views about the magnitude of the deterioration of terrestrial ecosystems are strongly diverging. The interpretations range from virtually no effects on terrestrial plants (e. g. Knoll, 1984; McElwain and Punyasena, 2007) to an almost complete devastation of terrestrial ecosystems (e. g. Utting et al., 2004; Visscher et al., 1996). The first hypotheses refers to a long-termed (25 Ma) gradual floristic transition across the Permian-Triassic boundary reflected in the fossil record by a gradual change from palaeophytic floras to mesophytic floras without evidence for a major plant biomass decay (Knoll, 1984). A long-term floristic turnover has been documented in the macrofossil data from the South African Karoo Basin. There, the diversity of the woody vegetation decreases already at the transition from the middle to the Late Permian. The succession of the Late Permian to Middle Triassic assemblages is marked by unchanged diversity and replacement of the glossopterids by other plant groups (cycads, benettitaleans, ginkgos and other seed ferns, Bamford, 2004). This does not exclude that ecosystems underwent significant short-term changes during the Palaeozoic-Mesozoic transition. To assess whether these short-term changes affected ecosystem functionality it is essential to incorporate abundance data and dominance structures of plant communities rather than relying solely on total biodiversity data (McElwain and Punyasena, 2007). Opposing scenarios relying on the so called fungal event (Visscher et al., 1996) instead advocate the total collapse of ecosystems after the end-Permian mass extinction. Some authors even attribute most of the Early Triassic palynofloral records to reworking (Utting et al., 2004).

The significance of palynofloral records for the reconstruction of terrestrial ecosystem responses to mass extinction has gained great attention in the last decades (e. g. Hochuli et al., 2010b; Looy et al., 1999; 2001; McLoughlin et al., 1997). Reviews of the floral records revealed that faunal mass extinctions are commonly associated with instabilities of terrestrial ecosystems (McElwain and Punyasena, 2007). The onsets of these instabilities are often marked by a short interval during which pteridophytes dominate terrestrial plant assemblages. The fern spike at the Cretaceous-Palaeogene boundary is assumed to represent the devastation of vegetation causes by the climatic and atmospheric perturbations of the impact event at this boundary (Vajda et al., 1999). High abundances of fern spores are also reported from the Triassic-Jurassic boundary (van de Schootbrugge et al., 2009). Pioneering studies documenting ecological perturbation around the Permian-Triassic boundary and in the Early Triassic have been published by Looy et al. (1999; 2001). They documented a spore peak close to the end-Permian extinction event in sections from Jameson Land in E-Greenland and inferred a great loss of plant diversity from their data. Furthermore they inferred that the recovery of plant communities took 4 – 5 Ma.

The aforementioned floral changes (spore spike) observed in the palynological records have been interpreted as responses of terrestrial ecosystems to palaeoenvironmental perturbations. For the Triassic-Jurassic spore spike Bonis et al. (2010) demonstrated that the high abundances of spores are related to climatic changes. Recent publications of Hochuli et al. (2010a; 2010b), and Lindström and McLoughlin (2007) also showed that the palynological turnover near the Permian-Triassic boundary are associated with changes in humidity. The striking recurrent patterns of high spore abundances, large perturbations of the global C-cycle and faunal mass extinctions suggest major and geologically rapid climatic changes affecting both marine and terrestrial biotas. The ultimate causes which triggered these global changes still need to be determined.

During the Late Permian and Triassic times, Gondwana provided a stable plate configuration

of the southern hemisphere continents that has established in the late Proterozoic and continued to exist until the Early Cretaceous (Comin-Chiaramonti et al., 2010; Meert and Liebermann, 2010; Renne et al., 1992). Despite the stable configuration of landmasses, physical environmental conditions fluctuated through time (Veevers, 2006) and environmental changes determined the Triassic vegetation history on Gondwana (Spalletti et al., 2003).

Here we present the composite palynological record from Nammal, Chhidru, Chitta-Landu, and Narmia in the Salt Range and Surghar Range in Pakistan (Fig. 1), spanning the latest Permian to early Middle Triassic time interval. The palynological assemblages record floral turnovers, which reflect profound changes of the composition of the terrestrial plant community. The detailed ammonoid age control of the studied sections allows a precise dating of the floral events. Our data provide detailed insights into terrestrial ecosystem turnovers associated with the environmental changes during the Palaeozoic-Mesozoic transition.

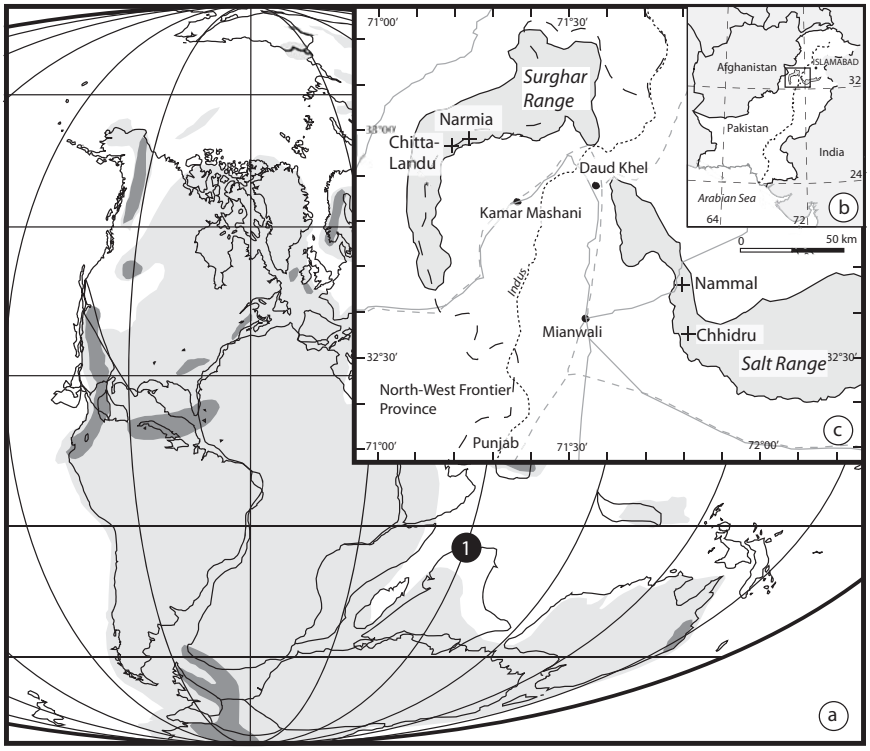

Figure 1. Location of the studied sites. a) Palaeogeographic position of the Salt Range and the Surghar Range in Pakistan after Smith et al., (1994) and Golonka and Ford, (2000) b) location of Nammal, Chhidru, Chitta-Landu, and Narmia gorge c) location of the Salt Range and Surghar Range in Pakistan.

2. Methods

Samples were preferably taken from the fine-grained siliciclastic intervals of the sections at Nammal, Chhidru, Chitta-Landu and Narmia. Siltstones and in few cases limestone and fine-grained sandstone have been sampled. The samples were crushed and weighed (5-25 g) and subsequently treated with hydrochloric and hydrofluoric acid according to standard palynological preparation techniques. A short oxidation with nitric acid was performed before the residues were sieved over an 11 µm mesh screen. From strew mounts a minimum of 300 spores and pollen per sample were counted. In few samples with high amorphous organic matter contents, low sporomorph concentration or poor preservation the intended 300 sporomorph counts could not be reached.

3. The palynological record and its significance

The excellently preserved organic walled microfossils at the Nammal, the Chhidru, the Chitta-Landu and the Narmia gorges in the Salt Range and Surghar Range allowed establishing a detailed succession of palynological assemblages for the first time. The assemblages range from the late Permian Chhidru Formation to the Early Triassic Mianwali Formation and the lower part of the Middle Triassic Tredian Formation and represent several distinct changes of the terrestrial ecosystem on North Gondwana within this time interval. Changes in the depositional environment and climatic conditions have been determined using sedimentological evidence, palynofacies and spore-pollen ratios (Hermann et al., subm.; in press).

In the quantitatively analysed palynological data seven floral phases have been distinguished, which are illustrated in Fig. 2 and referred to as numbers (1 to 7) in parentheses in the text. Permian assemblages (1) are characterised by high abundances of striate and non striate bisaccate pollen. These assemblages are substituted by spore rich assemblages of latest Permian to Griesbachian age (2), in which typical Permian forms (e. g. *Weylandites* spp.) are still present. Dienerian and early Smithian assemblages (3) are characterised by abundant cavate trilete spores (lycopods) with common fern spores and striate bisaccate pollen. This spore dominance culminates in an acme of *Densoisporites* spp. in the middle Smithian (4). The late Smithian assemblages (5) are dominated by striate bisaccate pollen. These are replaced in the Spathian (6) by assemblages characterised by non-striate bisaccate pollen combined with *Densoisporites* spp., *Aratrisporites* spp., and ornamented spores. At the turn of the Middle Triassic (Anisian) (7) the dominance of non-striate bisaccate pollen increases whereas cavate trilete spores and striate bisaccate pollen are reduced and occur only in low numbers.

For the reconstruction of Early Triassic plant communities these palynological data have to be translated into a parent plant record. Present-day surface pollen assemblages are known to represent surrounding plant communities (e. g. Lézine et al., 2009). According to numerous studies specific pollen spectra can be used for the reconstruction of past ecosystems. However, some reservations are indicated concerning quantitative reconstruction of plant communities inferred from pollen spectra (Fletcher and Thomas, 2007; McGlone and Moar, 1997; Stutz and Prieto, 2003). Palaeopalynological assemblages recovered from sedimentary basins are known to reflect the flora of the hinterland from which the spores and pollen have been transported into the basin (Muller, 1959; Traverse, 2007). For Holocene and Pleistocene palynological records analysed using modern analogue techniques, reconstructions of past vegetation produced convincing results (e. g. Delcourt and Delcourt, 1985; Pross et al., 2009). However, some physical aspects of transport and sedimentation have to be kept in mind. Due to the various morphologies of sporomorph taxa, they are liable to different buoyancy and transportation modes. Sporomorphs with higher buoyancy, e. g. bisaccate pollen, can be transported over longer distances, and are therefore generally more abundant in more distal settings (e. g. highstand system tracts; Tyson, 1995 and references therein).

Nevertheless, given the low taxa density and generally poor time resolution of plant macrofossil data, palynological records offer a more complete record of past vegetation with greater taxonomic richness and with high temporal resolution. For the Early Triassic succession from Pakistan it could be demonstrated that the floral changes are independent of sea-level changes as reflected in the sedimentary and palynofacies patterns (Hermann et al., subm.; in press).

For the Early Triassic palynological record the botanical affinities of sporomorphs are mainly

provided by *in-situ* occurrences of sporomorph taxa. These affinities are crucial for ecological reconstructions. For the present study spore-pollen representing major components of the Early Triassic vegetation of Gondwana have been assigned to major plant groups, essentially based on the compilation of Balme (1995) (Table 1). However, in some cases these assignments are not straightforward. *Alisporites* spp. for example has been assigned to Corystospermae by de Jersey and Hamilton (1967). In contrast this pollen type has been recovered from *in-situ* occurrences in the male conifer cone *Willsiostrobus* (Grauvogel-Stamm, 1978), the latter affinity is favoured herein.

Table 1: Botanical affinities of relevant sporomorph taxa (after Balme, 1995; Grauvogel-Stamm, 1978).

	Plant Phylum/Class	Plant Order	Sporomorph genera	
Pteridophytes	Bryophyta		*Maculatasporites* spp., alete spores	Spores
	Lycopodiopsida	Selaginellales, Pleuromeiales, Lycopodiales, Isoetales	*Densoisporites* spp. *Kraeuselisporites* spp. *Lundbladispora* spp. *Lycopodiacidites* spp *Aratrisporites* spp. *Uvaesporites* spp. *Endosporites* spp.	
	Equisetopsida		*Calamospora* spp.	
	Pteridopsida (ferns)		*Apiculatisporis* spp., *Leiotriletes* spp., *Lophotriletes* spp., *Apiculatisporites* spp., *Converrucosisporites* spp., *Cyclogranisporites* spp., *Osmundacidites* spp., *Verrucosisporites* spp., *Granulatisporites* spp., *Convolutispora* spp.,., *Concavisporites* spp., *Leschikisporis* spp., *Camptotriletes* spp., *Raistrickia* spp., *Triquitrites* spp., *Grandispora* spp., *Polycingulatisporites* spp., *Polypodiisporites* spp., *Laevigatosporites* spp	
	spores with uncertain botanical affinity		*Punctatisporites* spp., *Limatulasporites* spp., *Triplexisporites* spp., *Annulispora* spp., *Jerseyiaspora* spp. *Naumovaspora* spp., *Retusotriletes* spp., *Playfordiaspora* spp., and undifferentiated spores	
Gymnosperms	Lyginopteridopsida (Pteridospermae)		*Lunatisporites* spp., *Protohaploxypinus* spp., *Striatoabieites* spp., *Striatopodocarpites* spp., *Weylandites* spp., *Vitreisporites* spp., *Falcisporites* spp., *Striomonosaccites* spp., and undifferentiated striate bisaccate pollen	Pollen
	Coniferopsida		*Alisporites* spp., *Brachisaccus* spp., *Klausipollenites* spp., *Limitisporites* spp., *Platysaccus* spp., *Lueckisporites* spp,. *Cordaitina* spp., *Jugasporites* spp., *Chordasporites* spp., *Sulcatisporites* spp., and undifferentiated non-striate bisaccate pollen	
	Coniferopsida and pteridospermae		Undeterminable bisaccate pollen, due to their preservation or orientation in the slide.	
	Gnetopsida		*Ephedripites* spp.	
	Cycadopsida		*Cycadopites* spp., *Pretricopipollenites* spp.	

4. Discussion

4.1. Ecological changes

Seven distinct floral associations (floral phases 1 to 7) representing terrestrial ecosystem turnovers are reflected in the Early Triassic palynological record from Pakistan.

Phase (1). The palynological assemblages dominated by non-striate and striate bisaccate pollen indicate the proliferation of conifers and pteridosperms during the late Permian on North Gondwana. In contemporaneous coal-bearing sequences of Australia the last occurrences of glossopterid megafossil plant remains are documented (Foster et al., 1982). Ferns, lycopods and equisetopids are minor component of the late Permian vegetation.

Phase (2). Immediately before the documented end-Permian mass extinction, which coincides with the formational boundary between the Chhidru Formation and the Mianwali Formation (Schindewolf, 1954) the composition of the Gondwanan flora changes significantly. The increase abundance of cavate trilete spore (*Kraeuselisporites* spp.) in the latest Permian/Griesbachian assemblages reflects the establishment of a lycopod dominated vegetation prior to the faunal mass extinction. Since many of the typical Permian taxa (e. g. *Weylandites* spp., *Lueckisporites* spp.) are still present, floral diversity increases across the Permian-Triassic boundary (Fig. 2).

Phase (3). The Dienerian plant communities on North Gondwana are characterised by the dominance of lycopods as reflected in the in the low diversity assemblages of cavate trilete spores such as *Densoisporites* spp., and *Lundbladispora* spp. (Fig. 2). The predominance of lycopods continues into the early Smithian. However, ornamented spore diversity increases and reflects the prominent role of ferns within this interval. Pollen of the *Ephedripites* and *Cycadopites* groups and striate and non-striate bisaccate pollen document a mixed vegetation of conifers, pteridosperms, Gnetales and cycads.

Phase (4). A rapid and conspicuous floral changes is documented in the middle Smithian. The palynological assemblages up to the lower boundary of the *Wasatchites distractus* beds represent a spore spike. They are dominated by *Densoisporites* spp., intermittently reaching percentages higher than 90% of the total sporomorph count, thus suggesting monotonous stands of the lycopsid order Pleuromeiales (Abbink, 1998).

Phase (5). In the late Smithian, above the *Wasatchites distractus* beds, the monotonous lycopod assemblages are replaced by a pteridosperm dominated vegetation reflected in the high abundances of striate bisaccate pollen (*Lunatisporites* spp.). The diversity in the late Smithian plant communities is still low but increases rapidly in the beginning Spathian (Fig. 2).

Phase (6). The Spathian plant communities have a transitional character between the lycopod dominated Griesbachian to Smithian vegetation and the Middle Triassic conifer dominated vegetation. Lycopods mainly represented by *Densoisporites* spp., and *Aratrisporites* spp. are still a prominent component of the vegetation, but conifers begin to proliferate. The diversity of ornamented spores indicates that ferns also played a prominent role in these ecosystems.

Phase (7). Gymnosperm forests with conifers, Gentopsida, Cycadopsida, and pteridosperms associated with ferns and lycopods established in the Anisian. This interval records the highest palynofloral diversity of the studied time interval is reached.

In the Smithian the profound changes in the vegetation of North Gondwana are paralleled by synchronous changes in the ammonoid faunas of the North Indian Margin (southern Tethys). During the early Smithian (floral phase 3) the generic richness of ammonoids increases steadily and shows moderate to high turnover rates (Brühwiler et al., 2010). During the time of the middle Smithian spore spike, ammonoid turnover

rates are highest, and the peak values of generic richness of ammonoid faunas are reached. It is striking that the top of the Smithian spore spike (4) coincides with a major extinction event in the marine realm reflected in high extinction rates in the ammonoid faunas of the *Wasatchites distractus* beds (Fig. 2). During the late Smithian, extinction rates in ammonoid faunas of the North Indian Margin exceed the rates of origination.

4.2. Environmental context of ecosystem changes

One of the most widely discussed causes of the end-Permian mass extinction includes rapid climatic changes induced by the release of greenhouse gases by volcanic activities. The synchronicity of the extinction event and the emplacement of the Siberian Traps support speculations that greenhouse gases were released from volcanic degassing (e. g. Wignall, 2001). An additional source of CO_2 was C-rich sediments heated by intruding magma in Siberia and release by pipe structures that have been dated as 252 +-0.4 Ma (ID–

TIMS, Svensen et al., 2009). Additionally, Gondwana bound Permian volcanism is documented in the Argentinean Choiyoi igneous province. Here, the last major volcanic pulse with extensive rhyolitic ignimbrites and pyroclasitc flows has been dated as 251.9+-2.7 Ma (SHRIMP U–Pb zircon, Rocha Campos et al., 2010). The climate forcing potential of ignimbrite eruptions by enhancing primary productivity through iron fertilization has been previously suggested (Cather et al., 2009). Enhanced primary production and burial of organic carbon leads to a CO_2 drawdown and implies a global cooling (Cather et al., 2009). This contrasts with the warming effect caused by the large CO_2 amounts induced by the Siberian Trap volcanism. The CO_2 release from the Siberian Traps through pipe structures as described by Svensen et al. (2009) appears to be a relatively fast process, probably outpacing the CO_2 drawdown by enhanced primary productivity. Therefore the impact of the felsic volcanism in Argentina on global climate remains open for discussion. Nevertheless, the ejection of large amounts of volcanic ash might imply an additional source of environmental perturbations near the Permian-Triassic transition.

Carbon isotope records of Early Triassic sedimentary sequences are marked by recurrent excursions of high magnitude. These excursions have been interpreted to reflect the recurrent CO_2 pulses linked with the protracted Siberian trap volcanism (Ovtcharova et al., 2006; Payne and Kump, 2007). Such pulses might be responsible for additional extinction events that followed the main crisis at the Permian-Triassic boundary and for the repeatedly reset of the recovery of marine ecosystems (Brayard et al., 2006, Hautmann et al. in press).

The palynological records recovered from the sections of the Salt Range and Surghar Range reflects a series of changes in the North Gondwanan terrestrial ecosystems in the aftermath of the end-Permian mass extinction. Strikingly, major changes in the marine biota (ammonoids) are closely related to these ecosystem changes on land. In many Permian-Triassic sections from different palaeogeographic regions the onset of lycopod dominated plant communities reflected in a spore spike has been observed in association with the end-Permian mass extinction (Greenland, Looy et al., 2001; Stemmerik et al., 2001; Norway, Hochuli et al., 2010a; Australia, Foster, 1982). This end-Permian spore spike occurs within the global negative carbon isotope excursion that marks Permian-Triassic boundaries (Payne and Kump, 2007). In the North Gondwanan records of Pakistan the floral phases (1) and (2) have both been recovered from the uppermost Chhidru Formation, but from different localities. The discontinuity of the sampled succession prevents the firm identification of the end-Permian spore spike. However, the studied palynological assemblages show a distinct increase of spores in the uppermost Chhidru Formation from floral phase (1) to floral phase (2).

Figure 2: Late Permian to Middle Triassic vegetation history on North Gondwana, represented in seven floral phases. Ammonoid biostratigraphy after Brühwiler et al. (in press), Guex (1978), and ongoing work of Bucher, H. and Ware, D.: Prh = Prohungarites beds; Tr = Tirolites beds; Gly = Glyptophiceras sinatum beds; Was = Wasachites distractus beds; Nya = Nyalamites angustecostatus beds; Psc = Pseudoceltites multiplicatus beds; Nam = Nammalites pilatoides beds; Bry = Brayardites compressus beds; Fl. f. = Flemingites flemingianus beds; Fl. n. = Flemingites nanus beds; Xed = Xenodiscoides perplicatus beds; F. bh. Flemingites bhargavai beds; Prbl. = Prionolobus rotundatus beds; Gyr = Gyronites beds. Ammonoid evolutionary trends after Brühwiler et al. (2010). Carbon isotopes after Hermann et al. (in press).

The end-Permian spore spike has been interpreted as the signal for pioneering plant assemblages following the destruction and extinction of woody gymnosperms in Europe (Looy et al., 1999; 2001). Global compilations demonstrate that the reduction of floral diversity is a regional phenomenon and strongly biased by low numbers of fossiliferous localities at the Permian-Triassic transition (Rees, 2002). In other areas diversity increases (Hochuli et al., 2010a and references therein). Due to the plant specific physiological advantage to sprout after physical destruction or after dormancy from various parts (e. g. seeds, spores, and roots), plants are not subject to the same destructive effects than marine and terrestrial fauna. The competition for their basic requirements such as water, CO_2 and light is crucial for the determination of plant diversity patterns. Thus, climate changes have a great effect on floral diversity. A loss of diversity might be induced when the migration of plants can not keep the pace of climate change (Knoll, 1984). The Early Triassic carbon isotope perturbations are marked by an initial negative shift at the Permian-Triassic boundary signalling enhanced greenhouse gas releases and global warming (Wignall, 2001). Therefore, diverging from the interpretations of Looy et al., (2001), the end-Permian spore spike can be interpreted as consequence of a climate change to more humid conditions at the Permian-Triassic transition (Hochuli et al., 2010a). For the fern spike near the Triassic-Jurassic boundary van de Schootbrugge et al. (2009) suggested in addition to increased humidity the release of volcanic SO_2 affecting plants by generating acid rain. In contrast to seed plants, the physiological dispositions of pteridophytes growing under water saturated conditions enable these plants to cope with elevated levels of atmospheric volcanic pollutants (Page, 2002; van de Schootbrugge et al., 2009).

Another floral phenomenon of the Permian-Triassic boundary is the common occurrence of unseparated spore tetrads and anormal pollen grains, reflecting the prevailing environmental stress during the Permian-Triassic transition (Looy et al., 2001, Foster and Afonin, 2005). One of these environmental stress factors could be increase UV-B radiation induced by the depletion or destruction of the ozone layer. The increased UV-B radiation is thought to cause genetic changes so that spore tetrads of mutant pteridophytes loose the ability to separate and probably reduce the efficiency of reproduction (Beerling, 2007, Visscher et al. 2004). Probable causes for the ozone layer destruction are volcanically induced releases of H_2S and halocarbons (Kump et al., 2005, Svenson et al., 2009, Visscher et al., 2004). Another factor that might have lead to increased penetration of mutanogenic cosmic rays is a lowering of the geomagnetic field intensity, which together with the ozone layer protects the biosphere from harmful cosmic radiation. Low geomagnetic field intensity might be caused by an unstable magnetic dipole. The Illawarra Reversal in the late Guadalupian marks the onset of a period with an unstable magnetic dipole and probably intermittently low geomagnetic field intensity (Isozaki, 2009; Svensmark, 2007).

To the abrupt climate change near the Permian-Triassic boundary the flora reacted by entering into a “stress mode”, i.e. a time interval characterised by ecosystem instability caused by environmental stress and reflected in fast floral adaptations. The onset of these ecosystem instabilities is reflected in a spore spike (Greenland, Looy et al., 2001; Stemmerik et al., 2001; Norway, Hochuli et al., 2010a; Australia, Foster, 1982) and to a lesser degree in floral phase (2) of the present study. The synchronicity of the spore spike documented in northern hemisphere records with those observed in the southern hemisphere is still a matter of ongoing research. The global significance of this event is reflected in the fundamental floral changes in all sections straddling this time interval. However, even in the tropical successions of South China microfloral and macrofloral records of the Permian-Triassic transition are marked by increased abundances of Triassic lycopods associated with surviving Permian floral elements (Peng et al., 2005).

The aftermath of the end-Permian extinction is characterised by recurrent environmental perturbations (Hochuli et al., 2010b; Galfetti et al., 2007b). The ecosystem instabilities began with the initial end-Permian floral turnover (and faunal extinction) and continued into the Early Triassic from the Griesbachian up to the earliest Spathian. Ammonoid calibrated U-Pb radiometric ages suggest a duration of about 2.1 Ma for this time interval (Galfetti et al., 2007a; Ovtcharova et al., 2006). The changing climatic conditions caused a series of floral adaption reflected in our floral phases (2) to (5). After the end-Permian spore spike the vegetation of the Dienerian and especially of the early Smithian on North Gondwana experienced a slight relief from the initial perturbation. Floral diversity increased and gymnosperms were common, but pteridophytes were still the prominent component of the flora of phase (3). European palynological records of the same time interval are similarly dominated by lycopods (Kürschner and Herngreen, 2010; Vigran et al., 1998, Looy et al., 1999) with highest diversities in mid-latitudinal records (Hochuli et al., 2010a). Global ammonoid diversity patterns of this time interval do not match the resolution of the North Gondwana data but they show significant increases in diversity in the Dienerian and the Smithian (Brayard et al., 2006). Conodonts, which passed the Permian-Triassic boundary without a significant reduction in diversity, experienced a major radiation in the Dienerian and early Smithian time intervals (Orchard, 2007).

The second major ecological perturbation following the end-Permian spore spike is documented for the middle to late Smithian. In the middle Smithian a negative carbon isotope excursion is associated with a spore spike (4) and immediately followed by the proliferation of gymnosperms (5). Similar patterns have been observed from the Permian-Triassic boundary in Norway (Hochuli et al., 2010a). These high resolution records documented a spore spike coinciding with the onset of a major carbon cycle perturbation and followed by a rebound of gymnosperms (Hochuli et al., 2010a). Another similarity to the end-Permian spore spike is the association with a major and global extinction event. The late Smithian extinction event affected essentially the clades that had recovered rather quickly after the end-Permian extinction such as ammonoids and conodonts (Brayard et al., 2006; Orchard, 2007).

The environmental perturbations and the associated ecosystem upheavals finally weakened during the Spathian. The floral adaption rates slowed down back to a “normal mode”. Increased gymnosperm abundances are not only reflected in the palynological assemblage of the transitional phase (6) of the Spathian of North Gondwana but also in Australia (increased abundance of *Falcisporites* spp. e. g. Price, 1997) and in central Europe (increased abundance of *Voltziaceaesporites heteromorphus* Kürschner and Herngreen, 2010; Orłowska-Zwolińska, 1984). The “normal mode” in the terrestrial ecosystems is paralleled in the marine biosphere by a strong diversification of ammonoids (Brayard et al., 2006; 2009), conodonts (Orchard, 2007), and benthic organisms (Hautmann et al., 2008).

Looy et al. (1999) proposed a delayed recovery of conifer forests in Europe of 4 to 5 million years, spanning the entire Early Triassic. Our results demonstrate that the resurgences of prominent gymnosperm vegetation started already in the early Spathian with a transitional flora (6) composed of lycopods and conifers. Similar recovery patterns have been observed in the same time interval of mid-latitude succession of Norway (Hochuli and Vigran, 2010) and central Europe (Kürschner and Herngreen, 2010; Orłowska-Zwolińska, 1984). The Anisian palynological assemblages of North Gondwana reflect widespread conifer forests with a diverse fern understory and rare lycopods. Similar to our result gymnosperm pollen dominate the Anisian assemblages of central Europe showing even higher diversity (e. g. Orłowska-Zwolińska, 1984). In contrast to this, sites from mid-latitudes

of the northern hemisphere show remarkable abundances of lycopods associated with highly diversified gymnosperm pollen (Hochuli and Vigran, 2010).

Our observations combined with the radiometric ages for the Early Triassic stages allow the reassessment of the "delayed floral recovery". The ecosystem perturbation as reflected in the dominance of stress resistant lycopods encompasses the Griesbachian up the earliest Spathian corresponding to a time interval of ca. 2.1 Ma. The ecosystem perturbations waned during the Spathian comprising a time of ca. 2.4 Ma (Galfetti et al., 2007a, Ovtcharova et al., 2006) and diverse gymnosperm-rich plant communities established. We interpret the observed changes in the floral record of the Early Triassic as a signal of floral adaption to changing environments whereas the loss of plant diversity on a higher taxonomic level remained a minor phenomenon. Or in a nutshell, if the environmental conditions had turned to more favourable conditions earlier, gymnosperms could have proliferated at any time during the Early Triassic.

5. Conclusions

The Early Triassic palynological record and the inferred floral changes on North Gondwana shows a recurrent pattern of spore peaks associated with a negative excursions in the carbon isotope record and closely linked to extinction events in marine ecosystems.

The proliferation of pteridophytes during the Early Triassic, from the Griesbachian up to the Smithian and to minor extent in the Spathian is linked to climatic changes probably triggered by volcanism. The data supports that the major plant groups survived the end-Permian extinction event but might have been temporally absent from the palynological record depending on changes in the relative abundances driven by changing climatic/atmospheric conditions. We propose that the observed floral changes reflect the adaptation of the vegetation to profound and recurrent environmental changes in the Early Triassic and are not necessarily a signal of a global floral diversity decrease or disastrous extinction event. During a time period of about 2.1 Ma the vegetation on North Gondwana was forced into a mode of fast adaptations to abiotic environmental changes ("stress-mode" corresponding to ecological instability) reflected in fast changes in the dominance structure within the terrestrial flora. In the Spathian and Anisian these conditions were replaced by a "normal mode" and the development of stable ecosystems.

Acknowledgements

We acknowledge financial support from the Swiss National Science Foundation project 200020-127716/1 (to H. Bucher).

References

Abbink, O.A., 1998. Palynological investigation in the Jurassic of the North Sea region. Ph.D. thesis, Laboratory of Palaeobotany and Palynology, Utrecht.

Balme, B.E., 1970. Palynology of Permian and Triassic strata in the Salt Range and Surghar Range, West Pakistan. In: Kummel, B., Teichert, C. (Eds.): Stratigraphic boundary problems: Permian and Triassic of West Pakistan. University Press of Kansas, Lawrence, 305-453.

Balme, B.E., 1995. Fossil in situ spores and pollen grains: an annotated catalogue. Review of Palaeobotany and Palynology, 87, 81-323.

Bonis, N. R., Ruhl, M., Kürschner, W., 2010. Milankovitch-scale palynological turnover across the Triassic-Jurassic transition at St. Audries Bay, SW UK. Journal of the Geological Society, 167, 877-880.

Brayard, A., Bucher, H., Escarguel, G., Fluteau, F., Bourquin, S., Galfetti, T., 2006. The Early Triassic ammonoid recovery: Paleoclimatic significance of diversity gradients. Palaeogeography, Palaeoclimatology, Palaeoecology, 239, 374-395.

Brayard, A., Escarguel, G., Bucher, H., Monnet, C., Brühwiler, T., Goudemand, N., Galfetti, T. &

Guex, J. 2009. Good Genes and Good Luck: Ammonoid Diversity and the End-Permian Mass Extinction. Science, 325, 1118-1121.

Brühwiler, T., Bucher, H., Brayard, A., Goudemand, N., 2010. High-resolution biochronology and diversity dynamics of the Early Triassic ammonoid recovery: the Smithian faunas of the Northern Indian Margin. Palaeogeography, Palaeoclimatology, Palaeoecology, doi:10.1016/j.palaeo.2010.09.001.

Brühwiler, T., Bucher, H., Ware, D., Hermann, E., Hochuli, P.A., Roohi, G., ur-Rehman, K., and Yaseen, A., (in press), Smithian (Early Triassic) ammonoids from the Salt Range, Pakistan. Special Papers in Palaeontology.

de Jersey, N.J., Hamilton, M., 1967. Triassic spores and pollen grains from the Moolayember Formation. Geological Survey of Queensland, Brisbane, Publication No 336.

Delcourt, H.R., Delcourt, P.A., 1985. Comparison of taxon calibrations, modern analogue techniques, and forest-stand simulation models for the quantitative reconstruction of past vegetation. Earth Surface Processes and Landforms, 10, 293-304.

Fletcher, M.S., Thomas, I., 2007. Modern pollen-vegetation relationships in western Tasmania, Australia. Review of Palaeobotany and Palynology, 146, 146-168.

Foster, C.B., 1982. Spore-Pollen assemblages of the Bowen Basin, Queensland (Australia): Their relationship to the Permian/Triassic boundary. Review of Palaeobotany and Palynology, 36, 165-183.

Galfetti, T., Bucher, H., Ovtcharova, M., Schaltegger, U., Brayard, A., Brühwiler, T., Goudemand, N., Weissert, H., Hochuli, P.A., Cordey, F., Goudun, K., 2007a. Timing of the Early Triassic carbon cycle perturbations inferred from new U-Pb ages and ammonoid biochronozones. Earth and Planetary Science Letters, 258, 593-604.

Galfetti, T., Hochuli, P.A., Brayard, A., Bucher, H., Weissert, H., Vigran, J.O., 2007b. Smithian/Spathian boundary event: Evidence for global climatic change in the wake of the end-Permian biotic crisis. Geology, 35, 291-294.

Golonka, J., Ford, D., 2000. Pangean (Late Carboniferous-Middle Jurassic) paleoenvironment and lithofacies. Palaeogeography, Palaeoclimatology, Palaeoecology, 161, 1-34.

Grauvogel-Stamm, L., 1978. La flore du grès a Voltzia (Buntsandstein supérieur) des Vosges du Nord (France), morphologie, anatomie, interprétations phylogénique et paléogéographique, Université Louis Pasteur de Strasbourg - Institute de Géologie, Strasbourg.

Guex, J., 1978. Le Trias intérieur des Salt Ranges (Pakistan): problèmes biochronologiques. Eclogae geologicae Helvetiae, 71,. 105-141.

Hautmann, M., Bucher, H., Brühwiler, T., Goudemand, N., Kaim, A., Nützel, A., in press. And unusually divers mollusc fauna from the earliest Triassic of South China and its implication for benthic recovery after the end-Permian biotic crises. Geobios.

Hautmann, M., Bucher, H., Nützel, A., Brühwiler, T., Goudemand, N., Brayard, A., 2008. Recovery of benthos versus nekton after the end-Permian mass extinction event - A preliminary comparison. GSA Joint Annual Meeting, Houston, paper no. 285-14.

Hermann, E., Hochuli, P.A., Bucher, H., Brühwiler, T., Hautmann, M., Ware, D., Weissert, H., Roohi, G., Yaseen, A., ur-Rehman, K., subm. Climatic oscillations at the onset of the Mesozoic inferred from palynological records from the North Indian Margin. Journal of the Geological Society London.

Hermann, E., Hochuli, P.A., Méhay, S., Bucher, H., Brühwiler, T., Hautmann, M., Ware, D., Roohi, G., ur-Rehman, K., and Yaseen, A., in press. Organic matter and palaeoenvironmental signals during the Early Triassic biotic recovery: the Salt Range and Surghar Range records. Sedimentary Geology doi:10.1016/j.sedgeo.2010.11.003.

Hochuli, P.A., Vigran, J.O., 2010. Climate variations in the Boreal Triassic - Inferred from palynological records from the Barents Sea. Palaeogeography, Palaeoclimatology, Palaeoecology, 290, 20-42.

Hochuli, P.A., Hermann, E., Vigran, J.O., Bucher, H., Weissert, H., 2010a. Rapid demise and recovery of plant ecosystems across the end-Permian extinction-event. Global and Planetary Change 74 (3-4), 144-155.

Hochuli, P.A., Vigran, J.O., Hermann, E., and Bucher, H., 2010b. Multiple climatic changes around the Permian Triassic boundary event revealed by an expanded palynological record from Mid Norway. GSA Bulletin, 122, 884-896.

Knoll, A.H., 1984. Patterns of extinction in the fossil record of vascular plants. In: Nitecki, M. H. (Ed.): Extinctions. The University of Chicago Press, Chicago, 21-68.

Kürschner, W.M., Herngreen, G.F.W., 2010. Triassic palynology of central and northwestern Europe: A review of palynoflora diversity patterns and biostratigraphic subdivisions. Geological Society London, Special Publications, 334, 263-283.

Lézine, A.M., Watrin, J., Vincens, A., Hély, C., 2009. Are modern pollen data representative of west African vegetation? Review of Palaeobotany and Palynology, 156, 265-276.

Lindström, S., McLoughlin, S., 2007. Synchronous palynofloristic extinction and recovery after the end-Permian event in the Prince Charles Mountains, Antarctica: Implications for palynofloristic turnover across Gondwana. Review of Palaeobotany and Palynology, 145, 89-122.

Looy, C.V., Brugman, W.A., Dilcher, D.L., Visscher, H., 1999. The delayed resurgence of equatorial forests after the Permian-Triassic ecologic crisis. Proceedings of the National Academy of Sciences of the United States of America, 96, 13857-13862.

Looy, C.V., Twitchett, R.J., Dilcher, D.L., Van Konijnenburg-VanCittert, J.H.A., Visscher, H., 2001. Life in the end-Permian dead zone. Proceedings of the National Academy of Sciences, 98, 7879-7883.

McElwain, J.C., Punyasena, S.W., 2007. Mass extinction events and the plant fossil record. Trends in Ecology and Evolution, 22, 548-557.

McGlone, M.S., Moar, N.T., 1997. Pollen-vegetation relationship on the subantarctic Auckland Islands, New Zealand. Review of Palaeobotany and Palynology, 96, 317-338.

McLoughlin, S., Lindström, S., Drinnan, A.N., 1997. Gondwanan floristic and sedimentological trends during the Permian-Triassic transition: new evidence from the Amery Group, northern Prince Charles Mountains, East Antarctica. Antarctic Science, 9, 281-298.

Muller, J., 1959. Palynology of recent Orinoco delta and shelf sediments: Reports of the Orinoco Shelf Expedition. Micropaleontology, 5, 1-32.

Orłowska-Zwolińska, T., 1984. Palynostratigraphy of the Buntsandstein in sections of western Poland. Palaeontologia Polonica, 29, 161-194.

Orchard, M.J., 2007. Conodont diversity and evolution through the latest Permian and Early Triassic upheavals. Palaeogeography, Palaeoclimatology, Palaeoecology, 252, 93-117.

Ovtcharova, M., Bucher, H., Schaltegger, U., Galfetti, T., Brayard, A., Guex, J., 2006. New Early to Middle Triassic U-Pb ages from South China: Calibration with ammonoid biochronozones and implications for the timing of the Triassic biotic recovery. Earth and Planetary Science Letters, 243, 463-475.

Page, C.N., 2002. Ecological strategies in fern evolution: a neopteridological overview. Review of Palaeobotany and Palynology, 119, 1-33.

Payne, J.L., Kump, L.R., 2007. Evidence for recurrent Early Triassic massive volcanism from quantitative interpretation of carbon isotope fluctuations. Earth and Planetary Science Letters, 256, 264-277.

Peng, Y., Zhang, S., Yu, T., Yang, F., Gao, Y., Shi, G.R., 2005. High-resolution terrestrial Permian-Triassic eventostratigraphic boundary in western Guizhou and eastern Yunnan, southwestern China. Palaeogeography, Palaeoclimatology, Palaeoecology, 215, 285-295.

Price, P.L., 1997. Permian to Jurassic palynostratigraphic nomenclature. In: Green, P. M. (Ed.): The Surat and Bowen Basins, South-east Queensland Brisbane, Queensland Department of Mines and Energy, Brisbane, 137-178.

Pross, J., Kotthoff, U., Müller, U.C., Peyron, O., Dormoy, I., Schmiedl, G., Kalaitzidis, S., Smith, A.M., 2009. Massiv perturbation in terrestrial ecosystems of the Eastern Mediterranean region associated with the 8.2 kyr B.P. climatic event. Geology, 37, 887-890.

Rees, P., 2002. Land-plant diversity and the end-Permian mass extinction. Geology, 30, 827-830.

Schindewolf, O.H., 1954. Über die Faunenwende vom Paläozoikum zum Mesozoikum: Zeitschrift der Deutschen Geologischen Gesellschaft, 105, 154-183.

Smith, A.G., Smith, D.G., Funnell, B.M., 1994. Atlas of Mesozoic and Cenozoic Coastlines. Cambridge University Press, Cambridge.

Stemmerik, L., Bendix-Almgreen, S.E., Piasecki, S., 2001. The Permian-Triassic boundary in central East Greenland: past and present views. Bulletin of the Geological Society of Denmark, 48, 159-167.

Stutz, S., Prieto, A.R., 2003. Modern pollen and vegetation relationships in Mar Chiquita coastal lagoon area, southeastern Pampa grasslands, Argentina. Review of Palaeobotany and Palynology, 126, 183-195.

Svensen, H., Planke, S., Polozov, A.G., Schmidbauer, N., Corfu, F., Podladchikov, Y., Jamtveit, B., 2009, Siberian gas venting and the end-Permian environmental crisis. Earth and Planetary Science Letters, 277, 490-500.

Traverse, A., 2007. Paleopalynology. Springer Verlag, Dordrecht.

Tyson, R.V., 1995. Sedimentary organic matter - organic facies and palynofacies. Chapman & Hall, London.

Utting, J., Spina, A., Jansonius, J., McGregor, D.C., Marschall, J.E.A., 2004. Reworked miospores in the upper Paleozoic and Lower Triassic of the Northern circum-polar area and selected localities. Palynology, 28, 75-119.

van de Schootbrugge, B., Quan, T.M., Lindström, S., Püttmann, W., Heunisch, C., Pross, J., Fiebig, J., Petschick, R., Röhling, H.-G., Richoz, S., Rosenthal, Y., Falkowski, P.G., 2009. Floral changes across the Triassic/Jurassic boundary linked to flood basalt volcanism. Nature Geoscience, 2, 589-594.

Vajda, V., Raine, J.I., Hollis, C.J., 2001. Indication of global deforestation at the Cretaceous-Tertiary boundary by New Zealand fern spike. Science, 294, 1700-1702.

Vigran, J.O., Mangerud, G., Mørk, A., Bugge, T., Weitschat, W., 1998. Biostratigraphy and sequence stratigraphy of the Lower and Middle Triassic deposits from the Svalis Dome, Central Barents Sea, Norway. Palynology, 22, 89-141.

Visscher, H., Brinkhuis, H., Dilcher, D.L., Elsik, W.C., Eshet, Y., Looy, C.V., Rampino, M.R., Traverse, A., 1996. The terminal Paleozoic fungal event: Evidence of terrestrial ecosystem destabilization and collapse. Proceedings of the National Academy of Sciences, 93, 2155-2158.

Wignall, P.B., 2001. Large igneous provinces and mass extinctions. Earth-Science Reviews, 53, 1-33.

Chapter 5:

Early Triassic palynology of the Salt Range and Surghar Range, Pakistan

with Peter A. Hochuli, Hugo Bucher, Ghazala Roohi

submitted to Review of Palaeobotany and Palynology

Independently dated palynostratigraphic zonations of Early Triassic age are rare. One of the best opportunities to study Permian to Middle Triassic palynology together with contemporaneous marine faunas is found in the sedimentary successions of the Salt Range and Surghar Range, Pakistan.

Here, we present a new Early Triassic palynostratigraphic zonation of North Gondwana, based on the palynological records of the Chhidru Formation, the Mianwali Formation, and the Tredian Formation from section of the Nammal, Chhidru, Chitta-Landu and Narmia gorges in Pakistan. Eight palynological zones have been recognised, described and calibrated against ammonoid biostratigraphy and C-isotope chemostratigraphy. The two basal zones (PP, PTr 1) have been recovered from the uppermost Chhidru Formation. PP is dominated by gymnosperm pollen, whereas PTr 1 is characterised by abundant cavate trilete spores associated with conifer and pteridosperm pollen of Permian affinity. The Dienerian to early Smithian PTr 2 and PTr 3 assemblages are dominated by cavate spores. Compared to PTr 2 ornamented spores are more diverse in PTr 3 and striate bisaccate pollen are more abundant. The middle Smithian assemblages PTr 4 are marked by an acme of *Densoisporites* spp. The successive late Smithian to early Spathian PTr 5 assemblages are characterised by abundant striate bisaccate pollen. The Spathian and Anisian assemblages (PTr 6 and PTr 7) are characterised by the abundance non-striate bisaccate pollen, the common occurrence of *Aratrisporites* spp. in generally diverse spore assemblages. The new palynostratigraphic zonation could be correlated with several other Gondwanan records (Australia, India, and Madagascar). The palynological record allowed for reassessment of the floral recovery patterns in the aftermath of the end-Permian event. During periods with relative stable carbon isotope values (early Smithian, Spathian and Anisian) pulses of diversification have been observed. During episodes of high carbon cycle fluctuations reduced palynofloral diversity is combined with rapid changes in the abundance structure of the palynological assemblages. The palynoflora from North Gondwana shows a complex Early Triassic recovery pattern, which was most probably linked to changes in the atmospheric pCO_2.

Keywords: Early Triassic, palynology, floral recovery, Pakistan

1. Introduction

The sedimentary succession exposed in the Nammal, Chhidru, Chitta-Landu and Narmia gorges in the Salt Range and Surghar Range represents one of the most extensively studied Early Triassic successions on Northern Gondwana. The high density palaeontological and isotope data consolidate the importance of the region as a reference area for the Early Triassic of the Tethyan realm. The majority of the publications concerning the Early Triassic deal with the faunal content of the succession: Ammonoids have been studied e.g. by Waagen (1895), Kummel and Teichert (1970), Guex (1978), and Brühwiler et al., (2010; in press); brachiopods, foraminifera and conodonts e. g. by Grant (1970) and the Pakistani-Japanese Research Group (1985). Detailed organic and inorganic carbon isotope data have been published by Atudorei (1999), Baud et al. (1996), and Hermann et al. (in press). Most of these studies concentrate on the PT boundary and the associated stratigraphic problems as well as the recovery patterns of the marine biota in the aftermath of the end-Permian extinction event.

The macrofloral record of the Permian and Triassic succession in the Salt Range and Surghar Range were first studied by Reed et al. (1930) and Virkki (1939, 1946). A macroflora of the Middle Triassic Landa Member was decribed by Sitholey (1943) and Pant (1946). First micropalaeontolgical studies were published by Virkki (1937; 1939; 1946). A more recent and comprehensive work on the palynology of the Salt Range and Surghar Range has been published by Balme (1970). This author distinguished three assemblages, “Permian assemblages”, “early Scythian assemblages” and “late Sythian to middle Triassic assemblages” and established the first palynological zonation for the Early Triassic of this region. The most recent palynological and stratigraphic studies give a detailed description of the palynological assemblage of the middle Permian Sardhai Formation (Jan et al., 2009).

In the last decades several studies focused on the impact of the end-Permian extinction event on the terrestrial plant communities. The discussions about the magnitude of deteriorations are divergent (e. g. Knoll, 1984; Looy et al., 2001). In various Permian-Triassic successions such as in the Australian sedimentary successions the Permian-Triassic transition is marked by a distinct floral turnover. There the Permian peat-forming *Glossopteris* flora was replaced by the Triassic *Dicroidium* flora and abundant lycopod plants (Retallack, 1995). In numerous sections the floral turnover is marked by a compositional change from gymnosperm dominated flora to a lycopod dominated flora and a prolonged extinction of lingering Permian taxa (Looy et al., 1999; 2001; Lindström and McLoughlin, 2007; Hochuli et al., 2010b). Together with the floral turnover palaeobotanical provinces became blurred and were replaced by cosmopolitan flora (Retallack 1995; Foster et al., 1997). The presence of this low diversity cosmopolitan flora with prominent abundances of lycopods has been suggested to prevail unchanged during the entire Early Triassic. A delayed recovery of 4-5 million years of diverse plant communities has been proposed for the semi-arid region of Central Europe (Looy et al., 1999).

Based on the study of several sections, we present a refined palynostratigraphy of the Early Triassic succession of the Salt Range and Surghar Range calibrated against ammonoid biostratigraphy (Brühwiler et al., 2010; in press). This allows for reevaluation of the pace and causes of the recovery of the flora in the aftermath of the end-Permian mass extinction.

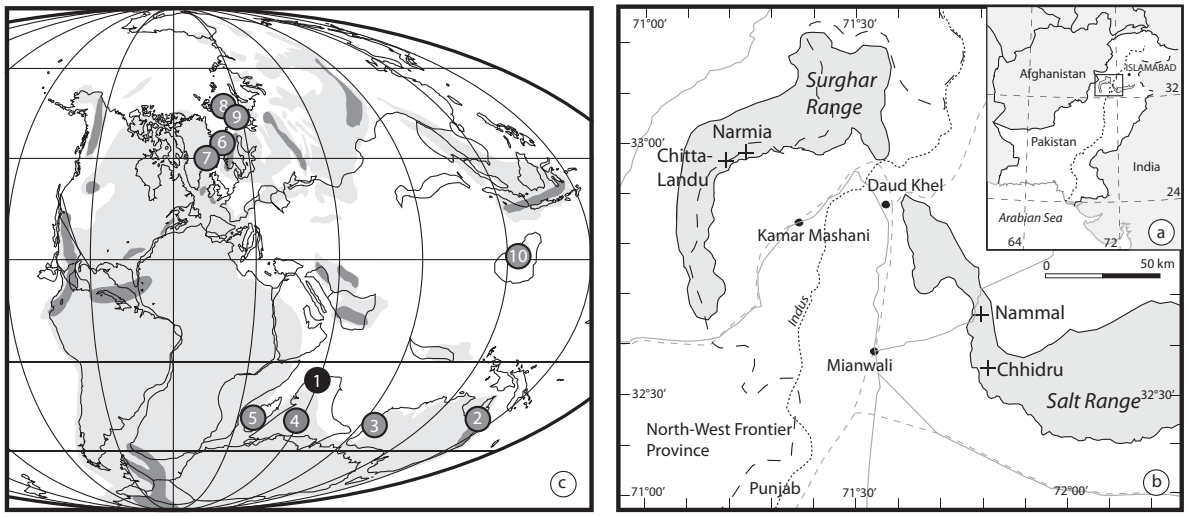

Figure 1: a) Locations of the Salt Range and Surghar Range in Pakistan, b) location of Nammal, Chhidru, Chitta-Landu, and Narmia gorge. c) Palaeogeographic position of mentioned sites (1) Salt Range and Surghar Range in Pakistan; (2) East Australia (Bowen Basin): (3) West Australia (Carnarvon and Perth Basin); (4) various basins in India; (5) Madagascar; (6) Trøndelag platform, Norway; (7) East Greenland; (8) Svalis Dome, Norway, (9) Finnmark platform, Norway; (10) South China. Modified after Smith et al., 1994 and Golonka and Ford, 2000.

2. Geological setting – lithostratigraphy – marine biostratigraphy

The Salt Range in the Punjab province of Pakistan is located on the southern margin of the Potwar Plateau and continues westward in the Surghar Range west of the Indus (Fig. 1). During the late Palaeozoic and Mesozoic palaeogeography was determined by the supercontinent Pangaea extending and the tropical Tethyan ocean (Ziegler et al., 1983; Stampfli and Borel, 2002). The sedimentary succession of the Salt Range and Surghar Range represent the depositional environment of the North Indian Margin (NIM) of the North Gondwana shelf. The sites were located at latitude of about 30° S (Smith et al., 1994; Golonka and Ford, 2000). Siliciclastics were shed from the Indian subcontinent into the Tethyan Ocean. Intermittent carbonate deposits are rich in marine macrofossils. With the subduction of the Indian subcontinent during the late Eocene and particularly during the Quaternary, the sedimentary sequence was thrusted southward along the Salt Range Thrust fault (Gee, 1989). Today Permian and Triassic rocks are cropping out in a stack of slabs roughly parallel to this thrust in the Salt Range and the Surghar Range, respectively. These strata are well exposed in several transecting gorges, among which we studied the Chitta-Landu and Narmia sections in the Surghar Range and the Nammal and Chhidru sections in the Salt Range (Fig. 1 b).

The mixed siliciclastic- carbonate sediments of Permian to Triassic age are represented by the Chhidru, Mianwali and the Tredian Formations. The Chhidru Formation consists of limestones and sandstones with intercalated siltstones. Above an unconformity representing a hiatus, it is overlain by the Early Triassic Mianwali Formation. This formation is subdivided into seven lithological units in ascending order: the Kathwai Member, the Lower Ceratite Limestone (LCL), the Ceratite Marls (CM), the Ceratite Sandstone (CS), the Upper Ceratite Limestone (UCL) ending with the Bivalve Beds (BB), the “Niveaux Intermédiaires” (NI) and the Topmost Limestone (TL) (Kummel and Teichert, 1966, Guex, 1978, Hermann et al., in press). LCL, CM, CS, UCL, and NI form the Mittiwali Member, whereas the TL corresponds to the Narmia Member. However, Kummel and Teichert (1966) and Balme (1970) included the NI as part of the Narmia Member.

The Kathwai Member is dominated by dolomites and limestone. It is followed by an alternation of siltstone and limestone of the LCL and the lower part of the CM at Nammal. The CM are dominated by siltstones, which are replaced by sandstone-siltstone and siltstone-limestone alternations in the CS and UCL. The BB (topmost part of the UCL) represents a fossil rich limestone interval, which is in turn overlain by the siliciclastic sequence of the NI. The NI is followed by the fossil-rich limestones of the TL. The Landa Member of the Anisian Tredian Formation is characterised by a predominant siltstone/sandstone alternation of reddish/brownish colour.

The Permian-Triassic boundary has been officially defined by the FAD (First Appearance Datum) of the conodont *Hindeodus parvus* at the GSSP in Meishan, South China (Yin et al., 2001). Occurrences of *H. parvus* have been described from the middle part of the Kathwai Member (Pakistani-Japanese Research Group, 1985). The main faunal turnover and the negative isotope excursion occur below the GSSP Permian-Triassic boundary (e. g. Jin et al., 2000). In the Salt Range and Surghar Range the main faunal turnover has also been recorded from below the FAD of *H. parvus* and coincides with the formational boundary between the Chhidru Formation and the Kathwai Member (Schindewolf, 1954). Herein, we follow the boundary definition of Kummel and Teichert (1970) as far as possible. They placed the Permian-Triassic boundary between the Chhidru Formation and the Kathwai Member. The Chhidru Formation was dated as late Wuchiapingian based on brachiopods and foraminifera (Pakistani-Japanese Research Group, 1985). Except for its uppermost part, the palynological assemblages from the Chhidru Formation described by Balme (1970) represent a diverse Permian flora. The new palynological data from the Salt Range and Surghar Range indicate diachronism of the formational boundary between the Chhidru Formation and the Kathwai Member. Except for the Chhidru Formation, ammonoids are the main biostratigraphic markers within the Mianwali Formation. The presence of *Ophiceras* in the Kathwai Member indicates a basal late Griesbachian age; the early Griesbachian ammonoid zone (*Otoceras woodwardi*) has not been recognised (Guex, 1978, D. Ware, ongoing work). Dienerian ammonoid faunas occur in the LCL, and the lower part of the CM at Nammal. The most accurate biostratigraphic scheme exists for the Smithian substage. It is composed of 13 unitary associations and allowed to subdivide the Smithian into early, middle and late Smithian part, respectively (Brühwiler et al., 2010; in press). The early Smithian comprises the entire CM at Chhidru, Chitta-Landu, the upper two thirds of the CM at Nammal, and the CS in all three sections. Palynological assemblages from the Kathwai Member up to the middle part of the CM (early Smithian) have been summarised as "Early Scythian Assemblage" by Balme (1970). The middle Smithian encompasses the UCL up to the base of the *Wasatchites distractus* beds. The late Smithian ammonoid faunas include the *Wasatchites distractus* and the *Glyptophiceras sinatum* beds. The middle to late Smithian interval has not been studied by Balme (1970). Within the Spathian biostratigraphic age control is limited because of the scarceness of ammonoids. Evidence for the position of the base and the top of the Spathian is provided by a positive shifts of carbon isotopes and the *Procolumbites* fauna in the BB at Nammal, and the *Tirolites* fauna in the basal NI at Chitta-Landu (Hermann et al., in press; H. Bucher, ongoing work). The lower boundary of the Landa member is marked by a second positive shift in the organic carbon isotope record (Hermann et al., in press). Balme (1970) summarised Spathian to Anisian palynological assemblages in the "late Scythian and Middle Triassic Assemblages".

3. Material and Methods

Samples were preferably taken from fine-grained siliciclastic interval of the sections. In few cases limestone and fine-grained sandstone have been

sampled. 180 cleaned samples (65 Nammal, 59 Chhidru, 7 Narmia, 49 Chitta-Landu) were crushed and weighed (5-25 g) and subsequently treated with hydrochloric and hydrofluoric acid according to standard palynological preparation techniques (Traverse, 2007). A short oxidation with nitric acid was performed before the residues were sieved over an 11 µm mesh screen. From strew mounts a minimum of 300 spores and pollen per sample were counted. Most samples contain well preserved palynological assemblages, only eight samples were barren. In few samples with high amorphous organic matter contents, low sporomorph concentration or poor preservation prevented reaching the intended 300 sporomorph counts.

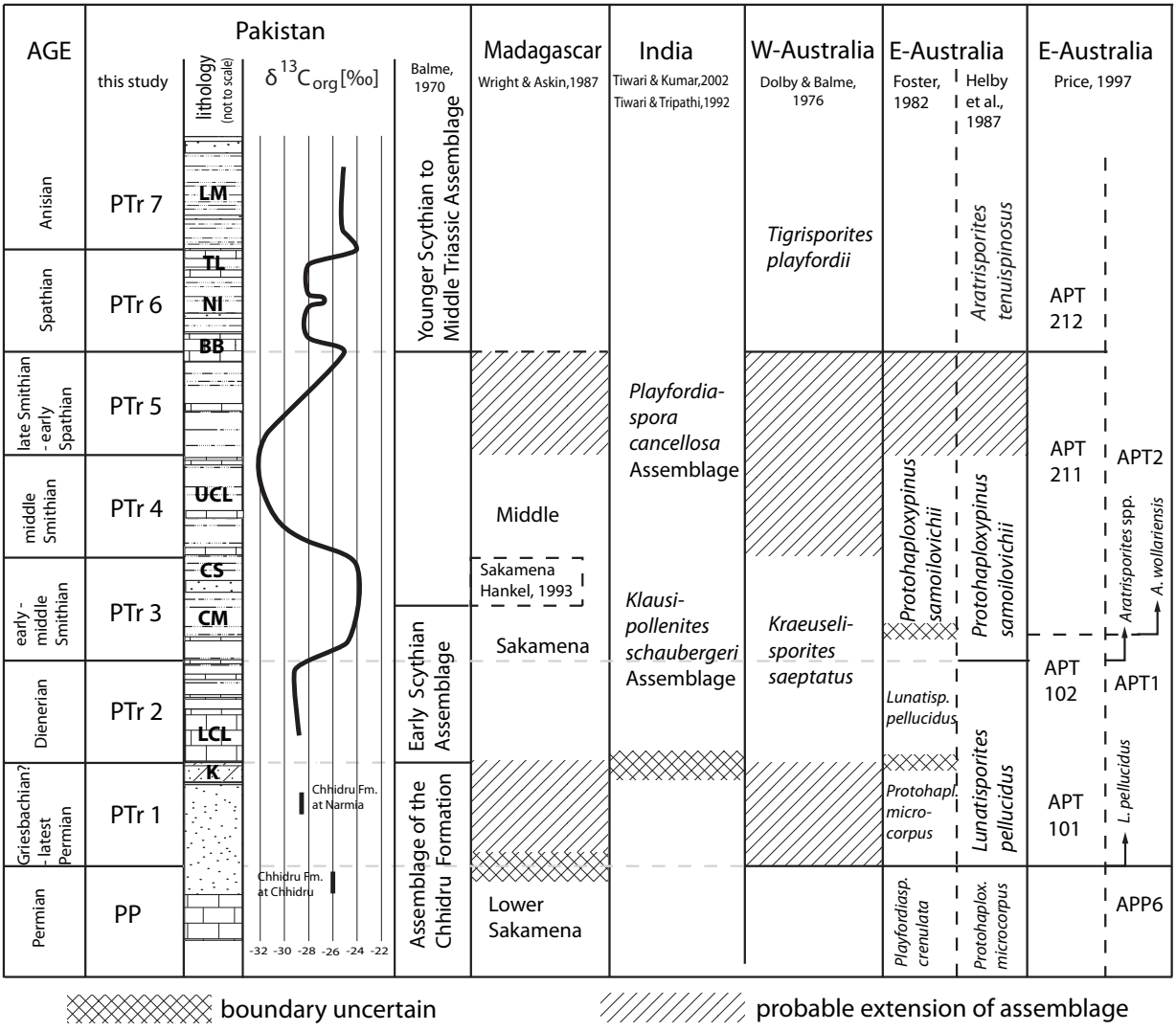

Figure 2: Correlation of Early Triassic palynostratigraphy of Pakistan with other Gondwanan palynological records – not to scale.

4. Palynological assemblages

Based on the quantitative distribution, the palynological record from the Late Permian to Middle Triassic deposits from the Nammal, Chhidru, Chitta-Landu, and Narmia sections has been subdivided into eight assemblage zones (Figs. 2 – 10). These zones are referred to as PP (Pakistan Permian) and PTr 1 to PTr 7 (Pakistan Triassic and numbered consecutively). They are defined by the relative sporomorph abundances of prominent taxa in the zone as well as top and base occurrences of selected taxa. Six zones could be calibrated with ammonoid biostratigraphy and C-isotope chemostratigraphy, respectively. For completeness of the palynological assemblage description, aquatic palynomorph taxa occurring in the specific zones are documented. Their presence or absence is a facies dependent local signal and not of stratigraphic importance. A summary description of the palynozones is given in Table 1.

Palaeogeographically located in Northern Gondwana the palynological assemblages are presented together with their potential correlation with other palynological records from the Gondwana floral province (Fig. 1 c). The most detailed palynological Permian to Triassic succession has been described for Australian records (de Jersey, 1970; Helby, 1973; de Jersey, 1979;). In Fig. 2 the zonation scheme from Pakistan is correlated to the zonation of E-Australia (Helby et al., 1987; Foster, 1979;Foster, 1982; Price, 1997), and W-Australia (Balme, 1963; Dolby and Balme, 1976). A close relationship also exists with the palynological records from Madagascar (Goubin, 1965; Wright and Askin, 1987; Hankel, 1993). A correlation with the Indian records is hampered by a different taxonomic approach and remains therefore rather tentative (Tiwari and Tripathi, 1992; Tiwari and Vijaya, 1995; Tiwari and Kumar, 2002).

PP: *Protohaploxypinus* spp. - *Weylandites* spp. Assemblage zone

Definition and description. The assemblages are characterised by the dominance of non-striate and striate bisaccate pollen and undifferentiated bisaccate pollen (Fig. 5, 6). The moderate preservation with a high portion of disintegrated pollen grains hampers in many cases a precise identification of individual taxa. Characteristic components of the assemblage are common *Klausipollenites* spp., *Protohaploxypinus* spp., *Weylandites lucifer*, and *Alisporites* spp. Spores are very rare. Marine acritarchs are mainly represented by low numbers of *Micrhystridium* spp.

The composition of the palynological assemblages of PP essentially confirms the previous description of the "Permian Assemblage from the Chhidru Formation" by Balme (1970). However, Balme (1970) noted abundant cavate trilete spores within the uppermost part of the Chhidru Formation. In this study we differentiate the uppermost spore rich part as a separate zone (PTr 1), as discussed below.

Occurrence of PP and age control. The base and the top of the zone are not recorded. The zone is represented by a unique assemblage of two samples in the uppermost Chhidru Formation at Chhidru. This formation has been dated late Wuchiapingian based on brachiopods (Pakistani-Japanese Research Group, 1985).

Correlation. Co-occurrence of *Klausipollenites* spp. (including *K. schaubergeri*) and *Protohaploxypinus* spp. (including *P. limpidus*) has been also reported from the *Playfordiaspora crenulata* zone from the Bowen Basin (W-Australia, Foster et al., 1982) and supports a correlation of PP and the *Playfordiaspora crenulata* zone. The latter represents the lower part of the *Protohaploxypinus microcorpus* zone of Foster (1979) and is associated with the youngest known macrofossils of *Glossopteris* (Foster, 1982). The Permian and Early Triassic flora from Madagascar is regarded to be very similar to the Pakistani assemblages (Balme, 1970; Hankel, 1993). Thus, the Lower Sakamena Assemblage from Madagascar described by

Wright and Askin, (1987) is in good agreement with the PP assemblage. However, the dominant taxon of the Lower Sakamena Assemblage, *Guttulapollenites hannonicus*, which has also been documented in Pakistan by Balme (1970), has not been observed in our samples.

PTr 1: Kraeuselisporites wargalensis – Protohaploxypinus spp. Assemblage zone

Definition and description. The palynological assemblages of PTr 1 are dominated by the cavate zonate spores *Kraeuselisporites wargalensis* and *Kraeuselisporites* spp. The range of *K. wargalensis* is restricted to this zone (Fig. 7-10). *K. cuspidus* and *Lunatisporites pellucidus* have their first appearances within PTr 1. Together with *K. wargalensis*, *Klausipollenites schaubergeri*, *Lueckisporites* spp., *Protohaploxypinus limpidus*, *P. varius*, have their highest stratigraphic occurrences within this zone. Long-ranging spores are accessory components of the assemblages (Table 1). Subdominant abundances of pollen include undifferentiated bisaccate pollen, striate bisaccate pollen, non-striate bisaccate pollen, and common occurrences of *Protohaploxypinus* spp. and *Alisporites* spp. (Fig. 9, Table 1). Marine palynomorphs represented by *Micrhystridium* spp. and *Veryhachium* spp.

Palynological assemblages from the uppermost Chhidru Formation have been described as part of the "Permian Assemblage" from Wargal (Salt Range) by Balme (1970). It is marked by increased spore abundances (about 60% *Kraeuselisporites* spp.).

Occurrence of PTr 1 and age control. The base of this zone is not recorded. The top is cut off by a hiatus.The assemblages representing PTr 1 are restricted to the uppermost Chhidru Formation at Narmia and Chitta-Landu. Bulk organic carbon isotope samples from the stratigraphic levels of PP and PTr 1 yield values of -28‰ for PP equivalent samples and -26‰ for PP 2 equivalent samples (Fig. 2). The low $\delta^{13}C_{org}$ values in the PTr 1 zone indicate a stratigraphic position near the negative shift marking the Permian-Triassic boundary (Hermann et al., in press). From the overlying Kathwai Member basal late Griesbachian ammonoid faunas with *Ophiceras* sp. have been reported (Guex, 1978, Schindewolf, 1954; D. Ware, ongoing work). For these reasons a latest Permian to early Griesbachian (?) age can be inferred for PTr 1.

Correlation. In Eastern Australia the base of APT 101 is defined by the first occurrence (FO) of *Lunatisporites pellucidus* and is interpreted to represent the Permian-Triassic boundary (Price, 1997). Taxa from the underlying APP 6 are still present. Thus APT 101 of Price (1997) and the *Lunatisporites pellucidus* zone of Helby et al. (1987), which is defined by the oldest common occurrence of *L. pellucidus* corresponds to PTr 1.

Abrupt increases of spore abundances near the Permian-Triassic boundary are recorded from numerous Permia-Triassic sections. This so-called spore spike is considered a distinct feature of the palynological turnover near the Permian-Triassic boundary (Stemmerik et al., 2001; Hochuli et al., 2010a; de Jersey, 1979). High spore abundances (44-80%) are also known from the *Protohaploxypinus microcorpus* zone of the Bowen Basin (Foster, 1982), which represents the upper part of the *Protohaploxypinus microcorpus* zone of Foster (1979). Unfortunately both zones have the same name but with different ranges. According to Foster (1982) *L. pellucidus* is not present in the *Protohaploxypinus microcorpus* zone. However the overall assemblage composition supports the correlation of the *P. microcorpus* zone (Foster, 1982) with PTr 1 from Pakistan (Fig. 2). Helby et al. (1987) suggested that the *P. microcorpus* zone (Foster, 1982) is a lateral facies equivalent of the *L. pellucidus* zone (Helby et al., 1987). The rare occurrences of *Lunatisporites pellucidus* in the uppermost samples of the Lower Sakamena Assemblage from Madagascar suggest that the uppermost part of these assemblages might be equivalent to PTr 1.

Table 1: Characterisation of the palynological assemblages from the Salt Range and Surghar Range, Pakistan.

AGE	Assem-blage Zone	Lithological unit	Age control: Ammonoids	Age control: Carbon isotopes	Range bases of selected palynomorphs	Range tops of selected palynomorphs	dominating sporomorph taxa	common sporomorph taxa	accessory sporomorph taxa
Anisian	PTr 7	Landa Member		heavy C-isotope values (-24‰)	*Aratrisporites* sp. A, *Jerseyaspora* sp.		*Aratrisporites* spp., non-striate bisaccate pollen and undifferentiated bisaccate pollen, *Alisporites* spp., *Falcisporites* spp.	*Calamospora* spp., *Densoisporites* spp. including *D. nejburgii, Endosporites papillatus*, *Leschikisporis* spp., *Osmundacidites* spp., *Punctatisporites* spp., *Verrucosisporites* spp., striate bisaccate pollen	*Apiculatisporis* spp., *Convolutispora* spp., *Cyclogranisporites* spp., *Converrucosisporites* spp., *Granulatisporites* spp., *Leiotriletes* spp., *Limatulasporites* spp. *Raistrickia* spp., *Retusotriletes* spp., monolete spores, monosaccate pollen, *Chordasporites* spp., *Duplicisporites verrucosus, Lunatisporites* spp. *Platysaccus* spp., *Sulcatisporites* spp.
Spathian	PTr 6	NI, TL	*Tirolites* sp.	C-isotope values around -28‰ positive shift towards the Anisian	*Aratisporites fischeri*, *A. paenulatus*, *A. tenuispinosus*, *Leschikisporis* spp. *Duplicisporites verrucosus*, *Jugasporites* spp.,	*Densoisporites playfordii*, *Lunatisporites noviaulensis*,	*Aratrisporites* spp., *Densoisporites* spp. including *D. nejburgii*, *Alisporites* spp., non-striate bisaccate pollen and undifferentiated bisaccate pollen	*Calamospora* spp., *Endosporites papillatus, Osmundacidites* spp., *Punctatisporites* spp., *Verrucosisporites* spp.	*Converrucosisporites* spp., *Convolutispora* spp., *Cyclogranisporites* spp., *Granulatisporites* spp., *Limatulasporites* spp. *Retusotriletes* spp., monosaccate pollen, *Chordasporites* spp., *Falcisporites* spp., *Platysaccus* spp., *Sulcatisporites* spp.
late Smithian-early Spathian	PTr 5	UCL above Wasatchites distractus beds	*Procolumbites* sp., *Glyptophiceras sinatus*, *Wasatchites distractus*	Positive shift across the Smithian-Spathian boundary			*Densoisporites* spp. including *D. nejburgii, Lunatisporites* spp. undifferentiated striate and non-striate bisaccate pollen	non striate bisaccate pollen	*Aratrisporites* spp., *Calamospora* spp., *Osmundacidites* spp., *Punctatisporites* spp.
middle Smithian	PTr 4	UCL up to Wasatchites distractus beds	*Nyalamites angustecostatus*, *Pseudoceltites multiplicatus*,	negative shift to (-32‰)			*Densoisporites* spp. (up to 90%) including *D. nejburgii*, *D. playfordii*	*Endosporites papillatus*	*Punctatisporites* spp., undifferentiated bisaccate pollen

Table 1: Characterisation of the palynological assemblages from the Salt Range and Surghar Range, Pakistan. - continued

AGE	Assem-blage Zone	Lithological unit	Age control: Ammonoids	Age control: Carbon isotopes	Range bases of selected palynomorphs	Range tops of selected palynomorphs	dominating sporomorph taxa	common sporomorph taxa	accessory sporomorph taxa
early to middle Smithian	PTr 3	CM,CS. At Chhidru and Chitta-Landu including lowermost part of UCL	*Nammalites pilatoides*, *Brayardites compressus*, *Flemingites flemingianus*, *Flemingites nanus*, *Xenodiscoides perplicatus*, *Flemingites bhargavai*	heavy C-isotope values (-24‰)	*Annulispora* spp., *Aratrisporites* spp., *Cyclogranisporites* spp., *Kraeuselisporites apiculatus, K. rallus*, *K. saeptatus*, *Maculatasporites* spp., *Naumovaspora striata*, *Polycingulatisporites* spp., *Retusotriletes* spp.	*Inaperturopollenites nebulosus*, *Kraeuselisporites apiculatus, K. rallus*, *K. saeptatus*, *Lundbladispora willmotti*, *L. obsoleta*, *L. brevicula*, *Maculatasporites* spp., *Naumovaspora striata*, *Polycingulatiyporites* spp., *Pretricolpipollenites* spp., *Uvaesporites* spp., *Weylandites spp.*	*Lundbladispora* including *L. obsoleta* and *L. brevicula*, *Densoisporites* spp. including *D. nejburgii*, *D. playfordii*	*Endosporites papillatus, Kraeuselisporites* spp., increased abundance of striate bisaccate pollen, *Lunatisporites* spp., and common occurrence of non-striate bisaccate pollen	*Annulispora* spp., *Calamospora* spp., *Convolutispora* spp., *Grandispora* spp., *Kraeuselisporites saeptatus*, *Osmundacidites* spp., *Punctatisporites* spp., *Retusotriletes* spp. *Uvaesporites* spp., *Verrucosisporites* spp., monosaccate pollen
Dienerian	PTr 2	At Narmia and Chitta-Landu: LCL, at Nammal: lower CM	*Prionolobus rotundatus*, *Gyronites* sp.	top of the zone falls within the positive shift, which marks the Dienerian-Smithian boundary	*Densoisporites nejburgii*, *D. playfordii*, *Lundbladispora brevicula*, *L. obsoleta*, *Uvaesporites* spp., *Chordasporites* spp.; first regular occurrence of *Lunatisporites noviaulensis*		*Densoisporites* spp. *Lundbladispora* spp. including *L. obsoleta* and *L. brevicula*	*Endosporites papillatus, Lunatisporites* spp. including *L. novialensis*, *L. pellucidus,* undifferentiated striate bisaccate pollen	*Calamospora* spp., *Kraeuselisporites* spp., non-striate bisaccate pollen
Griesbachian? /Latest Permian	PTr 1	Topmost Chhidru Formation		Light values around -29‰	*Kraeuselisporites cuspidus*, *K. wargalensis, Lunatisporites pellucidus*,	*K. wargalensis*, *Klausipollenites schaubergeri, Lueckisporites* spp., *Protohaploxypinus limpidus, P. varius*	*Kraeuselisporites wargalensis*, *Kraeuselisporites* spp., undifferentiated bisaccate pollen, striate bisaccate pollen, non-striate bisaccate pollen	*Alisporites* spp., *Protohaploxypinus* spp.	*Apiculatisporis* spp., *Calamospora* spp., *Endosporites papillatus, Punctatisporites* spp., *Verrucosisporites* spp., *Klausisporites* spp., *Lueckisporites* spp., *Lunatisporites pellucidus, Weylandites lucifer*
Permian	PP	Topmost Chhidru Formation		Values around -26‰			non-striate bisaccate pollen, striate bisaccate pollen, undifferentiated bisaccate pollen, *Alisporites* spp., *Protohaploxypinus* spp., *Weylandites lucifer*	*Klausipollenites* spp.	*Striatopodocarpites* spp., undifferentiated trilete spores

PTr 2: *Densoisporites* spp. – *Lundbladispora* spp. Assemblage zone

Definition and description. The base of the zone is defined by the base of the consistent occurrences of *Lunatisporites noviaulensis*. At Chitta-Landu rare occurrences of *L. pellucidus* are documented already within PTr 1 (Fig. 7), but the first stratigraphic common occurrences of the pollen taxon falls together with the base of PTr 2. The range bases of the following sporomorphs occur within PTr 2: *Densoisporites nejburgii*, *D. playfordii*, *Lundbladispora brevicula*, *L. obsoleta*, *Uvaesporites* spp., *Chordasporites* spp. The palynomorph assemblages of this zone are characterised by the dominance of cavate trilete spores, such as *Densoisporites* spp., *Lundbladispora* spp., including *L. obsoleta* and *L. brevicula.* The assemblage is distinguished from the overlying PTr 3 assemblage by lower spore diversity and lower abundances of striate bisaccate pollen. Spores include the long-ranging form *Calamospora* spp., Pollen are represented by *Lunatisporites* spp., *Lunatisporites pellucidus* and undifferentiated striate bisaccate pollen, and non-striate bisaccate pollen. Marine palynomorphs are constituted by *Micrhystridium* spp., *Veryhachium* spp. and pracinophyceae (*Leiospherida* spp., and *Tasmanites* spp.).

A palynological assemblage ranging from the Kathwai Member up into the middle of the CM has been described as "Early Scythian Assemblage" by Balme (1970). The assemblages include *Taeniaesporites* spp. (here recorded as *Lunatisporites* spp.), *Lundbladispora* spp., and *Densoisporites* spp. These taxa are very prominent in the palynological assemblages of PTr 2.

Occurrence of PTr 2 and age control. The assemblage zone spans the LCL at Chitta-Landu, Narmia, and lower part of the CM at Nammal. A Dienerian age for PTr 2 is indicated by the associated ammonoid faunas. Typical faunas containing *Gyronites sp*. have been described from the LCL at Nammal and Landu (Guex, 1978). The youngest Dienerian ammonoid fauna with *Prionolobus rotundatus* has been recorded near the top of assemblage PTr 2 (D. Ware, ongoing work).

Correlation. The *Lunatisporites pellucidus* zone of Foster (1982) is characterised by the dominance of cavate trilete spores and the first appearances of *L. pellucidus, Kraeuselisporites saeptatus, K. cuspidus,* and *L. obsoleta.* In our stratigraphic scheme (table 1) The FO of the mentioned taxa are distributed over the interval spanning the PTr 1 to PTr 3. The presence of *L. pellucidus, K. cuspidus,* and *L. obsolete* in PTr 2 suggests that the *L. pellucidus* zone (Foster, 1982) and PTr 2 are coeval. This supports Foster's (1982) correlation of the *L. pellucidus* zone (and the overlaying *Protohaploxypinus samoilovichii* zone) with the Pakistani "Early Scythian Assemblage" of Balme (1970). The sporomorph assemblages of the *Kraeuselisporites saeptatus* zone from the W-Australian Perth and Carnarvon Basins are marked by the presence of *Lunatisporites pellucidus*, *Lundbladispora* spp., *Densoisporites* spp., and *Kraeuselisporites* spp., which demonstrates close similarity with assemblages of PTr 2 (Fig. 2). The sporomorphs defining the PTr 2 assemblages are also well represented in the Middle Sakamena Assemblage from Madagascar of Wright and Askin (1987). In the Indian *Klausipollenites schaubergeri* assemblage (Tiwari and Tripathi, 1992) diverse and common cavate cingulate-zonate spores occur together with striate bisaccate pollen resembling the composition of assemblages of PTr 2. Marker species in the *Klausipollenites schaubergeri* assemblage are *L. pellucidus* and *L. brevicula*. *K. schaubergeri* is present together with *L. pellucidus* in our PTr 1, therefore the lower boundary of the *Klausipollenites schaubergeri* assemblage maybe lower within PTr 1.

PTr 3: *Lundbladispora* spp. – *Densoisporites* spp. Assemblage zone

Definition and description. The boundary between zone PTr 3 and PTr 2 is marked by the abrupt increase of bisaccate pollen abundance,

especially striate bisaccate pollen, together with a decrease of abundance of *Densoisporites* spp. The last consistent occurrence of *Lundbladispora* spp. defines the top of the zone. The ranges of several sporomorphs are restricted to this zone: *Kraeuselisporites apiculatus*, *K. saeptatus*, *Maculatasporites* spp., *Naumovaspora striata*, *Polycingulatisporites* spp. According to our study *K. rallus* is also restricted to PTr 3 but has previously been reported from the upper most part of the Chhidru Formation by Balme (1970) corresponding to our PTr 1. Characteristic for zone PTr 3 are the lowest occurrences of *Annulispora* spp., *Aratrisporites* spp., *Cyclogranisporites* spp., and *Retusotriletes* spp. The highest occurrences of the following taxa have been observed within the zone: *Inaperturopollenites nebulosus*, *L. obsoleta*, *L. brevicula, Pretricolpipollenites* spp., *Uvaesporites* spp., and *Weylandites* spp.

The dominance of cavate trilete spores of *Lundbladispora* spp. including *L. obsoleta* and *L. brevicula*, *Densoisporites* spp. including *D. nejburgii*, *D. playfordii* persists in this zone. Compared to the underlying PTr 2 the diversity of spores is remarkably higher but decreases again in the topmost samples (Table 1, Fig. 3, 4). The increased abundances of bisaccate pollen comprise mainly undifferentiated bisaccate and striate bisaccate pollen including *Lunatisporites* spp., *L. noviaulensis*, *L. pellucidus*. From the base of the zone and up-section non-striate bisaccate pollen are regularly observed (Fig. 3, 5). Pollen of Permian affinity such as *Weylandites lucifer*, and *Florinites* spp. are occasionally recorded. Except for the basal samples the marine assemblages are dominated by *Micrhystridium* spp. In the basal interval *Veryhachium* spp. represents the most abundant form.

Occurrence of PTr 3 and age control. Zone PTr 3 is recorded from the CM and CS at Nammal, Chhidru, and Chitta-Landu. At Chhidru the lowermost samples from the UCL yield palynological assemblages comparable to PTr 3. At Narmia it is represented by a single sample of the CM. The age of PTr 3 ranges from early Smithian to early middle Smithian. The oldest Smithian ammonoid faunas are documented from the base of the assemblage zone PTr 3. At Nammal and Chhidru the early Smithian and basal middle Smithian ammonoid succession of *Flemingites bhargavai*, *Xenodiscoides perplicatus*, *Flemingites nanus*, *Flemingites flemingianus Brayardites compressus*, and *Nammalites pilatoides* coincide with the zone range (Brühwiler et al., 2010). The change from Dienerian to Smithian ammonoid assemblages coincides with a positive shift of $\delta^{13}C_{org}$ values and the boundary between PTr 2 and PTr 3.

Correlation. The increase in striate bisaccate pollen, and first stratigraphic occurrence of *Aratrisporites* spp. defining the base of PTr 3 is also a characteristic of the E-Australian APT 102 zone (Price, 1997) and the *Protohaploxypinus samoilovichii* zone (Helby et al., 1987).

In E-Australia the APT 102 zone is overlain by the APT 2 zone corresponding to the *Protohaploxypinus samoilovichii* zone of Foster (1982). The base of this zone is defined by the FO of *Aratrisporites wollariensis* (Price, 1997). Since this taxon has not been observed in the Pakistani assemblages, the correlation of the APT 102 to APT 2 boundary to our stratigraphic scheme is indistinct. Based on the overall composition of the palynological assemblages from the Sakamena sediments in Madagascar, Hankel (1993) assigned his Sakamena assemblage to a position between the “Early Scythian Assemblage” and the “Late Scythian to Middle Triassic Assemblage” of Balme (1970).

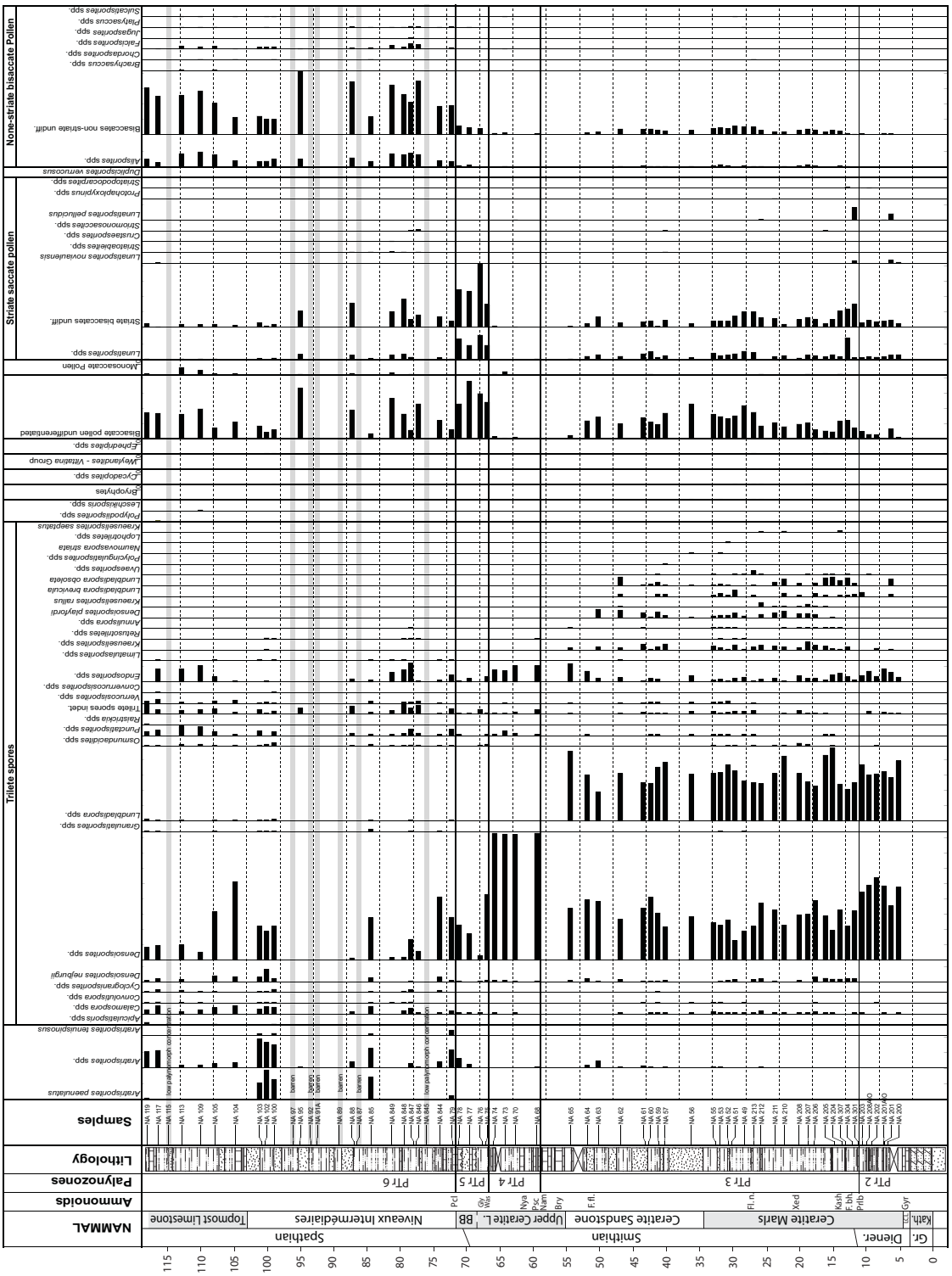

Figure 3: Relative abundances of relevant sporomorph taxa, Nammal gorge. Ammonoid biostratigraphy after Brühwiler et al., (2010; in press) and ongoing work of H. Bucher, and D. Ware,: Pcl = Procolumbites beds; Gly = Glyptophiceras sinatum beds; Was = Wasachites distractus beds; Nya = Nyalamites angustecostatus beds; Psc = Pseudoceltites multiplicatus beds; Nam = Nammalites pilatoides beds; Bry =

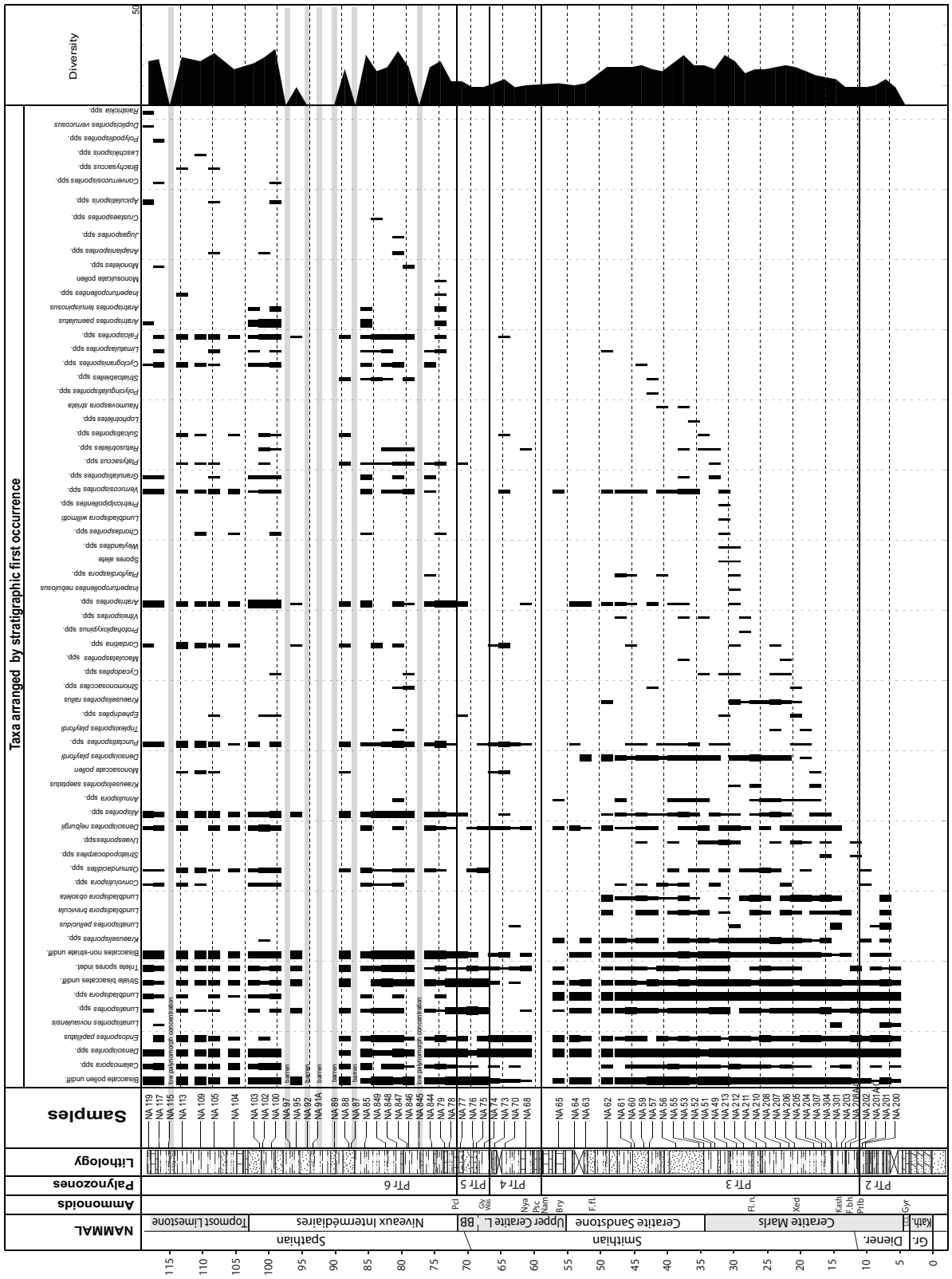

Figure 4: Ranges of palynomorphs at Nammal gorge section arranged by stratigraphic first occurrence.

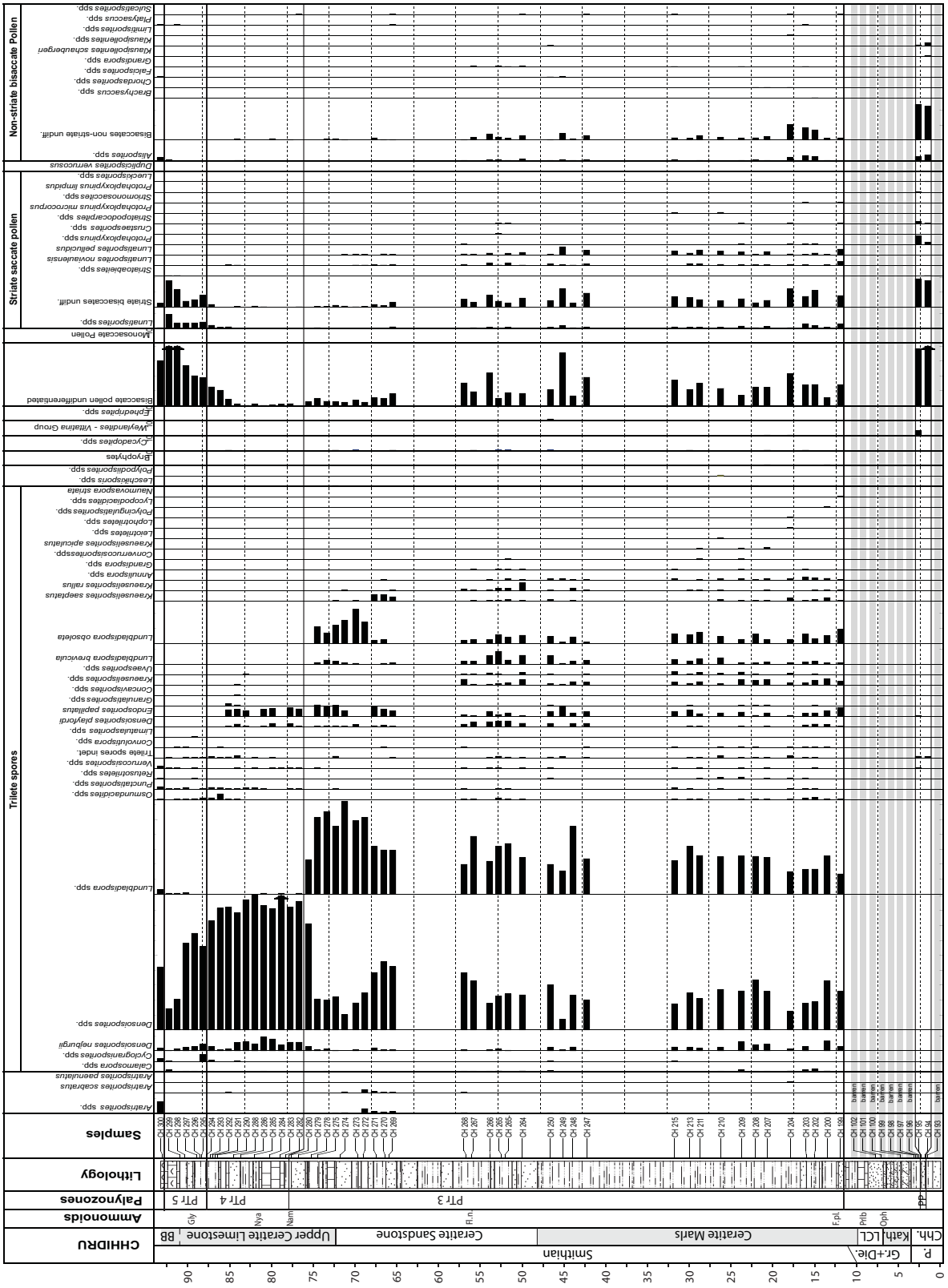

Figure 5: Relative abundances of relevant sporomorph taxa, Chhidru gorge. Ammonoid biostratigraphy after Brühwiler et al., (in press) and ongoing work of H. Bucher, and D. Ware: abbreviations see Fig. 4; Fl. p. = Flemingites planatus beds; Oph = Ophiceras sp. beds.

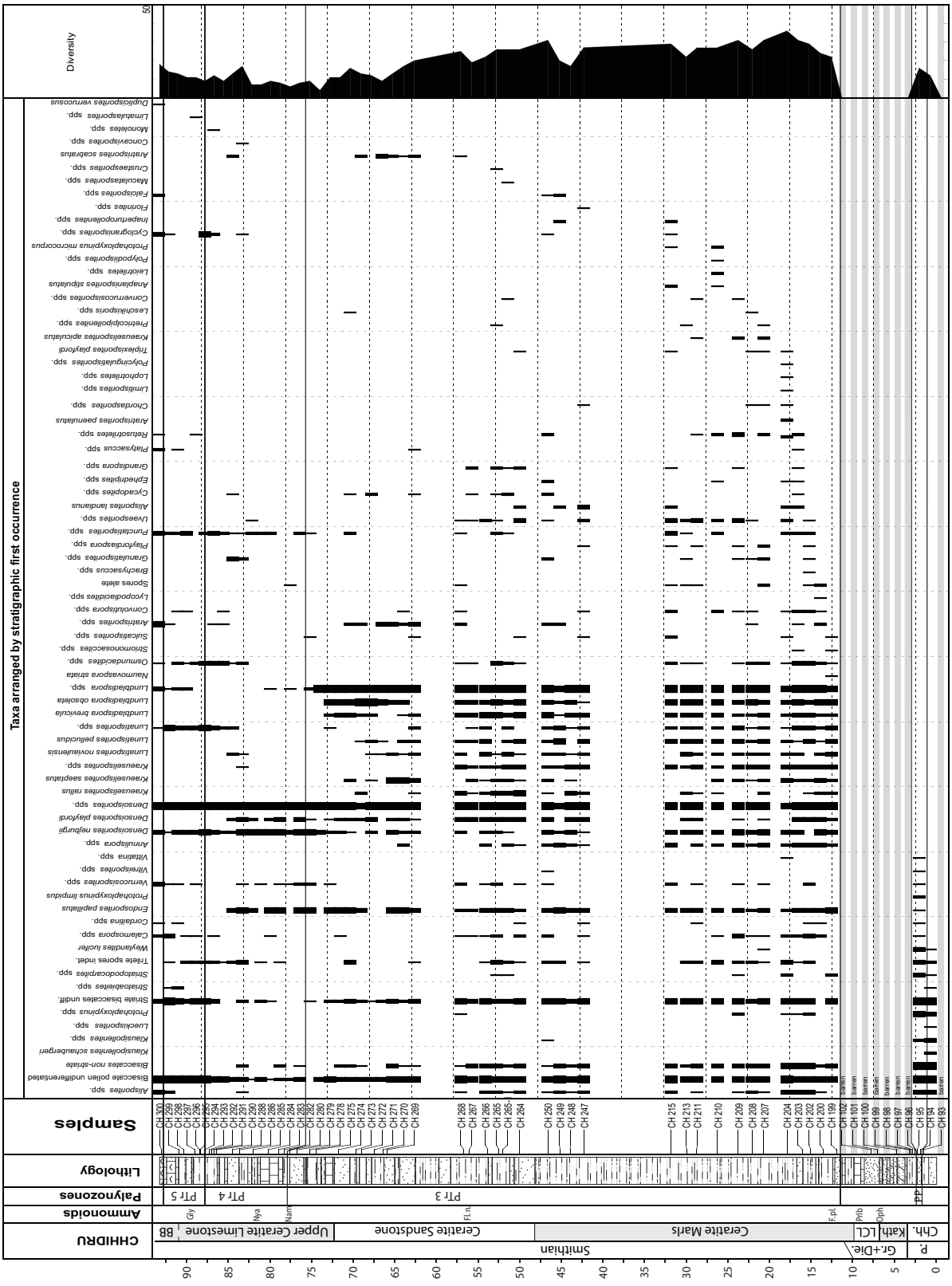

Figure 6: Ranges of palynomorphs at Chhidru gorge section arranged by stratigraphic first occurrence.

PTr 4: *Densoisporites* spp. Acme zone

Definition and description. The zone is defined by the acme of *Densoisporites* spp. The low diversity assemblages are dominated by *Densoisporites* spp. (up to 90%) including *D. nejburgii*, and *D. playfordii*. *Endosporites papillatus* is also common. Marine palynomoroph assemblages are dominated by *Micrhystridium* spp. with accessory occurrences of *Veryhachium* spp. and *Leiosphaeridia* spp.

Occurrence of PTr 4 and age control. The zone spans the UCL up to the *Wasatchites distractus* beds. A late middle Smithian age of zone PTr 4 is indicated by the associated ammonoid faunas assigned to the *Pseudoceltites multiplicatus* beds, and *Nyalamites angustecostatus* beds (Brühwiler et al., 2010; inpress).

Correlation. Due to a sampling gap the section corresponding to zone PTr 4 has not been reported by Balme (1970).The comparison with other Gondwana palynostratigraphic divisions suggest that PTr 4 corresponds to the Middle Sakamena Assemblage from Madagascar (Wright and Askin, 1987), the E-Australian *Protohaploxypinus samoilovichii* Assemblage (Foster, 1982; Helby et al., 1987) and probably also to the W-Australian *Kraeuselisporites seaptatus* Assemblage (Dolby and Balme, 1976) (Fig. 2).

PTr 5: *Lunatisporites* spp. – *Densoisporites* spp. Assemblage zone

Definition and description. The base of the zone is defined by the decrease in the abundance of *Densoisporites* spp. The high abundances of pollen, especially of striate bisaccate pollen including *Lunatisporites* spp. distinguish the assemblage from the underlying zone. The low diversity assemblages are characterised by high abundances of striate bisaccate pollen including *Lunatisporites* spp. and undifferentiated bisaccate pollen (Fig. 3, 5, 7). The cavate trilete spore content is reduced to low numbers of *Densoisporites* spp., and *D. nejburgii*. Compared to the underlying assemblages non-striate bisaccate pollen occur regularly. The rich plankton assemblage is characterised by high abundance of *Micrhystridium* spp. with accessory occurrences of *Veryhachium* spp., *Leiosphaeridia* spp. and foraminiferal test linings.

Occurrence of PTr 5 and age control. The zone PTr 5 is recorded from the UCL above the *Wasatchites distractus* beds and includes almost the entire BB. The base of the assemblage zone coincides with the onset of the positive C-isotope shift that marks the Smithian-Spathian boundary worldwide (Galfetti et al., 2007 a, c; Hermann et al., in press). A late Smithian to early Spathian age is indicated by the ammonoid succession of *Wasatchites distractus*, *Glyptophiceras sinatum*, and the positive C-isotope peak in the lowermost bed in the lowermost bed of the BB. Due to gaps the age of the BB above this C-isotope peak is different in the sections of Nammal and Chitta-Landu. At Nammal the ammonoid fauna with *Procolumbites* sp. indicates a early middle Spathian age for the topmost beds of the BB. At Chitta-Landu, however, the younger *Tirolites* fauna occurs within the lower part of the NI.

Correlation. Due to a sampling gap the section corresponding to zone PTr 4 has not been reported by Balme (1970). The taxa defining PTr 5 have their first appearances in PTr 1 to PTr 3. With the dominance of Lunatisporites spp. PTr 5 is distinctly different in its abundance structure from the underlying zones. Such a change in abundance structure has not been observed in most other Gondwanan records. A correlation with the Middle Sakamena Assemblage from Madagascar (Wright and Askin, 1987), the E-Australian *Protohaploxypinus samoilovichii* Assemblage (Foster, 1982; Helby et al., 1987), and the W-Australian *Kraeuselisporites seaptatus* Assemblage (Dolby and Balme, 1976) is therefore rather tentative only. The Indian *Playfordiaspora cancellosa* Assemblage zone has some similarities with the underlying *Klausipollenites schaubergeri* Assemblage. Marker species within *Playfordiaspora cancellosa* Assemblage zone are *L. pellucidus* and *D. playfordii*. Furthermore the

acme for *Lunatisporites* spp. and *Lundbladispora* spp. are recorded from this zone (Tiwari and Tripathi, 1992). However the exact stratigraphic position of the *Lunatisporites* spp. acme is not known. The position of the lower boundary *Playfordiaspora cancellosa* Assemblage with respect to our stratigraphic scheme is not determinable.

PTr 6: Aratrisporites spp. – Densoisporites spp. zone

Definition and description. The first stratigraphic abundance peak of *Aratrisporites* spp. including *A. paenulatus* and *A. tenuispinosus* defines the base of the zone. The range base of the two latter species coincides with the base of the zone. *A. fischeri*, *Duplicisporites verrucosus*, *Jugasporites* spp., *Leschikisporis* spp. appear within this zone. Range tops are recorded of the species *Densoisporites playfordii*, and *Lunatisporites noviaulensis*. The reduced numbers of striate bisaccate pollen and the increased spore diversity differentiates PTr 6 from PTr 5. The main spore taxa comprise *Densoisporites* spp., including *D. nejburgii*, *Aratrisporites* spp., including *A. paenulatus*, and *A. tenuispinosus.* In the lower part of the assemblage the *Aratrisporites* spp. group shows an abundance of up to 30 %, with a co-dominance of *Densoisporites* spp. In the upper part of the zone *Densoisporites* spp. dominates the assemblage. Smooth and ornamented spores include long ranging forms (Table 1). The bisaccate pollen are dominated by non-striate bisaccate pollen including *Alisporites* spp. together with *Falcisporites* spp., *Platysaccus* spp., *Sulcatisporites* spp., *Chordasporites* spp. Compared to the Chitta-Landu section pollen abundances are higher in the corresponding section at Nammal. Aquatic palynomoroph assemblages contain *Micrhystridium* spp., *Veryhachium* spp., *Botryococcus* spp. and algal remains of undetermined origin (Plate III, m-p).The "Late Scythian to Middle Triassic Assemblage" palynological assemblage described by Balme (1970) spans the NI, TL and the Landa Member. Balme (1970) demonstrated that the lower part of this zone is characterised by increased abundances of non-striate bisaccate pollen and *Aratrisporites* spp. and also by the persistent common abundance of *Densoisporites* spp., which is in agreement with the composition of the PTr 6 assemblage

Occurrence of PTr 6 and age control. The presence of this zone is documented at Nammal and Chitta-Landu and comprises the lithological unit NI and TL. Marine biostratigraphic markers are rather rare within this interval. The *Tirolites* sp. beds in the lower part of the NI at Chitta-Landu indicate an early Spathian age for the lower part of the palynozone. *Prohungarites* spp. have been observed in the lower part of the TL indicating a middle Spathian age for this interval (Guex, 1978).

Correlation. The consistent and abundant co-occurrence of *Aratrisporites* spp. and *Falcisporites* spp. are common characteristic of PTr 6 and the E-Australian APT 212 (defined by the FO *A. tenuispinosus,* Price, 1997) as well as the *Aratrisporites tenuispinosus* zone (Helby et al., 1987). From the latter additional common occurrences of *Leschikisporis* spp. have been described (Helby et al., 1987). Very close similarities also exist between the PTr 6 assemblages and the *Tigrisporites playfordii* assemblages of W-Australia (Dolby and Balme, 1976). Despite *T. playfordii* is rather rarely represented in Pakistani assemblages whereas it is abundant in W-Australia. The nominative species has been assigned to the new genus *Triplexisporites playfordii* by Foster (1979).

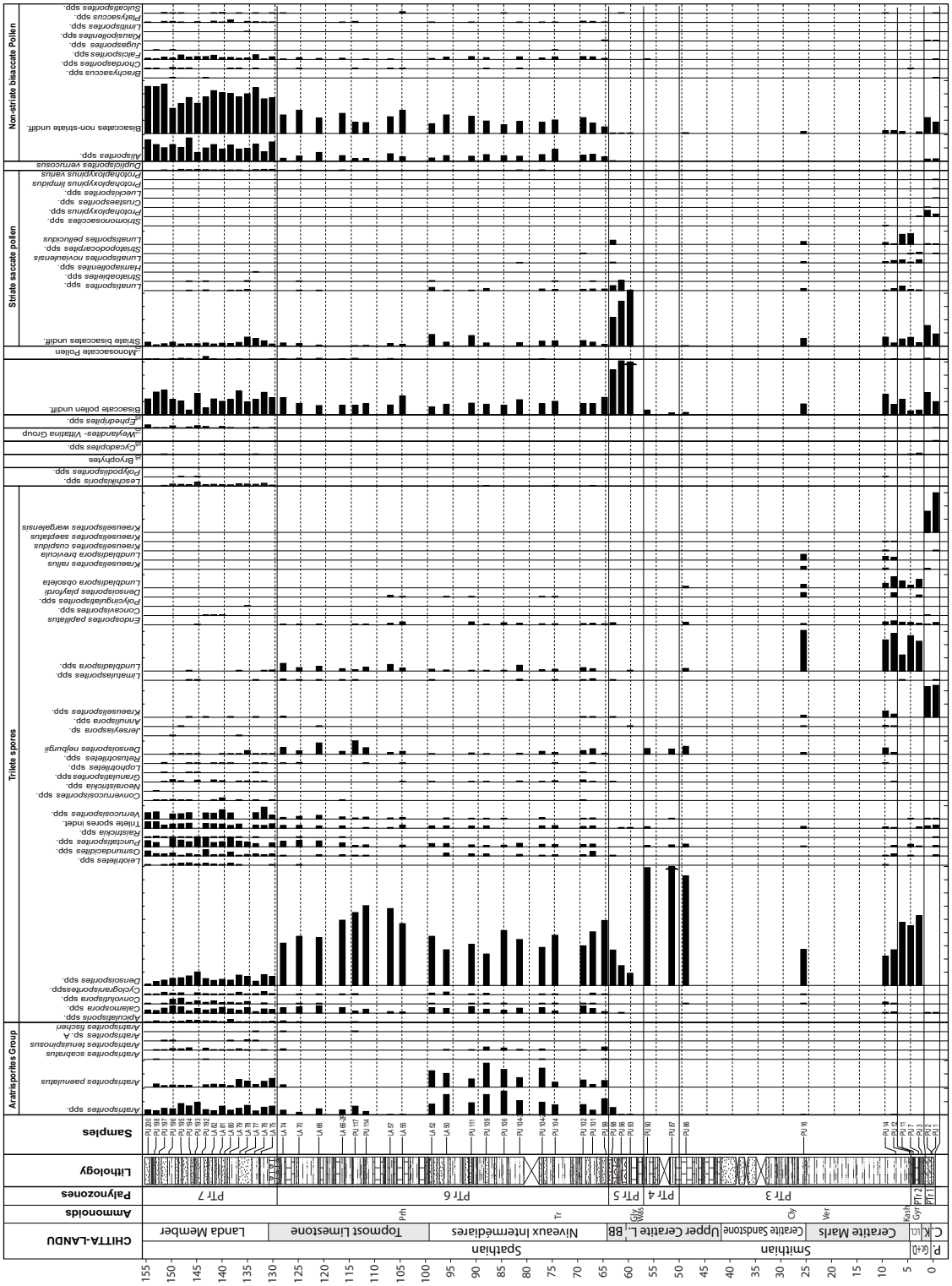

Figure 7: Relative abundances of relevant sporomorph taxa, Chitta-Landu gorge. Ammonoid biostratigraphy after Brühwiler et al., (in press), Guex (1978), and ongoing work of Bucher, H. and Ware, D.: abbreviations see Fig. 4; Prh = Prohungarites beds; Tr = Tirolites beds; Cly = Clypeoceras beds; Ver = Vercherites beds.

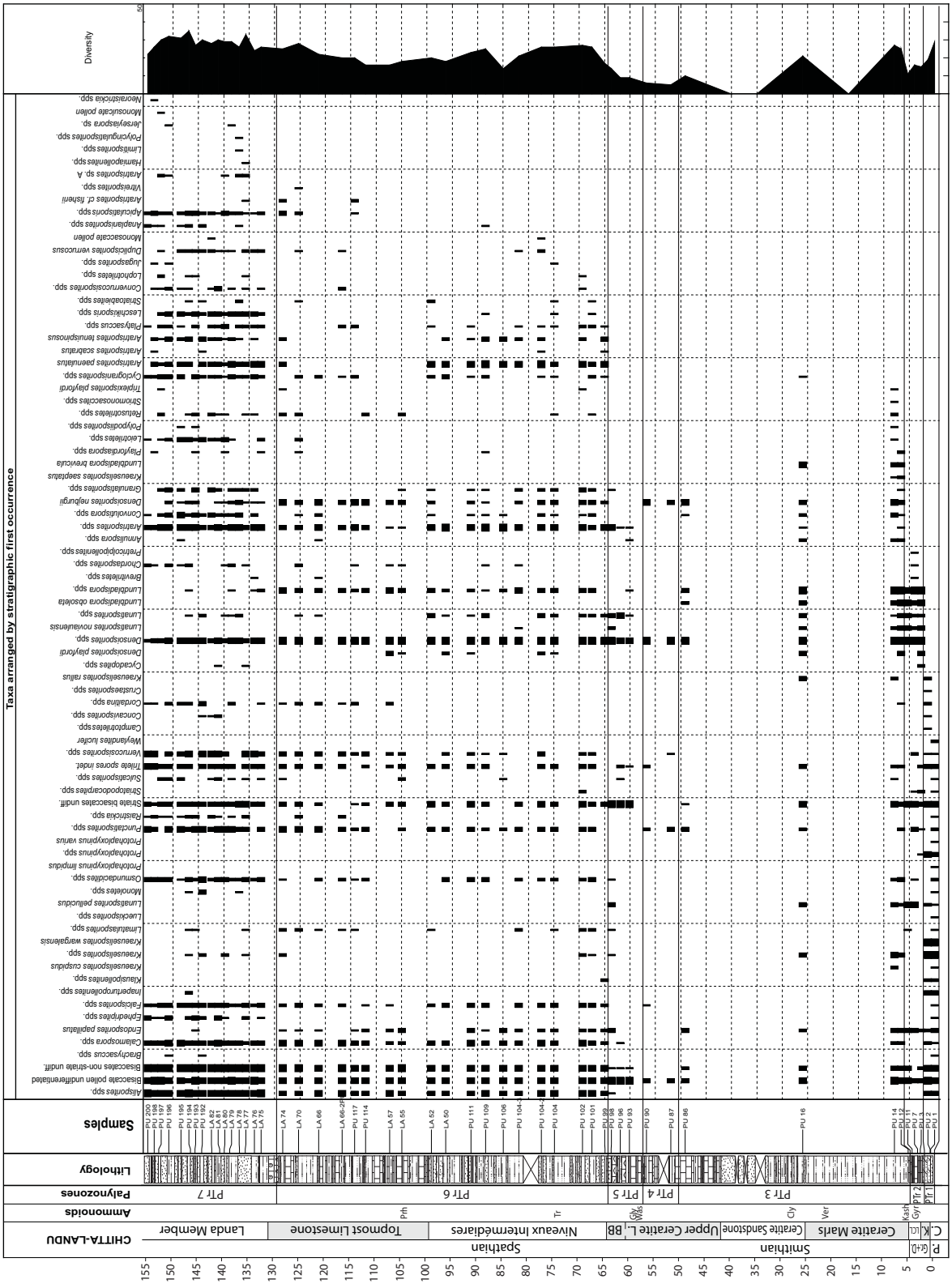

Figure 8: Ranges of palynomorphs at Chitta-Landu gorge section arranged by stratigraphic first occurrences.

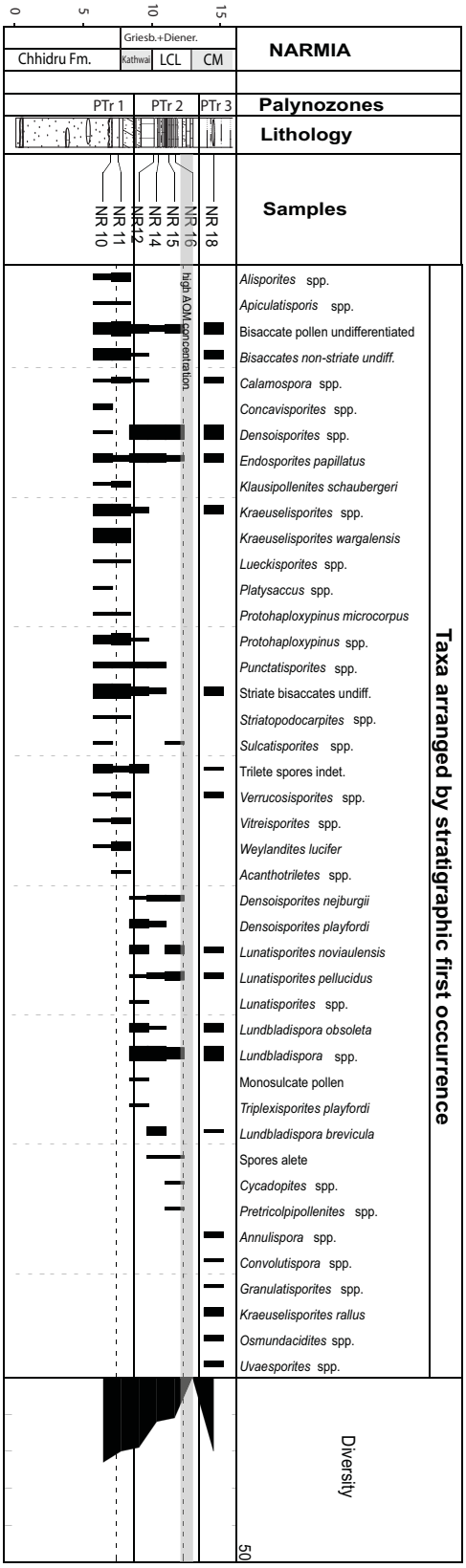

Figure 10: Ranges of palynomorphs around the boundary between the Chhidru Formation and the Mianwali Formation at Narmia gorge section arranged by stratigraphic first occurrence.

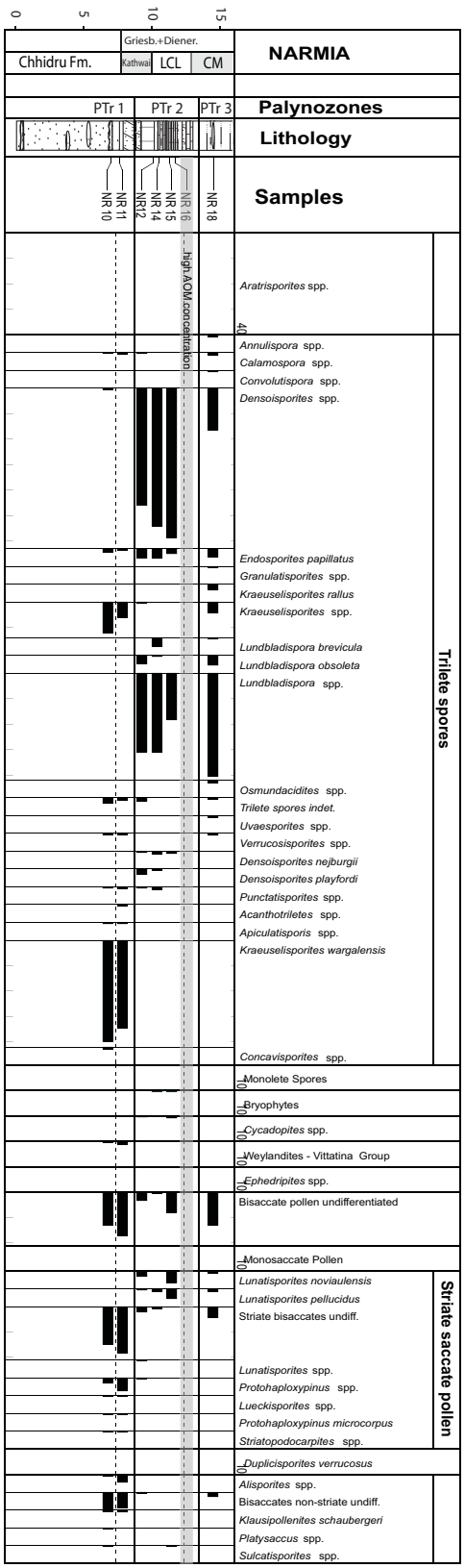

Figure 9: Relative abundances of relevant sporomorph taxa around the boundary between the Chhidru Formation and the Mianwali Formation, Narmia gorge.

PTr 7: *Alisporites* spp. – *Aratrisporites* spp. zone

Definition and Description. The base of the zone is defined by decreased abundances of *Densoisporites* spp. and increase in the abundance of non-striate bisaccate pollen. The increased abundance of ornamented trilete spores and the low abundance and diversity of cavate trilete spores distinguishes the PTr 7 from the underlying assemblages. The range base of *Aratrisporites* sp. A and *Jerseyiaspora* spp. and the first stratigraphic regular occurrences of monolete spores (*Leschikisporis* spp.). are recorded within this zone.

Characteristic for the PTr 7 assemblage is the dominance of non-striate bisaccate pollen including (*Alisporites* spp., *Falcisporites* spp., *Platysaccus* spp., *Sulcatisporites* spp., and *Chordasporites* spp.) together with striate bisaccate pollen and monosaccate pollen (Fig. 7, 8). Another characteristic feature is the common occurrence of *Duplicisporites verrucosus*. The rich and diverse spore assemblages comprise long ranging taxa (Table 1). Remains of megaspores are observed regularly, one completes specimen is illustrated on plate II, c Marine palynomoroph assemblages contain *Micrhystridium* spp., accessory occurrences of *Veryhachium* spp., and *Botryococcus* spp. (Plate III, q). Additionally algal remains of undetermined origin have been observed.

Occurrence of PTr 7 age control. Zone PTr 7 has been recorded from the Landa Member (Tredian Formation) at Chitta-Landu. Due to the shallow marine conditions, no marine invertebrate fossils are recorded with in this interval. Age constraints for the base of PTr 7 are indicated by the $\delta^{13}C_{org}$ record, which documents a positive shift near the lithological boundary between the Mianwali Formation and the Tredian Formation. The positive shift is interpreted to mark the Spathian-Anisian boundary in this section (Hermann et al., in press). Hence, we infer a Middle Triassic (Anisian) age for the PTr 7.

Correlation. The base of the E-Australian Middle Triassic APT 3 is defined by the FO of *Striatella scanica* (Price, 1997). This species has not been observed in the Pakistani sections. The co-occurrence of *Aratrisporites* spp. and *Falcisporites* spp. is a persistent feature of APT 2 which supports a correlation of PTr 7 with APT 2. Close similarities also exists with the *Triplexisporites playfordii* assemblages (Dolby and Balme, 1976) and the E-Australian *Aratrisporites tenuispinosus* zone (Helby et al., 1987).

5. Discussion

5.1. Implications for the dating of the Australian palynostratigraphy

Most Early Triassic sections in Gondwana are non-marine. The Perth and Carnarvon Basins in W-Australia represent two marine sedimentary archives of Early Triassic age. The sedimentary sequences of these basins have been dated based on conodont assemblages and ammonoids that have been studied from several cores (McTavish, 1973, McTavish and Dickens, 1974). These conodont assemblages are the basis for the independent dating of the W- Australian palynological zonation. The dating of the E-Australian palynological assemblages is based on the correlation with the W-Australian sites. In W-Australia the Early Triassic time interval is represented by the sedimentary sequences of the Locker Shales in the Carnarvon Basin and the Kockatea Shales and the overlying Woodada Formation in the Perth Basin, which is located south of the Carnarvon Basin. The Locker Shales and the Kockatea Shales overly unconformably Permian sediments. The completeness of the Early Triassic succession differs in these two basins. The Locker Shales in the Carnarvon Basin are dated late Dienerian to early Spathian, whereas the Griesbachian and early Dienerian is not preserved (Dolby and Balme, 1976). However, Griesbachian ammonoids are reported from near the base of the Kockatea Shales in the

Perth Basin (McTavish and Dickens, 1974). In the Carnarvon Basin, palynological assemblages from the Locker Shales have been assigned to the *Kraeuselisporites saeptatus* assemblage zone (Dolby and Balme, 1976). Based on conodont assemblages these shales could be dated late Dienerian to early Smithian and correspond to the upper part of the Kockatea Shales in the Perth Basin (Foster, 1982). The palynological assemblages from the Locker Shales include common occurrences of *Aratrisporites* spp., which has been reported to occur only rarely in the assemblages of the Kockatea Shales in the Perth Basin (Balme, 1963, Dolby and Balme, 1976). In our data, the FO of *Aratrisporites* spp. is recorded at the Dienerian-Smithian boundary in a similar stratigraphic position as in the Locker Shale assemblages. Based on the conodont assemblages Dolby and Balme (1976) inferred that the *Tigrisporites playfordii* zone in the Carnarvon Basin encompasses most of the Smithian, the entire Spathian and parts of the early Anisian. However, Smithian conodont assemblages are only reported from below the *T. playfordii* zone. Even in the core Cunaloo No 1 in which the *T. playfordii* zone ranges from 356.5 to 429.8 m (Dolby and Balme, 1976) the youngest Smithian conodonts including *Neospathodus waageni* are reported from below the range of the *T.playfordii* assemblages (530.4 m below the core top, McTavish, 1973). Spathian conodont associations are reported about 401 - 410 m below core top and confirm the Spathian age of the *T. playfordii* assemblages. With the assumption that the T. *playfordii* assemblage includes also parts of the Smithian Dolby and Balme (1976) compare the palynological assemblages of the Carnarvon Basin with palynological assemblages from the Narmia Member, which according to Balme (1970) include the lithological units NI and TL. Dolby and Balme (1976) conclude that the Pakistani assemblages of the Narmia Member resemble the *T. playfordii* assemblages of the Carnarvon Basin. This correlation is supported by the results of the present study. The increased abundances of *Aratrisporites* spp. and the regular occurrences of *Falcisporites* spp. characterise PTr 6 and PTr 7 and the *T. playfordii* assemblages. Dolby and Balme (1976) expected that these assemblages range down into the Smithian without palynological evidence since this interval has not been studied by Balme (1970). This correlation was based on the presence of the Smithian conodont *Neospathodus waageni*, which has been reported from the UCL in the Salt Range and Surghar Range (e.g. Pakistani-Japanese Research Group, 1985) and which is also known from below the *T. playfordii* zone in W-Australia. Due to the lack of a firm biostratigraphic evidence for the age of the basal part of the *T. playfordii* zone (Dolby and Balme, 1976) and the results of our study demonstrating that the PTr 4 and PTr 5 assemblages recovered from the UCL resemble rather those of the *Kraeuselisporites saeptatus* assemblage zone, we suggest that the *T. playfordii* assemblages of the Carnarvon Basin are probably restricted to the Spathian and the early Anisian. This interpretation has also consequences for the timing of the E-Australian *Aratrisporites tenuispinosus* zone, which has been regarded as equivalent to the W-Australian *T. playfordii* zone (Helby et al., 1987). Our results suggest that the E-Australian *A. tenuispinosus* zone is most probably also Spathian to early Anisian in age.

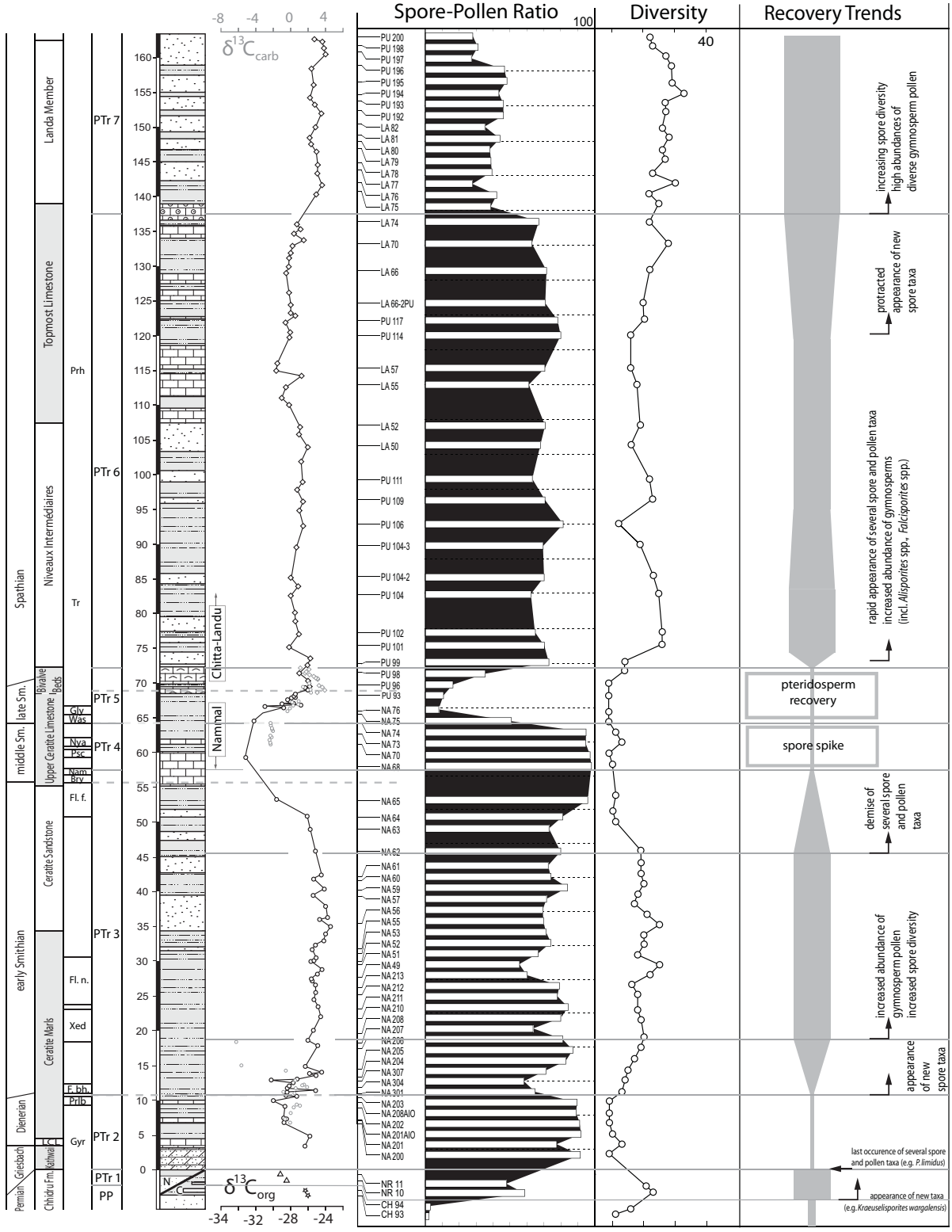

Figure 11: Composite record from the Nammal, Chhidru, Chitta-Landu and Narmia gorges. Relative abundances and the diversity pattern of the palynological data have been used to illustrate the palynofloral recovery trend on North Gondwana. Ammonoid biostratigraphy after Brühwiler et al. (2010; in press) and carbon isotopes after Hermann et al. (in press).

5.2. Implications for the recovery of the flora

The unique palynological record from the sedimentary successions of the Salt Range and Surghar Range allows reassessing of the recovery of floral diversity after the end-Permian event. The firm chronological framework for the floral succession is provided by the detailed ammonoid biostratigraphy of the sections (Brühwiler et al., in press). In Fig. 11 a composite record of the Nammal, Chhidru, Chitta-Landu and Narmia gorge is presented. Based on the palynological assemblages the diversity patterns of the Early Triassic floral succession are illustrated. Changes in the floral succession seem to be closely related to changes in the carbon isotope curve (Fig. 11). Early Triassic carbon isotope records are marked by recurrent excursions of high magnitude (e. g. Galfetti et al., 2007 a). Negative excursions have been interpreted to be triggered by pulses of volcanic activity releasing CO_2 from volcanic degassing or from metamorphosed organic deposits whereas the triggers of the positive excursions are still poorly understood (Payne and Kump, 2007). Since changes in the atmospheric CO_2 content are known to have a great influence on the global climate (Kump, 2002) the carbon isotope excursions probably reflect climatic changes within the Early Triassic (Galfetti et al., 2007 c). The spore pollen ratio displays changes in the relative abundances of the two major plant groups namely pteridophytes and gymnosperms (Fig. 11).

The Permian palynoflora (PP) is dominated by gymnosperm pollen. Due to the moderate preservation of the Permian assemblages the diversity in PP assemblages is rather low. Identified striate bisaccate pollen include common occurrences of *Protohaploxypinus* spp. representing the *Glossopteris* flora of the southern hemisphere (Balme 1995, Lindström and McLoughlin, 2007). A distinct floral turnover occurs between the PP and the PTr 1 assemblages. The spore pollen ratio shows a significant increase of spore abundances. With the FO of *Kraeuselisporites wargalensis* cavate trilete spores begin to be the dominant components of the palynoflora. From PTr 1 onward lycopod spores dominate the palynological assemblages up-section up to PTr 4. The diversity is moderately high, since the FOs of several sporomorph taxa occur within PTr 1 (e. g. *Kraeuselisporites* spp., *Lunatisporites pellucidus*) and typical Permian taxa (e. g. *Weylandites lucifer*) are still present. Abundances of gymnosperm pollen are reduced compared to the PP assemblages and several of the lingering Permian taxa have their last occurrence (LO) within or at the top of PTr 1. The $\delta^{13}C_{org}$ of bulk organic matter that have been measured in PP and PTr 1 assemblages indicate for the PTr 1 zone a stratigraphic position near the negative shift that marks Permian-Triassic section worldwide (Hermann et al., 2010). If we follow the model simulations of Payne and Kump (2007) this would imply volcanic activity and enhanced greenhouse gas concentrations. Increasing greenhouse gas concentrations for the Permian-Triassic transition have also been predicted by stomatal index data (Retallack, 2009) and climate models (Kiehl and Shields, 2005). A significant diversity decline marks the boundary between PTr 1 and the Dienerian PTr 2. Despite several lycopod spore taxa have their FO at the base of PTr 2 (e. g. *Lundbladispora brevicula*, *L. obsolete*) the diversity decreases because of the extinction of several Permian taxa at the top of PTr 1 (Fig. 8, 11). In the samples of the lower part of PTr 3 (beginning of the early Smithian, Fig. 11) several spore taxa have their FO (Table 1). The spore-pollen ratio displays increasing proportions of gymnosperm pollen. This interval coincides with a positive shift of the $\delta^{13}C_{org}$ record. Assemblages representing the main part of the early Smithian are characterised by an early recovered diversity (Fig. 11). The higher diversity is mainly caused by rich spore assemblages together with the common occurrences of gymnosperm pollen. This interval coincides with a period of relative stable carbon isotope values which may be interpreted to reflect a time period of relatively low volcanic activity and therefore stable environmental

conditions. The uppermost part of the early Smithian PTr 3 is marked by a gradual diversity decrease (Fig. 11, 6). The abundance of gymnosperm pollen declines synchronously and several spore species have their LO including *Lundbladispora brevicula* and *L. obsoleta* in this interval. Both species are very prominent in PTr 2 and PTr 3. The onset of the diversity decline coincides with the onset of a negative isotope shift. According to the studies of Payne and Kump (2007) this could be interpreted as a renewed pulse of volcanically induced CO_2 and the beginning of repeated environmental perturbations. The middle Smithian assemblages are almost exclusively dominated by cavate trilete spores. In PTr 4 the assemblages are even almost monogeneric. The diversity within this so called spore spike is very low. PTr 4 coincides with a negative isotope anomaly. A second distinct floral turnover marks the boundary between PTr 4 and PTr 5. The diversity remains low in PTr 5 but the abundance structure changes significantly as it can be observed in the spore-pollen ratios (Fig. 11). The *Densoisporites* spp. assemblages of PTr 4 are replaced by striate bisaccate pollen dominated assemblages indicating the proliferation of pteridosperms. The palynological turnover has been interpreted to reflect the adaptation of the vegetation to changing climatic conditions (Hermann et al., subm.). That would imply a change from relatively humid conditions in the time period from the Griesbachian to the middle Smithian and distinct change to dryer climates in the late Smithian and onwards. The boundary between PTr 4 and PTr 5 coincides with the onset of the positive carbon isotope shift that marks the Smithian-Spathian boundary. A rapid increase of the palynofloral diversity can be observed in the basal assemblages of the Spathian PTr 6. Gymnosperm pollen taxa are more abundant in PTr 6 indicating the recovery of conifers and pteridosperms. Several spore and pollen taxa have their FO at the base or within PTr 6 (Table 1). During the Spathian the $\delta^{13}C_{org}$ curve is relatively stable except for a slight negative trend. This could indicate that the volcanically induced environmental perturbations were fading during this time period. The recovery of gymnospermous pollen is extends into PTr 7. The abundance of gymnosperm pollen increases again and the palynofloral assemblages are characterised by high diversity. After a positive shift, which coincides with the lower boundary of PTr 7, $\delta^{13}C_{org}$ values are relatively stable.

The floral succession of the Early Triassic sequence from Pakistan reveals two distinct floral turnovers. The first occurs near the Permian-Triassic boundary and the second at the middle to late Smithian boundary.

Due to the diachronous boundary between the Chhidru Formation and the Kathwai Member and associated gaps, the study of the floral succession around the Permian-Triassic boundary in a continuous outcrop section has been hampered in Pakistan. However the distinct global floral turnover that marks the Permian-Triassic boundary in numerous sections is also recognised in our samples from the uppermost part of the Chhidru Formation. Detailed palynological studies in a continuous section that focuses on the effects of the end-Permian event on the Gondwana flora exist for the sedimentary succession of the Antarctic Prince Charles Mountains. Based on palynological data and the correlation with the Australian palynstratigraphic scheme the Antarctic Mc Kinnon Member and the Ritchie Member have been assigned a Permian and Griesbachian age, respectively (Lindström and McLoughlin, 2007). The palynological assemblages document the extinction of several Permian taxa near the formational boundary. This initial extinction is marked by a shift in the spore pollen ratio indicating higher abundances of pteridophytes in the assemblages of the Ritchie Member. Assemblages of the basal Ritchie Member record a continued floral change with the prolonged extinction of lingering Permian taxa (Lindström and McLoughlin, 2007). Similar patterns across the Permian-Triassic boundary have also been described from sections outside the Gondwanan floral province. In the

sedimentary sequence of Jameson Land in Greenland the onset of the palynofloral turnover is marked by a distinct spore spike in the palynological assemblages (Looy et al., 2001; Stemmerik et al., 2001). Synchronously, abundances of typical Permian gymnosperms taxa are reduced. The spore spike has been interpreted to represent the onset of the terrestrial ecosystem collapse. It is followed by the delayed extinction of Permian taxa and the intermittent increase in diversity (Looy et al., 2001). The same features have also been documented from another Permian-Triassic record in the northern mid latitudinal Atlantic province. The Permian palynoflora of the sedimentary sequence of the Trøndelag platform in Norway is characterised by the dominance of *Vittatina* spp. and striate bisaccate pollen (Hochuli et al., 2010a,b). At the Permian-Triassic boundary the abundance of *Vittatina* spp. is significantly reduced and numerous spore taxa appear. However typical Permian taxa such as *Vittatina* spp. and *Lueckisporites virkkiae* are still present in the Griesbachian and diversity is comparatively high (Hochuli et al., 2010b). In the detailed palynological study of the sedimentary sequence from the Finnmark platform (Norway) the onset of the floral turnover is characterised by a pronounced short lived spore spike. Gymnosperms recover immediately after this spore spike. These short-termed changes in the abundance structure of the Norwegian palynoflora occur prior to the Permian-Triassic negative carbon isotope spike. They have been interpreted to reflect the environmental perturbations caused by the onset of volcanic activity of the Siberian Traps (Hochuli et al., 2010a). Late Permian palynological assemblages from the Cathaysian province have been described from sections in Guizhou, Yunnan, and Zhejiang in South China (Ouyang and Utting, 1990; Peng et al., 2005; 2006). In contrast to the Late Permian flora of the mid-latitudes, these assemblages are dominated by fern spores including numerous endemic genera. Similar to the floral successions in Pakistan, Antarctica, Greenland and Norway, these Late Permian assemblages are replaced by assemblages with a transitional character. These transitional assemblages are still marked by high abundances of Late Permian taxa but include also taxa with Early Triassic affinity such as *Lundbladispora* spp., and *Taeniaesporites* spp. (here recorded as = *Lunatisporites* spp.). These mixed assemblages are followed by Early Triassic floral associations characterised by the common occurrences of spores (*Lundbladispora* spp., *Aratrisporites* spp.,) and bisaccate pollen grains (*Taeniaesporites* spp., *Protohaploxypinus* spp.) together with increased abundances of *Cycadopites* spp. (Ouyang and Utting, 1990; Peng et al., 2005; 2006). Differing from the mid-latitudes where lycopod spores dominate the palynological assemblages of Griesbachian age, the abundance of gymnosperm pollen increases with the beginning Early Triassic in the tropical Cathaysian province.

With the floral turnover near the Permian-Triassic boundary cavate trilete spore become the dominant component of palynological assemblages in the mid-latitudes of both hemispheres whereas in tropical floral assemblages ferns are partly replaced by gymnosperms and lycopod spores during the same time interval. A common feature of the floral turnover near the Permian-Triassic transition of the Gondwanan, the Atlantic and the Cathaysian floral province is the appearance of lycopod spore taxa such as *Lundbladispora* spp., *Aratrisporites* spp., and the gymnosperm pollen taxa *Lunatisporites* spp. The floral turnover near the Permian-Triassic boundary resulted in the establishment of more cosmopolitan plant communities with common or even dominating lycopod abundances (Retallack, 1995; Foster et al., 1997).

The second floral turnover occurs between the middle and late Smithian. The spore-pollen ratio documents an abrupt decrease of spore abundances in the Pakistani records. A similar distinct change from spore dominated assemblages to pollen dominated assemblages has

been observed in the same stratigraphic position in the palynological assemblages from the Svalis Dome area (Norway) (Galfetti et al., 2007 a, Hochuli and Vigran, 2010). This distinct shift in the palynofloral abundance structure coincides in both areas with the late Smithian extinction event that severely affected ammonoids and conodonts and is represented by the low diversity an cosmopolitan fauna of the *Wasatchites distractus* beds (Brayard et al., 2006, Orchard, 2007). The early Spathian assemblages in Pakistan are marked a rapid increase in palynofloral diversity and the consistent occurrence of *Falcisporites* spp. and *Alisporites* spp. These are characteristic gymnosperm pollen taxa in the Spathian and Anisian of Pakistan. Late Spathian pollen assemblages from the Svalis Dome area in Norway differ distinctly from those of the southern hemisphere. (Hochuli et al., 1989; Vigran et al., 1998). *Succinctisporites grandior* and *Illinites chitonoides*, which have their first appearance in the Norwegian Spathian (Hochuli et al., 1989; Vigran et al., 1998), have not been recovered in Pakistan. Around the Smithian-Spathian boundary provincialism of the palynological records from the mid latitudes of the northern and southern hemisphere increase significantly.

In contrast to our results, the Early Triassic palynofloral record from Europe has been interpreted to represent survival communities populating the ecological desert after the end-Permian event. It has been suggested that the pioneering lycopods and bryophyte dominated plant assemblages prevailed unchanged during the entire Early Triassic. The recovery of the terrestrial ecosystems is thought to be delayed by 4 - 5 Ma and began only in the late Spathian (Looy et al., 1999). This differs from our data in the two following points. Firstly, the palynological record from Pakistan documents more than one attempt of recovery within the Early Triassic (early Smithian and early Spathian). However these early recoveries are reset by recurrent environmental perturbations as documented in the interval from the middle Smithian to the early Spathian. Ammonoid calibrated U-Pb radiometric ages (Ovtcharova et al., 2006; Galfetti et al. 2007 b) suggest a duration of about 1.4 Ma for the interval from the Griesbachian to the Dienerian, and a duration of about 700 ka for the Smithian. This implies that the first recovery pulse as documented in the assemblages of the early Smithian (PTr 3) occurred approximately 1.4 Ma after the end-Permian event, and the second recovery pulse is documented in the early Spathian (PTr 6) about 2.1 Ma years after the end-Permian event.

Secondly, the changes in the abundance structure as well as in the qualitative data of the Pakistani records demonstrate that the vegetation on North Gondwana has not remained unchanged during the entire Early Triassic. In fact, the assemblages show multiple adaptations to flucuating environmental conditions during the Early Triassic.

Since a wide range of biomes seems to be subject to fundamental changes in floral composition across the Permian-Triassic boundary (Pakistan, Antarctica, Norway, Greenland, South China) and within the Early Triassic (Pakistan, Norway) the most probable causes for the observed floral changes are environmental changes such as climatic perturbations (Galfetti et al., 2007 c; Lindström and McLoughlin, 2007; Hochuli et al., 2010b; Hochuli and Vigran, 2010). The multiple carbon isotope excursions during the Early Triassic that have been interpreted to be caused by recurrent pulses of volcanic activity (Payne and Kump, 2007) suggest that these climatic changes are induced by volcanically triggered CO_2 releases. Additional environmental stress factors could have been the release of gases such as halocarbons and SO_2 by the heating of evaporite deposits during the Siberian Trap emplacement. These gases are thought to have had a great impact on the environmental conditions by causing ozone layer depletion and acid rain (Svensen et al., 2009, Wignall, 2001). The onset of the Early Triassic floral deteriorations are marked by a distinct spore spike in various

sections (Looy et al., 2001; Hochuli et al., 2010a). This spore spike marks also the onset of the low diversity, lycopod dominated flora that has been postulated to prevail during the Early Triassic (Looy et al., 1999). The new record from the Salt Range and the Surghar Range demonstrates that this flora has not remained unchanged during the Early Triassic. The extinction and diversification patterns are far more complex. The flora shows multiple adaptations to the recurrent Early Triassic environmental perturbations.

6. Conclusions

Based on terrestrial palynomorphs recovered from the Late Permian to Middle Triassic sedimentary succession of the Salt Range and Surghar Range, eight palynological assemblage zones are defined and calibrated against ammonoid and C-isotope chemostratigraphy. The proposed palynological zonation is based on the relative abundances of prominent taxa in the zone together with top and base occurrences of selected taxa. The high resolution of the palynological and ammonoid biostratigraphic record the Salt Range and Surghar Range sections represent a reference area for the palynological zonation of the North Gondwanan shelf. The two basal zones (PP, PTr 1) have been recovered from the uppermost Chhidru Formation. PP is dominated by gymnosperm pollen, whereas the diverse PTr 1 assemblages are characterised by abundant cavate trilete spores associated with conifer and pteridosperm pollen of Permian affinity. The Dienerian to early Smithian PTr 2 and PTr 3 assemblages are dominated by cavate spores. However a first palynofloral recovery is reflected in diverse spore assemblages and higher abundances of gymnosperm pollen in PTr 3. The middle Smithian assemblages PTr 4 are marked by an acme of *Densoisporites* spp. The successive late Smithian to early Spathian PTr 5 assemblages are characterised by abundant striate bisaccate pollen. A second palynofloral recovery is reflected in the basal part of PTr 6 where diversity increases. The Spathian and Anisian assemblages (PTr 6 and PTr 7) are characterised by the abundance non-striate bisaccate pollen, the common occurrence of *Aratrisporites* spp. The comparison with palynological records from Australia, India and Madagascar revealed a similar succession of palynological assemblages in these sites. This allowed correlating several palynological assemblages across Gondwana. From the correlation a new dating for the base of the W-Australian *Tigrisporites playfordii* zone and the E-Australian *Aratrisporites tenuispinosus* zone could be inferred. The lower boundary of these zones is most probably of early Spathian age rather than of Smithian age. A comparison with the microfloral records of mid latitudes from the northern hemisphere reveals two distinct microfloral turnovers reflected in the palynological assemblages in both hemispheres. The first turnover occurs near the Permian-Triassic boundary. There gymnosperm dominated assemblages are replaced by assemblages dominated by cavate trilete spores of lycopod affinity. This change can also be observed in tropical records. The dominance of lycopod spores is followed by the second palynofloral turnover near the Smithian-Spathian boundary.

Our quantitative and qualitative data demonstrate that the palynflora has not remained monotonously dominated by lycopod spore throughout the entire Early Triassic. The assemblages rather indicate that the recovery of palynofloral diversity started early (1.4 Ma) years after the end-Permian event, but was interrupted by repeated environmental perturbations.

Appendix A1: Annotated list of identified palynomorphs in alphabetical order

Spores

Anaplanisporites spp. JANSONIUS 1962

Annulispora spp.DE JERSEY 1959 (Plate I, ab)

Spores assigned to *Annulispora* are radial, trilete and cingulated with circumpolar thickening on the distal side. The laesura is

distinct extending to the cingulum and flanked by thin labra. On the proximal face a usually well defined curvaturae (perfectae or imperfectae) is present. In the original diagnosis of *Annulispora* DE JERSEY 1959 the laesura is of variable length, averaging two thirds of the spore diameter. The exine is smooth /laevigate. De Jersey (1962) notes that an extension of the laesura is not observed in *Annulispora*, however the some of the specimen illustrated in de Jersery (1962) seem to show trilete marks extending to the equator. Cingulum, circumpolar thickening and well defined curvaturae are also diagnostic of *Limatulasporites* HELBY AND FOSTER IN FOSTER 1979 but the observed spores lack the proximal sculptural elements characterising *Limatulasporites*. Discisporites is acingulate and with different ornamentation.

Apiculatisporis spp. POTONIÉ & KREMP 1954

Aratrisporites sp. A (Plate I, n)

A species of *Aratisporites* that corresponds to the emended genus diagnosis of Playford & Dettmann, 1965. The exoexine has a spongeous structure. The usually straight monolete mark extends the full length of the spore and is bordered by raised labra.

Aratrisporites fischeri (KLAUS) Playford& Dettmann 1965 (Plate I, a)

Aratrisporites paenulatus PLAYFORD & DETTMAN 1965 (Plate I, p)

Aratrisporites scabratus KLAUS 1960 (Plate I, q)

Aratrisporites spp. (LESCHIK) Playford & Dettmann 1965

Aratrisporites tenuispinosus PLAYFORD 1965 (Plate I, o)

Brevitriletes sp. BHARADWAJ & SRIVASTAVA 1969

Calamospora landiana BALME 1970 (Plate I, b)

Calamospora spp. SCHOPF, WILSON & BENTALL 1944

Camptotriletes spp. (NAUMOVA) ex Potonié & Kremp 1954

Concavisporites spp. PLUG in Thomson & Pflug 1953 (Plate II, a)

Converrucosisporites spp. POTONIÉ & KREMP 1954

Convolutispora sp. 1 (Plate I, d)

Spores assigned to *Convolutispora* sp. 1 show a circular to subcircular outline with a thin yellow exine. Thickness of individual elements of the anostomosing vermiculate closely packed ornamation is 1 of less µm. The trilete mark is usually distinct, spore dimension have been measured on two specimens (40 and 55 µm).

Convolutispora sp. 2 (Plate II, i)

Spores assigned to *Convolutispora* sp. 2 show a circular to subcircular outline with a thick orange to brown exine. Thickness of individual elements of the anostomosing vermiculate closely packed ornamation is 2 to 4 µm. The trilete mark is often distorted by the heavy ornamentation, spore dimension have been measured on four specimens (27 to 51 µm).

Convolutispora spp. STAPLIN & MALLOY 1955

Cyclogranisporites spp. POTONIÉ & KREMP 1954 (Plate I, m)

Densoisporites complicatus BALME 1970

Densoisporites nejburgii (SCHULZ) Balme 1970 (Plate II, f)

Densoisporites playfordii (BALME) Dettmann 1963 (Plate I, e)

Densoisporites spp. (WEYLAND & KRIEGER) Dettmann 1963

Endosporites papillatus JANSONIUS 1962

Represents the inner part of a multitude of cavate trilete spores.

Grandispora sp. (HOFFMEISTER, STAPLIN & MALLOY) Neves & Owens 1966 (Plate I, x)

Granulatisporites spp. (IBRAHIM) Schopf, Wilson & BentalI 1944 (Plate II, g,h)

Besides the laesura displays a curvaturae imperfectae, the encountered species correspond to the emended genus diagnosis of Schopf, Wilson and Bentall (1944).

Jerseyiaspora spp. KAR, KIESER & JAIN, 1973 (Plate I, e)

Kraeuselisporites apiculatus JANSONIUS 1962 (Plate I, s)

The dimension of the observed specimen ranges around the smaller size range of the original diagnosis of Jansonius, 1962.

Kraeuselisporites cuspidus BALME 1963 (Plate I, g)

The observed specimens are slightly smaller as described in the original diagnosis, this has also been noted by Balme (1970).

Kraeuselisporites rallus BALME 1970 (Plate I, r)

Kraeuselisporites saeptatus BALME 1963 (Plate I, h)

Kraeuselisporites wargalensis BALME 1970 (Plate I, l)

Kraeuselisporites spp. (Leschik) JANSONIUS 1962

Leiotriletes spp. (Naumova) ex POTONIÉ & KREMP 1954 (Plate I, u)

Leschikisporis spp. POTONIÉ 1958 (Plate I, ae)

Limatulasporites spp. HELBY & FOSTER IN FOSTER 1979 (Plate I, v)

Lophotriletes spp. (NAUMOVA) ex Potonié & Kremp 1954

Lundbladispora brevicula BALME 1963 (Plate I, j)

Lundbladispora obsoleta BALME 1970 (Plate I, f)

Lundbladispora spp. (BALME) Playford 1965

Lundbladispora willmotti BALME 1963 (Plate I, k)

Lycopodiacidites spp. COUPER 1953

Maculatasporites sp. TIWARI 1964 (Plate I, ad)

The specimens recovered resemble *Maculatasporites* sp. recovered in Griesbachian assemblages from Norway illustrated in Hochuli et al. (2010b, Fig. 5c).

Monoletes spp. IBRAHIM ex Schopf 1936

Naumovaspora striata JANSONIUS 1962 (Plate II, b)

Neoraistrikia spp. Potonié 1956

Osmundacidites spp. COUPER 1953 (Plate I, w)

Playfordiaspora crenulata (PLAYFORD & DETTMANN) Foster 1979 (Plate I, c)

Polycingulatisporites sp. SIMONCSICS & KEDVES 1961

Polypodiisporites spp. (POTONIÉ & GELLETICH) ex Potonié (Plate I, y)

Punctatisporites spp. (IBRAHIM) Potonié & Kremp 1954

Raistrickia spp. (SCHOPF, WILSON & BENTALL) Potonié & Kremp 1954 (Plate I, t)

Retusotriletes sp. (NAUMOVA) Streel 1964 (Plate I, ac)

Triplexisporites playfordii (DE JERSEY & HAMILTON) Foster 1979 (Plate I, aa)

Uvaesporites spp. DÖRING 1965 (Plate I, i)

Verrucosisporites spp. (IBRAHIM) Smith & Butterworth 1967

Trilete spore indeterminate

Trilete spores that could not be assigned to a specific genus of species due to poor preserveration.

Spores alete

Spores without distinct laesura have been assigned to this group. Exceptions are *Maculatasporites* spp. and *Naumovaspora striata*.

Pollen

Alisporites landianus BALME 1970 (Plate II, r)

Pollen grains assigned to *Alisporites landianus* BALME 1970 have similarities with *Voltziaceaesporites heteromorphus* KLAUS 1964 such as a round to oval body and semicircular finely reticulate sacci. The dimensions of the two taxa are comparable. However, the corpus outline of Voltziaceaesporites heteromorphus is usually distinct which is not the case in A. landianus the described crest (cappa) has never been observed, therefore we follow the diagnosis and terminology of Balme (1970).

Alisporites spp. (DAUGHERTY) Jansonius 1971

Specimens assigned to *Alisporites* spp. include non-striate bisaccate pollen grains that correspond to the emended genus diagnosis; specific differentiation has not been attempted.

Brachysaccus sp. MÄDLER 1964

Chordasporites sp. KLAUS 1960

Cordaitina gunyalensis (PANT & SRIVASTAVA) Balme 1970 (Plate III, a)

Cordaitina spp. SAMOILOVICH 1953

Specimens assigned to *Cordaitina* spp. are in most cases poorly preserved therefore a specific differentiation has not been attempted.

Crustaesporites sp. LESCHIK 1956 (Plate III, f)

Cycadopites spp. WODEHOUSE ex Wolson & Webster 1946

Duplicisporites verrucosus (LESCHIK) Scheuring 1978 (Plate II, o, p)

The observed pollen grains correspond to the emended species diagnosis of Scheuring (1978). *Duplicisporites verrucosus* has been described from late Ladinian and Carnian sequences (Middle to Late Triassic, Scheuring, 1970; 1978). One occurrence documented in the Early Triassic Buntsandstein has been questioned by Scheuring (1978). In the Chitta-Landu section the base range of this species is near the base of the Spathian.

Ephedripites spp. (BOLKHOVITINA) ex Potonié 1985

Falcisporites spp. (LESCHIK) Klaus 1963

Florinites sp. SCHOPF, WILSON & BENTALL 1944 (Plate II, aa)

Hamiapollenites sp. (WILSON) Tschudy & Kosanke 1966 (Plate II, w)

Inaperturopollenites nebulosus BALME 1970

*Inaperturopollenite*s spp. (THOMSON & PLUG) Potonié 1958

Jugasporites sp. LESCHIK 1956

Klausipollenites schaubergeri POTONIÉ & KLAUS 1954 (Plate II, g)

Klausipollenites spp. JANSONIUS 1962

Lueckisporites singhii? BALME 1970 (Plate II, l)
The recovered specimen is slightly contorted but corresponds to the species description of Balme (1970).
Lueckisporites spp. (POTONIÉ & KLAUS) Klaus 1963
Lueckisporites virkkiae POTONIÉ & KLAUS 1954 (Plate II, k)
Lunatisporites noviaulensis (LESCHIK) Foster 1979 (Plate II, n)
Lunatisporites pellucidus GOUBIN (Helby 1972) (Plate II, s)
Lunatisporites spp. LESCHIK 1956
Monosaccate Pollen
Pollen genera assigned to this group include *Cordaitina* spp., *Crustaesporites* spp., and *Striomonosaccites* spp.
Platysaccus spp. NAUMOVA ex Potonieé & Klaus 1954
Pretricolpipollenites spp. DANZÉ-CORSIN & LAVEINE 1963
Protohaploxypinus goraiensis POTONIÉ & LELE 1961 (Plate II, e)
Protohaploxypinus limpidus BALME & HENNELLY 1955 (Plate II, d)
Protohaploxypinus microcorpus SCHAARSCHMIDT 1963 (Plate II, c)
Protohaploxypinus spp. (SAMOILOVICH) Hart 1964
Protohaploxypinus varius (BHARADWAJ) Balme 1970
Striatoabieites spp. SEDOVA 1956
Striatopodocarpites spp. (ZORICHEVA & SEDOVA ex Sedova) Hart 1964 (Plate II, x)
Striomonosaccites sp. BHARADWAJ 1962 (Plate II, b)
Sulcatisporites spp. (LESCHIK) Nilsson 1958
Scheuringipollenites spp. see Tiwari, 1973 and Foster, 1979 for synonymy.
Vitreisporites spp. (LESCHIK) Jansonius 1962
Weylandites lucifer (BHARADWAJ & SALUJHA) Foster 1975 (Plate II, z)
Weylandites spp. BHARADWAJ & SALUJHA 1964
Undifferentiated bisaccate pollen
Bisaccate pollen grains that can not be assigned to a distinct genus or species due to poor preservation or orientation.
Undifferentiated non-striate bisaccate pollen
Bisaccate pollen grains that can not be assigned to a distinct genus or species due to poor preservation or orientation but are not striate.
Undifferentiated bisaccate pollen
Bisaccate pollen grains that can not be assigned to a distinct genus or species due to poor preservation or orientation but are clearly striate.

Aquatic palynomorphs

algae indeterminate (Plate III, m-p)
Botryococcus spp. KÜTZING 1849 (Plate III, q)
Cymatiosphaera spp. WETZEL ex Deflandre 1954 (Plate III, k)
foraminiferal test linings
Acid resistent inner organic linings of tests of foraminifera (Stancliffe, 1996). Uniserial, biserial and trochospiral forms have been observed.
Leiosphaeridia spp. EISENACK 1958
Micrhystridum spp. (DEFLANDRE) Sarjeant 1967 (Plate III, g,h)
Peltacystia venosa BALME & SEGROVES 1966
Quadrisporites horridus HENNELLY 1958 (Plate III, l)
Schizosporis sp. COOKSON & DETTMANN 1959
Tasmanites spp. NEWTON 1875
Veryhachium riburgense BROSIUS & BITTERLI 1961 (Plate III, j)
Veryhachium spp. DEUNFF ex Downie 1959 (Plate III, i)

Palynomorphs observed as single occurrences (not included in counts and charts)

Alisporites cf. *A. opii* DAUGHERTY 1941
Anaplanisporites stipulatus JANSONIUS 1962
Corisaccites alutas VENKATACHALA & KAR 1966
Ephedripites sp. 1 (Plate II, u)
Longitudinally oval, polyplicate pollen grains with numerous thin ribs 1-3µm in width.
Ephedripites sp. 2 (Plate II, v)
Polyplicate pollen grains with few broad rips 4-8 µm in width. In some specimen the ribs are spirally contorted comparable to the forms of *E. tortuosus* MÄDLER 1964
Falcisporites stabilis BALME 1970 (Plate II, ab)
Laevigatosporites spp. IBRAHIM 1933
Limatulasporites fossulatus (BALME) Helby & Foster in Foster 1979
Marsupipollenites sp. (BALME& HENNELLY) Balme 1970 (Plate II, t)
?Protodiploxypinus sp. SAMOILOVICH 1953
The observed specimen is in accordance with the genus diagnosis of Samoilovich (1953)

but differs in the presence of a thickened exinal fold.

Punctatosporites sp. IBRAHIM 1933

Reticuloidosporites cf *R. warchianus* BALME 1970

Striatopodocarpites pantii (JANSONIUS) Balme 1970

Sulcatisporites ovatus BALME & HENNELLY 1955

Scheuringisporites ovatus (BALME & HENNELLY) Foster 1975; see Tiwari, 1973 and Foster, 1979 for synonymy.

Triquitrites sp. WILSON & COE 1940 (Plate I, z)

Verrucosisporites narmianus BALME 1970 (Plate II, d)

Acknowledgements

We acknowledge financial support from the Swiss National Science Foundation project 200020-127716/1 (to H. Bucher).

References

Atudorei, V., 1999. Constraints on the Upper Permian to Upper Triassic marine carbon isotope curve. Case studies from the Tethys. PhD thesis University of Lausanne, Switzerland.

Balme, B.E., 1963. Plant microfossils from the lower Triassic of Western Australia. Palaeontology 6, 12-40.

Balme, B.E., 1970. Palynology of Permian and Triassic strata in the Salt Range and Surghar Range, West Pakistan. In: Kummel, B., Teichert, C. (Eds.): Stratigraphic boundary problems: Permian and Triassic of West Pakistan. The University Press of Kansas, Lawrence, pp. 305-453.

Balme, B.E., 1995. Fossil in situ spores and pollen grains: an annotated catalogue. Review of Palaeobotany and Palynology 87, 81-323.

Baud, A., Atudorei, V., Sharp, Z., 1996. Late Permian and Early Triassic evolution of the Northern Indian margin: carbon isotope and sequence stratigraphy. Geodinamica Acta 9, 57-77.

Brayard, A., Bucher, H., Escarguel, G., Fluteau, F., Bourquin, S., Galfetti, T., 2006. The Early Triassic ammonoid recovery: Paleoclimatic significance of diversity gradients. Palaeogeography, Palaeoclimatology, Palaeoecology 239, 374-395.

Brühwiler, T., Bucher, H., Brayard, A., Goudemand, N., 2010. High-resolution biochronology and diversity dynamics of the Early Triassic ammonoid recovery: the Smithian faunas of the Northern Indian Margin. Palaeogeography, Palaeoclimatology, Palaeoecology doi:10.1016/j.palaeo.2010.09.001.

Brühwiler, T., Bucher, H., Ware, D., Hermann, E., Hochuli, P.A., Roohi, G., ur-Rehman, K., Yaseen, A., in press, Smithian (Early Triassic) ammonoids from the Salt Range, Pakistan. Special Papers in Palaeontology.

de Jersey, N.J., 1962. Triassic spores and pollen grains from the Ipswich Coalfield. Geological Survey of Queensland, Publication No. 307, Brisbane.

de Jersey, N.J., 1970. Triassic miospores from the Blackstone Formation, Aberdare, Conglomerate and Raceview Formation. Geological Survey of Queensland, Publication No. 348, Brisbane.

de Jersey, N.J., 1979. Palynology of the Permian-Triassic transition in the Western Bowen Basin. Geological Survey of Queensland. Publication No. 374, Brisbane.

Dolby, J.H., Balme, B.E., 1976. Triassic palynology of the Carnarvon Basin, Western Australia. Review of Palaeobotany and Palynology 22, 105-168.

Foster, C. B., 1982. Spore-Pollen assemblages of the Bowen Basin, Queensland (Australia): Their relationship to the Permian/Triassic boundary. Review of Palaeobotany and Palynology 36, 165-183.

Foster, C.B., 1979. Permian plant microfossils of the Blair Athol Coal Measures, Baralaba Coal Measures, and basal Revan Formation of Queensland. Geological Survey of Queensland, Publication No. 372, Brisbane.

Foster, C.B., Logan, G.A., Summons, R.E., Gorter, J.D., Edwards, D.S., 1997. Carbon isotopes, kerogen types and the Permian-Triassic boundary in Australia: Implications for exploration. Australian Petroleum Production and Exploration Association Journal 37, 472-489.

Galfetti, T., Bucher, H., Brayard, A., Hochuli, P.A., Weissert, H., Goudun, K., Atudorei, V., Guex, J., 2007 a. Late Early Triassic climate change: Insights from a carbonate carbon isotopes, sedimentary evolution and ammonoid paleobiogeography. Palaeogeography,

Palaeoclimatology, Palaeoecology 243, 394-411.

Galfetti, T., Bucher, H., Ovtcharova, M., Schaltegger, U., Brayard, A., Brühwiler, T., Goudemand, N., Weissert, H., Hochuli, P.A., Cordey, F., Goudun, K., 2007 b. Timing of the Early Triassic carbon cycle perturbations inferred from new U-Pb ages and ammonoid biochronozones. Earth and Planetary Science Letters 258, 593-604.

Galfetti, T., Hochuli, P.A., Brayard, A., Bucher, H., Weissert, H., Vigran, J.O., 2007 c. Smithian/Spathian boundary event: Evidence for global climatic change in the wake of the end-Permian biotic crisis. Geology 35, 291-294.

Gee, E.R., 1989. Overview of the geology and structure of the Salt Range, with observations on related areas of northern Pakistan. Geological Society of America, Special Paper 232, 95-112.

Golonka, J., Ford, D., 2000. Pangean (Late Carboniferous-Middle Jurassic) paleoenvironment and lithofacies. Palaeogeography, Palaeoclimatology, Palaeoecology, 161, 1-34.

Goubin, N., 1965. Description et répartition des principaux pollenites Permians, Triasiques et Jurassiques des sondages du bassin de Morondava (Madagascar). Revue de L'Institute français du pétrole et annales des combustibles liquides 20, 1415-1461.

Grant, R.E., 1970. Brachipods form Permian-Triassic Boundary Beds and Age of Chhidru Formation, West Pakistan. In: Kummel, B., Teichert, C. (Eds.): Stratigraphic boundary problems: Permian and Triassic of West Pakistan, The University Press of Kansas, Lawrence, pp. 117-151.

Guex, J., 1978. Le Trias intérieur des Salt Ranges (Pakistan): problèmes biochronologiques. Eclogae geologicae Helvetiae 71, 105-141.

Hankel, O., 1993. Early Triassic plant microfossils from Sakamena sediments of the Majunga Basin, Madagascar. Review of Palaeobotany and Palynology 77, 213-233.

Helby, R., 1973. Review of Late Permian and Triassic palynology of New South Wales. In: Glover, J. E., Playford, G. (Eds.) Mesozoic and Cainozoic Palynology. Geological Society of Australia, Special Publication No. 4, pp. 141-155.

Helby, R., Morgan, R., Partridge, A.D., 1987. A palynological zonation of the Australian Mesozoic.In Jell, P. A. (Ed.) Studies in Australian Mesozoic Palynolgy, Association of Australasian Palaeontologists, Sydney.

Hermann, E., Hochuli, P.A., Bucher, H., Brühwiler, T., Hautmann, M., Ware, D., Weissert, H., Roohi, G., Yaseen, A., ur-Rehman, K., subm. Climatic oscillations at the onset of the Mesozoic inferred from palynological records from the North Indian Margin. Journal of the Geological Society of London.

Hermann, E., Hochuli, P.A., Bucher, H., Vigran, J.O., Weissert, H., Bernasconi, S.M., 2010. Close-up view on the Permian Triassic boundary based on extended organic carbon isotope records from Norway (Trøndelag and Finnmark Platform). Global and Planetary Change 74 (3-4), 156-167.

Hermann, E., Hochuli, P.A., Méhay, S., Bucher, H., Brühwiler, T., Hautmann, M., Ware, D., Roohi, G., ur-Rehman, K., Yaseen, A., in press. Organic matter and palaeoenvironmental signals during the Early Triassic biotic recovery: the Salt Range and Surghar Range records. Sedimentary Geology. doi:10.1016/j.sedgeo.2010.11.003.

Hochuli, P.A., Vigran, J.O., 2010. Climate variations in the Boreal Triassic - Inferred from palynological records from the Barents Sea. Palaeogeography, Palaeoclimatology, Palaeoecology 290, 20-42.

Hochuli, P.A., Collin, J.P., Vigran, J.O., 1989. Triassic biostratigraphy of the Barents Sea area. In: Collinson, J. D. (Ed.): Correlation in Hydrocarbon Exploration, Norwegian Petroleum Society (NPF), Graham & Trotman Ltd., London, pp 131-153.

Hochuli, P.A., Hermann, E., Vigran, J.O., Bucher, H., Weissert, H., 2010a. Rapid demise and recovery of plant ecosystems across the end-Permian extinction-event. Global and Planetary Change 74 (3-4), 144-155.

Hochuli, P.A., Vigran, J.O., Hermann, E., Bucher, H., 2010b. Multiple climatic changes around the Permian Triassic boundary event revealed by an expanded palynological record from Mid Norway. Geological Society of America Bulletin 122, 884-896.

Jan, I.U., Stephenson, M.H., Khan, F.R., 2009. Palynostratigraphic correlation of the Sardhai Formation (Permian) of Pakistan. Review of Palaeobotany and Palynology 158, 72-82.

Jin, Y.G., Wang, Y., Wang, W., Shang, Q.H., Cao, C.Q., Erwin, D.H., 2000. Pattern of marine mass extinction near the Permian-Triassic boundary in South China. Science 289, 432-436.

Kiehl, J.T., Shields, C.A., 2005. Climate simulation of the latest Permian: Implications for mass extinction. Geology 33, 757-760.

Knoll, A.H., 1984. Patterns of extinction in the fossil record of vascular plants, in: Nitecki, M. H. (Ed.): Extinctions. The University of Chicago Press, Chicago, pp. 21-68.

Kummel, B., Teichert, C., 1966. Relations between the Permian and Triassic formations in the Salt Range and Trans-Indus ranges, West Pakistan. Neues Jahrbuch für Geologie und Paläontologie, Abhandlungen 125, 297-333.

Kummel, B., Teichert, C., 1970, Stratigraphic boundary problems: Permian and Triassic of West Pakistan, The University Press of Kansas, Lawrence.

Kump, L.R., 2002. Reducing uncertainty about carbon dioxide as a climate driver. Nature 419, 188-190.

Lindström, S., McLoughlin, S., 2007. Synchronous palynofloristic extinction and recovery after the end-Permian event in the Prince Charles Mountains, Antarctica: Implications for palynofloristic turnover across Gondwana. Review of Palaeobotany and Palynology 145, 89-122.

Looy, C.V., Brugman, W.A., Dilcher, D.L., Visscher, H., 1999. The delayed resurgence of equatorial forests after the Permian-Triassic ecologic crisis. Proceedings of the National Academy of Sciences of the United States of America 96, 13857-13862.

Looy, C.V., Twitchett, R.J., Dilcher, D.L., Van Konijnenburg-VanCittert, J.H.A., Visscher, H., 2001. Life in the end-Permian dead zone.Proceedings of the National Academy of Sciences 98, 7879-7883.

McTavish, R.A., 1973. Triassic conodont faunas from Western Australia. Neues Jahrbuch für Geologie und Paläontologie, Abhandlungen 143, 275-303.

McTavish, R.A., Dickens, J.M., 1974. The age of the Kockatea shales (Lower Triassic), Perth Basin - a reassessment. Journal of the Geological Society of Australia 21, 195-201.

Orchard, M.J., 2007. Conodont diversity and evolution through the latest Permian and Early Triassic upheavals. Palaeogeography, Palaeoclimatology, Palaeoecology 252, 93-117.

Ouyang, S., Utting, J., 1990. Palynology of Upper Permian and Lower Triassic rocks, Meishan, Changxing County, Zhejiang Province, China. Review of Palaeobotany and Palynology 66, 65-103.

Pakistani-Japanese Research Group, 1985. Permian and Triassic systems in the Salt Range and Surghar Range, Pakistan. In: Nakazawa, K., and Dickins, J.M., (Eds.) The Tethys: Her Paleogeography and Paleobiogeography from Paleozoic to Mesozoic. Tokai University Press, Tokyo, pp. 221-312.

Pant, D.D., 1949. On some Triassic plant remains from the Salt Range in the Punjab. Nature 163, 914.

Payne, J.L., Kump, L.R., 2007. Evidence for recurrent Early Triassic massive volcanism from quantitative interpretation of carbon isotope fluctuations. Earth and Planetary Science Letters 256, 264-277.

Peng, Y., Yu, J., Gao, Y., Yang, F., 2006. Palynological assemblages of non-marine rocks at the Permian-Triassic boundary, western Guizhou and eastern Yunnan, South China. Journal of Asian Earth Sciences 28, 291-305.

Peng, Y., Zhang, S., Yu, T., Yang, F., Gao, Y., Shi, G.R., 2005. High-resolution terrestrial Permian-Triassic eventostratigraphic boundary in western Guizhou and eastern Yunnan, southwestern China. Palaeogeography, Palaeoclimatology, Palaeoecology 215, 285-295.

Playford, G., Dettmann, M. E., 1965. Rhaeto-Liassic plant microfossils from the Leigh Creek Coal Measures, South Australia. Senckenbergiana Lethaea 46 (2/3), 127-181.

Price, P.L., 1997. Permian to Jurassic palynostratigraphic nomenclature. In: Green, P. M. (Ed.) The Surat and Bowen Basins, South-east Queensland. Queensland Department of Mines and Energy, Brisbane, pp. 137-178.

Reed, F. R. C., Cotter, G. de P., Lahiri, H. M., 1930. The Permo-Carboniferous succession in the Warcha Valley, western Salt Range, Punjab. Records Geological Survey of India 62, 412-443.

Retallack, G.J., 1995. Permian-Triassic life crisis on land. Science 267, 77-80.

Retallack, G.J., 2009. Greenhouse crises of the past 300 million years. Geological Society of America Bulletin 121, 114-1455.

Scheuring, B.W., 1970. Palynologische und palynostratigraphische Untersuchungen des Keupers im Bölchentunnel (Solothurner Jura). Schweizerische Paläontologische Abhandlungen, 88, pp. 119.

Scheuring, B.W., 1978. Mikrofloren aus den Meridenkalken des Mte. San Giorgio (Kanton Tessin). Schweizerische Paläontologische Abhandlungen 100, pp. 205.

Schindewolf, O.H., 1954. Über die Faunenwende vom Paläozoikum zum Mesozoikum. Zeitschrift der Deutschen Geologischen Gesellschaft 105, 154-183.

Sitholey, R. V., 1943. Plant remains from the Triassic of Salt Range in the Punjab. Proceedings of the Indian Academy of Science 13, 300-327.

Smith, A.G., Smith, D.G., Funnell, B.M., 1994. Atlas of Mesozoic and Cenozoic Coastlines. Cambridge University Press, Cambridge.

Stancliffe, R. P. W., 1996. Microforaminiferal linings. In: Jansonius, J., and McGregor, D. C. (Eds.) Palynology: principles and applications I. American Association of Stratigraphical Palynologists Foundation, Salt Lake City, pp. 373-380.

Stampfli, G.M., Borel, G.D., 2002. A plate tectonic model for the Paleozoic and Mesozoic constrained by dynamic plate boundaries and restored synthetic oceanic isochrones. Earth and Planetary Science Letters 196, 17-33.

Stemmerik, L., Bendix-Almgreen, S.E., Piasecki, S., 2001. The Permian-Triassic boundary in central East Greenland: past and present views. Bulletin of the Geological Society of Denmark 48, 159-167.

Svensen, H., Planke, S., Polozov, A.G., Schmidbauer, N., Corfu, F., Podladchikov, Y., Jamtveit, B., 2009. Siberian gas venting and the end-Permian environmental crisis. Earth and Planetary Science Letters 277, 490-500.

Tiwari, R. S., 1973. *Scheuringipollenites*, a new name for the Gondwana palynomorphs so far assigned to "*Sulcatisporites* Leschik 1955". Senckenbergiana Lethaea 54 (1), 105-111.

Tiwari, R.S., Kumar, R., 2002. Indian Gondwana palynochronology: relationships and chronocalibration The Palaeobotanist 51, 13-30.

Tiwari, R.S., Tripathi, A., 1992. Marker Assemblage-Zones of spores and pollen species through Gondwana Palaeozoic and Mesozoic sequence in India. The Palaeobotanist, 40, 194-236.

Tiwari, R.S., Vijaya, 1995. Diffenrential morphographic identity of Gondwanic palynomorphs. The Palaeobotanist 44, 62-115.

Traverse, A., 2007. Paleopalynology. Springer Verlag, Dordrecht.

Vigran, J.O., Mangerud, G., Mørk, A., Bugge, T., Weitschat, W., 1998. Biostratigraphy and sequence stratigraphy of the Lower and Middle Triassic deposits from the Svalis Dome, Central Barents Sea, Norway. Palynology 22, 89-141.

Virkki, C., 1937. On the occurrence of winged spores in the Lower Gondwana rocks of India and Australia. Proceedings of the Indian Academy of Science Section B 6, 428-431.

Virkki, C., 1939. On the occurrence of winged spores in a Lower Gondwana glacial tillite from Australia and in Lower Gondwana shales in India. Proceedings of the Indian Academy of Science Section B 9, 7-12.

Virkki, C., 1946. Spores from the Lower Gondwanas of India and Australia. Proceedings of the Indian Academy of Science 15, 93-176.

Waagen, W., 1895. Salt Range fossils II. Fossils from the Ceratite formation. Palaeontologia Indica 2, 1-323.

Wignall, P.B., 2001. Large igneous provinces and mass extinctions. Earth-Science Reviews 53, 1-33.

Wright, R.P., Askin, R.A., 1987. The Permian-Triassic boundary in the southern Morondava basin of Madagascar as defined by plant microfossils. In: McKenzie, G. D. (Eds.) Gondwana six: Stratigraphy, Sedimentology, and Paleontology. Geophysical Monograph Series, Washington, pp. 157-166.

Yin , H., Zhang, K., Tong, J., Yang, Z., Wu, S., 2001. The Global Stratotype Section and Point

(GSSP) of the Permian-Triassic Boundary. Episodes 24, 102-114.

Ziegler, A.M., Scotese, C.R., Barrett, S.F., 1983. Mesozoic and Cenozoic Paleogeographic Maps. In: Brosche, P., Sündermann, J. (Eds.) Tidal Friction and the Earth's Rotation II. Springer Verlag, Berlin, pp. 240-252.

Plates

Plate I. Taxon name is followed by sample number (bold), slide number (brackets) and stage coordinates for an Olympus BX 51 microscope. Scale bar is 20 μm on all photomicrographs.

a) *Aratrisporites fischeri*, **PU 117** (2. Präp. a), 4.9/136.9
b) *Calamospora landiana*, **NA 103** (b), 14.1/124.3
c) *Playfordia crenulata*, **NA 202** (a), 14.8/126.3
d) *Convolutispora* sp. 1, **LA 78** (a), 11.5/124.2
e) *Jerseyiaspora* sp., **PU 192** (a), 5.7/126.2
f) *Lundbladispora obsoleta*, **CH 199** (a), 15.1/135.5
g) *Kraeuselisporites cuspidus*, **PU 17** (2. Präp. a), 11.0/127.0
h) *Kraeuselisporites saeptatus*, **PU 16** (a), 10.3/125.4
i) *Uvaesporites* sp., **CH 202** (a), 14.2/144.0
j) *Lundbladispora brevicula*, **CH 213** (a), 13.5/115.0
k) *Lundbaldispora willmotti*, **NA 213** ([2] a), 10.1/129.0
l) *Kraeuselisporites wargalensis*, **NR 10** (a); 18.5/144.2
m) *Cyclogranisporites* sp., **PU 102** (b), 9.1/143.2
n) *Aratrisporites* sp. A, **LA 77** (a), 7.4/145.4
o) *Aratrisporites tenuispinosus*, **PU 194** (a), 11.7/114.3
p) *Aratrisporites paenulatus*, **NA 85** (a), 10.8/147.9
q) *Aratrisporites scabratus*, **NA 207** (a), 8.8/130.3
r) *Kraeuselisporites rallus*, **NA 207** (2. Präp. a), 3.7/149.0
s) *Kraeuselisporites apiculatus*, **PU 14** (2. Präp. a), 11.0/142.3
t) *Raistrickia* sp., **PU 198** (a), 14.7/119.5
u) *Leiotriletes* sp., **PU 195** (a), 11.0/138.0
v) *Limatulasporites* sp., **NA 85** (a), 13.8/131.0
w) *Osmundacidites* sp., **NA 207** (2. Präp. a), 6.3/131.0
x) *Grandispora* sp., **CH 215** (a), 14.6/123.8
y) *Polypodiisporites* sp., **PU 193** (a), 10.2/131.3
z) *Triquitrites* sp., **NR 11** (2. Präp. a), 15.0/117.1
aa) *Triplexisporites playfordii*, **NA 847** (a), 8.2/134.9
ab) *Annulispora* sp., **NA 207** (2. Präp. a), 7.0/126.0
ac) *Retusotriletes* sp., **PU 117** (a), 9.4/115.1
ad) *Maculatasporites* sp., **NA 207** (2. Präp. a), 7.7/140.7
ae) *Leschikisporis* sp., **PU 101** (a), 10.0/130.0

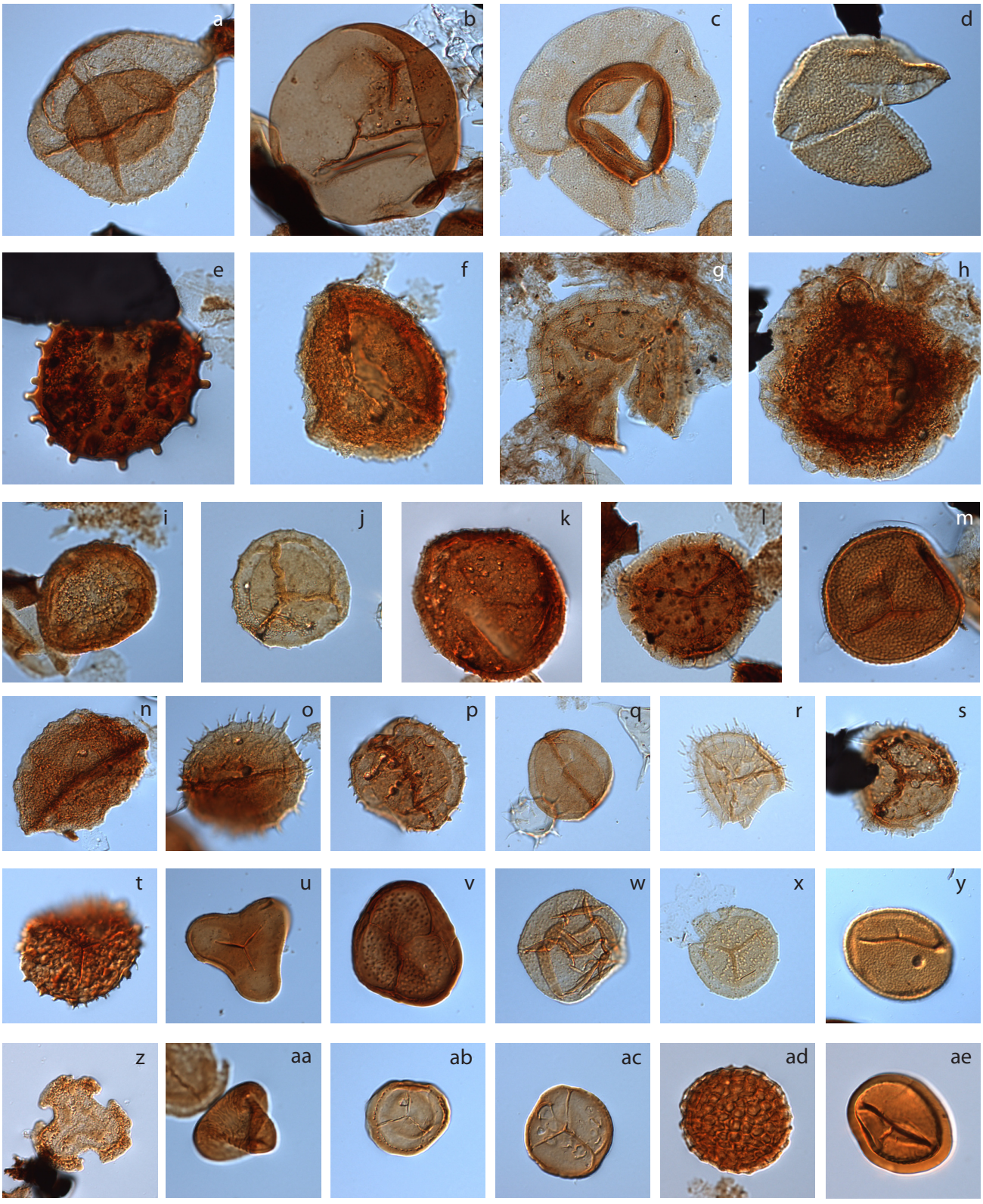

Plate I

Plate II. Taxon name is followed by sample number (bold), slide number (brackets) and stage coordinates for an Olympus BX 51 microscope. Scale bar is 20 μm on all photomicrographs.

a) *Concavisporites* sp., **CH 204** (a) 12.2/127.2

b) *Naumovaspora striata*, **CH 199** (a), 14.9/119.9

c) Megaspore, **LA 78** (a), 13.2/125.7

d) *Verrucosisporites narmianus*, **PU 114** (a), 6.5/115.2

e) *Densoisporites playfordii*, **NA 207** (2. Präp. a), 7.6/142.1

f) *Densoisporites nejburgii*, **PU 117** (a); 12.8/121.0

g) *Granulatisporites* sp., **NA 85** (a), 7.4/122.9

h) *Granulatisporites* sp., **NA 85** (a), 19.5/144.6

i) *Convolutispora* sp. 2, **PU 194** (a), 17.3/147.8

j) *Klausipollenites schaubergeri*, **CH 94** (2. Präp. a). 12.2/145.7

k) *Lueckisporites virkkiae*, **PU 1** (a), 14.5/129.3

l) *Lueckisporites singhii?*, **CH 95** (a) 18.8/109.6

m) *Sulcatisporites ovatus*, **PU 1** (a), 14.5/129.3

n) *Lunatisporites noviaulensis*, **NA 207** (2. Präp. b), 6.8/127.4

o, p) *Duplicisporites verrucosus*, **PU 119** (a), 11.7/122.0

q) *Alisporites* sp., **PU 193** (a) 14.3/142.0

r) *Alisporites landianus*, **PU 117** (2. Präp. a), 2.5/135.7

s) *Lunatisporites pellucidus*, **NA 74** (a), 7.7/137.4

t) *Marsupipollenites* sp., **CH 265** (a) 9.6/119.4

u) *Ephedripites* sp., 1 **CH 250** (a), 10.2/123.4

v) *Ephedripites* sp. 2, **LA 80** (a), 10.3/140.4

w) *Hamiapollenites* sp., **LA 77** (a), 15.0/136.4

x) *Striatopodocarpites* sp., **CH 95** (a), 18.2/128.4

y) *Platysaccus* sp., **NA 102** (b), 19.3/115.4

z) *Weylandites lucifer* **NR 11** (2. Präp. a), 13.8/133.8

aa) *Florinites* sp., **CH 247** (ρ, a), 12.1/129.5

ab) *Falcisporites stabilis*, **NA 103** (b), 14.2/114.6

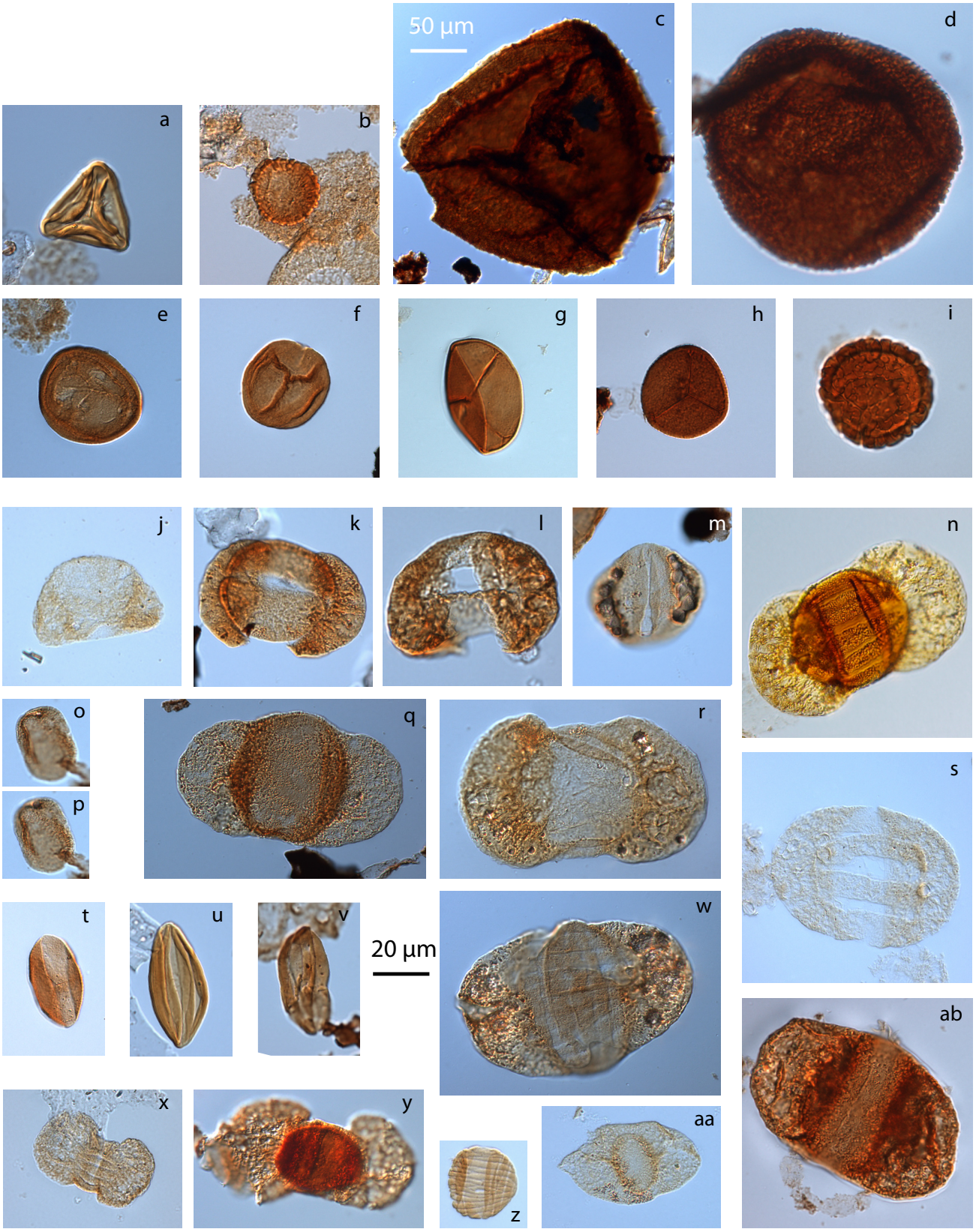

Plate II

Plate III. Taxon name is followed by sample number (bold), slide number (brackets) and stage coordinates for an Olympus BX 51 microscope. Scale bar is 20 μm on all photomicrographs.

a) *Cordaitina gunyalensis*, **NA 104** ([2] a), 7.9/124.0
b) *Striomonosaccites* sp., **NA 85** (a), 12.1/125.5
c) *Protohaploxypinus microcorpus*, **CH 203** (a), 15.7/121.2
d) *Protohaploxypinus limpidus*, **PU 1**(a), 19.4/127.7
e) *Protohaploxypinus goraiensis*, **CH 95** (a), 14.4/130.4
f) *Crustaesporites* sp., **NA 849** (a), 9.6/127.8
g) *Micrhystridium* sp., **NA 207** (2. Präp. a), 8.0/127.3
h) *Micrhystridium* sp., **NA 207** (2. Präp. b), 12.8/122.5
i) *Veryhachium* sp., **NA 207** (2. Präp. b), 4.3/127.9
j) *Veryhachium riburgense*, **NA 844** (a), 19.1/142.7
k) *Cymatiosphaera* sp., **NA 115** (a), 15.0/145.7
l) *Quadrisporites horridus*, **PU 1** (a), 20.3/147.3
m) undetermined algae, **NA 102** (b), 19.0/137.5
n) undetermined algae, **NA 102** (b), 14.9/133.6
o) undetermined algae, **NA 102** (b), 14.1/149.5
p) undetermined algae, **NA 102** (b), 13.7/140.8
q) *Botryococcus* sp., **CH 249** (ρ, a), 10.1/132.1

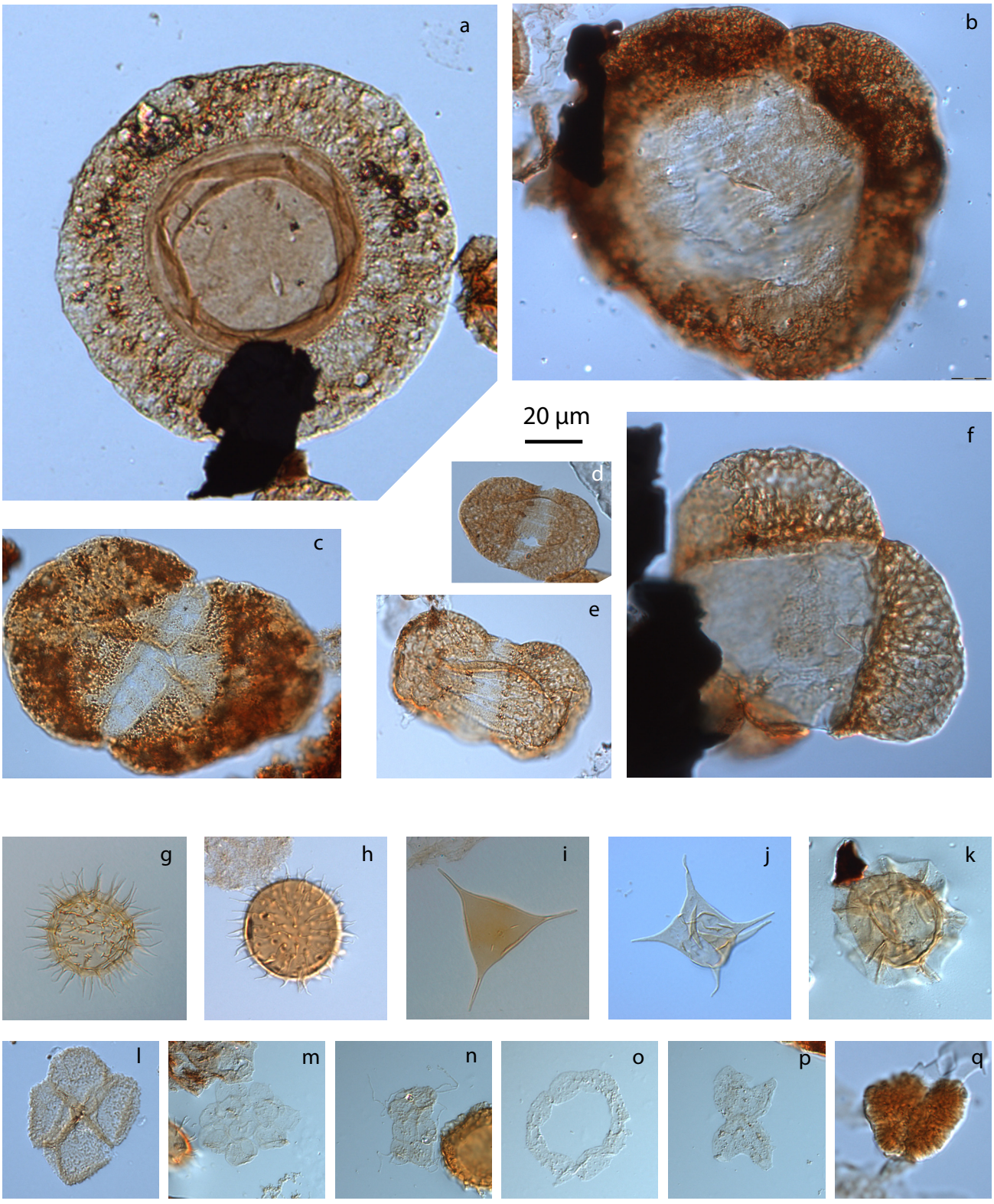

Plate III

Conclusions

In order to understand the interrelation between palaeoenvironmental perturbations and the extinction and recovery patterns during the Early Triassic time period, this thesis addressed the role of terrestrial ecosystems and marine depositional conditions during times of recurrent environmental perturbations. To use a multidisciplinary approach including sedimentology, palynology, palynofacies, carbon isotope studies, and organic geochemistry has proved to be a successful methodology, which integrates biotic and abiotic changes to describe responses of terrestrial ecosystems to major environmental changes. The most important findings of this study include the following conclusions:

- Based on bulk organic carbon isotope data a highly resolved chemostratigraphic framework for the Permian Triassic transition of the sedimentary archives from Norway is presented. The chemostratigraphic pattern near the Permian Triassic boundary is characterised by stepwise negative shift and allows for chemostratigraphic correlation of globally distributed Permian Triassic boundary sections.

- The distribution of end-Permian faunal events relative to the carbon isotope curve shows a series of extinctions in the marine realm coinciding with the stepwise negative shift. Major floral turnovers representing fast adaptations to the onset of environmental perturbations occur prior to the officially defined Permian Triassic boundary.

- The multiple excursions that characterise numerous Early Triassic carbon isotope records could be reproduced in bulk organic matter deposited in the sedimentary basins of the North Indian Margin. This allows establishing a continuous carbon isotope curve for the Early Triassic mixed siliciclastic-carbonate succession from the Salt Range and Surghar Range.

- Early Triassic changes in the marine depositional environment are documented in sea level changes as reflected in the sedimentological and palynofacies record from the Salt Range and Surghar Range in Pakistan. Two second order sequence boundaries, two third order sequence boundaries and five sequence boundaries of undetermined order could be differentiated. These rather short-termed sea-level changes are combined with a protracted shallowing upward trend.

- Based on the palynofacies and revised biostratigraphic data from the Salt Range and Surghar Range area a previously supposed marine anoxic event in the Griesbachian is shown to be Dienerian in age. Except for the Dienerian, well oxygenated conditions prevailed in the depositional environment of the North Indian Margin.

- The Early Triassic spore-pollen record from Pakistan and South Tibet provides new evidence for climatic changes within the Early Triassic. The most prominent climate change occurs near the Smithian Spathian boundary and is of global significance. It coincides with a prominent extinction event in the marine realm. Volcanically induced CO_2 and orbital forcing is suggested to have played a key role in determining the climatic conditions of the North Indian Margin.

- A spore spike in the middle Smithian coincides with a negative carbon isotope anomaly prior to the late Smithian marine extinction event. The short termed proliferation of pteridophytes (lycopods in this case) is a prominent feature during the initiation of environmental perturbations and faunal extinction events. A similar pattern has previously been observed from the Permian Triassic boundary.

- The palynofloral results from the Salt Range and Surghar Range question the commonly held view of a delayed recovery of terrestrial plant communities after the end-Permian mass extinction. Instead, it is shown that early recovery pulses during the early Triassic are reset by renewed environmental perturbations. These environmental perturbations are probably triggered by multiple volcanic activity phases and associated gas releases.

These findings contribute significantly to the understanding of past environmental changes and their influence on terrestrial ecosystems during the Early Triassic. The presented study emphasizes the value of a multidisciplinary approach for a better understanding of the causal relationships between carbon-cycle perturbations, climate, and terrestrial and marine ecosystem recovery in the aftermath of the end-Permian mass extinction.

Appendix 1:

Rapid demise and recovery of plant ecosystems across the end-Permian extinction-event

Peter A. Hochuli, Elke Hermann,
Jorunn Os Vigran, Hugo Bucher, Helmut Weissert

Global and Planetary Change 2010, 74 (3-4): 144-155

Global and Planetary Change 74 (2010) 144–155

Contents lists available at ScienceDirect

Global and Planetary Change

journal homepage: www.elsevier.com/locate/gloplacha

Rapid demise and recovery of plant ecosystems across the end-Permian extinction event☆

Peter A. Hochuli [a,b,*], Elke Hermann [a], Jorunn Os Vigran [c], Hugo Bucher [a,b], Helmut Weissert [b]

[a] Palaeontological Institute and Museum, University Zurich, Karl Schmid-Str. 4, CH-8006 Zurich, Switzerland
[b] Geological Institute, ETH Zurich, CH-8092 Zurich, Switzerland
[c] SINTEF Petroleum Research, NO-7465 Trondheim, Norway

ARTICLE INFO

Article history:
Received 6 July 2010
Accepted 14 October 2010

Keywords:
Late Permian
Early Triassic
chemostratigraphy
palynology
global correlation
paleoclimate

ABSTRACT

The end-Permian extinction event was the most pronounced biotic and ecological crisis in the history of the Earth. It is assumed that over 80% of marine genera disappeared, and that this event had a major impact on the evolution of marine organisms. The impact of this event on terrestrial biota is poorly known and a matter of controversial discussions. In contrast to the fundamental changes in marine fauna most major groups of plants range from the Late Palaeozoic into the Mesozoic. Consequently the impact of the end-Permian extinction event on the evolution of plants was often regarded as minor. However, major changes in the composition of the plant communities have been documented and a number of catastrophic scenarios have been envisioned — including the almost total destruction of plant ecosystems.

Based on expanded sections from the Southern Barents Sea (Northern Norway) we trace mid-latitudinal terrestrial ecosystems across the Permo–Triassic transition with a time resolution in the order of 10 kyr, based on a high resolution C_{org}-isotope stratigraphy. Our results show that the floral turnovers are linked with major changes in the C-isotope record and hence with global carbon cycling. The palynological records document the successive steps in the evolution of terrestrial ecosystems. After gradual changes during the latest Permian, plant ecosystems suffered from a major environmental perturbation leading to a rapid turnover from gymnosperm dominated ecosystems to assemblages dominated by lycopods. The dominance of the lycopods, expressed in a spore-spike, represents a relatively short-lived event in the order of 10 kyr. This perturbation of the terrestrial ecosystems preceded the globally recognized negative $\delta^{13}C_{org}$ isotope spike by up to 100 kyr. It coincides with a first end-Permian negative shift of the C-isotope curve and was probably induced by a first major perturbation of the chemistry of the atmosphere, related to the onset of the volcanic activity of the Siberian Traps. Gymnosperms recovered prior to the major isotopic shift. The fast recovery of terrestrial ecosystem explains why all major plant groups survived the end-Permian extinction event while the majority of marine organisms were wiped out.

The concordance of pattern of the $\delta^{13}C_{org}$ in globally distributed marine and terrestrial sequences enables us to link turnovers in the terrestrial environment with marine extinction events. It demonstrates that the demise and the onset of the recovery of the terrestrial ecosystems was a global phenomenon and occurred prior to the major isotopic shift. The successive negative shifts in $\delta^{13}C_{org}$ isotope values are thought to reflect CO_2 input into the atmosphere by multiphase volcanic activity (Siberian Traps) or other consecutive events (e.g. methane release).

1. Introduction

In contrast to the fundamental changes in marine faunas (Brayard et al., 2009; Erwin, 1993; MacLeod, 2003) the major plant groups range from the Late Palaeozoic into the Mesozoic. Consequently the impact of the end-Permian extinction event (e-PEE) on terrestrial ecosystems was often regarded as minor. However, major changes in the composition of plant communities have been documented and apocalyptic scenarios have been drawn (Retallack, 1999).

Since most previous palynological studies focused on biostratigraphy and the qualitative distribution of taxa detailed quantitative

☆ P.A.H. designed the project together with H.B and wrote the paper. P.A.H. studied the palynology and palynofacies of the cores together with E.H. and J.O.V. The isotopes were measured by E.H who also analysed the data together with H.W. All authors discussed the results and implications and commented on the manuscript at all stages.

* Corresponding author. Palaeontological Institute and Museum, University Zurich, Karl Schmid-Str. 4, CH-8006 Zurich, Switzerland. Tel.: +41 44 634 23 38; fax: +41 44 634 49 23.
E-mail address: Peter.Hochuli@erdw.ethz.ch (P.A. Hochuli).

0921-8181/$ – see front matter © 2010 Elsevier B.V. All rights reserved.
doi:10.1016/j.gloplacha.2010.10.004

data from stratigraphically controlled sections are rare. So far for the Northern hemisphere most of our perceptions of floral changes around the e-PEE were based upon condensed sections with an inherent strong preservational bias (Looy et al., 1999; Ouyang and Utting, 1990; Visscher and Brugman, 1986; Zhang et al., 2007). Compared to the relatively high diversity in the expanded sections of higher latitudes the extremely low diversity recorded in central and north-western European assemblages (Kürschner and Herngreen, 2010) is most probably another expression of this bias. Accordingly the e-PEE is supposed to have induced a heavy loss in plant diversity and the replacement of Late Palaeozoic plant assemblages dominated by woody gymnosperms by assemblages with prevailing herbaceous lycopods. Some authors even assumed an almost complete devastation of terrestrial ecosystems and interpreted most palynomorphs occurring in Early Triassic sediments as reworked from older sections, implying an evolutionary renewal as in marine ecosystems (Utting et al., 2004). Many sections covering the e-PEE are characterized by the abundance of the enigmatic palynomorph genus *Reduviasporonites* spp., which is considered by some authors of fungal (Eshet et al., 1995; Visscher, et al., 1996) and by others of algal origin (Foster et al., 2002). This feature, termed "fungal event", was interpreted to reflect the excessive dieback of the gymnosperm dominated ecosystems leading to their devastation and to proliferation of herbaceous lycopsids (Eshet et al., 1995; Visscher et al., 1996). The detailed records from the expanded sections from the Barents Sea, the Norwegian Sea and Greenland (Hochuli et al., 2010; Looy et al., 2001; Mangerud, 1994) show sporadic occurrences of *Reduviasporonites* spp. without any obvious link to the observed environmental and ecological changes. The data suggest that high abundances of *Reduviasporonites* spp. and the concomitant abundance of carbonized terrestrial plant debris (Eshet et al., 1995) are probably due to preferential preservation of this thick-walled palynomorph.

The most plausible evidence for massive environmental stress acting on plants around the e-PEE is the regular presence of unseparated spore tetrads (Visscher et al., 2004). The global occurrence of these tetrads has been explained by genetic damage of the spore-producing plants caused by increased radiation of UV-light possibly induced by the release of halocarbons or other pollutants into the atmosphere (Beerling, 2007; Visscher et al., 2004).

Some authors presume that plant ecosystems suffered from a major diversity loss and did not recover from the e-PEE until the onset of the Middle Triassic implying a recovery phase of about four million years (Looy et al., 1999; McElwain and Punyasena, 2007). Detailed studies of several expanded sections show that the loss of Palaeozoic taxa is counterbalanced by newly appearing species in the Early Triassic and that diversity increases (De Jersey, 1979; Hochuli et al., 2010; Lindström and McLoughlin, 2007; Mangerud, 1994). Here we present the results of an investigation comprising the spore–pollen and stable C-isotopes of organic matter from two extended sections from Northern Norway (Fig. 1) covering the interval around the e-PEE. These high resolution data show the direct link between changes in global carbon cycling and multiple floral turnovers including the impact of the catastrophic end-Permian event affecting the terrestrial ecosystems.

2. Stratigraphic terminology

In order to avoid terminological confusion the chronostratigraphic concept applied in this paper is shown in Fig. 2. Here we use the terms Late Permian and Griesbachian in the sense of Tozer (1994) based on

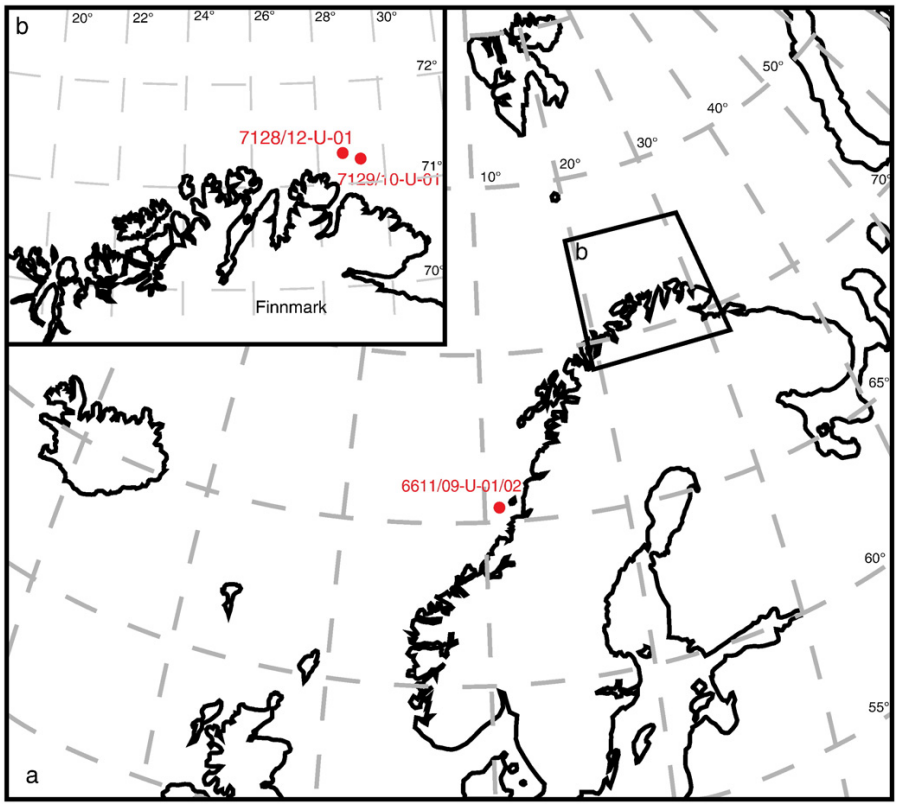

Fig. 1. Location of core holes 7128/12-U-01 and 7129/10-U-01 on the Finnmark Platform, Southern Barents Sea (Norway) and the shallow cores 6611/09-U-01 and 6611/09-U-02 on the Trøndelag Platform offshore mid-Norway.

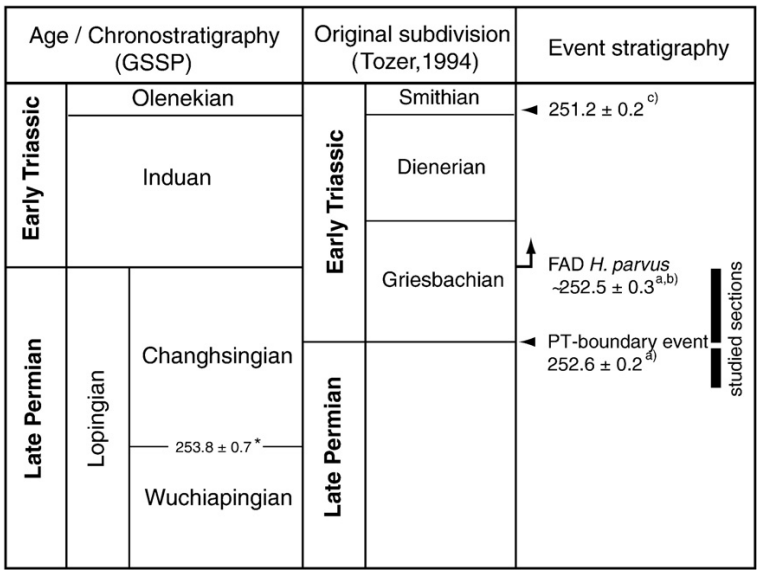

Fig. 2. Stratigraphic terminology: chronostratigraphic subdivision of the Late Permian and the Early Triassic with radiometric ages (not to scale), expressing the different views on the position of the Permian/Triassic boundary including the concept of the Griesbachian substage and the biostratigraphy events applied in this study. The U/Pb ages are taken from the following sources: a) Mundil et al. (2001), b) Mundil et al. (2004) and c) Galfetti et al. (2007b). The inferred age range of the studied cores is marked with a vertical line. Correlation between the boreal sections and the Tethyan GSSP section has been discussed by Twitchett et al. (2001) and Bjerager et al. (2006).

ammonoid biostratigraphy. Presently the Permian–Triassic boundary (PTB) is defined by the first appearance datum (FAD) of the conodont species *Hindeodus parvus* in the condensed global stratotype section and point (GSSP) of Meishan, South China (Yin et al., 2001). This biostratigraphic event considerably postdates the negative C-isotope spike and a series of marine extinction events traditionally associated with the PTB. According to the present definition of the boundary (GSSP) all the extinction events, which can be differentiated based on the high resolution chemostratigraphic $\delta^{13}C$ isotopic records, fall into the Late Permian (Changhsingian) (Hermann et al., 2010-this volume and references therein). Confusions with the occurrence and the range of *H. parvus* have been shirked by the introduction of new species such as *H. praeparvus* and *H. postparvus* (Korte et al., 2010) whereas other authors showed the diachronicity of this event (Hermann et al., 2010-this volume; Shevyrev, 2006).

3. Material and methods

Two cores, 7129/10-U-01 and 7128/12-U-01, have been drilled on the Finnmark Platform, offshore Northern Norway (Fig. 1) for the mapping program of IKU (today SINTEF Petroleum Research, Trondheim, Norway). For this study we sampled in detail the Late Permian and the Griesbachian part of the two cores and focused on lithologies suited for palynological studies (e.g. marls, clay- and siltstones).

38 samples have been collected from core 7128/12-U-01, and 7 from core 7129/10-U-01. All of them have been processed with standard palynological method (e.g. Traverse, 2007). Most of the samples yielded well preserved palynomorph assemblages. For the palynofacies analysis we counted a minimum of 350 (350–1550) organic particles. The quantitative palynological analysis has been carried out on the slightly oxidized residue. For the palynological study a minimum of 300 (304–490) palynomorphs has been counted for each sample. The critical interval showing the floral turnover between the Late Permian and the lowermost Griesbachian is represented in both cores.

For the $\delta^{13}C$ analysis the core samples have been ground and treated with 3 N HCl for at least 24 h to remove all carbonates. The residue was homogenised and analysed with a ThermoFisher Flash-EA1112 elemental analyser coupled with a Conflo IV interface to a ThermoFisher Delta V isotope ratio mass spectrometer (IRMS). The system was calibrated with NBS22 ($\delta^{13}C = -30.03$) and IAEA CH-6 ($\delta^{13}C = -10.46$). Reproducibility of the measurements is better than ± 0.15‰. The carbon-isotope ratios are expressed in the standard δ notation in per mil (‰) relative to the international VPDB isotope standard.

4. Palaeogeography and geological setting

For the Late Permian and the Early Triassic interval the two drill sites represented a mid-latitudinal (~45°N) palaeogeographic position (Larssen et al., 2005). They were located north of an extended landmass that shed siliciclastic material into the subsiding basin (Larssen et al., 2005). The sections are marked by a prominent change in lithology from the Late Permian limestone and chert dominated Isbjørn Formation to the Griesbachian siliciclastic sequence of the Røye Formation. The cores are biostratgraphically and chemostratigraphically dated (Mangerud, 1994; Hermann et al., 2010-this volume.); they cover the Late Permian (Changhsingian) interval immediately below the Permian–Triassic boundary (PTB), in the sense of the GSSP definition (Yin et al., 2001; see Fig. 2). The $\delta^{13}C_{org}$ isotope record shows a stepwise decrease of values to the characteristic minimum (negative spike) prior to the PTB (sensu GSSP). The essentially gradual changes in the isotope records suggest nearly continuous sedimentation.

The geological setting and the lithological succession of these sections have been described in several papers (Bugge et al., 1995; Larssen et al., 2005; Mangerud, 1994). The core holes have been drilled at a distance of about 1.5 km. According to seismic data and the lithological succession (Figs. 2 and 5 in Mangerud, 1994) core 7128/12-U-01 represents a more distal position and compared to core 7129/10-U-01 comprises a more complete section.

The Permian part of the section is marked by a predominance of carbonate deposition in a shallow to outer shelf depositional environments. In the present study only the upper part of the Permian section is considered. Based on palynology a Late Permian (Kazanian–?Tatarian–Wuchiapingian–Changhsingian (in updated terminology)) age has been assigned to it (Mangerud, 1994). In core 7129/10-U-01 the top of the carbonates is marked by a phosphoritic

layer, which coincides with a gamma ray peak that can be correlated with a corresponding peak in the unrecovered interval of core 7128/12-U-01. The phosphoritic layer is overlain by a brownish coloured conglomeratic bed characterizing the base of the Griesbachian section (Bugge et al., 1995). Palynological assemblages from this layer show peak abundances of acritarchs, which probably reflects the base Griesbachian transgression. The lithological interpretation of Larssen et al. (2005) implies that the uppermost Permian (Ørret Formation) is missing from the two cores. However, the consistently decreasing $\delta^{13}C$ curves suggest that only a minor hiatus exists at this level (Figs. 3 and 4).

The Griesbachian represents a siliciclastic unit consisting of bioturbated sandstones and siltstones, deposited in several fining upwards cycles. Coarse wood and other plant debris are common in the sandstones. The depositional environment has been interpreted as shallow storm influenced shelf (Bugge et al., 1995). The palynological data from this unit (Mangerud, 1994) indicate an early Griesbachian age, thus confirming ammonoid data from coeval sections from Svalbard and Greenland (Bjerager et al., 2006; Tozer and Parker, 1968; Korchinskaya, 1986). Mangerud (1994) differentiated three palynological zones assigning the Late Permian assemblages to the

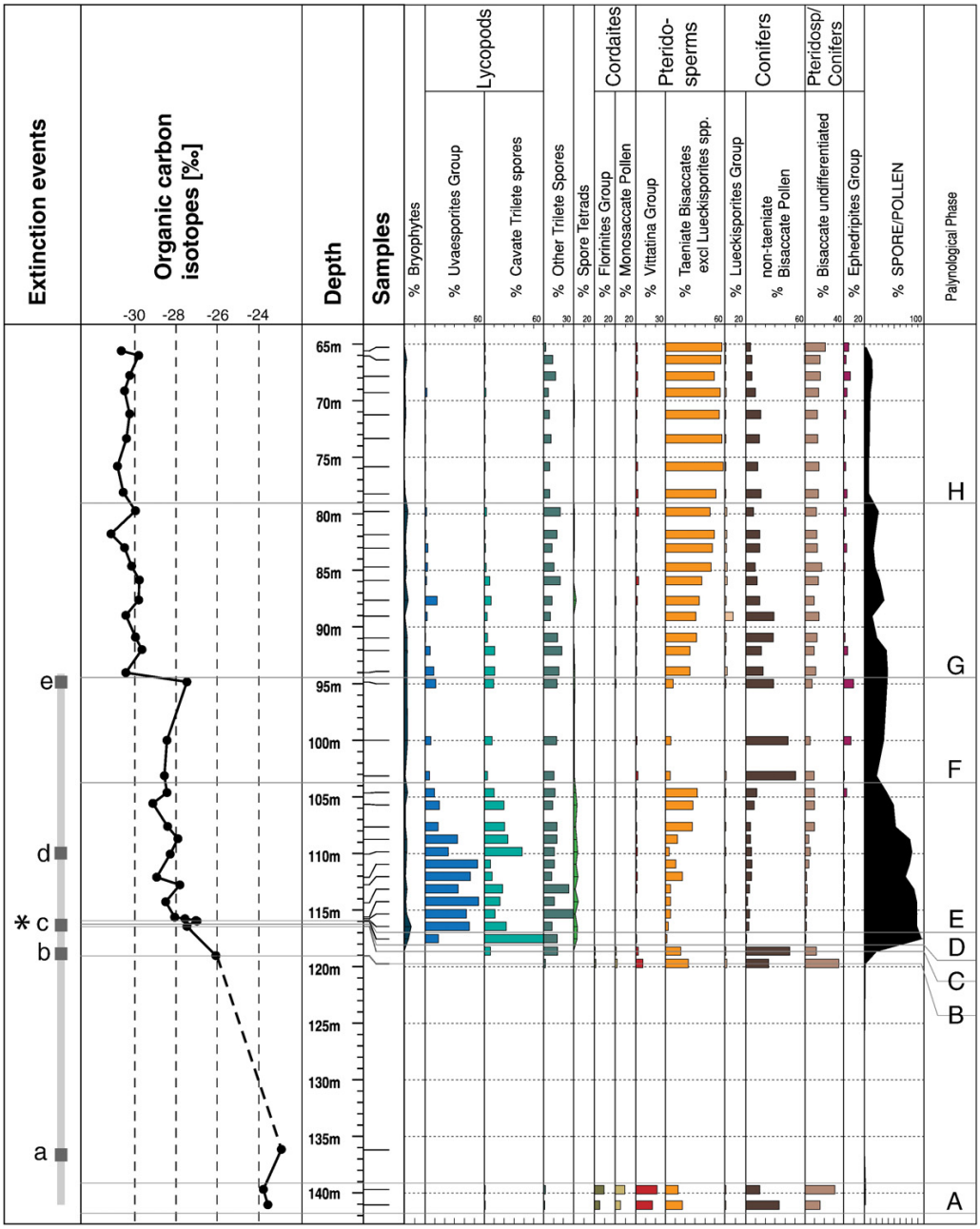

Fig. 3. $\delta^{13}C_{org}$ isotope and palynological records of core 7128/12-U-01 with published extinction events of the marine realm: a) E-Greenland (Twitchett et al., 2001); b) Iran (Heydari et al., 2008); c/d) E-Greenland (Stemmerik et al., 2001); e) Meishan, China (Jin, et al., 2000), Gartnerkofel, Austria (Holser et al., 1989); Canada, Buchanan Lake, (Grasby and Beauchamp, 2008); and * extinction of glossopterids on Gondwana (Morante, 1996).

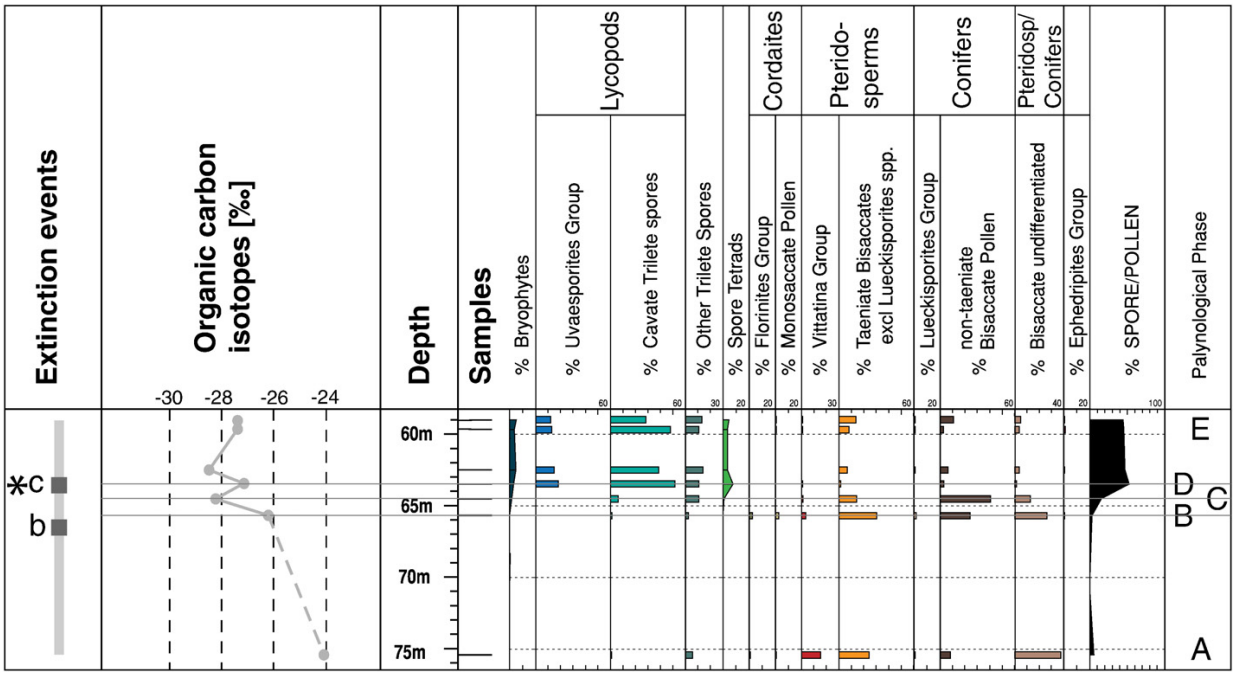

Fig. 4. $\delta^{13}C_{org}$ isotope and palynological records of core 7129/10-U-01 with published extinction events of the marine realm: b) Iran (Heydari et al., 2008); c) E-Greenland (Stemmerik et al., 2001); and * extinction of glossopterids (Morante, 1996).

Dyupetalum sp.-*Hamiapollenites bullaeformis* assemblage zone and to the *Scutasporites* sp. cf. S. *unicus*-*Lunatisporites* sp. concurrent range zone and those of the Griesbachian part of the section to the *Lundbladispora obsoleta*-*Tympanicysta stoschiana* assemblage zone.

Additional information including core photos can be found under:

doi:10.1594/GFZ.SDDB.7128-12u01-06
doi:10.1594/GFZ.SDDB.7129-10u01-01

5. Results

5.1. Palynofacies and C-isotope chemostratigraphy

In most samples the particulate organic matter is strongly dominated by terrestrial OM. Kerogen of marine origin is represented by the rare but continuous presence of acritarchs and a few prasinophycean algae (Figs. 5 and 6). An exception is found in the assemblage with abundant occurrence of acritarchs in lowermost part of the Griesbachian. In core 7128/12-U-01 this feature is restricted to a single sample; in 7129/10-U-01 the initial abundance is fading out in two subsequent samples. No amorphous organic matter (AOM) has been observed. The kerogen assemblages reflect well oxygenated depositional environments throughout the sections without any sign of oxygen deficient conditions. The consistent dominance of terrestrial organic matter precludes major impact on the isotopic composition of the organic matter ($\delta^{13}C_{org}$), therefore the $\delta^{13}C_{org}$ record reflects real changes and therefore major perturbations in the global carbon cycle.

The high resolution $\delta^{13}C_{org}$ record in the studied extended sections of the Finnmark platform reveals a stepwise decrease of C-isotope values between the Late Permian and the lowermost part of the Griesbachian. In most published sections the extinction event(s) affecting the marine realm are linked with a sharp negative $\delta^{13}C$ isotope shift (Grasby and Beauchamp, 2008; Jin et al., 2000; Krull et al., 2004). In the Finnmark cores as in other expanded sections the negative C-isotope shift is spread to a stepwise decrease with more stable phases separating the individual steps. In the Meishan (GSSP) section (Jin et al., 2000) the corresponding isotopic shifts take place within an interval of about 30.0 cm, while it comprises a 75 m thick sequence in core 7128/12-U-01. This distinct pattern (Fig. 7, and Hermann et al., 2010-this volume) allows for precise correlations between globally distributed records (e.g. Canada (Grasby, and Beauchamp, 2008), E-Greenland (Looy et al., 2001; Stemmerik et al., 2001; Twitchett et al., 2001), Austria (Holser et al., 1989), Iran (Heydari et al., 2008), Australia (Morante, 1996), and China (Krull et al., 2004)); some of them include well calibrated faunal extinction events.

5.2. Floral succession

In the palynological record (Figs. 3 and 4 and Table 1: list of floral elements) we differentiate eight spore–pollen assemblages. In core 7129/10-U-01 only the lower five are preserved. The match of our palynological results with records from E-Greenland (see later discussion) proves that the observed breaks in the assemblages reflect real floral turnovers which occur independently from changes in the depositional environment. This is also confirmed by the homogeneous composition of palynofacies throughout the sections (Figs. 5 and 6).

5.2.1. Floral succession of the Late Permian

The Late Permian assemblages (phase A) reveal an overwhelming dominance of gymnosperm pollen. They are composed of pteridosperms (*Vittatina* group and taeniate bisaccate pollen) and conifer pollen (non-taeniate pollen and *Lueckisporites* spp.). Subordinate elements are Cordaites (*Florinites* spp. and monosaccate pollen) and rare pteridophytes, essentially ferns. *Vittatina, Lueckisporites* spp. and the representatives of the Cordaites are generally considered typical Permian

Fig. 5. Palynofacies of core 7128/12-U-01: quantitative distribution of particulate organic matter (terrestrial palynomorphs, and phytoclasts) and *Reduviasporonites* spp. (semi-quantitative) together with the ratio of marine (black) to terrestrial (white) organic particles.

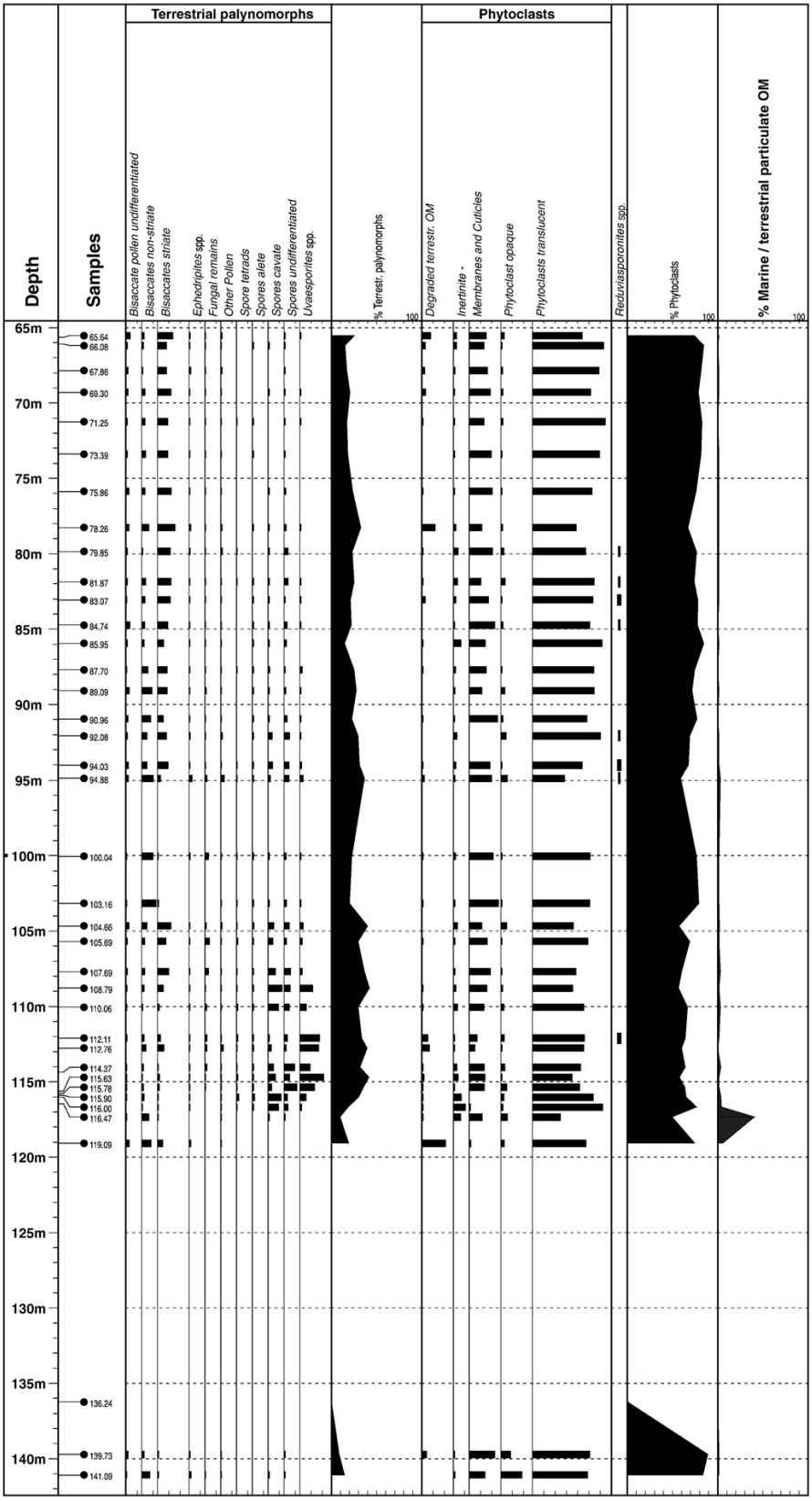
Terrestrial palynomorphs
Phytoclasts
Depth
Samples
Bisaccate pollen undifferentiated
Bisaccates non-striate
Bisaccates striate
Ephedripites spp.
Fungal remains
Other Pollen
Spore tetrads
Spores alete
Spores cavate
Spores undifferentiated
Uvaesporites spp.
% Terrestr. palynomorphs
Degraded terrestr. OM
Inertinite - Membranes and Cuticles
Phytoclast opaque
Phytoclasts translucent
Reduviasporonites spp.
% Phytoclasts
% Marine / terrestrial particulate OM
65m
70m
75m
80m
85m
90m
95m
100m
105m
110m
115m
120m
125m
130m
135m
140m
65.54
66.08
67.86
69.30
71.25
73.39
75.86
78.26
79.85
81.87
83.07
84.74
85.95
87.70
89.09
90.96
92.08
94.03
94.88
100.04
103.16
104.66
105.69
107.69
108.79
110.06
112.11
112.76
114.37
115.63
115.78
115.90
116.00
116.47
119.09
136.24
139.73
141.09

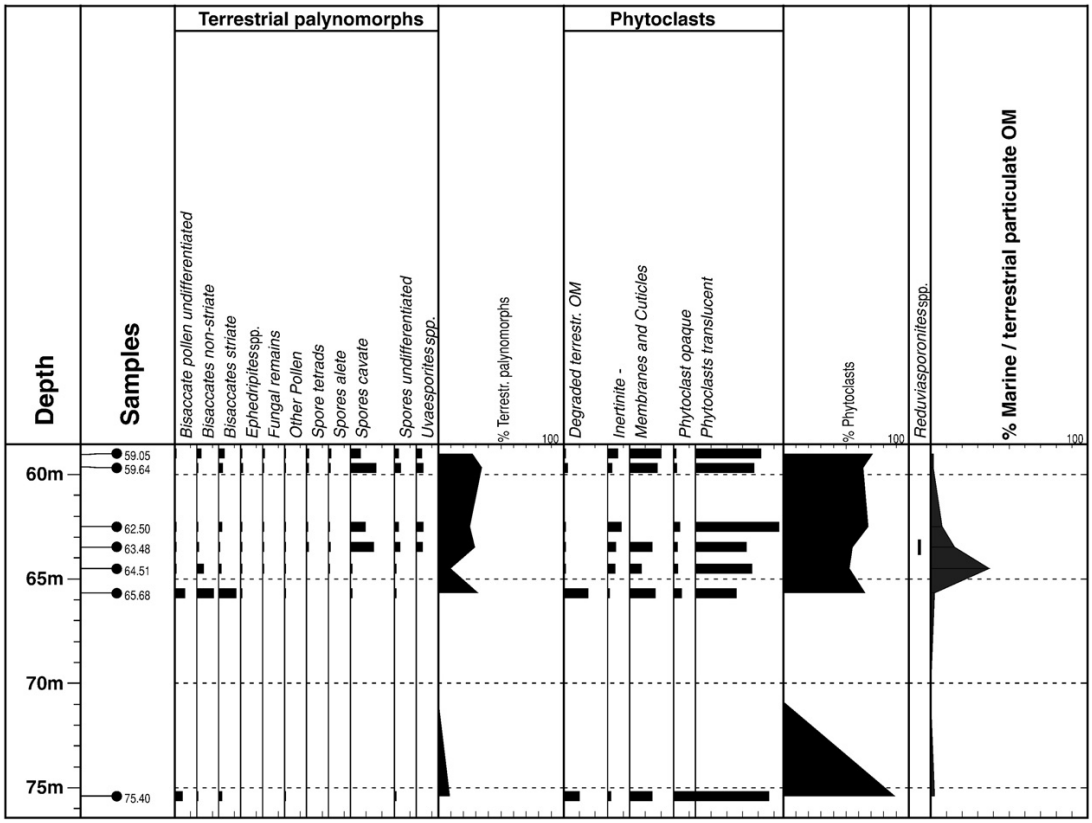

Fig. 6. Palynofacies of core 7129/10-U-01: quantitative distribution of particulate organic matter (terrestrial palynomorphs, and phytoclasts) and *Reduviasporonites* spp. (semi-quantitative) together with the ratio of marine (black) to terrestrial (white) organic particles.

elements. The interval covered by phase A is characterized by stable $\delta^{13}C_{org}$ values around −22‰. Due to a recovery gap in core 7128/12-U-01 and the lack of sediments sufficiently rich in organic matter in core 7129/10-U-01 our record is intermittent in phase A. According to Mangerud (1994) it corresponds to the *Dyupetalum* sp.-*Hamiapollenites bullaeformis* assemblage zone. The assemblage from the uppermost samples of the Late Permian (phase B), represented by one sample in both cores, reflects the demise of *Vittatina* spp. and of *Florinites* spp. Pteridosperms, other than *Vittatina*, and conifers are more common. Non-cavate trilete spores (ferns) are still rare; cavate forms (lycopods) are absent. Together with the two overlying phases (C/D) this interval falls within the first negative $\delta^{13}C_{org}$ shift towards values around −28‰. Phase B falls within the *Scutasporites* sp. cf. *S. unicus-Lunatisporites* sp. concurrent range zone (Mangerud, 1994).

5.2.2. Floral succession of the basal Griesbachian

Separated from the underlying interval by a lithological break the samples of the basal Griesbachian are characterized by overabundant marine acritarchs (Figs. 5 and 6) reflecting the basal Triassic transgression. The terrestrial assemblages (phase C) are distinguished by abundant conifers and in contrast to the underlying intervals by the appearance of rare lycopod and fern spores, as well as by a further decrease of *Vittatina* spp. and the disappearance of *Florinites* spp. The following phase (D) marks the most pronounced turnaround of the sequence. The representation of gymnosperms drops to the lowest level; they are replaced by the proliferating lycopod spores with *Uvaesporites* spp. as a new and common element. With the onset of this phase appear spore tetrads and bryophyte spores. The following phase E is characterized by a peak abundance of lycopods spores including the acme of the *Uvaesporites* group. The abundance of gymnosperm pollen (pteridosperms, conifers and *Ephedripites* spp.) being strongly reduced in the lower part of this interval gradually increases, marking a gradual change of the flora and the first step of the recovery of these plants. Within this interval and the following phase F $\delta^{13}C_{org}$ values stabilize around −28‰. A further decrease of the lycopod spores and a strong increase of conifer pollen characterizes phase F. Here pteridosperms are relatively uncommon; whereas the frequency of fern and bryophyte spores remains essentially unchanged. The significant $\delta^{13}C_{org}$ drop to values around −30‰ coincides with the limit between phases F and G; subsequently the values stabilize. With increasing percentages of pteridosperms, and a general decrease of conifers and lycopods phase G represents a transitional assemblage between phases F and H. Phase H is marked by a pronounced dominance of pteridosperms. During this phase bryophytes and pteridophytes become rare.

An extended floral record of Griesbachian age is known from the Trøndelag Platform offshore mid-Norway from the shallow cores 6611/09-U-01 and 6611/09-U-02 (Hochuli et al., 2010). According to the chemostratigraphic correlation (Hermann et al., 2010-this volume) the lower part of core 6611/09-U-01 overlaps with the upper part of core 7128/12-U-01. The interval between the upper part of Phase E up to the top of Phase H of the latter core corresponds to phase II in core 6611/09-U-01. In this core the distribution of floral elements shows little variation and the assemblages are characterized by a dominance of pollen, however with a considerable percentage of spores (average 40%). Probably due to the semi-quantitative approach used in this record the floral changes are less pronounced. However, the cavate spores (lycopods) show a distinct decrease during this interval, while gymnosperms (pteridosperms, conifers and *Ephedripites* spp.) dominate the assemblages. Diversity remains quite stable

Table 1
List of floral elements: spore–pollen groups applied in this paper with corresponding botanical affinity essentially based on the compilation of Balme (1995).

Floral elements	Taxa included	Affinity	Remarks
Bryophytes	*Maculatasporites* spp. *Proprisporites* spp. *"Apiculatisporis" lanjouwii* Alete spores	Bryophytes	
Uvaesporites group	*Uvaesporites* spp., *U. imperialis* *U.* cf. *imperialis*	Lycopsids	Group with variable morphology
Cavate spores	*Densoisporites* spp. *Kraeuselisporites* spp., *Endosporites* spp., *Lundbladispora* spp.	Lycopsids	
Other trilete spores	*Leiotriletes* spp., *Apiculatisporites* spp., *Converrucosisporites* spp., *Verrucosisporites* spp.	Mostly Filicales (ferns), but probably also including some additional Lycopsids	
	Calamospora spp.	Equisetopsids	
Spore tetrads	This group includes unseparated tetrads of several of the above mentioned genera (mostly lycopsids)	Lycopsids and Filicales	
Florinites group	*Florinites* spp.	Cordaites	
Monosaccate pollen	Undifferentiated monosaccate pollen *Cordaitina* spp. *Grebespora* spp.	Cordaites and some forms of uncertain botanical affinity	
Vittatina group	*Vittatina* spp. *Weylandites* spp.	Pteridosperms (Peltaspermales)	Diverse group in the Late Permian; regarded here as in place also in the Griesbachian.
Taeniate bisaccate pollen (exc. *Lueckisporites*)	*Lunatisporites* spp., *Protohaploxypinus* spp., *Striatoabieites* spp., *Striatopodocarpites* spp.	Pteridosperms	
Lueckisporites group	*Lueckisporites* spp. *L. virkkiae*	Conifers	Generally considered as restricted to the Late Permian; regarded here as in place also in the Griesbachian.
Non-taeniate bisaccate pollen	*Alisporites* spp., *Klausipollenites* spp., *Scutasporites* spp., *Limitisporites* spp., *Platysaccus* spp.	Mostly conifers, *Alisporites* have also been produced by pteridosperms (Peltaspermales)	
Undifferentiated bisaccate pollen		Pteridosperms or conifers	Undeterminable bisaccate pollen, due to their preservation or orientation in the slide.
Ephedripites group	*Ephedripites* spp.	Gnetales	

over this interval (Fig. 2 in Hochuli et al., 2010). The subsequent floral record, extending over another 300 m shows distinct variations in the hygrophyte/xerophyte ratio or the spore/pollen ratio, respectively. The phases D–H correspond to the *Lundbladispora obsoleta-Tympanicysta stoschiana* assemblage zone.

The duration of the Griesbachian and the Dienerian substages is estimated at 1.4 ± 0.4 myr (see Fig. 2). Within the Griesbachian the FAD of *H. parvus* is estimated to occur at about ~252.5 ± 0.3. Hence the Griesbachian part of the studied section has an estimated duration in the order of 100 kyr. Hence, we estimate that the main floral turnover – between the floral phases C and E – which is documented to occur in an interval of less than 2 m in both cores took place within a time span in the order of 10 kyr.

6. Discussion

6.1. Coeval floral records

Based on the correlation of the $\delta^{13}C_{org}$ isotope high resolution records we are able to compare coeval floral patterns on a global scale. Our data concur with the data from Late Permian/basal Griesbachian outcrop sections in E-Greenland (Stemmerik et al., 2001). The succession from the Schuchert Dal Formation of Jameson Land (Stemmerik et al., 2001) shows the same stepwise decrease of the $\delta^{13}C_{org}$ isotopes (Fig. 7) and the palynomorph assemblages are also characterized by a strong reduction of the *Vittatina* group leading to a bisaccate dominated assemblage with increased diversity of pteridophytes. The following sudden increase in pteridophyte abundance (spore peak) marking the "palynological P/T boundary" of Stemmerik et al. (2001) occurs near the top of this formation. At this level $\delta^{13}C_{org}$ isotope values stabilize after a first initial drop (Fig. 7). The sequence of events is identical to our phases A to D. The marine record of the uppermost Schuchert Dal Formation reflects two extinction events. The first one, affecting bivalves, brachiopods and bryozoans occurs prior to the spore peak during the phase of decreasing $\delta^{13}C_{org}$ values. The second one striking agglutinated foraminifera is located within the spore peak and coincides with the formation change (Stemmerik et al., 2001). A second record from Jameson Land (Looy et al., 2001; Twitchett et al., 2001) shows a more discontinuous C-isotope record, e.g. with an abrupt drop of $\delta^{13}C_{org}$ values at the boundary between the Schuchert Dal and the overlaying Wordie Creek Formation and also more abrupt changes in the palynological record. A collapse of the marine ecosystems has been reported to occur below the onset of the spore dominance in the interval with $\delta^{13}C_{org}$ values around $-24‰$ (Twitchett et al., 2001) corresponding to our phase A or B (Figs. 3 and 4).

Most European Tethyan sections are condensed and being deposited in carbonate dominated systems contain poorly preserved spore–pollen assemblages with an apparent preservational bias (Looy et al., 1999; Ouyang and Utting, 1990; Visscher and Brugman, 1986; Zhang et al., 2007). Numerous Tethyan records are known from China.

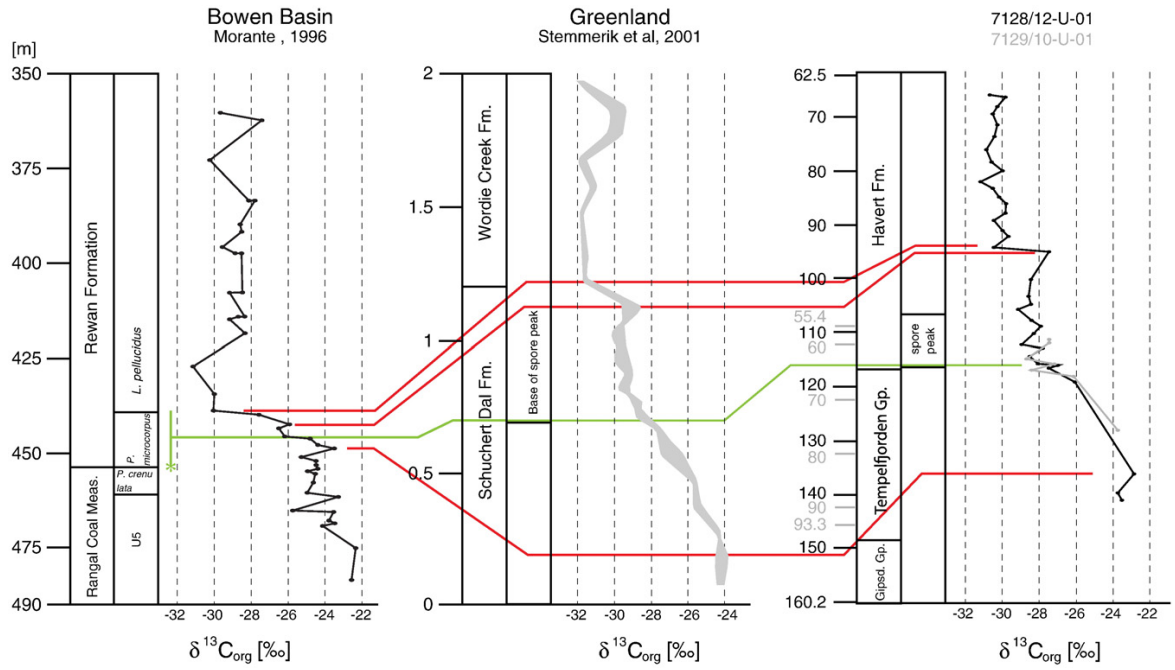

Fig. 7. Chemostratigraphic correlation ($\delta^{13}C_{org}$ isotope records) of the Bowen Basin (Queensland, Australia; Morante, 1996), E-Greenland (Stemmerik et al., 2001) and S-Barents Sea, shallow cores 7128/12-U-01 and 7129/10-U-01 (this study).

However, no detailed quantitative data are available and palynological data, averaged over entire formations are unsuitable to reflect short term floral changes. Several authors describe the transitional character of the palynomorph assemblages around the e-PEE of Northern China (Metcalfe et al., 2009; Ouyang and Utting, 1990; Peng et al., 2005).

Contrasting floral patterns have been described from the Cathaysian floral province in South China (Peng et al., 2006; Peng and Shi, 2009). Here the spore dominated assemblages of the Late Permian (sensu GSSP, Yin et al., 2001) were successively replaced by gymnosperm dominated assemblages. These changes, accompanied by a major loss of abundance and diversity, started in the early Late Permian (Wuchiapingian) and continued up to the earliest Triassic (sensu GSSP, Yin et al., 2001). According to the chemostratigraphic ($\delta^{13}C_{org}$) correlation the transitional zone corresponds to the interval covered by our phases E and F and is characterized by a continuous dominance of spores (Peng et al., 2006). A more pronounced change associated with an increase of gymnosperms coincides with the onset of the $\delta^{13}C_{org}$ minimum.

The detailed $\delta^{13}C_{org}$ record from the Bowen Basin (Queensland, Australia; Morante, 1996) combined with the palynological zonation (Foster, 1982; Helby et al., 1987) provide an overview of the mid-latitudinal floral succession of Southern Gondwana and allow for a correlation with Northern hemisphere records. The Late Permian *Playfordiaspora crenulata* zone covers the uppermost part of the pre-shift $\delta^{13}C_{org}$ interval (−24/−26‰). It is characterized by predominance of gymnosperm pollen. This interval contains the ultimate remains of the *Glossopteris* group and the youngest coals seams (Foster, 1982; Morante, 1996). Bounded by a lithological break, the overlaying *Protohaploxipinus microcorpus* zone corresponds to the first major shift of the $\delta^{13}C_{org}$ interval (−26/−28‰). This zone is characterized by the abundance of lycopod spores. A spore peak occurring immediately above the coal measures has also been documented from core samples from the Sydney Basin (N.S.W.) (Grebe, 1970; Retallack, 1995). As documented in several palynological records there is a minor change in diversity since the decreased diversity of gymnosperm pollen in the *P. microcorpus* zone is counterbalanced by numerous first appearances in the following zone (Foster, 1982; Grebe, 1970). In contrast to that the megafloral record from the Sydney Basin suggests a dramatic loss in plant diversity with the disappearance of 97% of fossil leaf species (Retallack, 1995). This contrasting evidence might be due to the different preservation potential of leaves compared to spore–pollen. The lower part of the overlying *Lunatisporites pellucidus* zone comprises the interval with minimal $\delta^{13}C_{org}$ values (−30/−32‰). Except for the presence of marker species, the assemblages of this zone are not well constrained. Originally characterized by the dominance of the eponymous gymnosperm pollen taxa (Helby et al., 1987) other authors report continuous high abundance of spores (De Jersey, 1979; Foster, 1982).

6.2. Inferred environmental impacts

The results from the Barents Sea (Figs. 3, 4 and 8) reflect the climatic evolution and environmental upheavals across the interval during which marine biota suffered the most extreme extinction of the Earth's history. Changes start during the Late Permian (Changhsingian) with the onset of the negative $\delta^{13}C$ shift and the gradual change in the floral assemblages (phases A and B). A more pronounced change of the flora, coinciding with the basal transgression of the Griesbachian Røye Formation and a further negative $\delta^{13}C$ shift, is indicated by a higher representation of conifers and ferns (phase C). These changes might be explained with an increase in pCO_2 inducing a first temperature and humidity increase. The most pronounced floral turnover leading to a dominance of the lycopods is documented in the overlaying interval (phase D). Chemostratigraphic correlations indicate that similarly expressed changes occur simultaneously in distant areas (e.g. Greenland (Stemmerik et al., 2001), China (Krull et al., 2004), and Australia (Metcalfe et al., 2009)) proving the global extent of this event. This interval falls within a phase of almost stable $\delta^{13}C_{org}$ values indicating stabilization of the C-cycle. Consequently the global turnover in terrestrial ecosystems

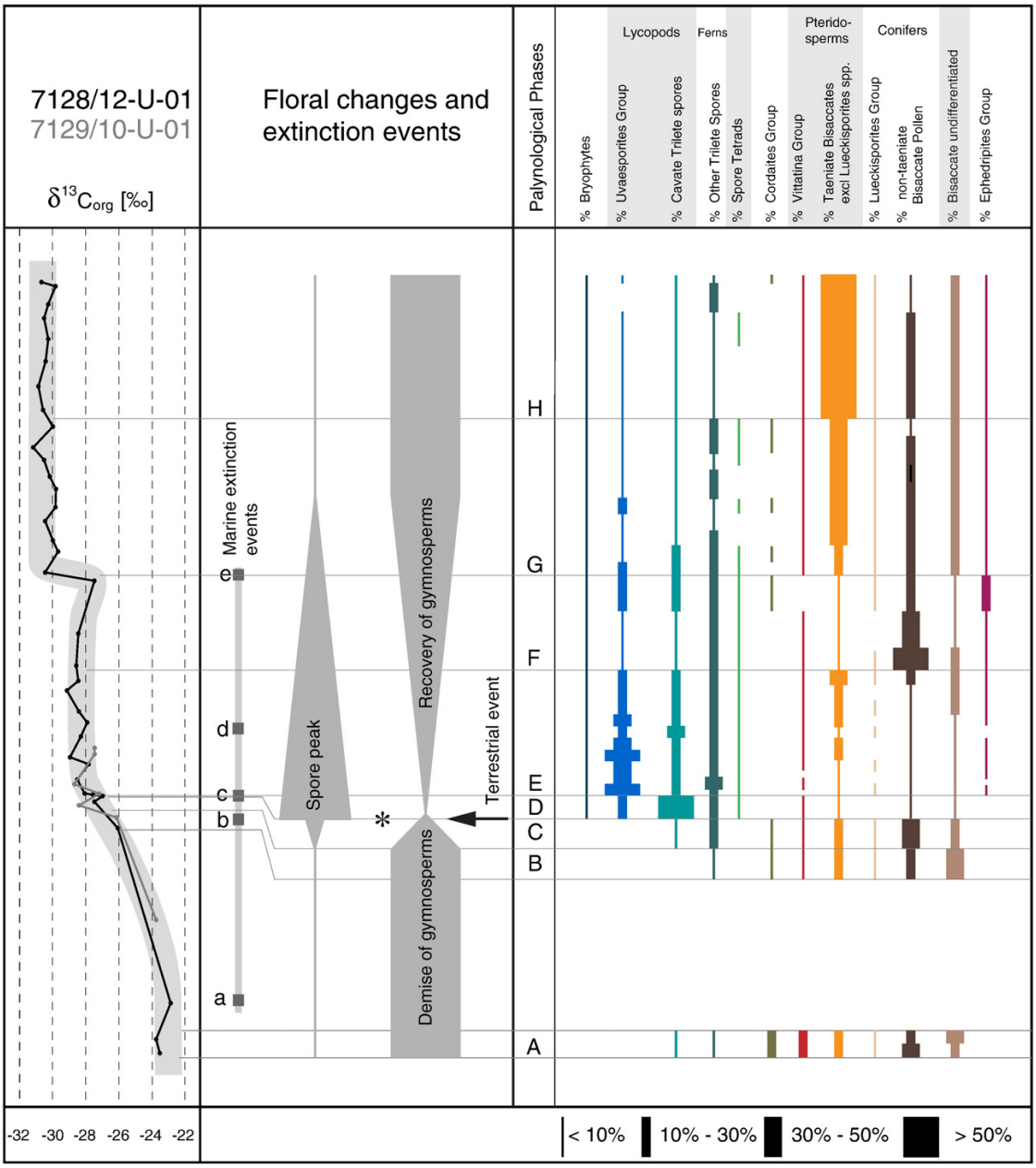

Fig. 8. Environmental changes across the end-Permian extinction event. $\delta^{13}C_{org}$ isotope record in cores 7128/12-U-01 and 7129/10-U-01 and quantitative distribution of spore–pollen with published extinction events of the marine realm: a) E-Greenland, Jameson Land (Twitchett et al., 2001); b) Iran (Heydari et al., 2008); c/d) E-Greenland, Jameson Land (Stemmerik et al., 2001); e) Meishan, China (Jin, et al., 2000); Gartnerkofel, Austria (Holser et al., 1989); Canada, Buchanan Lake (Grasby and Beauchamp, 2008); and * extinction of glossopterids (Morante, 1996).

was probably unrelated to a significant perturbation in the C-cycle; therefore other triggers must be considered. One plausible cause is the postulated pollution by halocarbons and other toxic aerosols produced by volcanic intrusions heating organic rich sediments and evaporites (Svensen et al., 2009). Unseparated spore tetrads of pteridophytes, first appearing at this level, possibly reflect genetic damage of the pteridophytes caused by increased UV-radiation as an effect of pollution (Beerling, 2007; Visscher et al., 2004). The dominance of pteridophytes per se indicates stressful conditions. Pteridophytes are known to rapidly colonize disturbed and polluted areas and to resist harmful conditions, potentially fatal to other plants (McElwain and Punyasena, 2007; Page, 2002). The abundance of lycopods is reminiscent of the "fern spike" observed at the Cretaceous/Tertiary boundary, which has been interpreted to reflect a post bolide impact winter (Vajda et al., 2001). A similar fern spike related to the extinction event at the Triassic/Jurassic boundary has been associated with atmospheric pollution (e.g. halocarbon and SO_2) caused by volcanic activity of the Central Atlantic Magmatic Province (Van de Schootbrugge et al., 2009).

Following the deterioration of the terrestrial ecosystem during the e-PEE our data suggest a rapid recovery of the gymnosperms following this event, since within the same interval of relatively stable $\delta^{13}C_{org}$

values (around −28‰) and within a second lycopod dominated assemblage (phase E) gradually increasing abundance of pteridosperms heralds their recovery. During the following phase (F) lycopods are gradually replaced by pteridosperms and conifers. The latter dominate the associations up to the most extreme negative $\delta^{13}C_{org}$ shift. In the interval with the most negative but relatively stable $\delta^{13}C_{org}$ values (phase G/H) pteridosperms become the dominant group and the low representation of pteridophytes may be associated with decreased humidity. In our record as in other expanded sections (Norwegian Sea and Greenland) there is no trace of the putative "fungal event"; the rare occurrence of *Reduviasporonites* shows no obvious link to the observed environmental and ecological changes (compare Hochuli et al., 2010; Looy et al., 2001; Mangerud, 1994., and present study Figs. 5 and 6).

7. Conclusions

The simultaneous global floral turnover of plant assemblages suggests that the terrestrial ecosystems were affected by a major perturbation of the chemistry of the atmosphere and by successive climatic changes. The effects of these changes varied depending on the palaeogeographic position and the particular boundary conditions of the terrestrial ecosystems. On Southern Gondwana it led to the most dramatic plant extinction event causing the disappearance of the cool-temperate adapted *Glossopteris* flora (Retallack, 1995). The climatic conditions following this event are described as more equable, warmer and less seasonal (Kidder and Worsley, 2004; Lindström and McLoughlin, 2007; Retallack, 1999; Retallack et al., 2003).

The duration of the described ecological changes is difficult to assess. However, based on the radiometric ages from the GSSP section (Meishan) the interval between the End-Permian extinction event and the FAD of *H. parvus* (PTB sensu GSSP) is in the order of 100 kyr (Mundil et al., 2001, 2004). However, according to the latter record the time span between the two events is at the limit of the resolution of radiometric measurements. In the studied cores the turnover of the flora documented in phase C up to the onset of phase E, representing a few meters of sediments, probably happened within a time span in the order of 10 kyr. The short-lived heavily disturbed conditions, reflected in the spore peak, were followed by a recovery phase of the gymnosperms within a comparable time span (Phase F and lower part of phase G). In contrast to the marine realm the impact of the e-PEE on the terrestrial ecosystem was apparently too short to cause a major impact on the evolution of plants. The documented rapid revival of gymnosperm dominated plant communities apparently contradicts the postulated delayed recovery of the demised ecosystems with the continuous lycopods dominance during the Early Triassic (Looy et al., 1999). However, new paleontological and chemostratigraphic data from Early Triassic reveal reiterated crises throughout this epoch, including major disturbances in the C-cycle, which affected not only marine but also terrestrial ecosystems (Brühwiler, 2010; Galfetti et al., 2007a; Hermann et al., 2010; Hochuli et al., 2010; Payne et al., 2004) and caused the apparently delayed recovery of the plant assemblages.

Acknowledgments

This paper is a contribution to project #200020-113554 of the Swiss National Science Foundation. We thank SINTEF Petroleum Research, Trondheim for the possibility to sample the cores and H. Weiss for his help. We acknowledge the help of the editor H. Oberhänsli and the comments of two anonymous reviewers.

References

Balme, B.E., 1995. Fossil in situ spores and pollen grain: an annotated catalogue. Rev. Palaeobot. Palyno. 87, 81–323.
Beerling, D., 2007. The Emerald Planet — How Plants Changed Earth's History. Oxford University Press, Oxford.
Bjerager, M., Seidler, L., Stemmerik, L., Surlyk, F., 2006. Ammonoid stratigraphy and sedimentary evolution across the Permian–Triassic boundary in East Greenland. Geol. Mag. 143 (5), 635–656.
Brayard, A., Escarguel, G., Bucher, H., Monnet, C., Brühwiler, T., Goudemand, N., et al., 2009. Good genes and good luck: ammonoid diversity and the end-Permian mass extinction. Science 325, 1118–1121.
Brühwiler, T., 2010. Smithian (Early Triassic) ammonoids faunas of the Tethys: Taxonomy, biochronology, diversity dynamics and paleoenvironments. PhD thesis Univ. Zürich (unpublished).
Bugge, T., Mangerud, G., Elvebakk, G., Mørk, A., Nilsson, I., Fanavoll, S., et al., 1995. The Upper Palaeozoic succession on the Finnmark Platform, Barents Sea. Nor. Geol. Tidsskr. 75, 3–30.
De Jersey, N.J., 1979. Palynology of the Permian–Triassic transition in the Western Bowen Basin. Geol. Surv. Queensl. Publ. 374, 1–67.
Erwin, D.H., 1993. The Great Paleozoic Crisis; Life and Death in the Permian. Columbia University Press, New York.
Eshet, Y., Rampino, M.R., Visscher, H., 1995. Fungal event and palynological record of ecological crisis and recovery across the Permian–Triassic boundary. Geology 23 (11), 967–970.
Foster, C.B., 1982. Spore–pollen assemblages of the Bowen Basin, Queensland (Australia). Rev. Palaeobot. Palyno. 36, 165–183.
Foster, C.B., Stephensen, M.H., Marshall, C., Logan, G.A., Greenwood, P.F., et al., 2002. A revision of *Reduviasporonites* Wilson 1962: description, illustration, comparison and biological affinities. Palynology 26, 165–183.
Galfetti, T., Hochuli, P.A., Brayard, A., Bucher, H., Weissert, H., Vigran, J.O., 2007a. The Smithian/Spathian boundary event: evidence for global climatic change in the wake of the end-Permian biotic crisis. Geology 35 (4), 291–294.
Galfetti, T., Bucher, H., Ovtcharova, M., Schaltegger, U., Brayard, A., Brühwiler, T., et al., 2007b. Timing of the Early Triassic carbon cycle perturbations inferred from new U–Pb ages and ammonoid biochronozones. Earth Planet. Sci. Lett. 258, 593–604.
Grasby, S.E., Beauchamp, B., 2008. Intrabasin variability of the carbon-isotope record across the Permian–Triassic transition, Sverdrup Basin, Arctic Canada. Chem. Geol. 253, 141–150.
Grebe, H., 1970. Permian plant microfossils from the Newcastle coal measures/ Narrabeen group boundary, Lake Munmorah, New South Wales. Rec. Geol. Surv. NSW 12 (2), 125–136.
Helby, R., Morgan, R., Partridge, A.D., 1987. A palynological zonation of the Australian Mesozoic. In: Jell, P.A. (Ed.), Studies in Australian Mesozoic Palynology: Assoc. Austral. Palaeont. Mem., 4, pp. 1–94.
Hermann, E., Hochuli, P.A., Bucher, H., Brühwiler, T., Ware, D., Hautmann, M., Weissert, H., Bernasconi, S., Roohi, G., Reman, K., Yaseen, A., 2010. Climatic changes in the aftermath of the end-Permian mass extinction – evidence from palynological records of Pakistan. Geophysical Research Abstracts Vol. 12, EGU2010-2394-5.
Hermann, E., Hochuli, P.A., Bucher, H., Vigran, J.O., Weissert, H., 2010. A close-up view of the Permian Triassic boundary based on expanded organic carbon isotope records from Norway (Trøndelag and Finnmark Platform). Global and Planetary Change 74, 156–167 (this volume).
Heydari, E., Arzani, N., Hassanzadeh, J., 2008. Mantle plume: the invisible serial killer — application to the Permian–Triassic boundary mass extinction. Palaeogeogr. Palaeoclim. Palaeoecol. 264, 147–162.
Hochuli, P.A., Vigran, J.O., Hermann, E., Bucher, H., 2010. Multiple climatic changes around the Permian Triassic boundary event revealed by an expanded palynological record from Mid Norway. Geol. Soc. Am. B. 122 (5/6), 884–896.
Holser, W.T., Schönlaub, H.-P., Attrep, M., Boekelmann, K., Klein, P., Magaritz, M., et al., 1989. A unique geochemical record at the Permian/Triassic boundary. Nature 337, 39–44.
Jin, Y.G., Wang, Y., Wang, W., Shang, Q.H., Cao, C.Q., Erwin, D.H., 2000. Pattern of marine mass extinction near the Permian–Triassic boundary in South China. Science 289, 432–436.
Kidder, D.L., Worsley, T.R., 2004. Causes and consequences of extreme Permo–Triassic warming to globally equable climate and relation to the Permo–Triassic extinction and recovery. Palaeogeogr. Palaeoclim. Palaeoecol. 203, 207–237.
Korchinskaya, M.V., 1986. In: Krasil'shchikov, A.A., Miraev, M.N. (Eds.), Geology of the Sedimentary Blanket of the Archipelago of Svalbard, pp. 77–93 (Coll. Sci. Pap., Leningrad, 1986).
Korte, C., Pande, P., Kalia, P., Kozur, H.W., Joachimski, M.M., Oberhänsli, H., 2010. Massive volcanism at the Permian–Triassic boundary and its impact on the isotopic composition of the ocean and atmosphere. J. Asian Earth Sci. 37, 293–311.
Krull, E.S., Lehrmann, D.J., Druke, D., Kessel, B., Yu, Y., Li, R., 2004. Stable carbon isotope stratigraphy across the Permian–Triassic boundary in shallow marine carbonate platforms, Nanpanjiang Basin, South China. Palaeogeogr. Palaeoclim. Palaeoecol. 204, 297–315.
Kürschner, W.M., Herngreen, G.F.W., 2010. Triassic palynology of central and northwestern Europe: a review of palynofloral diversity patterns and biostratigraphic subdivisions. Geol. Soc. Lond. Spec. Publ. 334, 263–283.
Larssen, G.B., Elvebakk, G., Henriksen, L.B., Kristensen, S.-E., Nilsson, I., Samuelsberg, 2005. Upper Palaeozoic lithostratigraphy of the southern part of the Norwegian Barents Sea. Norg. Geol. Unders. B. 444, 3–43.
Lindström, S., McLoughlin, S., 2007. Synchronous palynofloristic extinction and recovery after the end-Permian event in the Prince Charles Mountains, Antarctica. Implications for palynofloristic turnover across Gondwana. Rev. Palaeobot. Palyno. 145, 89–122.
Looy, C.V., Brugman, W.A., Dilcher, D.L., Visscher, H., 1999. The delayed resurgence of equatorial forests after the Permian–Triassic ecologic crisis. Proc. Natl Acad. Sci. USA 96 (24), 13857–13862.

Looy, C.V., Twitchett, R.J., Dilcher, D.L., van Konijnenburg-van Cittert, J.H.A., Visscher, H., 2001. Life in the end-Permian dead zone. Proc. Natl Acad. Sci. USA 98 (14), 7879–7883.
MacLeod, N., 2003. The causes of Phanerozoic extinctions. In: Rothschild, L.J., Lister, A.M. (Eds.), Evolution of Planet Earth. Academic Press, Amsterdam, pp. 253–277.
Mangerud, G., 1994. Palynostratigraphy of the Permian and lowermost Triassic succession, Finnmark Platform, Barents Sea. Rev. Palaeobot. Palyno. 82, 317–349.
McElwain, J.C., Punyasena, S.W., 2007. Mass extinction and the plant fossil record. Trends Ecol. Evol. 22 (10), 548–557.
Metcalfe, I., Foster, C.B., Afonin, S.A., Nicoll, R.S., Mundil, R., Xiaofeng, W., et al., 2009. Stratigraphy, biostratigraphy and C-isotopes of the Permian–Triassic non-marine sequence at Dalong and Lucaogou, Xinjiang Province, China. J. Asian Earth Sci. 36, 503–520.
Morante, R., 1996. Permian and Early Triassic isotopic records of carbon and strontium in Australia and a scenario of events about the Permian–Triassic boundary. Hist. Biol. 11, 289–310.
Mundil, R., Metcalfe, I., Ludwig, K.R., Renne, P.R., Oberli, F., Nicoll, R.S., 2001. Timing of the Permian–Triassic biotic crisis: implications from new zircon U/Pb age data (and their limitations). Earth Planet. Sci. Lett. 187, 131–145.
Mundil, K.R., Ludwig, I., Metcalfe, P.R., Renne, P.R., 2004. Age and timing of the Permian mass extinction: U/Pb dating of close-system zircons. Science 305, 1760–1763.
Ouyang, S., Utting, J., 1990. Palynology of Upper Permian and Lower Triassic rocks, Meishan, Changxing County, Zhejiang Province, China. Rev. Palaeobot. Palyno. 66, 65–103.
Page, C.N., 2002. Ecological strategies in fern evolution: a neopteridological overview. Rev. Palaeobot. Palyno. 119, 1–33.
Payne, J.L., Lehrmann, D.J., Wei, J.Y., Orchard, M.J., Schrag, D.P., Knoll, A.H., 2004. Large perturbations of the carbon cycle during recovery from the end-Permian extinction. Science 305, 506–509.
Peng, Y., Shi, G.R., 2009. Life crises on land across the Permian–Triassic boundary in South China. Glob. Planet. Change 65, 155–165.
Peng, Y., Zhang, S., Yu, T., Yang, F., Gao, Y., Shi, G.R., 2005. High-resolution terrestrial Permian–Triassic eventostratigraphic boundary in western Guizhou and eastern Yunnan, southwestern China. Palaeogeogr. Palaeoclim. Palaeoecol. 215, 285–295.
Peng, Y., Yu, J., Gao, Y., Yang, F., 2006. Palynological assemblages of non-marine rocks at the Permian–Triassic boundary, western Guizhou and eastern Yunnan, South China. J. Asian Earth Sci. 28, 291–305.
Retallack, G.J., 1995. Permian–Triassic life crisis on land. Science 267, 77–80.
Retallack, G.J., 1999. Postapocalyptic greenhouse paleoclimate revealed by earliest Triassic paleosols in the Sydney Basin, Australia. Geol. Soc. Am. B. 111 (1), 52–70.
Retallack, G.J., Smith, R.M.H., Ward, P.D., 2003. Vertebrate extinction across Permian–Triassic boundary in Karoo Basin, South Africa. Geol. Soc. Am. B. 15 (9), 1133–1152.
Shevyrev, A.A., 2006. Triassic biochronology: state of the art and main problems. Stratigr. Geol. Correl. 14, 6, 629–641.
Stemmerik, L., Bendix-Almgreen, S.E., Piasecki, S., 2001. The Permian–Triassic boundary in East Greenland: past and present views. B. Geol. Soc. Denmark 48, 159–167.
Svensen, H., Planke, S., Polozov, A.G., Schmidbauer, N., Corfu, F., Podladchikov, Y., et al., 2009. Siberian gas venting and the end-Permian environmental crisis. Earth Planet. Sci. Lett. 277, 490–500.
Tozer, E.T., 1994. Canadian Triassic ammonoid faunas. Geol. Surv. Can. B. 467, 1–663.
Tozer, E.T., Parker, J.R., 1968. Notes on the Triassic biostratigraphy of Svalbard. Geol. Mag. 105 (6), 526–542.
Traverse, A., 2007. Paleopalynology2nd ed. Springer Verlag, Dordrecht.
Twitchett, R.J., Looy, C.V., Morante, R., Visscher, H., Wignall, P.B., 2001. Rapid and synchronous collapse of marine and terrestrial ecosystems during the end-Permian biotic crisis. Geology 29, 4, 351–354.
Utting, J., Spina, A., Jansonius, J., McGregor, D.C., Marshall, J.E.A., 2004. Reworked miospores in the upper Paleozoic and lower Triassic of the Northern circum-polar area and selected localities. Palynology 28, 75–119.
Vajda, V., Raine, J.I., Hollis, C.J., 2001. Indication of global deforestation at the Cretaceous–Tertiary boundary by New Zealand fern spike. Science 294, 1700–1702.
Van de Schootbrugge, B., Quan, T.M., Lindström, S., Püttmann, W., Heunisch, C., Pross, J., et al., 2009. Floral changes across the Triassic/Jurassic boundary linked to flood basalt volcanism. Nat. Geosci. 2, 589–594.
Visscher, H., Brugman, W.A., 1986. The Permian–Triassic boundary in the southern Alps: a palynological approach. Mem. Soc. Geol. Ital. 34, 121–128.
Visscher, H., Brinkhuis, H., Dilcher, D.L., Elsik, W.C., Eshet, Y., Looy, C.V., et al., 1996. The terminal Paleozoic fungal event: evidence of terrestrial ecosystem destabilization and collapse. Proc. Natl Acad. Sci. USA 93, 2155–2158.
Visscher, H., Looy, C.V., Collison, M.E., Brinkhuis, H., van Konijnenburg-van Cittert, J.H.A., Kürschner, W., et al., 2004. Environmental mutagenesis during the end-Permian ecological crisis. Proc. Natl Acad. Sci. USA 101 35, 12952–12956.
Yin, H., Zhang, K., Tong, J., Yang, Z., Wu, S., 2001. The global stratotype section and point (GSSP) of the Permian–Triassic boundary. Episodes 24 (2), 102–114.
Zhang, K., Tong, J., Shi, G.R., Lai, X., Yu, J., He, W., et al., 2007. Early Triassic conodont-palynological biostratigraphy of the Meishan D Section in Changxing, Zhejiang Province, South China. Palaeogeogr. Palaeoclim. Palaeoecol. 252, 4–23.

Appendix 2:

Smithian (Early Triassic) ammonoids from the Salt Range, Pakistan

Thomas Brühwiler, Hugo Bucher, David Ware, Elke Hermann,
Peter A. Hochuli, Ghazala Roohi, Khalil-ur-Rehman, Aamir Yaseen

Special Papers on Palaeontology, in press

Intensive sampling of the Early Triassic successions at the Chiddru, Nammal and Zaluch localities in the Salt Range (Pakistan) has yielded abundant and well-preserved Smithian (Early Triassic) ammonoid faunas that are of prime importance for ammonoid taxonomy and biostratigraphy. The Salt Range is the type area of many Smithian taxa, and it has played a central role in Early Triassic ammonoid zonation since the pioneer works of Waagen and Mojsisovics et al. in the late 19th century. Our data allow the construction of a highly-resolved ammonoid succession spanning the entire Smithian. Boundary faunas with the older Dienerian and the younger Spathian are also well documented. The new biostratigraphical sequence comprises the following 12 distinct ammonoid faunas (in ascending order): the Flemingites bhargavai beds, the Shamaraites rursiradiatus beds, the Xenodiscoides perplicatus beds, the Flemingites nanus beds, the Radioceras evolvens beds, the Flemingites flemingianus beds, the Brayardites compressus beds, the Nammalites pilatoides beds, the Pseudoceltites multiplicatus beds, the Nyalamites angustecostatus beds, the Wasatchites distractus beds, and the Glyptophiceras sinuatum beds. Biostratigraphic correlations between Nammal and Chiddru reveal diachroneity of the lithological boundaries between the Lower Ceratite Limestone and the Ceratites Marls on one hand, and between the Ceratite Marls and the Ceratite Sandstone on the other. The faunal succession from the Salt Range correlates well with that of other Tethyan sequences such as Tulong (South Tibet), Spiti (India) and South China.

Six new genera (*Koiloceras*, *Monneticeras*, *Truempyceras*, *Punjabites*, *Hochuliites*, *Mianwaliites*) and 13 new species (*Koiloceras romanoi*, *Monneticeras compressum*, *Punjabites punjabiensis*, *Hochuliites retrocostatus*, *Mianwaliites multiradiatus*, *Paraspidites obesus*, *Flemingites hautmanni*, *F. hofmanni*, *F. planatus*, *Rohillites pakistanensis*, *Prionites nammalensis*, *Shamaraites rursiradiatus*, *Subinyoites punjabiensis*) are described.

Keywords: Ammonoidea, Early Triassic, Smithian, Salt Range, Pakistan, biostratigraphy.

Introduction

The end-Permian mass extinction event, which resulted in the most severe crisis in the history of life, wiped out more than 90 percent of all marine species (e.g. Raup and Sepkoski 1982). During the Early Triassic, ammonoids and conodonts recovered very fast in comparison with other marine clades (Brayard et al. 2006, 2009b; Orchard 2007). Early Triassic ammonoid evolution during this recovery is characterized by the following main developments: (i) very low diversity in the Griesbachian, (ii) a moderate diversity increase in the Dienerian, (iii) an explosive radiation in the early Smithian, and (iv) a late Smithian extinction event followed by a second explosive radiation in the early Spathian (Tozer 1981a, b; Brayard et al. 2006, 2009b). Recently published U-Pb ages from South China and their calibration with ammonoid faunas (Ovtcharova et al. 2006; Galfetti et al. 2007b) indicate a maximum duration of the Griesbachian-Dienerian interval of 1.4±0.4 my, 0.7±0.6 my for the Smithian and ca. 3 my for the Spathian (Text-fig. 1). Therefore, the first Early Triassic major ammonoid diversification phase in the early Smithian occurred no later than 2 my after the Permo/Triassic Boundary (PTB) and ended less than 1 my later with the extinction event in the late Smithian.

Although the first Early Triassic ammonoids from the Salt Range were described by de Koninck (1863), Waagen's contribution in the late 19th century (1895) was of immense importance for the study of Early Triassic ammonoids. In his master work entitled Fossils from the Ceratite Formation, he described a large number of new ammonoid taxa, thus making the Salt Range a classic Early Triassic locality. Moreover, Waagen established a detailed lithostratigraphic succession, and precisely recorded the occurrence of the taxa he described within this lithostratigraphic scheme. Therefore, the biostratigraphic subdivision of the Early Triassic for the Tethys given by Mojsisovics et al. (1895), which was based on Waagen's data, is basically correct in its main lines (see below). Subsequently, Frech (1905) and Spath (1934) carried out additional work on Early Triassic ammonoids from the Salt Range, but did not provide much new information. Griesbachian ammonoids in the Salt Range were first discovered by Schindewolf (1953), and then later duplicated by Kummel (1970). Kummel (1966) also described some rather poorly preserved ammonoids of Spathian age. Guex (1978) provided a well-documented distribution of Dienerian, Smithian and Spathian ammonoids from the Salt Range, but his work was based on a relatively small amount of material collected during a single field campaign. Later, a few additional Early Triassic ammonoids were found by the Pakistani-Japanese Research Group (1985).

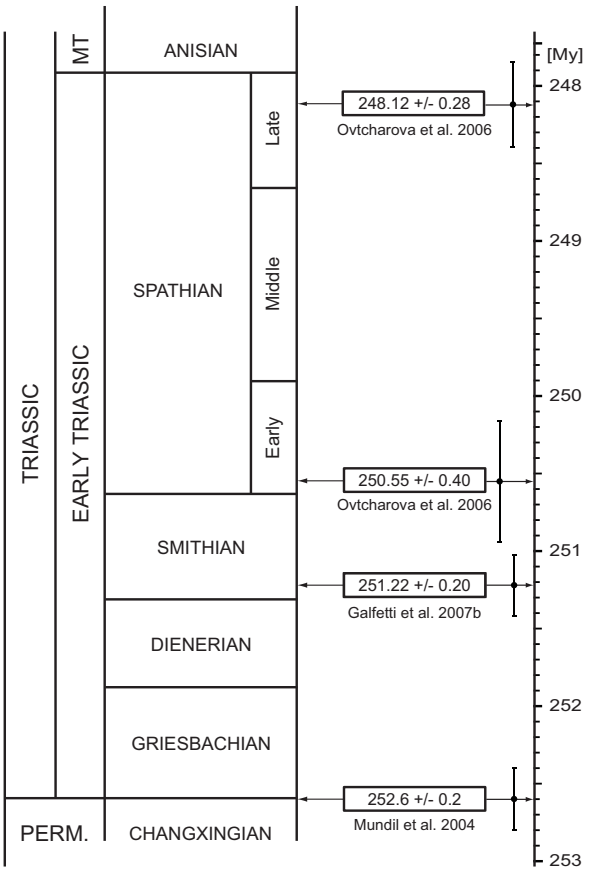

TEXT-FIG. 1. *Early Triassic stage subdivision (Tozer, 1967) calibrated with recently published radiometric ages (Mundil et al. 2004, Ovtcharova et al. 2006, Galfetti et al. 2007b).*

Our extensive investigations in the Salt Range have yielded abundant, well-preserved ammonoid faunas of earliest to latest Smithian age. This new material enables us to revise the taxonomy of Smithian ammonoids, and to establish a high-resolution biostratigraphical sequence for the Smithian of the Salt Range. Such data are crucial for establishing a precise and laterally reproducible biochronological subdivision of the Smithian within the Tethys and within the Early Triassic tropics (Brayard and Bucher 2008; Brühwiler et al. accepted, submitted [b]). Dienerian and Spathian ammonoid faunas from the Salt Range will be discussed in forthcoming papers (Ware et al. ongoing work; Bucher et al. ongoing work).

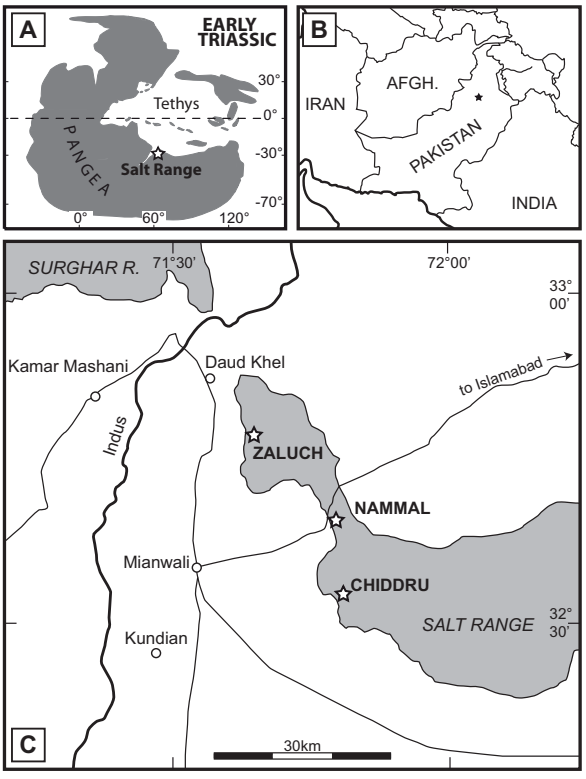

TEXT-FIG. 2*. A) Palaeogeographical map of the Early Triassic with the palaeoposition of the Salt Range (modified after Brayard et al. 2006). B) Map of Pakistan with indication of the studied area. C) Location map of sampled sections in the Salt Range.*

Palaeogeographical and geological settings

During the Early Triassic, the Pangean supercontinent was surrounded by two wide oceans, namely the Panthalassa and the Tethys, and several microcontinents (e.g. Cimmerian and Cathaysian) crossed these two oceans (e.g. Tozer 1982; Ricou 1994; Ehiro *et al.* 2005). During this period, the Salt Range area was located on the northern Gondwanan margin, about 30° south of the equator on the southern side of the Tethys Ocean (e.g. Smith *et al.* 1994; Stampfli and Borel 2002) (Text-fig. 2A). Typically, Lower Triassic successions on the Northern Indian Margin consist of mixed siliciclastic - carbonate series (Galfetti *et al.* 2007*a*; Brühwiler *et al.* 2009).

Waagen (1895) subdivided the Lower Triassic sediments of the Salt Range as follows (from bottom to top): Lower Ceratite Limestone (LCL), Ceratite Marls (CM), Ceratite Sandstone (CS), Upper Ceratite Limestone (UCL), Bivalve Beds (BB), Dolomitic Beds, and Topmost Limestone. These lithological subdivisions can easily be identified in all studied sections, and we use them in this paper (Text-fig. 3). A few minor modifications have been adapted from Kummel and Teichert (1970; Kathwai Member [KM]) and Guex (1978; "Niveaux Intermédiaires" [NI]). For a thorough description of the Lower Triassic sedimentary evolution of the Salt Range, see Hermann *et al.* (in press).

Sampled localities

The Salt Range is located about 170 km southwest of Islamabad, and three localities (Chiddru, Nammal and Zaluch) in the western part of the range were studied (Text-fig. 2B, C).

The area near the village of Chiddru, 25 km ESE of Mianwali (Text-fig. 2C), is one of the main localities studied by Waagen (1895), and he described numerous ammonoid taxa from the LCL, the CS, the UCL and the BB from this locality. Later, Schindewolf (1953) and Kummel

Waagen, 1895			Kummel and Teichert, 1970		Guex, 1978	PJRG, 1985		This work	
Ceratite Formation	Dolomite Group	Topmost Limestone	Mianwali Formation	Narmia Member	TL	Mianwali Formation	Narmia Mb.		TL	TRIASSIC
		Dolomitic Beds			NI		Mittiwali Member	Unit 5	NI	
	Bivalve Limestone	Bivalve Beds			UCL			Unit 4	BB	
		Upper Ceratite Limestone		Mittiwali Member					UCL	
	Ceratite Beds	Ceratite Sandstone			CS			Unit 3	CS	
		Ceratite Marls			CM			Unit 2	CM	
		Lower Ceratite Limestone			LCL			Unit 1	LCL	
Upper Productus Limestone				Kathwai Member	KM		Kathwai Mb.		KM	
			Chhidru Formation			Chhidru Fm.				P.

TEXT-FIG. 3. *Stratigraphic nomenclature of the Early Triassic sediments in the Salt Range according to different authors. In this work we use Waagen's (1895) subdivisions with some minor adaptations from Kummel and Teichert (1970; Kathwai Member) and Guex (1978; NI = Niveaux Intermédiaires ["Intermediate Horizons"]).*

(1970) documented ammonoids of Griesbachian age in the KM at Chiddru, and in 1985 the Pakistani-Japanese Research Group described some rather poorly preserved Dienerian and Smithian ammonoids from the same locality. In addition to the sections at the entry of the gorge examined by Kummel (1966), we also studied a site about 1km to the east, where sections of the entire succession from the LCL to the BB are well exposed (Text-fig. 4). Abundant and well-preserved Smithian ammonoid faunas were collected from the base of the CM, from throughout the CS, from the UCL and from the base of the BB. Ammonoids are particularly abundant in the CS, and several species reach remarkably large size of up to more than 30 cm in diameter (Text-fig. 5). All ammonoid occurrences from Chiddru are given in Text-figures 6-8.

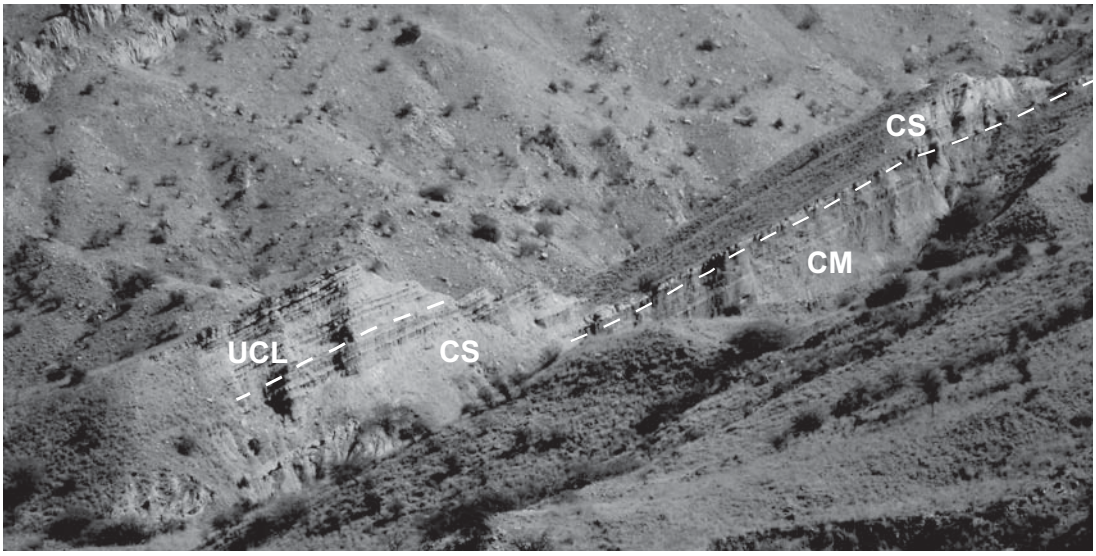

TEXT-FIG. 4. *Section near the village of Chiddru; 1km ESE of the sections at the entry of the gorge described by Kummel and Teichert (1966, 1970) and Kummel (1966), seen from NW. CM Ceratite Marls; CS Ceratite Sandstones; UCL Upper Ceratite Limestone.*

TEXT-FIG. 5*. A block from the Ceratite Sandstones of Chiddru containing several very large specimens of Paranorites ambiensis (Waagen, 1895). From Sample Chi10, Flemingites nanus beds.*

The Nammal Gorge section, located 25 km ENE of Mianwali (Text-fig. 2C), was described by Kummel (1966), who reported the occurrence of a few Spathian ammonoids but it was Guex (1978) who first described Dienerian and Smithian ammonoids from this locality. Excellent exposures of the entire Lower Triassic succession occur in the Nammal Gorge section (Text-fig. 9). Our intensive sampling of this section has yielded abundant and well preserved Smithian ammonoids from the middle and upper third of the CM, from the uppermost part of the CS and from numerous horizons throughout the UCL. All ammonoid occurrences from Nammal are given in Text-figures 10-12.

As a complement to the extensively studied localities of Chiddru and Nammal, we also investigated a third locality near the village of Zaluch, 24 km NNE of Mianwali (Text-fig. 2C). The Zaluch section was first described by Kummel (1966), but again, it was Guex (1978) who first described its Smithian ammonoids. Our sampling at this locality has yielded ammonoids from the upper part of the CS and from the UCL. All ammonoid occurrences from Zaluch are given in Text-figure 13.

Biostratigraphical discussion

Based on our extensive, bed-rock controlled sampling, we recognize a total of twelve distinct ammonoid faunas of earliest to latest Smithian age in the studied area (Text-figs 14-15). The resulting informal zonation presented herein is entirely new. Only a preliminary version was previously presented in a conference abstract (Brühwiler *et al.* 2007). A description of the ammonoid faunas as well as a discussion of their correlation with ammonoid zonations from other areas is provided, and synthetic range charts for Smithian ammonoid species and genera from the Salt Range are given in Text-figs 16 and 17, respectively. No formal zone names are introduced since we prefer to use the term "beds" at the present time to describe the local faunal sequence. The usage of formal zones would imply a well-established lateral reproducibility of the faunal sequence between various basins, which is still a subject of ongoing work.

Latest Dienerian ammonoid faunas

***Prionolobus rotundatus* beds.** The Dienerian ammonoid faunas of the Salt Range are currently being revised by our group (Ware *et al.*, ongoing work). The latest Dienerian ammonoid fauna in the studied area is characterized by *Prionolobus rotundatus* and *Clypites typicus* and has been found at Chiddru and at Nammal (Text-figs 6, 10, 15). A correlative of this fauna has recently been found near Mud in Spiti, India (Brühwiler *et al.* submitted [b]).

Early Smithian ammonoid faunas

***Flemingites bhargavai* beds.** In the Nammal section, the oldest fauna of typical Smithian affinity occurs at the top of the lower third of the CM and is characterized by *Flemingites bhargavai*, *F. hautmanni* sp. nov. and *Radioceras* cf. *kraffti*. *Kashmirites* sp. indet. and poorly preserved specimens possibly belonging to *Koiloceras romanoi* gen. et sp. nov. occur slightly higher in the section.

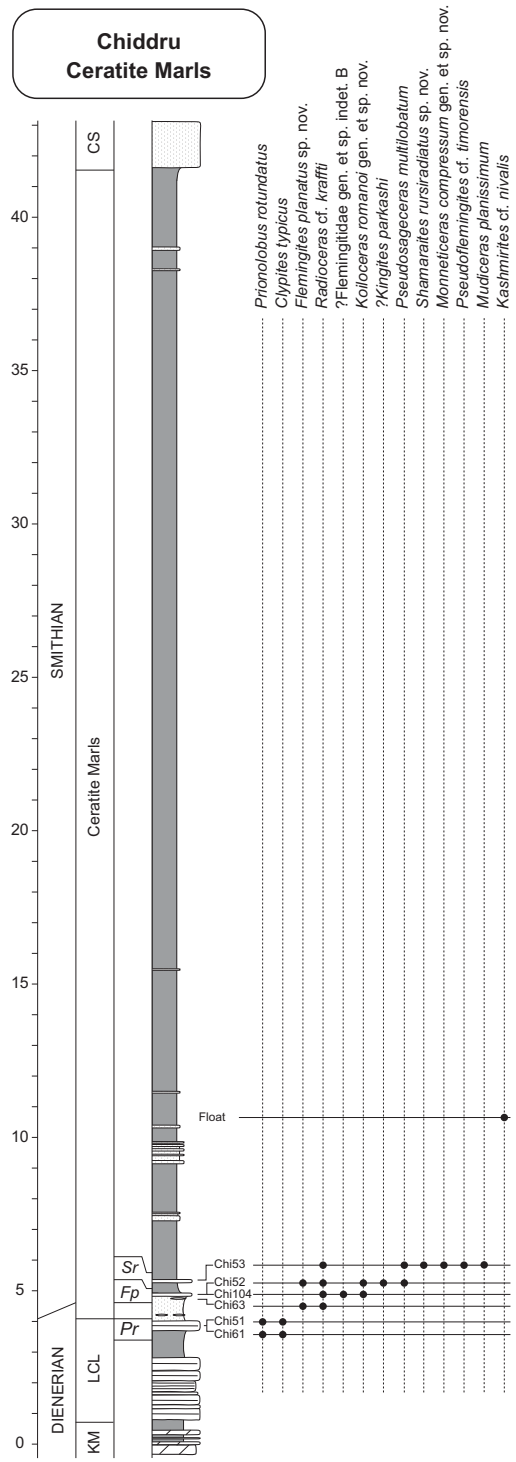

***TEXT-FIG. 6**. Distribution of ammonoids in the Ceratite Marls in the Chiddru section. Abbreviations as in Text-figure 15.*

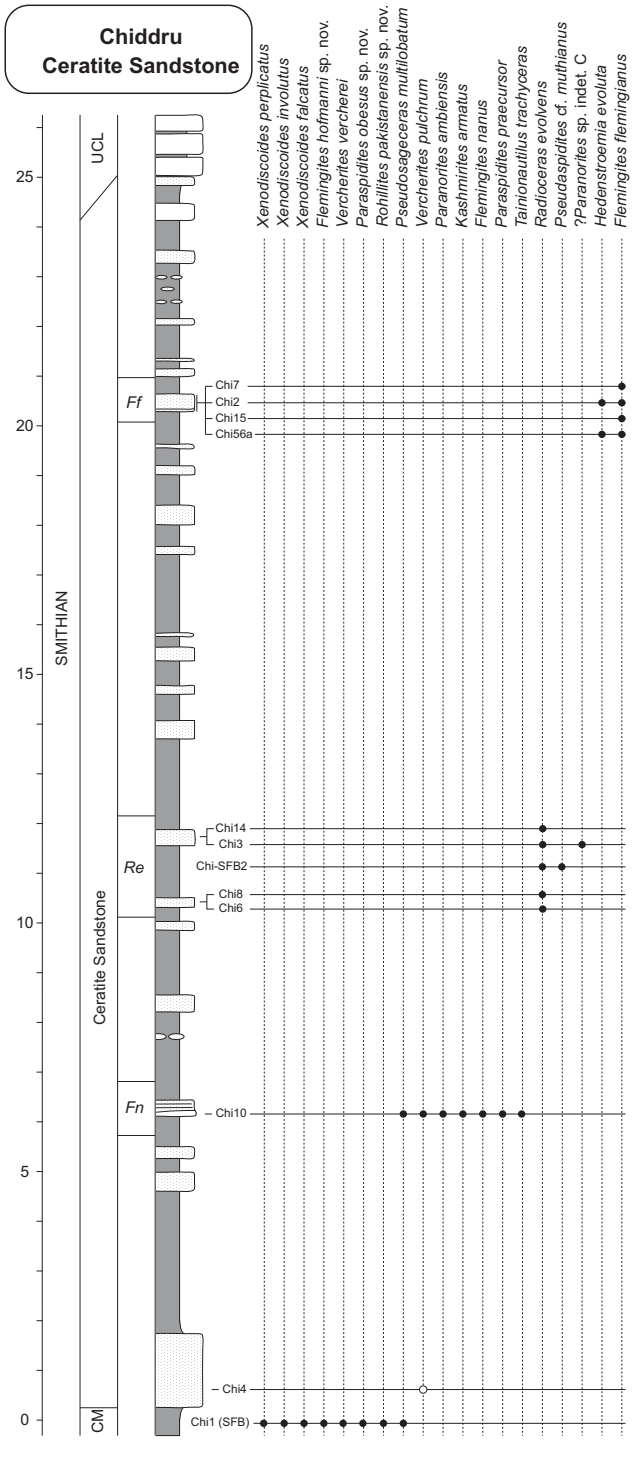

***TEXT-FIG. 7**. Distribution of ammonoids and nautiloids in the Ceratite Sandstones in the Chiddru section. Abbreviations as in Text-figure 15.*

At Chiddru, a similar fauna occurs in the first limestone beds at the base of the CM and is characterized by the association of *Koiloceras romanoi* gen. et sp. nov., *Radioceras* cf. *kraffti*, *Flemingites planatus* sp. nov. and ?*Kingites parkashi*. The beds containing the Chiddru fauna are termed the *Flemingites planatus* beds, and they probably correlate with the *Flemingites bhargavai* beds from Nammal. This biostratigraphic correlation is further supported by the directly underlying *Prionolobus rotundatus* assemblage both at Nammal and Chiddru. It reveals an important diachronism of the lithological boundaries between the LCL and the CM between these two areas (Text-fig. 15).

An equivalent fauna including *Flemingites bhargavai*, *Koiloceras romanoi* gen. et sp. nov. and ?*Kingites parkashi* has recently been found near Mud in Spiti, India (Brühwiler *et al.*, submitted [b]). This particular section had been proposed as a GSSP candidate for the Induan-Olenekian boundary (Krystyn *et al.* 2007*a*, *b*), but the discovery of the *Flemingites bhargavai* fauna below the horizon of the proposed GSSP has led us to suggest that the boundary level should be lowered by ca. 1m (Brühwiler *et al.* submitted [b]).

***Shamaraites rursiradiatus* beds.** This ammonoid fauna was found only in a single bed, i.e. in the second limestone bed within the base of the CM at Chiddru. It is characterized by the association of *Shamaraites rursiradiatus* sp. nov., *Monneticeras compressum* gen. et sp. nov., *Pseudoflemingites* cf. *timorensis* and *Radioceras* cf. *kraffti*.

The occurrence of *Shamaraites* in this association indicates that it correlates at least partly with the early Smithian "*Clypeoceras timorense*" Zone from Primorye (Shigeta *et al.* 2009). Note that "*Clypeoceras timorense*" from Primorye as described by Shigeta and Zakharov (2009) is a not true *Clypeoceras*, but is here assigned to *Radioceras* (see systematic section).

***Xenodiscoides perplicatus* beds.** This subdivision has been found in the middle part of the CM at Nammal and in a single float block most likely derived from the base of the CS at Chiddru (sample Chi1). The fauna is characterized by the association of *Xenodiscoides perplicatus*, *X. involutus*, *X. falcatus*, *Vercherites vercherei*, *Paraspidites obesus* sp. nov., *Kashmirites* sp. indet., *Flemingites hofmanni* sp. nov. and *Rohillites pakistanensis* sp. nov. The latter two species were found only in the single float block from Chiddru.

***Flemingites nanus* beds.** These beds are well-documented from the lower part of the CS at Chiddru and from the upper part of the CM at Nammal. They are characterized by the association of *Flemingites nanus*, *Kashmirites armatus*, *Paranorites ambiensis*, *Paraspidites praecursor* and *Vercherites pulchrum*. The nautilid *Tainionautilus trachyceras*, a Permian holdover, is here documented from these beds. Biostratigraphic correlation based on this ammonoid assemblage reveals an important diachronism of the lithological boundaries between the CM and the CS between these two areas (Text-fig. 15).

The *Flemingites nanus* beds probably correlate with the lowest part of the *Flemingites* beds of Spiti (Bed 12 in Krystyn *et al.* 2007*a*, *b*; *Vercherites* cf. *pulchrum* beds in Brühwiler *et al.* submitted [b]), and with part of the *Flemingites rursiradiatus* beds from South China (Brayard and Bucher 2008).

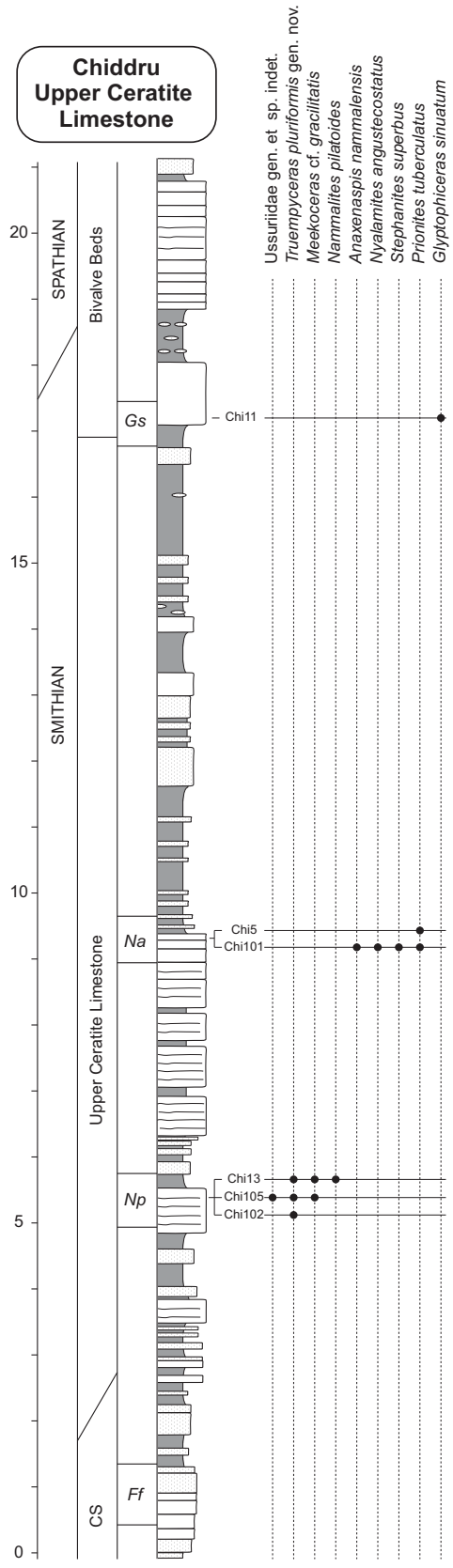

TEXT-FIG. 8*. Distribution of ammonoids in the Upper Ceratite Limestone in the Chiddru section. Abbreviations as in Text-figure 15.*

***Radioceras evolvens* beds.** This subdivision occurs in the middle part of the CS at Chiddru, and its fauna is characterized by the occurrence of *Radioceras evolvens*, *Pseudaspidites* cf. *muthianus* and ?*Paranorites* sp. indet. A. Note that according to Waagen (1895), *R. radiosum*, which is herein considered as a synonym of *R. evolvens*, occurs in the lower part of the CS. Moreover, *Radioceras* appears to be a long-ranging genus, since it occurs as low as the *Flemingites bhargavai* beds. Thus, this subdivision may be only of local significance.

***Flemingites flemingianus* beds.** The uppermost part of the Ceratite Sandstone at Chiddru, Nammal and Zaluch contains a distinctive fauna dominated by large-sized ammonoid specimens, and it is mainly characterized by the association of *Flemingites flemingianus* and *Hedenstroemia evoluta*. At Zaluch, these beds also contain *Clypeoceras superbum*, *Kashmirites baidi*, Arctoceratidae gen. et sp. indet. and Gen. et sp. indet. A.

The occurrence of *Flemingites flemingianus* and *Clypeoceras superbum* at this level has already been described by Waagen (1895) from several other localities in the Salt Range. This fauna correlates with at least part of the *Flemingites* beds of Spiti (Krystyn *et al.* 2007*a*, *b*) and the *Flemingites rursiradiatus* beds from South China (Brayard and Bucher 2008).

Middle Smithian ammonoid faunas

***Brayardites compressus* beds.** This subdivision occurs in the lower part of the Upper Ceratite Limestone at Nammal and Zaluch and is characterized by the association of *Brayardites compressus* and *Juvenites* sp. indet.

Brayardites compressus was recently described from the middle Smithian *Brayardites compressus* beds of Tulong (South Tibet) (Brühwiler *et al.* accepted), and it has also been found in Spiti, Northern India (Brühwiler *et al.*

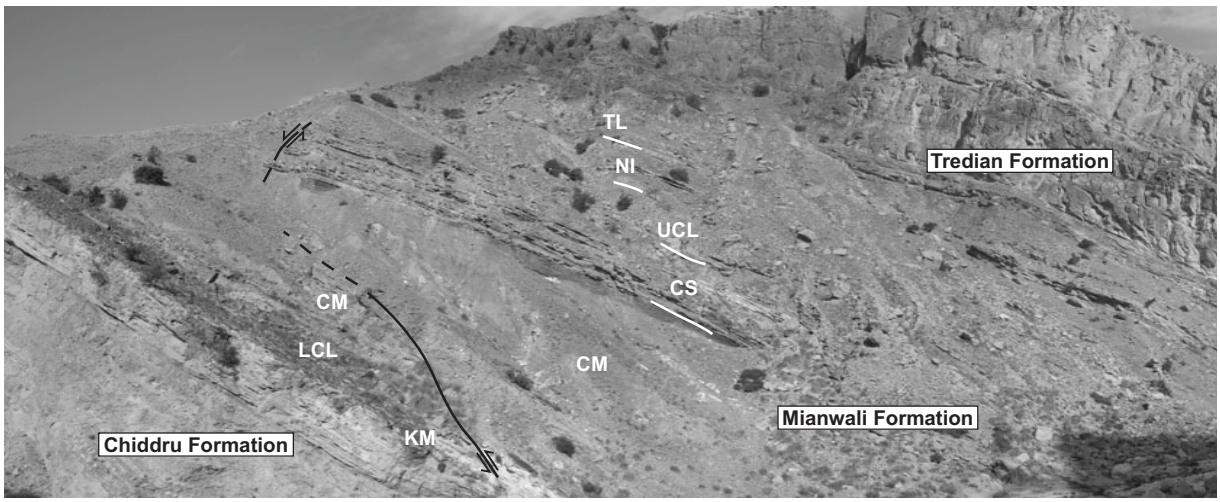

TEXT-FIG. 9*. Northwestern slope of the Nammal Gorge. KM Kathwai Member; LCL Lower Ceratite Limestone; CM Ceratite Marls; CS Ceratite Sandstones; UCL Upper Ceratite Limestone; NI Niveaux Intermédiaires; TL Topmost Limestone. Note the presence of normal and low angle reverse faults (black lines).*

submitted [b]). In these two regions, *Brayardites* co-occurs with a distinctive faunal association that includes *Jinyaceras hindostanus*, *Tulongites xiaoqiaoi* and *Urdyceras tulongensis*. In the Salt Range, this fauna is apparently less diverse, but the occurrence of *Brayardites compressus* nevertheless allows correlation with Tulong and Spiti.

***Nammalites pilatoides* beds.** This subdivision occurs in the UCL at Chiddru, Nammal and Zaluch. It is characterized by the association of *Nammalites pilatoides*, *Meekoceras* cf. *gracilitatis*, *Truempyceras pluriformis*, *Juvenites* cf. *kraffti*, Ussuriidae gen. et sp. indet. and Proptychitidae gen. et sp. indet. B.

This association correlates with the middle Smithian *Nammalites pilatoides* beds recently described from Tulong (Brühwiler *et al.* accepted), with the fauna of an exotic block of Hallstatt facies from Oman (Brühwiler *et al.* submitted [a]) and with the "new prionitid B beds" in Spiti (Brühwiler *et al.*, 2007). As shown by Brühwiler *et al.* (accepted) the *Nammalites pilatoides* beds of South Tibet correlate with the lower part of the middle Smithian *Owenites koeneni* beds of South China (i.e. *Ussuria* and *Hanielites* horizons; Brayard and Bucher 2008) with which they share the common occurrence of *Owenites simplex* and *Paranannites spathi*. The occurrence of Ussuriidae gen. et sp. indet. in the *Nammalites pilatoides* beds from the Salt Range may also corroborate this correlation.

The occurrence of *Meekoceras* cf. *gracilitatis* in these beds indicates that a portion of the *Meekoceras gracilitatis* Zone of the USA (Silberling and Tozer 1968; Jenks 2007; Brayard *et al*. 2009a) correlates with the *Nammalites pilatoides* beds. However, the presence of several genera, such as *Guodunites*, *Inyoites* and *Lanceolites*, in the *Meekoceras gracilitatis* Zone indicates that this zone comprises the entire middle Smithian (Brühwiler *et al.* accepted), and the presence of *Euflemingites* may even indicate that part of the *M. gracilitatis* Zone may be of early Smithian age.

***Pseudoceltites multiplicatus* beds**. Hitherto, this subdivision has been found only in the UCL at Nammal, and it is characterized by the association of *Pseudoceltites multiplicatus*, *Prionites nammalensis* sp. nov. and *Hochuliites retrocostatus* gen. et sp. nov. In addition, rare specimens of *Punjabites punjabiensis* gen. et sp.

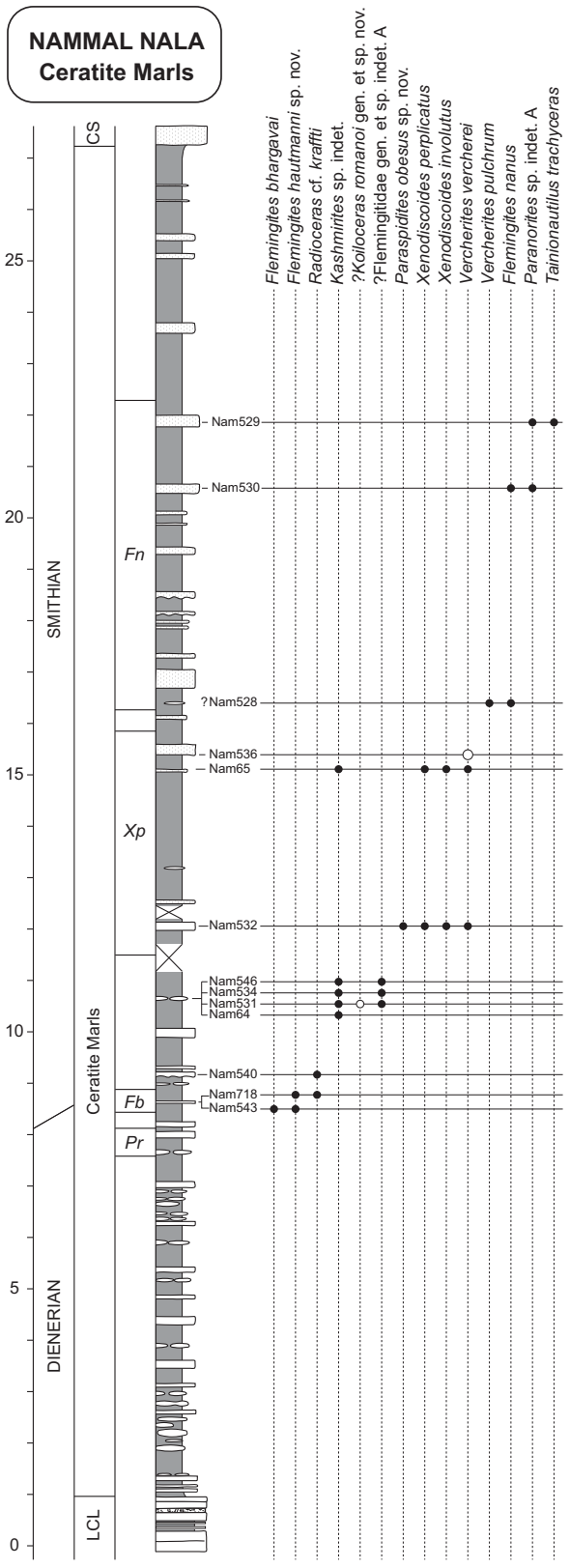

***TEXT-FIG. 10**. Distribution of ammonoids and nautiloids in the Ceratite Marls in the Nammal Gorge section. Abbreviations as in Text-figure 15.*

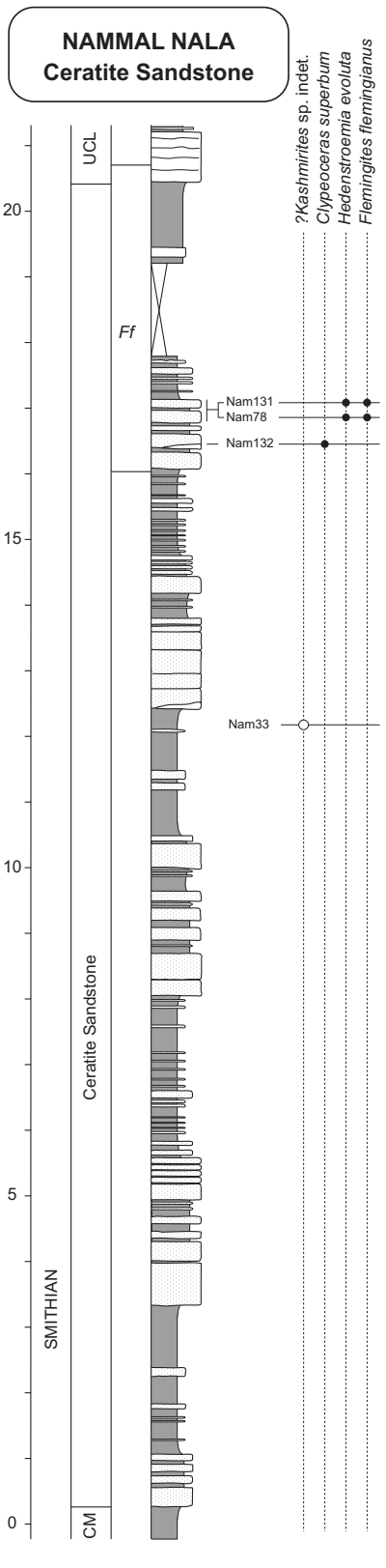

***TEXT-FIG. 11**. Distribution of ammonoids in the Ceratite Sandstones in the Nammal Gorge section. Abbreviations as in Text-figure 15.*

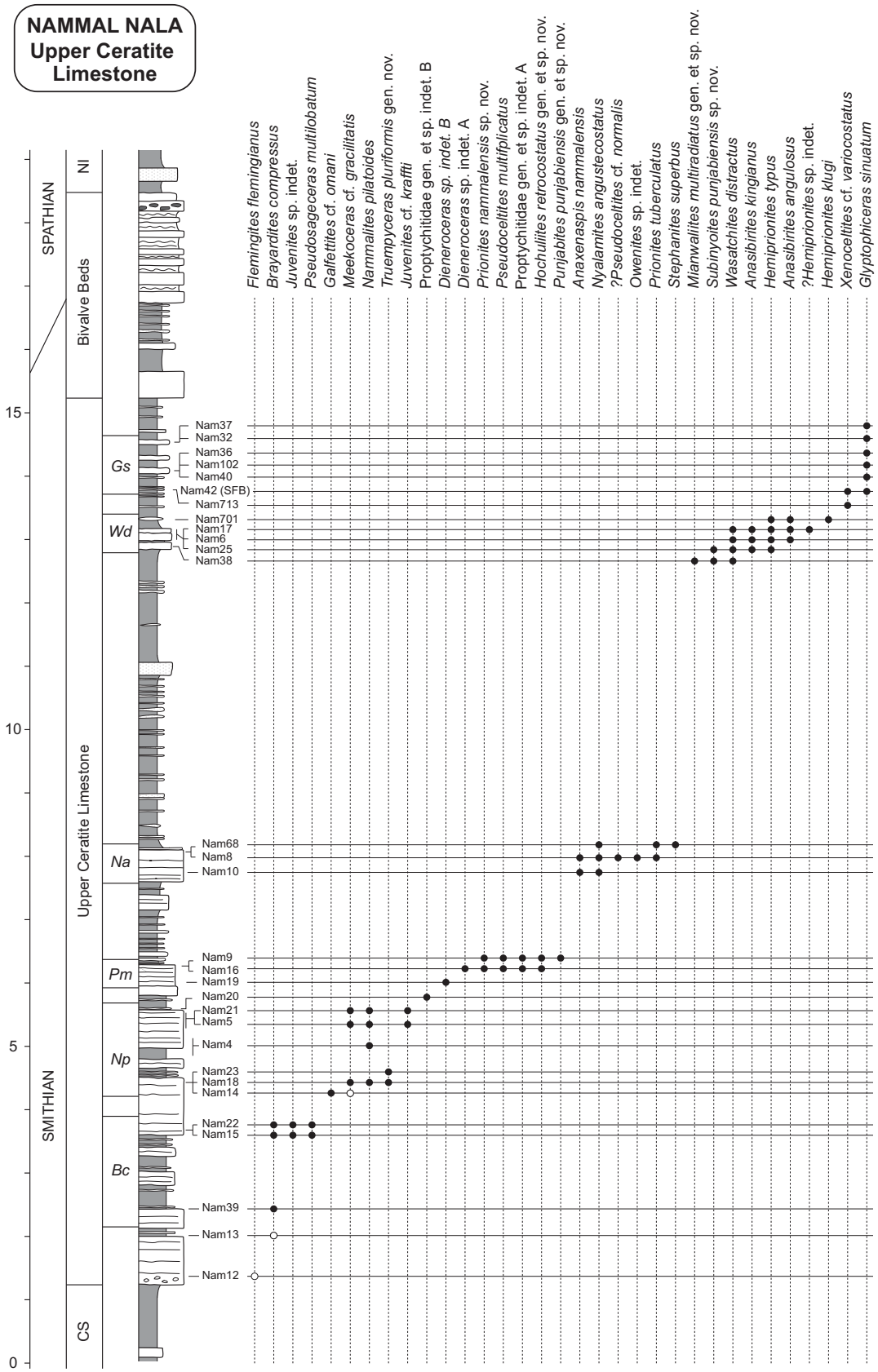

TEXT-FIG. 12*. Distribution of ammonoids in the Upper Ceratite Limestone in the Nammal Gorge section. Abbreviations as in Text-figure 15.*

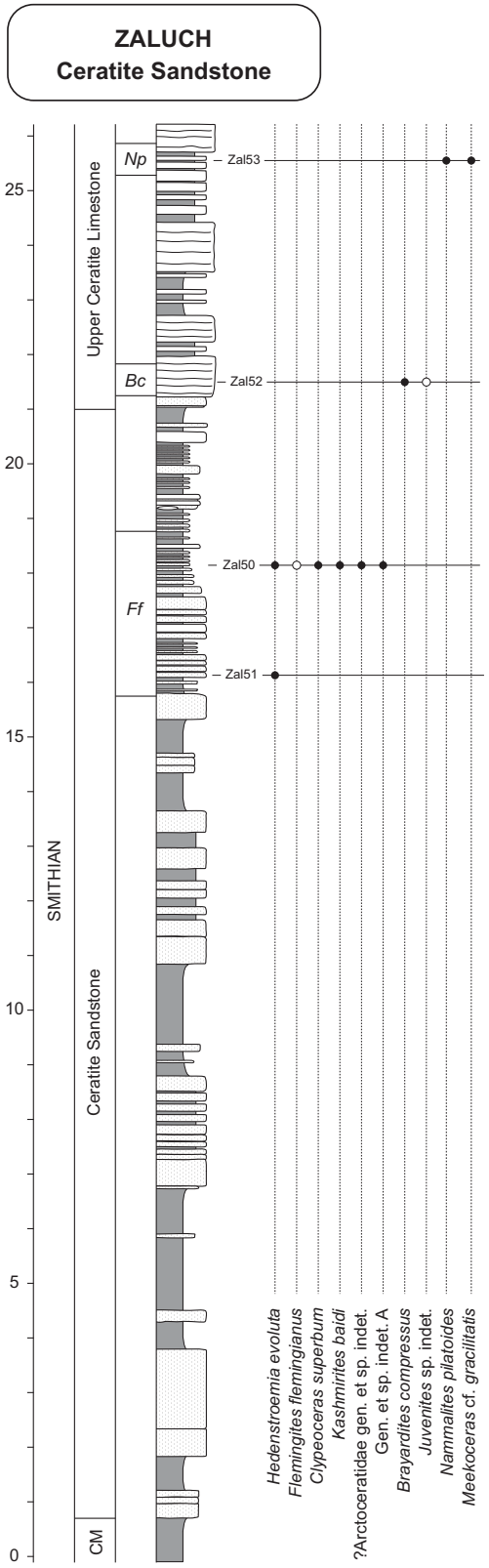

TEXT-FIG. 13*. Distribution of ammonoids in the Ceratite Sandstones in the Zaluch section. Abbreviations as in Text-figure 15.*

nov., Proptychitidae gen. et sp. indet. A, *Dieneroceras* sp. indet. A and *Dieneroceras* sp. indet. B have also been found in these beds.

This fauna also occurs at Tulong (Brühwiler *et al.*, accepted) and at Spiti ("Flemingitid A beds" in Brühwiler *et al.*, 2007). An exact correlative is not known from South China.

***Nyalamites angustecostatus* beds.** This subdivision, well known from Chiddru and Nammal, occurs in the uppermost beds of the massive limestones in the middle part of the UCL. Its fauna is characterized by the association of abundant *Anaxenaspis nammalensis*, *Nyalamites angustecostatus* and *Prionites tuberculatus*. *Stephanites superbus* also occurs, but is less abundant. Additionally, a single, very small specimen described as *Owenites* sp. indet. as well as a single specimen referred to as ?*Pseudoceltites* cf. *normalis* has been found in these beds.

This fauna is also known from Tulong (Brühwiler *et al.* accepted), Spiti (Brühwiler *et al.* subm. [b]) and Oman (Brühwiler *et al.* submitted [a]). It correlates with the *Inyoites* horizon in the upper part of the *Owenites koeneni* beds of South China (Brayard and Bucher 2008).

Late Smithian ammonoid faunas

Wasatchites distractum beds. This subdivision occurs in the upper part of the UCL and thus far, has been documented only from Nammal. The fauna contains very abundant Wasatchites distractus, Anasibirites kingianus, Anasibirites angulosus and Hemiprionites typus. Hemiprionites klugi, Subinyoites punjabiensis sp. nov. and Mianwaliites multiradiatus gen. et sp. nov. also occur, but are relatively rare.

Correlatives of this late Smithian fauna, which contain Anasibirites and/or Wasatchites, are known from many Tethyan localities such as Oman (Brühwiler et al., submitted [a]), Tulong (Brühwiler et al., accepted), Spiti (Bhargava et

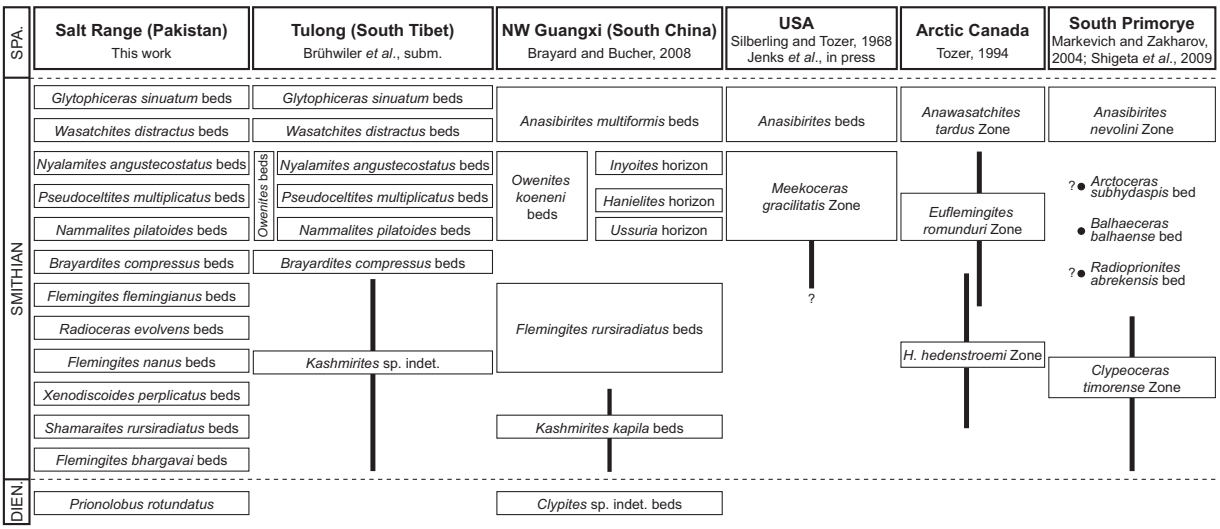

***TEXT-FIG. 14**. Biostratigraphical subdivisions of the Smithian of the Salt Range and correlation with zonations of other regions. Thick black bars indicate uncertainty intervals for correlations. See text for discussion.*

al. 2004; Brühwiler et al. submitted [b]), Timor (Welter 1922) and South China (Brayard and Bucher 2008). The fauna is also known from other worldwide localities such as Primorye (Markevich and Zakharov 2004), the USA (Silberling and Tozer 1968) and Arctic Canada (Tozer 1994).

Glyptophiceras sinuatum beds. This subdivision occurs in the uppermost part of the UCL at Nammal and in the lowest bed of the Bivalve Beds at Chiddru. Its fauna is characterized by Glyptophiceras sinuatum and Xenoceltites cf. variocostatus.

This latest Smithian fauna also occurs in Spiti (Brühwiler et al. submitted [b]) and in Tulong (Brühwiler et al. accepted). In South China the Xenoceltites variocostatus fauna also occurs above the horizons with Anasibirites, but was included in the Anasibirites multiformis beds by Brayard and Bucher (2008). Note that the genus Glyptophiceras was originally considered to be of Griesbachian age, but is now known to be restricted to the latest Smithian (Brühwiler et al. accepted).

Comparison with previous work

Based on the data of Waagen (1895), Mojsisovics *et al.* (1895) provided the first biostratigraphic subdivision of the Early Triassic of the Salt Range. In comparison with our new data, their subdivisions are correct in a general sense, but further refinement and some corrections are required (Text-fig. 18). Their first two zones, i.e. the *Gyronites frequens* Zone (LCL) and the *Proptychites lawrencianus* Zone (lower part of CM) contain typical Dienerian ammonoid faunas, and the subsequent *Proptychites trilobatus* Zone (CM) appears to contain a mixture of Dienerian taxa (such as *Ambites*, *Clypites*) and Smithian taxa (such as *Vercherites vercherei* and *V. pulchrum*). However, our extensive bed-rock controlled sampling has not revealed such associations. The following *Ceratites normalis* Zone (lower part of CS) is also problematic, since we found a specimen that probably belongs to this index species in a much higher horizon (i.e. in the *Nyalamites angustecostatus* beds). Moreover, most other species reported by Waagen (1895) from this zone are based on rather poorly preserved material. The subsequent *Flemingites radiatus* Zone (middle part of CS) and the *Flemingites flemingianus* Zone (upper part of CS) correspond to our *Flemingites nanus* beds

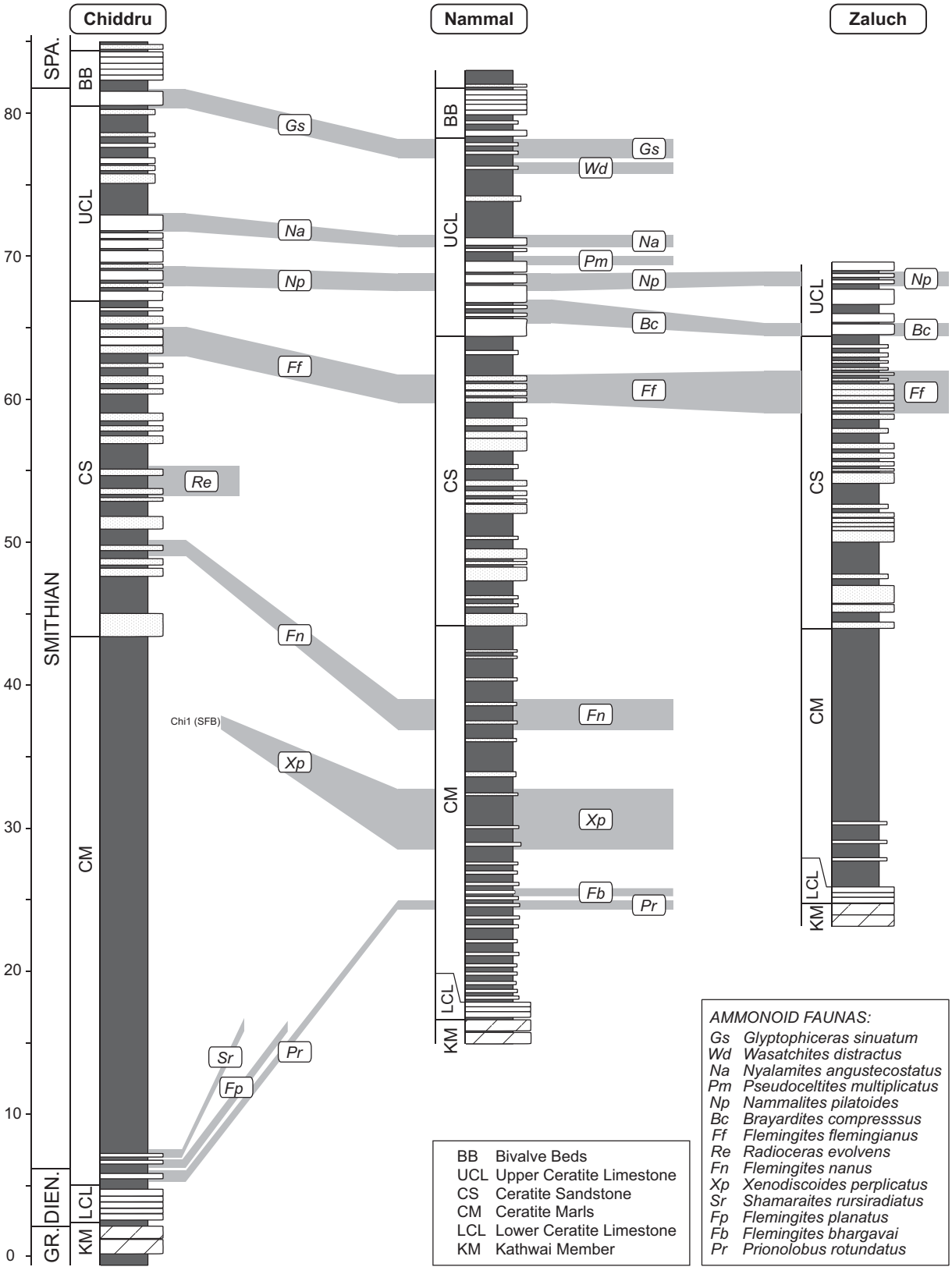

***TEXT-FIG. 15**. Biostratigraphical correlation of Chiddru, Nammal and Zaluch sections. Note the diachronism of the LCL/CM and CM/CS lithological boundaries between Chiddru and Nammal.*

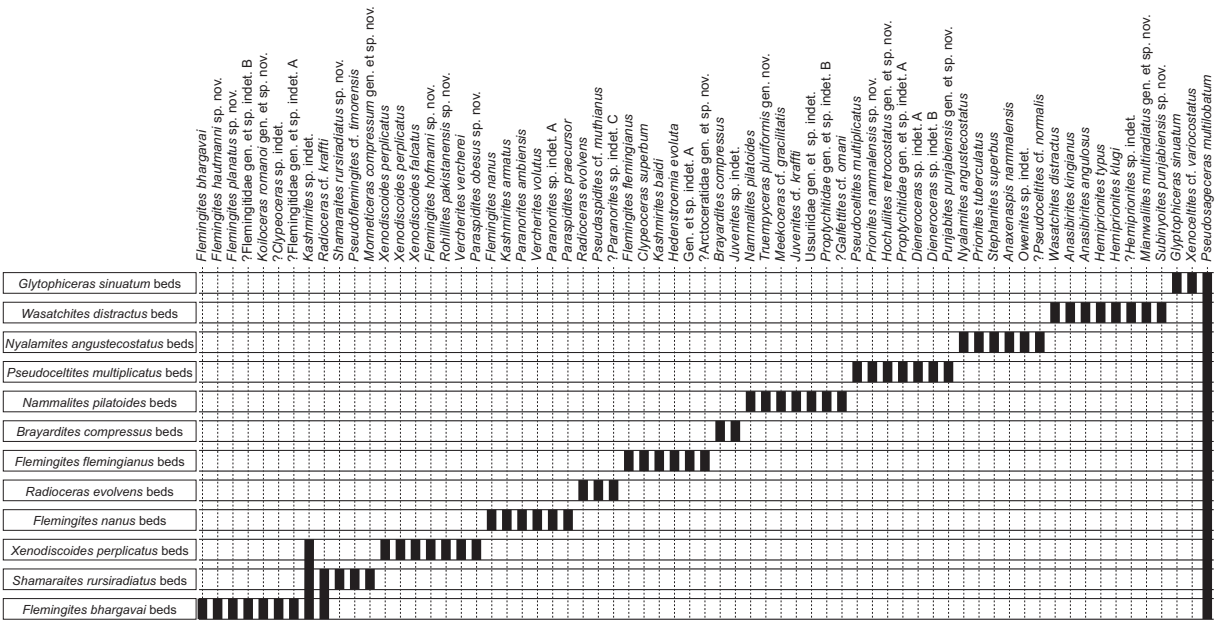

TEXT-FIG. 16. *Synthetic range chart showing the biostratigraphical distribution of Smithian ammonoid species in the Salt Range.*

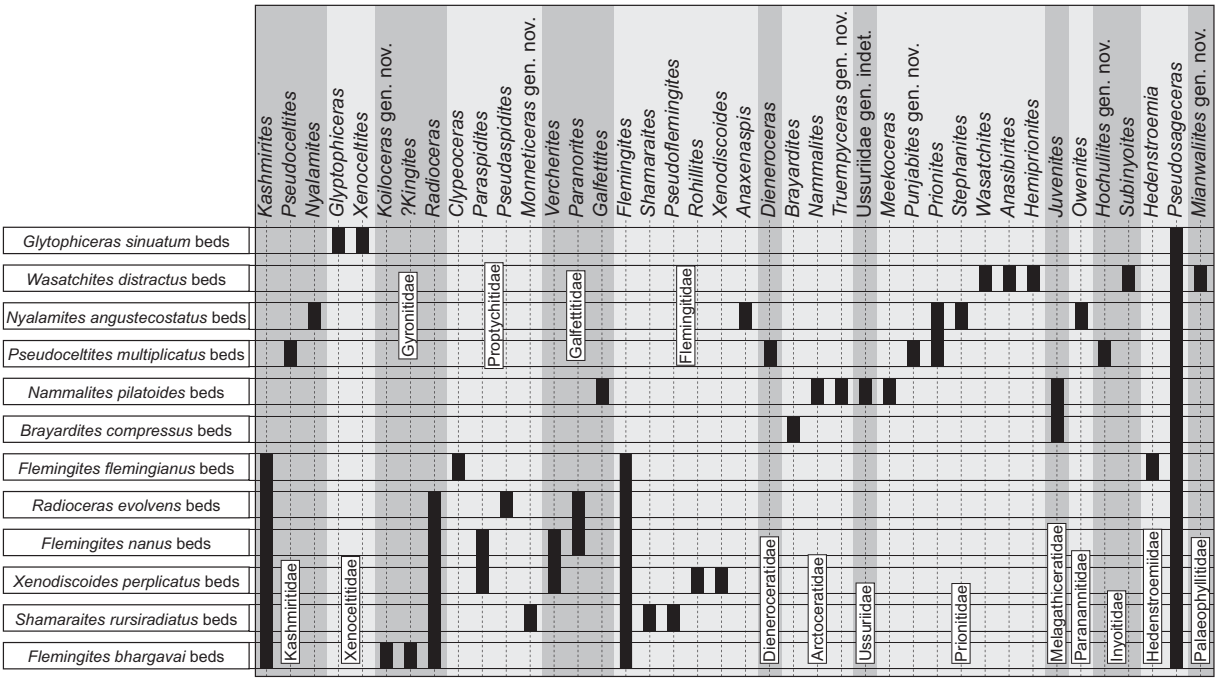

TEXT-FIG. 17. *Synthetic range chart showing the biostratigraphical distribution of Smithian ammonoid genera (grouped by families) in the Salt Range.*

and *Flemingites flemingianus* beds, respectively. The *Stephanites superbus* Zone (UCL) includes the middle and late Smithian interval from our *Brayardites compressus* beds to the *Wasatchites distractus* beds.

Noetling's (1905) zonation of the Lower Triassic of the Salt Range was based on non-bedrock controlled material collected from Chiddru and Virgal. Consequently, due to possible lateral diachronism of lithological boundaries (compare Text-fig. 15), some of Noetling's zones appear to be mixtures of faunas that cannot be directly compared with our data. A tentative correlation of Noetling's zonation with our data is given in Text-fig. 18. Noetling's lowermost zone, the *Celtites radiosus* Zone, contains Kashmiritidae and is possibly of earliest Smithian age. The second zone, the *Prionolobus rotundatus* Zone, contains a mixture of Dienerian and earliest Smithian ammonoids. The *Celtites fallax* Zone contains *Xenodiscoides* and is equivalent to our *Xenodiscoides perplicatus* beds. Noetling's *Prionolobus volutus* Zone corresponds more or less to our *Flemingites nanus* beds. However, the *Flemingites flemingianus* Zone as defined by Noetling encompasses the entire CS, which spans the interval from our *F. nanus* beds to the *F. Flemingianus* beds. Noetling's *Stephanites superbus* Zone includes all faunas from the UCL.

Our new biostratigraphic data have revealed important diachronisms of the lithological boundaries between the LCL and the CM, and between the CM and the CS, whereas the boundaries between the CS and UCL and between the UCL and the BB are relatively synchronous in the studied area (Text-fig. 15). When establishing their early ammonoid zonations for the Salt Range, Mojsisovics *et al.* (1895) and Noetling (1905) did not account for such lateral diachronisms of Waagen's (1895) lithological subdivisions, which may explain most of the inconsistencies of their zonations.

Guex (1978) formally introduced the late Griesbachian *Ophiceras connectens* Zone (based on the data from Schindewolf [1953] and Kummel [1970]), the early Dienerian *Gyronites frequens* Zone and the "*Anasibirites*" *pluriformis* Zone, which he correlated with the late Smithian *Tardus* Zone (Tozer 1967; Silberling and Tozer 1968). However, as we show here, the index species (herein transferred to *Truempyceras* gen. nov.) of the "*Anasibirites*" *pluriformis* Zone is not of late Smithian age, but instead occurs in the middle Smithian *Nammalites pilatoides* beds. Therefore, the *Pluriformis* Zone as defined by Guex (1978) corresponds to the entire interval from our *Nammalites pilatoides* beds to the end of the Smithian (Text-fig. 18).

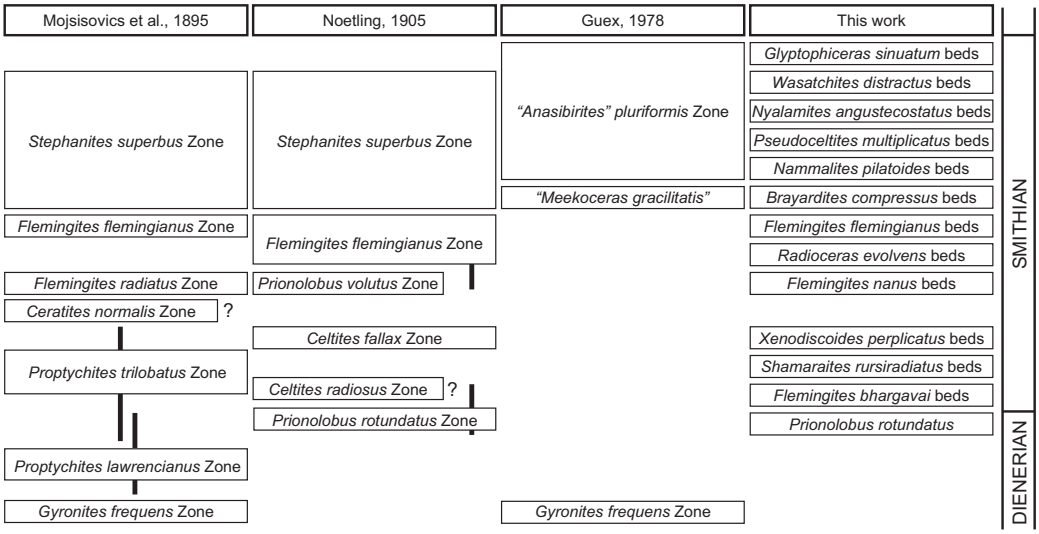

TEXT-FIG. 18*. Comparison of previous biostratigraphic subdivisions of the Early Triassic of the Salt Range. Thick black bars indicate the range of uncertainty of some correlations.*

Conclusions

Detailed sampling of the Lower Triassic succession at the Chiddru, Nammal and Zaluch localities in the Salt Range (Pakistan) has yielded abundant and well preserved ammonoid faunas of earliest to latest Smithian age. These faunas enable us to revise the taxonomy of Smithian ammonoids and also to address the important aspects of intraspecific variation and ontogenetic changes. The majority of Smithian ammonoid species from the Salt Range was insufficiently known due to small numbers of individuals and/or poor preservation.

Our data have enabled us to establish a high-resolution biostratigraphic sequence for the Smithian of the Salt Range, consisting of a total of 12 successive, well differentiated ammonoid assemblages. Thus, the Salt Range provide the most complete record of Smithian ammonoids presently known world-wide. Such detailed documentations of ammonoid successions are a prerequisite for the establishment of a precise, laterally reproducible and robust chronostratigraphic framework for the Smithian and subsequent diversity and phylogenetic analyses.

References

BHARGAVA, O. N., KRYSTYN, L., BALINI, M., LEIN, R. and NICORA, A. 2004. Revised litho- and sequence stratigraphy of the Spiti Triassic. *Albertiana*, 30, 21-39.

BRAYARD, A. and BUCHER, H. 2008. Smithian (Early Triassic) ammonoid faunas from northwestern Guangxi (South China): taxonomy and biochronology. *Fossils and Strata*, 55, 1-179.

BRAYARD, A., BUCHER, H., ESCARGUEL, G., FLUTEAU, F., BOURQUIN, S. and GALFETTI, T. 2006. The Early Triassic ammonoid recovery: Paleoclimatic significance of diversity gradients. *Palaeogeography, Palaeoclimatology, Palaeoecology*, 239, 374-395.

BRAYARD, A., BRÜHWILER, T., BUCHER, H., JENKS, J., 2009a. Guodonites, a low-palaeolatitude and trans-Pahynthalassic Smithian (Early Triassic) ammonoid genus: Palaeontology, 52 (2), 471-481.

BRAYARD, A., ESCARGUEL, G., BUCHER, H., MONNET, C., BRÜHWILER, T., GOUDEMAND, N., GALFETTI, T. and GUEX, J. 2009b. Good Genes and Good Luck: Ammonoid Diversity and the End-Permian Mass Extinction. *Science*, 325, 1118-1121.

BRÜHWILER, T., BUCHER, H and GOUDEMAND, N. accepted. Smithian (Early Triassic) ammonoids from Tulong, South Tibet. *Geobios*.

BRÜHWILER, T., BUCHER, H., GOUDEMAND, N and BRAYARD, A. 2007. Smithian (Early Triassic) ammonoid faunas of the Tethys: new preliminary results from Tibet, India, Pakistan and Oman. *New Mexico Museum of Natural History and Science Bulletin*, 41, 25-26.

BRÜHWILER, T., BUCHER, H., GOUDEMAND, N and GALFETTI, T. (submitted [a]). Smithian (Early Triassic) ammonoid faunas from Exotic Blocks from Oman: taxonomy and biochronology. *Palaeontographica*.

BRÜHWILER, T., WARE, D., BUCHER, H., KRYSTYN, L. and GOUDEMAND, N. (submitted [b]). New Early Triassic ammonoid faunas from the Dienerian/Smithian boundary beds at the Induan/Olenekian GSSP candidate at Mud (Spiti, Northern India). *Journal of Asian Earth Sciences*.

DE KONINCK, L. G. 1863. Description of some fossils from India, discovered by Dr. A. Fleming, of Edingburgh. *The quarterly Journal of the Geological Society of London*, 19, 1-19.

EHIRO, M., HASEGAWA, H. and MISAKI, A. 2005. Permian ammonoids *Prostacheocers* and *Perrinites* from the Southern Kitakami Massif, Northeast Japan. *Journal of Paleontology*, 79, 1222-1228.

FRECH, F. 1905. Das Mesozoicum. *Lethaea geognostica. II, Trias*. Stuttgart, 623 pp.

GALFETTI, T., BUCHER, H., BRAYARD, A., HOCHULI, P. A., WEISSERT, H.,

GUODUN, K., ATUDOREI, V. and GUEX, J. 2007*a*. Late Early Triassic climate change: Insights from carbonate carbon isotopes, sedimentary evolution and ammonoid paleobiogeography.

Palaeogeography, Palaeoclimatology, Palaeoecology, 43, 394-411.

GALFETTI, T., BUCHER, H., OVTCHAROVA, M., SCHALTEGGER, U., BRAYARD, A., BRÜHWILER, T., GOUDEMAND, N., WEISSERT, H., HOCHULI, P. A., CORDEY, F. and GUODUN, K. A. 2007*b*. Timing of the Early Triassic carbon cycle perturbations inferred from new U-Pb ages and ammonoid biochronozones. *Earth and Planetary Science Letters*, 258, 593-604.

GUEX, J. 1978. Le Trias inferieur des Salt Ranges, Pakistan: problemes biochronologiques. *Eclogae Geologicae Helvetiae*, 71, 105-141.

HERMANN, E., HOCHULI, P.A., MÉHAY, S., BUCHER, H., BRÜHWILER, T., HAUTMANN, M., WARE, D., ROOHI, G., UR-REHMAN, K., and YASEEN, A. in press. Organic matter and palaeoenvironmental signals during the Early Triassic biotic recovery: the Salt Range and Surghar Range records. *Sedimentary Geology,* doi:10.1016/j.sedgeo.2010.11.003.

JENKS, J. 2007. Smithian (Early Triassic) ammonoid biostratigraphy at Crittenden Springs, Elko County, Nevada and a new ammonoid from the *Meekoceras gracilitatis* zone. *New Mexico Museum of Natural History and Science Bulletin*, 40, 81-90.

KRYSTYN, L., BHARGAVA, O. N. and RICHOZ, S. 2007*a*. A candidate GSSP for the base of the Olenekian Stage: Mud at Pin Valley; district Lahul & Spiti, Himachal Pradesh (Western Himalaya), India. *Albertiana*, 35, 5-29.

KRYSTYN, L., RICHOZ, S. and BHARGAVA, O. N. 2007*b*. The Induan-Olenekian Boundary (IOB) in Mud – an update of the candidate GSSP section M04. *Albertiana*, 36, 33-45.

KUMMEL, B.1966. The Lower Triassic formations of the Salt Range and Trans-Indus Ranges, West Pakistan. *Bulletin of the Museum of Comparative Zoology, Harvard University*, 134, 361-429.

KUMMEL, B.1970. Ammonoids from the Kathwai Member, Mianwali Formation, Salt Range, West Pakistan. 177-192. *In* KUMMEL, B. and TEICHERT, C. (eds). *Stratigraphic Boundary Problems: Permian and Triassic of West Pakistan*. Department of Geology, University of Kansas, Special Publication 110 pp.

KUMMEL, B. and TEICHERT, C. 1966. Relations between the Permian and Triassic formations in the Salt Range and Trans-Indus ranges, West Pakistan. *Neues Jahrbuch für Geologie und Paläontologie. Abhandlungen*, 125, 297-333.

KUMMEL, B. and TEICHERT, C. 1970. Stratigraphy and Paleontology of the Permian-Triassic Boundary Beds, Salt Range and Trans-Indus Ranges, West Pakistan. 1-110. *In* KUMMEL, B. and TEICHERT, C. (eds). *Stratigraphic Boundary Problems: Permian and Triassic of West Pakistan*. Department of Geology, University of Kansas, Special Publication 110 pp.

MARKEVICH, P. V. and ZAKHAROV, Y. 2004. *Triassic and Jurassic of the Sikhote-Alin*. Dalnauka, Vladivostok, Russia. [In Russian with English summary]. 420 pp.

MOJSISOVICS, E. VON (1873, 1875, 1902): Das Gebirge um Hallstatt. 1. Abtheilung. Die Cephalopoden der Hallstatter Kalke. 1. Band. *Abhandlungen der geologischen Reichsanstalt*, 6/1, 1. Lief. (1873): 1–82, Taf. 1–32; 2. Lief. (1875): 83–174, Taf. 33– 70; 3. Lief. (Supplement, 1902): 175–356, Taf. 1–23; Wien.

MOJSISOVICS, E. 1896. Beitrage zur Kenntnis der obertriadischen Cephalopoden-Faunen des Himalaya. *Denkschriften der Akademie der Wissenschaften in Wien*, 63, 573-701.

MOJSISOVICS, E., WAAGEN, W. and DIENER, C. 1895. Entwurf einer Gliederung der pelagischen Sedimente des Trias-Systems. *Sitzungsberichte der Akademie der Wissenschaften in Wien (I)*, 104, 1271-1302.

MUNDIL, R., LUDWIG, K. R., METCALFE, I. and RENNE, P. R. 2004. Age and timing of the Permian mass extinctions: U/Pb dating of closed-system zircons. *Science*, 305, 1760-1763.

NOETLING, F. 1905. Die asiatische Trias. 107-221. *In* FRECH, F. (ed.) *Lethaea geognostica. Das Mesozoicum, 1. Band, Trias. Lethaia Mesozoica 1*. Schweizerbart, Stuttgart, 623 pp.

ORCHARD, M. J. 2007. Conodont diversity and evolution through the latest Permian and Early Triassic upheavals. *Palaeogeography, Palaeoclimatology, Palaeoecology*, 252, 93-117.

OVTCHAROVA, M., BUCHER, H., SCHALTEGGER, U., GALFETTI, T., BRAYARD, A. and GUEX, J. 2006. New Early to Middle Triassic U-Pb ages from South China: Calibration with ammonoid biochronozones and implications for the timing of the Triassic biotic recovery. *Earth and Planetary Science Letters*, 243, 463-475.

PAKISTANI-JAPANESE RESEARCH GROUP 1985. Permian and Triassic systems in the Salt Range and Surghar Range, Pakistan. 221-312. *In* NAKAZAWA, K. and DICKINS, J. M. (eds). *The Tethys: Her Paleogeography and Paleobiogeography from Paleozoic to Mesozoic*. Tokai University Press, Tokyo, 317 pp.

RAUP, D. M. and SEPKOSKI, J. J. 1982. Mass Extinctions in the Marine Fossil Record. *Science*, 215, 1501-1503.

RICOU, L. E. 1994. Tethys reconstructed - plates, continental fragments and their boundaries since 260 Ma from Central-America to South-Eastern Asia. *Geodinamica Acta*, 7, 169-218.

SCHINDEWOLF, O. 1953. Uber die Faunenwende vom Palaozoikum zum Mesozoikum. *Zeitschrift der Deutschen Geologischen Gesellschaft*, 105, 153-182.

SHIGETA, Y., MAEDA., H. and ZAKHAROV, Y. 2009. Biostratigraphy: ammonoid succession. 24-27. *In* SHIGETA, Y., ZAKHAROV, Y., MAEDA, H. and POPOV, A. M. (eds). *The Lower Triassic system in the Abrek Bay area, South Primorye, Russia.* National Museum of Nature and Science Monographs 38, Tokyo, 218 pp.

SILBERLING, N. J. and TOZER, E. T. 1968. *Biostratigraphic classification of the marine Triassic in North America*. Special Paper - Geological Society of America (GSA), Boulder, CO, United States, 63 pp.

SMITH, A. G., SMITH, D. G. and FUNNELL, B. M. 1994. *Atlas of Mesozoic and Cenozoic Coastlines*. Cambridge University Press, Cambridge, 109 pp.

SPATH, L. F. 1934. *Part 4: The ammonoidea of the Trias, Catalogue of the fossil cephalopoda in the British Museum (Natural History)*. The Trustees of the British Museum, London, 521 pp.

STAMPFLI, G. M. and BOREL, G. D. 2002. A plate tectonic model for the Paleozoic and Mesozoic constrained by dynamic plate boundaries and restored synthetic oceanic isochrons. *Earth and Planetary Science Letters*, 196, 17-33.

TOZER, E. T. 1967. A standard for Triassic time. *Geologic Survey of Canada Bulletin*, 156, 141 pp.

TOZER, E. T. 1981*a*. Triassic ammonoidea: geographic and stratigraphic distribution. 397–431. *In* HOUSE, M. R., SENIOR, J.R. (ed.) *The Ammonoidea*. The Systematics association, Academic Press, London, 593 pp.

TOZER, E. T.1981*b*. Triassic Ammonoidea; classification, evolution and relationship with Permian and Jurassic forms. 65-100. *In* HOUSE, M. R. and SENIOR, J. R. (eds). *The Ammonoidea*. The Systematics association, Academic Press, London, 593 pp.

TOZER, E. T. 1982. Marine Triassic Faunas of North-America - Their Significance for Assessing Plate and Terrane Movements. *Geologische Rundschau*, 71, 1077-1104.

TOZER, E. T. 1994. *Canadian Triassic ammonoid faunas*. Geological Survey of Canada, Ottawa, ON, Canada, 663 pp.

WAAGEN, W. 1879. Salt-Range fossils Vol 1: Productus limestone fossils. *Palaeontologia Indica*, 13, 1-72.

WAAGEN, W. 1895. Salt-Range fossils. Vol 2: Fossils from the Ceratite Formation. *Palaeontologia Indica*, 13, 1-323.

WELTER, O. A. 1922. Die Ammoniten der unteren Trias von Timor. *Paläontologie von Timor*, 11, 83-154.

ZAKHAROV, Y. D. 1968. *Biostratigraphiya i amonoidei nizhnego triasa Yuzhnogo Primorya (Lower Triassic biostratigraphy and ammonoids of South Primorye)*. Nauka, Moskva, 175 pp. [in Rusian].

Appendix 3:

Multiple climatic changes around the Permian-Triassic boundary event revealed by an expanded palynological record from mid-Norway

Peter A. Hochuli, Jorunn Os Vigran,
Elke Hermann, Hugo Bucher,

GSA Bulletin, 2010. 122 (5/6): 884–896

Multiple climatic changes around the Permian-Triassic boundary event revealed by an expanded palynological record from mid-Norway

Peter A. Hochuli[1,2,†], Jorunn Os Vigran[3], Elke Hermann[1], and Hugo Bucher[1,2]
[1]*Paleontological Institute and Museum, University Zürich, Karl Schmid-Strasse 4, CH-8006 Zürich, Switzerland*
[2]*Geological Institute ETH-Zürich, CH-8092 Zürich, Switzerland*
[3]*Sintef Petroleum Research, Trondheim NO-7465, Norway*

ABSTRACT

Here, we present the palynological record from two shallow core holes (6611/09-U-01 and -02) from the Trøndelag Platform offshore mid-Norway consisting of 750 m of Upper Permian and Lower Triassic sediments. The relatively homogeneous assemblages recovered from the Upper Permian deposits are dominated by gymnosperm pollen, mainly pteridosperms. At the base of the Griesbachian, numerous spore species appear in the record, leading to an increased diversity. The change at this boundary is also marked by the massive reduction of one group of pteridosperm pollen (*Vittatina*). Together with other typical Permian elements (e.g., *Lueckisporites virkkiae*), this group is rare but consistently present in the lower part of the Griesbachian, and it gradually disappears in its upper part. The distribution of other groups such as taeniate and non-taeniate bisaccate gymnosperm pollen (pteridosperms and conifers) shows no significant change across the boundary, whereas spores and other gymnosperm pollen increase in diversity and abundance. These changes coincide with the formational change between the Schuchert Dal Formation (Upper Permian) and the Wordie Creek Formation (Griesbachian) equivalents.

Late Permian and Griesbachian palynomorph assemblages display different patterns. The former show a homogeneous composition of low diversity, whereas the latter reflect diverse and variably composed floras. The data suggest that the arid phase of the Late Permian was followed by a humid phase at the base of the Griesbachian. In the Griesbachian section, a succession of six distinct palynological assemblages (phase II–VII) can be inferred. Comparable changes have been described from East Greenland. The variations in the palynological record are interpreted to reflect changing ecological conditions (e.g., changing humidity). Comparable variations in the distribution of $\delta^{13}C$ isotope values reported from various sections from Greenland and China, showing stable values during the Late Permian and highly variable values during the Griesbachian, suggest common causes for the observed fluctuations. Multiphase volcanic activity of the Siberian traps seems to be the most likely candidate to have caused the variations in the $\delta^{13}C$ isotope as well as in the palynological record.

In contrast to the common claim that marine and terrestrial biota both suffered a mass extinction related to the Permian-Triassic boundary event, the studied material from the Norwegian midlatitudinal sites shows no evidence for destruction of plant ecosystems. The presence of diverse microfloras of Griesbachian age supports the idea that the climate in this area allowed most plants to survive the Permian-Triassic boundary event.

INTRODUCTION

The Upper Permian and Griesbachian sequence from mid-Norway (Fig. 1) covers 750 m of clastic sediments. Detailed palynological study of these deposits allows a new look at the development of terrestrial ecosystems during the Permian-Triassic boundary interval, showing evidence for changing climatic conditions during one of the most critical intervals in Earth's history.

The end-Permian mass extinction is considered to be the largest biotic and ecological crisis recorded in Earth's history. It is generally accepted that more than 90% of the marine organisms went extinct during the Permian-Triassic boundary event (Erwin et al., 2002; Bottjer and

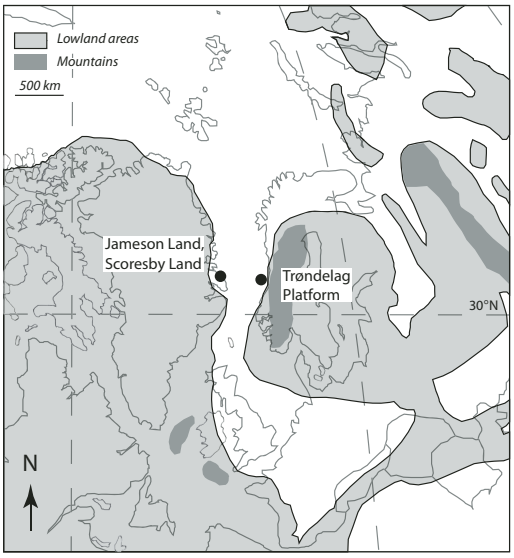

Figure 1. Paleogeographic position and location of the discussed sections, e.g., cores 6611/09-U-01 and -02 on the Trøndelag Platform, offshore mid-Norway, and the section from East Greenland (Jameson Land). The paleogeography is based on the compilation of Smith et al. (1994).

†E-mail: peter.hochuli@erdw.ethz.ch

GSA Bulletin; May/June 2010; v. 122; no. 5/6; p. 884–896; doi: 10.1130/B26551.1; 6 figures; 1 table.

Gall, 2005). Its impact on the terrestrial ecosystems is less evident and is still a matter of dispute (Metcalfe et al., 2008; Utting et al., 2004). The diverse plant assemblages, as documented in the relatively complete succession in East Greenland and the more expanded marine section in mid-Norway, suggest that changes were less dramatic than proposed in apocalyptic scenarios of some authors and demonstrate why none of the major plant lineages became extinct during the Permian-Triassic boundary event. The idea of decimated plant ecosystems seems to be influenced by low-latitudinal records, which are sparse, mostly incomplete, and often biased due to their preservation in red beds (Grauvogel-Stamm and Ash, 2005). The fragmentary terrestrial records also prevent the establishment of reliable temporal frameworks and hamper assessment of the turnover or possible extinction events in plant assemblages.

Most Early Triassic palynomorph assemblages are dominated by pteridophyte spores, especially of lycopsids, in contrast with Late Permian as well as Middle Triassic assemblages, which are dominated by gymnosperm pollen grains. The poorly diversified monotonous pollen-spore assemblages recovered from low latitudes of the Euramerican province have led to the idea that during the Permian-Triassic boundary event, terrestrial ecosystems suffered a mass extinction of similar magnitude as marine biotas and that only a few plants could survive the extremely hostile conditions. Mostly based on palynological records, several theories on the events affecting the terrestrial ecosystems have been put forward. Utting et al. (2004, p. 100) presented the most extreme position in stating that "some Lower Triassic rocks may be virtually barren of in situ pollen and spores and reworked material is dominant." A more moderate view was expressed by Visscher et al. (1996, p. 2155), who attributed "…world-wide destruction of standing woody biomass [as] resulting from excessive dieback of dominant gymnosperm vegetation." Other authors have mentioned devastated terrestrial ecosystems (Visscher and Brugman, 1986), or they have indirectly implied the collapse of the late Paleozoic floras in the statement of "post-collapse colonization by herbaceous pioneers" (Twitchett et al., 2001, p. 353). Several authors consider the abundance of *Reduviasporonites*, a putative fungal spore, as a witness for a dieback of the woody vegetation (Eshet et al., 1995; Visscher et al., 1996; Sandler et al., 2006). They are ignoring the probable affiliation of this taxon to the algae (Foster et al., 2002, and references therein) and the fact that destroyed or etiolated ecosystems might be attacked by more than one species of fungi.

The floral changes at the Permian-Triassic boundary transition are best observed from continuous palynological records with good age control. Well-preserved palynomorph assemblages have been described from the expanded marine sections from the Boreal realm, e.g., Canada (Utting, 1994; Utting et al., 2005), Greenland (Balme, 1979; Looy et al., 2001; Stemmerik et al., 2001; Bjerager et al., 2006), Norway (Mangerud, 1994), and Russia (Tuzhikova, 1985; Afonin, 2000). With the temporal resolution provided by marine fauna in the deposits, the palynological records of these sections represent the most complete archives of plant ecosystems of the Northern Hemisphere. From the Griesbachian records, we can infer that diversified plant assemblages existed during the Permian-Triassic boundary interval in which the abundant lycopsids coexisted with well-diversified assemblages of gymnosperms (e.g., pteridosperms and conifers).

The famous, supposedly sudden disappearance of glossopterids, and the subsequent appearance of *Dicroidium* on Gondwana, which support the idea of a catastrophic event affecting the terrestrial ecosystems at the Permian-Triassic boundary, have been challenged recently. Late Permian records of *Dicroidium* (Kerp et al., 2006) and reports of *Glossopteris* in the Triassic (e.g., Holmes, 1992) support the palynological evidence from Antarctica, which also suggests a gradual disappearance of Permian species (Lindström and McLoughlin, 2007).

Possible evidence for stressful conditions acting on terrestrial ecosystems might be inferred from the frequency of spore tetrads and the increased occurrence of abnormal pollen found in the Permian-Triassic boundary interval (Visscher et al., 2004; Beerling, 2007; Metcalfe et al., 2008). According to these authors, the peculiar shape and the type of preservation of some spores and pollen might have been caused by elevated ultraviolet (UV) radiation. Increased radiation was probably induced by the destruction of the ozone layer due to the effect of increased CO_2 and halocarbons released into the atmosphere through volcanic activity of the Siberian traps (Svensen et al., 2009). However, the data presented in this study and the fact that most plant groups range across the Permian-Triassic boundary suggest that plants must have survived in refuge areas where they faced less harsh conditions, or, alternatively, conditions on land were not as hostile as imagined by some authors. Plausible scenarios for the changes in the plant ecosystems include climatic changes induced by increased levels of CO_2 caused by volcanic activity and methane release (e.g., Kidder and Worsley, 2004), as well as possibly temporarily increased radiation.

STRATIGRAPHIC TERMINOLOGY

The chronostratigraphic concept and terminology applied in this paper are shown in Figure 2. Ignoring all important physical and biological changes (e.g., extreme isotope excursions, transgressions, faunal turnover), the new definition of the Permian-Triassic boundary is based on the first appearance datum (FAD) of the conodont species *Hindeodus parvus* in the extremely condensed global stratotype section and point (GSSP) section of Meishan (South China; Yin et al., 2001). Due to the facies dependence of the marker, this boundary can be identified only in limestone-dominated sections. In expanded sections with strong clastic influx, it is not recognizable. According to this biostratigraphically defined boundary, all significant changes related to the Permian-Triassic boundary event took place during the latest Permian (Changhsingian). The changes occur at the base or within the interval, which used to be recognized as the base of the Early Triassic or the Griesbachian substage (Tozer, 1994; Bjerager et al., 2006). Although this substage needs to be redefined, it is used in this paper in the traditional sense, since it is well defined by ammonoid (*Otoceras*) faunas in the Boreal realm and represents the initial transgressive sequence following the global Late Permian regression.

LOCATION, GEOLOGICAL SETTING, AND DATING

Two shallow cores were drilled in 1992 by IKU (now SINTEF Petroleum Research) as part of the bedrock mapping program of the Norwegian shelf (Bugge et al., 2002). The sections drilled on the Trøndelag Platform (Fig. 1) include 370 m of Upper Permian and 400 m of Griesbachian deposits recovered in the cores 6611/09-U-01 and 6611/09-U-02, with an overlap of 60 m. The perfect correlation of the two boreholes drilled 1200 m apart allows one to compile/assemble a 400-m-thick Griesbachian composite sequence (Figs. 3 and 4). The following brief overview over the lithological succession is based on the descriptions published by Bugge et al. (2002). The latter publication includes descriptions of depositional environments and well-log information (gamma, sonic, neutron porosity, and dipmeter logs) as well as seismic lines (figs. 3,5, and 15 in Bugge et al., 2002) and a cross section. Additional information including core photos is available on the Web site at http://www.sintef.no/static/pe/produkt/shadripro/corephotos/area_pages/helgeland.htm.

Core 6611/09-U-01 ended at a depth of 560 m in Upper Permian deposits. Starting from the bottom, the sequence consists of 170 m of

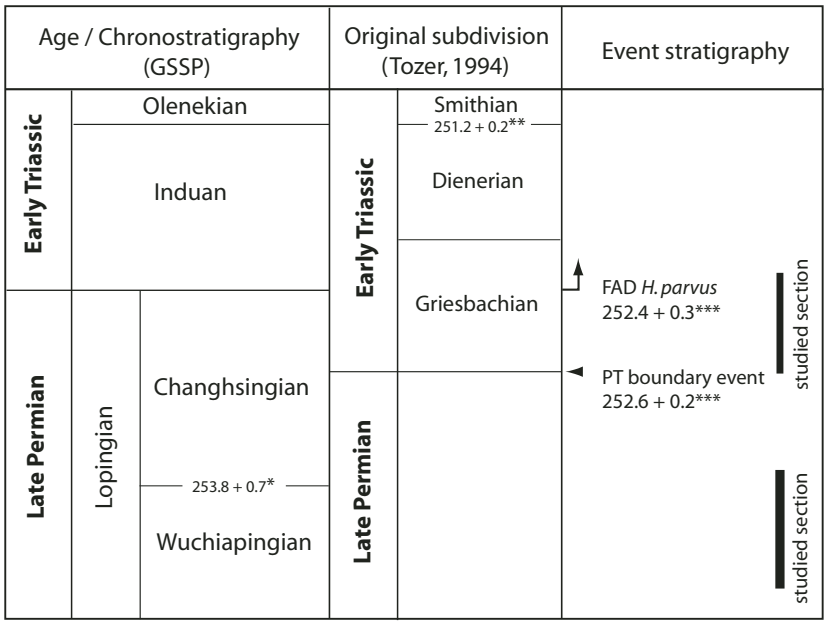

Figure 2. Chronostratigraphic subdivision of the Late Permian and the Early Triassic with radiometric ages (not to scale), expressing the different views on the position of the Permian-Triassic (PT) boundary, including the concept of the Griesbachian substage and the biostratigraphy events applied in this study. The ages are taken from the following sources: *interpolated age of Wardlaw et al. (2004), **U/Pb age after Galfetti et al. (2007), ***U/Pb ages according to Mundil et al. (2004). The inferred age range of the studied cores is marked with the vertical lines. Correlation between the Boreal sections and the Tethyan global stratotype section and point (GSSP) section has been discussed by Twitchett et al. (2001) and Bjerager et al. (2006). FAD—first appearance datum.

shallow-marine sandstones, characterized by reddish color. The ~15.5-m-thick Anhydrite unit following above reflects a change in the depositional environment and is characterized by anhydritic sandstones with reworked sabkha and tidal-flat deposits. In the Norwegian section, deepening of the basin is marked by the overlying 166-m-thick turbidite sequence (Lower Turbidite unit), which consists of series of fining-upward sandstone beds interbedded with dark-gray siltstone layers. Organic-rich intervals with laminated siltstones and mudstones occurring within the upper part of this unit are associated with dysoxic conditions.

Equivalent sections have been described from East Greenland. Thus, the shallow-marine red sandstones are considered to be equivalent to the Huledal Formation, the Anhydrite Unit corresponds to the Karstryggen Formation, the main part of the Lower Turbidite unit corresponds to the Ravenefjeld Formation, and its uppermost part corresponds to the Schuchert Dal Formation (Bugge et al., 2002). The upper part of the Schuchert Dal Formation has been dated as Dzulfian (late Wuchiapingian) based on ammonoids (Nassichuk, 1995). According to Bugge et al. (2002), the top of the Lower Turbidite unit represents the upper part of the Upper Permian (see Fig. 2).

The overlying series consisting of 400 m of turbidites (Upper Turbidite unit) was recovered in core 6611/09-U-01 and -02. It is characterized by 50–100-m-thick coarsening-upward sequences composed of laminated siltstones interbedded with gradually upward-increasing numbers of massive and individually fining-upward sandstone beds. In both cores, this sequence is interrupted by a distinct 10-m-thick interval composed of numerous thin evaporate layers, allowing precise correlation of the cores. The Upper Turbidite unit is considered equivalent of the Griesbachian Wordie Creek Formation in East Greenland.

Although they were deposited in a similar, fully marine environment, the Upper Permian and the Griesbachian units are separated by a distinct sedimentary break (Bugge et al., 2002, their fig. 9A). This break is marked by a pronounced change in the sedimentation pattern of the turbidites. Based on relatively homogeneous sporomorph assemblages, Bugge et al. (2002) attributed an Ufimian to early Tatarian? (Lopingian) age to the entire Upper Permian section. The hiatus between the Late Permian and the Griesbachian is supposed to span the late Tatarian (Changhsingian). The distinct change in the palynomorph assemblages between the Lower and the Upper Turbidite unit confirms the presence of a relatively long hiatus at this level. Correlation of the palynological data suggests that in the studied section, the hiatus between the Lower and Upper Turbidite units might be more important than in the correlative sections in East Greenland. According to Stemmerik et al. (2001), the major turnover in the floral record occurs within the uppermost Schuchert Dal Formation.

In core 6611/09-U-01, the lowermost 43 m of the Griesbachian are devoid of any fauna, and the interval above contains macrofauna with ammonoids (*Ophiceratidae* sp., *Tompophiceras*? sp. and *Lytophiceras*? sp.) indicating a late Griesbachian age. The bivalve *Claraia* sp. has been recognized at 200 m. The 81 fossiliferous samples covering 400 m of section contain palynomorph assemblages that are typical for a Griesbachian age. There is no evidence for a hiatus within this interval. According to the seismic data, the section recovered in well 6611/09-U-02 might be truncated, missing the top of the Griesbachian (Bugge et al., 2002).

The composition of the palynological assemblages indicates the presence of the basal Griesbachian palynostratigraphic zone defined in the Barents Sea area as assemblage P (Hochuli et al., 1989) or as *Lundbladispora obsoleta–Chordecystia chalasta* zone (Mangerud, 1994). These assemblages are closely comparable with those from the Wordie Creek Formation of Eastern Greenland (cf. Stemmerik et al., 2001; Looy et al., 2001). Similar assemblages from Arctic Canada have been defined as *Tympanicysta stoschiana–Striatoabieites richteri* zone (Utting, 1994). The late Griesbachian zone Svalis-1 (Vigran et al., 1998) or assemblage O (Hochuli et al., 1989) defined in the Barents Sea area is probably younger.

FLORAL ELEMENTS OBSERVED WITHIN CORE 6611/09-U-01 AND -02

The present discussion of the evolution of the Late Permian and Griesbachian floras is based on the quantitative distribution of 13 groups of spore-pollen (Fig. 4). The components of these groups are listed in Table 1 together with some remarks on their probable botanical attributions and ecological affinities. Botanical assignments

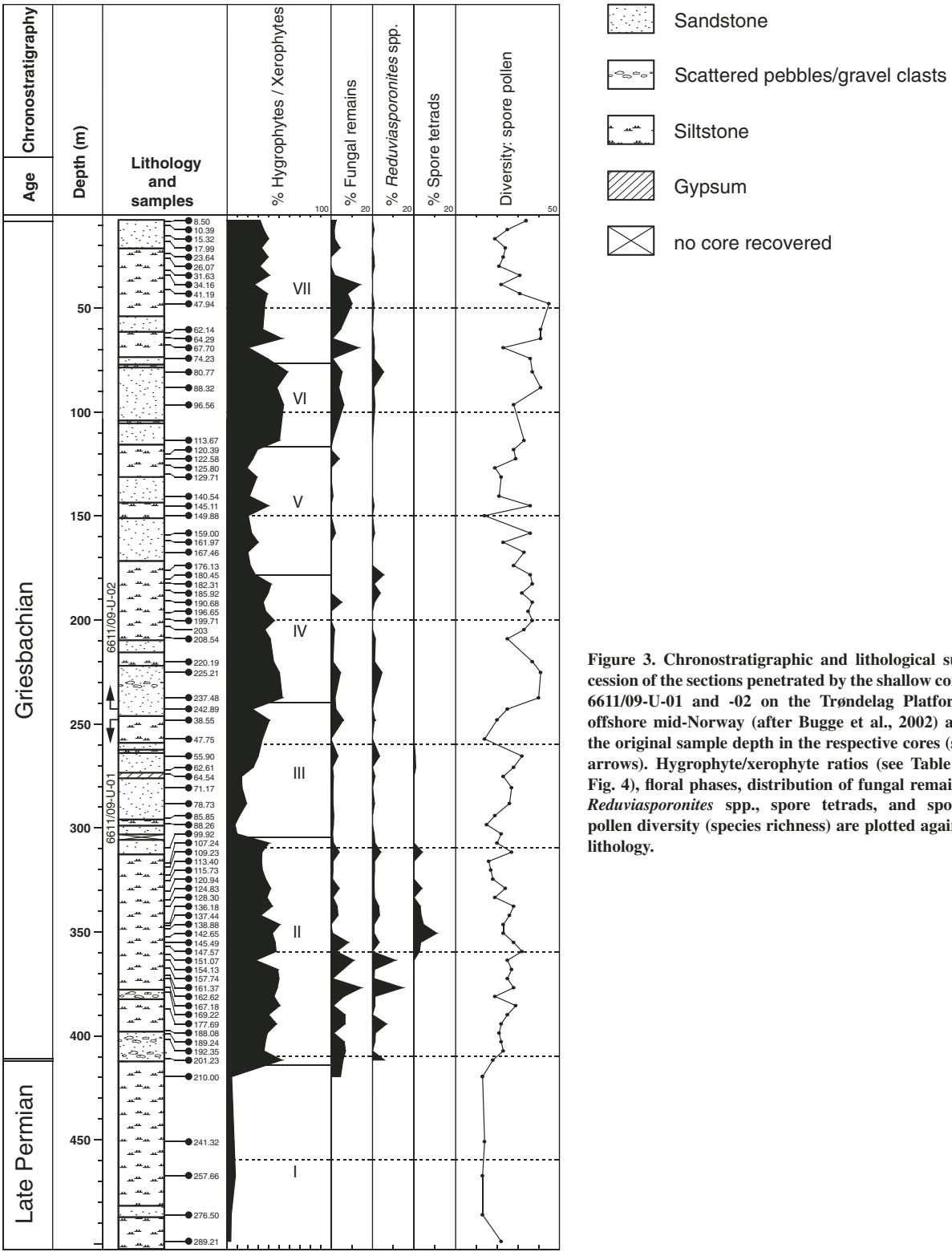

Figure 3. Chronostratigraphic and lithological succession of the sections penetrated by the shallow cores 6611/09-U-01 and -02 on the Trøndelag Platform, offshore mid-Norway (after Bugge et al., 2002) and the original sample depth in the respective cores (see arrows). Hygrophyte/xerophyte ratios (see Table 1; Fig. 4), floral phases, distribution of fungal remains, *Reduviasporonites* spp., spore tetrads, and spore-pollen diversity (species richness) are plotted against lithology.

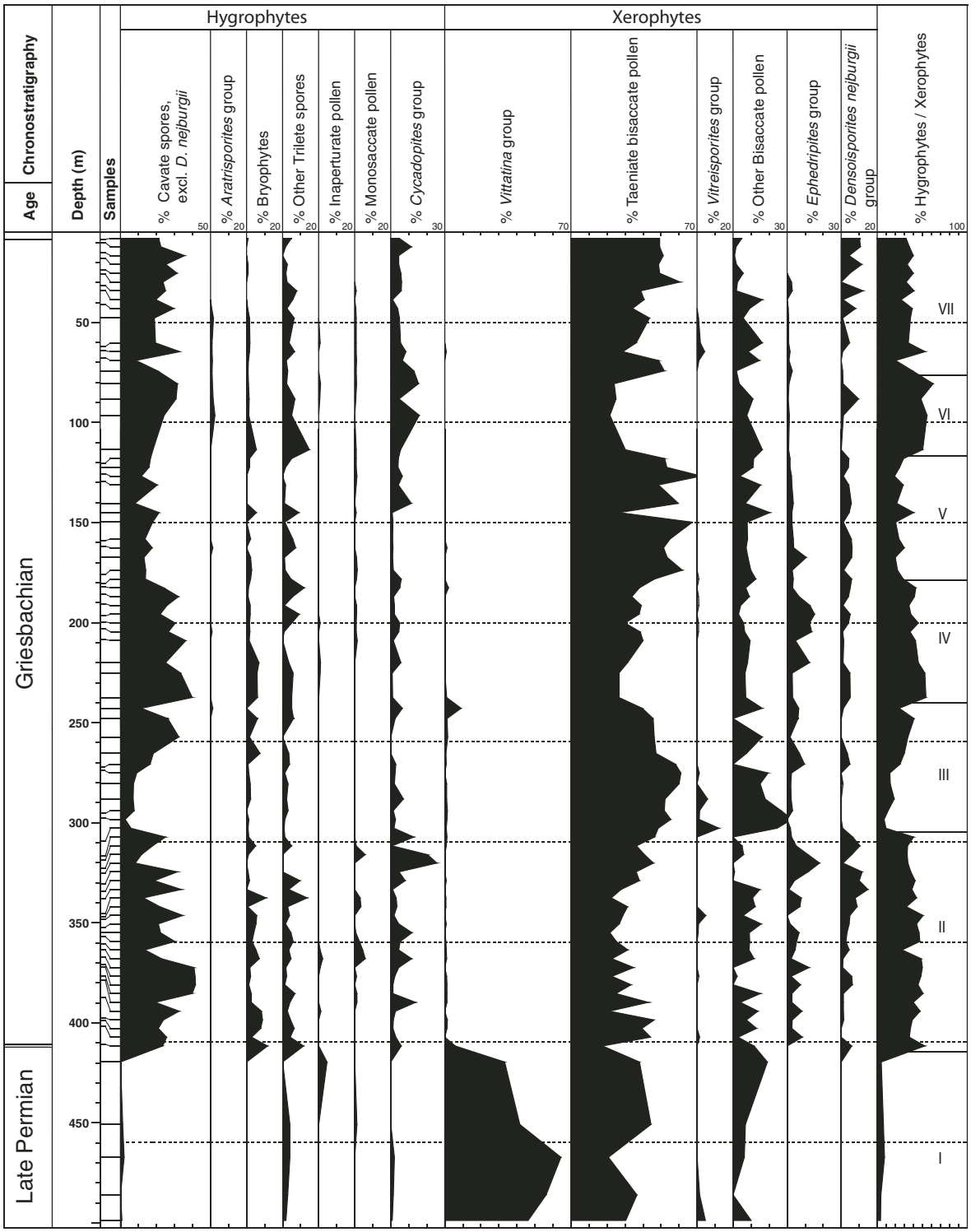

Figure 4. Composite section of the shallow cores 6611/09-U-01 and -02 showing chronostratigraphy, distribution of the main floral elements (see Table 1; Fig. 5), hygrophyte/xerophyte ratios, and floral phases I to VII as defined in this study.

TABLE 1. SPORE-POLLEN GROUPS APPLIED IN THIS PAPER AND CORRESPONDING BOTANICAL AFFINITY AND ECOLOGICAL ATTRIBUTION (HYGROPHYTES AND XEROPHYTES)

Floral elements	Genera included	Affinity	Remarks
Cavate spores (see Fig. 5H)	*Densoisporites*, *Kraeuselisporites*, *Pechorosporites*, *Endosporites*, *Lundbladispora*	Lycopsids	Hygrophytes
Aratrisporites	*Aratrisporites*	Lycopsids (Pleuromeiaceae)	First appearance datum (FAD) in the Griesbachian (see comments on reworking); Hygrophytes
Bryophytes (see Fig. 5C)	*Maculatasporites*, *Proprisporites*		Hygrophytes
Other trilete spores (see Figs. 5D, 5E, 5F)	*Leiotriletes*, *Apiculatisporites*, *Converrucosisporites*, *Verrucosisporites*	Filicales	Hygrophytes
	Calamospora	Equisetopsids	
	Uvaesporites	? Bryophytes	
Monosaccate pollen (see Fig. 5I)	*Tsugaepollenites*, *Grebespora*	Uncertain botanical affinity	Hygrophytes
	Florinites, *Cordaitina*	Cordaites	
Cycadopites (see Fig. 5M)	*Cycadopites*	Cycadales, Bennettitales, Ginkgoales	Hygrophytes
Inaperturopollenites (group)	*Inaperturopollenites*, *Pilasporites*	Pteridophytes, Conifers, ?Bryophytes (hygrophytes)	Xerophytes
Vittatina (see Fig. 5S)	*Vittatina*	Pteridosperms (Peltaspermales)	Xerophytes
Taeniate bisaccate pollen (see Figs. 5O, 5P, 5R)	*Lunatisporites*, *Protohaploxypinus*, *Striatoabieites*, *Striatopodocarpites*	Pteridosperms	Xerophytes
	Lueckisporites	Conifers	
Vitreisporites group (see Fig. 5Q)	*Vitreisporites*, *Falcisporites*	Pteridosperms, Caytoniales	Xerophytes
Non-taeniate bisaccate pollen (see Figs. 5J, 5L, 5N, 5T)	*Alisporites*, *Klausipollenites*, *Scutasporites*, *Bharadwajisporites*, *Limitisporites*, *Platysaccus*	Conifers *Alisporites* have also been produced by pteridosperms (Peltaspermales)	Xerophytes
Ephedripites group (see Fig. 5K)	*Ephedripites*, *Gnetaceaepollenites*	Gnetales	Xerophytes
Densoisporites nejburgii (see Fig. 5G)	*Densoisporites nejburgii*, *D.* cf. *nejburgii*	Lycopsids, *Pleuromeia* including *P. sternbergii*	Xerophytes

are essentially based on the compilation of in situ occurrences by Balme (1995). The distribution of *Reduviasporonites*—here regarded as an alga—fungal remains and spore tetrads are plotted separately (Fig. 3).

Hygrophytes/Xerophytes

The aforementioned groups are classified according to their assumed ecological requirements into two entities, hygrophytes and xerophytes, respectively, following the concept of Visscher and van der Zwan (1981). With the exception of *Densoisporites nejburgii*, all spores are regarded as hygrophytes. Among gymnosperm pollen, *Cycadopites*, monosaccate pollen, and the *Inaperturopollenites* group are attributed to the hygrophytes; all other pollen groups are classified as xerophytes. The hygrophyte-xerophyte ratio is plotted in Figures 3 and 4. Consistent changes of this ratio are interpreted as changes in the humidity available to the parent plants. This ratio essentially corresponds to the spore/pollen ratio used by other authors (e.g., Looy et al., 2001, their fig. 6).

***Reduviasporonites*, Fungal Remains, and Spore Tetrads (Figs. 3, 5A, and 5B)**

Reduviasporonites (syn. *Tympanicysta* and *Chordecystia*) is here considered to be of algal origin (cf. Foster et al., 2002). In the studied material, it first occurs at the base of the Griesbachian (Upper Turbidite unit) and in varying frequency upsection. It reaches over 5% of the total sporomorph count only in two samples.

Fungal remains, essentially hyphae, appear in the uppermost part of the Late Permian and are regularly noted throughout the Griesbachian section.

Spore tetrads have been found in significantly increased numbers in the lower part of the Griesbachian unit.

PALYNOLOGICAL RESULTS

The present compilation is based on the distribution of over 100 taxa in 117 samples. The data, originally represented in a semiquantitative

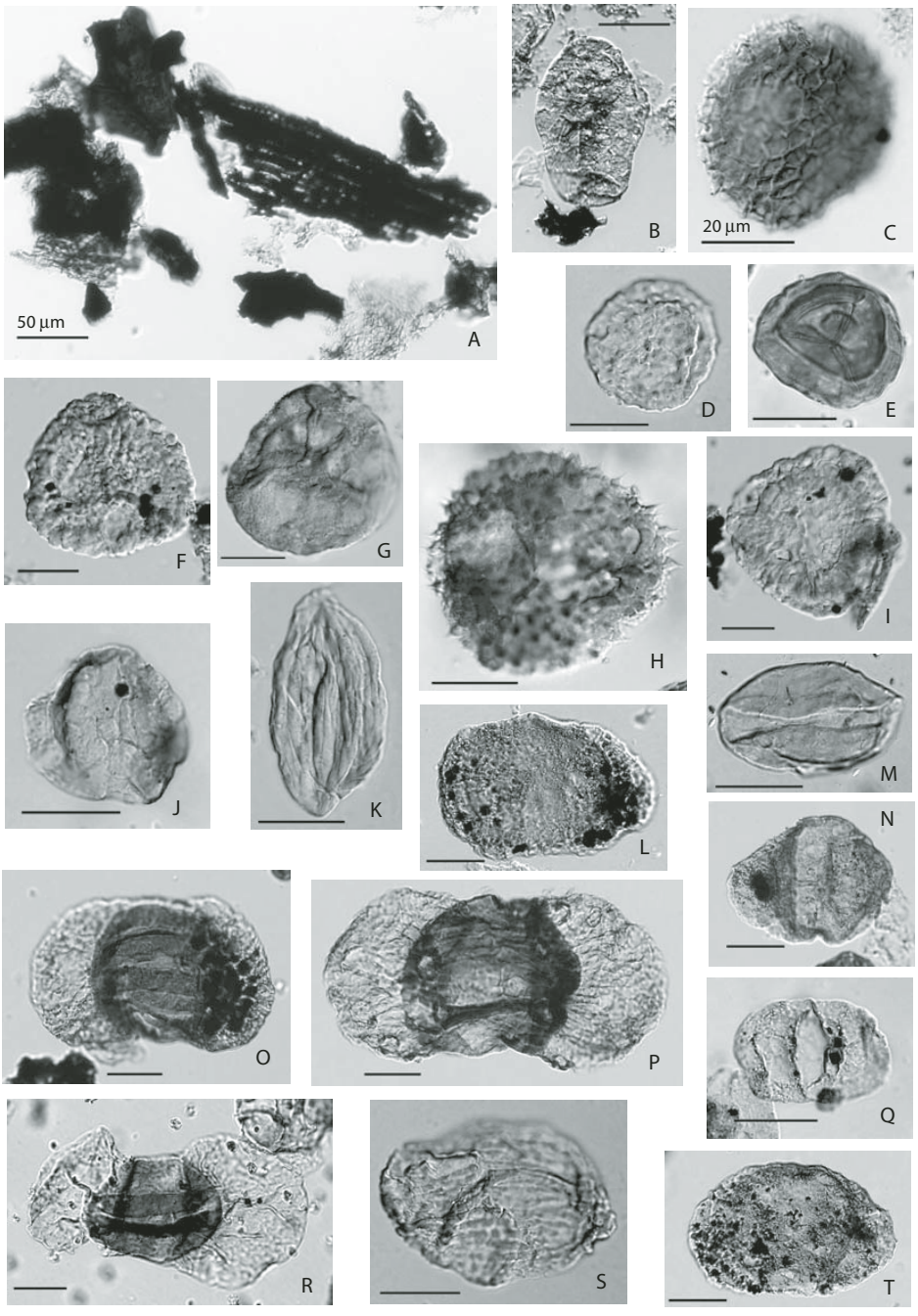

Figure 5. Palynofacies and selected palynomorphs from the shallow cores 6611/09-U-01 and -02. The number following the well number indicates the depth. It is followed by the reference number of the Palaeontological Museum Oslo (PMO), Norway, where the corresponding slides are housed. The last number refers to the England finder coordinates. Scale bars: A and B = 50 µm, all other figures = 20 µm. (A) Typical palynofacies with a dominance of woody phytoclasts; 6611/09-U-01, 185.64 m, PMO 214.019, P49. (B) *Reduviasporonites* sp.; 6611/09-U-01, 137.44 m, PMO 214.015, J44/2. (C) *Maculatasporites* sp.; 6611/09-U-01, 138.88 m, PMO 214.016, K49/2. (D) *Anaplanisporites stipulatus*; 6611/09-U-01, 151.07 m, PMO 214.017, P55/3. (E) *Polycingulatisporites densatus*; 6611/09-U-02, 47.94 m, PMO 214.020, B42. (F) *Uvaesporites* sp.; 6611/09-U-01, 151.07 m, PMO 214.017, C49/4. (G) *Densoisporites nejburgii*; 6611/09-U-01, 137.44 m, PMO 214.015, O51. (H) *Pechorosporites disertus*; 6611/09-U-01, 137.44 m, PMO 214.015, L48/3. (I) *Cordaitina* sp.; 6611/09-U-01, 151.07 m, PMO 214.017, T38/1. (J) *Klausipollenites staplinii*; 6611/09-U-01, 138.88 m, PMO 214.016, F53/2. (K) *Ephedripites* sp.; 6611/09-U-01, 151.07 m, PMO 214.017, C39/2. (L) *Falcisporites zapfei*; 6611/09-U-02, 47.94 m, PMO 214.020, K53. (M) *Cycadopites follicularis*; 6611/09-U-01, 138.88 m, PMO 214.016, E44/3. (N) *Limitsporites* sp.; 6611/09-U-02, 47.94 m, PMO 214.020, O44/3. (O) *Protohaploxypinus samoilovichii*; 6611/09-U-02, 47.94 m, PMO 214.020, L49. (P) *Striatoabieites richteri*; 6611/09-U-01, 185.64 m, PMO 214.019, K55. (Q) *Vitreisporites koenigswaldii*; 6611/09-U-02, 47.94 m, PMO 214.020, G44/3. (R) *Striatoabieites richteri*; 6611/09-U-01, 185.64 m, PMO 214.019, K55. (S) *Vittatina* sp.; 6611/09-U-01, 162.62 m, PMO 214.014, R49. (T) *Klausipollenites schaubergeri*; 6611/09-U-02, 47.94 m, PMO 214.020, M41/4.

manner (Vigran, 1992, personal commun.), have been transferred into a quantitative scheme by attributing figures to the following semiquantitative classification: abundant/common = 25, frequent = 10, present = 2. The original distribution charts were produced for confidential reports to the participants in the 1992 IKU shallow drilling project (see http://www.sintef.no/static/pe/produkt/shadripro/index.html). The number of counted specimens in each slide was restricted to 200; subsequently, the slides were scanned for rare species. Poor samples with counts below 200 have been excluded from the present compilation. Within the studied interval, the quantitative distribution of the aforementioned groups shows distinct changes. For the following discussion, we subdivide the palynological succession into seven distinct floral phases (I–VII, see Figs. 3 and 4) based on the distribution of the main floral elements. The distribution of these phases and the lithological succession show that the distribution of the spore-pollen groups and the inferred hygrophyte/xerophyte (H/X) ratios are independent of the lithology (cf. Figs. 3 and 4). All the phases comprise intervals with predominance of both sandstones and siltstones.

Late Permian

The Late Permian palynological record (core 6611/09-U-01) is based on the study of over 20 reasonably rich samples that represent over 200 m of deposits. For graphical reasons, only the highest part of this interval (phase I: 498.76–419.55 m) has been represented in Figures 3 and 4. The assemblages show relatively homogeneous composition with rather low diversity. Beside the abundance of *Vittatina*, they are characterized by the common occurrence of taeniate and non-taeniate bisaccate pollen. Typical taxa are *Protohaploxypinus* spp., *P. samoilovichii*, *Falcisporites* spp., and *Scutasporites* spp., while *Cycadopites* spp., monosaccate pollen, representatives of the *Inaperturopollenites* group, and spores are rare. The top of the Late Permian is marked by the disappearance of a number of species, such as *Vittatina costabiliz*, *V. vittifera*, and *V. simplex*, as well as *Florinites luberae* and *Protohaploxypinus minor.* Due to their homogeneous composition, the assemblages are considered of approximately the same age and reflecting uniform environments.

Griesbachian

The Griesbachian record is based on the study of well-preserved palynomorph assemblages from 75 samples. The assemblages are characterized by the abundance and diversity of pteridophyte spores. The numerous taxa appearing at the base or within this interval include several characteristic species of taeniate bisaccate pollen, lycopsid (cavate) spores, and bryophytes. The relevance of the presence of supposedly typical Late Permian elements such as *Lueckisporites virkkiae*, or several species of *Vittatina*, is a matter of dispute. Numerous authors regard them as reworked (Utting et al., 2004, and references therein). However, because of their consistent presence in the lower part of the Griesbachian and their subsequent disappearance higher in the section in mid-Norwegian and numerous Arctic records, we consider them here as being in place. This concurs with the opinion of several other authors (e.g., Looy et al., 2001; Stemmerik et al., 2001).

Influenced by the catastrophic effect of the Permian-Triassic boundary event on marine ecosystems, some authors try to find evidence for similar effects on terrestrial ecosystems (Visscher et al., 1996; Benton and Twitchett, 2003; Utting et al., 2004; Sandler et al., 2006). According to Utting et al. (2004) most—if not all—palynomorphs recorded in Lower Triassic sections are interpreted as reworked. Thus, the genus *Aratrisporites* has been considered to represent a synonym of the Devonian spore *Archaeoperisaccus*, and its Triassic records are considered reworked (Utting et al., 2004). These authors suppress the fact that the representatives of the genus *Aratrisporites* are abundant and diverse throughout the Triassic, including several species of restricted range (Hochuli et al., 1989; Vigran et al., 1998). Additionally, in situ finds have been reported from numerous Triassic locations (see compilation of Balme, 1995). According to Utting et al. (2004), cavate trilete spores (e.g., *Densoisporites*, *Lunbladispora*, and *Pechorosporites*), one of the main elements of Early Triassic floral assemblages, supposedly represent reworked spores from the Devonian. Again, many of these forms have been isolated from sporangia of macrofossils of lycopsid affinity found in Triassic sediments (for references, see Balme, 1995). Taeniate bisaccate pollens (e.g., *Lunatisporites*), which are regarded to be reworked from the Permian (Utting et al., 2004), have also been reported from Triassic in situ finds (Balme, 1995). This pollen group is common throughout the Early and Middle Triassic, becomes rare in the Late Triassic, and disappears at the Triassic-Jurassic boundary. One species of this group, *Lueckisporites virkkiae*, has its main distribution in the Late Permian, but it has been consistently observed in the lower part of the Griesbachian (Balme, 1979; Hochuli et al., 1989; Mangerud, 1994; Looy et al., 2001). So far, it has not been recorded in Late Griesbachian assemblages (Hochuli et al., 1989; Vigran et al., 1998). Its distribution pattern suggests that it is in place in the assemblages from the lower part of the Griesbachian. In the present record, the *Vittatina* group represents the main floral element of the Late Permian. Since its distribution in the Griesbachian is similar to that of *L. virkkiae*, we suggest that it probably is also in place. Other authors consider *L. virkkiae* in place and *Vittatina* spp. as reworked (Mangerud, 1994; Bugge et al., 2002). Similar patterns of gradual disappearance of Permian sporomorphs have been recorded in other areas, such as in boundary sections of Antarctica (Lindström and McLoughlin, 2007). Evidence of gradual change of the flora is also provided by macroflora, with the records of supposedly Triassic elements in Upper Permian sediments (Kerp et al., 2006) and Permian elements in the Triassic (Holmes, 1992).

Most changes observed within the Griesbachian section are gradual and subtle (see Fig. 4). The assemblages from the basal part (phase II: 410.78–316.79 m) are characterized by the abundance and diversity of spores, especially cavate spores. In a short part of the section (376.73–367.29 m), these spores dominate the assemblages. Taeniate pollen seem to decrease consistently toward the middle part of this interval and increase again toward the transition to phase III. The upper part of phase II is marked by common occurrence of *Cycadopites* as well as higher percentages of *Ephedripites* and *Densoisporites nejburgii.* Non-taeniate bisaccate pollens are relatively rare. The abundance of spores results in a consistently high percentage of hygrophytes. Another obvious change between the Late Permian and the Griesbachian section includes the appearance of the algae *Reduviasporonites* (Fig. 3).

A next distinct phase (III) can be differentiated between 309.47 and 242.89 m. It is characterized by the strong dominance of taeniate pollen, in parts together with relatively strong representation of non-taeniate bisaccates and *Ephedripites*. With the exception of four samples (between 272.16 and 248.10 m), percentages of cavate spores are reduced. Compared to the interval below, *Cycadopites* and *D. nejburgii* are rare. *Vittatina* is consistently present up to the top of this interval. This phase is characterized by relatively low hygrophyte/xerophyte ratios.

Similar to phase I, cavate spores are abundant in the following phase IV (237.48–180.45 m). Near the base of this interval, the cavate spores dominate. Upsection, they decrease corresponding with an increase of the taeniate pollen. In contrast to the basal Griesbachian (phase II), *Vittatina* occurs only sporadically. The hygrophyte/xerophyte ratio is high in the

lower part of this interval and decreases toward the transition to phase V.

The highest abundances of taeniate pollen are reached in the following phase V (176.13–120.39 m).

Another distinct decrease of taeniate pollen combined with an increase of spores and *Cycadopites* characterizes the following phase VI (113.67–80.77 m). Another characteristic feature of this interval is the rare but consistent occurrence of *Aratrisporites*.

The uppermost part of the section (phase VII: 74.23–8.05 m) is again characterized by abundant taeniate pollen together with very common spores. Compared to the interval below, *D. nejburgii* is relatively common.

The distributions of fungal remains, *Reduviasporonites*, and spore tetrads are plotted in Figure 3 together with the hygrophyte/xerophyte ratio. Fungal remains seem to be more consistently represented and more common within the humid phases (II, IV, and VI). *Reduviasporonites* is most consistently found in the lower part of the section (phase II), where it also reaches relatively high numbers. The occurrence of spore tetrads is restricted to a relatively short interval within phase II.

COMPARISON WITH OTHER RECORDS

The section of Jameson Land in East Greenland is the most important point of reference (cf. Figs. 1 and 6). As for lithology and fauna, the palynological data are comparable to those presented in this study. Palynological and palynofacies records from East Greenland have been published by several authors (Balme, 1979; Oberhänsli et al., 1989; Piasecki, 1984; Stemmerik et al., 2001; Looy et al., 2001; Twitchett et al., 2001). The record documented by the last two publications covers a section of ~10 m of Upper Permian (Schuchert Dal Formation) and ~30 m of Griesbachian deposits (Wordie Creek Formation), including a considerable sampling gap in the upper part of the latter formation. Based on variations in the composition of the palynological assemblages, Looy et al. (2001) distinguished five phases (a–e) within the succession. The lowest phase, a, of Late Permian age, is characterized by abundances of *Inaperturopollenites* spp., which the authors attribute to cordaites. Other common floral elements include taeniate bisaccate pollen, non-taeniate bisaccate pollen ("alete bisaccoid pollen"), and genera attributed to the *Vittatina* group (*Vittatina* and *Weylandites*). Pteridophyte spores are rare. Relying on the very uncertain affiliation of *Inaperturopollenites* to cordaites, this phase supposedly reflects the "decline of cordaite-pteridosperm woodland" (Looy et al., 2001, p. 7881).

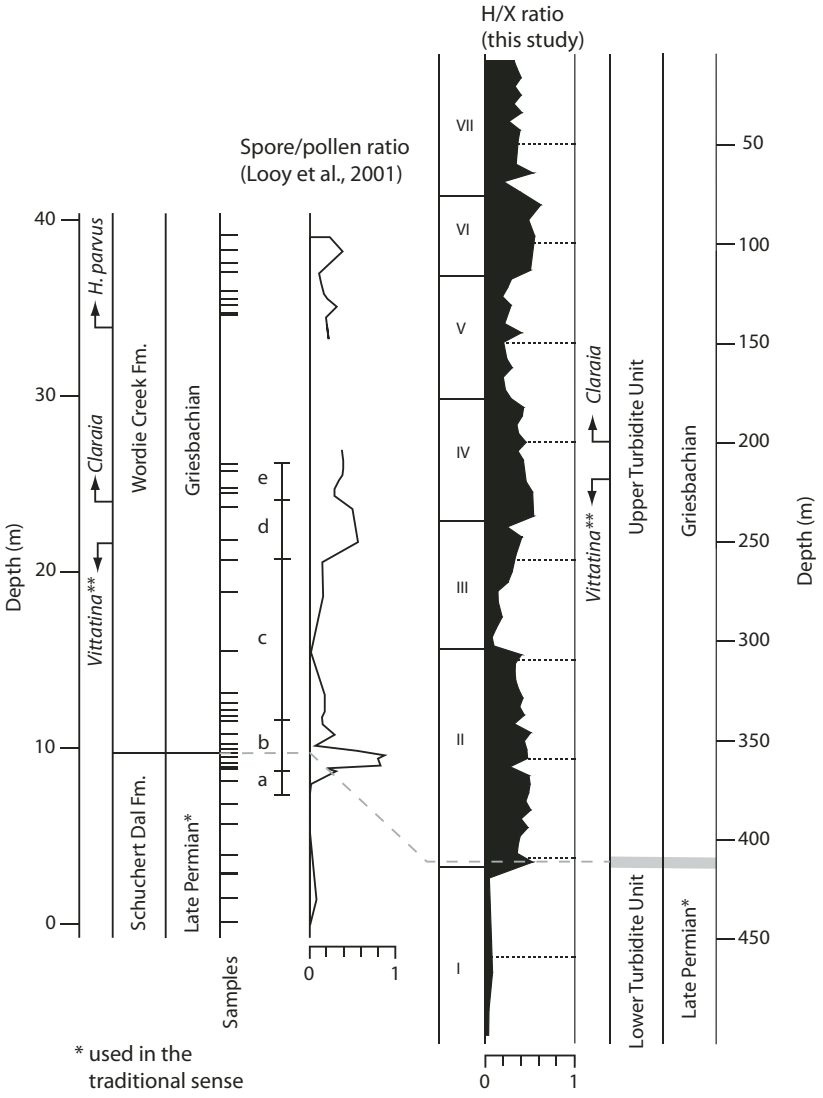

Figure 6. Chronostratigraphic succession and lithostratigraphic units in East Greenland (Jameson Land) and mid-Norway sections (Trøndelag section, cores 6611/09-U-01 and -02) with floral phases, spore/pollen and hygrophytic/xerophytic (H/X) ratios (see Table 1), and biostratigraphic events (first appearance datum [FAD] of *Claraia* sp., *Hindeodus parvus*, and the last consistent occurrence (**) of *Vittatina* spp.). East Greenland record is according to Looy et al. (2001, their fig. 2). The biostratigraphic events from mid-Norway include the last consistent occurrence (**) of *Vittatina* spp. as recorded in the present study and the FAD of *Claraia* sp. as reported by Bugge et al. (2002). Direct correlation of the FAD of *Claraia* sp. is unreliable due to the accidental record of the bivalves in the core 6611/09-U-02.

Distinct changes are recorded in the assemblages from three samples of the uppermost Schuchert Dal Formation (lower part phase b). Here, spores, essentially of lycopsid origin are abundant, and the previously mentioned pollen groups show a corresponding strong reduction. These samples are placed in the Late Permian pre–Permian-Triassic boundary interval, prior to the main isotopic shift and faunal change (Twitchett et al., 2001). This change has been

defined as the palynological Permian-Triassic boundary by Stemmerik et al. (2001).

The assemblages from the base of the Griesbachian (Wordie Creek Formation) are different, showing again a dominance of pteridosperms, here represented by taeniate bisaccate pollen. Spores are more common than in the main part of the Schuchert Dal Formation, but their abundance is drastically reduced compared to the samples below. Despite this contrast, Looy et al. (2001, p. 7881) considered the assemblages of the uppermost Schuchert Dal Formation and the lowermost Wordie Creek Formation as one phase (phase b), which they interpreted to reflect the "proliferation of herbaceous lycopsids." In our view, this interpretation can only apply to the samples of the topmost Schuchert Dal Formation, but not to the assemblages of the basal Griesbachian (Wordie Creek Formation).

The Wordie Creek Formation can be differentiated from the Schuchert Dal Formation by a lithological change, a marked shift in isotopic composition (>5‰), and the composition of the palynological assemblages. The assemblages from the first 10 m of the Wordie Creek Formation (representing upper part of phase b and phase c of Looy et al., 2001) are characterized by the dominance of gymnosperm pollen (taeniate pollen) with varying numbers of spores. Here, representatives of the *Vittatina* and *Inaperturopollenites* group are rarely but consistently reported. These assemblages have been interpreted to reflect the "establishment of diverse shrubland communities" (Looy et al., 2001, p. 7881). Following this interval, a distinct increase in the abundance of spores—with two samples where they dominate—is interpreted as a "renewed lycopsid proliferation" (phase d). *Vittatina*, *Lueckisporites*, and *Inaperturopollenites* have their highest occurrence at the top of this interval. The supposedly synchronous disappearance of the aforementioned genera in phase e, classified as "extinction of typical Late Permian Subangaran gymnosperms," is most probably amplified by a considerable sampling gap above this level. The assemblages from the interval above this gap are again dominated by taeniate pollen. The base of this interval is marked by the FAD of *H. parvus*, which is of Early Triassic age according to the GSSP Permian-Triassic boundary concept.

Although detailed correlations of the palynological assemblages from mid-Norway and East Greenland are not straightforward, common features include the varying percentages of the main floral elements (e.g., pteridosperms and lycopsids), as well as the fast decline and the subsequent disappearance of *Vittatina*. In Greenland, the basal part of the Griesbachian (upper part phase b) is characterized by common spores and taeniate bisaccate pollen. The assemblages following above (main part of phase c), with rare spores and dominance of taeniate bisaccate pollen, can be interpreted to reflect a relatively dry period. This interval is followed by a segment with renewed abundance of spores (phase d, e), which could be explained by more humid conditions. Detailed correlation of the East Greenland section with the studied succession is hampered by the lack of reliable and independent biostratigraphic constraints. The faunal record in the cores (e.g., FAD of *Claraia* sp.) is too fortuitous to be used for the correlation with the outcrop sections.

Based on the study of several sections in East Greenland, Stemmerik et al. (2001) described the gradual change of floral assemblages within the Schuchert Dal Formation as a transition from the *Vittatina*-dominated assemblages of the main part of the formation to the spore-dominated assemblages in its uppermost part. The palynological turnover—palynological Permian-Triassic boundary according to Stemmerik et al. (2001)—occurs 50 cm below the formation change and precedes the major shift in $C_{(carb)}$ isotopes occurring at the base of the Wordie Creek Formation

In the Barents Sea area, palynological records covering the Permian-Triassic boundary interval have been published by Mangerud (1994). Apart from Late Permian assemblages that are characterized by comparatively high diversity of pteridophyte spores and monosaccate pollen, the palynological development reveals the same tendencies as seen in the material from mid-Norway, with an increase in diversity of lycopsid spores. Possibly due to preservational bias, Griesbachian assemblages from Arctic Canada are poorly diversified, contrasting with diverse microfloras of Late Permian age (Utting, 1994; A. Baud, 2008, personal commun.). Quantitative data from the Griesbachian of Western Canada (Utting et al., 2005) show a distinct and continuous dominance of gymnosperm pollen; spores, especially lycopsids, are rare. Additionally, the Canadian records are biased by the presence of high numbers of reworked species.

Most records from the Tethyan realm are either based on very few samples or on records suffering from strong preservational bias. However, even fragmentary records derived from a few samples suggest a transition rather than a radical change between Late Permian and Early Triassic assemblages (Ouyang and Norris, 1999). Data from the condensed GSSP boundary section of Meishan show a distinct increase in diversity of spore-pollen at the Permian-Triassic boundary (in the traditional sense), whereas there are no significant changes at the level of the FAD of *H. parvus* (Ouyang and Utting, 1990). Here, the assemblages are also dominated by gymnosperm pollen.

The results from Upper Permian continental sections from South China, representing the typical Cathaysian Province, show diversified plant assemblages with strong dominance of spores. The Early Triassic assemblages show predominance of pollen; spore diversity appears to be considerably diminished (Peng et al., 2005, 2006). Based on this material, the authors draw the catastrophic scenario, where "…already depressed ecological conditions on land might have limited the chances for the sprout of plant roots (hence severely reducing the possibility of having full-grown trees with leaves)" (Peng et al., 2005, p. 292).

An expanded terrestrial record from North China has been published by Metcalfe et al. (2008). It is thought to represent an essentially complete section covering the latest Permian and the earliest Triassic. Three assemblages (A1–A3) have been distinguished. Assemblage A1 shows a common record of *Potonieisporites* and monosaccate pollen and is incommensurate with the records discussed in this paper. Assemblage A2 shares a few features with assemblages from Norway or Greenland (e.g., common occurrence of *R. chalasta* and presence of key taxa such as *Lueckisporites virkkiae*, *Lunatisporites transversundatus*, and *L. pellucidus*), but it differs by the common record of non-taeniate bisaccate pollen. In contrast to that, assemblage A3 shows close similarities with the Griesbachian record presented in this study, such as the dominance of cavate spores and taeniate bisaccate pollen as well as the presence of typical markers such as *Otynisporites eotriassicus* and *Pechorosporites disertus*. So far, some distinct feature of A3, namely, the presence of frequent abnormal pollen, has not been observed in our material. According to Metcalfe et al. (2008), the distribution of sporomorphs in assemblages A2 and A3 documents the transitional nature of the palynofloras across the Permian-Triassic boundary in northern China. A record reflecting similar trends has been published by Afonin (2000) from Permian-Triassic deposits of European Russia.

DISCUSSION

The so-far most expanded Late Permian–Griesbachian palynological succession recorded from shallow cores of the Trøndelag Platform (mid-Norway) reveals distinct changes in the quantitative distribution of spore-pollen. The Late Permian (Lopingian) spore-pollen assemblages show a homogeneous composition with a pronounced dominance of pteridosperms

associated with conifers contrasting with those from the Griesbachian, which are characterized by an association of pteridosperms and pteridophytes, the latter being dominated by lycopsids. In contrast to the uniform composition of the Late Permian assemblages, those of the Griesbachian show distinct variations. Within the 400-m-thick interval, six discrete phases of floral development can be differentiated based on varying percentages of the main plant groups (e.g., pteridosperms, conifers, and lycopsid spores). The ratio of hygrophytes/xerophytes suggests that there are three phases with increased humidity (phase II, IV, VI; cf. Figs. 3 and 4).

Late Permian Assemblages

The Late Permian assemblages are dominated by pollen of the *Vittatina* group accompanied by taeniate pollen. Spores are rare. Thus, during this interval, the vegetation was dominated by pteridosperms. Essentially based on the sparseness of spores, the climate of this interval is interpreted as dry. This result contrasts with the findings from East Greenland, where Looy et al. (2001) recorded in the Upper Permian section an abundance peak of inaperturate pollen, which they assigned to cordaites, implying more humid conditions. The morphologically indistinct genus *Inaperturopollenites* spp. could represent many other groups, including conifers or even bryophytes (cf. Balme, 1995). However, the data from Greenland show the same scarceness of spores, and verified cordaitalean pollen (e.g., *Florinites* or *Cordaitina*) have not been recorded. In the Norwegian material, these forms are very rare. Thus, the interpretation of Looy et al. (2001) stating that the Late Permian assemblage from Greenland reflects the "decline of the cordaite and pteridosperm woodland" is unsubstantiated and cannot be confirmed in this study.

Griesbachian Assemblages

In the studied cores, the assemblages from the over 400-m-thick base of the Griesbachian interval are characterized by abundance of spores. The distributions of other groups, e.g., pteridosperms, other than *Vittatina*, and conifers show only insignificant changes. The abundance as well as the diversification of spore taxa and percentages of hygrophytes reaching ~50% are interpreted to reflect increased humidity. There is, however, no equivalent of the peak abundance of spores as observed in East Greenland (spore/pollen ratio up to 0.8). According to the lithological correlation and to the C isotope values, this event occurs in the Upper Permian Schuchert Dal Formation (Twitchett et al., 2001; Stemmerik et al., 2001). This suggests that the corresponding interval might be missing in the studied cores and that here the hiatus between the Upper Permian and the Griesbachian might be more important.

The consistent trends reflected in the composition of the palynomorph assemblages in the well-documented sections from mid-Norway and East Greenland is a clear counterargument against the theory claiming that "The Early Triassic environment was so hostile to plant growth that few plants survived" (Utting et al., 2004, p. 100). In contrast to the Canadian material on which this hypothesis is based, no obviously reworked palynomorphs were found in the studied material. In numerous sites, the typical Permian taxa such as *Lueckisporites virkkiae* or the species of the *Vittatina* group are consistently present in the lower part of the Griesbachian. For this reason and in accordance with other authors (Balme, 1979; Hochuli et al., 1989; Looy et al., 2001), we assume that they are in place. The continuous presence of *Vittatina* recorded in core 01 and its sporadic occurrences afterwards suggest that the parent plants disappeared not suddenly during the Permian-Triassic boundary event, but that they survived during the lower part of the Griesbachian. The distribution pattern of this group could be interpreted in terms of ecological requirements of the parent plants, suggesting that they were adapted to dry conditions. Thriving during the Late Permian, they barely survived the more humid conditions of the early Griesbachian up to the second humid phase, where their continuous record ends. A similar pattern can be observed in the record of East Greenland, where *Vittatina* also disappears with onset of a second phase (phase d) dominated by spores (Looy et al., 2001).

Environmental Changes

According to the data from mid-Norway as well as the previous records from East Greenland and the Barents Shelf, the widely accepted image of the lowermost Triassic flora, after which herbaceous lycopsids invaded the devastated terrestrial ecosystems and became the globally dominant group, has to be revised. Our data show that, although the vegetation changed significantly during the Permian-Triassic boundary interval, there is no evidence for the disappearance of woody vegetation in mid- and high-latitudinal sites. Herbaceous lycopsids seem to have appeared as additional elements in vegetations dominated by gymnosperms. In East Greenland, the dominance of spores (spore/pollen ratio >0.5) is restricted to short intervals. Absence of woody plants has been inferred from the lack of coal deposits during the Early Triassic (Retallack et al., 1996). However, since formation of coal depends, beside the production of considerable amounts of organic matter, also on climatic conditions, the existence of the so-called coal gap postulated for the Early Triassic could be ascribed to the global climate. Additionally, Early Triassic palynofacies almost continuously dominated by woody and coaly particles indicate common occurrence of woody plants (cf. Fig. 5A and Hermann et al., 2008a).

A characteristic feature of many palynomorph assemblages of Permian-Triassic boundary sections is the common occurrence of *Reduviasporonites* (Eshet et al., 1995). Interpreting this taxon to be of fungal origin, and more precisely to represent a saprophytic fungus, its abundance stimulated several authors to prove the enfeebled nature of the plant ecosystems with the so-called "fungal event" (Sandler et al., 2006, and references therein). The solid evidence for the algal origin of this taxon published by several authors (Foster et al., 2002, and references therein) has been refuted without any further clue (Sandler et al., 2006). The fact that numerous sites representing the Permian-Triassic boundary show severely impoverished sporomorph assemblages has been attributed to decimated plant ecosystems, without considering possible preservational bias. Impoverished assemblages dominated by preferentially preserved thick-walled palynomorphs such as *Reduviasporonites* and dark woody particles (declared as reworked) appear for some authors as plausible evidence for apocalyptic scenarios (e.g., Sandler et al., 2006; Benton and Twitchett, 2003; Peng et al., 2005).

In search for the causes for the drastic changes in terrestrial ecosystems in the Permian-Triassic boundary interval, the common occurrence of tetrads of pteridophyte spores has been used as indication for increased radiation (Visscher et al., 2004; Beerling, 2007). This hypothesis is essentially based on the fact that pollen or spores tetrads of irradiated plants might lose through mutagenesis their ability to separate and on the observation of peak abundance of tetrads in the material from East Greenland. One peak has been observed at the top of the Schuchert Dal Formation, prior to the main isotopic shift and the collapse of the marine ecosystem and the second, less pronounced one, in the middle part of the Wordie Creek Formation. Other possible evidence for environmental stress affecting plants during the Permian-Triassic boundary event has been published by Foster and Afonin (2005) and Metcalfe et al. (2008). Increased abundance of abnormal morphological variations of pollen, found at distant localities (e.g.,

Russia and northern China), might have been caused by various environmental stress factors. Beside increased radiation, air pollution related to volcanic activity has been considered as possible causes.

The climate of the Griesbachian is generally characterized as being very warm and uniform. Latitudinal gradients of generic richness (LGGR) of ammonoids are very flat during this substage. This parameter has been interpreted to correspond to extremely low sea-surface temperatures (SST) gradients (Brayard et al., 2006; Galfetti et al., 2007). The distribution of plants with diversified assemblages at high latitudes (e.g., Mangerud, 1994; Vigran et al., 1998) also suggests minimal latitudinal temperature gradients. The distinct differences of Late Permian assemblages from northern China compared to those from Norway and the relative similarity of Griesbachian assemblages from the two areas (Metcalfe et al., 2008) also suggest minimal latitudinal gradients during the latter substage. Our data suggest the existence of short-term fluctuations of the climate during the Griesbachian. For the same interval, radically changing environmental conditions have been interpreted from distinct short-term shifts of $\delta^{13}C$ isotope values, which contrast with the almost constant values of the preceding interval (Foster et al., 1997; Twitchett et al., 2001; Xie, et al., 2007; Grasby and Beauchamp, 2008). Pronounced negative shifts in $\delta^{13}C$ values are generally related to massive releases of ^{13}C-depleted carbon into the ocean-atmosphere reservoir, either by volcanic activity or by methane release. The strongly varying values observed in the Permian-Triassic boundary interval suggest correspondence to the multiphase volcanic eruption of the Siberian traps (Kamo et al., 2003; Xie et al., 2007). Volcanic activity of this magnitude can be expected to have a direct impact on terrestrial ecosystems. Thus, the observed variations in the distribution of palynomorphs might reflect climatic changes caused by volcanic eruptions.

Changes in floral assemblages of similar magnitude have been documented for the mid-Olenekian event (Smithian-Spathian boundary), where they also coincide with a pronounced shift in $\delta^{13}C$ isotope compositions (Galfetti et al., 2007; Hermann et al., 2008b). These changes have been interpreted to be related to volcanic activity of the Siberian traps. Within the Permian-Triassic boundary interval, other possible indications for environmental changes have been put forward, such as increased weathering interpreted from the distribution of black organic particles (Xie et al., 2007), or temporarily increased humidity based on the distribution of lake sediments in the Germanic Basin (Bachmann and Kozur, 2004).

CONCLUSIONS

The studied section of Late Permian and Griesbachian age from mid-Norway covers the critical interval of the Permian-Triassic boundary during which terrestrial biotas supposedly suffered from extremely hostile conditions. The Upper Permian section, interpreted as equivalent to the Schuchert Dal Formation, has been dated as Ufimian to early Tatarian? (Lopingian) based on palynomorphs (Bugge et al., 2002). The palynological assemblages of the Wordie Creek Formation can be assigned to the basal zone of the Early Triassic (Griesbachian) of the Boreal realm, assemblage P of Hochuli et al. (1989), or to the *Lundbladispora obsoleta–Chordecystia chalasta* zone of Mangerud (1994). Thus, the studied interval section covers an important hiatus between the Late Permian and the Griesbachian (cf. Fig. 2). Except for the disappearance of one group (*Vittatina*) and the appearance of the *Aratrisporites* group, there are no major changes in the qualitative composition of Griesbachian palynological assemblages. The palynological as well as the lithological successions suggest continuous sedimentation of this part of the section (Bugge et al., 2002). Comparison with assemblages of a dated late Griesbachian section from the Barents Sea (Vigran et al., 1998) suggests that the upper part of the Griesbachian might be missing from the studied cores.

The quantitative distribution of spore-pollen reveals not only a radical change between the Late Permian and the Griesbachian interval, but also considerable variations within the Griesbachian succession, which may reflect climatic changes. The poorly diversified Late Permian sporomorph assemblages point to stable pteridosperm-dominated vegetation with rare pteridophytes. With the onset of the Griesbachian transgression, diversity increases considerably, essentially due to the appearance of numerous pteridophyte and bryophyte spores (cf. Figs. 3 and 4). Only one group of pteridosperms, represented by the pollen genus *Vittatina*, shows a drastic reduction at the boundary and subsequently disappears during the Griesbachian. Some groups seem to be barely affected by the effect of the Permian-Triassic boundary event, whereas others such as *Cycadopites* and *Ephedripites* thrive during the Griesbachian.

In contrast to the relatively monotonous Late Permian palynological record, the Griesbachian succession shows distinct changes, essentially reflected by varying abundances of cavate spores (lycopsids) and bisaccate pollen (pteridosperms and conifers). Here, these variations are expressed in the ratio of hygrophytes and xerophytes and are interpreted as reflecting variations in humidity. Like the pronounced shifts in $\delta^{13}C$ isotope values observed by several authors (e.g., Oberhänsli et al., 1989; Foster et al., 1997; Xie et al., 2007), these variations suggest strongly varying environmental conditions, possibly related to volcanic activity. Our results are incompatible with the catastrophic scenarios, according to which terrestrial ecosystems suffered complete devastation during the Permian-Triassic boundary event to recover only during the Middle Triassic (e.g., Looy et al., 1999; Utting et al., 2004). Instead, as suggested by the continuum in the distribution of the major plant groups, the data from the Griesbachian show that in some areas, diverse plant assemblages survived the Permian-Triassic boundary event.

ACKNOWLEDGMENTS

We thank two anonymous reviewers and Brian Pratt (associate editor) for their valuable comments and for improving the English language. We also thank Atle Mørk and Hermann Weiss (Sintef Petroleum Research, Trondheim) for their constructive input and help during this study. This paper is a contribution to the Swiss National Science Foundation (SNF, project 200020-113554).

REFERENCES CITED

Afonin, S.A., 2000, A palynological assemblage from the transitional Permian-Triassic deposits of European Russia: Paleontological Journal, v. 34, p. 29–34.

Bachmann, G.H., and Kozur, H.W., 2004, The Germanic Triassic: Correlations with the international chronostratigraphic scale, numerical ages and Milankovitch cyclicity: Hallesches Jahrbuch für Geowissenschaften, v. 26, p. 17–62.

Balme, B.E., 1979, Palynology of the Permian Triassic boundary bed at Kap Stosch, East Greenland: Meddelelser om Grønland, v. 20, no. 6, p. 1–37.

Balme, B.E., 1995, Fossil in situ spores and pollen grain: An annotated catalogue: Review of Palaeobotany and Palynology, v. 87, no. 2–4, p. 81–323, doi: 10.1016/0034-6667(95)93235-X.

Beerling, D., 2007, The Emerald Planet—How plants Changed Earth's History: New York, Oxford University Press, 288 p.

Benton, M.J., and Twitchett, R.J., 2003, How to kill (almost) all life—The end-Permian extinction event: Trends in Ecology & Evolution, v. 18, no. 7, p. 358–365, doi: 10.1016/S0169-5347(03)00093-4.

Bjerager, M., Seidler, L., Stemmerik, L., and Surlyk, F., 2006, Ammonoid stratigraphy and sedimentary evolution across the Permian-Triassic boundary in East Greenland: Geological Magazine, v. 143, no. 5, p. 635–656, doi: 10.1017/S0016756806002020.

Bottjer, D.J., and Gall, J.C., 2005, The Triassic recovery, the dawn of the modern biota: Comptes Rendu Palévol, v. 4, p. 453–461, doi: 10.1016/j.crpv.2005.08.001.

Brayard, A., Bucher, H., Escarguel, G., Fluteau, F., Bourquin, S., and Galfetti, T., 2006, The Early Triassic ammonoid recovery: Paleoclimatic significance of diversity gradients: Palaeogeography, Palaeoclimatology, Palaeoecology, v. 239, p. 374–395, doi: 10.1016/j.palaeo.2006.02.003.

Bugge, T., Ringås, J.E., Leith, D.A., Mangerud, G., Weiss, H.M., and Leith, T.L., 2002, Upper Permian as a new play model on the mid-Norwegian continental shelf: Investigated by shallow drilling: American Association of Petroleum Geologists Bulletin, v. 86, no. 1, p. 107–127.

Erwin, D.H., Bowering, S.A., and Yugan, J., 2002, End-Permian mass extinctions: A review, *in* Koeberl, C.,

and MacLeod, K.G., eds., Catastrophic Events and Mass Extinction: Impacts and Beyond: Geological Society of America Special Paper 356, p. 363–383.

Eshet, Y., Rampino, M.R., and Visscher, H., 1995, Fungal event and palynological record of ecological crisis and recovery across the Permian-Triassic boundary: Geology, v. 23, no. 11, p. 967–970, doi: 10.1130/0091-7613(1995)023<0967:FEAPRO>2.3.CO;2.

Foster, C.B., and Afonin, S.A., 2005, Abnormal pollen grains: An outcome of deteriorating atmospheric conditions around the Permian-Triassic boundary: Journal of the Geological Society of London, v. 162, p. 653–659, doi: 10.1144/0016-764904-047.

Foster, C.B., Logan, G.A., Sommons, R.E., Gorter, J.D., and Edwards, D.S., 1997, Carbon isotopes, kerogen types and the Permian-Triassic boundary in Australia: Implications for exploration: Australian Petroleum Production and Exploration Association Journal, v. 37, p. 472–489.

Foster, C.B., Stephenson, M.H., Marshall, C., Logan, G.A., and Greenwood, P.F., 2002, A revision of *Reduviasporonites* Wilson 1962: Description, illustration, comparison and biological affinities: Palynology, v. 26, p. 165–183, doi: 10.2113/0260035.

Galfetti, T., Hochuli, P.A., Brayard, A., Bucher, H., Weissert, H., and Vigran, J.O., 2007, The Smithian/Spathian boundary event: Evidence for global climatic change in the wake of the end-Permian biotic crisis: Geology, v. 35, no. 4, p. 291–294, doi: 10.1130/G23117A.1.

Grasby, S.E., and Beauchamp, B., 2008, Intrabasin variability of the carbon-isotope record across the Permian-Triassic transition, Sverdrup Basin, Arctic Canada: Chemical Geology, v. 253, p. 141–150, doi: 10.1016/j.chemgeo.2008.05.005.

Grauvogel-Stamm, L., and Ash, S.R., 2005, Recovery of the Triassic land flora from the end-Permian life crisis: Comptes Rendu Palévol, v. 4, p. 593–608, doi: 10.1016/j.crpv.2005.07.002.

Hermann, E., Hochuli, P.A., Bucher, H., and Roohi, G., 2008a, Palynofacies of the Early Triassic section of Nammal Nala, Salt Range, Pakistan: Terra Nostra, v. 2008, no. 2, p. 112.

Hermann, E., Hochuli, P.A., Bucher, H., Brühwiler, T., Goudemand, N., and Roohi, G., 2008b, Major climatic change at the Smithian/Spathian boundary—Evidence from low palaeolatitudinal records: Geological Society of America Abstracts with Programs, v. 40, no. 6, p. 505.

Hochuli, P.A., Colin, J.P., and Vigran, J.O., 1989, Triassic biostratigraphy of the Barents Sea area, *in* Collinson, J.D., ed., Correlation in Hydrocarbon Exploration: London, Graham and Trotman, p. 131–153.

Holmes, W.B.K., 1992, *Glossopteris*-like leaves from the Triassic of Western Australia: Geophytology, v. 22, p. 119–125.

Kamo, S.L., Czamanske, G.K., Amelin, Y., Fedorenko, V.A., Davis, D.W., and Trofimov, V.R., 2003, Rapid eruption of Siberian flood volcanic rocks and evidence for coincidence with the Permian-Triassic boundary and mass extinction at 251 Ma: Earth and Planetary Science Letters, v. 214, p. 75–91, doi: 10.1016/S0012-821X(03)00347-9.

Kerp, H., Hamad, A.A., Vörding, B., and Bandel, K., 2006, Typical Triassic Gondwanan floral elements in the Upper Permian of the paleotropics: Geology, v. 34, no. 4, p. 265–268.

Kidder, D.L., and Worsley, T.R., 2004, Causes and consequences of extreme Permo-Triassic warming to globally equable climate and relation to the Permo-Triassic extinction and recovery: Palaeogeography, Palaeoclimatology, Palaeoecology, v. 203, p. 207–237, doi: 10.1016/S0031-0182(03)00667-9.

Lindström, S., and McLoughlin, S., 2007, Synchronous palynofloristic extinction and recovery after the end-Permian event in the Prince Charles Mountains, Antarctica: Implications for palynofloristic turnover across Gondwana: Review of Palaeobotany and Palynology, v. 145, p. 89–122, doi: 10.1016/j.revpalbo.2006.09.002.

Looy, C.V., Brugman, W.A., Dilcher, D.L., and Visscher, H., 1999, The delayed resurgence of equatorial forests after the Permian-Triassic ecologic crisis: Proceedings of the National Academy of Sciences of the United States of America, v. 96, no. 24, p. 13,857–13,862, doi: 10.1073/pnas.96.24.13857.

Looy, C.V., Twitchett, R.J., Dilcher, D.L., van Konijnenburg-van Cittert, J.H.A., and Visscher, H., 2001, Life in the end-Permian dead zone: Proceedings of the National Academy of Sciences of the United States of America, v. 98, no. 14, p. 7879–7883, doi: 10.1073/pnas.131218098.

Mangerud, G., 1994, Palynostratigraphy of the Permian and lowermost Triassic succession, Finnmark Platform, Barents Sea: Review of Palaeobotany and Palynology, v. 82, p. 317–349, doi: 10.1016/0034-6667(94)90082-5.

Metcalfe, I., Foster, C.B., Afonin, S.A., Nicoll, R.S., Mundil, R., Wang, X., and Lucas, S.G., 2008, Stratigraphy, biostratigraphy and C-isotopes of the Permian-Triassic non-marine sequence at Dalong and Lucaogou, Xinjiang Province, China: Journal of Asian Earth Sciences (in press), doi: 10.1016/j.jseaes.2008.06.005.

Mundil, R., Ludwig, K.R., Metcalfe, I. and Renne, P.R., 2004, Age and timing of the Permian mass extinction: U/Pb dating of close-system zircons: Science, v. 305, p. 1760–1763.

Nassichuk, W.W., 1995, Permian ammonoids of the Arctic regions, *in* Scholle, P.A., et al., eds., The Permian of Northern Pangea: Berlin, Springer Verlag, p. 210–235.

Oberhänsli, H., Hsu, K., Piasecki, S., and Weissert, H., 1989, Permian-Triassic carbon-isotope anomaly in Greenland and in the Southern Alps: Historical Biology, v. 2, p. 37–49, doi: 10.1080/08912968909386489.

Ouyang, S., and Norris, G., 1999, Earliest Triassic (Induan) spores and pollen from the Junggar Basin, Xinjiang, northwestern China: Review of Palaeobotany and Palynology, v. 106, p. 1–56, doi: 10.1016/S0034-6667(98)00078-5.

Ouyang, S., and Utting, J., 1990, Palynology of Upper Permian and Lower Triassic rocks, Meishan, Changxing county, Zhejiang Province, China: Review of Palaeobotany and Palynology, v. 66, p. 65–103, doi: 10.1016/0034-6667(90)90029-I.

Peng, Y., Zhang, S., Yu, T., Yang, F., Gao, Y., and Shi, G.R., 2005, High-resolution terrestrial Permian-Triassic eventostratigraphic boundary in western Guizhou and eastern Yunnan, southwestern China: Palaeogeography, Palaeoclimatology, Palaeoecology, v. 215, p. 285–295, doi: 10.1016/j.palaeo.2004.09.009.

Peng, Y., Yu, J., Gao, Y., and Yang, F., 2006, Palynological assemblages of non-marine rocks at the Permian-Triassic boundary, western Guizhou and eastern Yunnan, South China: Journal of Asian Earth Sciences, v. 28, p. 291–305, doi: 10.1016/j.jseaes.2005.10.007.

Piasecki, S., 1984, Preliminary palynostratigraphy of the Permian–Lower Triassic sediments in Jameson Land and Scoresby Land, East Greenland: Bulletin of the Geological Society of Denmark, v. 32, p. 139–144.

Retallack, G.J., Veevers, J.J., and Morante, R., 1996, Global coal gap between Permian-Triassic extinction and Middle Triassic recovery of peat-forming plants: Geological Society of America Bulletin, v. 108, no. 2, p. 195–207, doi: 10.1130/0016-7606(1996)108<0195:GCGBPT>2.3.CO;2.

Sandler, A., Eshet, Y., and Schilman, B., 2006, Evidence for a fungal event, methane-hydrate release and soil erosion at the Permian-Triassic boundary in southern Israel: Palaeogeography, Palaeoclimatology, Palaeoecology, v. 242, p. 68–89, doi: 10.1016/j.palaeo.2006.05.009.

Smith, A.G., Smith, D.G., and Funnell, B.M., 1994, Atlas of Mesozoic and Cenozoic Coastlines: Cambridge, Cambridge University Press, 109 p.

Stemmerik, L., Bendix-Almgreen, S.E., and Piasecki, S., 2001, The Permian-Triassic boundary in East Greenland: Past and present views: Bulletin of the Geological Society of Denmark, v. 48, p. 159–167.

Svensen, H., Planke, S., Polozov, A.G., Schmidbauer, N., Corfu, F., Podladchikov, Y.Y., and Jamtveit, B., 2009, Siberian gas venting and the end-Permian environmental crisis: Earth and Planetary Science Letters, v. 277, p. 490–500, doi: 10.1016/j.epsl.2008.11.015.

Tozer, E.T., 1994, Canadian Triassic Ammonoid Faunas: Geological Survey of Canada Bulletin 467, 663 p.

Tuzhikova, V.I., 1985, Miospores and Stratigraphy of Key Reference Sections of the Triassic of the Urals: Lower Triassic–Upper Permian: Sverdlovsk, Akademiia Nauk SSSR, Publishing House, 232 p.

Twitchett, R.J., Looy, C.V., Morante, R., Visscher, H., and Wignall, P.B., 2001, Rapid and synchronous collapse of marine and terrestrial ecosystems during the end-Permian biotic crisis: Geology, v. 29, no. 4, p. 351–354, doi: 10.1130/0091-7613(2001)029<0351:RASCOM>2.0.CO;2.

Utting, J., 1994, Palynostratigraphy of Permian and Lower Triassic Rocks, Sverdrup Basin, Canadian Arctic Archipelago: Geological Survey of Canada Bulletin 478, 107 p.

Utting, J., Spina, A., Jansonius, J., McGregor, D.C., and Marshall, J.E.A., 2004, Reworked miospores in the Upper Paleozoic and Lower Triassic of the northern circum-polar area and selected localities: Palynology, v. 28, p. 75–119, doi: 10.2113/28.1.75.

Utting, J., Zonneveld, J.P., MacNaughton, R.B., and Fallas, K.M., 2005, Palynostratigraphy, lithostratigraphy and thermal maturity of the Lower Triassic Toad and Grayling, and Montney Formations of western Canada, and comparisons with coeval rocks of the Sverdrup Basin, Nunavut: Bulletin of Canadian Petroleum Geology, v. 53, no. 1, p. 5–24, doi: 10.2113/53.1.5.

Vigran, J.O., Mangerud, G., Mørk, A., Bugge, T., and Weitschat, W., 1998, Biostratigraphy and sequence stratigraphy of the Lower and Middle Triassic deposits from the Svalis Dome, central Barents Sea, Norway: Palynology, v. 22, p. 89–141.

Visscher, H., and Brugman, W.A., 1986, The Permian–Triassic boundary in the Southern Alps: A palynological approach: Memorie della Societa Geologica Italiana, v. 34, p. 121–128.

Visscher, H., and van der Zwan, W.A., 1981, Palynology of the circum-Mediterranean Triassic: Phytogeographical and palaeoclimatological implications: Geologische Rundschau, v. 70, p. 625–636, doi: 10.1007/BF01822140.

Visscher, H., Brinkhuis, H., Dilcher, D.L., Elsik, W.C., Eshet, Y., Looy, C.V., Rampino, M.R., and Traverse, A., 1996, The terminal Paleozoic fungal event: Evidence of terrestrial ecosystem destabilization and collapse: Proceedings of the National Academy of Sciences of the United States of America, v. 93, p. 2155–2158, doi: 10.1073/pnas.93.5.2155.

Visscher, H., Looy, C.V., Collinson, M.E., Brinkhuis, H., van Konijnenburg-van Cittert, J.A.H., Kürschner, W.M., and Sephton, M.A., 2004, Environmental mutagenesis during the end-Permian ecological crisis: Proceedings of the National Academy of Sciences of the United States of America, v. 101, no. 35, p. 12952–12956, doi: 10.1073/pnas.0404472101.

Wardlaw, B.R., Davydov, V., and Gradstein, F.M., 2004, The Permian period, *in* Gradstein, F.M., Ogg, J., and Smith, A., eds., A Geological Timescale: Cambridge, Cambridge University Press, p. 249–270.

Xie, S., Pancost, R.D., Huang, J., Wignall, P.B., Yu, J., Tang, X., Chen, L., Huang, X., and Lai, X., 2007, Changes in the global carbon cycle occurred as two episodes during the Permian–Triassic crisis: Geology, v. 35, no. 12, p. 1083–1086, doi: 10.1130/G24224A.1.

Yin, H., Zhang, K., Tong, J., Yang, Z., and Wu, S., 2001, The global stratotype section and point (GSSP) of the Permian-Triassic boundary: Episodes, v. 24, no. 2, p. 102–114.

Manuscript Received 24 September 2008
Revised Manuscript Received 11 March 2009
Manuscript Accepted 29 April 2009

Printed in the USA

Appendix 4:

The Lower Triassic sedimentary and carbon isotope records from Tulong (South Tibet) and their significance for Tethyan palaeoceanography

Thomas Brühwiler, Nicolas Goudemand, Thomas Galfetti, Hugo Bucher, Aymond Baud, David Ware, Elke Hermann, Peter A. Hochuli, Rossanna Martini

Sedimentary Geology 2009. 222: 314–332

Sedimentary Geology 222 (2009) 314–332

Contents lists available at ScienceDirect

Sedimentary Geology

journal homepage: www.elsevier.com/locate/sedgeo

The Lower Triassic sedimentary and carbon isotope records from Tulong (South Tibet) and their significance for Tethyan palaeoceanography

Thomas Brühwiler [a,*], Nicolas Goudemand [a], Thomas Galfetti [b], Hugo Bucher [a,c], Aymon Baud [d], David Ware [a], Elke Hermann [a], Peter A. Hochuli [a,c], Rossanna Martini [e]

[a] Paläontologisches Institut und Museum der Universität Zürich, Karl Schmid-Strasse 4, 8006 Zürich, Switzerland
[b] Holcim Group Support Ltd, Materials Technology, 5113 Holderbank, Switzerland
[c] Department of Earth Sciences, ETH, Universitätsstrasse 16, 8092 Zürich, Switzerland
[d] BGC, Parc de la Rouvraie 28, 1018 Lausanne, Switzerland
[e] Department of Geology and Paleontology, University of Geneva, Rue des Maraîchers 13, 1205 Geneva, Switzerland

ARTICLE INFO

Article history:
Received 18 June 2009
Received in revised form 23 September 2009
Accepted 11 October 2009

Keywords:
Early Triassic
South Tibet
Microfacies
Palaeoenvironments
Carbon isotopes

ABSTRACT

The Lower Triassic sedimentary and carbonate/organic carbon isotope records from the Tulong area (South Tibet) are documented in their integrality for the first time. New age control is provided by ammonoid and conodont biostratigraphy. The basal Triassic series consists of Griesbachian dolomitic limestones, similar to the Kathwai Member in the Salt Range (Pakistan) and to the *Otoceras* Beds in Spiti (India). The overlying thin-bedded limestones of Dienerian age strongly resemble the Lower Ceratite Limestone of the Salt Range. They are followed by a thick series of dark green, silty shales of Dienerian–early Smithian age without fauna that strikingly resemble the Ceratite Marls of the Salt Range. This interval is overlain by thin-bedded, light grey fossil-rich limestones of middle to late Smithian age, resembling the Upper Ceratite Limestone of the Salt Range. These are followed by a shale interval of early Spathian age that has no direct counterpart in other Tethyan sections. Carbonate production resumes during the late early and middle Spathian with the deposition of red, bioclastic nodular limestone ("Ammonitico Rosso" type facies). Apart from its colour this facies is similar to the one of the Niti Limestone in Spiti and of the Spathian nodular limestone in Guangxi (South China). As in other Tethyan localities such as Spiti, the early–middle Anisian part of the Tulong section is strongly condensed and is characterized by grey, thin-bedded limestones with phosphatized ammonoids. As for many other Tethyan localities the carbon isotope record from Tulong is characterized by a late Griesbachian–Dienerian positive $\delta^{13}C_{carb}$ excursion (2‰), and a very prominent positive excursion (5‰) at the Smithian–Spathian boundary, thus confirming the well-documented perturbations of the global carbon cycle following the Permian–Triassic mass extinction event.

1. Introduction

The end-Permian mass extinction is the biggest known crisis in life history and wiped out more than 90% of all marine species (e.g. Raup and Sepkoski, 1982). The subsequent Early Triassic recovery of marine and terrestrial ecosystems is considered to have been delayed when compared with other mass extinctions and to have lasted until the end of the Early Triassic (e.g. Erwin, 1998). Many marine clades such as corals (Stanley, 2003), foraminifers (Tong and Shi, 2000) or radiolarians (Racki, 1999) did not completely recover until the Spathian or the Anisian, and poorly diversified and small-sized benthonic shelly faunas predominated during the Early Triassic (e.g. Fraiser and Bottjer, 2004; Fraiser et al., 2005). Metazoan reef communities were completely absent in the Early Triassic (Pruss and Bottjer, 2005). On the other hand, ammonoids and conodonts recovered very fast in comparison with other marine clades (Brayard et al., 2006, 2009; Orchard, 2007). Moreover, recent analysis of outer platform paleoenvironments from South China reveals that increasing rates of diversity and abundance of skeletal material occurred already during well-oxygenated carbonate episodes of early Smithian and Spathian age, respectively (Galfetti et al., 2008).

Stable carbon isotope studies have shown that the global carbon cycle was profoundly perturbed at the Permian–Triassic boundary and that several large and short-lived fluctuations occur in the Early Triassic, before the carbon cycle stabilizes in the Middle Triassic (Baud et al., 1996; Atudorei and Baud, 1997; Atudorei, 1999; Payne et al., 2004; Richoz, 2004; Corsetti et al., 2005; Galfetti et al., 2007a,b,c; Horacek et al., 2007a,b). The coincidence of carbon isotope cycle instabilities with the Early Triassic delayed recovery suggests a relationship between carbon cycling and biological rediversification in the aftermath of the extinction (Payne et al., 2004). Indeed, for instance, the major positive $\delta^{13}C$ excursion at the Smithian–Spathian

* Corresponding author. Tel.: +41 44 634 26 98; fax: +41 44 634 49 23.
E-mail address: bruehwiler@pim.uzh.ch (T. Brühwiler).

0037-0738/$ – see front matter © 2009 Elsevier B.V. All rights reserved.
doi:10.1016/j.sedgeo.2009.10.003

boundary coincides with the most severe ammonoid and conodont intra-Triassic extinction event (Brayard et al., 2006; Galfetti et al., 2007a,c; Orchard, 2007), associated with major climatic change (Brayard et al. 2006; Galfetti et al. 2007b). CO_2 degassing via volcanism, possibly related to a late eruptive phase of the Siberian Traps, has been proposed as a trigger for these global disturbances (Payne et al., 2004; Ovtcharova et al. 2006). Such an explanation is favoured also by carbon cycle modelling which suggests that the Early Triassic perturbations result from continuing environmental disturbances rather than from lingering effects from a single disturbance at the Permian–Triassic boundary (Payne and Kump, 2007).

Recent analysis of the late Early Triassic sedimentary facies evolution has revealed striking similarities between the South China Block and the widely distant Northern Indian Margin suggesting a common, at least Tethys-wide control on outer platform sedimentary environment evolution (Galfetti et al., 2007a). On the other hand, during the Early Triassic the Northern Indian Margin was characterized by extensional tectonics related to the opening of the Neothetys (e.g. Stampfli et al., 1991). Therefore, successions from closely spaced localities such as Selong and Tulong in South Tibet may show pronounced differences regarding facies and thickness (Garzanti et al., 1998; and Section 7.1. hereafter). Thus, additional detailed descriptions of well-dated successions from various paleogeographic settings are essential in order to differentiate between local patterns related to synsedimentary tectonics and large-scale patterns such as shown by Galfetti et al. (2007a). Deciphering such large-scale patterns may provide new insights into the processes related to the Early Triassic biotic recovery.

Various sections from South Tibet (Wang and He, 1976; Rao and Zhang, 1985; Wang et al., 1989; Liu and Einsele, 1994; Yugan et al., 1996; Garzanti et al., 1998; Shen et al., 2006) and adjacent North Nepal (Bassoullet and Colchen, 1976; Garzanti et al., 1994; von Rad et al., 1994; Baud et al., 1997) are known for their Lower Triassic sedimentary and palaeontological records. However, for the area of Tulong previously published documentations of the Lower Triassic succession were incomplete and/or poorly or incorrectly dated (see Section 7 below). Here we document for the first time the complete and well-dated Lower Triassic sedimentary record from this area and compare it with other Tethyan successions. We also present a new high-resolution carbonate carbon isotope record. The comparison of this new C-isotope record with other Lower Triassic profiles described in the literature (Baud et al., 1996; Payne et al., 2004; Galfetti et al., 2007a,b,c) provides additional evidence for the global character of the instabilities of the carbon cycle during the Early Triassic recovery interval.

2. Geologic background

2.1. Palaeogeography

During Early Triassic times the Tulong area was located in a distal position on the peri-Gondwanan margin, on the southern side of the Tethys Ocean (Ogg and von Rad, 1994) (Fig. 1). As shown by different authors (Marcoux and Baud, 1996; Ricou, 1996; Garzanti and Sciunnach, 1997) at least two rifting processes affected the North Indian plate. The first event is linked to the detachment of the Quiantang block from Gondwana during the Early Carboniferous. With a second rifting phase during the Early Permian the Lhasa block detached from the Gondwanan margin and the Neotethys developed. In this process the southern Neotethyan Indian margin was acting as upper plate inducing basalt flows (Panjal Traps) and volcanism (Stampfli et al., 1991; Baud et al., 1996; Garzanti et al., 1996). During the expansion of the Neotethys in the Early Triassic, the Indian margin underwent thermal subsidence and was characterized by large tilted blocks. This may explain the differences in lithological

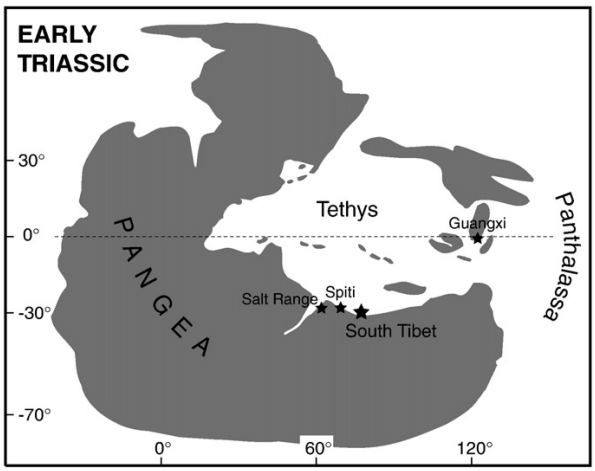

Fig. 1. Simplified Early Triassic palaeogeography (modified after Brayard et al., 2006) showing the location of South Tibet (Northern Indian Margin) and other localities cited in the text.

successions between presently closely spaced localities such as Tulong and Selong (35 km apart) in South Tibet (see Section 7.1.).

2.2. Thermal alteration

Based on conodont and palynomorph alteration indexes it appears that the Lower Triassic sediments of the studied area experienced some low-grade thermal metamorphism during the Himalayan orogeny. Conodonts recovered throughout the section are dark to very dark brown in colour, corresponding to a CAI (i.e. Conodont Alteration Index) of 3 to 4 (Epstein et al., 1977). This indicates an exposure to temperatures close to 200 °C (the temperature range of CAI 3/resp. 4 is 110–200/resp. 190–300 °C (Nowlan and Barnes, 1987). Palynological investigations from the studied area yield dark brown to almost opaque black palynomorphs, indicating a value of 6–7 on the thermal alteration scale (TAS) of Batten (1996). This value corresponds to exposure to temperatures of 170–200 °C confirming the values inferred from the CAI.

3. Lower Triassic sections

In addition to the classic section located near the village of Tulong (section Tu in this paper) (Garzanti et al., 1998; Shen et al., 2006), several new and more complete sections are reported here (Figs. 2 and 3). The stratigraphic successions obtained from several scattered outcrops can be correlated bed-by-bed, allowing establishment of an almost complete composite section spanning the Late Permian to Early Anisian time interval (Fig. 4). Only the total thickness of the Dienerian–early Smithian shale interval (Unit II; see Section 4.3.2. hereafter) remains uncertain. Biostratigraphic and facies description of each lithologic unit is provided below. Detailed descriptions of ammonoids, conodonts, palynomorphs and ostracods will be addressed in forthcoming papers.

4. Upper Permian to Lower Triassic litho-/biostratigraphic and microfacies description

4.1. Upper Permian

In the studied area the uppermost Permian consists of about 30 m of dark to black shales containing cm to dm-sized, black, phosphatic nodules. No macrofossils have been found within this interval, and our palynological samples from this interval proved to be barren.

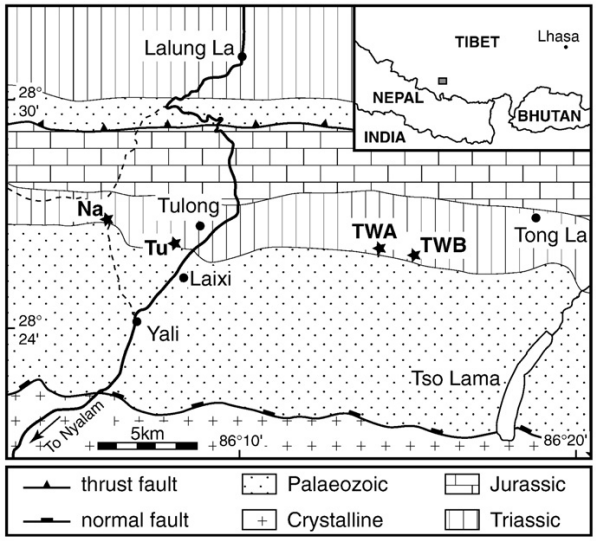

Fig. 2. Geologic sketch map of the study area (modified after Burg, 1983) and location of studied sections. Tu: classical section near the village of Tulong; Na: Nazapuo section; TWA: Tong La West A section; TWB: Tong La West B section.

These shales strikingly resemble the late Permian Kuling Shales of Spiti (Northern India) (Bucher et al., 1997).

4.2. Lower Triassic — Unit I

4.2.1. Description

In the studied area the basal Triassic deposits unconformably overlie the Kuling Shales. They consist of 3 m of carbonate rocks, which are here subdivided into two subunits (i.e. *Subunit Ia* and *Subunit Ib*).

Subunit Ia — 2 m of rusty, yellowish-reddish, thin-bedded dolomitic limestones intercalated with few, thin shale layers (Fig. 5a). The basal bed has an irregular base (Fig. 5b). The first 80 cm of the Subunit consists of thin-bedded dolomitic mudstone with thin shale interbeds showing the progressive appearance of thin-shelled bivalves, rare crinoid fragments and foraminifera (*Earlandia* sp., *Rectocornuspira* sp., microlagenids and other microforaminifera) (Fig. 5c). The upper part of *Subunit Ia* consists of essentially barren, thin-bedded dolomitic mudstone with thin shale interbeds.

In *Subunit Ia* ammonoids are very rare and too poorly preserved for identification. The occurrence of the conodont species *Hindeodus parvus* in the upper part of the first carbonate bed (sample TWB5) suggests a probable basal Early Triassic (Griesbachian) age. Besides the occurrence of *Hindeodus* spp. conodont assemblages of this subunit are mostly dominated by *Neogondolella* spp. including *Ng. planata*, *Ng. taylorae*, and *Ng. tulongensi*. This assemblage unambiguously indicates a Griesbachian age.

Subunit Ib — 1 m of light grey, thin-bedded limestone (Fig. 5d). Although partly recristallized and slightly dolomitized, this horizon yields juvenile ammonoids, rare ostracods and peculiar spherical bioclasts (i.e. "microspheres", possibly radiolaria; compare discussion in Galfetti et al., 2008, p. 42) (Fig. 5e). The upper part of *Subunit Ib* consists of shelly mudstones–wackestones with thin-shelled microbivalves (Fig. 5f) and contains abundant ammonoids. In the topmost bed abundant framboidal pyrite is preserved in ammonoid body chambers.

The horizon located 20 cm below the top of *Subunit Ib* (sample TWB32) yielded rather poorly preserved specimens of *Proptychites* sp., *Gyronites undatus* and *Gyronites* aff. *planissimus*. The uppermost bed (sample TWB35) contains an assemblage characterized by *Ambites* cf. *discus*, ?*Pleurambites* sp., *Gyronites* aff. *planissimus*, *Proptychites haydeni* and ?*Meekophiceras* sp., indicating a Dienerian age (Spath, 1934; Tozer, 1994; Brühwiler et al., 2008).

The presence of *Ng.*? *discreta* in the lower part (sample TWB25) of this subunit indicates a latest Griesbachian age (*discreta* conodont Zone/*Bukkenites strigatus* ammonoid Zone). Note that one reworked specimen of *Jinogondolella* of Guadalupian age has been observed in this sample. The occurrence of *Sweetospathodus kummeli* in the sample above (TWB29) confirms a succession already observed at Guling (Spiti, India) (Orchard and Krystyn, 1998) and at Chhidru (Salt Range, Pakistan; Goudemand et al., ongoing work). Although *Sw. kummeli* is commonly regarded as a Dienerian species, it may appear as early as in the Strigatus Zone from Otto Fjord as observed in the Canadian Arctic (Orchard, 2008). The beginning of the first major radiation of conodonts in the Early Triassic is well expressed within samples TWB32 and TWB35 with the noticeable appearance of *Neospathodus* species. Numerous P1 elements of the *Ns. dieneri* group, including *Ns. svalbardensis* confirm a Dienerian age for the uppermost part of this subunit.

4.2.2. Interpretation

The Permian–Triassic boundary in the study area is marked by an erosive boundary as shown by the irregular base of Unit I (Fig. 5a). No evidence for reworked Permian rocks (e.g. pebbles derived from the Kuling phosphate nodules) has been found. It is interesting to note the presence of foraminifera disaster taxa such as *Earlandia* sp. and *Rectocornuspira* sp. in *Subunit Ia*. This corresponds to the well-known bloom of these disaster taxa that occur in the extinction interval and continue well into the basal Triassic sediments as shown by Altiner et al. (1980), Baud et al. (1997, 2005) and Groves and Altiner (2005). With the appearance of abundant ammonoids and possibly radiolarians ("microspheres") the biomicrites in *Subunit Ib* indicate a probable drowning. The topmost bed of this subunit possibly suggests a low sedimentation rate, but without any indication of paleontological condensation.

4.3. Lower Triassic — Unit II

4.3.1. Description

The basal Triassic carbonates of Unit I are overlain by an interval of barren, dark green shales. Since no continuous outcrop has been found in these strongly faulted and folded shales, the thickness of Unit II can roughly be estimated to be greater than 50 m and probably less than 100 m (Fig. 3a). In the upper part the shales of Unit II contain very thin lenses of cross-bedded siltstone (Fig. 5g) showing dolomitization and fracturation in thin section (Fig. 5h).

So far, no ammonoids or conodonts have been found in this unit. Its age ranges from Dienerian to early Smithian. However, the precise position of the Dienerian–Smithian boundary remains unknown.

4.3.2. Interpretation

It is unclear whether or not the lenticular cross-bedded dolomitized siltstones in the upper part of this unit are part of distal turbidites or not. Cross-bed laminations found within these lenses suggest the presence of bottom currents. However, given the absence of hummocky cross stratification it is suggested that this unit was deposited below storm wave base.

4.4. Lower Triassic — Unit III

4.4.1. Description

The shale interval of Unit II is followed by about 9 m of mostly grey limestone beds alternating with thin shale intervals. They are here subdivided into four subunits.

Subunit IIIa — 1 m of red-weathering ferruginous, dolomitized coarse grained limestone containing silt- to sand-sized skeletal debris

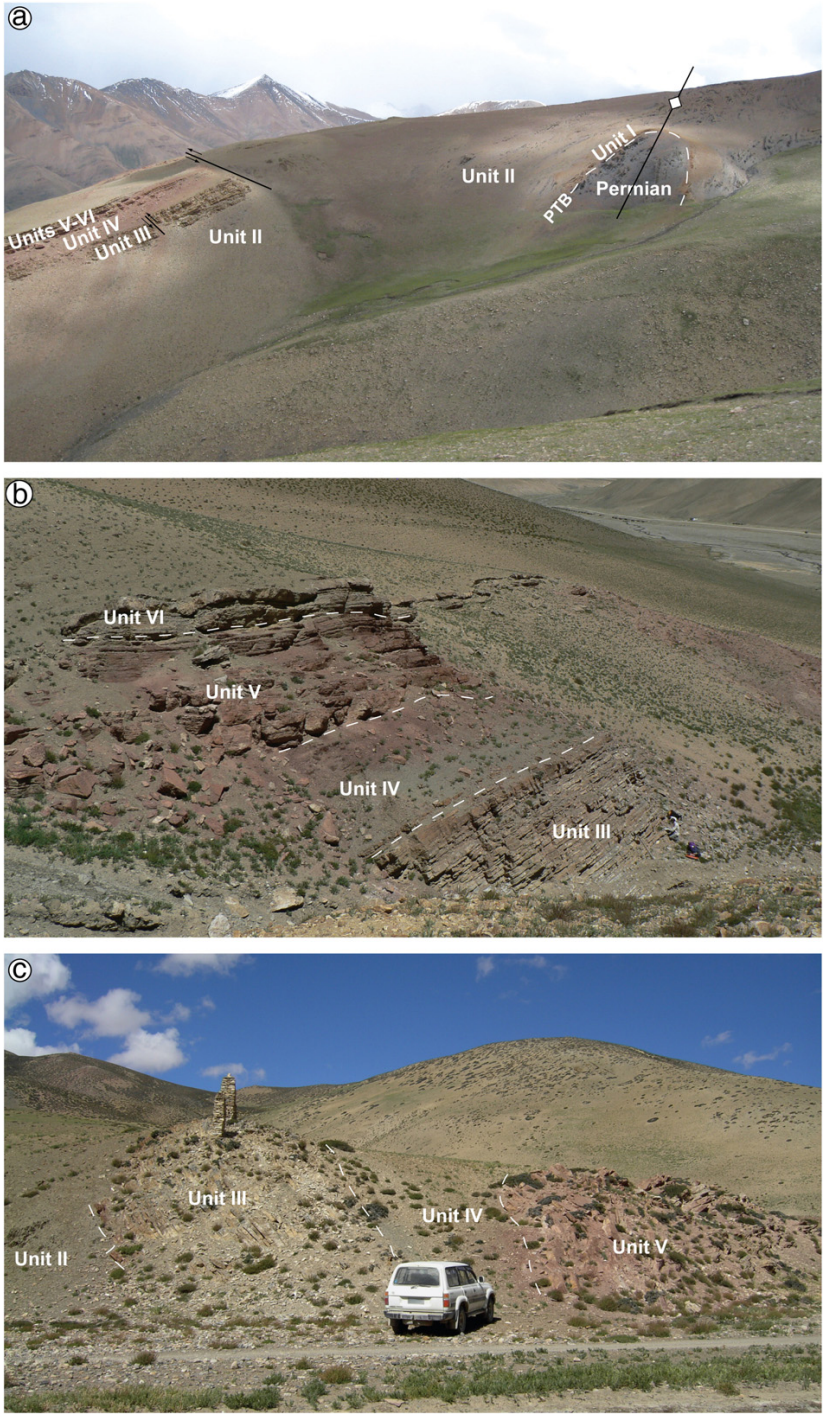

Fig. 3. Outcrop photographs with indicated Lower Triassic lithologic units. (a) Section TWB. Unit II is discontinuously exposed, folded and faulted. (b) Classical section (Tu) near the village of Tulong. (c) Nazapuo section (Na).

(thin-shelled microbivalves, echinoids, spicules) (Fig. 6a–b). This is followed by 60 cm of dm-scale-bedded grey lime packstones consisting of packed, partly oriented thin-shelled microbivalves.

Ammonoids are rare in *Subunit IIIa* and too poorly preserved for unambiguous identification. Conodonts are also relatively rare in this subunit but the occurrence of *Novispathodus waageni* in its lower part (sample Na3) indicates a Smithian age.

Subunit IIIb — 2 m of mostly thin-bedded, platy to nodular, grey or light red limestone alternating with shale interbeds (Fig. 6c). It starts with packstones with a microfacies similar to *Subunit IIIa*, containing

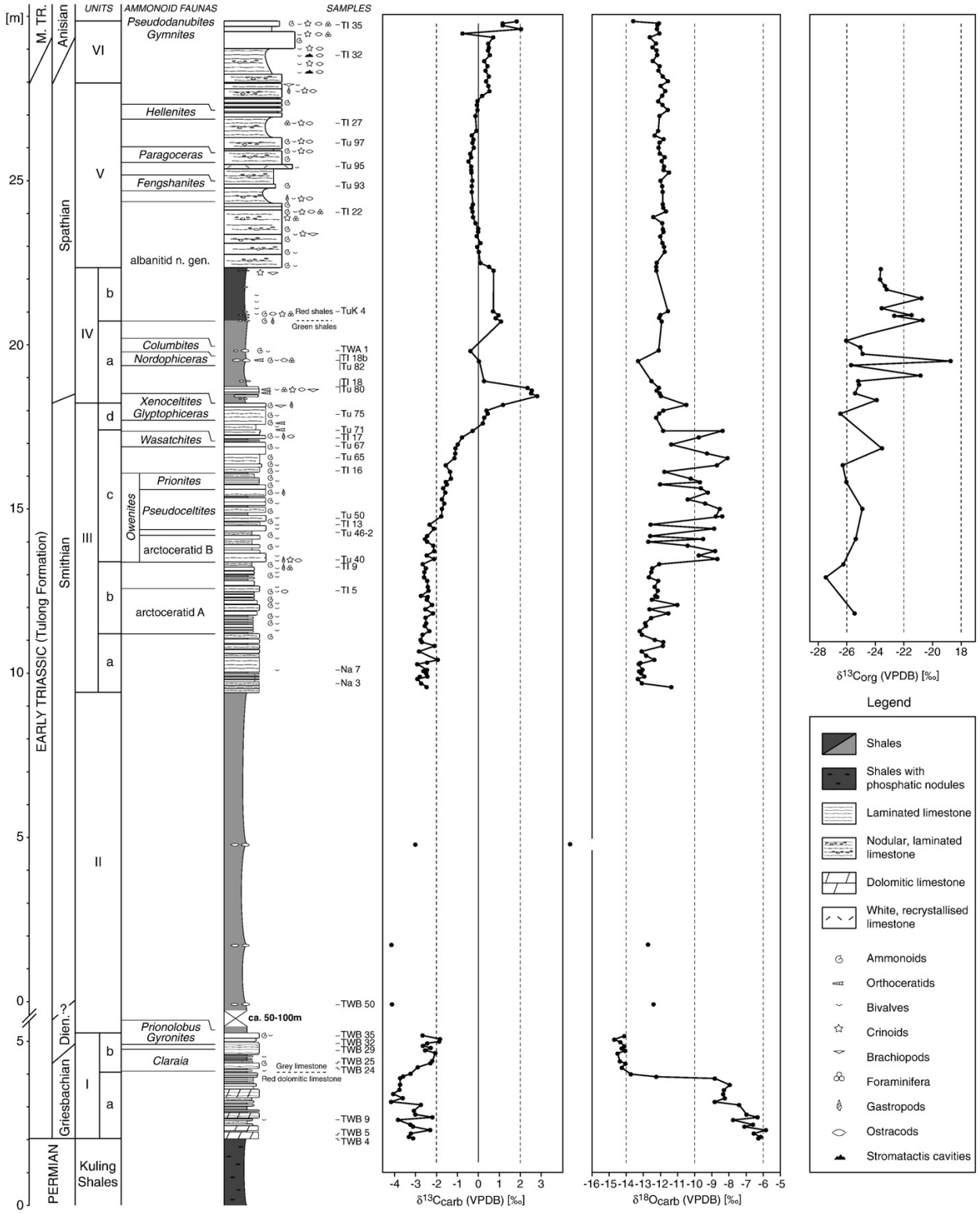

Fig. 4. Composite section of the Tulong Formation (Tulong area, South Tibet) showing lithology, microfossil content, distribution of ammonoid faunas, carbonate carbon/oxygen and organic carbon isotopes, as well as ammonoid, conodont and microfacies samples mentioned in the text. Note the large gap in the record of about 50–100 m in Unit II (see also Fig. 3a). Abbreviations: Dien.: Dienerian; M. TR.: Middle Triassic.

cemented thin-shelled microbivalves. This interval is followed by packstones with completely preserved bivalves (Fig. 6d). The upper part of *Subunit IIIb* is largely dominated by mudstones–wackestones containing microgastropods, juvenile ammonoids, echinoids and calcitic spheres (Fig. 6e).

Subunit IIIb yields a distinct ammonoid fauna including a new taxon here provisionally referred to as arctoceratid A, associated with *Jinyaceras hindostanus* and *Aspenites acutus*. This association has also been recently discovered in beds of middle Smithian age in the Salt Range (Pakistan) and in Northern India (provisionally termed "new prionitid A beds", cf. Brühwiler et al., 2007). However, no correlative of these beds is known from Guangxi (South China) (Brayard and Bucher, 2008).

The occurrence of conodont species like *Wapitiodus robustus*, *Novispathodus spitiensis* or *Ns.* n. sp. S (Orchard, unpublished) confirms a middle Smithian age for this subunit.

Subunit IIIc — 4 m of medium-bedded grey limestone, alternating with shales or distinctly nodular, marly limestone (Fig. 6f). Limestone microfacies are represented by (i) sparitic packestones-grainstones, packed with crushed thin-shelled microbivalves with a few microgastropods and juvenile ammonoids (Fig. 6g); and (ii) wackestones with thin-shelled microbivalves and microgastropods in a nodular muddy matrix (Fig. 6h). The first occurrence of sparitic cement in the Lower Triassic series of the studied area is recorded in this subunit.

Occasionally *Subunit IIIc* contains beds or nodules that have been referred to as "pseudostromatolithic structures" by Garzanti et al. (1998) (Fig. 7a). However, no typical microbial structures are visible in thin section. These structures consist of thin, alternating laminae of lime mudstone and of lime wackestone/packstone containing thin-shelled microbivalves, ostracods and probably sponge spicules (Fig. 7b).

The lower and middle parts of *Subunit IIIc* are characterized by typical ammonoid faunas of middle Smithian age, i.e. the *Owenites* beds. These beds can be subdivided into three parts. The lower part contains a new genus here provisionally referred to as arctoceratid B, together with *Owenites simplex*, *Paranannites spathi*, and *Kashmirites* sp. In the middle part *Owenites koeneni*, *Pseudoceltites multiplicatus* and ?*Anaxenaspis* sp. indet. occur. The upper part contains the association of *Prionites* sp., "*Pseudoceltites*" *angustecostatus*, *Owenites koeneni*, *Owenites carpentieri*, ?*Subflemingites* n. sp., and *Stephanites superbus*. Differing from these middle Smithian faunas, one bed in the uppermost part of *Subunit IIIc* (sample Tu67) contains the ammonoid *Wasatchites distractum*, which indicates a late Smithian age (Tozer, 1994; Brühwiler et al., 2007).

Besides the rare specimens of the conodont genus *Discretella*, various forms of *Nv. waageni* and *Nv. pakistanensis* largely dominate the assemblages of *Subunit IIIc*. New, very short segminate platform elements (similar but shorter than *Ns. soleiformis*) may characterize its lower part (samples Tu40 to Tu50). Conodont faunas start to change strikingly from sample Tu65 on, where the *waageni*/*pakistanensis* group almost disappears and is replaced by coniform elements and ellisonids. Above (sample Tu67) we observe a fauna dominated by specimens of *Guangxidella? robustus*, also found in South China and which correlates well with the late Smithian *Wasatchites*/*Anasibirites* ammonoid beds. The next conodont sample (sample Tu71) contains again a distinct, characteristically late Smithian assemblage, including *Scythogondolella mosheri* and *Sc. milleri*.

Subunit IIId — 1 m of massive, nodular, marly orange to grey limestone (Fig. 7c). Distinct orange bands appear on weathered surfaces. Brachiopods are very abundant in these beds.

In *Subunit IIId* ammonoids are abundant but are usually poorly preserved. *Glyptophiceras sinuatus* and *Xenoceltites* sp. have been found, both genera indicate a latest Smithian age (Brühwiler et al., 2007; Brayard and Bucher, 2008). This subunit contains the conodonts *Nv. pingdingshanensis* as well as *Borinella* aff. *buurensis*, two species which occur worldwide (Goudemand et al., ongoing work) just below the Smithian–Spathian boundary as here defined by ammonoids. From the horizon Tu75 on, *Borinella* becomes the dominant conodont genus.

4.4.2. Interpretation

Abundant benthic and nectonic fossils throughout Unit III indicate well-oxygenated conditions. The highly fragmented shelly material in *Subunit IIIa* indicates a high-energy depositional environment. The changes in the paleoenvironment within *Subunit IIIb* indicate a marked decrease in water energy related to deepening. This modification is coincident with a diversification of the biotas as indicated by the appearance of microgastropods, calcispheres and abundant ammonoids. Water energy increases in the basal part of *Subunit IIIc* as indicated by crushed shells and a sudden shift from micritic matrix to sparry calcite cement. Alternatively, sparry calcite cement could indicate increasing carbonate saturation. Water energy is relatively low again in the remaining part of Unit III as indicated by many complete shells.

4.5. Lower Triassic — Unit IV

4.5.1. Description

This Unit consists of about 4 m of early Spathian shales with a few limestone beds and nodules (Fig. 7d). They can readily be subdivided into a lower green part (*Subunit IVa*) and an upper red part (*Subunit IVb*).

Subunit IVa — 2.5 m of dark green shales At its base it contains a few thin limestone beds made of wackestone with skeletal fragments, thin-shelled bivalves, ostracods, crinoid spines and plates and foraminifera of lagenid type as well as *Glomospirella* cf. *jefimowae* (Fig. 7e–f). In these beds orthoceratids and brachiopods are very abundant. In its middle part, *Subunit IVa* contains ammonoid-rich limestone nodules. One of these nodules consists of lime mudstone and contains thin skeletal fragments, rare ostracods and the benthic foraminifer *Meandrospira pusilla* (Fig. 7. g–h).

The lowermost beds of *Subunit IVa* yields only the ammonoid? *Pseudaspidites* sp., which is not of great age significance because *Peudaspidites* is a long-ranging genus. Two different ammonoid faunas of early Spathian age have been sampled in limestone nodules from about the same horizon in the middle part of the subunit at two different outcrops, i.e. a *Nordophiceras* fauna (sample Tu 82 from outcrop Tu) containing *Nordophiceras* sp., *Paranoritoides* n. sp., columbitid n. gen. and *Hedenstroemia augusta*; and a probably slightly younger *Columbites* fauna (sample TWA 1 from outcrop TWA) containing *Columbites* cf. *parisianus*, *Nordophiceratoides* n. sp., *Evenites* n. sp. and two new genera belonging to Xenoceltitidae. Note that the relative stratigraphic position of these two samples is not known.

The lowermost beds (Tu80) of *Subunit IVa* contain typical Spathian conodonts like *Borinella*? n. sp. C (Orchard, unpublished), transitional forms to *Gladigondolella*, as well as early forms of *Icriospathodus*. The nodules in the middle part of the subunit are almost barren. The presence of *Spathicuspus spathi* in sample Tu82 confirms a Spathian age.

Subunit IVb — 1.8 m of red shale containing abundant, but poorly preserved bivalves. At its base the subunit contains small limestone nodules with abundant but poorly preserved ammonoids. The reddish lime wackestone is slightly dolomitized and contains broken thin-shelled bivalves, crinoid plates, echinoids, microgastropods, ostracods and phantoms of foraminifera (Fig. 8a).

The nodules at the base of *Subunit IVb* contain the ammonoids *Evenites* n. sp. and a new early representative of Albanitidae, which is also known from NW Guangxi (Bucher et al, unpublished data). The occurrence of the conodont *Columbitella elongatus* in these nodules indicates an early Spathian age (*Columbites* beds).

4.5.2. Interpretation

The minor carbonate content in Unit IV may be explained by an increased input of siliciclastics, possibly related to tectonic instability

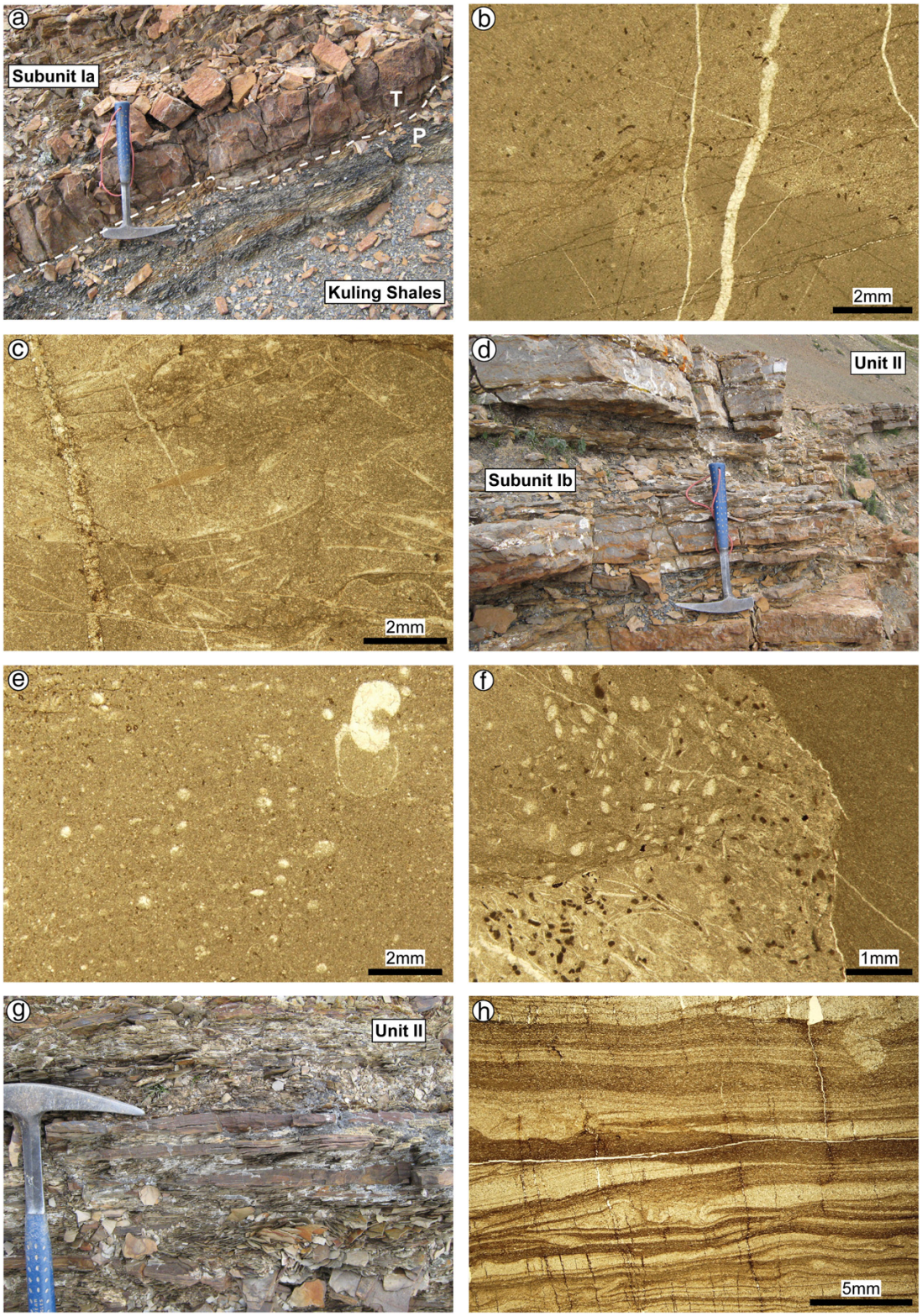
a
Subunit Ia
T
P
Kuling Shales
b
2mm
c
2mm
d
Unit II
Subunit Ib
e
2mm
f
1mm
g
Unit II
h
5mm

of the passive margin (e.g. tilting of blocks). The striking change from barren, dark green shales in *Subunit IVa* to red, bivalve-rich shales in *Subunit IVb* probably corresponds to a change in redox conditions caused by a change from a suboxic to a well-oxygenated sediment-water interface.

4.6. Lower Triassic — Unit V

4.6.1. Description

This red coloured, distinctive unit is about 6 m thick and consists of nodular, marly and bioturbated limestone resembling an "Ammonitico Rosso" facies (Fig. 8b; Garzanti et al., 1998). Due to its characteristic red colour it can very easily be recognized in the field. This unit consists of slightly to strongly bioturbated wackestones/packstones containing abundant thin-shelled bivalves, ostracods, crinoid spines and plates, microgastropods, lagenid and biseriammidid foraminifera, calcitic spheres (i.e. calcitized radiolarians) as well as rare brachiopods (Fig. 8c, e). Clay seams and stylolites are frequent and in some levels, microdolomite (neodolomite) occurs as spots. Discrete stromatactis cavities appear in the lower part of the unit, and become more frequent in the upper part.

The middle part of Unit V is marked by the presence of a peculiar white coquinoid limestone bed (sample Tu95; Fig. 8b). This 20 to 30 cm thick and distinct white bed consists of an accumulation of packed, cemented thin-shelled bivalves with some lenses rich in brachiopods at its top (Fig. 8d).

The same ammonoid fauna as in *Subunit IVb* was found in the lower part of Unit V. In a horizon just below the white coquinoid bed an association with *Fengshanites*, *Procarnites* and *Albanites* was found, indicating the early part of the *Hellenites* Beds of the middle Spathian (Guex et al., 2005a,b). The horizon just above the white bed yielded *Paragoceras*. The upper part of Unit V contains the ammonoids *Hellenites* and *Albanites*, indicating a middle Spathian age (Guex et al., 2005a,b).

The lower part of Unit V still contains the conodont *Columbitella elongatus*. The middle part (from Tu93) contains forms of the *Neogondolella regalis* group. A distinct fauna with *Triassospathodus* aff. *chionensis* appears in Tu97, indicating again a middle Spathian age. From this bed upward, the previously dominating elongate forms (neogondolellids) almost disappear, which may signal the return of shallower and/or warmer waters (Orchard, 2007). *Tr. homeri* dominates the upper part of the unit together with *Spathicuspus* spp.

4.6.2. Interpretation

The Ammonitico Rosso facies is well-known from the Jurassic of the Mediterranean (e.g. Jenkyns, 1974). In the Lower Triassic of the Tethys–Himalaya a similar facies was first described by von Rad et al. (1994) at Thini (Thakkhola area, Nepal), and later by Garzanti et al. (1998) at Tulong. This facies has been interpreted as having been deposited on a deep outer shelf plateau (upper bathyal pelagic carbonates), under well-oxygenated conditions (von Rad et al., 1994). It differs from the more distal, red Hallstatt Limestone facies (Lower to Upper Triassic, Tethyan realm; Tozer and Calon, 1990), by its high clay content and its nodular fabric. In the Himalayas, the Hallstatt facies is only known from exotic blocks (Heim and Gansser, 1939; Bassoulet et al., 1978). As reported from the Smithian ammonoid-rich Hallstatt limestones from Oman Exotics (Woods and Baud, 2008), the stromatactis cavities observed in Unit V at Tulong probably indicate microbial activity. Ammonoid and conodont biostratigraphy indicates that sedimentation rates were low, and the upper part of Unit V is condensed.

4.7. Middle Triassic — Unit VI

4.7.1. Description

The lower part of Unit VI consists of 1 m of yellowish, thin-bedded, nodular limestone (Fig. 8f). The microfacies is composed of biomicritic wacke/packstones showing remains of thin-shelled bivalves with some ostracods and crinoid spines (Fig. 8g). Microdolomite (neodolomite) occurs as spots. Some stromatactis cavities also occur. This interval is followed by a very prominent, ca. 50 cm thick grey limestone bed (Fig. 8f), overlain by two 15–20 cm thick ammonoid-rich, yellowish limestone beds showing phosphatic preservation of ammonoids. In this upper part of the unit the bioclastic content is identical to the one in the lower part (Fig. 8h). Small stromatactis cavities are present in all the microfacies of this unit. Unit VI is overlain by a thick series of dark to greenish turbiditic sandstones and shales of the Qudenggongba Formation (Liu and Einsele, 1994; Garzanti et al., 1998).

No ammonoids have been found in the lower part of Unit VI. The prominent thick limestone bed in the upper part yields representatives of *Gymnites* of Anisian age. From the two beds above this horizon Garzanti et al. (1998) mentioned the Early Anisian ammonoid *Japonites* sp. indet. In the upper of these two beds the ammonoids *Pseudodanubites* sp. and *Acrochordiceras hyatti* were found, an association diagnostic of the upper part of the early Middle Anisian Hyatti Zone (Bucher, 1992).

The lower part of Unit VI is still dominated by *Triassospathodus homeri* and *Cratognathus* spp. An Anisian fauna strongly dominated by *Chiosella timorensis* appears in the uppermost two beds.

4.7.2. Interpretation

As suggested by the phosphatic preservation of ammonoids and indicated by ammonoid and conodont biostratigraphy, Unit VI is highly condensed. No late Spathian ammonoid faunas have been documented from this unit.

5. Comparison with previous stratigraphic work

Our study, which includes several new sections and detailed biostratigraphical data, modifies and improves our knowledge of the Lower Triassic successions in the Tulong area. It reveals that previously published documentations of the Lower Triassic succession in this area were incomplete and/or poorly or incorrectly dated. The first report of Lower Triassic ammonoids from South Tibet was provided by Wang and He (1976) from the Mount Everest region. However, these authors did not publish any stratigraphical succession, which hampers the interpretation of their data. Moreover, preservation of their material is partly rather poor.

The stratigraphic profile of the Permian–Triassic boundary at Tulong provided by Rao and Zhang (1985) corresponds to our Units I and II. However, their ammonoid identifications seem dubious since they mention unusual associations of Dienerian and Smithian taxa, which are unknown from any other section in the world (e.g. Tozer, 1994; Brühwiler et al., 2007, 2008; Brayard and Bucher, 2008).

Fig. 5. (a) Outcrop photograph showing the Permian–Triassic boundary and *Subunit Ia* at section TWB. Hammer (33 cm) for scale. (b) Thin-section photomicrograph of sample TWB4 (lowest bed of *Subunit Ia*) from section TWB. Fractured and dolomitized micritic mudstone with possible phantoms of microfossils. (c) Photomicrograph of sample TWB9 (*Subunit Ia*) from section TWB. Dolomitized biomicritic mudstone, with abundant thin-shelled bivalves and broken echinoid plates. (d) Outcrop photograph showing *Subunit Ib* near section TWB. Hammer (33 cm) for scale. (e) Photomicrograph of sample TWB24 (*Subunit Ib*) from section TWB. Dolomitized biomicritic mudstone, containing ammonoids and spherical microfossils ("microspheres"; possibly radiolarians). (f) Photomicrograph of sample TWB35 (topmost bed of *Subunit Ib*) from section TWB. Recrystallized wackestone with abundant thin-shelled bivalves and ammonoids (not figured on the photo) on the left side, mudstone on the right side. Nodular texture, Stylolites and pyrite common. (g) Outcrop photograph showing thin cross-bedded dolomitic siltstone lenses in the upper part of Unit II from section TWB. Hammer (33 cm) for scale. (h) Photomicrograph of sample TWB50 (Unit II) from section TWB. Dolomitized, wavy laminated siltstone.

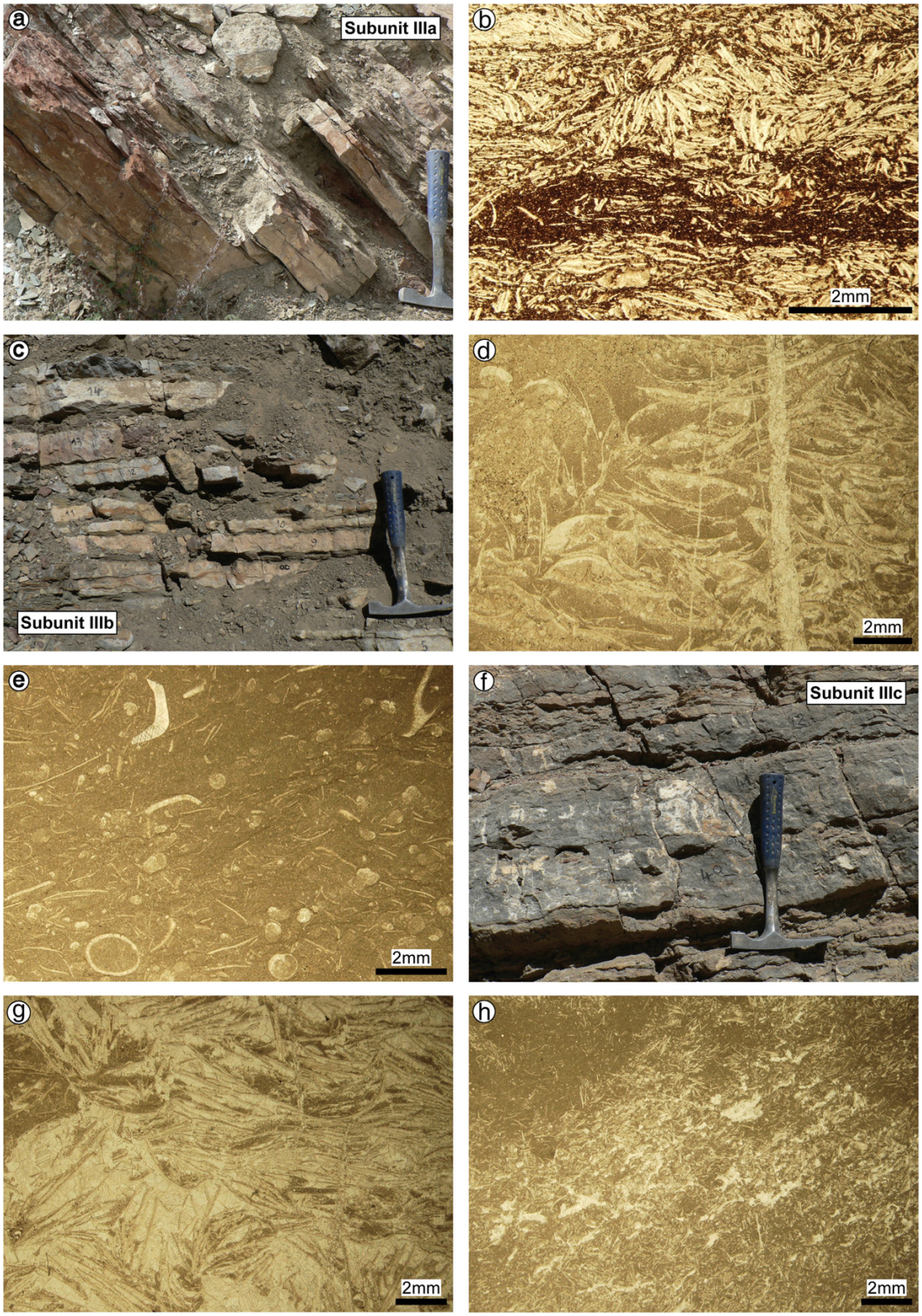
a
Subunit IIIa
b
2mm
c
Subunit IIIb
d
2mm
e
2mm
f
Subunit IIIc
g
2mm
h
2mm

Liu (1992) and Liu and Einsele (1994) provided a general overview on the Permian to Tertiary sedimentary history of South Tibet. They described the Lower Triassic Tulong Formation as 100–300 m thick, consisting in the lower part of dark, grey to purple shale, limestone and dolomite, and in the upper part of limestone and grey shale. They also mention the presence of the ammonoids *Otoceras*, *Owenites*, *Pseudosageceras* and *Procarnites* in this formation. However, it turns out to be difficult to compare their stratigraphic section with our observation of the sedimentary succession. Liu's (1992) Unit 3 probably corresponds to the Spathian red nodular limestone (i.e. our Unit V). In this case, his Lower–Middle Triassic boundary is placed some 100 m too high, and our Units I and II would be missing.

The classic Tulong section reported by Garzanti et al. (1998) shows no Permian–Triassic boundary since the Kuling shales and the entire Griesbachian and Dienerian parts of the section (Units I and II) are not exposed. Moreover, the conodont-based biostratigraphic interpretation of the section of these authors turns out to be erroneous: (i) the base of the outcrop is not Dienerian, but Smithian in age, and (ii) their Smithian–Spathian boundary is placed about 4 m too high, at the base of Unit V instead of the base of Unit IV.

The data on the Permian–Triassic boundary at Tulong reported by Shen et al. (2006) were based on Tian (1982) and Rao and Zhang (1985). However, this boundary as indicated on their photographs of the Tulong section (Shen et al., 2006, fig. 2E, p. 5) corresponds in fact more or less to the Lower–Middle Triassic boundary. Our extensive investigations did not reveal any exposed Permian–Triassic boundary on this hillside.

6. Carbonate carbon/oxygen and organic carbon isotope profiles

6.1. Samples and methods

High-resolution sampling (5–20 cm) was carried out throughout the entire Lower Triassic Tulong Formation. We analyzed the micritic matrix of 160 carbonate rock samples for the carbonate carbon and oxygen isotope ratios. Thirteen of these samples were also analyzed for the organic carbon isotope ratios. Additionally, 16 shale samples from Unit IV were analyzed for the organic carbon isotope ratios. Heterogeneous samples, containing visibly weathered parts, calcite veins or voids were carefully cleaned and cut into thin slabs. The visually least altered spots were selectively drilled with a diamond-tipped drill to produce a fine powder. All samples have been analyzed for their isotopic composition at the Institute of Mineralogy and Geochemistry of Lausanne University.

Stable carbonate carbon and oxygen isotope ratios were measured using a Thermo–Finnigan GasBench II equipped with a CTC Combi-Pal autosampler and linked to a Delta Plus XL mass spectrometer. Runs were calibrated with Carrara Marble as internal standard (+2.05‰ for C and −1.7‰ for O), which in turn has been calibrated against NBS-19 (see procedure described in Spötl and Vennemann, 2003). Reproducibility of replicate analyses was better than 0.1‰ for standards and 0.15‰ for whole rock sediment samples for both carbon and oxygen isotope ratios.

The organic carbon isotope ratio has been measured using a Carlo Erba EA-1500 connected to a Finnigan MAT Delta-S mass spectrometer. The samples were individually wrapped in tin foil cups and dropped into the reactor while a small dose of oxygen gas was mixed into the He stream. The samples have then been oxidized in the reactor held at about 1050 °C and filled with cobalt oxide as a catalyst for the oxidation. Excess oxygen from the He stream was adsorbed in another reactor column filled with metallic Cu held at 500 °C. The residual gases of CO_2, (N_2), and H_2O were then passed over a water trap of magnesium perchlorate [$Mg_4(ClO_4)_2$] and into a gas chromatograph filled with a molecular sieve (5 Å) to separate N_2 and CO_2. CO_2 was then transported by the He stream via a CONFLO III (open split) system into the mass spectrometer for isotopic analyses.

Reproducibility of the internal graphite standard used was better than ±0.12‰ and USGS-24 graphite (−16.0‰ VPDB) and NBS-22 oil (−29.6‰ VPDB) were used as calibration standards. All isotope results are reported using the conventional δ notation, defined as per mil (‰) deviation vs. VPDB (i.e. Vienna Pee Dee Belemnite).

6.2. Results

All analytical data ($\delta^{13}C_{carb}$–$\delta^{18}O_{carb}$–$\delta^{13}C_{org}$) are provided in the Supplementary Online Material (Table 1). The measured ratios are plotted against the composite profile, which combines the four sampled sections in the Tulong area (Fig. 4).

6.2.1. Carbonate carbon isotope record

Between the Permian–Triassic boundary and the Lower–Middle Triassic boundary the Lower Triassic carbonate carbon isotope record ($\delta^{13}C_{carb}$) of the Tulong Formation shows essentially 3 positive and 3 negative excursions. Its trend varies over a broad range comprised between −4.2‰ and +2.8‰ and displays a well-defined curve along the section.

Low and highly variable values ranging between −4.2‰ and −2.2‰ are obtained from the dolomitic limestones of the Griesbachian interval (*Subunit Ia*). Subsequently an increase in the C_{carb}-isotope values from −4.2‰ to −2.4‰ is observed from the Griesbachian–Dienerian boundary up to the limestone horizon at the top of *Subunit Ib* yielding the *Pleurambites* and *Proptychites* ammonoid fauna. This maximum is followed by a large gap which is due to the shales of Unit II lacking any limestone beds in the lower part. The few small dolomitic siltstone lenses in the upper part of Unit II yield C_{carb}-isotope values around −4‰. Nearly constant C_{carb}-isotope values around −2.5‰ characterize the lower part of the Smithian carbonates (*Subunits IIIa–b*). The most prominent positive C_{carb}-isotope excursion of the entire Lower Triassic Tulong Fm. starts around the horizon in *Subunit IIIc* yielding the first *Owenites* fauna, i.e. the Arctoceratid B fauna. This excursion is characterized by a gradual increase from −2.5‰ up to −1‰ (e.g. in the bed yielding *Wasatchites*), then rises abruptly and reaches peak values of up to 2.8‰ at the base of *Subunit IVa* (earliest Spathian). This well-defined, latest Smithian to earliest Spathian positive shift in C_{carb}-isotope values is then followed by a major drop ranging from −0.4‰ to 1‰, which coincides with the change to siliciclastics (Unit IV). Following this interval the C_{carb}-isotope values remain essentially stable between −0.2‰ and 0‰ during most of the Spathian limestone deposition (Unit V). A slightly positive excursion starts with the onset of the thin-bedded limestones in the uppermost part of Unit V yielding *Hellenites* and *Albanites* faunas and reaches maximum values around +2‰.

Fig. 6. (a) Outcrop photograph showing *Subunit IIIa* at section Na. Hammer (28 cm) for scale. (b) Thin-section photomicrograph of sample Na7 (*Subunit IIIa*) from section Na. Dolomitized, laminated biomicrosparitic packstone–grainstone containing densely packed, mostly broken, thin-shelled bivalves. Dolomitic matrix. (c) Outcrop photograph showing *Subunit IIIb* at section Tu. Hammer (28 cm) for scale. (d) Thin-section photomicrograph of sample Tl5 (*Subunit IIIb*) from section Tu. Packstone containing thin-shelled bivalves and probably ostracods. Note geopetal structures. (e) Thin-section photomicrograph of sample Tl9 (*Subunit IIIb*) from section Tu. Biomicritic mudstone–wackestone containing microspheres (probably microgastropods) and ammonitellas. (f) Outcrop photograph showing *Subunit IIIc* at section Tu. Hammer (28 cm) for scale. (g) Thin-section photomicrograph of sample Tl13 (*Subunit IIIc*) from section Tu. Biosparitic grainstone with packed, thin-shelled bivalves. (h) Thin-section photomicrograph of sample Tl16 (*Subunit IIIc*) from section Tu. Wackestone–packstone containing thin-shelled bivalves.

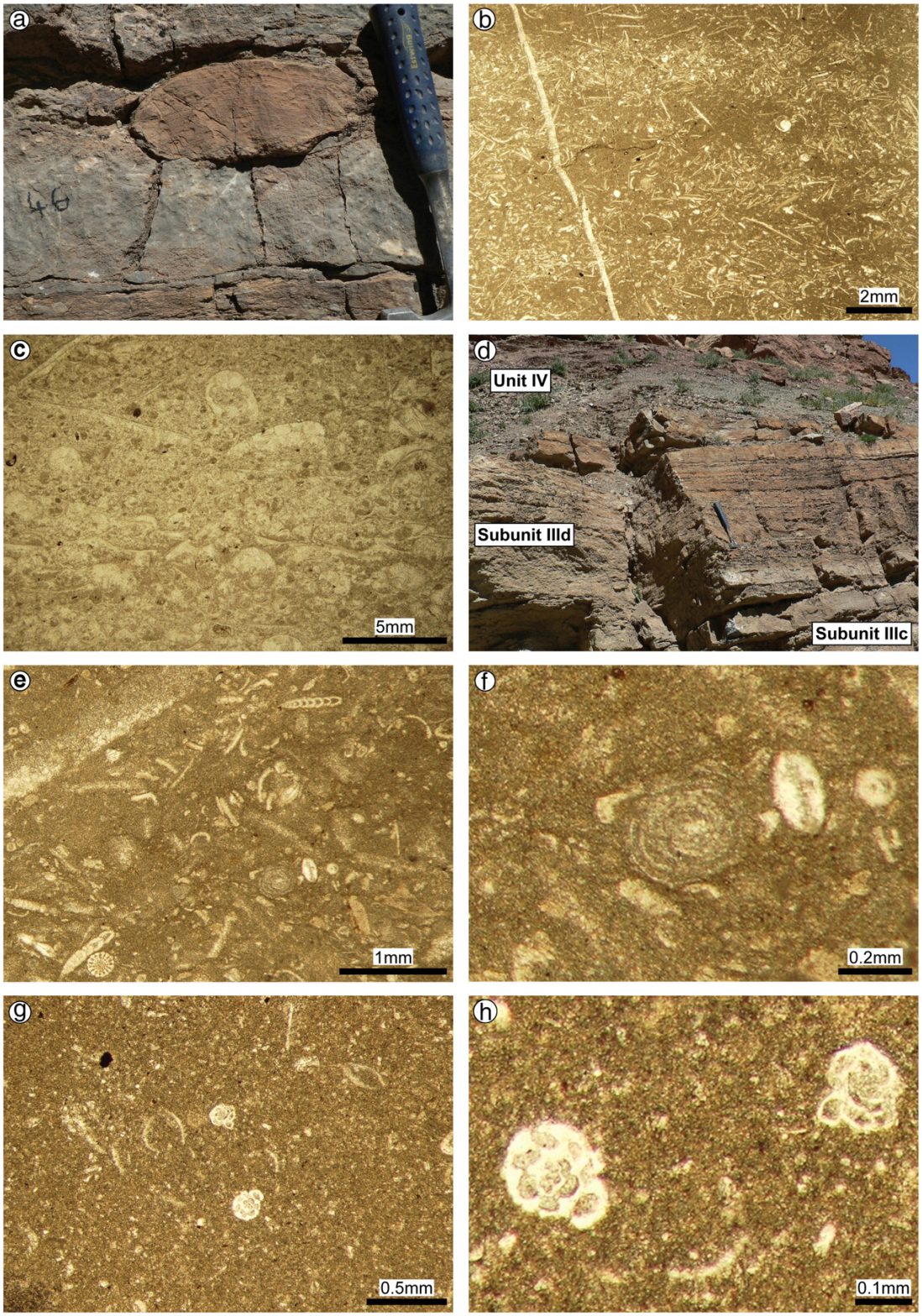
a
b
2mm
c
5mm
d
Unit IV
Subunit IIId
Subunit IIIc
e
1mm
f
0.2mm
g
0.5mm
h
0.1mm

6.2.2. Organic carbon isotope record

The organic carbon isotope record from the Lower Triassic Tulong Fm. has been obtained from the Smithian–early Spathian interval (*Subunit IIIb*–Unit IV). Its values vary over a wide range from −18.7‰ to −27.5‰. While the late Smithian record displays a slight increase in the $\delta^{13}C_{org}$ composition, the latest Smithian–earliest Spathian interval shows a highly fluctuating record. The $\delta^{13}C_{carb}$–$\delta^{13}C_{org}$ cross-plot for the carbonate samples, for which both $\delta^{13}C_{carb}$ and $\delta^{13}C_{org}$ have been analyzed, shows no covariance (Pearson's correlation coefficient $r = 0.386$, $p = 0.192$) (Fig. 9c). Due to the erratic nature of the signal, especially in Unit IV, the $\delta^{13}C_{carb}$ record appears as inconclusive. Therefore, any interpretation in terms of isotope excursions and correlations with the measured C_{carb} and O_{carb} isotope profiles would be rather speculative.

6.2.3. Carbonate oxygen isotope record

The $\delta^{18}O_{carb}$ values of the Lower Triassic Tulong Fm. are generally very low ranging from −5.8‰ to −14.2‰ for the Griesbachian–Dienerian and from −8‰ to −13.6‰ for the Smithian–Spathian time intervals. Extremely low values around −17‰ are detected within the carbonate lenses in the upper part of Unit II. Two major oxygen isotope anomalies are identified. The first one is a sharp, well-defined, negative excursion dropping from −5.8‰ to −14.2‰. It coincides with a lithologic change from dolomitic limestone to limestone around the Griesbachian/Dienerian boundary (*Subunits Ia–b*). The second one, less well-marked, is a change from relatively stable oxygen isotope values in *Subunits IIIa–b* to a strongly erratic signal in *Subunits IIIc–d*, coinciding with the onset of the major positive $\delta^{13}C_{carb}$-isotope shift within the middle-late Smithian time interval. Background values, ranging from −12‰ to −13.5‰, shift toward more positive values up to −8‰ during this interval. Following this perturbation constant oxygen isotope values around −12‰ are observed throughout the Spathian.

6.3. Diagenetic alteration of the isotope record

Since samples of the Lower Triassic Tulong Fm. display very low $\delta^{18}O_{carb}$ values (i.e. average: −12‰) and unusually low $\delta^{13}C_{carb}$ values (e.g. essentially during the Griesbachian–early/middle Smithian: average −2.5‰) one may question whether the primary marine signature has been preserved or if the measured isotope values represent diagenetic features. The comparison between the $\delta^{13}C_{carb}$ and $\delta^{18}O_{carb}$ profiles (see cross-plots in Fig. 9a–b) shows that $\delta^{18}O_{carb}$ covaries with $\delta^{13}C_{carb}$ values in some parts of the section (i.e. mostly the Griesbachian/Dienerian interval; the Smithian shows also a slight covariance [i.e. Unit III]). This suggests some influence of diagenesis on the isotope records (e.g. Glumac and Walker, 1998).

Oxygen isotope values are known to be more prone to alteration during diagenesis than carbon isotope values (Marshall, 1992). For instance, in other Tethys–Himalayan sections of Kashmir, Spiti and Nepal, very low $\delta^{18}O$ values (similar to those from Tulong) have been found and explained by a thermal metamorphism process of up to 300 °C (Baud et al., 1996; Atudorei, 1999). It is interesting to note that even in such conditions of low-grade metamorphism the relative changes in the carbon isotopic signal are preserved and correlate with other records for the same time span, although the changes in oxygen isotopes have been completely obliterated.

Another interesting case is the lithological change from dolomite to limestone at the *Subunit Ia/Ib* boundary, concomitant with a strong negative shift of the $\delta^{18}O$ values from −8 to −14.5‰ without affecting the $\delta^{13}C$ values. Similarly, an even more negative shift of the $\delta^{18}O$ values from −9 to −23‰ is recorded at exactly the same lithological change of Thini Chu section (Nepal), 300 km to the west with no influence on the $\delta^{13}C$ values (Baud et al., 1996).

Considering that rocks of the Tulong area experienced regional metamorphism with temperatures up to about 200 °C (see Section 2.2.) we suspect an overprint of the isotope signal by deep burial diagenesis, shifting both carbon and oxygen isotope ratios toward more negative values (e.g. Galfetti et al., 2007a). The oxygen isotope record of Tulong is very unlikely to preserve any primary signal. It is probably completely controlled by diagenetic processes. However, taking into consideration the striking similarity with other age-constrained, Lower Triassic sections from the Tethys (see Corsetti et al. (2005) and Galfetti et al. (2007a) for reviews; and discussion and correlations hereafter) it is assumed that all the relative fluctuations in the $\delta^{13}C_{carb}$ signal of the Lower Triassic Tulong Formation are reliable.

7. Discussion

7.1. Comparison with the Lower Triassic section of Selong, South Tibet

The described lithological Late Permian to Lower Triassic succession from Tulong shows distinct differences to the sections from the area of Selong which is located only 35 km to the NW (cf. Wang et al., 1989; Yugan et al., 1996; Garzanti et al., 1998; Wignall and Newton, 2003). At Selong the late Permian consists of fossil-rich limestones of Djulfian and Changhsingian age (Garzanti et al., 1998; Orchard et al., 1994), contrasting with the Kuling Shales at Tulong. The Griesbachian–Dienerian interval is similar to Tulong regarding facies and thickness. A shale interval similar to Unit II also exists in Selong, but is has an extremely reduced stratigraphic thickness (ca.1.5 m). The Smithian–Spathian interval of the Selong section is much less developed than in Tulong and is only about 4.5 m thick. At Selong the "Ammonitico Rosso" facies is missing.

Such facies and thickness changes appear to be compatible with large-scale tilted blocks that developed on the northern Gondwana passive, extensional margin (Stampfli et al., 1991). Tulong and Selong belong to two contiguous thrust sheets (Burg, 1983). Because of the unknown amount of N–S tectonic shortening between these two thrust sheets, it cannot be established whether the two areas were part of a single tilted block or belonged to two distinct blocks.

7.2. Comparison with other Lower Triassic Tethyan sections

Griesbachian — The dolomitic facies of *Subunit Ia* from Tulong seems not uncommon in the earliest Triassic. It is known from other Tethyan localities, such as in (i) the *Otoceras latilobatum* beds at Selong (Wignall and Newton, 2003); (ii) the Panjang unit of the Thakkhola area of N central Nepal, about 300 km to the West (Hatleberg, 1982; Baud et al., 1996); (iii) the brown, ferruginous, dolomitic limestone of the lower part of the Lower Limestone Member (*Otoceras* beds) in Spiti, Northern India (Bhargava et al., 2004; pers. observation); and in (iv) the dolomitic Kathwai Member of the Salt Range, Pakistan (Kummel, 1970; Guex, 1978; pers. observation).

For the Selong area Wignall and Newton (2003) suggested that the common formation of pyrite and dolomite in the Griesbachian *Otoceras latilobatum* beds may be caused by anoxic pore-waters during deposition of anoxic sediments in the Dienerian ("diagenetic anoxia

Fig. 7. (a) Outcrop photograph showing a nodule with so-called "pseudostromatolithic structures" (Garzanti et al., 1998) (*Subunit IIIc*, section Tu). Hammer (28 cm) for scale. (b) Photomicrograph of a thin-section through the same nodule (sample Tu46-2, section Tu). Note alternating domains of lime mudstone and of lime wackestone with thin-shelled microbivalves, ostracods and spicules. (c) Thin-section photomicrograph of sample Tl17 (*Subunit IIIc*) from section Tu. Recristallized packstone with juvenile ammonoids, thin-shelled bivalves, microgastropods, ostracods, peloids and geopetal structures. (d) Outcrop photograph showing *Subunit IIId* and Unit IV at section Tu. Hammer (28 cm) for scale. (e) Thin-section photomicrograph of sample Tl18 (*Subunit IVa*) from section Tu. Wackestone–packstone containing thin-shelled bivalves, ostracods, crinoid spines and plates together with Nodosariids foraminifera. (f) Detail of previous figure showing the foraminifer *Glomospirella* cf. *jefimowae*. (g) Thin-section photomicrograph of sample Tl18b (*Subunit IVa*) from section Tu. Mudstone containing small bioclasts and rare ostracods and foraminifera. (h) Detail of previous figure showing the foraminifer *Meandrospira pusilla*.

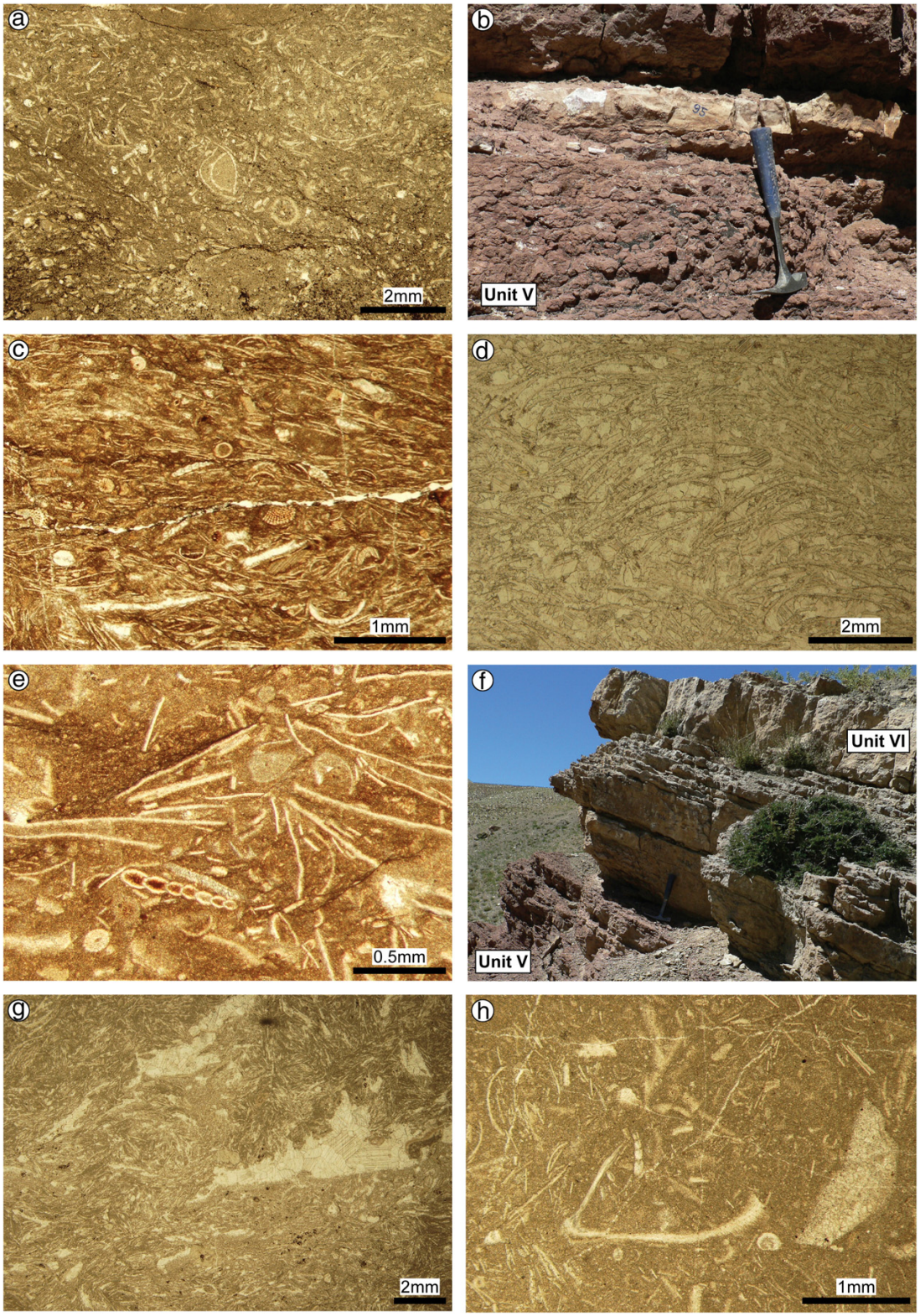
a
2mm
b
Unit V
c
1mm
d
2mm
e
0.5mm
f
Unit VI
Unit V
g
2mm
h
1mm

imposed upon a bed deposited in fully oxygenated conditions" (Wignall and Newton, 2003, p. 158)). However, this explanation is at variance with the widespread and synchronous distribution of dolomites in the Griesbachian in Tulong, Spiti and the Salt Range and the absence of evidence for anoxia in the overlying Dienerian carbonates in all of these areas (see below).

Microbial limestones, a common feature of the earliest Triassic as shown by Baud et al. (1997, 2002, 2005, 2007), Kershaw et al. (1999, 2002, 2007) and Galfetti et al. (2008) (e.g. South China, Japan, Iran, Turkey, Hungary, Armenia, Greenland and possibly Madagascar), are not present in the Tulong section. However, the synchroneity of widespread dolomite and microbial limestone deposition in the aftermath of the Permian/Triassic extinction may suggest a relationship between the two facies. In present-day hypersaline, anoxic environments microbial sulfate-reducing activity can induce an environment favouring the precipitation of dolomite (Vasconcelos and McKenzie, 1997). Burns et al. (2000) suggested that throughout the Phanerozoic the amount of dolomite formation is negatively correlated with the amount of atmospheric oxygen. Thus, they proposed that oxygen is the primary factor controlling widespread dolomite formation and suggested that sulfate-reducing microbial communities associated with seafloor hydrothermal systems may be an ultimate factor controlling massive dolomite formation on a global scale. Similarly, widespread and possibly sulfate-reducing microbial communities as exemplified by the global occurrence of microbial limestone (Baud et al., 2007) as well as deep oceanic anoxia (Isozaki, 1997; Kakuwa, 2008) might have favoured dolomite formation during the Griesbachian. However, further investigation is needed to test this hypothesis.

Dienerian — Regarding facies as well as thickness, the late Griesbachian to Dienerian ammonoid-rich, thin-bedded, grey carbonates of *Subunit Ib* strongly resemble the Lower Ceratite Limestone from the Salt Range (Waagen, 1895; Guex, 1978; pers. observation) and the age-equivalent carbonates of the upper Lower Limestone Member in Spiti (Bhargava et al., 2004; pers. observation). The overlying shales of Unit II (Dienerian and early Smithian) are strikingly similar to the Ceratite Marls of the Salt Range (Waagen, 1895; Guex, 1978; pers. observation). During the Dienerian clastic sedimentation also predominates in Guangxi (South China) and Spiti.

Smithian — As in many other Tethyan sections such as Guangxi, Spiti and in the Salt Range, the Smithian series in Tulong (Unit III) are dominated by carbonate rocks (Waagen, 1895; Guex, 1978; Galfetti et al., 2007a; pers. observation). However, detailed comparison reveals important differences between these areas. In Guangxi and in Spiti the early Smithian is marked by a conspicuous episode of carbonate deposition (i.e. the *Flemingites* beds; Galfetti et al., 2007a). However, in Tulong and in the Salt Range the early Smithian is still characterized by clastic deposition (Unit II; Ceratite Marls/Ceratite Sandstones), and massive carbonate sedimentation starts only in the middle Smithian (Unit III; Upper Ceratite Limestone). The middle and late Smithian parts of the Tulong and the Salt Range sections contain more carbonates than in Guangxi and Spiti, where the *Owenites* beds and the *Anasibirites* beds consist of dark, organic rich shales with interbedded limestones or limestone nodules. In the late Smithian (*Anasibirites* beds) these shales often show signs of anoxia or dysoxia (Galfetti et al., 2007a), a feature which is absent in Tulong and in the Salt Range (pers. observation).

Spathian — The early Spathian shales of Unit IV have no known direct counterpart in other Tethys–Himalaya sections. Time-equivalent rocks usually consist of nodular limestone similar to those of Unit V. This local absence of carbonates may be the result of an increased input of clastic sediments, possibly related to tectonic instability of the passive margin (e.g. tilting of blocks). The colour change from green to red in the shales in the Early Spathian Unit IV indicates a change in redox conditions.

The Middle Spathian red nodular limestone of Unit V ("Ammonitico Rosso" facies) has also been described from the Thakkhola (north of the Anapurna, Nepal) (von Rad et al., 1994). This facies also resembles the Lower to Upper Spathian Niti Limestone from the Indian Himalayas and the Lower to Upper Spathian nodular limestone from Guangxi (South China) (Galfetti et al., 2007a), differing only by its red colour. This colour is probably caused by fine Fe-rich terrigenous material (Liu, 1992) and an oxidizing water-sediment interface.

Anisian — In the studied area the interval ranging from the late Spathian to the middle Anisian is strongly condensed. Although less extreme, similar low sedimentation rates and/or hiatuses in this time interval are observed also in other Tethyan localities such as Spiti (India) (Bhargava et al., 2004).

7.3. Carbon isotope correlations

Fig. 10 shows the late Permian to late Spathian part of the carbonate carbon isotope record from northwestern Guangxi (South China), which has recently been calibrated by means of high-precision U–Pb ages and ammonoid biochronozones (Ovtcharova et al., 2006; Galfetti et al., 2007b). The correlation of the new carbon isotope record from Tulong with South China by means of ammonoid faunas results in a strong contraction of the Smithian part of the Tulong record and reveals striking similarities between the two records.

The observed positive shift around the Griesbachian/Dienerian boundary correlates well with coeval positive shift shown by Baud et al. (1996) from the Guryul Ravine section (lower Khunamuh Formation) and from the Thini Chu section (basal Tamba Kurkur Formation) and can be compared with the late Griesbachian positive shift observed in other localities such as South China (Fig. 10; Galfetti et al., 2007a).

The large positive excursion at the Dienerian–Smithian boundary, which has been documented in various areas such as South China, Spiti and Italy (Payne et al., 2004; Galfetti et al., 2007a; Horacek et al., 2007a; Krystyn et al., 2007; Richoz et al., 2007) is missing in our record (Fig. 10). Therefore, the corresponding time interval may lie within Unit II, and the excursion was not documented because of the lack of carbonates. Consequently, Unit III does not include the base of the Smithian and the Dienerian/Smithian boundary lies within Unit II.

Like in other sections the middle Smithian is characterized by low $\delta^{13}C_{carb}$ values (Galfetti et al., 2007a). The following well-defined positive $\delta^{13}C_{carb}$ excursion at the Smithian–Spathian boundary correlates well with that from other Tethyan and boreal profiles (Baud et al., 1996; Payne et al., 2004; Galfetti et al., 2007a,c; Horacek et al., 2007a,b). Differing from other profiles there is an unexpected and sudden $\delta^{13}C_{carb}$ drop following the Smithian–Spathian boundary excursion (*Subunit IVa*), which does not appear in other Tethyan

Fig. 8. (a) Thin-section photomicrograph of sample TuK4 (*Subunit IVb*) from section Tu. Nodular, dolomitized biomicritic wackestone–packstone, containing fragments of thin-shelled bivalves and echinoids and phantoms of foraminifera and ostracods. (b) Outcrop photograph showing Unit V with the peculiar white bed in its middle part (section Tu). Hammer (28 cm) for scale. (c) Thin-section photomicrograph of sample Tl22 (Unit V) from section Tu. Reddish packstone–grainstone, packed with thin-shelled bivalves, crinoids, ostracods and foraminifera. (d) Thin-section photomicrograph of the white bed (sample Tu95, Unit V) from section Tu. Biosparitic packstone containing bivalves. (e) Thin-section photomicrograph of sample Tl27 (Unit V) from section Tu. Reddish packstone with thin-shelled bivalves, ostracods, crinoid spines and plates as well Nodosariids foraminifera. (f) Outcrop photograph showing Unit VI at section Tu. Hammer (28 cm) for scale. (g) Thin-section photomicrograph of sample Tl32 (Unit VI) from section Tu. Packstone containing thin-shelled bivalves, rare ostracods and stromatactis cavities. (h) Thin-section photomicrograph of sample Tl35 (Unit VI) from section Tu. Grey mudstone–wackestone with thin-shelled bivalves, crinoid plates, ostracods and Nodosariids foraminifera.

Table 1
Analytical data for carbonate carbon/oxygen and organic carbon isotopes (relative to VPDB) from the Lower Triassic Tulong Formation, South Tibet.

Section	Sample	Unit	$\delta^{13}C_{carb}$ (‰)	$\delta^{18}O_{carb}$ (‰)	Section	Sample	Unit	$\delta^{13}C_{carb}$ (‰)	$\delta^{18}O_{carb}$ (‰)	$\delta^{13}C_{org}$ (‰)
TWB	4	Ia	−3.11	−6.26	Tu	7	IIIb	−2.36	−13.21	
TWB	5a	Ia	−3.32	−6.12	Tu	9	IIIb	−2.58	−12.85	
TWB	5b	Ia	−3.22	−6.53	Tu	11	IIIb	−2.51	−12.90	
TWB	7a	Ia	−2.31	−5.82	Tu	13	IIIb	−2.54	−12.52	
TWB	7b	Ia	−3.12	−7.08	Tu	14	IIIb	−2.18	−11.54	−25.44
TWB	8	Ia	−3.25	−6.57	Tu	16.1	IIIb	−2.55	−12.64	
TWB	9	Ia	−3.83	−7.74	Tu	16.2	IIIb	−2.23	−11.01	
TWB	10	Ia	−2.20	−6.27	Tu	18	IIIb	−2.48	−12.50	
TWB	11	Ia	−3.01	−6.95	Tu	22	IIIb	−2.44	−12.19	
TWB	12	Ia	−3.08	−7.11	Tu	26	IIIb	−2.76	−12.30	
TWB	14	Ia	−2.75	−7.39	Tu	29	IIIb	−2.40	−12.16	
TWB	15	Ia	−4.16	−8.82	Tu	30	IIIb	−2.43	−12.34	
TWB	16	Ia	−3.61	−8.23	Tu	33	IIIb	−2.46	−12.13	
TWB	17	Ia	−4.07	−8.32	Tu	35	IIIb	−2.59	−12.68	−27.46
TWB	18	Ia	−3.78	−8.28	Tu	37	IIIb	−2.60	−12.53	
TWB	20	Ia	−3.74	−7.94	Tu	38	IIIb	−2.53	−12.48	
TWB	21	Ia	−3.73	−8.82	Tu	39	IIIb	−2.68	−12.07	−26.24
TWB	22	Ia	−3.60	−12.25	Tu	40	IIIc	−2.14	−8.67	
TWB	23	Ia	−3.24	−13.75	Tu	41	IIIc	−2.49	−9.77	
TWB	24	Ib	−2.90	−14.29	Tu	42	IIIc	−2.13	−8.80	
TWB	25	Ib	−2.29	−14.06	Tu	44	IIIc	−2.17	−10.42	
TWB	26	Ib	−2.20	−14.39	Tu	45	IIIc	−2.46	−12.71	
TWB	28	Ib	−2.06	−14.52	Tu	46.1	IIIc	−2.55	−9.50	−25.37
TWB	29	Ib	−2.54	−14.07	Tu	46.2	IIIc	−2.45	−12.60	
TWB	30	Ib	−2.27	−14.28	Tu	47	IIIc	−2.14	−8.86	
TWB	31	Ib	−2.65	−14.13	Tu	48	IIIc	−2.35	−12.58	
TWB	32	Ib	−2.45	−14.27	Tu	50	IIIc	−1.79	−8.39	
TWB	33	Ib	−1.88	−14.36	Tu	52.1	IIIc	−1.77	−8.76	−24.91
TWB	34	Ib	−1.84	−14.72	Tu	52.2	IIIc	−1.76	−8.53	
TWB	35	Ib	−2.67	−14.13	Tu	53	IIIc	−1.65	−9.38	
TWB	50	II	−4.13	−12.41	Tu	54	IIIc	−1.76	−10.41	
TWB	51	II	−4.15	−12.73	Tu	55	IIIc	−1.60	−9.23	
TWB	52	II	−3.00	−17.35	Tu	56	IIIc	−1.70	−9.64	
TWB	54	IIIa	−2.79	−13.03	Tu	57	IIIc	−1.52	−12.02	
TWB	55	IIIa	−2.62	−13.26	Tu	58	IIIc	−1.56	−9.65	−26.02
TWB	56	IIIa	−2.44	−13.19	Tu	59	IIIc	−1.33	−10.23	
					Tu	61	IIIc	−1.37	−11.77	
Na	2	IIIa	−2.48	−11.36	Tu	63	IIIc	−1.58	−8.70	−26.28
Na	3	IIIa	−2.74	−13.08	Tu	64	IIIc	−1.16	−8.08	
Na	4	IIIa	−2.92	−13.32	Tu	66.1	IIIc	−1.12	−9.28	
Na	5	IIIa	−2.45	−12.94	Tu	66.2	IIIc	−1.11	−10.47	−23.54
Na	6	IIIa	−2.49	−13.14	Tu	67	IIIc	−1.01	−11.37	
Na	7	IIIa	−2.46	−13.05	Tu	69	IIIc	−0.80	−9.76	
Na	8	IIIa	−2.92	−13.27	Tu	71	IIIc	−0.29	−8.37	
					Tu	72	IIId	0.21	−11.84	
Tu	202	IIIa	−1.96	−12.36	Tu	73.1	IIId	0.26	−12.25	
Tu	201	IIIa	−2.41	−12.83	Tu	73.2	IIId	0.43	−12.07	−26.44
Tu	200	IIIa	−2.85	−13.10	Tu	74	IIId	0.37	−11.83	
Tu	1	IIIa	−2.09	−11.86	Tu	75	IIId	1.15	−10.49	
Tu	2.1	IIIa	−2.71	−11.83	Tu	P1	IVa			−23.91
Tu	2.2	IIIa	−2.76	−12.33	Tu	77	IVa	2.78	−11.97	
Tu	5	IIIb	−2.66	−13.08	Tu	78	IVa	2.49	−12.04	−25.42
Tu	91	V	−0.28	−11.86	Tu	79	IVa	2.52	−12.22	
Tu	92.2	V	−0.34	−11.87	Tu	80	IVa	2.32	−12.09	
Tu	93	V	−0.32	−11.90	Tu	P2	IVa			−25.14
Tu	94.1	V	−0.31	−12.00	Tu	81	IVa	0.25	−12.53	−25.20
Tu	94.2	V	−0.35	−11.50	Tu	P3	IVa			−20.84
Tu	94.3	V	−0.37	−11.81	Tu	P4	IVa			−25.67
Tu	95	V	−0.36	−11.79	Tu	82	IVa	0.03	−13.31	−18.74
Tu	96.1	V	−0.49	−11.93	Tu	P5	IVa			−24.89
Tu	96.2	V	−0.36	−11.75	TWA	1	IVa	−0.40	−12.08	
Tu	96.3	V	−0.41	−12.03	Tu	P6	IVa			−25.05
Tu	97.1	V	−0.24	−12.11	Tu	P7	IVa			−26.04
Tu	97.2	V	−0.30	−12.05	Tu	P8	IVa			−24.57
Tu	97.3	V	−0.25	−11.81	Tu	K1	IVb	1.06	−11.93	
Tu	98	V	−0.34	−12.34	Tu	P10	IVb			−20.70
Tu	99.1	V	−0.11	−12.13	Tu	K2	IVb	0.80	−12.07	
Tu	100	V	−0.16	−12.05	Tu	P11	IVb			−22.68
Tu	101	V	−0.07	−11.57	Tu	K3	IVb	0.94	−12.01	−21.47
Tu	102	V	−0.08	−11.89	Tu	K4	IVb	0.70	−11.57	
Tu	103	V	−0.07	−12.14	Tu	P12	IVb			−23.56
Tu	104.1	V	0.16	−11.91	Tu	P13	IVb			−20.78
Tu	104.2	V	0.50	−11.72	Tu	P14	IVb			−23.21
Tu	105	V	0.45	−11.99	Tu	P15	IVb			−23.34

Table 1 (*continued*)

Section	Sample	Unit	$\delta^{13}C_{carb}$ (‰)	$\delta^{18}O_{carb}$ (‰)	Section	Sample	Unit	$\delta^{13}C_{carb}$ (‰)	$\delta^{18}O_{carb}$ (‰)	$\delta^{13}C_{org}$ (‰)
Tu	106.1	VI	0.35	−11.56	Tu	P16	IVb			−23.67
Tu	106.2	VI	0.48	−11.88	Tu	86	IVb	0.71	−12.24	
Tu	107	VI	0.32	−12.12	Tu	P17	IVb			−23.62
Tu	108.1	VI	0.41	−12.05	Tu	87.1	V	0.49	−12.24	
Tu	108.2	VI	0.26	−12.44	Tu	87.2	V	0.08	−12.22	
Tu	108.3	VI	0.52	−12.19	Tu	87.3	V	−0.01	−11.76	
Tu	108.4	VI	0.44	−12.23	Tu	87.4	V	−0.08	−11.79	
Tu	109.1	VI	0.48	−12.46	Tu	87.5	V	0.08	−11.88	
Tu	109.2	VI	0.46	−12.26	Tu	87.6	V	−0.08	−12.01	
Tu	109.3	VI	0.68	−12.62	Tu	88.1	V	−0.02	−11.82	
Tu	109.4	VI	−0.78	−12.06	Tu	88.2	V	−0.03	−11.86	
Tu	110	VI	2.01	−12.20	Tu	88.3	V	−0.16	−11.90	
Tu	111.1	VI	1.14	−12.18	Tu	89.1	V	−0.27	−12.42	
Tu	111.2	VI	1.13	−12.09	Tu	89.2	V	−0.29	−11.68	
Tu	111.3	VI	1.82	−13.60	Tu	90	V	−0.34	−11.83	

profiles. This drop may represent a lithologic effect related to a conspicuous input of clastic material rather than a primary signature, i.e. decarbonation reactions in presence of siliciclastic components (Kaufman and Knoll, 1995).

Like in all known localities the Spathian interval is characterized by equilibrium $\delta^{13}C_{carb}$ values fluctuating only slightly around zero. The comparison of the new record from Tulong with the one from South China reveals strong similarities in these minor fluctuations during the Spathian, both in terms of variations and of absolute values (Fig. 10). At both localities the $\delta^{13}C$ values show a slight decrease in the early Spathian and reach a minimum in the middle Spathian. From there on values show a continuous increase. The few data points

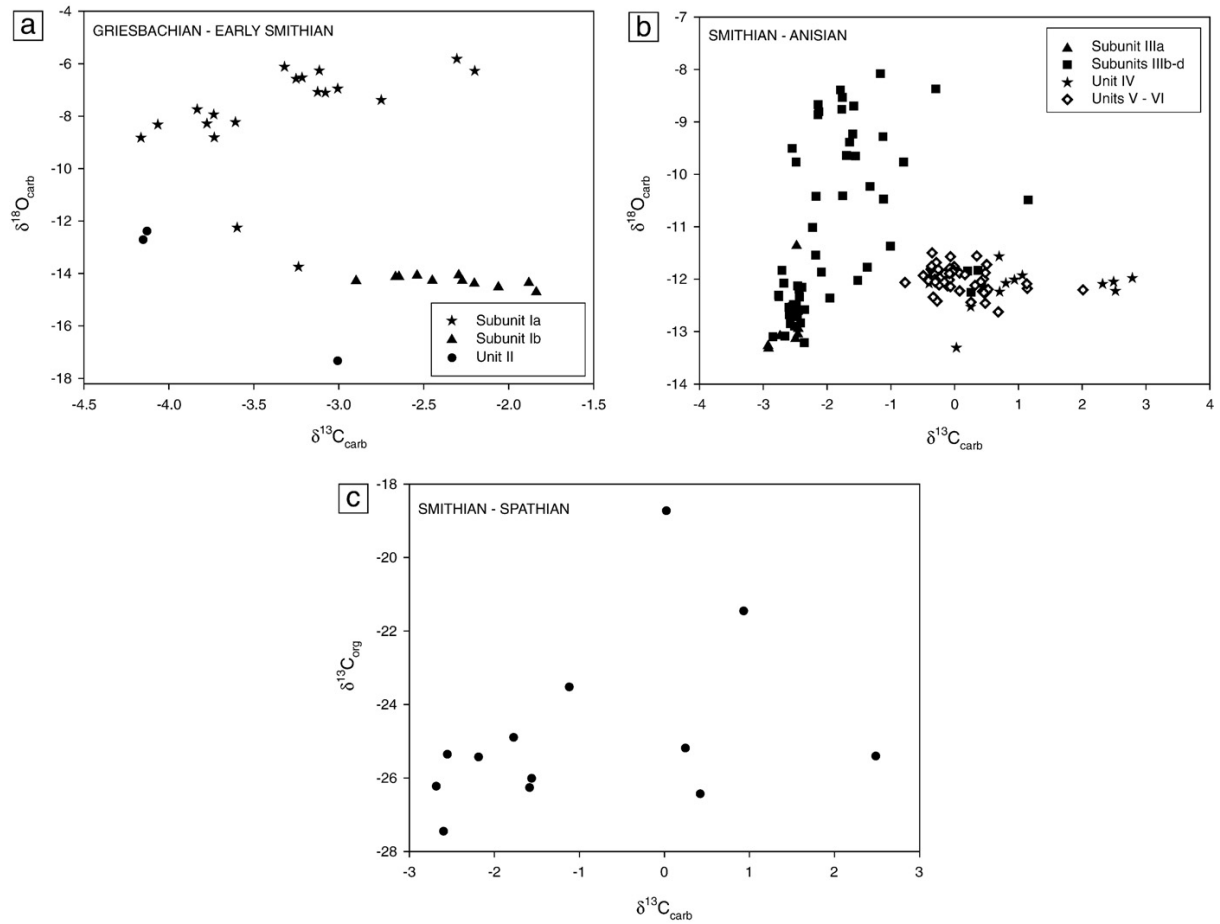

Fig. 9. Isotopic cross-plots of the Tulong Formation. All isotope values are expressed in ‰ deviation vs. VPDB. (a) $\delta^{13}C_{carb}$ versus $\delta^{18}O_{carb}$ for the Griesbachian–early Smithian. (b) $\delta^{13}C_{carb}$ versus $\delta^{18}O_{carb}$ for the Smithian–Anisian. (c) $\delta^{13}C_{carb}$ versus $\delta^{13}C_{org}$ values from carbonate samples.

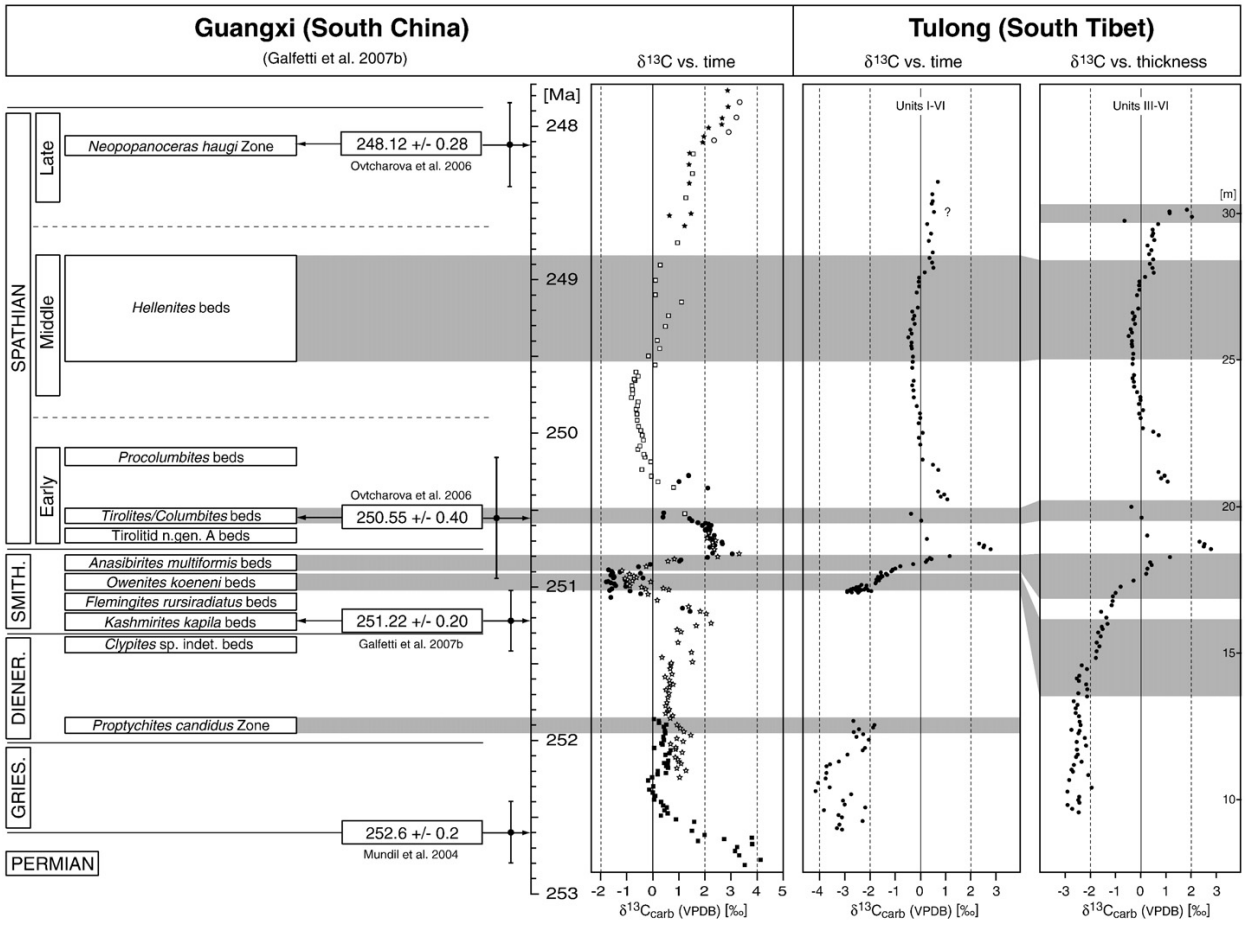

Fig. 10. $\delta^{13}C$ record from Tulong against stratigraphical thickness (Units III–VI only), and versus time (Units I–VI) by means of comparison with the record from northwestern Guangxi (South China), calibrated against U–Pb ages and ammonoid biochronozones (Galfetti et al., 2007b). The middle Smithian Arcoceratid A beds from Tulong (*Subunit IIIb*) have hitherto no direct counterpart in the South Chinese ammonoid succession; they probably correlate with a stratigraphic level between the Chinese *Flemingites rursiradiatus* beds and the *Owenites koeneni* beds (Brühwiler et al., 2007). Note the strong contraction of the Smithian part of the Tulong record resulting from calibration with time. Abbreviations: Gries.: Griesbachian; Diener.: Dienerian; Smith.: Smithian.

around the Spathian–Anisian boundary interval from Tulong indicate a positive $\delta^{13}C_{carb}$ shift as in other localities such as South China (Payne et al., 2004; Galfetti et al., 2007a), but due to condensation and possible hiatuses these data remain too spotty for a sound interpretation.

8. Conclusions

Our work provides a first precise and complete description of the Lower Triassic sedimentary record from the area of Tulong (South Tibet). Extensive bedrock-controlled sampling yields detailed ammonoid and conodont biostratigraphy that allows precise dating of the succession. The differences in the sedimentary evolution of the Lower Triassic section from Tulong with nearby sections such as Selong (i.e. prominent thickness and facies changes) reveal that sedimentation was influenced by large-scale block-faulting tectonics of the northern Gondwanian extensional margin. More importantly, comparison of the Tulong record with other Tethyan localities (Waagen, 1895; Guex, 1978; Bhargava et al., 2004; Galfetti et al., 2007a, 2008; pers. observation) reveals striking similar facies in parts of the Lower Triassic record. These similarities include (i) dolomites in the Griesbachian (Tulong, Spiti, Salt Range); (ii) thin-bedded, ammonoid-rich limestones in the early Dienerian (Tulong, Spiti, Salt Range); (iii) predominant clastic sedimentation in the late Dienerian (Tulong, Spiti, Salt Range, South China) which continues into the early Smithian in the Salt Range and in Tulong; (v) fossil-rich limestones in the middle Smithian (Tulong, Salt Range); and (vi) massive, fossil-rich nodular limestones in the Spathian (Tulong, Spiti, South China).

The striking similarities of the late Early Triassic sedimentary evolution from two widely distant localities in South China and Spiti were recently described by Galfetti et al. (2007a). Here, two distinct carbonate deposition episodes occur in the early Smithian (i.e. *Flemingites* beds) and in the Spathian, respectively. These are coeval with two major ammonoid and conodont diversification phases during the Early Triassic recovery (Brayard et al., 2006; Orchard, 2007). These carbonate episodes are characterized by increased levels of diversity and abundance of skeletal material, and therefore reflect an increasing recovery of the biosphere during favourable oceanographic conditions (Galfetti et al., 2008). In contrast with these well-oxygenated episodes, two Early Triassic dysoxic/anoxic episodes occur in South China in the late Dienerian and in the late Smithian, respectively, concomitant with large global positive carbon isotope excursions (Galfetti et al., 2007a, 2008). The late Smithian event was accompanied by a severe ammonoid and conodont extinction event (Brayard

et al., 2006; Orchard 2007) and major climatic change (Brayard et al., 2006; Galfetti et al., 2007a,c). However, our new data indicate that well-oxygenated waters and carbonate production persisted in the middle and late Smithian in Tulong. Only the earliest Spathian green shales suggest some indications of possible oxygen-poor bottom waters.

High-resolution sampling throughout the entire Tulong Formation yields a new ammonoid and conodont age-constrained, carbonate carbon isotope record for the Early Triassic in South Tibet. It confirms the well-documented perturbations of the global carbon cycle following the Permian–Triassic mass extinction event (Baud et al., 1996; Atudorei and Baud, 1997; Atudorei, 1999; Payne et al., 2004; Richoz, 2004; Corsetti et al., 2005; Galfetti et al., 2007a,b,c; Horacek et al., 2007a,b), such as a late Griesbachian positive shift and a major positive carbon isotope excursion at the Smithian/Spathian boundary. However, the well-known positive carbon isotope excursion at the Dienerian/Smithian boundary could not be replicated because of the lack of carbonates in this time interval. In combination with previously published carbon isotope records and new ammonoid data from several other Tethyan sections such as the Salt Range (Pakistan), Spiti (Northern India), and NW Guangxi (South China) (Brühwiler et al., 2007, ongoing work; Brayard and Bucher, 2008), our new data from Tulong provide additional evidence for the synchronicity of the positive carbon isotope excursion at the Smithian/Spathian boundary. The Smithian/Spathian boundary C-isotope excursion therefore represents a global perturbation of the carbon cycle as well as a key chemostratigraphic marker. Finally, minor fluctuations of carbonate carbon isotopes during the Spathian (i.e. a slight decrease of $\delta^{13}C$ values until the middle Spathian and a subsequent continuous increase) represent an at least Tethys-wide signal.

Acknowledgments

W. Xiaoqiao (Beijing) and Li Guobiao (Lhasa) are thanked for facilitating the field work in Tibet. T. Vennemann (Lausanne) is thanked for measuring carbon and oxygen isotopes at the Institute of Mineralogy and Geochemistry of the University of Lausanne. We are grateful to the Geological Institute of the University of Lausanne for providing the thin sections. P. Moix and S. Crasquin (Paris) helped one of us (A.B.) in the field and in lab preparation of samples. T. Algeo (Cincinnati) and an anonymous referee are thanked for their useful reviews of the manuscript. R.M. wishes to thank the Swiss NSF (project 200021–113816). This work was supported by the Swiss NSF project no. 200020-113554 (to H.B.).

References

Altiner, D., Baud, A., Guex, J., Stampfli, G., 1980. La limite Permien–Trias dans quelques localités du Moyen–Orient: recherches stratigraphiques et micropaléontologiques. Rivista Italiana di Paleontologia e Stratigrafia 85, 683–714.

Atudorei, N.–V., 1999. Constraints on the upper Permian to upper Triassic marine carbon isotope curve. Case studies from the Tethys. PhD Thesis, Lausanne, 155 pp.

Atudorei, N.-V., Baud, A., 1997. Carbon isotope events during the Triassic. Albertiana 20, 45–49.

Bassoullet, J.P., Colchen, M., 1976. La limite Permien–Trias dans le domaine tibétain de l'Himalaya du Népal. In: Jest, C. (Ed.), Himalaya. Colloques internationaux du CNRS. CNRS, Sèvres-Paris, pp. 41–52.

Batten, D.J., 1996. Palynofacies and petroleum potential. In: Jansonius, J., McGregor, D.C. (Eds.), Palynology: Principles and Applications. American Association of Stratigraphic Palynologists Foundation, pp. 1065–1084.

Baud, A., Atudorei, V., Sharp, Z., 1996. Late Permian and Early Triassic evolution of the Northern Indian margin: carbon isotope and sequence stratigraphy. Geodinamica Acta 9, 57–77.

Baud, A., Cirilli, S., Marcoux, J., 1997. Biotic response to mass extinction: the lowermost Triassic microbialites. Facies 36, 238–242.

Baud, A., Richoz, S., Cirilli, S. and Marcoux, J., 2002. Basal Triassic carbonate of the Tethys: a microbialite world. In: IAS (Ed.), 16th International Sedimentological Congress. RAU University, Johannesburg, pp. 24–25.

Baud, A., Richoz, S., Marcoux, J., 2005. Calcimicrobial cap rocks from the basal Triassic units: western Taurus occurrences (SW Turkey). Comptes Rendus Palevol 4, 569–582.

Baud, A., Richoz, S., Pruss, S., 2007. The lower Triassic anachronistic carbonate facies in space and time. Global and Planetary Change 55, 81–89.

Bassoulet, J.-P., Colchen, M., Guex, J., Lys, M., Marcoux, J., Mascle, G., 1978. Permien terminal néritique, Scythien pélagique et volcanisme sousmarin, indices de processus tectono-sédimentaires distensifs à la limite Permien-Trias dans un bloc exotique de la suture de l'Indus (Himalaya du Ladakh). Comptes Rendues de l'Académie des Sciences 287, 675–678.

Bhargava, O.N., Krystyn, L., Balini, M., Lein, R., Nicora, A., 2004. Revised litho- and sequence stratigraphy of the Spiti Triassic. Albertiana 30, 21–39.

Brayard, A., Bucher, H., 2008. Smithian (Early Triassic) ammonoid faunas from northwestern Guangxi (South China): taxonomy and biochronology. Fossils and Strata 55, 1–179.

Brayard, A., Bucher, H., Escarguel, G., Fluteau, F., Bourquin, S., Galfetti, T., 2006. The Early Triassic ammonoid recovery: paleoclimatic significance of diversity gradients. Palaeogeography, Palaeoclimatology, Palaeoecology 239, 374–395.

Brayard, A., Escarguel, G., Bucher, H., Monnet, C., Brühwiler, T., Goudemand, N., Galfetti, T., Guex, J., 2009. Good Genes and Good Luck: Ammonoid Diversity and the End-Permian Mass Extinction. Science 325, 1118–1121.

Brühwiler, T., Brayard, A., Bucher, H., Guodun, K., 2008. Griesbachian and Dienerian (Early Triassic) ammonoid faunas from northwestern Guangxi and southern Guizhou (South China). Palaeontology 51, 1151–1180.

Brühwiler, T., Bucher, H., Goudemand, N., Brayard, A., 2007. Smithian (Early Triassic) ammonoid faunas of the Tethys: new preliminary results from Tibet, India, Pakistan and Oman. New Mexico Museum of Natural History and Science Bulletin 41, 25–26.

Bucher, H., 1992. Ammonoids of the Hyatti Zone (Middle Anisian, Middle Triassic) and the Anisian transgression in the Star Peak Group (northwestern Nevada). Palaeontographica Abt. A 223, 137–166.

Bucher, H., Nassichuk, W.W., Spinosa, C., 1997. A new occurrence of the upper Permian ammonoid *Stacheoceras trimurti* Diener from the Himalayas; Himachal Pradesh, India. Eclogae Geologicae Helvetiae 90, 599–604.

Burg, J.P., 1983. Carte géologique du sud du Tibet / Ministère de la Géologie – Pékin (République Populaire de Chine); Contours synth. par J.P. Burg. China. Ministry of Geology and Mineral Resources, Paris.

Burns, S.J., McKenzie, J.A., Vasconcelos, C., 2000. Dolomite formation and biogeochemical cycles in the Phanerozoic. Sedimentology 47, 49–61.

Corsetti, F.A., Baud, A., Marenco, P.J., Richoz, S., 2005. Summary of Early Triassic carbon isotope records. Comptes Rendus Palevol 4, 405–418.

Epstein, A.G., Epstein, J.B., Harris, L.D., 1977. Conodont color alteration — an index to organic metamorphism. U.S. Geological Survey Professional Paper 995, 1–27.

Erwin, D.H., 1998. The end and the beginning: recoveries from mass extinctions. Trends in Ecology & Evolution 13, 344–349.

Fraiser, M.L., Bottjer, D.J., 2004. The non-actualistic Early Triassic gastropod fauna: a case study of the Lower Triassic Sinbad Limestone Member. Palaios 19, 259–275.

Fraiser, M.L., Twitchett, R.J., Bottjer, D.J., 2005. Unique microgastropod biofacies in the Early Triassic: indicator of long-term biotic stress and the pattern of biotic recovery after the end-Permian mass extinction. Comptes Rendus Palevol 4, 543–552.

Galfetti, T., Bucher, H., Brayard, A., Hochuli, P.A., Weissert, H., Guodun, K., Atudorei, V., Guex, J., 2007a. Late Early Triassic climate change: insights from carbonate carbon isotopes, sedimentary evolution and ammonoid paleobiogeography. Palaeogeography, Palaeoclimatology, Palaeoecology 243, 394–411.

Galfetti, T., Bucher, H., Ovtcharova, M., Schaltegger, U., Brayard, A., Brühwiler, T., Goudemand, N., Weissert, H., Hochuli, P.A., Cordey, F., Guodun, K.A., 2007b. Timing of the Early Triassic carbon cycle perturbations inferred from new U–Pb ages and ammonoid biochronozones. Earth and Planetary Science Letters 258, 593–604.

Galfetti, T., Hochuli, P.A., Brayard, A., Bucher, H., Weissert, H., Vigran, J.O., 2007c. Smithian–Spathian boundary event: evidence for global climatic change in the wake of the end-Permian biotic crisis. Geology 35, 291–294.

Galfetti, T., Bucher, H., Martini, R., Hochuli, P.A., Weissert, H., Crasquin-Soleau, S., Brayard, A., Goudemand, N., Brühwiler, T., Guodun, K., 2008. Evolution of Early Triassic outer platform paleoenvironments in the Nanpanjiang Basin (South China) and their significance for the biotic recovery. Sedimentary Geology 204, 36–60.

Garzanti, E., Angiolini, L., Sciunnach, D., 1996. The Permian Kuling Group (Spiti, Lahaul and Zanskar; NW Himalaya): sedimentary evolution during rift/drift transition and initial opening of Neo-Tethys. Rivista Italiana di Paleontologia e Stratigrafia 102, 175–200.

Garzanti, E., Nicora, A., Rettori, R., 1998. Permo-Triassic boundary and lower to middle Triassic in South Tibet. Journal of Asian Earth Sciences 16, 143–157.

Garzanti, E., Nicora, A., Tintori, A., 1994. Triassic stratigraphy and sedimentary evolution of the Anapurna Tethys Himalaya (Manang area, central Nepal). Rivista Italiana di Paleontologia e Stratigrafia 100, 195–226.

Garzanti, E., Sciunnach, D., 1997. Early Carboniferous onset of Gondwanian glaciation and Neo-Tethyan rifting in Southern Tibet. Earth and Planetary Science Letters 148, 359–365.

Glumac, B., Walker, K.R., 1998. A Late Cambrian positive carbon-isotope excursion in the southern Appalachians: relation to biostratigraphy, sequence stratigraphy, environments of deposition, and diagenesis. Journal of Sedimentary Research 68, 1212–1222.

Groves, J.R., Altiner, D., 2005. Survival and recovery of calcareous foraminifera pursuant to the end-Permian mass extinction. Comptes Rendus Palevol 4, 419.

Guex, J., 1978. Le Trias inferieur des Salt Ranges, Pakistan; problemes biochronologiques. Eclogae Geologicae Helvetiae 71, 105–141.

Guex, J., Hungerbühler, A., Jenks, J., Taylor, D., Bucher, H., 2005a. Dix-huit nouveaux genres d'ammonites du Spathien (Trias inférieur) de l'Ouest américan (Idaho, Nevada, Californie): Note préliminaire. Bulletin de Géologie Lausanne 362.

Guex, J., Hungerbühler, A., Jenks, J., Taylor, D., Bucher, H., 2005b. Dix-neuf nouvelles espèces d'ammonites du Spathien (Trias inférieur) de l'Ouest américan (Idaho, Nevada, Californie): Note préliminaire. Bulletin de Géologie Lausanne 363.

Hatleberg, E.W., 1982. Conodont biostratigraphy of the lower Triassic at Van Keulenfjorden, Spitsbergen and Thakhola Valley, Nepal. Wisconsin University, Madison. 148 pp.
Heim, A., Gansser, A., 1939. Central Himalaya: geological observations of the Swiss expedition 1936. Denkschriften der Schweizerischen Naturforschenden Gesellschaft 73 (Abh. 1, 245 pp.).
Horacek, M., Brandner, R., Abart, R., 2007a. Carbon isotope record of the P/T boundary and the Lower Triassic in the Southern Alps: evidence for rapid changes in storage of organic carbon. Palaeogeography, Palaeoclimatology, Palaeoecology 252, 347–354.
Horacek, M., Richoz, S., Brandner, R., Krystyn, L., Spötl, C., 2007b. Evidence for recurrent changes in Lower Triassic oceanic circulation of the Tethys: the $\delta^{13}C$ record from marine sections in Iran. Palaeogeography, Palaeoclimatology, Palaeoecology 252, 355–369.
Isozaki, Y., 1997. Permo-Triassic boundary superanoxia and stratified superocean: record from lost deep sea. Science 276, 235–238.
Jenkyns, H.C., 1974. Origin of red nodular limestone (Ammonitico Rosso, Knollenkalke) in the Mediterranean Jurassic: a diagenetic model. Special Publication of the International Association of Sedimentologists 1, 249–271.
Kakuwa, Y., 2008. Evaluation of palaeo-oxygenation of the ocean bottom across the Permian–Triassic boundary. Global and Planetary Change 63, 40–56.
Kaufman, A.J., Knoll, A.H., 1995. Neoproterozoic variations in the C-isotopic composition of seawater: stratigraphic and biogeochemical implications. Precambrian Research 73, 27–49.
Kershaw, S., Guo, L., Swift, A., Fan, J.S., 2002. Microbialites in the Permian–Triassic boundary interval in Central China: structure, age and distribution. Facies 47, 83–89.
Kershaw, S., Li, Y., Crasquin-Soleau, S., Feng, Q.L., Mu, X.N., Collin, P.Y., Reynolds, A., Guo, L., 2007. Earliest Triassic microbialites in the South China block and other areas: controls on their growth and distribution. Facies 53, 409–425.
Kershaw, S., Zhang, T.S., Lan, G.Z., 1999. A ?microbialite carbonate crust at the Permian–Triassic boundary in South China, and its palaeoenvironmental significance. Palaeogeography, Palaeoclimatology, Palaeoecology 146, 1–18.
Krystyn, L., Richoz, S., Bhargava, O.N., 2007. The Induan–Olenekian boundary (IOB) in mud — an update of the candidate GSSP section M04. Albertiana 36, 33–45.
Kummel, B., 1970. Ammonoids from the Kathwai Member, Mianwali Formation, Salt Range, West Pakistan. In: B. Kummel and C. Teichert (Eds.), Stratigraphic Boundary Problems: Permian and Triassic of West Pakistan. Department of Geology, University of Kansas, Special Publication pp. 177–192.
Liu, G., 1992. Permian to Eocene sedimenst and Indian passive margin evolution in the Tibetan Himalayas. Tübinger Geowissenschaftliche Arbeiten. Reihe A 13, 1–268.
Liu, G., Einsele, G., 1994. Sedimentary history of the Tethyan basin in the Tibetan Himalayas. Geologische Rundschau 83, 32–61.
Marcoux, J., Baud, A., 1996. Late Permian to Late Triassic Tethyan paleoenvironments. Three snapshots: Late Murgabian, Late Anisian, Late Norian. In: Nairn, X., Ricou, L.E., Vrielynck, B., Dercourt, J. (Eds.), The Tethys Ocean. The Ocean Basins and Margins. Plenum Press, New York, pp. 153–190.
Marshall, J.D., 1992. Climatic and oceanographic isotopic signals from the carbonate rock record and their preservation. Geological Magazine 129, 143–160.
Nowlan, G.S., Barnes, C.R., 1987. Application of conodont colour alteration indices to regional and economic geology. In: Austin, R.L. (Ed.), Conodonts : Investigative Techniques and Applications. Bristish Micropalaeontological Society Series. Ellis Horwood Limited, Chichester, West Sussex, PO19 1EB, England, pp. 188–202.
Ogg, J.G., von Rad, U., 1994. The Triassic of the Thakkola (Nepal). II: Paleolatitudes and comparison with other Eastern Tethyan Margins of Gondwana. Geologische Rundschau 83, 107–129.
Orchard, M.J., 2007. Conodont diversity and evolution through the latest Permian and Early Triassic upheavals. Palaeogeography, Palaeoclimatology, Palaeoecology 252, 93–117.
Orchard, M.J., 2008. Lower Triassic conodonts from the Canadian Arctic, their intercalibration with ammonoid-based stages and a comparision with other North American Olenekian faunas. Polar Research 27, 393–412.
Orchard, M.J., Krystyn, L., 1998. Conodonts of the Lowermost Triassic of Spiti, and New Zonation Based on *Neogondolella* Successions. Rivista Italiana di Paleontologia e Stratigrafia 104, 341–368.
Orchard, M.J., Nassichuk, W.W., Rui, L., 1994. Conodonts from the Lower Griesbachian *Otoceras Latilobatum* bed of Selong, Tibet and the Position of the Permian – Triassic Boundary, Pangea: global environments and resources. Canadian Society of Petroleum Geologists, pp. 823–843.
Ovtcharova, M., Bucher, H., Schaltegger, U., Galfetti, T., Brayard, A., Guex, J., 2006. New Early to Middle Triassic U–Pb ages from South China: calibration with ammonoid biochronozones and implications for the timing of the Triassic biotic recovery. Earth and Planetary Science Letters 243, 463–475.
Payne, J.L., Kump, L.R., 2007. Evidence for recurrent Early Triassic massive volcanism from quantitative interpretation of carbon isotope fluctuations. Earth and Planetary Science Letters 256, 264–277.
Payne, J.L., Lehrmann, D.J., Wei, J.Y., Orchard, M.J., Schrag, D.P., Knoll, A.H., 2004. Large perturbations of the carbon cycle during recovery from the end-Permian extinction. Science 305, 506–509.
Pruss, S.B., Bottjer, D.J., 2005. The reorganization of reef communities following the end-Permian mass extinction. Comptes Rendus Palevol 4, 553–568.
Racki, G., 1999. Silica-secreting biota and mass extinctions: survival patterns and processes. Palaeogeography, Palaeoclimatology, Palaeoecology 154, 107–132.
Rao, R.B., Zhang, Z.G., 1985. A discovery of Permo–Triassic transitional fauna in the Qomolangma Feng area: its implications for the Permo–Triassic boundary. Xizang Geology 1, 19–31.
Raup, D.M., Sepkoski, J.J., 1982. Mass Extinctions in the Marine Fossil Record. Science 215, 1501–1503.
Richoz, S., 2004. Stratigraphie et variations isotopiques du carbone dans le Permian supérieur et le Trias inférieur de la Néotéthys (Turquie, Oman et Iran). PhD., University of Lausanne, Switzerland. 281pp.
Richoz, S., Krystyn, L., Horacek, M., Spötl, C., 2007. Carbon isotope record of the Induan–Olenekian candidate GSSP Mud and comparison with other sections. Albertiana 35, 35–40.
Ricou, L.E., 1996. The plate tectonic history of the past Tethys ocean. In: Nairn, X., Ricou, L.E., Vrielynck, B., Dercourt, J. (Eds.), The Tethys Ocean. The Ocean Basins and Margins. Plenum Press, New York, pp. 3–70.
Shen, S.Z., Cao, C.Q., Henderson, C.M., Wang, X.D., Shi, G.R., Wang, Y., Wang, W., 2006. End-Permian mass extinction pattern in the northern peri-Gondwanan region. Palaeoworld 15, 3–30.
Spath, L.F., 1934. Part 4: The ammonoidea of the Trias, catalogue of the fossil cephalopoda in the British Museum (Natural History). The Trustees of the British Museum, London. 521 pp.
Spötl, C., Vennemann, T.W., 2003. Continuous-flow isotope ratio mass spectrometric analysis of carbonate minerals. Rapid Communications in Mass Spectrometry 17, 1004–1006.
Stampfli, G., Marcoux, J., Baud, A., 1991. Tethyan margins in space and time. Palaeogeography, Palaeoclimatology, Palaeoecology 87, 373–409.
Stanley, G.D., 2003. The evolution of modern corals and their early history. Earth Science Reviews 60, 195–225.
Tian, C.R., 1982. Triassic conodonts in the Tulong section from Nyalam County, Xizang (Tibet), China. Contributions to Geology Qinghai-Xizang (Tibet) Plateau 8, 153–165.
Tong, J., Shi, G.R., 2000. Evolution of the Permian and Triassic foraminifera in south China. In: Yin, H., Dickins, J.M., Shi, G.R., Tong, J. (Eds.), Permian–Triassic Evolution of Tethys andWestern Circum-Pacific. Developments in Palaeontology and Stratigraphy. Elsevier, Amsterdam, pp. 291–307.
Tozer, E.T., 1994. Canadian Triassic ammonoid faunas. Bulletin — Geological Survey of CanadaGeological Survey of Canada, Ottawa, ON, Canada. 663 pp.
Tozer, E.T., Calon, T.J., 1990. Triassic ammonoids from Jabal Safra and Wadi Alwa, Oman, and their significance. In: Robertson, A.H.F., Searle, M.P., Ries, A.C. (Eds.), The geology and tectonics of the Oman region. Geological Society Special Publications. Geological Society of London, London, United Kingdom, pp. 203–211.
Vasconcelos, C., McKenzie, J.A., 1997. Microbial mediation of modern dolomite precipitation and diagenesis under anoxic conditions (Lagoa Vermelha, Rio de Janeiro, Brazil). Journal of Sedimentary Research 67, 378–390.
von Rad, U., Dürr, S.B., Ogg, J.G., Wiedmann, J., 1994. The Triassic of the Thakhola (Nepal). I: stratigraphy and paleoenvironment of a north-east Gondwana rifted margin. Geologische Rundschau 83, 76–106.
Waagen, W., 1895. Salt-range fossils. Vol 2: fossils from the Ceratite Formation. Palaeontologia Indica 13, 1–323.
Wang, Y.G., Chen, C., Rui, L., Wang, Z., Liao, Z., He, J., 1989. A potential global stratotype of Permian–Triassic boundary. In: Zengquan, L., Fa'er, J. (Eds.), Developments in geoscience: Contribution to 28th International Geological Congress, July 1989, Washington, D. C., USA. Science Press, Beijing, pp. 221–230.
Wang, Y.G., He, G.X, 1976. Triassic ammonoids from the Mount Jolmo Lungma region. A report of scientific expedition in the Mount Jolmo Lungma region (1966–1968).
Wignall, P.B., Newton, R., 2003. Contrasting deep-water records from the Upper Permian and Lower Triassic of South Tibet and British Columbia: evidence for a diachronous mass extinction. Palaios 18, 153–167.
Woods, A.D., Baud, A., 2008. Anachronistic facies from a drowned Lower Triassic carbonate platform: lower member of the Alwa Formation (Ba'id Exotic), Oman Mountains. Sedimentary Geology 209, 1–14.
Yugan, J., Shuzhong, S., Zili, Z., Silong, M., Wei, W., 1996. The Selong section, candidate of the Global Stratotype section and point of the Permian–Triassic boundary. In: Yin, H. (Ed.), The Palaeozoic–Mesozoic Boundary Candidates of Global Stratotype Section and Point of the Permian–Triassic Boundary. China University Press, Wuhan, pp. 127–137.

Appendix 5:

Conference Abstracts

by Elke Hermann et al.

2008–2010

EARLY TRIASSIC RECORDS IN LOW PALAEOLATITUDES – EVIDENCE FOR A GLOBAL AND MAJOR CLIMATIC CHANGE AT THE SMITHIAN/SPATHIAN BOUNDARY

Elke Hermann[1], Peter A. Hochuli[1], Hugo Bucher[1], Ghazala Roohi[2]

[1]Institute and Museum of Palaeontology, University of Zurich, Karl Schmid-Str. 4, 8006 Zurich, Switzerland

[2]Pakistan Museum of Natural History, Garden Avenue, Islamabad 44000, Pakistan

ehermann@pim.uzh.ch

The Early Triassic is characterized by a delayed recovery of terrestrial and marine ecosystems. Especially the Smithian/Spathian boundary is marked by a significant global ammonoid and conodont turnover as well as a change in the palynological associations of the Boreal realm. There, the Smithian/Spathian transition is marked by a conspicuous change from a hygrophyte dominated assemblage in the Smithian to a xerophyte dominated Spathian spore/pollen association. (Galfetti et al., 2007 Geology).

In order to test the global significance of this signal, it is necessary to gain a better knowledge of palynological records from the low palaeolatitudes. Here, we present the composition of the Early Triassic microfloras of Nammal Nala, Salt Range, Pakistan. Ammonoids and conodonts provide the high resolution age control at Nammal Nala.

The Smithian palynological assemblage is characterized by a general dominance of hygrophytic elements. The proportion ranges between 80% in the lower Smithian, 60 % in the middle Smithian and 95% in the upper Smithian. Slightly below the Smithian/Spathian boundary, between the *Anasibirites/Wasatchites* horizon and the *Glyptophiceras* horizon, the composition changes dramatically. The assemblages show an increased proportion of xerophytic elements, which varies between 40 % and around 95% within the Spathian. This event coincides with the onset of a positive shift in the $\delta^{13}C$ record which marks the Smithian/Spathian boundary (Galfetti et al., 2007 EPSL). The Smithian/Spathian boundary climatic event can thus be traced from high to low latitudes, thus demonstrating its global significance.

References:

Galfetti, T, et al. (2007). Timing of the Early Triassic carbon cycle pertubations inferred from new U-Pb ages and ammonoid biochronozones. EPSL 258: 593-604.

Galfetti, T., Hochuli, P. A., Brayard, A., Bucher, H., Weissert, H., Virgan, J. O., (2007) Smithian/Spathian boundary event: Evidence for global climatic change in the wake of the end-Permian biotic crisis. Geology 35: 291-294.

XII IPC/VIII IOPC, Bonn (Germany) 30 Aug. – 5 Sept. 2008
Terra Nostra, 2008/2 – No 276

PALYNOFACIES OF THE EARLY TRIASSIC SECTION OF NAMMAL NALA, SALT RANGE, PAKISTAN - EVIDENCE FOR HOSTILE ENVIRONMENTAL CONDITIONS OR EVEN EARLY TRIASSIC ANOXIA?

Elke Hermann[1], Peter A. Hochuli[1], Hugo Bucher[1], Ghazala Roohi[2]

[1]Institute and Museum of Palaeontology, University of Zurich, Karl Schmid-Strasse 4, 8006 Zurich, Switzerland

[2]Pakistan Museum of Natural History, Garden Avenue, Islamabad 44000, Pakistan

Following the end-Permian extinction, the biotic recovery was globally delayed until the Middle Triassic. The recovery process appears to be linked to palaeoclimatic and palaeoenvironmental changes throughout the Early Triassic. In order to find new evidence for environmental changes in the Early Triassic, the classical section of Nammal Nala in the Salt Range (Pakistan) has been studied with respect to the content and composition of the particulate organic matter (POM).

The 118 m thick Mianwali Formation can be divided into six lithological units, which are from base to top Kathwai, Lower Ceratite Limestone (LCL), Ceratite Marls (CM), Ceratite Sandstone (CS), Upper Ceratite Limestone (UCL), "Niveaux Intermédiaires" (NI) and Topmost Limestone (TL). The lithologies consist of siltstones, sandstones, limestones and dolomites. LCL, UCL and TL include several carbonate beds, whereas the CM, CS and the NI are dominated by silt- and sandstones. Several erosional horizons underlined by intraformational breccias can be observed throughout the section.

Palynofacies analysis of the section show that two trends are interfering with each other. A general regressive trend is overlain by four smaller transgressive-regressive cycles. The lowermost cycle starts in the Kathwai (upper Griesbachian) and LCL (Dienerian) with a strong terrestrial signal with 100% phytoclasts (mostly opaque particles). Marine oxygen deficient conditions are indicated in the lower part of the CM (Dienerian) where AOM is dominant. Assemblages from the middle part of the CM (Smithian) are dominated by terrestrial kerogen (phytoclasts and sporomorphs), which reflect well oxygenated conditions and can be interpreted as a second lowstand. Well oxygenated conditions continue up to the top of the Early Triassic Mianwali Formation. The following transgressive cycle is reflected by increased numbers of acritarchs, reaching 50% of the POM. A third lowstand at the transition from CS to UCL (Smithian) is reflected again by abundant spores combined with low numbers of acritarchs. The forth lowstand in the middle part of the NI (Spathian) is represented by fully terrestrial conditions with 100% phytoclasts, which is followed by a minor trangressive signal (< 10% acritarchs) in the TL.

The total organic carbon (TOC) content ranges between 0 and 0.6%. Even in the AOM-rich Dienerian rocks TOC does not exceed 0.6%. Thus there is no evidence for a prolonged Early Triassic anoxia and oxygenated environmental conditions prevailed during most of the Early Triassic.

GSA Annual Meeting, Houston (USA) 5 – 9 Oct. 2008
Paper no. 318-1

MAJOR CLIMATIC CHANGE AT THE SMITHIAN/SPATHIAN BOUNDARY – EVIDENCE FROM LOW PALAEOLATITUDINAL RECORDS

Elke Hermann[1], Peter A. Hochuli[1,2], Hugo Bucher[1, 2], Thomas Brühwiler[1], Nicolas Goudemand[1], Ghazala Roohi[3]

[1]Institute and Museum of Palaeontology, University of Zurich, Karl Schmid-Str. 4, 8006 Zurich, Switzerland
[2] Department of Earth Sciences, ETH Zürich, Switzerland
[3]Pakistan Museum of Natural History, Garden Avenue, Islamabad 44000, Pakistan
ehermann@pim.uzh.ch

The delayed recovery of marine and terrestrial ecosystems after the end-Permian extinction event is still up for debate. Focusing on the Smithian/Spathian boundary, palaeoecological changes are reflected by a significant global faunal turnover as indicated by ammonoids (Brayard et al. 2006) and conodonts (Orchard 2007) as well as a change in the palynological associations of the Boreal realm. There, the Smithian/Spathian transition is marked by a conspicuous change from spore dominated assemblages in the Smithian to gymnosperm dominated assemblages in the Spathian (Galfetti et al. 2007a).
Here, we present the composition of the Early Triassic microfloras of Nammal, Salt Range, Pakistan. Ammonoids and conodonts provide the high resolution age control of the studied section (Brühwiler et al. 2007).
The late Smithian palynological assemblages are characterized by a general dominance of hygrophytic elements. Slightly below the Smithian/Spathian boundary, between the *Anasibirites* beds and the *Glyptophiceras* beds, the composition changes dramatically with a drastically increasing proportion of xerophytic elements. This event coincides with the onset of a positive shift in the $\delta^{13}C$ record marking the Smithian/Spathian boundary (Galfetti et al. 2007b). Preliminary results from southern Tibet also indicate a similar trend from hygrophyte-dominated to xerophyte-dominated assemblages across the boundary.
Thus the Smithian/Spathian boundary climatic event can be traced from high to low latitudes, demonstrating its global significance.

Brayard, A. et al. 2006: PPP 239:374-395.
Brühwiler, T. et al. 2007: New Mexico Mus. Nat.Hist.& Sci. Bull. 41: 26-26.
Galfetti, T. et al. 2007a: Geology 35: 291-294.
Galfetti, T. et al. 2007b: EPSL 258: 593-604.
Orchard, M.J. 2007: PPP 252: 93-117.

6th Swiss Geoscience Meeting, Lugano (Switzerland) 21 – 23 Nov. 2008

EVIDENCE FOR MAJOR CLIMATIC CHANGE AT THE SMITHIAN-SPATHIAN BOUNDARY FROM LOW PALAEOLATITUDINAL RECORDS

Hermann Elke*, Hochuli Peter A.*,**, Bucher Hugo*,**, Brühwiler Thomas*, Goudemand Nicolas* & Ghazala Roohi***

*Paläontologisches Institut und Museum, University of Zurich, Karl Schmid-Strasse 4, CH-8006 Zürich (ehermann@pim.uzh.ch)

**Geologisches Institut, Universitätsstrasse 16,CH-8050 Zürich

***Pakistan Museum of Natural History, Garden Avenue, PK-44000 Islamabad

The delayed recovery of marine and terrestrial ecosystems after the end-Permian extinction event is still up for debate. Focusing on the Smithian-Spathian boundary, palaeoecological changes are reflected by a significant global faunal turnover as indicated by ammonoids (Brayard et al. 2006) and conodonts (Orchard 2007) as well as a change in the palynological associations of the Boreal realm. There, the Smithian-Spathian transition is marked by a conspicuous change from spore dominated assemblages in the Smithian to gymnosperm dominated assemblages in the Spathian (Galfetti et al. 2007a).

Here, we present the composition of the Early Triassic microfloras of Nammal, Salt Range, Pakistan. Ammonoids and conodonts provide the high resolution age control of the studied section (Brühwiler et al. 2007). The late Smithian palynological assemblages are characterized by a general dominance of hygrophytic elements. Slightly below the Smithian-Spathian boundary, between the *Anasibirites* beds and the *Glyptophiceras* beds, the composition changes dramatically with a drastically increasing proportion of xerophytic elements. This event coincides with the onset of a positive shift in the $\delta^{13}C$ record marking the Smithian-Spathian boundary (Galfetti et al. 2007b). Preliminary results from southern Tibet also indicate a similar trend from hygrophyte-dominated to xerophyte-dominated assemblages across the boundary. Thus, there is evidence for the Smithian-Spathian boundary climatic event from high as well as from low palaeolatitudes, demonstrating its global significance.

REFERENCES

Brayard, A., Bucher, H., Escarguel, G., Fluteau, F., Bourquin, S., Galfetti, T. 2006: The Early Triassic ammonoid recovery: Paleoclimatic significance of diversity gradients, Palaeogeography, Palaeoclimatology, Palaeoecology, 239, 374-395.

Brühwiler, T., Bucher, H., Goudemand, N., Brayard, A. 2007: Smithian (Early Triassic) Ammonoid successions of the Tethys: New preliminiary results from Tibet, India, Pakistan and Oman, New Mexico Museum of Natural History and Science Bulletin, 41, 25-26.

Galfetti, T., Hochuli, P. A., Brayard, A., Bucher, H., Weissert, H., Virgan, J. O., 2007a: Smithian/Spathian boundary event: Evidence for global climatic change in the wake of the end-Permian biotic crisis, Geology, 35, 291-294.

Galfetti, T., Bucher, H., Ovtcharova, M., Schaltegger, U., Brayard, A., Brühwiler, T., Goudemand, N., Weissert, H., Hochuli, P.A., Cordey, F., Goudun, K. 2007b: Timing of the Early Triassic carbon cycle perturbations inferred from new U-Pb ages and ammonoid biochronozones, Earth and Planetary Science Letters, 258, 593-604.

Orchard, M.J. 2007: Conodont diversity and evolution through the latest Permian and Early Triassic upheavals, Palaeogeography, Palaeoclimatology, Palaeoecology, 252, 93-117.

EGU General Assembly, 2 – 7 May 2010
Geophysical Research Abstracts Vol.12, EGU2010-2394-5

CLIMATIC CHANGES IN THE AFTERMATH OF THE END-PERMIAN MASS EXTINCTION - EVIDENCE FROM PALYNOLOGICAL RECORDS OF PAKISTAN

Elke Hermann[1], Peter A. Hochuli1, Hugo Bucher[1], Thomas Brühwiler[1], David Ware[1], Michael Hautmann[1], Helmut Weissert[2], Stefano Bernasconi[2], Ghazala Roohi[3], Khalil Reman[3], Aamir Yaseen[3]

[1]Institute and Museum of Palaeontology, University of Zurich, Karl Schmid-Str. 4, 8006 Zurich, Switzerland
[2] Department of Earth Sciences, ETH Zürich, Switzerland
[3]Pakistan Museum of Natural History, Garden Avenue, Islamabad 44000, Pakistan

Early Triassic fossil records feature the varied responses of the biosphere to the greatest mass extinction in the Phanerozoic. Few marine clades recovered relatively quickly (e.g. ammonoids, Brayard et al., 2009 and conodonts, Orchard, 2007) whereas benthic organisms showed a comparatively slow recovery (Hautmann et al., 2008). Environmental perturbations such as climatic changes are thought to be the cause for the delayed recovery of some clades (Galfetti et al., 2007). A climatic framework of this interval can be inferred from the palynological data of the sedimentary archives of the thermally unaltered Salt Range and Surghar Range sections in Pakistan.

Spore-pollen records from four sections provide new evidence for climatic perturbations in the aftermath of the end-Permian mass extinction. The palynological record encompasses isolated assemblages from the Permian and the Griesbachian and a continuous from the middle Dienerian up to the Anisian. Concomitant organic carbon isotope data allow for correlation with other Early Triassic sections. Age control is provided by ammonoids and conodonts.

Two markedly different assemblages have been recovered from the Chhidru Formation:
One assemblage is dominated by typical Permian floral elements such as conifer and pteridosperm pollen indicating dry climates in the late Permian. The second is dominated by lycopod spores (up to 60%). In comparison with other records this assemblage can be assigned to the Griesbachian indicating more humid climates and the diachrony of the boundary between Chhidru Formation and Mianwali Formation.
Middle to late Dienerian palynological assemblages are characterised by the dominance of spores indicating humid climates. Lower Smithian assemblages show a continuous increase pollen abundance indicating a trend towards dryer climates. This trend is reversed in the middle Smithian, with increasing dominance of spores towards the upper Smithian. A distinct and abrupt change from spore-dominated to pollen-dominated assemblages marks the onset of dryer climates in the Spathian and Anisian. This change coincides with the Anasibirites/Wasatchites beds and the onset of a global positive shift in the organic and inorganic carbon isotopes. It can be correlated with a similar climatic change in the Boreal realm (Galfetti et al., 2007).

Values of bulk organic C-isotopes from the samples with Permian affinity range around -26‰. Whereas $\delta^{13}C_{org}$ values of samples with Griesbachian affinity display values around -29‰ indicating a stratigraphic level near the negative carbon isotope minimum that marks PT boundary sections worldwide.
Middle Dienerian $\delta^{13}C_{org}$ values around -28‰ are followed by an increase across the Dienerian-Smithian boundary with peak values of -24‰ during the middle Smithian. The following steady decrease to values around -32‰ reached at the level of the Anasibirites/Wasatchites beds is followed by a pronounced positive shift at the Smithian-Spathian boundary. Stable Spathian values (around -28‰) are followed by another positive shift at the Spathian-Anisian boundary (-25‰).

The three positive shifts (Dienerian-Smithian, Smithian-Spathian, and Spathian Anisian) coincide with or seem to be closely related to changes in the spore/pollen - ratio implying a close relationship between environmental changes and ecological responses. C-isotope perturbations in the Early Triassic are thought to be caused by recurring CO_2 releases probably by late protracted pulses of the Siberian Trap emplacement (Payne & Kump, 2007).The close relationship between positive C-isotope excursions, extinctions of ammonoids, and climatic changes proposed by Galfetti et al. (2007) for the Smithian/Spathian boundary and can be confirmed for the most pronounced shifts of the Early Triassic.

References

Brayard, A., Escarguel, G., Bucher, H., Monnet, C., Brühwiler, T., Goudemand, N., Galfetti, T., Guex, J. (2009). Good Genes and Good Luck: Ammonoid Diversity and the End-Permian Mass Extinction. Science 325: 1118-1121.

Galfetti, T., Hochuli, P. A., Brayard, A., Bucher, H., Weissert, H., Vigran, J. O. (2007) Smithian/Spathian boundary event: Evidence for global climatic change in the wake of the end-Permian biotic crisis: Hautmann, M., Bucher, H., Nützel, A., Brühwiler, T., Goudemand, N., Brayard, A. (2008) Recovery of Benthos versus Nekton after the End-Permian Mass Extinction Event - A Preliminary Comparison, GSA annual meeting: Houston, Tx, p. no. 285-14.

Orchard, M.J. (2007) Conodont diversity and evolution through the latest Permian and Early Triassic upheavals: Palaeogeography, Palaeoclimatology, Palaeoecology, 252: 93-117.

Payne, J.L., Kump, L. R. (2007) Evidence for recurrent Early Triassic massive volcanism from quantitative interpretation of carbon isotope fluctuations: Earth and Planetary Science Letters 256: 264-277.

Appendix 6:

Organic matter and palaeoenvironmental signal during the Early Triassic biotic recovery: the Salt Range and Surghar Range records

with Peter A. Hochuli, Sabine Méhay, Hugo Bucher, Thomas Brühwiler, David Ware, Michael Hautmann, Ghazala Roohi, Khalil-ur-Rehman, Aamir Yaseen

Supplementary Table 1

Supplementary Table 1 $\delta^{13}C_{org}$ and $\delta^{13}C_{org}$ values of the Nammal, Chhidru, Chitta-Landu and Narmia section.

$\delta^{13}C_{org}$ Nammal section				
Lithological unit		**sample**	**m to Chhidru Fm./Kathwai Member**	**$\delta^{13}C_{org}$ [‰]**
	1	NA 119	118.12	-24.115
TL	**2**	NA 117	116.40	-27.413
	3	NA 115	114.92	-27.042
	4	NA 113	112.90	-27.378
	5	NA 109	110.05	-27.635
	6	NA 105	107.90	-28.541
	7	NA 104	104.80	-28.353
NI	**8**	NA 103	100.90	-26.764
	9	NA 102	100.40	-26.483
	10	NA 100	99.00	-26.626
	11	NA 97	96.12	-25.309
	12	NA 95	95.10	-26.307
	13	NA 92	93.45	-26.149
	14	NA 91A	92.60	-23.466
	15	NA 89	89.20	-25.721
	16	NA 88	87.00	-26.504
	17	NA 87	86.57	-26.381
	18	NA 85	84.45	-26.911
	19	NA 849	81.30	-26.485
	20	NA 846	77.70	-27.332
	21	NA 845	76.15	-27.716
	22	NA 844	74.12	-27.505

	23	NA 651	72.40	-27.743
	24	NA 79	72.17	-27.045
	25	NA 650	72.10	-25.939
	26	NA 649	71.10	-27.275
UCL	**27**	NA 78	71.32	-27.023
	28	NA 77	69.65	-25.974
	29	NA 648	69.33	-26.353
	30	NA 647	69.07	-26.112
	31	NA 646-5	68.48	-27.492
	32	NA 646-4	68.23	-27.642
	33	NA 646-3	68.15	-27.662
	34	NA 646-2	68.03	-27.547
	35	NA 646-1	67.92	-27.965
	36	NA 76	67.70	-28.365
	37	NA 646	67.45	-28.109
	38	NA 75	67.15	-27.789
	39	NA 645	67.08	-29.027
	40	NA 401	66.86	-26.42
	41	NA 644	66.68	-31.023
	42	NA 400	66.58	-28.802
	43	NA 74	66.05	-26.16
	44	NA 643	64.60	-32.291
	45	NA 73	64.30	-25.81
	46	NA 70	62.75	-26.265
	47	NA 68	59.50	-26.58
	48	NA 642	59.35	-33.285
CS	**49**	NA 65	54.45	-29.647
	50	NA 64	51.97	-26.036
	51	NA 63	50.30	-25.761
	52	NA 62	46.95	-25.285
	53	NA 61	43.25	-24.499
	54	NA 60	42.70	-25.338
	55	NA 58	41.25	-24.144
	56	NA 57	40.35	-25.400
	57	NA 318	38.16	-23.943
	58	NA 317	36.49	-23.773
	59	NA 56	36.30	-24.634
CM	**60**	NA 316	35.24	-23.423
	61	NA 315	34.15	-23.985
	62	NA 314	33.20	-24.219
	63	NA 55	32.67	-25.162
	64	NA 53	31.92	-25.521
	65	NA 52	30.75	-25.092
	66	NA 313	30.60	-25.102
	67	NA 312	30.42	-25.308
	68	NA 51	30.22	-25.682
	69	NA 311-2	29.08	-24.405
	70	NA 49	28.37	-24.940
	71	NA 311-1	27.82	-25.597
	72	NA 310	27.55	-25.556
	73	NA 213	26.90	-25.168
	74	NA 212	25.85	-25.099
	75	NA 309	24.73	-25.340
	76	NA 211	23.75	-24.841
	77	NA 210	22.30	-24.539
	78	NA 208	20.10	-25.342
	79	NA 207	18.68	-26.032
	80	NA 206	17.85	-24.908
	81	NA 205	14.85	-26.308
	82	NA 501	14.07	-24.433
	83	NA 500	13.90	-25.845
	84	NA 204	13.65	-25.107
	85	NA 307	13.10	-27.267
	86	NA 306	12.90	-30.241

	87	NA 305	12.57	-27.721
	88	NA 304	12.17	-28.152
	89	NA 303	11.78	-28.388
	90	NA 302	11.52	-25.158
	91	NA 301	11.24	-28.388
	92	NA 300	10.70	-28.527
	93	NA 203	10.60	-27.286
	94	NA 208AIO	9.92	-29.969
	95	NA 202	9.15	-28.627
	96	NA 201AIO	7.40	-28.786
	97	NA 201	7.30	-28.566
	98	NA 200	6.80	-28.781
LCL	**99**	NA 19	4.78	-25.798
Kathwai	**100**	NA 10A	3.44	-26.372

$\delta^{13}C_{carb}$ Nammal section

Lithological unit		**sample**	**m to Chhidru Fm./Kathwai Member**	**$\delta^{13}C_{org}$ [‰]**	**$\delta^{18}O_{carb}$ [‰]**
	1	BV 11	73.22	-1.07	-7.90
	2	BV 10	72.07	-1.08	-8.44
	3	NA2-9a	71.99	-1.326	-7.928
	4	BV 9	71.79	-0.43	-7.13
	5	BV 8a	71.60	1.468	-8.287
	6	BV 7a	71.34	0.816	-6.391
	7	BV 7	71.15	1.63	-8.01
	8	BV 6a	70.92	1.58	-6.76
	9	BV 6	70.82	2.03	-8.25
	10	BV 5	70.69	1.86	-7.52
	11	BV4	70.22	2.06	-8.12
	12	BV 3	70.02	1.28	-8.70
	13	BV 2a	69.62	1.40	-6.15
	14	BV 2	69.19	2.27	-7.20
	15	BV 1	68.80	2.35	-7.52
UCL	**16**	NA 2-15	67.59	0.95	-6.04
	17	NA 2-14	67.39	0.16	-6.65
	18	NA 2-13	67.05	0.87	-7.72
	19	NA 2-12	66.87	0.28	-8.69
	20	NA 2-11	66.49	-0.09	-8.53
	21	NA 2-10	66.12	-0.39	-7.93
	22	NA 2-9	65.16	-1.653	-8.136
	23	NA 2-8	64.40	-2.35	-8.65
	24	NA 2-7	64.09	-2.28	-8.01
	25	NA 2-5	63.69	-2.15	-8.39
	26	NA 2-4	63.46	-2.14	-8.21
	27	NA 2-3	63.24	-2.02	-8.10
	28	NA 2-2	62.64	-2.36	-8.20
	29	NA 2-1	62.37	-2.18	-7.78
	30	NA 2-1a	61.92	-2.43	-8.28
	31	NA 2-1b	61.58	-2.34	-8.27
	32	NA 2-1c	61.30	-2.31	-8.38
CM	**33**	NAM 532 ISO	18.55	-6.28	-5.78
	34	NA 214 AIO	15.10	-5.64	-6.73
	35	NA 213 AIO	14.38	-0.55	-7.63
	36	NAM 534I	14.00	-1.872	-4.654
	37	NAM 545I	13.00	0.53	-4.23
	38	NAM 541I	12.35	1.50	-5.15
	39	NAM 540I	12.25	1.34	-5.14
	40	NAM 542I	12.06	1.84	-4.69
	41	NAM 543I	11.83	0.58	-5.38

42	NAM 544I	11.40	-0.86	-5.19
43	NAM 101I	11.12	0.44	-4.71
44	NA 208 AIO	9.92	0.632	-6.668
45	NA 207 AIO	9.55	0.68	-5.31
46	NA 206 AIO	9.35	1.06	-5.55
47	NA 205 AIO	9.10	0.36	-5.85
48	NA 203 AIO	8.68	0.106	-5.162
49	NA 202 AIO	8.28	-0.01	-5.13
50	NA 201 AIO	7.40	-0.64	-6.25
51	NA 200 AIO	6.90	-0.07	-5.48

$\delta^{13}C_{org}$ Chhidru section

Lithological unit		**sample**	**m to Chhidru Fm./Kathwai Member**	**$\delta^{13}C_{org}$ [‰]**
UCL	**1**	CH 300	88.68	-28.624
	2	CH 299	86.63	-27.329
	3	CH 298	86.04	-25.335
	4	CH 297	84.69	-31.212
	5	CH 296	84.22	-30.689
	6	CH 295	84.05	-30.404
	7	CH 294	83.50	-30.273
	8	CH 293	83.00	-30.747
	9	CH 292	82.73	-31.531
	10	CH 291	82.45	-31.644
	11	CH 290	82.15	-30.783
	12	CH 289/CH 288	80.27	-31.732
	13	CH 287	80.09	-32.087
	14	CH 286	79.40	-32.348
	15	CH 285	77.82	-32.981
	16	CH 284	76.04	-31.147
	17	CH 283	74.78	-32.551
	18	CH 282	74.10	-29.77
	19	CH 281	73.80	-31.936
	20	CH 280	73.40	-31.363
	21	CH 279	72.55	-31.253
	22	CH 278	71.05	-31.123
	23	CH 277	70.85	-30.484
	24	CH 276	70.58	-31.776
	25	CH 275	70.32	-30.915
CS	**26**	CH 274	67.63	-30.353
	27	CH 273	65.55	-29.6
	28	CH 272	64.95	-28.656
	29	CH 271	63.40	-27.382
	30	CH 270	62.30	-28.377
	31	CH 269	61.90	-28.185
	32	CH 268	52.78	-26.273
	33	CH 267	52.10	-24.785
	34	CH 266	49.88	-24.696
	35	CH 265	48.55	-24.438
	36	CH 265-1	47.13	-24.096
	37	CH 264	46.08	-25.682
CM	**38**	CH 250	42.75	-25.751
	39	CH 249	41.30	-25.558
	40	CH 248	40.08	-25.211
	41	CH 247	38.45	-26.34
	42	CH 215	28.08	-26.527
	43	CH 214	27.10	-26.248
	44	CH 213	26.25	-26.28
	45	CH 212	25.73	-26.758

	46	CH 211	25.05	-26.254
	47	CH 210	22.55	-26.539
	48	CH 209	20.10	-26.804
	49	CH 208	18.42	-26.631
	50	CH 207	17.02	-26.707
	51	CH 206	15.80	-25.551
	52	CH 205	15.28	-25.429
	53	CH 204	14.30	-27.795
	54	CH 203	12.42	-27.74
	55	CH 202	11.50	-27.768
	56	CH 201	10.33	-26.432
	57	CH 200	9.93	-27.74
	58	CH 199	8.40	-27.886
LCL	**59**	CH 102	4.26	-24.35
	60	CH 101	3.59	-24.911
	61	CH 100	1.25	-26.349
Chhidru	**62**	CH 99	-0.31	-26.147
	63	CH 98	-0.45	-25.495
	64	CH 97	-0.65	-26.632
	65	CH 96	-0.91	-26.089
	66	CH 95	-1.17	-26.157
	67	CH 94	-1.60	-26.025
	68	CH 93	-1.96	-25.485

$\delta^{13}C_{carb}$ Chhidru section

Lithological unit		**sample**	**m to Chhidru Fm./Kathwai Member**	**$\delta^{13}C_{carb}$ [‰]**	**$\delta^{18}O_{carb}$ [‰]**
	1	CH 300A	88.57	1.29	-7.13
TL	**2**	CH 298A	88.20	-0.14	-7.91
	3	CH 297A	87.90	1.89	-6.72
	4	CH 296A	87.48	0.14	-7.18
	5	CH 295A	87.20	0.93	-2.38
	6	CH 294A	86.73	0.44	-2.73
	7	CH 293A	84.95	3.80	-1.82
NI	**8**	CH 292A	82.00	-1.77	-6.63
	9	CH 291A	80.88	-2.50	-7.36
	10	CH 290A	80.37	-2.60	-7.25
	11	CH 289A	79.74	-2.70	-7.11
	12	CH 288A	77.68	-2.34	-6.07
	13	CH 287A	77.18	-2.87	-7.56
	14	CH 286A	76.68	-2.58	-6.82
	15	CH 284A	75.14	-2.55	-7.30
	16	CH 283A	74.49	-2.54	-7.17
	17	CH 282A	72.93	-2.21	-6.86
	18	CH 281A	71.85	-2.41	-7.38
	19	CH 280A	70.38	-2.36	-7.54
	20	CH 279A	69.38	-2.14	-6.71
	21	CH 277A	58.38	-1.88	-7.88
BL	**22**	CH 8A	8.94	-1.75	-7.42
	23	CH 7-1A	8.70	0.35	-7.36
	24	CH 7-2A	8.32	-0.59	-6.66
	25	CH 7A	6.25	-0.09	-8.08
	26	CH 6A	6.02	-0.93	-7.48
	27	CH 5A	5.85	-0.06	-7.68
	28	CH 4A	5.77	0.04	-6.99
	29	CH 3A	5.60	0.11	-7.93
	30	CH 2A	5.43	0.20	-7.15
	31	CH 1A	5.30	-0.06	-7.93

$\delta^{13}C_{org}$ Chitta-Landu section

Lithological unit		sample	m to Chhidru Fm./Kathwai Member	$\delta^{13}C_{org}$ [‰]
Landa Mmb.	**1**	PU 200	154.06	-25.294
	2	PU 199	153.72	-24.357
	3	PU 198	152.75	-24.214
	4	PU 197	151.84	-24.017
	5	PU 196	149.89	-25.651
	6	PU 195	147.50	-25.384
	7	PU 194	145.66	-25.804
	8	PU 193	144.70	-25.271
	9	PU 192	143.40	-24.502
	10	LA 82	141.44	-25.183
	11	LA 81	139.85	-25.835
	12	LA 80	138.95	-25.691
	13	LA 79	137.90	-25.095
	14	LA 78	135.97	-24.912
	15	LA 77	134.80	-24.975
	16	LA 76	133.03	-24.414
	17	LA 75	131.72	-25.096
TL	**18**	LA 74	127.45	-27.302
	19	LA 73	126.84	-26.879
	20	LA 72	126.12	-27.633
	21	LA 71	125.16	-26.512
	22	LA 70	124.31	-27.785
	23	LA 69	123.25	-28.037
	24	LA 68	122.50	-28.211
	25	LA 67	121.36	-28.253
	26	LA 66	120.40	-28.514
	27	LA 65	117.60	-28.184
	28	LA 64-2 PU	115.78	-27.998
	29	PU 120	114.73	-28.015
	30	PU 119	114.25	-27.502
	31	PU 117	113.29	-28.616
	32	PU 115	111.90	-28.084
	33	PU 114	111.15	-28.156
	34	LA 58	107.40	-29.541
	35	LA 57, PU 113-2	106.38	-29.68
	36	LA 56	105.60	-26.768
	37	LA 55	103.98	-28.581
	38	LA 54	102.40	-29.059
	39	LA 53	101.42	-28.218
NI	**40**	LA 52	98.20	-26.936
	41	LA 51	97.20	-27.041
	42	LA 50	95.32	-26.071
	43	PU 112	93.23	-26.817
	44	PU 111	90.40	-26.635
	45	PU 110	89.20	-27.289
	46	PU 109	87.49	-26.602
	47	PU 108	86.20	-27.038
	48	PU 106	84.00	-26.551
	49	PU 104-3	80.93	-27.345
	50	PU 104-2	76.50	-27.937
	51	PU 104-1	75.30	-27.139
	52	PU 104	73.93	-28.046
	53	PU 103-1	71.52	-27.516
	54	PU 103	70.29	-27.49
	55	PU 102	68.42	-27.047
	56	PU 101	66.55	-28.209
	57	PU 100	64.94	-25.754

	58	PU 99	63.97	-26.091
UCL	**59**	PU 98	62.78	-27.037
	60	PU 97	61.70	-25.987
	61	PU 96	60.95	-25.864
	62	PU 95	59.77	-26.107
	63	PU 94	59.64	-26.34
	64	PU 93	59.15	-27.179
	65	PU 92	57.45	-32.859
	66	PU 91	56.55	-30.235
	67	PU 90	55.80	-31.636
	68	PU 89	54.45	-26.773
	69	PU 88	53.58	-29.166
	70	PU 87	51.00	-28.392
	71	PU 86	48.20	-30.17
	72	PU 85	44.90	-30.512
CS	**73**	PU 19	31.14	-23.682
	74	PU 18	29.13	-24.881
	75	PU 17	28.02	-25.069
	76	PU 16	25.05	-25.288
CM	**77**	PU 15	23.62	-24.336
	78	PU 14-6	21.58	-24.636
	79	PU 14-5	18.63	-25.121
	80	PU 14-4	15.64	-25.743
	81	PU 14-3	12.70	-25.833
	82	PU 14-2	10.60	-26.458
	83	PU 14-1	8.64	-26.559
	84	PU 14	6.98	-26.392
	85	PU 13-1	5.95	-26.612
	86	PU 13	5.18	-25.421
	87	PU 12	4.25	-25.476
LCL	**88**	PU 11	3.50	-28.563
	89	PU 10	3.25	-27.64
	90	PU 9	3.07	-28.301
	91	PU 8	2.60	-28.856
	92	PU 7	2.42	-29.592
	93	PU 6	2.17	-29.133
	94	PU 5	2.09	-29.286
	95	PU 4	1.95	-29.966
	96	PU 3	1.88	-27.752
Chhidru	**97**	PU 2	-0.05	-25.398
	98	PU 1	-0.18	-25.63

$\delta^{13}C_{carb}$ Chitta-Landu section

Lithological unit		**sample**	**m to Chhidru Fm./Kathwai Member**	**$\delta^{13}C_{carb}$ [‰]**	**$\delta^{18}O_{carb}$ [‰]**
UCL	**1**	PU 100A	63.63	1.108	-5.695
	2	PU 99A	63.40	2.113	-6.985
	3	PU 98A	63.12	1.757	-4.607
	4	PU 97-1A	62.88	1.659	-5.762
	5	PU 97A	62.67	2.173	-5.502
	6	PU 96A	62.48	2.639	-6.049
	7	PU 95-1A	62.26	2.856	-6.808
	8	PU 95A	62.14	3.1	-5.786
	9	PU 94A	61.95	3.113	-6.411
	10	PU 93A	61.47	2.115	-5.956
	11	PU 92-1A	61.15	3.241	-4.676
	12	PU 92A	60.75	3.763	-5.022
	13	PU 91-1A	60.38	4.067	-5.054
	14	PU 91A	60.05	3.207	-4.601
	15	PU 90A	59.37	3.654	-4.047

	16	PU 89A	58.90	3.174	-4.773
	17	PU 88A	58.65	2.413	-5.374
	18	PU 87-1A	58.43	0.783	-7.042
	19	PU 87A	57.90	-0.427	-7.944
	20	PU 86-1A	57.58	-0.553	-8.226
	21	PU 86A	57.32	-1.544	-8.487
	22	PU 85-1A	56.65	-1.407	-8.146
	23	PU 85A	56.27	-1.486	-8.260
	24	PU 84-1A	55.94	-1.638	-8.511
	25	PU 84A	55.53	-2.055	-8.544
	26	PU 83A	55.12	-1.959	-7.990
	27	PU 82A	54.28	-2.244	-8.323
	28	PU 81A	51.53	-2.335	-8.191
	29	PU 80A	50.28	-2.218	-8.372
	30	PU 79A	48.05	-2.118	-7.088
	31	PU 78-1A	47.25	-2.047	-7.908
	32	PU 78A	45.87	-1.762	-8.130
	33	PU 77A	44.08	-1.608	-8.075
	34	PU 76A	41.90	-1.558	-8.990
LCL	**35**	PU 8A	3.97	2.29	-7.577
	36	PU 7A	3.80	3.392	-3.287
	37	PU 6A	3.35	2.011	-8.254
	38	PU 5A	3.13	2.348	-7.764
	39	PU 4-2A	3.00	2.415	-7.709
	40	PU 4-1A	2.90	2.105	-7.399
	41	PU 4A	2.78	2.135	-8.270
	42	PU 3-1A	2.68	1.956	-7.129
	43	PU 3A	2.55	2.065	-7.599
	44	PU 2A	2.28	2.191	-6.985
	45	PU 1-1A	2.02	2.247	-6.862
	46	PU 0A	1.63	2.442	-5.351

$\delta^{13}C_{org}$ Narmia section

Lithological unit		**sample**	**m to Chhidru Fm./Kathwai Member**	**$\delta^{13}C_{org}$ [‰]**
CM	**1**	NR 22	9.75	-26.39
	2	NR 21	8.97	-26.259
	3	NR 20	8.22	-26.383
	4	NR 19	7.52	-26.33
	5	NR 18	6.92	-25.131
	6	NR 17	6.22	-25.108
LCL	**7**	NR 16	4.10	-29.057
	8	NR 15	3.65	-28.671
	9	NR 14	2.88	-29.231
	10	NR 13	2.65	-29.823
	11	NR 12	2.50	-28.697
Chhidru/Kathw.	**12**	NR 11	-0.05	-29.059
Chhidru	**13**	NR 10	-0.66	-28.379
	14	NR 9	-7.32	-23.789

Acknowledgements

Thanks go to Prof. Hugo Bucher. The results of this thesis are based on the opportunity to work at the Institute and Museum of Palaeontology at University of Zurich (PIMUZ) and to participate in the Early Triassic research group. I am very thankful for his supervision and helpful and enthusiastic support during my work. I am enormously indebted to Prof. Peter A. Hochuli, for constructive discussions and manuscript reviews. Without his expertise in palynology I would have been lost in the palynomorph taxanomy.

The financial support from the Swiss National Science Foundation project 200020-127716/1 (to H. Bucher) is gratefully acknowledged.

I wish to thank Prof. Helmut Weissert and Dr. Stefano Bernasconi from ETH Zurich (ETHZ) for offering me the possibility to use the isotope lab at the ETHZ and their collaboration on this specific topic and to get a deep insight into the world of chemostratigraphy. Additionally Helmut Weissert is thanked for his willingness to referee my theses.

Many thanks go also to Prof. Peter Linder from the Institute of Botany, University of Zurich for his willingness to co-examine the thesis. Prof. Ulrich Heimhofer from the Institute for Geology, Mineralogy and Geophysics, Ruhr Univerity Bochum is thanked for his commitment to write and expertise for my PhD thesis.

During the field seasons in Pakistan, I had the pleasure to get in touch with Ghazala Roohi, Latif Khan, Khalil-ur-Rehman and Aamir Yaseen. Without the administrational efforts of Ghazala, field work would not have been possible. She also offered me insights into the Pakistani culture and traditions and a deep friendship developed for which I want to express my gratefulness. The staff of the Pakistan Museum of Natural History is thanked for their support during our stays in Pakistan.

I would also like to thank the administrational staff at PIMUZ, their support allowed working free of bureaucratic, computer caused, and library related barriers. Further I would like to thank the laboratory staff of PIMUZ and ETHZ, Markus Hebeisen, Julia Huber, Leonie Pauli, Maria Coray Strasser, Stewart Bishop for their collaboration.

I also want to thank all my colleagues at the PIMUZ and the Geological Institute at ETHZ, in particular Dr. Thomas Brühwiler, Kenneth de Baets, Jasmina Hugi, Richard Hofmann, David Ware, Carlo Romano, Dr. Michael Hautmann, Christian Kolb, Nicolas Goudemand, and Dr. Christian Klug. They made the time during my PhD studies enjoyable and unforgettable for me. Peter Hochuli, Thomas Brühwiler, David Ware and Michael Hautmann participated also in the field work. Special thanks go to Christina Keller; she shared with me the ups and downs of PhD student's life.

Thanks go as well to all my good friends with whom I have enjoyed many great moments.

Without the persistent love and support of Hannes Schneebeli and my family this work would not have been possible.

Curriculum Vitae

HERMANN, Elke

Date of birth:	17 July 1977
Nationality:	German
Place of birth:	Stuttgart (Germany)

Education

1994–1997 1997	Ferdinand von Steinbeis Gymnasium, Tuttlingen, Germany Abitur (A-levels)
1997–2001 2001	Student at the Weingarten University of Education, Germany State examination for teaching profession
2001–2005	Diploma student (Geology) at the University of Karlsruhe, Germany
2005	Diploma thesis: Geology and Tectonics of the upper Murg-Valley, Baiersbronn, SW-Germany. Supervisors: Prof. Dr. H. G. Stosch, Dr. W. Fielitz
2006	Assistant geologist at gbm – Gesellschaft für Baugeologie und –messtechnik mbH, Baugrundinstitut, Ettlingen, Germany
2007–2010	PhD student at the Institute and Museum of Palaeontology, University of Zurich, Switzerland Dissertation: Early Triassic palaeoenvironmental and floral changes on North Gondwana Supervisors: Prof. Dr. Peter A. Hochuli Prof. Dr. Hugo Bucher Prof. Dr. Helmut Weissert